# COMPARATIVE ANALYSIS OF THE DISCORDANCE BETWEEN THE GLOBAL TRANSCRIPTIONAL AND PROTEOMIC RESPONSE OF THE YEAST *SACCHAROMYCES CEREVISIAE* TO DELETION OF THE F-BOX PROTEIN, *GRR1*

Joshua William Heyen

Submitted to the faculty of the University Graduate School
in partial fulfillment of the requirements
for the degree
Doctor of Philosophy
in the Department of Biochemistry and Molecular Biology,
Indiana University

May 2010

Accepted by the Faculty of Indiana University, in partial fulfillment of the requirements for the degree of Doctor of Philosophy.

_____

Mark G. Goebl, Ph.D., Chair

_____

Peter J. Roach, Ph.D.

Doctoral Committee

_____

David E. Clemmer, Ph.D.

January 15th, 2010

_____

Mu Wang, Ph.D.

_____

Jake Yu Chen, Ph.D.

DEDICATED TO
MY WIFE, CANDY, MY SON, NATHANIEL,
AND MY DAUGHTER, ADDISON
FOR THEIR UNCONDITIONAL LOVE
AND SUPPORT

ACKNOWLEDGMENTS

The proceeding volume is the culmination of several years where not only my blood, sweat, and tears were sacrificed in the pursuit of scientific discovery but also the very core of my being. What is the core of one's being? I define it as an immense network of life instances through which a person's psyche develops an awareness of who they are and what they stand for. Of course, being the scientist that I am, I believe that one is pre-disposed by genetics at the beginning of life to interpret life circumstances with a certain shade of color or temperament. However, the initial hue of one's perspective is only the base coat for a lifetime that is susceptible to artistic license from many different painters. In this way a person's psyche is like a canvas, a sentient, emotionally predisposed canvas that can choose to accept or deny strokes (life instances) of color from any person or situation they may encounter. Thus, I wholeheartedly believe that the people I have met are painters from which many strokes of perception I have received and have attempted to add to my "core". This volume is the manifestation of a tremendous amount of effort that at times seemed beyond my capacity; the completion of which can only be attributable to not just me but the myriad of people who have contributed to my "core".

I would like to acknowledge each of my immediate and extended family members that have each had to sacrifice in some way for me to pursue this endeavor. "Thank you" seems inappropriate in this instance since the sacrifices made warrant much more than words commonly uttered in passive conversation. At the risk of sounding soft and hokey, which for those that know me is a tremendous risk to take on my part; the only word that seems applicable here is love. So to each of whom I mention here I give my love. To my wife, Candy, who despite her own frustrations, put up with me these past eight years and never waned in her belief that I am exceptional. To my kids, Nathaniel and Addison, whose smiles infect me every day with the energy to do my best in all aspects of life. To my mother and father, who have molded me into the person I am today and have taught me too many things to mention. To my sister and my brother, whom I admire more than they can possibly imagine. To my

grandparents, who always have believed in me and encouraged me to aim high. To my extended family, who all have contributed greatly to my maturation and development as a person. Finally, to my in-laws and friends, who have supported my wife and me through this long journey. To all of you I give my deepest gratitude and love.

I would also like to express my extraordinary gratitude to my mentor, Mark Goebl, who showed me what it is to be a real scientist. Also, to my committee I extend my deepest gratitude for our thoughtful discussions and their wise guidance along this journey.

ABSTRACT

Joshua William Heyen

COMPARATIVE ANALYSIS OF THE DISCORDANCE BETWEEN THE GLOBAL TRANSCRIPTIONAL AND PROTEOMIC RESPONSE OF THE YEAST *SACCHAROMYCES CEREVISIAE* TO DELETION OF THE F-BOX PROTEIN, *GRR1*

The Grr1 (Glucose Repression Resistant) protein in *Saccharomyces cerevisiae* is an F-box protein for the E3 ubiquitin ligase protein complex known as the $SCF^{Grr1}$ (Skp, Cullin, F-box). F-box proteins serve as substrate receptors for this complex and in this capacity Grr1 serves to promote the ubiquitylation and subsequent proteasomal degradation of a number of intracellular protein substrates. Substrates of $SCF^{Grr1}$ include the G1-S phase cyclins, Cln1 and Cln2, the Cdc42 effectors and cell polarity proteins, Gic1 and Gic2, the FCH-bar domain protein, Hof1, required for cytokinesis, the meiosis activating serine/threonine protein kinase, Ime2, the transcriptional regulators of glucose transporters, Mth1 and Std1, and the mitochondrial retrograde response inhibitor Mks1. Stabilization of these substrates lead to pleiotrophic phenotypic defects in *grr1Δ* strains including resistance to glucose repression, accumulation of *grr1Δ* cells in G2 and M phase of the cell cycle, sensitivity to osmotic stress, and resistance to divalent cations. However, many of these phenotypes are not reflected at the gene expression level. We conducted a quantitative genomic

and proteomic comparison of 914 loci in a *grr1Δ* and wild-type strain grown to early log-phase in glucose media. These loci encompassed 16.7% of the *Saccharomyces* proteome of which 22.3% exhibited discordance between gene and protein expression. GO process enrichment analysis revealed that discordant loci were enriched in the processes of “trafficking”, “mitosis”, and “carbon/energy” metabolism. Here we show that these instances of discordance are biologically relevant and in fact reflect phenotypes of *grr1Δ* strains not evident at the transcriptional level. Additionally, through combined biochemical and network analysis of discordant loci among “carbon and energy metabolism” we were able to not only construct a model for central carbon metabolism in *grr1Δ* strains but also were able to elucidate a novel molecular event that may serve to regulate glucose repression of genes needed for respiration in response to changes in glucose concentration.

Mark G. Goebl, Ph.D., Chair

## SUMMARY OF PROPOSED RESEARCH

The goal of my thesis project was to develop and apply a global proteomics strategy to discover novel mechanisms by which the *Saccharomyces cerevisiae* F-box protein, Grr1, acts to regulate multiple cellular processes in *Saccharomyces*. The Grr1 protein is a member of a class of proteins known as F-box proteins. F-box proteins are found in all eukaryotic organisms and serve to regulate multiple cellular processes such as development, endocytosis, transcription, translation, and targeted protein degradation. Many of these essential functions for the F-box proteins are carried out through a conserved mechanism by which the F-box protein serves as a receptor to target various protein substrates for ubiquitin modification. Most F-box proteins discovered to date facilitate protein ubiquitylation in conjunction with a well conserved complex of proteins collectively known as the SCF (Skp, Cullin, F-box). The archetype of the SCF complex is the *S. cerevisiae* SCF composed of the proteins Skp1, Cdc53, Rbx1, Cdc34, and a variable F-box protein. Multiple F-box proteins can associate with this core group of four SCF components adding modularity to the complex and the ability to recognize multiple cellular substrates. The attachment of ubiquitin to SCF substrates has been extensively shown to result in the substrate's degradation. It is through this targeted degradation that the SCF can control numerous cellular processes including transcription (by targeting transcription factors for degradation), translation, and cell signaling. As one can imagine the function of this complex is critical to the cell and alterations in its function could lead to disease and indeed diseases such as Parkinson's, Huntington's, and Alzheimer's have all been linked to defects in the ubiquitylation machinery.

The importance of the SCF complex in maintaining cellular homeostasis underscores the need to characterize each of its components as they relate to the cell as a whole. Recently, through the development of global assays and screens the molecular toolbox available to biologists has expanded allowing researchers to begin to probe the cell and measure its molecular response on a global system wide level. Micro-arrays allow for the measurement of all actively

transcribed genes in a cell providing a snapshot of the cell at the transcriptional level. This valuable tool allows scientists to probe the transcriptional framework that dictates genes expression; however the molecular state of the cell at the protein level can only be inferred. Thus, a method to assay global protein expression is needed to complement the gene expression data. Consistencies and paradoxes between these two data sets will aid in our understanding of the cell on a system wide level.

Global proteomic strategies based on liquid chromatography followed by mass spectrometry have really just begun to be used as a method to analyze complex protein mixtures. Development in this field has been rapid, still major hurdles are yet to be overcome. First, researchers are still unable to detect and quantify the entire proteome of an organism reliably. This is due to limitations with the current resolving power of liquid chromatography and the sensitivity of widely available mass spectrometers. Second, scoring algorithms for accurately matching experimental MS/MS spectra to the correct peptide are inefficient, leaving many spectra unidentified, and sometimes inaccurate, containing many false positives. Third, quantification of a peptide and/or protein is limited by the fact that post-translational modification of a peptide can skew the relative ratios obtained for the peptide resulting in inaccurate quantification. Finally, software to efficiently and effectively mine the results of the data generated to arrive at interesting biological discoveries are in short supply and those that are available, though useful, fall short of the mark.

Thus, a significant part of my thesis will detail the development of a global proteomics strategy that generates valid and accurate LC-MS based results and allows for the efficient and effective analysis of this data to uncover novel scientific discoveries. This method will be applied to discovering novel roles for the F-box Grr1 in *S. cerevisiae* cell biology. For my thesis I hope to contribute to the development of LC-MS based global proteomic strategies and apply these developments to a significant biological question (the system wide role of the F-box protein Grr1) using the biology to validate my strategy and the strategy to uncover novel biological roles for SCF based functions.

TABLE OF CONTENTS

LIST OF TABLES

LIST OF FIGURES

# LIST OF ABBREVIATIONS

ATP ..... Adenosine TriPhosphate

*CDC4*..... Cell Division Cycle four

*CDC34*..... Cell Division Cycle thirty four

*CDC53*..... Cell Division Cycle fifty three

CDK..... Cyclin Dependent Kinase

DNA..... DeoxyriboNucleic Acid

*GRR1* ..... Glucose Repression Resistant one

GO..... Gene Ontology

GTP ..... Guanosine Tri-Phosphate

HECT..... Homologous to E6-AP Carboxyl Terminus

HIV ..... Human Immunodeficiency Virus

HPV ..... Human Papillomavirus

HSV ..... Herpes Simplex Virus

LC-MS ..... Liquid Chromatography coupled to Mass Spectrometry

LTQ ..... Linear Trapping Quadrupole

*MET30*..... Methionine requiring thirty

MudPIT..... MUltiDimensional Protein Identification Technology

RING ..... Really Interesting New Gene

*RSP5*..... Reverses Spt- Phenotype five

*RUB1*..... Related to Ubiquitin one

SCF ..... Skp, Cullin, F-box

SILAC..... Stable Isotope Labeling of Amino acids in Cell culture

*SKP1* ..... Suppressor of Kinetochore Protein mutant one

SPS ..... Ssy1, Ptr3, Ssy5 amino acid sensor

TCA ..... TriCarboxylic Acid

*UBA1* ..... UBiquitin Activating enzyme one

*UBI4* ..... UBIquitin four

UFD ..... Ubiquitin Fusion Degradation

# CHAPTER 1: INTRODUCTION TO UBIQUITYLATION AND *GRR1*

## 1.1. The Process of Ubiquitylation and its Multifarious Role in Eukaryotes

The molecular regulatory process of ubiquitylation, as the name implies, is ubiquitously conserved in all eukaryotic cells. Defects in this process in mammalian cells lead to the manifestation of complex human diseases. In mammalian cells, ubiquitylation plays a critical role in axonal morphogenesis in the brain [1], the control of cellular aging [2], innate and adaptive immunity [3], angiogenesis [4], and many other processes. Given the eclectic nature of ubiquitylation, it is not surprising that multiple diseases are intimately linked to defects in the molecular machinery that carry out the reactions of ubiquitylation (for review, see [5]). Breast, ovarian [6,7], colorectal [8-10], as well as HPV linked cervical cancers [11,12] display alterations in the ubiquitylation system. Viruses such as HIV [13-18] and HSV [19-22] possess genes that encode components of the ubiquitylation machinery. Finally, the development of neurodegenerative diseases such as Alzheimer's [23-26], Parkinson's [27,28,26], and Huntington's [29,30] has been linked to defects in components of the ubiquitylation system.

The multitude of processes that rely on a functional ubiquitylation system and the prevalence of diseases caused by a defective ubiquitylation system underscore the need to understand not only the molecular mechanism of protein ubiquitylation but also the cellular response to perturbations of this system. The fact that the core molecular mechanism of ubiquitylation is conserved in the yeast, *Saccharomyces cerevisiae*, enables researchers to utilize this single celled eukaryote as a model system for studying this process. The ease with which *S. cerevisiae* can be grown in the laboratory and manipulated genetically, as well as its eukaryotic nature has made this organism a vital contributor to our understanding of many cellular processes, not the least of which is ubiquitylation. It is through research using this organism that much of our current understanding of the molecular processes necessary for a proteins ubiquitylation were revealed.

## 1.2. Ubiquitin and the Molecular Mechanism of Ubiquitylation

Ubiquitin is a 76 amino acid protein. In 1980, it was discovered as an essential post-translational modification necessary for the targeted degradation of many intracellular protein substrates by the 26S proteasome [31,32]. Since that time, we have found that the role ubiquitin plays in the biology of eukaryotic cells is vast and it is clear that the nature of the ubiquitin modification and the processes it facilitates are far more diverse than first hypothesized. Classically, ubiquitin has been defined by its role in targeting protein substrates for degradation by the 26S proteasome. Targeting of substrates to the 26S proteasome occurs through the oligomeric addition of ubiquitin moieties to the protein substrate in the form of lysine 48 linked ubiquitin chains [33]. It was later shown that the multimeric addition of at least four covalently linked ubiquitin molecules facilitated the efficient degradation of modified substrates [34]. Ubiquitin chains are formed by covalent attachment of the C-terminal glycine of a free ubiquitin to an acceptor lysine on the substrate associated ubiquitin [35]. Initial investigations primarily focused on the mechanism of lysine 48 linkage formations but it soon became clear that other lysine residues on the ubiquitin molecule could also serve as acceptor sites for chain formation. These various chains facilitate diversified cellular processes and this fact emphasizes the multifarious role of ubiquitin in cell biology.

Ubiquitin contains eight lysines available for chain formation and three (Lysine 48, 63, and 29) have been found to form multi-ubiquitin chains [36]. Additionally, ubiquitin can be added to substrates without forming a chain. Each of these types of ubiquitin modifications has been shown to participate in unique intracellular processes. Lysine 63 linked ubiquitin chains are necessary for DNA repair, mitochondrial DNA inheritance, ribosome function, stress adaptation, and endocytic trafficking of some integral membrane proteins [37]. Lysine 29 linked ubiquitin chains have been shown to play a role in the UFD (Ubiquitin Fusion Degradation) pathway [38] and mono-ubiquitylation is necessary for retroviral budding, endocytosis, and histone regulation [39]. Thus, each of these different ubiquitin modifications has been shown to facilitate distinct cellular processes

and thus the nature of the ubiquitin modification determines to some extent the effect that ubiquitin attachment will have on a protein substrate (Figure 1.1). However, in all cases the purpose of ubiquitylation is to promote protein/protein interactions that commonly culminate in the altered sub-cellular localization of the protein substrate.

It is clear that these different ubiquitin modifications are critical to facilitating the diverse cellular functions in which ubiquitin participates. However, the eclectic nature of the ubiquitin signal is not solely explained by the presence of its alternative forms. Mechanistic studies have revealed that various modular complexes of proteins interchangeably work together to facilitate substrate recognition, ubiquitin attachment, and chain formation. Even though the nature of the ubiquitin modification and the cellular fate of the substrates modified by this protein are highly variable, remarkably, the core mechanism of ubiquitin attachment is highly conserved.

Through an enzymatic cascade involving three essential enzyme types, free intracellular ubiquitin is activated and covalently attached to a protein substrate (Figure 1.1). First, an E1 ubiquitin activating enzyme catalyzes, in an ATP dependent manner, the covalent attachment of ubiquitin to itself through formation of a thiolester bond between the C-terminal glycine of ubiquitin and the catalytic cysteine of the E1 [40]. Three gene products in *S. cerevisiae* have been classified as E1s, however only the product of the essential *UBA1* gene participates in ubiquitin activation [41]. Following ubiquitin activation, transfer of ubiquitin to an E2 conjugating enzyme is facilitated by an ATP dependent transacylation reaction. Eleven E2's have been discovered to catalyze ubiquitin modifications in *S. cerevisiae*, each thought to be required for ubiquitin modification of different intracellular substrates in different intracellular locations. However, hundreds or possibly thousands of different proteins are modified by ubiquitin in *S. cerevisiae* and the nature of the ubiquitin modification for each of these substrates varies.

To enable the modification of multiple substrates by a specific E2, the E2 enzymes associate with different complexes of proteins collectively known as E3

ubiquitin ligases. Together a particular E3 complex and the E2 recognize and ubiquitylate specific substrates. Therefore, the number of substrates ubiquitylated by a specific E2 is often substantial since one E2 can associate with multiple different E3 ubiquitin ligases. The number of E3 ubiquitin ligases in yeast and humans is unknown since little sequence homology exists between the constituent proteins in these complexes. However, known E3 complexes can be broadly divided into two categories based on the presence of a RING (really interesting new gene) finger domain or a HECT (homologous to E6-AP carboxyl terminus) domain containing protein in the complex [37]. Perhaps the best characterized of these complexes is the RING Finger E3, SCF (Skp1, Cdc53/Cullin, and F-box receptor) complex.

### 1.3. The SCF (Skp, Cullin, F-Box) Complex

The *S. cerevisiae* SCF complexes consist of five proteins that each facilitates specific aspects of SCF function (Figure 1.2). Cdc53, Skp1, Rbx1, and F-box proteins work in collaboration with the E2, Cdc34, which together are responsible for the recognition and ubiquitylation of protein substrates. Domain characterization of the Skp1 protein has emphasized its role as a molecular bridge (or chaperone) linking F-box proteins to the core enzymatic proteins, Cdc53 and Rbx1 [42]. The Cdc53 protein contains three domains which enable its interaction with Skp1, the RING Finger protein Rbx1, and the E2 ubiquitin conjugating enzyme Cdc34, respectively [43,44]. A scaffolding role for Cdc53 in the SCF complex is well established but limiting Cdc53 to this functional definition seems premature at this time. The extreme C-terminus of Cdc53 is the most conserved region of the protein and serves as the site of Rub1 (an ubiquitin-like protein) modification, yet no functional significance to this region has been assigned [45]. The RING Finger protein, Rbx1, directly interacts with Cdc53, Cdc34, and the F-box protein [46]. Rbx1 is essential to the SCF for ubiquitylation of substrates. The RING Finger motif of Rbx1 promotes interaction with the E2; Cdc34. Rbx1 is thought to position Cdc34 next to the substrate, promoting

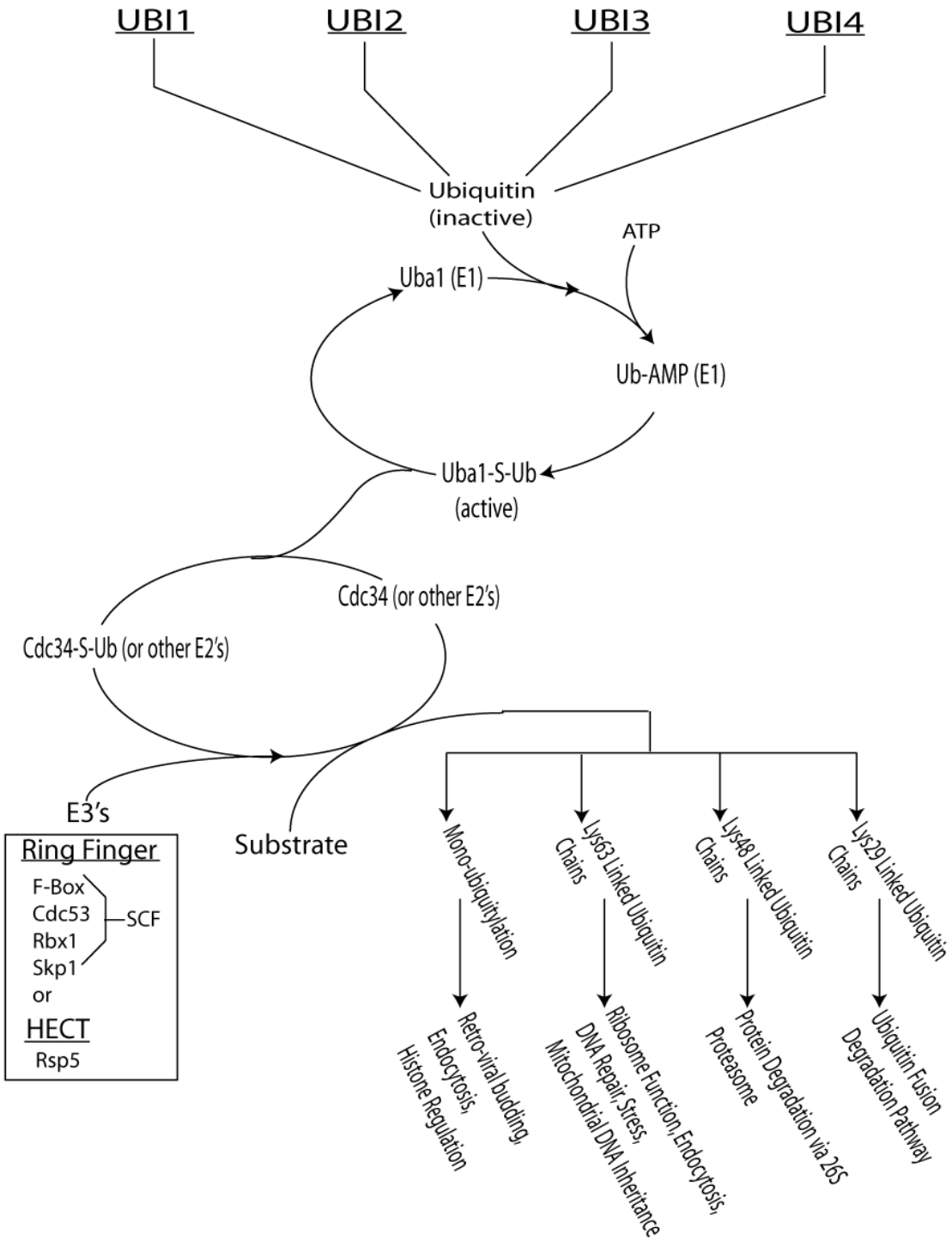


**Figure 1.1. Ubiquitylation in *Saccharomyces cerevisiae*.** The intracellular pool of ubiquitin is supplied by four genes in yeast. Free ubiquitin is then activated by Uba1 and transferred to any one of 13 E2 enzymes which in conjunction with a RING Finger or HECT type complex from an E3 ubiquitin ligase. The E3 then recognizes and catalyzes the ubiquitylation of the protein substrate. Alternative ubiquitin modifications can be appended on the substrate and have been shown to be important for diversified cellular processes.

efficient substrate modification [44]. Substrate recognition is the responsibility of a class of proteins called the F-box proteins. These proteins serve as adapters for the core SCF complex enabling multiple substrates to be ubiquitylated by the same core machinery. Cdc4, Grr1, and Met30 are three such proteins that have been identified in S. cerevisiae and each promotes the ubiquitylation and subsequent degradation of unique substrates.

### 1.4. F-Box Proteins

The F-box proteins comprise a growing class of proteins detected in multiple eukaryotic organisms. Members of this class of proteins are similar in that they possess a highly conserved domain termed the F-box. Mutations in this F-box region abrogate interaction with Skp1 [47] supporting the role of this domain in promoting F-Box protein association with the SCF. Multiple F-box proteins can associate interchangeably with the core SCF components. Thus, the SCFs are considered modular complexes and the associated F-box defines the repertoire of substrates that may be ubiquitylated. Hence, many different SCF complexes are possible and are usually distinguished by a nomenclature that denotes the F-box associated, for example $SCF^{Cdc4}$ indicates the Cdc4 associated complex. Factors regulating the temporal and spatial association of different F-box proteins with the core SCF complex have not been identified.

A C-terminal truncation of an F-box protein results in the inability to degrade the appropriate substrate and thus has been determined to mediate F-box substrate interactions [48]. The presence of WD-40 or leucine-rich repeats in the C-termini of most F-box proteins initially suggested the presence of two distinct signals mediating F-box/substrate interaction. However, both regions have been found to recognize phosphorylated substrates and no conserved recognition sequences have been found that would distinguish the substrates of these two domains [49]. In fact, phosphorylation of the target protein is required to initiate most interactions between substrate and F-box proteins [50].

Seventeen F-box proteins exist in *S. cerevisiae* [51], but only three have been extensively characterized both biochemically and genetically. Through

these studies it became apparent that a single F-box protein can promote the ubiquitylation of multiple substrates resulting in yet another level of SCF modularity. Among the *Saccharomyces* E3's, more substrates have been discovered for the $SCF^{Grr1}$ than any other SCF complex. The reason for this partially stems from the fact that *S. cerevisiae* cells harboring null mutations at the *GRR1* locus are viable (null mutations of *CDC4* as well as *MET30* are lethal) making *grr1Δ* cells particularly amenable to biochemical and genetic analysis. Substrates for the $SCF^{Grr1}$ complex include the cyclins, Cln1 and Cln2 [52], the meiosis activating kinase Ime2 [53], the Hof1 protein required for cytokinesis [54], the Cdc42 effectors Gic2 and Gic1 [55], the glucose responsive transcriptional repressors, Mth1 and Std1 [56], the retrograde signaling regulator Mks1 [57], and the Snf1 kinase interacting protein Gis4 [58]. Additionally, Grr1 has been shown to be indirectly involved in controlling the targeted degradation of nutrient transporters [59,60] and to be required for SPS (Ssy1, Ptr3, Ssy5) signaling in response to external amino acids [61-63] suggesting that more substrates have yet to be uncovered.

### 1.5. Grr1

Much of what is known about the role of Grr1 in yeast physiology has been discovered either directly or indirectly through characterization of yeast strains containing deleted (*grr1Δ*) or crippled alleles of the *GRR1* gene. Yeast deleted for *GRR1,* remarkably, remain viable despite pleiotrophic defects. Originally, mutations in *GRR1* (glucose repression resistant) were isolated in 1982 [64] and subsequently characterized in 1984 as mutations conferring resistance to glucose repression [65]. Concurrently, as *GRR1* mutant alleles were isolated and characterized it was also noted that these strains possess a distinct multiple elongated bud morphology. Cloning of the *GRR1* gene allowed for a more thorough investigation of *grr1Δ* strains that revealed a number of additional phenotypic defects. Strains fully deleted for *GRR1* display a decreased rate of growth on glucose media [66,67], a severely decreased rate of respiratory growth [68], defects in high affinity glucose transport [69,70], defects in divalent cation

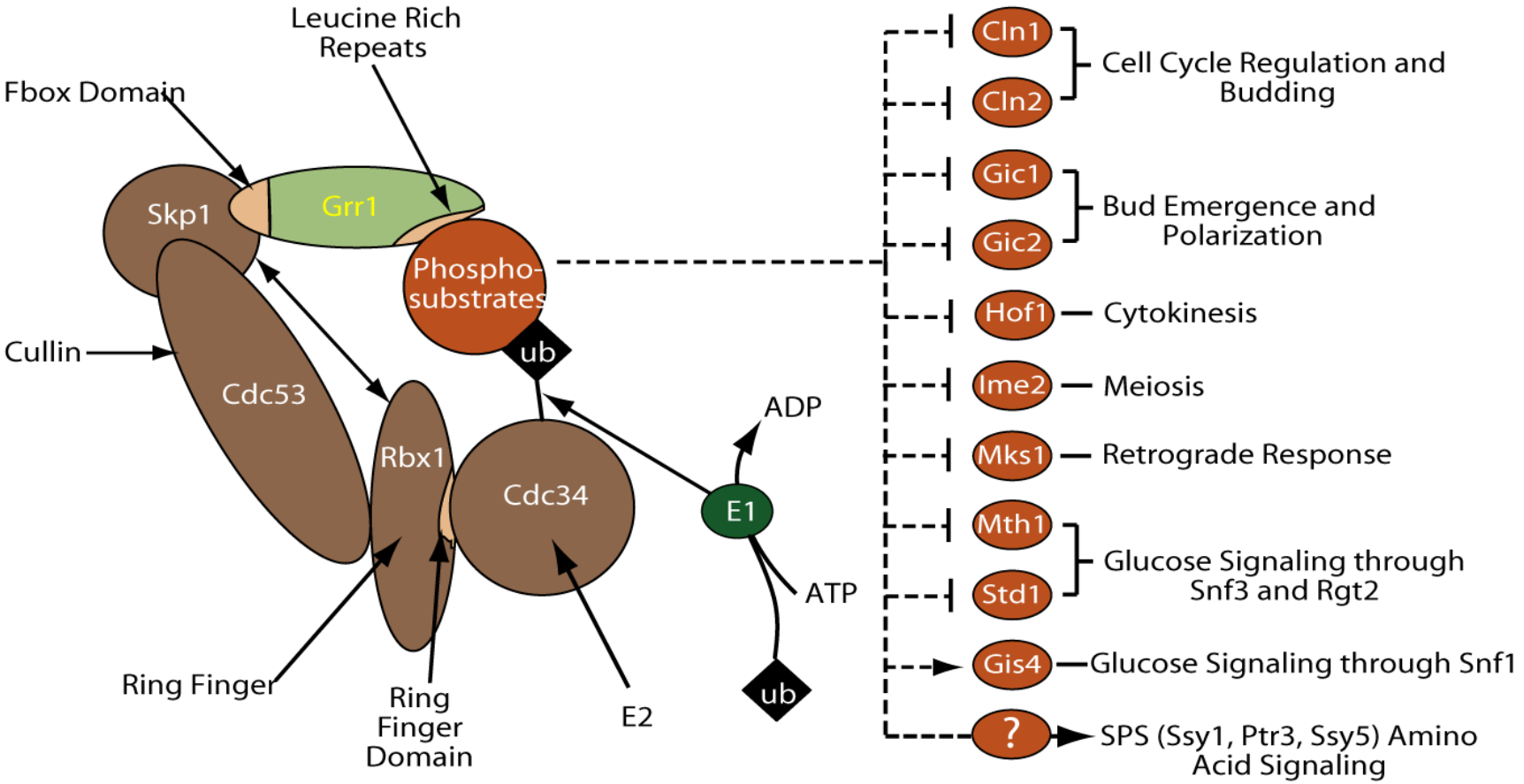


**Figure 1.2. The SCF$^{Grr1}$ Complex, Substrates, and Regulated Processes.** The SCF$^{Grr1}$ E3 ubiquitin ligase consists of the cullin, Cdc53, Skp1, the Ring Finger, Rbx1, the E2, Cdc34, and the F-box protein, Grr1. Together these proteins recognize and catalyze the covalent attachment of ubiquitin to a protein substrate. Grr1 is the substrate receptor for the SCF$^{Grr1}$ and has been shown to mediate the ubiquitylation and subsequent degradation of nine protein substrates involved in various cellular processes. Additionally, Grr1 has been shown to positively regulate SPS signaling through an unknown mechanism as well as Snf1 signaling by mediating ubiquitin dependent stabilization of Gis4. All SCF$^{Grr1}$ substrates must be phosphorylated to be recognized by the leucine rich repeat domain of Grr1 and are shown in orange. Vertical bars indicate Grr1 dependent inhibition of the substrate through enhanced protein degradation while arrows indicate Grr1 dependent activation.

transport [71], defects in amino acid transport [72], defects in cytokinesis [73], and resistance to mating pheromone [74]. They also are sensitive to osmotic [66] and oxidative [75] stresses as well as the microtubule destabilizing drug benomyl [76]. Furthermore, in multiple studies it has been noted that *grr1Δ* cells accumulate with 2N DNA [77,78] with 10% of the cells undergoing defective nuclear segregation [78,76]. The pleiotrophic defects exhibited by *grr1Δ* cells underscore the multifarious roles of Grr1 in the molecular biology of *Saccharomyces*.

As indicated in Section 1.4, Grr1 has been discovered to target a number of intracellular proteins for proteasomal degradation and the molecular functions of these substrates are in many cases consistent with the observed phenotypes of *grr1Δ* cells (Figure 1.2). For instance, the observed slow growth on glucose and high affinity glucose transport defects in *grr1Δ* cells have been attributed to stabilization of Mth1 and Std1; two membrane-bound proteins responsible for transcriptional repression of hexose transporter genes in the absence of glucose. Additionally, as seen in Figure 1.2, the Cln's as well as the Gic's are $SCF^{Grr1}$ substrates that are positively involved in bud emergence. Expression of stabilized forms of these proteins causes hyperpolarized growth, resembling that seen in *grr1Δ* strains. Though a direct substrate for the $SCF^{Grr1}$ complex linking its function to the control of amino acid transport has not been found, it is well known that $SCF^{Grr1}$ is required for transcriptional expression of amino acid transporters through the membrane bound sensor known as the SPS (Ssy1, Ptr3, and Ssy5). Defects in respiratory metabolism in *grr1Δ* may partially be due to the inability to degrade the negative regulator of the retrograde response, Mks1. Finally, at least some of the defects in cytokinesis observed in *grr1Δ* strains are explained by a role for Grr1 in degrading Hof1.

The various roles that Grr1 plays in the molecular biology of Saccharomyces present a high level of complexity when attempting to delineate the direct causality of its pleiotrophic defects. As indicated above, a number of phenotypes are readily explainable in the context of known Grr1 substrates; however the nuclear segregation defects, the sensitivity to osmotic and oxidative stresses, as well as the sensitivity to benomyl observed in *grr1Δ* cells are not

easily linked to known substrates of $SCF^{Grr1}$, suggesting that undiscovered substrates for $SCF^{Grr1}$ exist. Additionally, conflicting evidence exists that suggests that the role of Grr1 in glucose signaling may not be limited to its role in the Snf3/Rgt2 pathway. In order to delineate these discrepancies it is first necessary to understand what is already known about Grr1. With this in mind the remaining sections will be dedicated to describing the known roles for Grr1 in the context of its characterized substrates. Since the role of Grr1 in glucose repression is the central subject of this volume its role in this process will be reserved for Chapter 2.

### 1.6. The Role of Grr1 in the G1 to S Phase Transition through Targeted Degradation of the G1 Cyclins, Cln1 and Cln2

The propagation of viable offspring in all eukaryotic cells occurs through a sequential process known as the cell cycle (Figure 1.3). Through this process genetic as well as biosynthetic material necessary for life are replicated and segregated to spawn an independent daughter cell. The successful execution of the cell cycle relies on the temporal and spatial perpetration of consecutive molecular events and as a result can be divided into four phases known as G1, S, G2, and M. These four phases have been defined through biochemical, genetic, and cytological assays that permitted the elucidation of the chronological order of key molecular events such as DNA replication and chromosome condensation. At the molecular level, the chronological initiation of each of these events is tightly controlled through a control system that monitors and integrates environmental and intracellular cues to insure cell cycle fidelity.

The initial phase of the cell cycle is considered to be “Gap 1” or G1 and is the phase in which *Saccharomyces* spends most of its time. During G1 yeast cells undergo cell growth in response to the availability and type of nutrients present in the environment. In the absence of essential nutrients yeast cells in G1 phase can enter a differentiated state termed quiescence. Additionally, if yeast cells of opposite mating type are present, yeasts in G1 will respond to mating pheromone and will enter another differentiated process known as

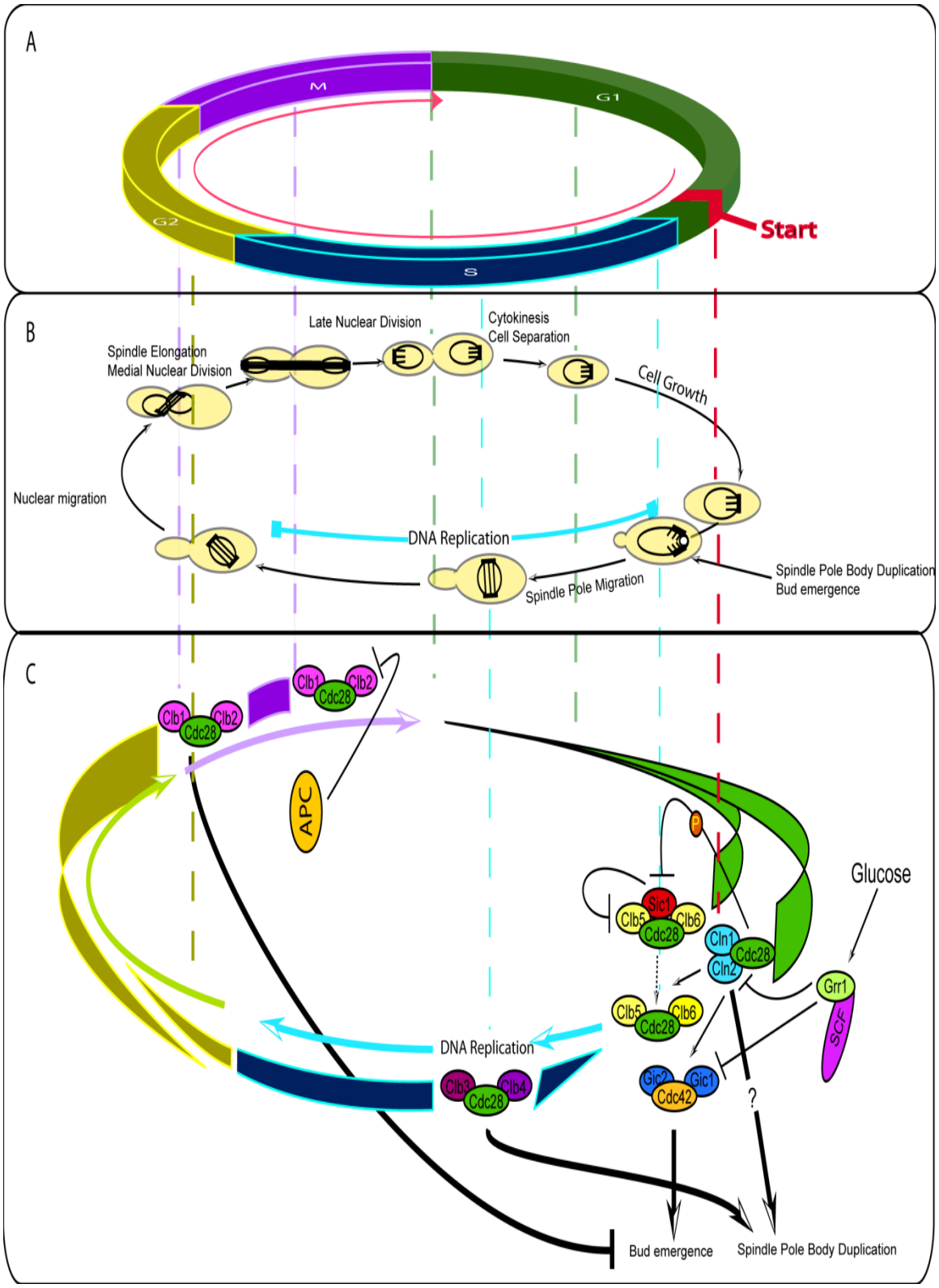
A
M
G1
G2
S
Start
B
Late Nuclear Division
Cytokinesis
Cell Separation
Spindle Elongation
Medial Nuclear Division
Cell Growth
Nuclear migration
DNA Replication
Spindle Pole Body Duplication
Bud emergence
Spindle Pole Migration
C
Clb1
Clb2
Cdc28
APC
Glucose
Sic1
Clb5
Clb6
Cln1
Cln2
Grr1
SCF
Gic2
Gic1
Cdc42
Clb3
Clb4
?
Bud emergence
Spindle Pole Body Duplication

**Figure 1.3. The *Saccharomyces* Cell Cycle.** **A.** The cell cycle can be divided into four distinct phases known as G1, S, G2, and M. Normally, the longest phase of the cell cycle in *Saccharomyces* is G1 (Green). Once cells progress past START (Red) they are committed to cell division and must wait until the next G1 phase to enter into differentiated cell fates such as mating. **B.** Each phase of the cell cycle is marked by distinct physiological events. In G1 phase of the cell cycle the cell grows to a cell size defined by quality of external nutrients. Once the optimal cell size is reached the cell passes START and shortly thereafter DNA replication is initiated, the bud begins to emerge, and the spindle pole body is duplicated. The cell is now in S phase where DNA replication and spindle pole migration proceed. After S phase the cell enters G2. In G2 the spindle pole migrates to the mother bud neck. Once the spindle pole reached the mother bud neck, mitosis or M phase begins. In this phase the spindle elongates, segregating chromosomes to mother and bud. The end of M phase and the beginning of G1 of the next cell cycle is marked by cytokinesis and cell separation. **C.** Progression through the cell cycle is regulated by modulating the kinase activity of the cyclin dependent kinase, Cdc28, by altering its association with any of the nine cyclins in *Saccharomyces.* At the beginning of G1, Cdc28 associates with the G1 cyclin, Cln3 (not shown), which drives the transcriptional expression of the G1-S phase cyclins, Cln1 and Cln2. Cln1 and Cln2 protein levels abruptly accumulate at START at which time Cln associated Cdc28 kinase activity peaks and catalyzes the phosphorylation of the cyclin dependent kinase inhibitor, Sic1. Phosphorylation of Sic1 results in Sic1 ubiquitylation by the $SCF^{Cdc4}$ and its degradation by the proteasome which results in the activation of Clb5/6-Cdc28 kinase activity and the initiation of DNA replication. Cln1/2/3-Cdc28 activity during G1 is required for spindle pole body duplication, bud emergence, and DNA replication. Premature accumulation of Cln1 and Cln2 and thus premature progression through START is prevented by maintaining low levels of Cln protein through $SCF^{Grr1}$ dependent ubiquitylation which promotes Cln degradation. The $SCF^{Grr1}$ is stimulated by glucose to promote Cln ubiquitylation and thus prolong G1 phase to promote cell growth. Throughout S phase, Cdc28 is primarily associated with Clb3 and Clb4 and then subsequently associates with Clb2 and Clb1 to promote G2 to M phase progression. Clb2-Cdc28 activity is required for M phase but must be inactivated to promote mitotic exit. Inactivation of Clb2-Cdc28 activity is achieved through ubiquitylation of Clb2 by the E3 ubiquitin ligase, anaphase promoting complex, and its subsequent degradation in the proteasome.

mating. In environmentally favorable nutrient conditions and in the absence of mating pheromone, wild-type yeast will progress through G1 past START, a point at which the cell is committed to DNA replication and cell division. Once past START, the cell cannot enter the quiescent or mating state until the subsequent G1 phase of the next cell cycle. Progression through START in yeast is marked phenotypically by resistance to mating pheromone, spindle pole body duplication, bud emergence, inactivation of B-type cyclin proteolysis, and the initiation of DNA replication.

Progression through START is driven by the kinase activity of the cyclin dependent kinase, Cdc28. Cdc28 is the central kinase that drives almost all stages of the cell cycle in *S. cerevisiae* and given this function Cdc28 protein levels remain constant throughout the cell cycle. Control of this kinase is achieved through post-translational modification and its association with any of

the nine cyclins present in *S. cerevisiae* (Cln1-3, Clb1- 6). Cdc28 interacts with each of these cyclins in a highly coordinated temporal manner which is achieved through timed regulation of cyclin transcription and perhaps more importantly cyclin degradation. Therefore, precise control of Cdc28 activity is achieved through its association with different cyclins and the availability of these cyclins to Cdc28 is a result of coordinately controlled cyclin synthesis and degradation. At the G1 to S phase transition, Cdc28 associates with the G1 cyclins, Cln1, Cln2, and Cln3. These cyclins have half lives in the range of 3 to 10 minutes, emphasizing the transient association of these proteins with Cdc28 [79-81]. Deletion of any two of these cyclins is permitted; however in the absence of all three, yeast cells arrest at START [82-84]. Association of the Cln proteins with Cdc28 activates its kinase activity at START which initializes the post START processes of budding [85], spindle pole body duplication, and DNA replication [1]. Initialization of DNA replication is realized through Cln-Cdc28 dependent phosphorylation of the Clb-Cdk inhibitor, Sic1. Phosphorylation of Sic1 leads to its ubiquitylation by the $SCF^{Cdc4}$ complex and subsequent degradation of Sic1 by the 26S proteasome, which activates Clb-Cdc28 kinase activity [87]. Thus active Cln-Cdc28 kinase activity promotes a cascade of events that ultimately drive the cell past START and into S-phase of the cell cycle.

The association of the Clns with Cdc28 in late G1 is primarily controlled by their ubiquitylation by the $SCF^{Grr1}$ which targets them for degradation by the 26S proteasome. Evidence supporting this role for Grr1 is provided by the fact that Cln1 and Cln2 protein levels, which normally accumulate sharply at the G1 to S phase transition and abruptly drop ten minutes later [88], are stabilized in a *GRR1* deleted strain [78]. Similar results were found for yeast strains harboring temperature sensitive mutations in *CDC34*, *CDC53*, and *SKP1* implicating the $SCF^{Grr1}$ complex in controlling the regulated degradation of Cln1 and Cln2 [89-92]. Additionally, Cln1 and Cln2 degradation by $SCF^{Grr1}$ can be reconstituted in vitro [93,94]. Degradation of Cln1 and Cln2 by $SCF^{Grr1}$ requires their phosphorylation through a Cdc28 dependent mechanism in regions of the proteins known as PEST sequences [81,80,90].

The role of Grr1 in G1 phase of the cell cycle through ubiquitylation and degradation of the Clns plays a role in coupling nutrient sensing (specifically glucose) to progression through the cell cycle. In a rich nutrient environment, both haploid and diploid yeast cells grow and divide at rates specific to the available nutrient profile. Thus, yeast not only coordinate growth and division strictly to the availability of nutrients but also to the quality of these nutrients. For example, the average doubling time of yeast grown in the presence of glucose (high quality carbon source) is ~75 minutes with cell volumes reaching ~38um$^3$ before the transition from G1 to S. However, the average doubling time on glycerol (low quality carbon source) is ~160 minutes with cell volumes reaching ~23um$^3$ before transition from G1 to S [95,96]. Thus, an inverse correlation between doubling time and the extent of growth is observed as the quality of nutrients available depreciates. A number of observations suggest that the role of Grr1 in degrading the Clns is important in the coupling of nutrient signals to progression through the cell cycle. First, Grr1 interaction with Skp1 is enhanced approximately four fold by high glucose [97] suggesting that glucose somehow promotes Grr1 interaction with the SCF which would presumably lead to enhanced Cln instability. Second, cells expressing stabilized forms of Cln2 cause shortened G1 phases, premature progression through START, a decreased ability to arrest in response to mating pheromone and nitrogen deprivation, and an increased percentage of cells with 2N DNA content [82]. Most of these phenotypes have been described for *grr1Δ* cells [98,77,74] and thus it is highly likely that *grr1Δ* cells also exhibit premature progression through START. Finally, Grr1 function is required for multiple nutrient signaling pathways including Snf3/Rgt2 glucose signaling [99,56], amino acid signaling through the SPS sensor [63], and mitochondrial retrograde response [57]. Each of these functions for Grr1 will be discussed in later sections.

## 1.7. The Role of Grr1 in Bud Emergence and Polarity through Targeted degradation of Cln1,2 and Gic1,2

For some time the role of Grr1 in cell cycle progression was believed to be limited to its control of G1 to S phase progression; however, it has become clear that there is a definitive role for Grr1 in the processes of budding and cytokinesis. Upon the transition from G1 to S phase of the cell cycle yeast cells begin to polarize the actin cytoskeleton to produce the daughter cell. This process is highly regulated and mainly facilitated by the small GTPase known as Cdc42 [100]. Through a signaling cascade that remains enigmatic the Cln1/2/3-Cdc28 complex stimulates the formation of the active GTP bound Cdc42 protein, promoting its binding to an effector known as Gic2 [101]. This active Cdc42/Gic2 complex is thought to be important for the initiation of bud formation and appears to need only be active for a small window of time to perform this function [101,102]. Cells that harbor a stabilized form of Gic2 exhibit defects in cytoskeletal polarization with some of these cells possessing multiple buds [55]. A similar phenotype is exhibited in *GRR1* deleted strains and it has been shown that Gic2 protein levels which normally abruptly disappear after bud emergence are stabilized in the absence of $SCF^{Grr1}$ [55]. The phosphorylation of Gic2 has also been shown to be necessary for Gic2 destabilization, but the mechanism of Gic2 action and its regulation have yet to be discovered. Interestingly, as stated previously, the Cln1/Cln2-Cdc28 protein kinase complex has been shown to induce polarization of the actin cytoskeleton through an unknown mechanism affecting Cdc42 activity [103,104] and thus would indirectly control Gic2 activity since it is downstream effector of Cdc42. It is not known how Grr1 can serve to promote degradation of both the cyclins and a downstream effector of the cyclins but nonetheless this interaction suggests that the processes of cell cycle progression and bud emergence are intimately coordinated through the $SCF^{Grr1}$ complex.

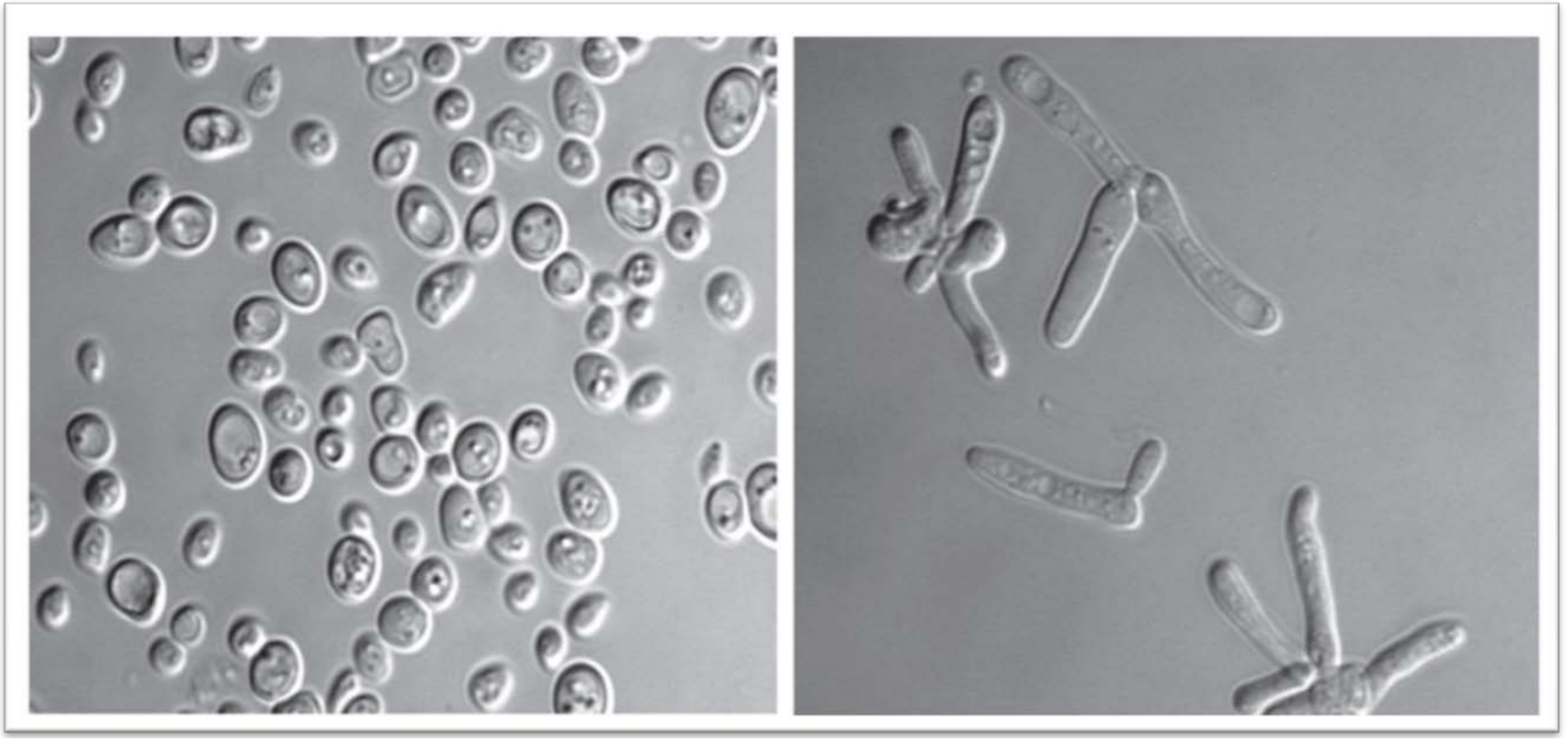

wild-type *grr1Δ*

**Figure 1.4. Morphology of wild-type and *grr1Δ* Yeast.** Phenotype of wild-type (left) and *grr1Δ* (right) cells grown on YPD-2% glucose media. As can be seen, the *grr1Δ* strains exhibit multiple hyperpolarized buds that remain attached. This morphology is most likely a manifestation of a corollary of defects associated with stabilization of substrates normally targeted for ubiquitylation by the $SCF^{Grr1}$.

## 1.8. The Role of Grr1 in Cytokinesis through Targeted Degradation of Hof1

Before the mother cell can re-enter G1 of the cell cycle, separation of the mother from the daughter cell must occur through cytokinesis. Most eukaryotic cells facilitate cytokinesis through the formation of an actomyosin-based contractile ring, however *S. cerevisiae* possesses a cell wall and cytokinesis can occur through the formation of a chitin septum as well [105,106]. The protein Hof1 has been shown to be necessary for both of these processes in *S. cerevisiae* [73] and over-expression of this protein interferes with cell separation in *S. pombe* [107]. Hof1 localizes to the bud neck during cytokinesis [108], a cellular location shared by Grr1 at this stage of the cell cycle [73]. This observation led to the implementation of a two hybrid screen where Grr1 was found to bind with Hof1 [73]. In this same study it was found that Hof1 protein stability is regulated in a $SCF^{Grr1}$ dependent manner since Hof1 is stabilized in *grr1Δ*, *cdc53-1*, and *cdc34-2* strains. It is interesting to note that *grr1Δ* strains exhibit multiple elongated buds that contain independent nuclei (Figure 1.4). This phenotype is probably a result of impaired cytokinesis due to Hof1 stabilization and hyper-polarization due to Gic2 stabilization.

The substrates identified for the $SCF^{Grr1}$ complex involved in cell cycle progression implicate Grr1's role in the cell cycle as diversified and complicated. Despite the complicated nature of the role of Grr1 in the cell cycle it has been hypothesized that the sequential and timely degradation of each of these substrates is necessary to coordinate the appropriate sequence of events that are required to efficiently and correctly divide. However, this coordination must not be essential since *GRR1* deleted strains are still viable. These mutants are, however, slow to divide with doubling times more than twice that of wild-type strains and these mutant strains seem to be inefficient at adapting to changing nutrient environments [78,66,109]. This has led many to hypothesize that Grr1 may be involved in regulating the cell cycle in response to external nutrient conditions and that the delayed division times and inefficient adaptability exhibited by *GRR1* deleted strains is a result of an impaired ability to change a subset of transporters and metabolizing enzymes necessary to efficiently utilize nutrients available in

the environment. Evidence supporting this hypothesis is best supplied by elaborating on the other known Grr1 substrates. It is indeed observed that the remaining substrates are involved in coupling external and internal nutrient sensing to the transcriptional and post-transcriptional regulatory machinery.

### 1.9. The Role of Grr1 in Amino Acid Signaling Through the SPS Sensor

The yeast *S. cerevisiae* possesses the ability to synthesize all twenty amino acids necessary for protein biosynthesis but when amino acids are present in the environment *Saccharomyces* will first utilize the extra-cellular amino acid supply in order to conserve the cellular energy and co-factors needed for their synthesis. Additionally, *Saccharomyces* can also utilize a large subset of amino acids as sources of ammonia for the biosynthesis of other amino acids and metabolites. The ability to utilize extra-cellular sources of amino acids directly for protein biosynthesis and/or as sources of ammonia is dependent on *Saccharomyces'* ability to sense and respond appropriately to the particular amino acid(s) present. The appropriate transport proteins and metabolic enzymes must be coordinately regulated in response to the extra-cellular nitrogen composition to ensure efficient utilization of the available nutrients. This coordinate regulation is in part realized through a plasma membrane localized amino acid sensor known as the SPS (Ssy5, Ptr3, and Ssy1). Through this sensor, external amino acids stimulate a signaling cascade that culminates in the transcriptional regulation of amino acid permeases and catabolic enzymes needed for their metabolism. Grr1 plays an essential role in propagating this response and thus the absence of Grr1 leads to an inability to respond to extra-cellular amino acids through this pathway. Therefore, the mechanism of SPS signaling and the consequences of defective SPS signaling will be discussed in the following section.

The presence of extra-cellular amino acids is initially sensed through a plasma membrane localized amino acid sensor known as Ssy1. Similar to the glucose sensors, Rtg2 and Snf3, Ssy1 was revealed as an amino acid sensor based on its similarities and marked differences to the amino acid permease

family [110]. Ssy1 is comprised of 12 transmembrane-spanning domains flanked by a large N-terminal cytoplasmic region not found in the 17 remaining amino acid permease family members [111]. This N-terminal extension is required for Ssy1 function [112] and strains harboring non-functional *SSY1* alleles were initially shown to exhibit defects in amino acid uptake [110]. The induced expression in response to extra-cellular amino acids occurs for genes encoding both broad specificity and high affinity amino acid permeases. Agp1, Bap2, Bap3, Gnp1, Tat1, Tat2, and Mup3 as well as the peptide transporter, Ptr2, have been shown to be dependent on Ssy1 (Figure 1.5) [111,112,110]. This dependency does not rely on facilitated amino acid transport by Ssy1 and occurs specifically in response to extra-cellular amino acids [110,111].

The mechanism for sensing extracellular amino acids by Ssy1 remains a mystery; however the intracellular events that occur in response to amino acid sensing have begun to be revealed. What is known about the molecular events that facilitate amino acid dependent induction of amino acid permeases through the SPS is summarized in Figure 1.5 and briefly discussed here. Disruption of *PTR3* or *SSY5*, like *SSY1,* leads to defects in amino acid uptake attributable to the inability to induce expression of amino acid permeases in these cells [112,113]. It was subsequently shown that the cytoplasmic N-terminal extension of Ssy1 physically interacts with both Ptr3 and Ssy5, suggesting that these three proteins together comprise the functional amino acid sensor responsible for transcriptional regulation of amino acid permease genes (hence the name SPS for Ssy1, Ptr3, Ssy5) [114,112]. The N-terminal association of Ptr3 with Ssy1promotes hyper-phosphorylation of Ptr3 by the plasma membrane bound casein kinases, Yck1 and Yck2, in response to the presence of extra-cellular amino acids. Hyper-phosphorylation of Ptr3 is essential for sensor signaling and has been shown to require Ssy1, at least one functional, and Grr1 [114]. The role of Grr1 in this pathway is ill-defined but like *ssy1Δ, ptr3Δ,* or *ssy5Δ* strains, *grr1Δ* cells exhibit amino acid uptake defects and complete loss of SPS signaling [111]. Through an unknown mechanism, hyper-phosphorylated Ptr3 stimulates cleavage of the inhibitory Ssy5 N-terminal pro-domain. Cleavage of the pro-domain is believed

to activate the C-terminal chymotrypsin-like serine protease activity of Ssy5 [115]. This protease activity is required for release of two functionally redundant, plasma membrane bound, transcription factors, known as Stp1 and Stp2, through cleavage of their N-terminal membrane targeting sequences. Interestingly, cleavage of Stp1 and Stp2 is also dependent on phosphorylation by Yck1 or Yck2 [116,117]. Finally, cleaved Stp1 and Stp2 are free to translocate to the nucleus where, in conjunction with Uga35/Dal81, they induce the transcription of amino acid permeases [118,119].

Deletion of GRR1 or SSY1 leads to complete loss of amino acid induced signaling through the SPS and this deficiency culminates at the physiological level with the inability to transport certain amino acids effectively across the plasma membrane. However, in the absence of GRR1 or SSY1, the general amino acid transporter, Gap1, can support, to a limited extent, uptake of all amino acids for protein synthesis and nitrogen supplementation [111,120,121,72]. Therefore, Grr1 as well as Ssy1 specific effects on amino acid transport were revealed by characterizing gap1Δ, grr1Δ gap1Δ, and ssy1Δ gap1Δ cells on multiple single amino acid nitrogen sources [111,72]. Through these studies it was revealed that Grr1 and Ssy1 are required for Gap1 independent transport of isoleucine, leucine, valine, phenylalanine, tyrosine, tryptophan, and methionine at 1mM concentrations. However, growth of ssy1Δ gap1Δ strains was restored on leucine, valine, methionine, and phenylalanine at 10mM [111] whereas no growth of the grr1Δ gap1Δ strain was supported on 10mM leucine or methionine [72]. Additionally, grr1Δ gap1Δ strains exhibited no growth on 1mM threonine whereas ssy1Δ gap1Δ strains grew robustly. Together, these data indicate that Grr1 is not only required for SPS mediated amino acid permease induction in response to external amino acids but also SPS independent control of amino acid transport.

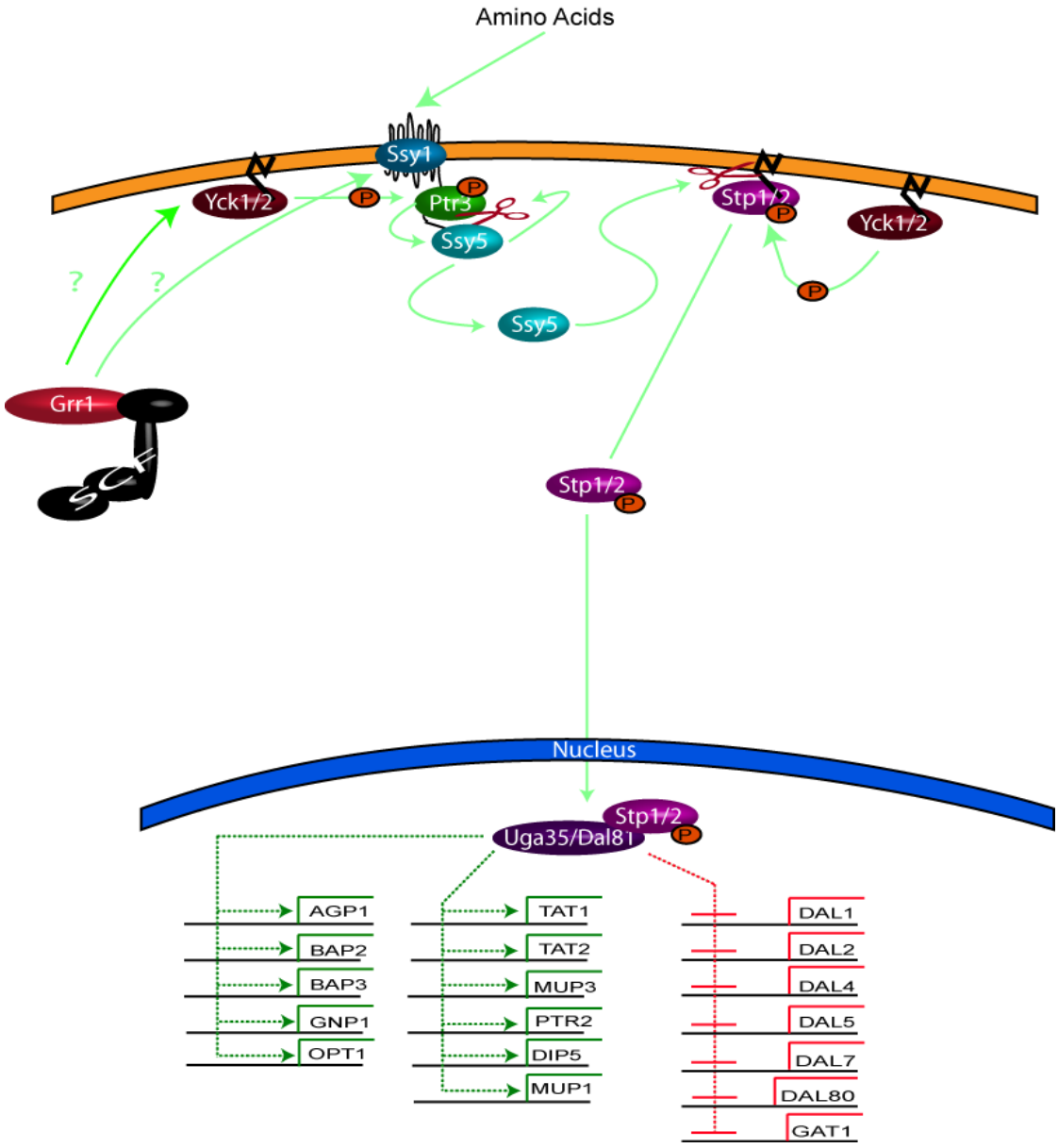


**Figure 1.5. Amino Acid Signaling through the SPS (Ssy1, Ptr3, Ssy5) Sensor.** Through an unknown mechanism, the presence of extracellular amino acids is believed to induce a conformational change in the integral plasma membrane sensor of the SPS known as Ssy1. This conformational change promotes phosphorylation of Ptr3 by either of the plasma membrane bound casein kinases, Yck1 or Yck2. Ptr3 is bound to the C-terminal cytoplasmic tail of Ssy1 along with the serine protease, Ssy5. Phosphorylation of Ptr3 leads to autocatalytic cleavage of the inhibitory domain of Ssy5 which activates its serine protease activity towards two redundant, plasma membrane bound, transcription factors, known as Stp1 and Stp2. Interestingly, Stp1 and Stp2 also must be phosphorylated by either of the Ycks in order to be proteolytically cleaved by Ssy5. Cleavage of Stp1 and Stp2 leads to their translocation to the nucleus where they, in conjunction with the Uga35/Dal81 transcription factor, induce or repress a number of amino acid transporters and genes involved in allantoin, allantoate, and urea metabolism, respectively. The role of Grr1 in SPS signaling is ill defined but it is known that Grr1 is required for phosphorylation of Ptr3 by the Ycks. Transcriptional control of all SPS targets in response to amino acids is non-functional in *grr1Δ* strains.

### 1.10. The Role of Grr1 in Mitochondrial Retrograde Signaling through Targeted Degradation of Mks1

In response to mitochondrial dysfunction, mitochondria influence nuclear gene expression in order to promote adaptation to decreased respiratory capacity. Decreased respiratory capacity can be attributable to defects in TCA cycle or respiratory protein function, changes in intracellular ion pools, or decreases in other cofactors needed by the mitochondrial respiratory chain such as ubiquinone. In *Saccharomyces,* these deficiencies indirectly influence nuclear gene expression through a signaling pathway known as the retrograde response pathway [122]. The repertoire of nuclear encoded genes affected by this pathway is extensive and includes genes of enzymes needed to provide necessary metabolites that are normally provided by the TCA cycle, which would fail to function as a full cycle in respiratory deficient mitochondria since succinate would fail to be oxidized to fumarate. Thus, genes of anapleurotic pathways that function to supply mitochondria with TCA cycle intermediates such as oxaloacetate, acetyl-CoA, and malate are all induced through the retrograde signaling pathway. These genes include enzymes of the glyoxylate cycle, peroxisomal enzymes, and enzymes involved in fatty acid oxidation [123]. A key metabolite provided by the TCA cycle is glutamate and respiratory deficiencies that compromise flux through the TCA cycle lead to decreased intracellular glutamate pools [124]. Therefore, an essential function of the retrograde response is to increase expression of genes needed to provide intracellular glutamate, which is synthesized from the TCA cycle intermediate, α-ketoglutarate. Consistent with this function, the retrograde response pathway is strongly activated by glutamate starvation [125].

Much of what is known about *Saccharomyces* retrograde signaling has been revealed through gene expression analysis of the *CIT2* gene [126]. *CIT2* encodes the peroxisomal citrate synthase in *Saccharomyces* and catalyzes the peroxisomal condensation of oxaloacetate and acetyl-CoA to form citrate. Thus, *CIT2* activity provides an alternative source of citrate through fatty acid oxidation in the peroxisome. Since *CIT2* expression is primarily controlled through the

retrograde pathway, many of the proteins responsible for retrograde signaling have been revealed by studying the effects of their mutation on *CIT2* expression.

*CIT2* expression is controlled directly by Rgt1 and Rgt3, which are basic helix-loop-helix-leucine zipper transcription factors that bind as a hetero-dimer to R box (GTCAC) sequences present in the promoters of retrograde pathway regulated genes [127]. Transcriptional activity of the hetero-dimer is regulated through both phosphorylation of Rtg3 and sequestration of Rtg1/3 in the cytoplasm. In the absence of retrograde signaling, Rtg3 is hyper-phosphorylated and both Rtg1 and Rtg3 are sequestered in the cytoplasm [128]. Activation of retrograde signaling requires the partial de-phosphorylation of Rtg3 which results in the nuclear accumulation of both Rtg1 and Rtg3, where the hetero-dimer is free to bind to R box sites of retrograde regulated genes. The kinase(s) and phosphatase(s) acting to regulate Rtg3 have not been identified; however the phosphorylation state and intracellular location of Rtg3 is intimately controlled by another retrograde protein, Rtg2 [124]. Cells deleted for *RTG2* contain hyper-phosphorylated Rtg3. Thus, the Rtg1/3 hetero-dimer remains cytoplasmic and as a result, retrograde signaling is defective in *rtg2Δ* cells [129]. Therefore, the key event regulating retrograde control of gene expression is the positive control of Rgt1/3 localization to the nucleus by Rtg2.

The molecular events that act to regulate Rtg2 and thus Rtg1/3 nuclear-cytoplasmic distribution have begun to be elucidated. Rtg2 has been found to interact with the retrograde signaling negative regulator, Mks1, when the retrograde signaling pathway is on [129]. When the pathway is off, Mks1 no longer interacts with Rtg2 but interacts with the 14-3-3 proteins, Bmh1 and Bmh2 [129]. Deletion of *MKS1* results in constitutive activation of retrograde response genes such as *CIT2* and gene expression is insensitive to glutamate repression [124]. Thus, Mks1 in complex with Bmh1/2 inhibits Rtg3 de-phosphorylation and/or promotes Rtg3 hyper-phosphorylation resulting in sequestration of Rtg1/3 in the cytoplasm when glutamate is plentiful or when respiratory competence is normal. In response to glutamate depletion and/or respiratory deficiency, the Mks1 phospho-protein becomes de-phosphorylated promoting interaction of Mks1 with

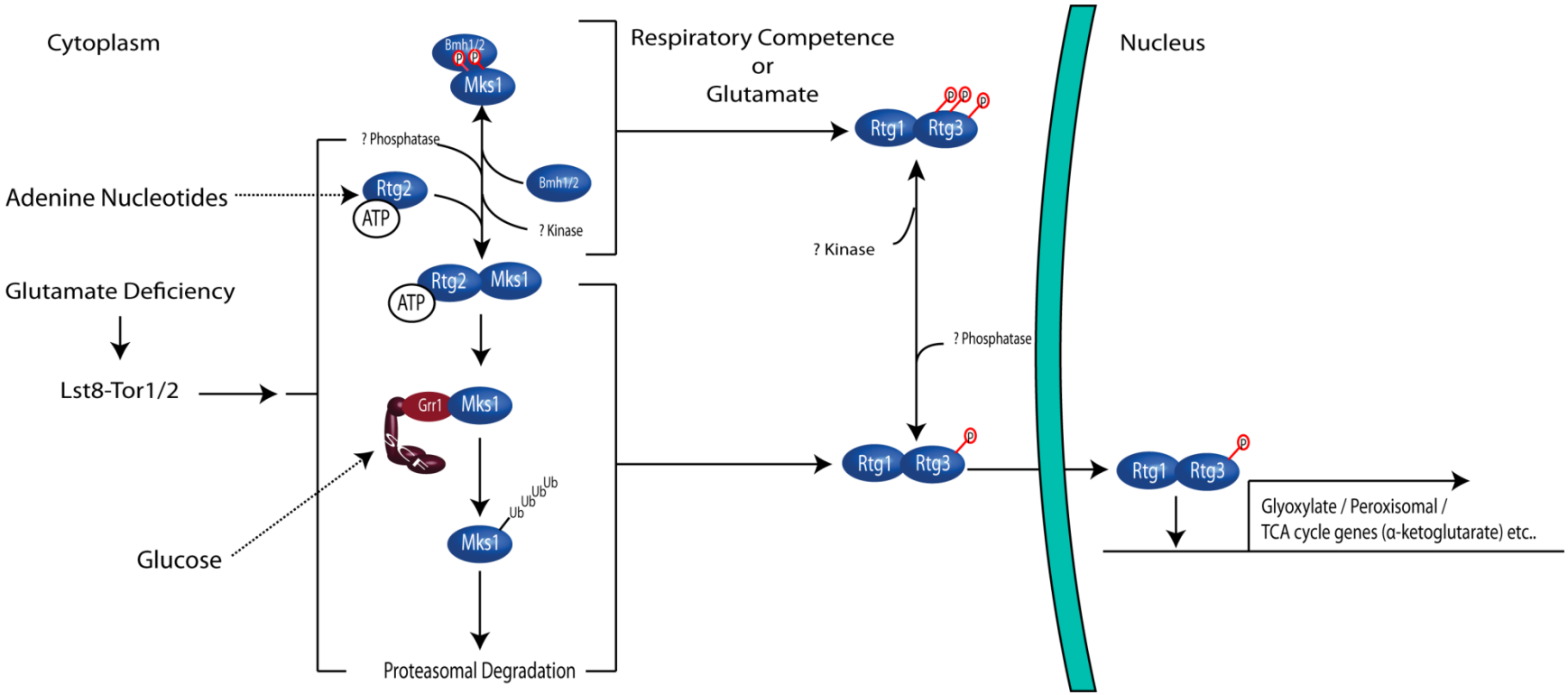


**Figure 1.6. Mitochondrial Retrograde Signaling in *Saccharomyces*.** Mitochondrial dysfunction promotes changes in nuclear gene expression necessary for adaptation to respiratory deficiency through the retrograde signaling pathway. Multiple intracellular nutrient cues act through unknown mechanisms to control retrograde signaling. Normally, during periods of respiratory competence and adequate glutamate concentrations, two transcription factors, Rtg1 and Rtg3, are sequestered in the cytoplasm resulting in the inability of these two transcription factors to induce retrograde target gene expression. Sequestration of Rtg1 and Rtg3 in the cytoplasm correlates with Rtg3 hyper-phosphorylation. Localization of Rtg1 and Rtg3 is controlled through an unknown mechanism mediated by the dynamic interplay between Rtg2, Mks1, and Bmh1/2. In nutrient replete conditions in the absence of mitochondrial dysfunction Mks1 is hyper-phosphorylated which promotes Mks1 interaction with Bmh1/2. Bmh1/2-Mks1 inhibits retrograde signaling by promoting the hyper-phosphorylation and cytoplasmic retention of Rtg3. In respiratory deficient cells, Mks1 is de-phosphorylated which promotes its interaction with Rtg2. Rtg2 inhibits Mks1 interaction with Bmh1/2 and thus inhibits the ability of Bmh1/2-Mks1 to inhibit de-phosphorylation and nuclear translocation of Rtg1 and Rtg3. Bmh1/2 interaction with Mks1 prevents Mks1 ubiquitylation by $SCF^{Grr1}$ which promotes degradation of Mks1 and subsequent activation of the retrograde signaling pathway.

Rtg2. De-phosphorylated Mks1 is also subject to $SCF^{Grr1}$ dependent ubiquitylation and subsequent degradation by the 26S proteasome [57]. Consistent with the requirement for Grr1 in positively regulating the retrograde response, dominant mutations in *GRR1* bypass the requirement for Rtg2 in retrograde signaling and deletion of *GRR1* in *rtg2Δ* cells exacerbates the growth defect of *rtg2Δ* cells on synthetic minimal media lacking glutamate [57]. The kinases and phosphatases which regulate the phosphorylation state of Mks1 are currently unknown. Additionally, the molecular events leading to Mks1 degradation by $SCF^{Grr1}$ are also currently unknown; however hypo-phosphorylated Mks1 recognition by the $SCF^{Grr1}$ complex is most likely not bridged by Rtg2 as $SCF^{Grr1}$ dependent ubiquitylation of Mks1 is not specific for Rtg2-Mks1 but for unbound Mks1 [57]. Thus, many of the details regarding retrograde signaling regulation through Rtg2, Mks1, Rtg1/3, and $SCF^{Grr1}$ remain to be determined; nevertheless, the role for Grr1 in this signaling pathway is well substantiated.

The intracellular signals which indicate mitochondrial dysfunction and/or glutamate starvation and lead to activation of the retrograde signaling pathway have not been deciphered. Most likely, multiple intracellular signals act through different retrograde signaling proteins to modulate the response. Rgt2 contains an ATP binding domain that is required for Rtg2 interaction with Mks1 [129]. Thus, the intracellular ATP/ADP ratio may influence retrograde response activation through Rtg2. Rapamycin inhibition of the PI kinase related kinase, Tor1 and Tor2, also promotes induction of the retrograde signaling response. Activation of retrograde signaling through Tor inhibition requires Rtg2 [130] and Tor dependent inactivation of retrograde signaling promotes Mks1 hyper-phosphorylation [131]. Tor kinase activity is regulated by multiple nutritional cues including the intracellular concentration of glutamate [132,133]. Thus, glutamate deficiency may induce retrograde signaling through inactivation of the Tor kinase. It is interesting to speculate that glucose dependent regulation of Grr1 interaction with Skp1 and the SCF may serve as an additional regulatory mechanism to control retrograde signaling. Grr1 interaction with Skp1 is enhanced four fold in the presence of glucose [97] which would most likely promote enhanced degradation of

Mks1. Thus, regulation of the retrograde response is highly complex with multiple nutrient signals acting through multiple regulatory proteins to fine tune the molecular response to mitochondrial dysfunction.

The role of Grr1 in *Saccharomyces* physiology is extremely complex. This complexity is underscored by the eclectic substrates targeted for ubiquitylation by the $SCF^{Grr1}$. However, as illustrated throughout this chapter, the roles for Grr1 in *Saccharomyces* fall into two major categories; cell cycle related processes and nutrient signaling processes. The multifaceted role for Grr1 in regulating multiple aspects of these processes suggests that Grr1 function is intimately involved in coordinating progression through the cell cycle in response to various alterations of the extracellular and intracellular nutrient profile. Consistent with this role, *grr1Δ* cells are additionally resistant to the repressive affects of glucose on the expression of genes needed for the utilization of alternative carbon sources. The molecular response of yeast to the presence of glucose underlies the ability of *Saccharomyces* to preferentially ferment glucose to ethanol, an attribute of yeast that has been exploited by man for centuries. Given this attribute, much attention has been devoted to determining the molecular events that dictate *Saccharomyces* response to glucose and thus the literature encompassing this subject is vast. Therefore the following chapter will be devoted to this subject and the role of Grr1 in the process of glucose repression

# CHAPTER 2: GLUCOSE TRANSPORT, SIGNALING, AND METABOLISM IN *SACCHAROMYCES*

## 2.1. Introduction to Glucose Signaling and Metabolism

Unlike mammalian cells, the preferred metabolic pathway to generate ATP in the yeast, *S. cerevisiae,* is through aerobic fermentation of glucose. Once glucose has been transported into the cell it is converted to two pyruvates through a series of enzymatic reactions that together comprise a nearly universally conserved metabolic pathway, termed glycolysis. In mammalian cells and other respiratory organisms, pyruvate is funneled into the citric acid cycle to produce electron carriers which are subsequently utilized to generate a proton gradient and produce ATP through oxidative phosphorylation. This process is efficient, since 32 ATPs are generated from one molecule of glucose. *Saccharomyces,* on the other hand, during growth on glucose, preferentially converts pyruvate to ethanol which produces only two ATPs for every molecule of glucose catabolized. Though inefficient, fermentive growth is fast, supporting a growth rate of 0.34 doublings per hour whereas the growth rate on galactose or ethanol is 0.26 and 0.087 doublings per hour, respectively [134]. Despite its inefficiencies, the preference to ferment glucose to ethanol most likely evolved in *Saccharomyces* to establish a competitive advantage in the environment. The fast growth rate allows for yeast to keep pace with faster growing microbes and the production of ethanol concurrently decreases the growth rate of these microbes as most are ethanol intolerant.

After the complete consumption of glucose, *Saccharomyces* will begin to utilize other fermentable carbon sources and finally non-fermentable carbon sources in order to maintain viability. A good example of *Saccharomyces* preference for glucose and its nutrient adaptability can be seen in the fermentation profile presented in Figure 2.1. When yeast is gown in the presence of glucose and maltose at equal concentrations (% weight to volume), the glucose is fermented first and completely before the maltose begins to be metabolized. After complete utilization of glucose *Saccharomyces* prefers to

ferment other hexose sugars, such as maltose. In the absence of other fermentable sugars, as maltose is depleted, *Saccharomyces* diverts more and more pyruvate generated from glycolysis away from ethanol production to the TCA cycle where it is respired to produce ATP more efficiently. Finally, after complete utilization of fermentable sugars *Saccharomyces* once again alters its metabolism to utilize C2 and C3 carbon sources such as ethanol and glycerol.

The versatility of yeast to grow on a wide variety of carbon sources is facilitated by their ability to reprogram their metabolic state. Metabolic state, as used here, is defined by the active subset of transporters and enzymes needed to metabolize a given carbon source for energy production. Though this re-programming occurs at all molecular regulatory levels the alterations in the transcriptional profile of yeast in batch culture as they progress from fermentative to respiratory based growth provides a descriptive representation of this complex process [135]. In the presence of glucose, multiple molecular pathways responsive to both internal and external glucose concentrations act to both repress (glucose repression) and inactivate genes and proteins responsible for the metabolism of other “non-preferred” carbon sources and to induce and activate genes and proteins needed for glucose fermentation. As seen in Figure 2.1 B, on glucose, genes and proteins needed for maltose utilization as well as respiration are suppressed in order to favor ethanol production from glucose. As glucose is usurped the regulatory pathways acting to repress maltose transporters and enzymatic proteins are de-activated allowing for fermentation of maltose (Figure 2.1 C). The depletion of a fermentable sugar (in this case maltose) leads to a gradual increase in respiratory genes needed to support ATP production as the metabolic flux through glycolysis is reduced (Figure 2.1 D). Finally, the complete depletion of maltose leads to de-repression of genes involved in the glyoxylate cycle, gluconeogenesis, and respiration in order to support growth on C2 and C3 carbon sources such as ethanol.

The ability to reprogram the metabolic state is conferred by the concerted action of a network of regulatory pathways that act to coordinate transcriptional and post-transcriptional processes in response to the internal and external

nutrient composition. Among the different carbon sources, the molecular response of yeast to glucose has drawn the most attention and as a result the regulatory pathways which facilitate the molecular response to glucose have been extensively characterized, especially at the level of gene expression [135,136,67,137-140]. Three regulatory pathways with seemingly redundant and non-redundant functions contribute to the transcriptional and post-transcriptional re-programming of the metabolic state of the cell in response to glucose. First, activation of the Ras/cAMP/PKA pathway has been shown to result in the activation and inactivation of almost the entire subset of glucose responsive genes through a mechanism that most likely is initiated by the phosphorylation of glucose to glucose-6-phosphate by one of the hexose kinases (Hxk1, Hxk2, or Glk1) [141]. The Snf3/Rgt2 pathway has been shown to almost exclusively regulate the transcriptional de-repression of hexose transporters in response to external glucose concentrations [142-144]. Finally, the Glc7/Snf1 pathway regulates the transcriptional induction of *MAL* (maltose), *GAL* (galactose), and *SUC* (sucrose) genes [145,146] as well as genes involved in gluconeogenesis, respiration, and the glyoxylate cycle in response to glucose depletion [147-151]. Inhibition of Snf1 catalytic activity in the presence of glucose is also dependent on Hxk2 activity [152-156,136]. Through integration of these three regulatory pathways the molecular response to glucose is elicited.

### 2.2. Grr1 and Glucose Repression

Mutant alleles of GRR1 were first isolated when ethylmethanesulfonate (EMS) mutagenized yeast were screened for mutations that conferred resistance to 2-deoxyglucose [65]. 2-Deoxyglucose is a non-metabolizable glucose analogue that retains the ability to exert glucose repression [157]. Thus, wild-type yeast strains lack the ability to grow on media containing non-glucose carbon sources in the presence of 2-deoxyglucose because the production of the enzymes necessary for utilization of these carbon sources is inhibited by glucose repression while 2-deoxyglucose itself cannot be metabolized to produce energy.

However, multiple non-allelic mutations have been isolated that abrogate the sensitivity of *S*. *cerevisiae* to 2-deoxyglucose and thus, these strains grow robustly on non-glucose carbon sources in its presence. The resistance to 2-deoxyglucose displayed by these mutants is conferred by their ability to produce the enzymes needed to grow on non-glucose carbon sources despite the presence of a signal to induce glucose repression and as a result yeast strains harboring these mutations have been deemed glucose repression resistant. Yeast deficient for the GRR1 gene exhibit this glucose repression resistance and as a result this gene was aptly named for the phenotype it conferred (Glucose Repression Resistant).

A diverse array of glucose repressed transcripts is observed to exhibit glucose insensitive expression in *grr1Δ* strains. Invertase (*SUC2*), maltase (*MAL12, 22, 32, 42, 62*), galactokinase (*GAL1*), and cytochrome c oxidase (COX genes) were among the first genes characterized to be insensitive to glucose repression in *grr1Δ* strains [64,158]; however micro-array analysis of *grr1Δ* strains reveal that a large number of glucose repressed transcripts are actively expressed despite the presence of glucose. Enzymes needed for the utilization of other fermentable carbon sources (i.e. maltose, galactose, and sucrose) as well as respiratory, gluconeogenic, and glyoxylate cycle genes needed for growth on C2 and C3 carbon sources (i.e. glycerol, ethanol, and acetate) all show increased gene expression in grr1Δ strains ([159] and present study). Additionally, previous studies revealed that Grr1 activity was necessary for induction of a number of glucose transporters in response to the presence of glucose in the external environment [69,56,160]. The signaling mechanism for the control of these transporters has been eloquently revealed and it is now known that defects in hexose transporter induction in *grr1Δ* strains is a result of the positive role of Grr1 in glucose signaling through the Snf3/Rgt2 pathway [161-165]. Thus, the glucose repression resistant effects of a *GRR1* deletion influence genes under the control of both the Snf3/Rgt2 pathway and the Hxk/Glc7/Snf1 pathway.

Currently, the lack of glucose repression exerted on genes under the control of the Hxk2/Glc7/Snf1 pathway in *grr1Δ* strains is hypothesized to be an

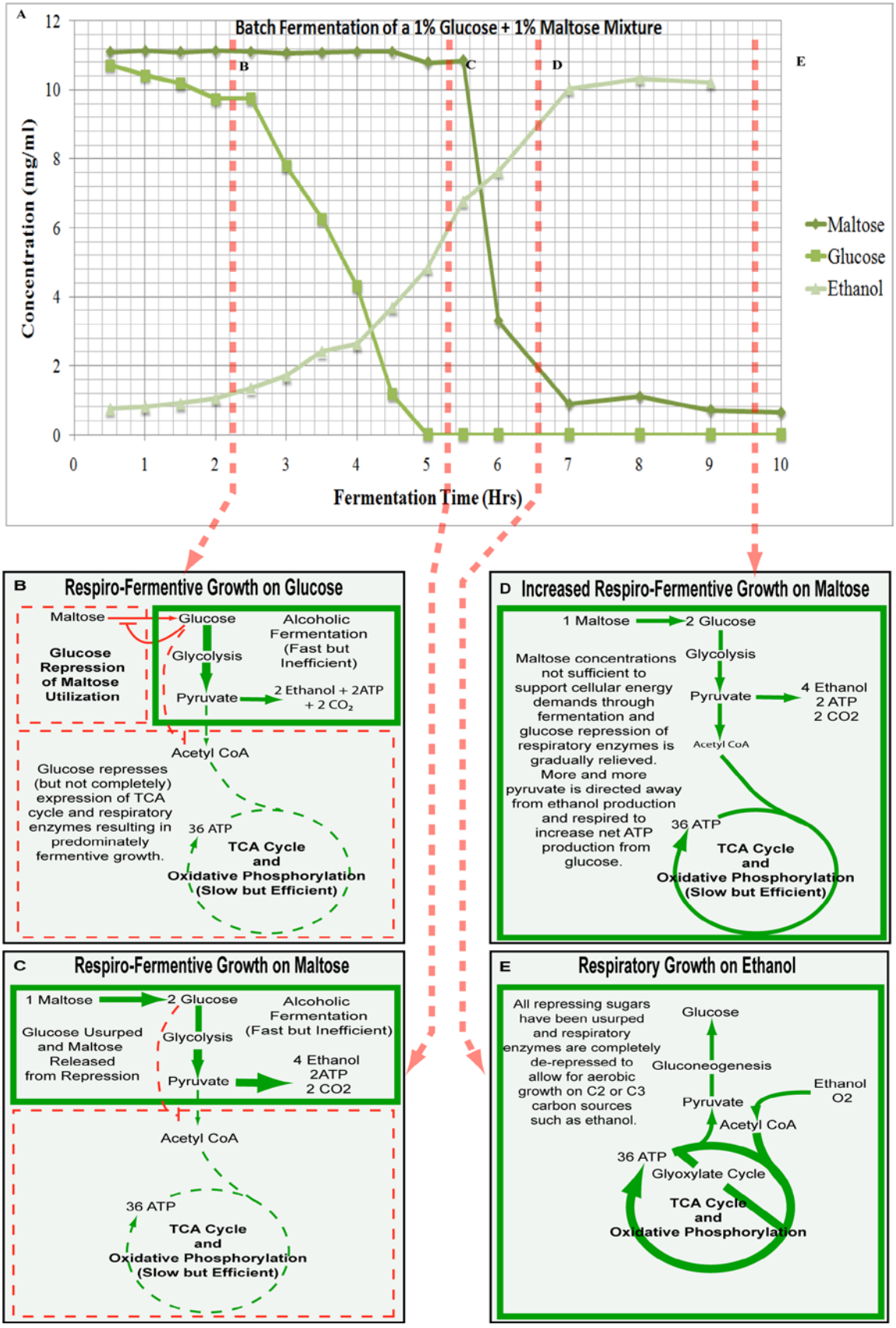
A
Batch Fermentation of a 1% Glucose + 1% Maltose Mixture
Concentration (mg/ml)
Fermentation Time (Hrs)
Maltose
Glucose
Ethanol
B
C
D
E
B Respiro-Fermentive Growth on Glucose
Maltose
Glucose
Glycolysis
Alcoholic Fermentation (Fast but Inefficient)
Glucose Repression of Maltose Utilization
Pyruvate
2 Ethanol + 2ATP + 2 CO2
Acetyl CoA
Glucose represses (but not completely) expression of TCA cycle and respiratory enzymes resulting in predominately fermentive growth.
36 ATP
TCA Cycle and Oxidative Phosphorylation (Slow but Efficient)
D Increased Respiro-Fermentive Growth on Maltose
1 Maltose
2 Glucose
Glycolysis
Maltose concentrations not sufficient to support cellular energy demands through fermentation and glucose repression of respiratory enzymes is gradually relieved. More and more pyruvate is directed away from ethanol production and respired to increase net ATP production from glucose.
Pyruvate
4 Ethanol 2 ATP 2 CO2
Acetyl CoA
36 ATP
TCA Cycle and Oxidative Phosphorylation (Slow but Efficient)
C Respiro-Fermentive Growth on Maltose
1 Maltose
2 Glucose
Alcoholic Fermentation (Fast but Inefficient)
Glucose Usurped and Maltose Released from Repression
Glycolysis
Pyruvate
4 Ethanol 2ATP 2 CO2
Acetyl CoA
36 ATP
TCA Cycle and Oxidative Phosphorylation (Slow but Efficient)
E Respiratory Growth on Ethanol
All repressing sugars have been usurped and respiratory enzymes are completely de-repressed to allow for aerobic growth on C2 or C3 carbon sources such as ethanol.
Glucose
Gluconeogenesis
Pyruvate
Ethanol O2
Acetyl CoA
36 ATP
Glyoxylate Cycle
TCA Cycle and Oxidative Phosphorylation

**Figure 2.1. Metabolic States of Saccharomyces throughout the Fermentation Process.** **A.** Fermentation profile of a wild-type Saccharomyces strain grown in batch culture in YP 1% glucose 1% maltose. Panes **B-E** represent simplified schematic diagrams of the metabolic state of the cell at the times on the fermentation profile as indicated. Green boxes in the panels encapsulate the metabolic pathway of greatest flux at the time point indicated while red dashed boxes represent repressed metabolic pathways. Red lines represent glucose repressed pathways. **B.** Saccharomyces prefers to ferment glucose before any other carbon/energy source. This preference for glucose is realized at the molecular level through integration of multiple signaling pathways which ultimately repress genes necessary for the utilization of other carbon sources (in this case maltose) and respiration. **C.** As glucose is usurped, the repression of genes needed for fermentation of secondary sugars such as maltose is lifted while repression of TCA cycle and respiratory genes is maintained. **D.** As Saccharomyces usurps all the fermentable sugars, repression of respiratory and TCA cycle genes is gradually lifted and coordinately more pyruvate generated from glycolysis is diverted from ethanol production to respiratory metabolism in order to support the energy demands of the cell. **E.** Once all fermentable sugars have been utilized, Saccharomyces goes through a dramatic alteration in its metabolic state known as the diauxic shift where fermentive growth is no longer supported. At this point, TCA cycle, respiratory, gluconeogenic, and glyoxylate cycle genes are completely de-repressed and Saccharomyces growth is fully supported through utilization of C2 and C3 carbon energy sources (in this case ethanol).

indirect consequence of defective glucose transport [69,70,67,166,167]. Defective glucose transport in *grr1Δ* strains is attributed to an inability to de-repress hexose transporter gene expression in response to glucose due to the positive role of Grr1 in relieving *HXT* repression through Snf3/Rgt2 [167,168,56]. It is thought that defective glucose transport in *grr1Δ* strains results in decreased flux through the glycolytic pathway which thereby releases glucose repression of genes affected by the Hxk2/Glc7/Snf1 pathway through an unknown mechanism [69,169,67]. However, a number of observations suggest that this explanation is not sufficient to explain the glucose repression defects of *grr1Δ* strains. First, though *grr1Δ* strains do show defects in high affinity glucose transport (needed for growth on low glucose), only a 30% reduction in low affinity transport (needed for growth on moderate to high glucose) has been observed and transcriptional studies measuring glucose insensitive expression of gluconeogenic and glyoxylate cycle genes have been performed utilizing samples from *grr1Δ* strains grown on moderate to high glucose concentrations (~1-2%) [159]. A number of studies suggest that a 30% transport reduction is insufficient to de-repress the gluconeogenic genes observed to be expressed in *grr1Δ* strains [170-173]. Second, *grr1Δ* strains are observed to have increased doubling times on glucose media which has been hypothesized to be a consequence of increased respiratory

metabolism in these strains [174]. However, while fermentation profiles performed on *grr1Δ* strains in glucose media have revealed decreased glucose uptake in these strains, they have not revealed significant decreases in ethanol yield [67]. These observations present a number of questions regarding the role of Grr1 in glucose signaling and metabolism. First, are the changes in gene expression observed for the *HXT*s as well as the *MAL, GAL, SUC,* respiratory, and gluconeogenic genes reflected at the protein level? Second, if so, how do *grr1Δ* cells maintain glucose fermentation despite increases in enzymes that would divert pyruvate from ethanol production and into respiratory metabolism? Lastly, does the decrease in glucose flux associated with the decreased glucose uptake in *grr1Δ* cells lead to de-repression of the internal glucose sensing pathway (Hxk/Glc7/Snf1) or is there an additional direct role for Grr1 in the internal glucose signaling pathway? In order to answer these questions it is first necessary to understand the mechanisms by which glucose is transported in wild-type yeast as well as the signaling pathways which affect their regulation and the regulation of other normally glucose repressed genes. Additionally, it is necessary to understand the current knowledge pertaining to the role of Grr1 in these processes. With this in mind, in the following sections, a detailed description of glucose transport and control of glucose transporter transcription through the Snf3/Rgt2 pathway will be presented. The role of Grr1 in this pathway as well as the phenotypes exhibited by *grr1Δ* cells as a result of defective signaling through this pathway will be emphasized. Additionally, glucose signaling through the internal Hxk/Glc7/Snf1 pathway will be reviewed.

### 2.3. Glucose Transport in *S. cerevisiae*

There are 20 genes in the *S. cerevisiae* genome that encode products with similarities to glucose transporters (*HXT1-HXT17*, *GAL2*, *SNF3*, and *RGT2*) underscoring the importance of glucose to *Saccharomyces* [175]. Interestingly, only Hxt1, Hxt2, Hxt3, Hxt4, Hxt6, and Hxt7 have been shown to be necessary for glucose transport since a yeast strain deleted for all six of these transporters (known as the *hxt* null*, hxt1-hxt7Δ*) exhibits no glucose uptake and no growth on

glucose media [176,177]. *GAL2* encodes for the galactose transporter, but *GAL2* over-expression restores normal glucose transport to the *hxt* null strain [177]. However, expression of this gene is regulated dualistically through glucose repression and galactose dependent induction and is therefore not actively expressed in media devoid of galactose. The physiological role of the remaining hexose transporter genes (*HXT8-HXT17*) has yet to be determined but it has been hypothesized that these genes may encode for transporters specific to other sugars [178]. Thus, the primary hexose transporters responsible for glucose transport under normal laboratory conditions (~1% glucose or above) are encoded by *HXT1-HXT7* and what is known about their transport kinetics, transcriptional regulation, and post-transcriptional regulation will be discussed further.

*S. cerevisiae* possesses the ability to grow on a variety of glucose concentrations and this ability is conferred by multiple transport systems with varying affinities for glucose [179]. Originally, two glucose uptake systems were described for *S. cerevisiae;* a constitutive low affinity uptake system acting on moderate to high glucose concentrations and a glucose repressible high affinity system acting at low glucose concentrations [180]. Genetic as well as biochemical characterization of yeast expressing only one of the seven hexose transporters at a time in the *hxt* null strain showed that each of these strains exhibited varying abilities to grow at different glucose concentrations [176] and that each of these transporters possesses a distinct affinity for glucose [173,181]. *HXT1*, *HXT3*, or *HXT4* expressing strains exhibited normal growth on high glucose concentrations (5%, or 278mM) but have impaired growth on low glucose concentrations (0.1% or 5.5mM). The growth defect on low glucose was especially pronounced in *HXT1* strains with a growth defect obvious at even 1% (55.5mM) glucose. This phenotype is explained by the fact that the Hxt1 transporter shows the lowest affinity for glucose (Km = ~107mM), implicating Hxt1 in the transport of glucose at high extra-cellular glucose concentrations. *HXT3* and *HXT4* growth defects on 0.1% glucose were more subtle and these phenotypes were consistent with their measured affinities (measured Km-values of ~28mM and 6mM respectively) and

thus Hxt3 and Hxt4 are also considered moderate to low affinity glucose transporters. Three of the remaining individual hexose transporter strains (*HXT2*, *HXT6*, or *HXT7* expressing) display opposite growth properties from the low affinity hexose transporters, exhibiting wild-type growth on low glucose concentrations and growth defects on high glucose concentrations. Thus, Hxt2, Hxt6, and Hxt7 were characterized as high affinity transporters with Km values for glucose of ~4mM, .9mM, and 1.3mM respectively. Finally, the *HXT5* expressing strain did not restore glucose transport to the *hxt* null and thus was deemed to possess no glucose transport capacity [173,176]. Thus, the combined action of these various glucose transporters enables yeast to support growth on fluctuating glucose concentrations.

### 2.4. Transcriptional Expression of Glucose Transporter Genes in Response to Fluctuating Glucose Concentrations

Over a broad range of glucose concentrations it has been observed that the maximal rates of glucose transport remain constant yet the affinity for glucose increases as the glucose concentration decreases for *S .cerevisiae* [182]. This ability to maintain relatively steady glucose influx over varying glucose concentrations is the manifestation of a corollary of regulatory mechanisms that modulate the transport capacity of *S. cerevisiae* in response to the external glucose concentration. These regulatory mechanisms ultimately control the subset of active glucose transporters present at the plasma membrane and their transport activities by directly controlling the transcriptional expression of hexose transporter genes and the stability, localization, and activity of Hxt proteins. Thus through the integration of these regulatory mechanisms yeast cells only actively express the subset of hexose transporters appropriate for growth on the actual external glucose concentration.

Though regulation of each of the hexose transporters is ultimately achieved by integration of transcriptional and post-transcriptional regulatory mechanisms the majority of work has been devoted to understanding the factors contributing to *HXT* gene regulation. Through this work, it was established that

the transcriptional regulation of each of the hexose transporters in response to glucose is consistent with the measured uptake kinetics for each transporter [181]. Thus, for *HXT1*, a low affinity glucose transporter, gene expression increases linearly with increasing glucose concentrations reaching maximal expression at 4% glucose where it shows an ~300 fold induction compared to transcript levels measured in galactose grown yeast cells (repressing) [167]. The expression levels of *HXT3* (encoding a moderate to low affinity transporter) in response to glucose are more moderate, increasing ~10 fold at 1% glucose concentrations, again consistent with Hxt3 uptake kinetics, with induction observed at glucose levels between 0.1 and 1%. It is also interesting to note that *HXT3* expression varies the least of any functional glucose transporter with high expression observed over the broadest range of glucose concentrations [167]. The transcriptional expression of *HXT1* and *HXT3* are not subject to glucose repression and this fact along with their measured uptake kinetics suggest that they are the major transporters comprising the low affinity glucose uptake system that was initially detected for this *Saccharomyces*.

The remaining functional glucose transporter genes (*HXT2*, *HXT4*, *HXT6* and *HXT7*) are subject to glucose repression with maximal expression observed at low glucose concentrations and thus together comprise the high affinity uptake system. *HXT2* and *HXT4*, encoding high affinity hexose transporters, show similar expression profiles, with *HXT4* transcription showing greater sensitivity to glucose repression. Gene expression profiles for these transcripts show induction between 0.1 and 0.5% glucose with reduction in expression observed at glucose concentrations greater than 0.75%. Basal levels for *HXT2* are reached at 4% glucose while *HXT4* expression reaches basal level at 1% glucose [167]. The *HXT6* and *HXT7* genes encode for highly similar proteins that only differ at two amino acid residues (293 Val/Ile and 556 Thr/Ala) [176]. Furthermore, these two genes are located in tandem on the right arm of chromosome IV and in some strains are fused into a single chimeric gene [176,177]. Thus, *HXT6* and *HXT7* gene expression is strikingly similar as both are highly glucose repressible at glucose concentrations greater than 0.5%. Interestingly,

*HXT7* exhibits the strongest level of expression of any *HXT* gene during growth on extremely low levels of glucose or on non-fermentable carbon sources, suggesting that this transporter is critical for re-establishment of glucose fermentation after prolonged periods of non-fermentative growth [183].

## 2.5. Glucose Signaling and Control of Hexose Transporters by the Rgt2 and Snf3 Pathway

The extracellular nutrient composition in both nature and the laboratory environment is in a constant state of flux and thus in order to support growth in this, vacillating environment, organisms must be able to adapt accordingly. *S. cerevisiae,* glucose transport capacity is adjusted to maintain an optimal influx of glucose in response to external glucose fluctuations. As reviewed earlier, the ability of yeast to maintain adequate glucose transport as glucose concentrations vary is realized, in part, by the presence of multiple glucose transporters with varying affinities for glucose. However, in order to maintain optimal glucose transport rates across a wide range of glucose concentrations, the subset of active transporters present at the plasma membrane must be coordinated in response to the external and internal glucose concentrations. Coordination of hexose transporter gene expression with external glucose concentrations is partially realized through a regulatory pathway that monitors extracellular glucose concentrations utilizing two glucose sensors known as Snf3 and Rgt2. These two glucose sensors initiate a signal that is propagated in a Grr1 dependent manner to ultimately alter the activity of a transcriptional repressor known as Rgt1 which binds the promoter region of a number of *HXT* genes.

### 2.5.1. The Snf3 and Rgt2 Extracellular Glucose Sensors

Snf3 and Rgt2 are high and low affinity glucose sensors, respectively, that lack the ability to transport glucose [144] but nevertheless influence glucose transport by coordinating hexose transporter transcription in response to extracellular glucose concentrations. Null mutations in *SNF3* (sucrose non-fermenting) were first isolated in screens searching for spontaneous mutations

that conferred the inability to grow on sucrose or raffinose [184]. These two polysaccharides are hydrolyzed in the periplasmic space by a secreted enzyme known as invertase, encoded by *SUC2*, which provides glucose to the cell. It was found that *snf3Δ* cells show no aberrations in the amount of secreted invertase activity [185] but show drastic defects in growth on low glucose due to defective high affinity glucose uptake [186]. Originally, it was suspected that *SNF3* encoded a high affinity glucose transporter; a conclusion supported by the high degree of Snf3 protein sequence homology to hexose transporters (~48%), the presence in the Snf3 protein sequence of 12 predicted transmembrane domains [161], and the fact that Snf3 localizes to the plasma membrane [187]. However, over-expression of *SNF3* in the *hxtΔ* mutant does not restore growth of this mutant on glucose [161] and thus, Snf3 possesses no glucose transport capacity of its own. Interestingly, *snf3Δ* cells are unable to induce transcriptional expression of the high affinity glucose transporters *HXT2* and *HXT4* in low glucose conditions [167]. Also, in *snf3Δ* cells, expression of the low affinity glucose transporter, *HXT3*, is reduced by greater than threefold on low glucose (raffinose) but is fully induced on high glucose concentrations (~4% glucose). However, the transcriptional expression of *HXT1,* another low affinity hexose transporter is only partially affected by the absence of *SNF3* [167]. Taken together, these results suggest that Snf3 functions as a high affinity glucose sensor that primarily influences the transcriptional expression of high affinity glucose transporters.

The transcriptional expression of the low affinity glucose transporters (*HXT1* and *HXT3*) on high glucose concentrations requires another plasma membrane localized protein known as Rgt2. Rgt2 is 60% similar in sequence identity to Snf3 and also like Snf3 possesses 12 predicted transmembrane domains. A dominant mutation in *RGT2*, named *RGT2-1*, was isolated as a suppressor that restores high affinity glucose uptake to *snf3*Δ cells [188]. This dominant *RGT2* allele restored, through a glucose and *SNF3* independent mechanism, the transcriptional expression of *HXT2* and *HXT4*, and displayed constitutive expression of *HXT1*. Interestingly, introduction of the same mutation into the *SNF3* locus (known as *SNF3-1*) also caused constitutive transcriptional

expression of *HXT2* and *HXT1* [144]. Strains deleted for *RGT2* display normal induction of *HXT2* and *HXT4* on low levels of glucose but are unable to fully induce *HXT1* transcription on high levels of glucose [144]. Taken together, these data suggest that Rgt2 and Snf3 coordinate the transcriptional expression of low and high affinity glucose transporter genes, respectively, in response to external glucose concentrations. Consistent with a role for these two proteins in the positive regulation of *HXTs* in response to glucose, *snf3Δrgt2Δ* strains exhibit extremely slow growth on glucose media and no growth at all on glucose media in the presence of the respiratory inhibitor, Antimycin A [99].

### 2.5.2. Std1 and Mth1

Though the precise mechanism by which glucose may be sensed through Snf3 and Rgt2 has not been elucidated, the molecular events initiated by these two sensors that ultimately coordinate hexose transporter transcription to external glucose levels have been revealed. Unlike the other members of the hexose transporter family, Snf3 and Rgt2 possess an additional long C-terminal cytoplasmic tail of 218 and 303 amino acids, respectively. Interestingly, deletion of these C-terminal tails abolishes the ability of these two sensors to induce the expression of their respective glucose transporter genes and chimeric Hxt1 and Hxt2 proteins with Snf3 and Rgt2 tails fused to their C-terminus restore this ability [161]. These cytoplasmic tails have been found to mediate binding of two proteins known as Std1 and Mth1 [189,190]. *STD1* (Suppressor of TBP Deletion) was originally discovered as a high copy suppressor of the growth defect associated with over-expression of a dominant negative *SPT15* (known as TBPΔ57; first 57 amino acids on the N-terminus are deleted) allele that encodes a yeast TFIID protein [191]. Deletion of *STD1* (aka *MSN3*) confers no observable phenotype on glucose media; however, a highly redundant functional paralog that shared 61% sequence similarity [192] with *STD1* was discovered through low stringency cross hybridization to the *STD1* coding sequence. This gene was aptly named *MTH1* (*MSN* Three Homolog) [192]. Like *std1Δ* strains, *mth1Δ* strains have no observable phenotypic defects on glucose media; however, deletion of *MTH1* in the

*snf3Δrgt2Δ* strain restores wild-type rates of growth to this strain on glucose as well as glucose/Antimycin A media [99]. Restoration of glucose based growth in the *mth1Δrgt2Δsnf3Δ* strain was subsequently shown to be a result of glucose insensitive transcriptional expression of *HXT2, HXT3,* and *HXT4* in this strain but *HXT1* expression was unaffected [99]. Deletion of *STD1* does not restore *HXT* expression or wild-type growth rates to *snf3Δrgt2Δ* cells but only a *std1Δmth1Δsnf3Δrgt2Δ* strain exhibited glucose insensitive expression of *HXT1* [99]. Together this data suggested that Std1 and Mth1 served to negatively regulate low and high affinity *HXT* expression, respectively, and that these two proteins are negatively regulated by the glucose sensors, Snf3 and Rgt2.

### 2.5.3. Rgt1

Mth1 and Std1 together cause repression of *HXT* genes by activating the transcriptional repressor, Rgt1, in the absence of glucose. Recessive mutations in *RGT1* were discovered in the same screen as dominant mutations in *RGT2* by their ability to restore growth on low glucose to *snf3Δ* strains [188]. It was subsequently shown that deletion of *RGT1* also restored glucose transport to *grr1Δ* strains [69,166] and that this restoration was due to relief of the constitutive repression of *HXT2, HXT3,* and *HXT4* observed in *grr1Δ* strains [167]. Rgt1 directly binds to the promoters of *HXT1, HXT2, HXT3,* and *HXT4* when glucose is absent and DNA binding activity towards these promoters requires Rgt1 association with Mth1 or Std1 [193-195,56,196]. Loss of either *MTH1* or *STD1* leads to glucose insensitive expression of *HXT1, HXT2, HXT3,* and *HXT4* and increased expression correlates directly with loss of Rgt1 association at these promoters and with Rgt1 hyper-phosphorylation [56]. In the absence of glucose, Rgt1 has been found to physically associate with Mth1 and Std1 by two-hybrid and pull-down assays and its association with Mth1 is required for DNA binding at *HXT* promoters [197]. Mth1 does not directly participate in transcriptional repression in conjunction with Rgt1 but is thought to prevent inhibitory phosphorylation of Rgt1 by the cAMP dependent protein kinases (Tpk1-Tpk3) [143]. Interestingly, though Tpk phosphorylation is required for inhibition of Rgt1 repressor activity on low

glucose, it is also required for hyper-phosphorylation of Rgt1 on high glucose where it acts to induce *HXT1* expression [198,199,143]. However, Rgt1 does not directly bind the *HXT1* promoter on high glucose and thus the role of Rgt1 in *HXT1* induction occurs through an indirect mechanism; possibly through induction of a transcription factor responsible for *HXT1* induction on high glucose [198].

### 2.5.4. The Role of Grr1 in the Snf3/Rgt2 Pathway

Rgt1 repressor activity towards the *HXT* genes is inactivated through Grr1 targeted ubiquitin dependent degradation of Mth1 and Std1in response to glucose. Strains deleted for *GRR1,* like *snf3Δrgt2Δ* strains, exhibit slow growth on glucose and have defects in high affinity glucose transport that are attributable to the inability to de-repress *HXT* gene expression in response to glucose availability [162,198,48,66]. This defect, also like *snf3Δrgt2Δ* strains, is abrogated by deletion of *RGT1* suggesting that Grr1 participates positively in conjunction with Snf3 and Rgt2 to negatively regulate Rgt1 repression of *HXT* genes [188,167,69]. It was originally posited that Grr1 mediates the degradation and/or sub-cellular localization of Rgt1 directly yet Rgt1 protein levels remain stable and nuclear regardless of glucose concentration. However, Rgt1 is found to be hypo-phosphorylated in *grr1Δ* cells and constitutively bound to *HXT1, HXT2, HXT3,* and *HXT4* promoters [56]. Deletion of both *STD1* and *MTH1* restore expression of *HXT* genes in *grr1Δ* cells and this restoration correlates with hyper-phosphorylation of Rgt1 and loss of Rgt1 association with *HXT* gene promoters [56]. Mth1 protein levels are rapidly reduced when wild-type cells grown on galactose are exposed to glucose and this rapid loss of Mth1 is not observed in *grr1Δ* strains [56]. It was subsequently shown that Mth1 and Std1 are targeted for ubiquitin dependent degradation by Grr1 in response to glucose [48,162]. Glucose induced ubiquitylation of Mth1 and Std1 requires not only Grr1 but also Snf3 or Rgt2, and either of the membrane bound casein kinases, Yck1 and Yck2 [162,142].

### 2.5.5. Model for Control of Hexose Transporter Gene Transcription through Integration of the Snf3/Rgt2, Hxk2/Glc7/Snf1, and Ras/cAMP Pathways

Considering all of the genetic and biochemical evidence regarding each of these elements influence on *HXT* gene expression, a model for how glucose stimulates de-repression of *HXT* genes through the Snf3/Rgt2 pathway has been proposed [200,163,197]. In the presence of low to moderate amounts of glucose (0.1-1%) (Figure 2.2 B and C), it is thought that glucose binding to Snf3 or Rgt2 may induce a conformational change in these proteins that stimulates phosphorylation of cytoplasmic C-terminally bound Mth1 and Std1 by the membrane bound casein kinases, Yck1 and Yck2 [142]. Phosphorylated Mth1 and Std1 are then recognized by Grr1 which facilitates their ubiquitylation and subsequent degradation by the 26S proteasome [56,48]. Degradation of Mth1 and Std1 inhibits their association with Rgt1 resulting in the exposure of inhibitory phosphorylation sites on Rgt1 that are targeted by cAMP dependent protein kinases (Tpks). Phosphorylated Rgt1 no longer associates with *HXT* promoters and thus repression is lifted in the presence of glucose. In the absence of glucose or in *grr1Δ* strains (Figure 2.2 A), Std1 and Mth1 phosphorylation, ubiquitylation, and degradation is absent allowing Std1 and Mth1 to translocate to the nucleus and bind Rgt1 [195]. Std1 and Mth1 mask Tpk phosphorylation sites on Rgt1 leading to Rgt1 hypo-phosphorylation. This active complex is then free to bind the promoters of a number of *HXT*s resulting in their transcriptional repression. While this model provides a basic description of the events that occur along the Snf2/Rgt2 pathway to control *HXT* transcription, full control of *HXT* expression is actually achieved through the combined action of the Hxk/Glc7/Snf1, Ras/cAMP, and the Snf3/Rgt2 pathways. Through integration of these pathways, expression of the appropriate subset of *HXT* genes is intricately coordinated in response to the external and internal glucose concentrations. When no glucose is present, as indicated above, transcription of *HXT1,2,3* and 4 is repressed by Rgt1 in association with Mth1 and Std1 [201]. On high glucose, the high affinity transporters Hxt2, 4, and 6/7 are not needed and therefore are transcriptionally repressed. However, repression of their respective genes is not exerted by Rgt1

on high glucose but by another repressor known as Mig1 [167]. Mig1 repressor activity is inactivated by Snf1 dependent phosphorylation [202,203]. On high glucose, Snf1 kinase activity is inactivated by a signaling mechanism that requires Hxk2 and the PP1 phosphatase, Glc7, in association with one of its targeting proteins, Reg1. Through an unknown mechanism, Hxk2 phosphorylation of glucose to glucose-6-phosphate promotes Glc7 association with Reg1 which targets Glc7 phosphatase activity to de-phosphorylate and subsequently inactivate Snf1 kinase [204]. Inactivation of Snf1 kinase on high glucose prevents Snf1 dependent inactivation of Mig1 which binds to the *HXT2, HXT4,* and *HXT6/7* promoters [160]. On high glucose, full de-repression of the low affinity transporter genes, *HXT3* and *HXT1* is achieved because these two transporter genes are not subject to Mig1 mediated repression and Rgt1 repressor activity is fully inactive due to Rgt1 hyper-phosphorylation by the cAMP dependent protein kinases [197,143].

On low glucose, the intracellular signals which lead to high affinity transporter gene expression and low affinity transporter gene repression are only partially defined and the events that dictate full expression of *HXT1* on high glucose and repression of *HXT1* on low glucose remain unclear. High glucose concentrations promote Tpk dependent hyper-phosphorylation of Rgt1 which leads to activation of *HXT* expression [198]. However, Rgt1 does not directly bind the *HXT1* promoter under these conditions [198]. Additionally, Std1 exclusively inhibits *HXT1* expression in conjunction with Rgt1 on low glucose, suggesting that Mth1 and Std1 function are not completely redundant [189]. A mechanism that completely describes how Rgt1 repressor activity is maintained at low affinity transporter gene promoters (specifically *HXT1)* but is inactivated on high affinity hexose transporter genes on low glucose has not been described. Here we propose a new model based on our interpretation of the current literature. On low glucose, the high affinity glucose sensor, Snf3, is activated, signaling for the Grr1 dependent degradation of Std1 and Mth1 which have both been found to bind the cytoplasmic C-terminal tail of Snf3. However, we propose that signaling through the low affinity sensor, Rgt2, is not active on low glucose conditions and

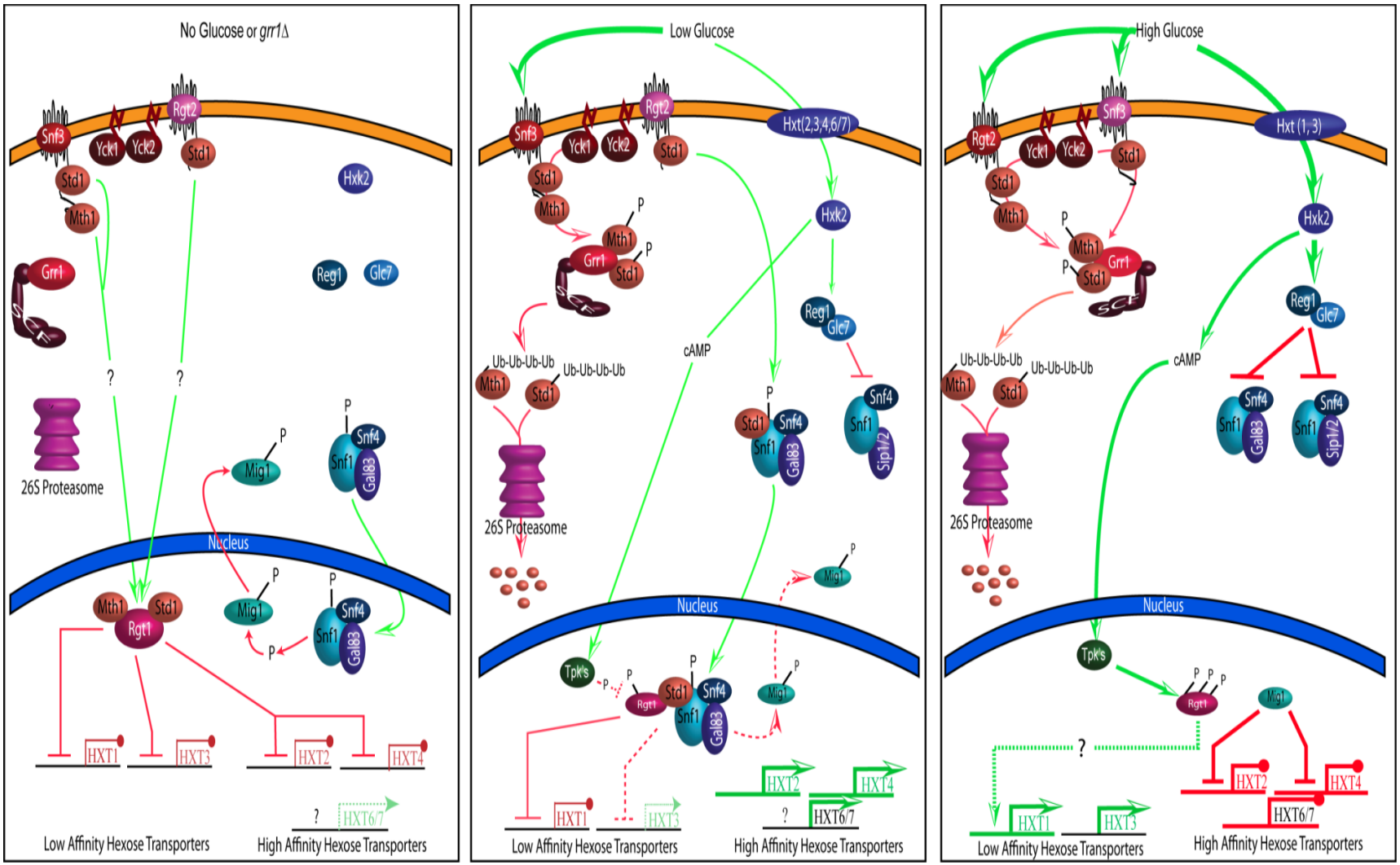
No Glucose or grr1Δ
Snf3
Rgt2
Yck1
Yck2
Std1
Mth1
Grr1
Hxk2
Reg1
Glc7
26S Proteasome
Mig1
Snf4
Snf1
Gal83
Nucleus
Rgt1
HXT1
HXT3
HXT2
HXT4
HXT6/7
Low Affinity Hexose Transporters
High Affinity Hexose Transporters
Low Glucose
Hxt(2,3,4,6/7)
cAMP
Ub-Ub-Ub-Ub
Tpk's
Sip1/2
High Glucose
Hxt (1, 3)

**Figure 2.2. Transcriptional Regulation of Hexose Transport.** **A.** On low glucose or in *grr1Δ* cells, degradation of Std1 and Mth1 is prevented and through and unknown mechanism Std1 and Mth1 translocate to the nucleus where they physically interact with the Rgt1 repressor. Association of Std1 and Mth1 with Rgt1 leads to repression of both low affinity (*HXT1* and *HXT3*) and high affinity (*HXT2* and *HXT4*) hexose transporter genes. At the same time Hxk2/Reg1-Glc7 inhibition of Snf1 kinase activity is prevented leading to phosphorylation and inhibition of the transcriptional repressor Mig1. **B.** Low extracellular glucose is sensed through the high affinity glucose sensor, Snf3, which promotes Yck1/2 (casein kinases) dependent phosphorylation of Snf3-C terminally bound Std1 and Mth1. Phosphorylation of Std1 and Mth1 leads to their ubiquitylation by $SCF^{Grr1}$ which targets Std1 and Mth1 for proteasomal degradation. However, the low affinity glucose sensor, Rgt2, is not active and C-terminally bound Std1 is free to associate and activate the Snf1 kinase. The active, nuclear localized, Std1-Snf1 kinase complex associates with Rgt1, preventing Rgt1 hyper-phosphorylation by the cAMP dependent protein kinases (Tpk1-3). The Std1-Rgt1-Snf1 complex fully represses *HXT1* expression, partially represses *HXT3* gene expression, and inhibits Mig1 dependent repression of high affinity (*HXT2* and *HXT4)* hexose transporter expression. **C.** High glucose is sensed by both the high affinity glucose sensor, Snf3, and the low affinity glucose sensor, Rgt2, which leads to Yck1/2 dependent phosphorylation of both Snf3 C-terminally associated Std1 and Mth1 and Rgt2 C-terminally associated Std1. Mth1 and Std1 are then ubiquitylated by $SCF^{Grr1}$ which targets them for proteasomal degradation. Degradation of Std1 and Mth1 leads to hyper-phosphorylation and inactivation of the Rgt1 transcriptional repressor which subsequently leads to inhibition of Rgt1 dependent repression of the low affinity hexose transporters, *HXT1* and *HXT3*. Concurrently, the high rate of glucose transport leads to inactivation of Snf1 through Reg1-Glc7 de-phosphorylation of Thr210 in the Snf1 catalytic domain. Inhibition of Snf1 kinase activity leads to Mig1 hypo-phosphorylation promoting Mig1 dependent repression of the high affinity hexose transporters, *HXT2, HXT4,* and possibly *HXT6/7* [205-209].

that only Std1 binds to its cytoplasmic C-terminal tail. This hypothesis is based on a number of genetic and biochemical assays described here. It was originally discovered through two-hybrid analysis that while Std1 interacted with both glucose sensors, Mth1, only interacted with the high affinity sensor, Snf3 [189]. Consistent with these observations, Snf3 contains two copies of a conserved, C-terminal, 25 amino acid, sequence which serve as binding sites for Std1 and Mth1, whereas Rgt2 contains only one such sequence [161]. Furthermore, mutations in Rgt2 have been found to exclusively prevent high glucose activation of *HXT1* expression [161] and glucose insensitive expression of *HXT1* requires deletion of both *STD1* and *MTH1,* whereas glucose insensitive expression of *HXT2* and *HXT4* only requires *MTH1* deletion [189]. Interestingly, Std1 has been discovered to interact with Snf1 [210,192] and Snf1 activity is required for *HXT1* repression on low glucose [189,210].

Taking these observations into account; the following model for de-repression of the high affinity hexose transporter genes and repression of the low

affinity hexose transporter, *HXT1,* on low glucose is proposed (Figure 2.2 B). Low external glucose concentrations activate the high affinity glucose sensor, Snf3, leading to Grr1 dependent ubiquitylation and degradation of Snf3 associated, Std1 and Mth1. On the other hand, low glucose does not lead to complete degradation of Std1 and it alone binds to Rgt2 which is not activated by low glucose. Stabilized Std1 is free to interact with Snf1 preventing Snf1 inactivation by Reg1-Glc7 and leading to the nuclear localization of a Std1-Snf1-Gal83-Snf4 complex. The absence of Mth1 bound Rgt1 leads to phosphorylation of Rgt1 by the cAMP dependent protein kinases (TPKs) which inhibits the repressor activity of Rgt1 towards the high affinity hexose transporter genes, *HXT2, HXT4,* and *HXT6,7*. At the same time, Mig1 repression of these genes is relieved through inactivation of Mig1 by Std1-Snf1-Gal83-Snf4 dependent phosphorylation. Full repression of *HXT1* and partial repression of *HXT3* is achieved through the Std1 dependent interaction of Rgt1 with the Snf1-Gal83-Snf4 complex.

## 2.6. The Hxk/Glc7/Snf1 Dependent Intracellular Glucose Signaling Pathway

### 2.6.1. Hxk2 and Glucose Phosphorylation

Once glucose has been transported into the cell by any of the functional hexose transporters it is quickly and irreversibly phosphorylated by one of three hexose kinases in yeast to form glucose-6-phosphate. There are three hexose kinases in yeast that possess the ability to phosphorylate glucose including Hxk1, Hxk2, and Glk1 [211]. Though each of these enzymes is capable of glucose phosphorylation, both transcriptional and protein expression studies suggest that Hxk2 provides most of the glucose phosphorylation activity in cells growing exponentially on glucose [212,213]. As the first and predominate enzyme in the metabolism of glucose, it is not surprising that Hxk2 plays a major regulatory role in glucose repression that cannot be ascribed to either Hxk1 or Glk1 [154,155] Genes resistant to glucose repression in strains deleted for *HXK2* include *SUC2* [153,152], *HXK1* and *GLK1* [152,214], *MAL* and *GAL* genes [215-217], *HXT2* and *HXT4* [218], and genes involved in respiratory metabolism [215,216,219]. The altered expression of

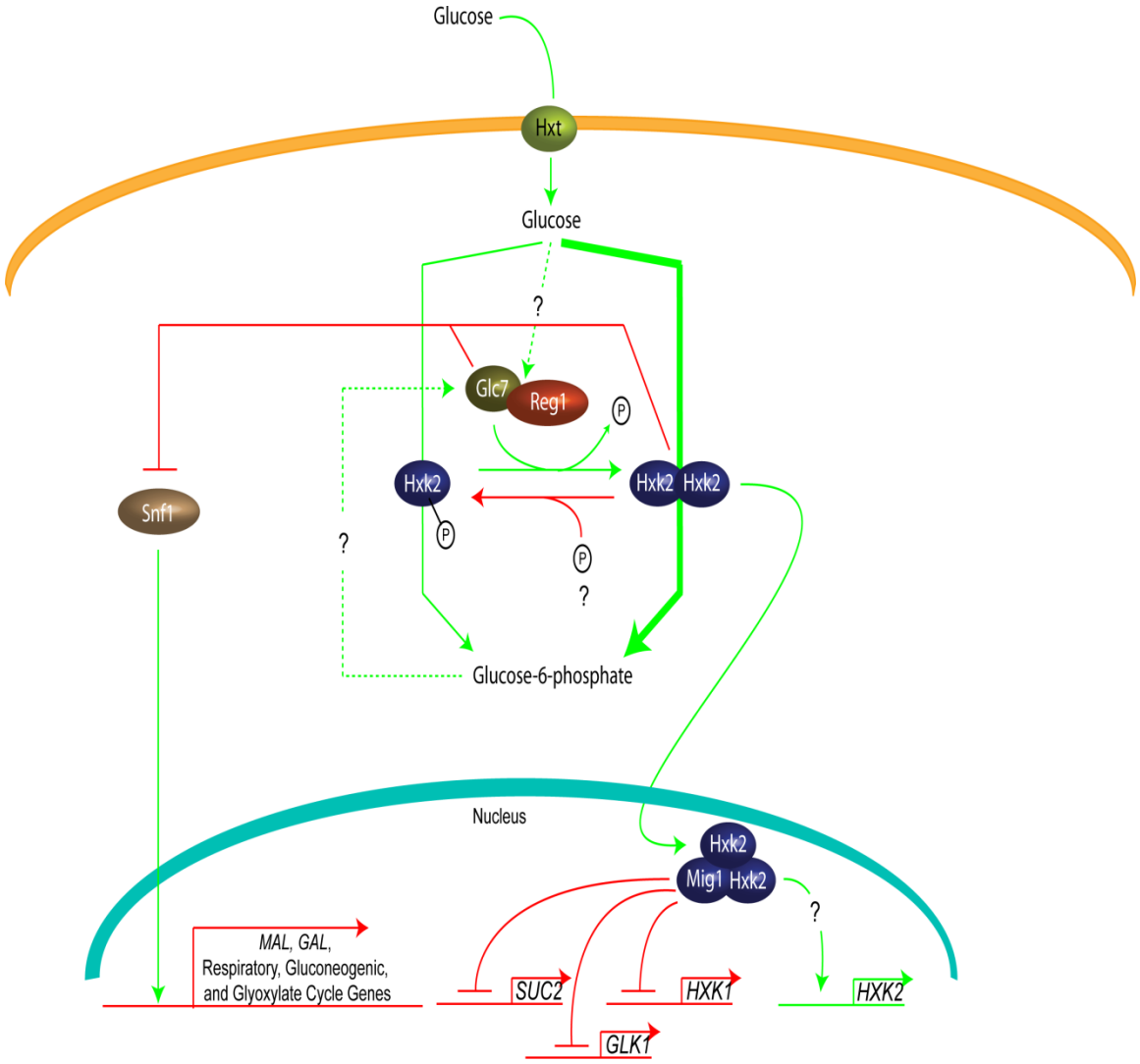


**Figure 2.3. Control of Hxk2 Dimerization and Hxk2 Dependent Transcriptional Repression in Response to Glucose.** In the absence of glucose, Hxk2 is found primarily in a hyper-phosphorylated form that possesses a higher Km for glucose (indicated by thin green line). The kinase acting to phosphorylate Hxk2 is currently unknown. Through an unknown signal, increased concentrations of glucose or glucose-6-phosphate induce Reg1-Glc7 dependent de-phosphorylation of Hxk2 (green dashed lines) which leads to Hxk2 dimerization. Dimerized Hxk2 possesses a lower Km for glucose and thus possibly supports greater glycolytic flux (thick green line). It is presumed that the dimerized form of Hxk2 interacts with the Mig1 repressor which promotes nuclear localization of Hxk2. Nuclear Mig1-Hxk2 binds directly to the *SUC2, GLK1,* and *HXK1* promoters to repress these genes transcription in response to glucose. Nuclear Hxk2-Mig1 also is required through an unknown mechanism to induce *HXK2* transcription on high glucose. Repression of *MAL*, *GAL*, respiratory, gluconeogenic, and glyoxylate cycle genes is inhibited through an Hxk2 and Reg1-Glc7 dependent pathway that acts to inhibit Snf1 catalytic activity which is responsible for induction of these genes in response to glucose exhaustion. (Figure 2.4)

respiratory genes are commensurate with an increased respiratory capacity in this stain, since *hxk2Δ* strains have been shown to grow 30% slower on glucose as well as have a 41% decrease in ethanol yield [215,219]. Additionally, *hxk2Δ* strains have been shown to co-consume multiple sugars and ethanol in the presence of glucose [220]. Genes encoding gluconeogenesis enzymes are unaffected by *HXK2* deletion [216,215].

Recent evidence suggests that, in addition to the catalytic activity of Hxk2, Hxk2 serves a direct role in transcriptional regulation of glucose repressed genes. Support for this role is supplied by a number of independent observations. Though most of Hxk2 protein is localized in the cytoplasm, a significant fraction has been determined to be nuclear localized (~14%) on glucose media [221-223]. Translocation of Hxk2 to the nucleus requires a putative nuclear localization sequence within the N-terminal sequence, $K^{7}$ –$M^{16}$, since a strain containing an Hxk2 construct lacking these amino acids (*HXK2Δ* $K^{7}M^{16}$) does not localize to the nucleus [223]. The nuclear localization of Hxk2 has been shown to be induced by the presence of glucose and is dependent on Hxk2 interaction with Mig1 which is a transcriptional repressor of many glucose repressed genes [222]. Nuclear localized Hxk2 is required for *SUC2* repression and has been shown to associate with a complex of proteins in the upstream promoter of this gene that includes the transcriptional repressor Mig1 and the mediator protein Med8 [222]. Taken together, the evidence supporting a direct role for Hxk2 in controlling transcriptional expression of at least *SUC2, HXK1, GLK1,* and itself is incontrovertible.

Hxk2 has been shown to be phosphorylated in vivo on Serine 15 and enhanced phosphorylation of this site correlates to increased levels of the monomer form of Hxk2. This monomer form of Hxk2 is more prevalent when cells are grown on non-repressive carbon sources such as galactose, raffinose, and ethanol. The phosphorylation and dimerization state of Hxk2 has been shown to be affected by mutations in Grr1, Reg1, and Glc7 [224]. While the increased phosphorylation of Hxk2 leading to the prevalence of the monomer form of Hxk2 has been shown to be attributable to reduced glucose transport in

*grr1* strains, this is not the case for *reg1* and *glc7* mutations and thus the Reg1-Glc7 phosphatase complex is proposed to regulate the phosphorylation state of Hxk2 directly. In a subsequent study comparing the phospho-proteome of *reg1Δ* strains and *reg1* mutant strains defective in the ability to bind Glc7 to wild-type strains; phosphorylation of Hxk2 was found to be enhanced and this was subsequently shown to be due to reduced de-phosphorylation of Hxk2 by Reg1-Glc7 [204].

Given the mounting evidence for a direct role for Hxk2 in transcriptional control, it is now undeniable that Hxk2 has both a regulatory and metabolic functions in response to the presence of glucose (for an overview of the role of Hxk2 in glucose repression see Figure 2.2). However, the inability to separate catalytic activity and regulatory modules of Hxk2 as well as the fact that Hxk1 and Glk1 cannot substitute for Hxk2 to reduce respiratory metabolism, has led to a controversial debate over the role Hxk2 catalytic function plays in regulation of glucose repression. Mutations in Hxk2 that abrogate glucose repression (as defined by the extent of *SUC2* de-repression) while maintaining wild-type or increased levels of glucose phosphorylation activity have been isolated and thus Hxk2 catalytic activity is not sufficient for regulation [223]. However, whether Hxk2 catalytic activity is necessary for exerting glucose repression is another question that remains to be answered. The effect on glucose repression (again in the context of *SUC2* repression) utilizing mutations which alter Hxk2 catalytic activity have been obtained with mixed results as multiple groups found catalytic activity to be required for eliciting glucose repression [156,225] while others have isolated Hxk2 mutants with low catalytic activity that retained the ability to induce glucose repression [226,227]. It should be noted that the effects on glucose repression for the various *HXK2* mutants have been primarily performed using *SUC2* transcription as a reporter with little attention devoted to other Hxk2 repressed genes such as respiratory enzymes. A role for Hxk2 catalytic activity in their repression and de-repression could be primarily dependent on Hxk2 catalytic activity since reduced phosphorylation of glucose would lead to an increased dependence on respiration to support the energy demands of the cell. It is also

interesting that Hxk1 is 75% identical at the sequence level to Hxk2 and also possesses the $K^{7}$-$M^{16}$ sequence as well as other regulatory sequences that have been shown to be important for Hxk2 regulatory function [163]. The controversy is further compounded by the fact that the levels of sugar phosphates can be completely supplied by the glucose phosphorylation activity of Hxk1 and Glk1 in *hxk2Δ* strains [228,211,156]. For further review regarding the controversy surrounding the mechanism by which Hxk2 induces glucose repression see the following excellent reviews [229,230,163,165,164].

### 2.6.2. Reg1-Glc7 and Snf1

In the absence of fermentable sugars, genes required for respiration, gluconeogenesis, and the glyoxylate cycle are relieved from repression in order to prepare the cell for growth on C2 and C3 carbon sources such as glycerol, ethanol, and acetate. At the protein level, enzymes and transporters responsible for the metabolism of these alternative energy sources are activated through post-translational events that modify the enzymatic activity and cellular location of these proteins. The integration of these processes requires a complicated coordination of multiple molecular signaling events that are all dependent to some degree on the activity of the Snf1 kinase. As glucose is exhausted, Snf1 kinase activity is elevated through an unknown intracellular signal. Though the origin of this signal remains elusive, the molecular events that occur to regulate Snf1 activity and the consequences of Snf1 activation have been elucidated through eloquent genetic and biochemical studies. Given the centralized role for Snf1 in the response to glucose limitation and the fact that *grr1Δ* mutants exhibit glucose independent changes in transcriptional and post-transcriptional events controlled by Snf1, what is known about Snf1's regulation and the consequences of its activation will be reviewed in this section.

Snf1 is the catalytic subunit of a serine/threonine kinase with significant homology to the mammalian AMP activated protein kinase (AMPK) [231-233]. As in mammals, Snf1 kinase functions in vivo within any of three hetero-trimeric protein complexes consisting of an α subunit (Snf1), a γ subunit (Snf4), and one of three

alternate β subunits (Gal83, Sip2, and Sip1) [234,235,163,164,229]. Snf1 is constitutively expressed and protein levels remain constant across diverse growth conditions [236]. Thus, the catalytic activity of Snf1 towards its various substrates is regulated primarily through post-translational mechanisms. Post-translational regulation of Snf1 is achieved through both regulation of its phosphorylation state on threonine 210 [237-241] and control of its sub-cellular localization through its interchangeable association with the β subunits [242-245]. Together these regulatory mechanisms differentially direct the kinase activity of Snf1 towards a myriad of intracellular substrates and these regulatory mechanisms are highly influenced by the presence or absence of glucose. (Figure 2.4)

### 2.6.3. Glucose Dependent Control of Snf1 Catalytic Activity by Regulation of the Phosphorylation Status of Thr210

Phosphorylation of threonine 210 found in the activation loop of the N-terminal kinase domain of the Snf1 catalytic subunit is required for its catalytic activity and is regulated in a glucose dependent manner [239,238,246]. On high glucose, this phosphorylation site is masked through auto-inhibition by a motif present in the C-terminal domain of Snf1 known as the AIS (Auto-Inhibitory Sequence) [247,241]. Autoinhibition is counteracted by association of the β subunit, Snf4, with the C-terminal regulatory region of Snf1 [241]. It is proposed that on low glucose, Snf4 binds to this regulatory region and inhibits interaction of the C-terminal AIS with the kinase domain thereby maintaining Snf1 in an open configuration to allow uninhibited phosphorylation of threonine 210 by activating kinases [248-250]. Consistent with this reasoning is the fact that glucose strongly inhibits Snf4 and Snf1 association [241]. Though Snf4 is required for catalytic activity of full length Snf1 it is not required for activity of Snf1 lacking the C-terminal regulatory domain [249,241]. However, in the absence of Snf4, in strains expressing truncated Snf1, the ability of glucose to modulate Snf1 phosphorylation on threonine 210 is preserved, suggesting that the glucose dependent phosphorylation and/or de-phosphorylation of Snf1 at threonine 210 do not require Snf4 for function [239,251,252]. Nevertheless, Snf4 is required for the

catalytic activation of Snf1 in the context of the functional hetero-trimeric complex.

Phosphorylation of threonine 210 is carried out by any of three upstream kinases known as Elm1, Tos3, and Sak1 [251]. With regard to Snf1 phosphorylation at threonine 210 these three kinases seem to be redundant since Snf1 catalytic activity is completely abolished in only an *elm1Δ tos3Δ sak1Δ* triple deleted strain [251]. In addition, this strain, like *snf1Δ* strains, does not grow on raffinose or ethanol/glycerol medium [251,237]. Despite the functional redundancy of these kinases towards Snf1 activation, other non-redundant cellular functions for these kinases have been described. Elm1 for instance localizes to the bud neck and is involved in regulating cytokinesis as well as cell morphogenesis [253-255]. Lack of *TOS3,* on the other hand, has been shown to lead to growth defects and reduced Snf1 catalytic activity after prolonged growth on ethanol-glycerol medium [256]. Due to their roles in discrete cellular functions, it seemed likely that each of these kinases was responsible for activating a specific hetero-trimeric Snf1 complex, specified by the particular β subunit of each complex. However, this is not the case as both Sak1 and Elm1 were found to participate in phosphorylating Gal83-Snf1 and Sip2-Snf1 kinase complexes [257,258]. The different hetero-trimeric Snf complexes do seem to exhibit kinase specific preferences dependent on the particular stress [257,258]. Interestingly, as of yet, there is no evidence that Snf1 activating kinase activity is regulated in response to glucose. In fact, it has been determined that kinase activity towards threonine 210 of Snf1 may be constitutive and that the glucose specific signal regulating the phosphorylation state of Snf1 is dependent on the rate of de-phosphorylation catalyzed by the Reg1-Glc7 phosphatase [237].

### 2.6.4. The Role of the Reg1-Glc7 Phosphatase in Regulating the Snf1 Kinase in Response to Glucose

The Glc7 protein is the yeast equivalent of the PP1 phosphatase of mammalian cells and like its homologs has been found to regulate a multitude of intracellular functions [259-267]. Glc7 is a stable protein with a half life of ~180

minutes and regulation of Glc7 activity through transcriptional and/or translational mechanisms has not been observed [261,259]. The specificity and catalytic activity of the PP1 catalytic subunit is partially determined by controlling its physical association with one of a number of regulatory proteins [262,268,263,264,269,270,266,267], including Reg1 [207]. Due to its central role in a number of critical cellular processes, null mutations in the *GLC7* locus result in the loss of viability. However, mutations that do not inhibit total Glc7 catalytic activity but result in the inability for a particular targeting subunit to interact with Glc7 have been isolated [271]. One such mutant, *glc7-T 152K* (known at that time as *cid1-226*), was isolated in a mutagenesis screen for mutants resistant to 2-deoxyglucose [272]. This mutant also exhibited glucose repression resistant expression of *SUC2* as well as the *MAL* genes which suggested that Glc7 may counteract the effects of Snf1 activity [273]. This mutation was later shown to cause a defect in the ability of Glc7 to associate with its regulatory subunit, Reg1 [207].

Strains lacking functional Reg1 were also isolated based on their resistance to 2-deoxyglucose (2-DOG) and show similar glucose repression resistant/Snf1 dependent gene expression as that observed for strains harboring the *glc7-T152K* allele [274]. It was later shown that Reg1 interacts strongly with protein phosphatase type 1 (Glc7) [207] through a PP1-binding motif found in Reg1 with the sequence $RHIHF_{468}$ [275,276]. Genetic complementation tests indicated that Reg1-Glc7 acted upstream of the Snf1 kinase in the intracellular glucose signaling pathway since mutations in *SNF1* are epistatic to *REG1* mutations [277,278]. Additionally, Reg1 physically interacts with Snf1 through a C-terminal sequence that is distinct from the Glc7 interaction domain [279]. This interaction requires phosphorylation of threonine 210 in the activation loop of the Snf1 kinase. Furthermore, *reg1Δ* strains exhibit glucose independent constitutive Snf1 kinase activity, hyper-phosphorylation of Snf1 at threonine 210, and glucose independent Snf1 interaction with Snf4 [241,280]. This data suggests that Reg1 serves to target Glc7 phosphatase activity to de-phosphorylate Snf1 at threonine 210 and that Reg1-Glc7 de-phosphorylation prevents activation of the Snf1-Snf4 kinase complex in response to glucose availability.

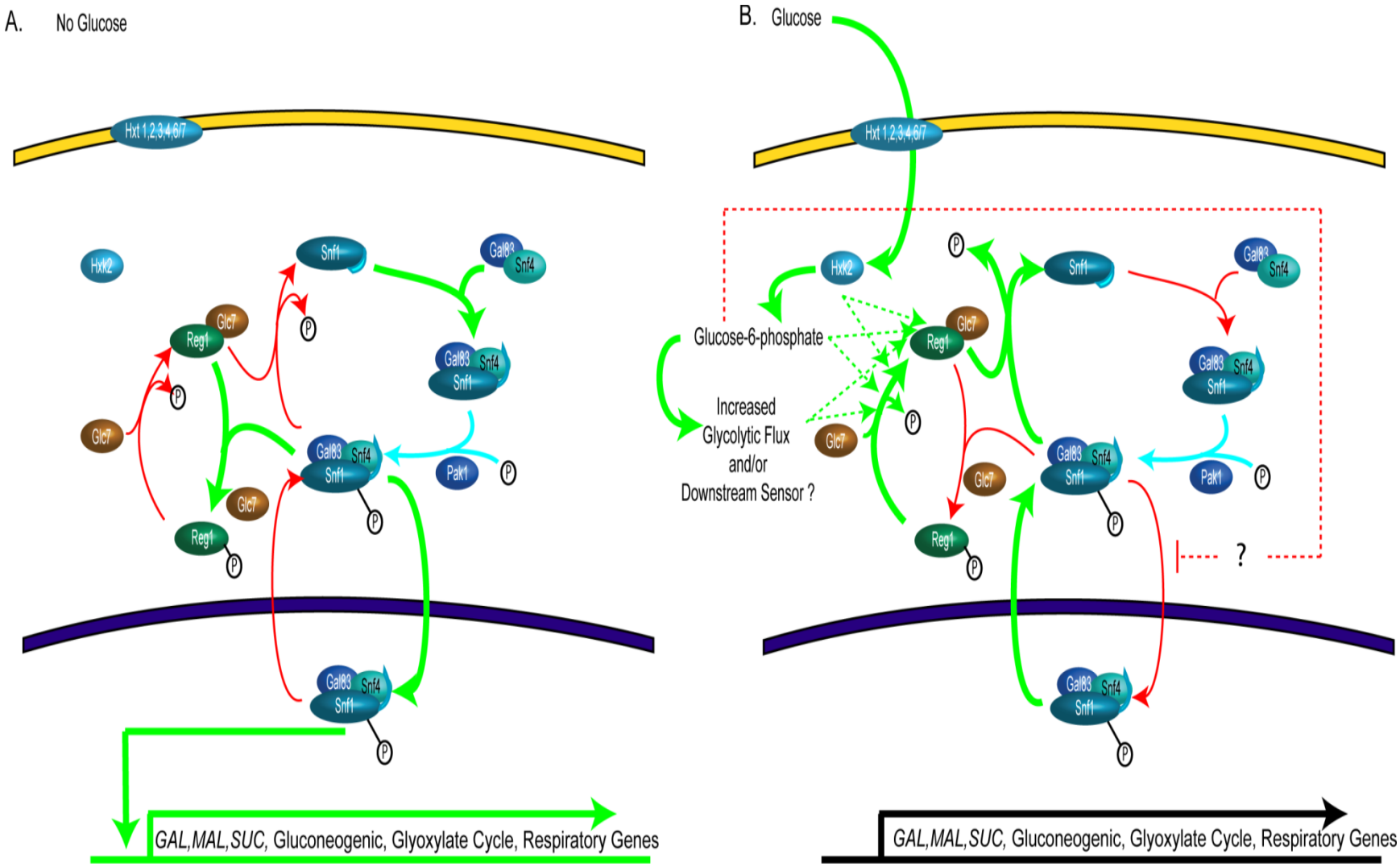
A. No Glucose
Hxt 1,2,3,4,6/7
Hxk2
Snf1
Gal83
Snf4
Glc7
Reg1
P
Pak1
GAL,MAL,SUC, Gluconeogenic, Glyoxylate Cycle, Respiratory Genes
B. Glucose
Glucose-6-phosphate
Increased
Glycolytic Flux
and/or
Downstream Sensor ?
?

**Figure 2.4. Regulation of Gal83-Snf4-Snf1 Kinase Activity.** **A.** Glucose exhaustion results in activation and nuclear accumulation of the Gal83-Snf4-Snf1 kinase hetero-trimer. Through an unknown mechanism that is inhibited by glucose, Gal83 associates with and promotes formation of the active Snf1 kinase hetero-trimer (Molecular events which are active or increased are shown in Green, inactive or decreased molecular events are shown in Red, constitutive molecular events are shown in powder blue). Activation is partially achieved through Snf4 association with the Snf1 auto regulatory domain (shown in powder blue on Snf1). Snf4 inhibits association of the auto regulatory domain with the kinase domain thereby exposing threonine 210 to phosphorylation by the Snf1 activating kinase Pak1. Phosphorylation of Snf1 on Thr210 is required to activate Snf1 kinase activity and Pak1 kinase activity towards Snf1 is not regulated by glucose. Phosphorylation and Gal83 association of Snf1 is also required for cytoplasmic to nuclear translocation of the complex. Once nuclear, the Gal83-Snf4-Snf1 hetero-trimer inhibits and activates transcription factors through phosphorylation which leads to de-repression and induction of glucose repressed genes. **B.** In the presence of glucose. Hxk2, glucose-6-phosphate, or increased glycolytic flux leads to activation of Reg1-Glc7 phosphatase activity through an unknown mechanism that either acts to promote Reg1/Glc7 interaction or to regulate Reg1-Glc7 catalytic activity directly through post-translational modification. Through Reg1, Glc7 phosphatase activity is targeted to de-phosphorylate threonine 210 on Snf1 which inactivates Snf1 kinase activity and promotes formation of the Snf1 auto-inhibited state. The auto-inhibited α subunit of Snf1 can no longer interact with Gal83 and therefore is retained in the cytoplasm. Through an unknown mechanism, glucose-6-phosphate also inhibits Gal83 dependent nuclear localization of Snf1.

Notwithstanding the inability to decipher the precise mechanism through which Hxk2, Reg1, and Glc7 regulate Snf1 activity in response to glucose, a number of results emphasize that glucose regulation of Snf1 occurs by governing the complex interplay between Glc7- Reg1 and Snf1. First, the phosphorylation state of Reg1 has been found to be regulated in a glucose dependent manner. On low glucose or in the absence of glucose, Reg1 is found in a hyper-phosphorylated state that is dependent on Snf1 catalytic activity [209]; whether Snf1 kinase phosphorylates Reg1 directly or through an indirect mechanism remains unanswered. Second, de-phosphorylation of Reg1 in response to the presence of glucose is directly dependent on Glc7 phosphatase activity [209]. Biochemical evidence suggests that Reg1 phosphorylation leads to its disassociation from Snf1 and thus is a mechanism for Snf1 to modulate its own activity. Third, this phosphorylation event has also been shown to be influenced by Hxk2 since Reg1 was not found to be phosphorylated in an *hxk2*Δ strain [209]. Fourth, analysis of the phosphorylation state of threonine 210 utilizing phospho-specific antibodies has revealed that the glucose dependent phosphorylation of this residue is not a result of regulated kinase activity but phosphatase activity [237]. *In vitro* kinase assays conducted utilizing each of the

three SAKs isolated from cells grown on low and high glucose concentrations showed high activity regardless of the glucose concentration [281]. However, inhibition of Reg1-Glc7 activity through deletion of *REG1* results in a tremendous increase in Snf1 phosphorylation, even at high glucose concentrations [281,207,282,283]. Despite the lack of a precise mechanism describing how each of these events are carried out in response to glucose the evidence supporting that the glucose signal acts to modulate Reg1-Glc7 activity towards Snf1 is compelling.

### 2.6.5. Spatial Regulation of Snf1

Among the postulated mechanisms for directing Reg1-Glc7 catalyzed inactivation of Snf1, the most probable involves modulation of Snf1 by controlling its sub-cellular localization and thus its exposure to Reg1-Glc7. Strains deleted for any single β subunit exhibit no traceable phenotype, but a triple null mutant, *sip1Δ gal83Δ sip2Δ*, is unable to grow on glycerol-ethanol and raffinose-Antimycin A medias and show slower growth than wild-type strains on rich glucose and galactose medias [242]. These phenotypes are indistinguishable from those exhibited by *snf1Δ* strains [231]. Consistent with the genetic data, each of the β subunits interact with both α and γ subunits of the Snf1 kinase complex, suggesting that the β subunits are important for formation of the Snf1 hetero-trimer [284,285,242]. These data suggest that the β subunits may be redundant in function and that the sole purpose of the β subunit is to serve as a molecular scaffold for hetero-trimer formation. However, genetic analysis of cells harboring various combinations of β subunit double mutations revealed that certain Snf negative phenotypes could be separated genetically. For example, while the *sip1Δ sip2Δ* and *sip1Δ gal83Δ* strains exhibit normal wild-type growth on various media, a *sip2Δgal83Δ* strain grew normally on raffinose-Antimycin A media but grew slowly on glycerol-ethanol media [242]. Additionally, Snf1 interaction and phosphorylation of the Sip4 transcription factor, whose function is important for glycerol-ethanol based growth, is exclusively mediated by Gal83 [244].

Utilizing GFP-fusion constructs of each of the β subunits Vincent et.al determined the intracellular location of each of these subunits, that nuclear localization of Snf1 was dependent on Gal83, and that Gal83 nuclear localization was controlled in a glucose dependent manner independent of Reg1-Glc7 and Hxk2 function [245]. In response to glucose availability and glucose phosphorylation by any one of the three hexose kinases, all β subunits are found predominately in the cytoplasm. However, in the absence of glucose, on glycerol-ethanol media, the Sip1 subunit localizes predominately to the vacuole, the Sip2 subunit localizes predominately to the cytoplasm, and the Gal83 subunit is found predominately nuclear [245]. The fact that the Gal83 isoform is the most highly expressed of all Snf1 β subunits and the fact that Gal83 directs nuclear localization of Snf1 in response to glucose exhaustion [245] together suggest that the affects of Snf1 activity on transcriptional processes are primarily carried out by the Gal83-Snf1-Snf4 hetero-trimer. Interestingly, while Glc7 is found in various sub-cellular compartments including the nucleus and nucleolus [286], Reg1 is exclusively found in the cytoplasm [276], limiting Glc7 phosphatase activity towards Snf1 to the cytoplasmic fraction of Snf1. Thus, the glucose dependent modulation of Gal83-Snf1 nuclear-cytoplasmic distribution may serve as another regulatory mechanism to control Snf1 kinase activity towards intracellular substrates.

## 2.7. Downstream Transcription Factors Directly Regulated by the Hxk2/Reg1-Glc7/Snf1 Glucose Signaling Pathway

### 2.7.1. Mig1

The *MIG1* gene was first isolated as a high copy suppressor of *GAL1* (glucose repressed gene encoding galactokinase catalyzing the first step in galactose catabolism) over-expression and was revealed to encode a C2H2 zinc finger type transcriptional repressor which binds to GC boxes (GC rich DNA sequences) present in the promoter regions of glucose repressed transcripts [287]. Since that time the Mig1 repressor has been discovered to repress a number of genes subject to glucose repression, including *GAL* [288-290] , *MAL* [291-293], hexose

transporter [167,160,176], *HXK1* [294], respiratory [295], gluconeogenic [296-300], and glyoxylate cycle [301,302] genes [303]. Interestingly, many of the genes directly repressed by Mig1 are glucose signaling proteins or transcription factors which induce expression of glucose repressed genes. The gluconeogenic transcription factor, Cat8 [300,304], the respiratory transcription factor, Hap4 [305,295,306,307], and the Snf3/Rgt2 pathway proteins, Snf3 and Mth1 [308], are all repressed at the transcriptional level by Mig1 in the presence of glucose. Thus, the Mig1 repressor plays a major role in glucose repression by directly repressing metabolic and regulatory genes necessary for growth on alternative carbon sources.

The regulatory mechanism acting to control Mig1 dependent repression has been partially revealed. In the presence of glucose, the Mig1 protein is found predominately in the nucleus and upon glucose depletion Mig1 translocates rapidly (~2 to 3 minutes) to the cytoplasm [309] which correlates with a rapid release of glucose repression of Mig1 transcriptional targets. Removal of Mig1 from the nucleus in response to glucose depletion requires Mig1 phosphorylation and the nuclear exportin, Msn5 [310,311]. Re-establishment of nuclear localized Mig1 in response to glucose repletion requires Mig1 de-phosphorylation [309]. It was subsequently revealed that Mig1 phosphorylation and nuclear localization is increased in the presence of glucose under conditions which lead to glucose insensitive activation of Snf1 kinase activity, including in *reg1Δ* and *hxk2Δ* cells [202]. Additionally, deletion of *MIG1* in *snf1Δ* cells relieves gene de-repression defects of *snf1Δ* cells and thus, *MIG1* deletion is epistatic to *SNF1* deletion [312]. These observations led to the discovery that Snf1 directly phosphorylates and thus inactivates Mig1 repression in response to glucose depletion [313,203,314]. Thus, active Snf1 kinase activity has been found to directly modulate the transcriptional repressor Mig1 through phosphorylation and Mig1 phosphorylation is a key regulatory event responsible for relieving glucose repression of a number of glucose repressed genes. Though Snf1 dependent modulation of Mig1 repressor activity seems to be the primary mechanism

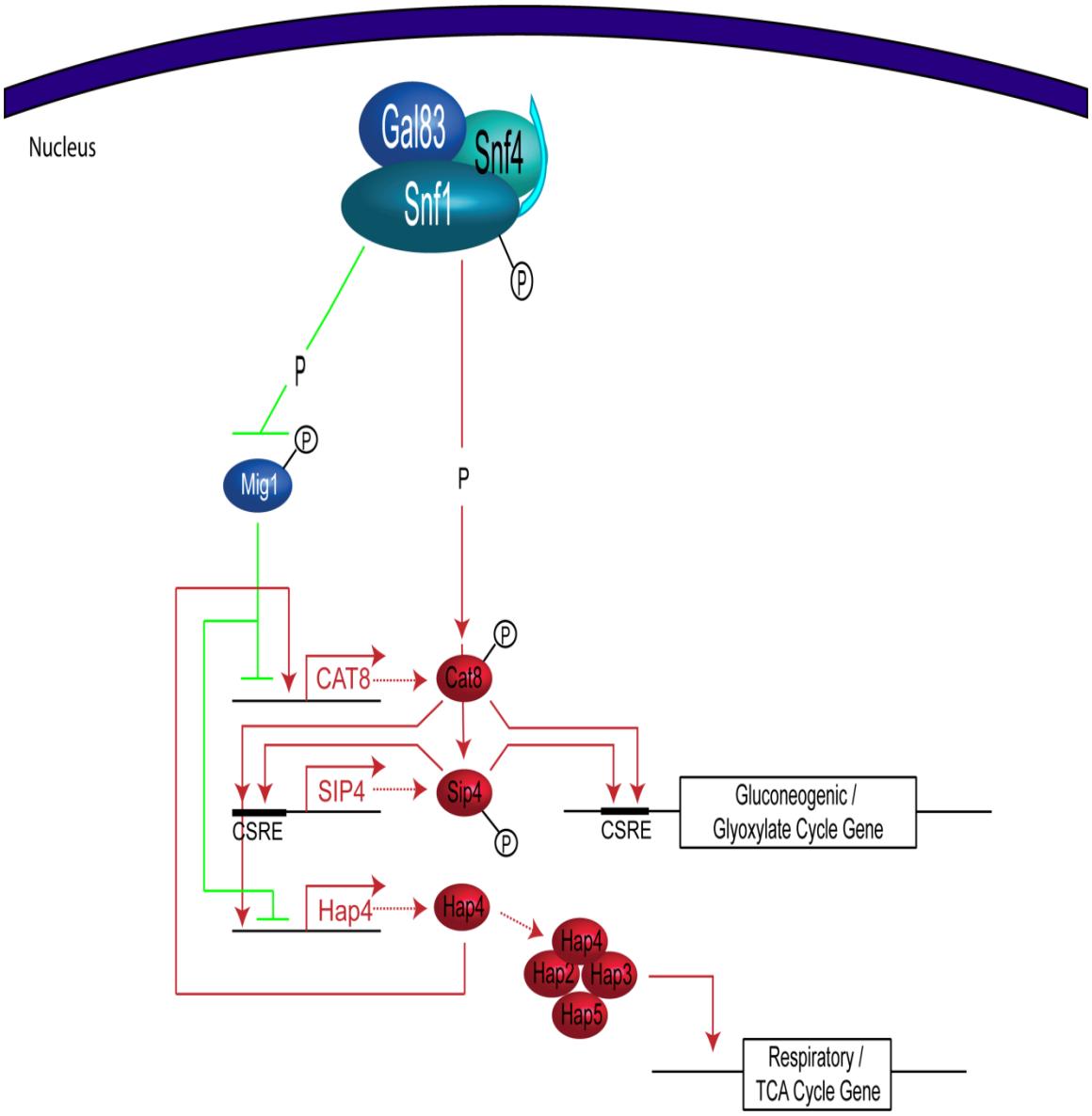


**Figure 2.5. Snf1/Mig1/Cat8/Sip4 Dependent Control of Respiratory, Gluconeogenic, and Glyoxylate Cycle Genes in Response to Glucose Exhaustion.** In the absence of fermentable sugars the Gal83/Snf4/Snf1 kinase complex traverses to the nucleus and catalyzes the phosphorylation of three transcription factors known as Mig1, Cat8, and Sip4 that together promote transcriptional activation of genes needed for growth on respiratory carbon sources. Phosphorylation of Mig1 by Snf1 leads to deactivation of its transcriptional repressor activity which relieves Mig1 dependent repression of *CAT8* and *HAP4*. *HAP4* de-repression leads to transcription and production of Hap4, which is a transcription factor that activates transcription of respiratory and TCA cycle genes. Additionally, Hap4 activates transcription of *CAT8* and transcriptional activation of *CAT8* by Hap4 leads to Cat8 synthesis. Cat8 dependent transcriptional activation of gluconeogenic and glyoxylate cycle genes is then activated through phosphorylation of Cat8 by the Snf1 kinase. Phosphorylated Cat8 also activates *SIP4* transcription leading to synthesis of Sip4. Activation of transcription by Sip4 is also dependent on Sip4 phosphorylation by the Snf1 kinase and active Sip4 promotes further activation of gluconeogenic and glyoxylate cycle genes.

governing Mig1 dependent repression in response to glucose depletion, other regulatory events have been shown to regulate Mig1 repressor function. First, Hxk2 directly interacts with Mig1 and this interaction is required for Hxk2 sequestration in the nucleus [222]. Additionally, The Hxk2-Mig1 complex has been demonstrated to form a repressor complex on the *SUC2* promoter [222]. It has been postulated that Hxk2 may inhibit Snf1 phosphorylation and nuclear export of Mig1 on high glucose (Figure 2.3) [315].

### 2.7.2. Cat8 and Sip4

Genes encoding enzymes of the glyoxylate cycle and gluconeogenesis are among the most sensitive to glucose repression as their gene expression is only de-repressed and induced when glucose has been completely exhausted [171,135]. The glucose sensitivity of gluconeogenic and glyoxylate cycle gene expression is conferred through the Hxk2/Reg1-Glc7/Snf1 glucose signaling pathway. Snf1 kinase is responsible for modulating both de-repression and induction of gluconeogenic and glyoxylate cycle genes by inhibiting their glucose induced repression [300,299,298,297,296,304] and by activating the transcriptional activity of the transcriptional activators, Cat8 and Sip4 [316-318]. In the presence of glucose, Mig1, and most likely other glucose controlled transcriptional repressors [297,319], bind to and repress *CAT8* transcription [316]. As indicated above, exhaustion of glucose leads to Snf1 activation and nuclear localization which subsequently leads to inactivation of Mig1 repression by Snf1 dependent phosphorylation. Snf1 dependent inactivation of Mig1 as well as other glucose regulated repressors leads to de-repression of *CAT8* gene expression which allows Hap2/3/4/5 (respiratory transcription factor complex) to activate *CAT8* gene expression [316]. Activation of Cat8 dependent transcription requires Cat8 to be phosphorylated and phosphorylation of Cat8 is also dependent on Snf1 kinase activity [316,320]. Thus, Snf1 modulates Cat8 dependent transcription by controlling *CAT8* gene expression and Cat8 transcriptional activity. Transcriptionally active Cat8 binds to an upstream activation sequence, known as the carbon source response element (CSRE with the consensus sequence

YCCRTTNRNCCG), present in gluconeogenic and glyoxylate cycle genes [321]. Additionally, the CSRE element is present in *SIP4* and *SIP4* expression is also Cat8 dependent [318]. Like Cat8, Sip4 transcriptional activity is activated through phosphorylation by the Snf1 kinase and Sip4 dependent gene expression is also facilitated through Sip4 binding to CSRE sequences [318]. Together, Cat8 and Sip4 are primarily responsible for the induction of gluconeogenic and glyoxylate cycle genes possessing CSRE sequences in their promoters, including *FBP1* [322], *ICL1* [321], *PCK1* [323], *MLS1* [323], *MDH2* [324], *ACS1* [325], *SFC1* [326], *IDP2* [327] and the respiratory transcription factor, *HAP4* [328]. Thus, the exquisite sensitivity of gluconeogenic and glyoxylate cycle genes to glucose repression is in part conferred by the extensive role of the Snf1 kinase in modulating their expression at multiple stages. Through modulation of Cat8 and Sip4 transcriptional activity, the Hxk2/Reg1-Glc7/Snf1 signaling pathway regulates the transcriptional re-programming of carbon metabolism in response to glucose exhaustion.

# CHAPTER 3: MATERIALS AND METHODS

## 3.1. Global Proteomic Analysis

### 3.1.1. Strain Construction

Two strains were utilized exclusively for both global proteomic as well as microarray experiments. Strain DBY2059 (MATα *leu2-3, 112)* served as the comparative wild-type strain in these experiments and is derived directly from S288C. Strain JH001 (MATα *grr1Δ*::NAT), also derived from S288C, was constructed by adaptamer mediated gene disruption as previously described [329]. Briefly, forward (5'-CGTGAAATCTTGAAATTTCTCATTGATTTCGGCACAATAAT TATCATTGGTAGTGAGGCTAAACAGTTTTGCGGTTTCCTTTATACTAAGAAG GTCTATACAGCTGAAGCTTCGTAC-3') and reverse (5'-TCAAAGTGAATGCAT TATGTATTTATATGTAAATAAGTAGAAAAGTGGGATTTTGAAAATAAAGGTGT AGTAGGACAGTAAGTATTCAATGAAATACAAGCATAGGCCACTAGTGGATCT G-3') adaptamers of ~120bp in length were designed and purchased from MWG Biotech™ with ~20bp of DNA sequence at the 3' ends of each oligonucleotide complementary to flanking sequences of the gene conferring dominant resistance to the aminoglycoside, nourseothrycin (*NATMX*). The remaining 100bp of 5' sequence on the forward and reverse oligonucleotides contains DNA sequence complementary to the 5' and 3' non-coding regions of the *GRR1* locus, respectively. Utilizing these adaptamers, a *GRR1* specific disruption cassette was PCR-amplified from the plasmid pAG25, harboring the *NATMX* gene. This cassette was then utilized to transform the S288c prototrophic strain, BL2, utilizing the lithium acetate method [330]. Following transformation, strains harboring the *NATMX* gene were selected by incubating transformed cells on YPD supplemented with 90ug/ml nourseothrycin at 30°C for 3 to 4 days. Clones harboring a complete disruption of the *GRR1* locus with this cassette were confirmed by PCR utilizing primer sets which flanked both the 5' and 3' ends of the cassette and the endogenous *GRR1* gene.

| Strain | Genotype |
|---|---|
| DBY2059 | *Mat α leu2-3, 112* |
| JH001 | *Mat α grr1Δ*::NAT |
| CenPK113-7D | *Mat A MAL2-8c, SUC2, RHO+* |
| JH015 | *Mat A MAL2-8c, SUC2, RHO+, grr1Δ::NAT* |
| BY4741 | *MATA his3Δ1 leu2Δ0 met15Δ0 ura3Δ0* |
| BY4741 (XXX:TAP) | *MATA his3Δ1 leu2Δ0 met15Δ0 ura3Δ0 XXX::TAP::HIS3* |
| MT2112 | *mfα1Δ::MFα1pr-LEU2 can1Δ::MFA1pr-HIS3, his3Δ1, leu2Δ0, ura3Δ0, met15Δ0, lys2Δ0* |
| JH002 | *mfα1Δ::MFα1pr-LEU2 can1Δ::MFA1pr-HIS3, his3Δ1, leu2Δ0, ura3Δ0, grr1Δ::URA3, met15Δ0, lys2Δ0* |
| JH006 | *mfα1Δ::MFα1pr-LEU2 his3Δ1 leu2Δ0 met15Δ0 ura3Δ0 grr1Δ::URA3 CAT8::TAP::HIS3* |
| JH007 | *mfα1Δ::MFα1pr-LEU2 his3Δ1 leu2Δ0 met15Δ0 ura3Δ0 grr1Δ::URA3 GLC7::TAP::HIS3* |
| JH008 | *mfα1Δ::MFα1pr-LEU2 his3Δ1 leu2Δ0 met15Δ0 ura3Δ0 grr1Δ::URA3 INO2::TAP::HIS3* |
| JH009 | *mfα1Δ::MFα1pr-LEU2 his3Δ1 leu2Δ0 met15Δ0 ura3Δ0 grr1Δ::URA3 INO4::TAP::HIS3* |
| JH010 | *mfα1Δ::MFα1pr-LEU2 his3Δ1 leu2Δ0 met15Δ0 ura3Δ0 grr1Δ::URA3 SOL1::TAP::HIS3* |

**Table 3.1. *S. cerevisiae* Strains Utilized in this Volume**

### 3.1.2. Growth Conditions and Sample Preparation

Mass labeling for MS analysis was performed using a customized SILAC approach [331]. *S. cerevisiae* strain DBY2059 (MAT α *leu2-3*) was cultured overnight to stationary phase in two replicate 10ml batches of modified SD media consisting of 2% glucose, 0.17% yeast nitrogen base minus amino acids and ammonium sulfate, 0.25% glutamine, 0.025% magnesium sulfate, and 0.05mg/ml $C_6^{13}$ leucine (Cambridge Isotope Laboratories, Inc., Andover, MA, USA). Concurrently, strain JH001 (MAT α, *grr1Δ::NAT*MX) was also cultured overnight to stationary phase in two replicate 10ml batches of the same media supplemented with $C_6^{12}$ leucine. Each 10ml culture was then used to inoculate a 500ml culture of the same media and cells were grown for nine population doublings to mid-log phase (~$5x10^6$cells/ml). Cell density was determined by cell counting using a hemacytometer (Reichert, Buffalo, NY, USA.). Cells were harvested by centrifugation in a Beckman JA-14 rotor at 4000Xg for 10 minutes, washed three times in ice cold water, and immediately re-suspended in 5ml of extraction buffer (8M Urea, .1M ammonium bicarbonate). Cells were then immediately flash frozen in liquid nitrogen and stored at -80°C overnight.

Protein extract was prepared the following day by manual bead beating using 300μm acid washed glass beads (Sigma, St. Louis, MO.). Specifically, samples were subjected to 10 cycles consisting of 30 seconds on ice and 30 seconds of vortexing in the presence of glass beads. Glass beads and cellular debris were then spun down at 2000Xg and the supernatant was placed in 15ml conical tubes. Protein concentrations were determined using the Bradford protein assay and protein samples were mixed in a 1:1 ratio (DBY2059 $C_6^{13}$ leucine: JH001 $C_6^{12}$ leucine) producing two replicate protein mixes from four independently grown batch cultures.

### 3.1.3. Reduction, Alkylation, and Trypsinization

Each protein mixture was diluted with 100mM ammonium bicarbonate to a final urea concentration of 4M. Protein disulfide bond reduction was carried out by adding a 40 fold molar excess of dithiothreitol (DTT) to each protein mixture

followed by a three hour incubation at 36°C. Reduced protein mixtures were then alkylated using a 1:80 molar ratio of protein to iodoacetamide (IAM) followed by incubation on ice in complete darkness for 2 hours. The reduced and alkylated protein mixture was then diluted to 2M urea using an equal volume of 100mM ammonium bicarbonate and subjected to trypsin digestion using 2% (weight/weight) of TPCK-treated trypsin. Digestion was carried out at 37°C for twenty four hours. Peptide samples were then dried down in a speed vac and resuspended in a buffer consisting of 5% acetonitrile, 95% EMD water, 0.025% formic acid, and .0025% HFBA.

### 3.1.4. Peptide Separation and Mass Spectrometry

The two replicate peptide mixtures were analyzed 3 times each through an automated de-salt/2DLC/MS system. Peptide de-salting and separation were performed in tandem using the Paradigm MG4 HPLC System (Michrom Biosciences, Inc.). Initially, approximately 150µg of the tryptic peptide mixture was loaded directly onto a C-18 microtrap (Michrom Biosciences, Inc.) and desalted by flushing the trap with 20 column volumes of mobile phase A (2% acetonitrile, 98% water, 0.025% formic acid) at a flow rate of 50µl/min. Peptides were then eluted onto an SCX microtrap (Michrom Biosciences, Inc.) using 20 volumes of mobile phase B (98% acetonitrile, 2% water, 0.025% formic acid, 0.001% HFBA). Peptides were then eluted from the SCX microtrap in a stepwise fashion using increasing concentrations of ammonium formate. Ten steps of 0, 4, 8, 12, 15, 18, 21, 25, 50, and 100mM ammonium formate were used in our analysis followed by two identical steps of 1M ammonium formate. Each population of peptides eluted off the SCX micro-trap onto a C8 nano-trap (Michrom Biosciences, Inc.) coupled directly to a hand packed C18 column with a hand pulled tip. A homemade high pressure bomb was used to pack 15cm of 5µm-100Å Magic C18 resin (Michrom Biosciences, Inc.). Peptides were then eluted off this column at 500ηl/min using an acetonitrile gradient from 5-50% and analyzed by an LTQ Mass Spectrometer (Thermo Electron Corporation) on the fly.

The LTQ-MS was set for data dependent MS/MS acquisition with a total ion count threshold of 1000. Dynamic exclusion was used to only collect two MS/MS spectra on a single parent ion every 45 seconds. Two types of data collection were performed in this analysis termed gas phase fractionation and full scan analysis. Typically, the LTQ-MS is set to scan across an m/z range from 500-2000 throughout the course of the analysis. This type of analysis was done in replicate for both replicate peptide mixtures culminating in four, 12 step full scan analyses. Each of the peptide mixtures was also subjected to a single gas phase fractionation analysis. This analysis is essentially equivalent to three full scan analyses but the mass spectrometer is set to scan 1/3 of the m/z scan range. This allows for greater m/z resolution and increased peptide detection sensitivity due to the fact that MS/MS spectra are only being collected for a smaller fraction of the peptide population eluting from the column. However, this process is time consuming given that three separate analyses must be performed to acquire data across the whole scan range and thus we only conducted a single gas phase analysis for each peptide mixture. The scan ranges for gas phase fractionation were 500-1000m/z, 900-1500m/z, and 1400-2000m/z. In all, each of the two replicate peptide mixes were loaded and analyzed five times through the 2D-LC-MS system for a total of ten different runs. A schematic summarizing our analysis is shown in Figure 3.1.

### 3.1.5. Data Analysis and Validation

Peptide assignments for experimental MS/MS spectra were made using the SEQUEST™ program (Thermo Electron Corporation). Peptide assignments were then analyzed for validity using a suite of software available from the Institute for Systems Biology termed the Trans-Proteomic Pipeline. This analysis toolkit provides computational tools that validate peptide assignments (PeptideProphet™) [332], protein assignments (ProteinProphet) [333], and quantify relative peptide and protein abundance ratios (ASAPRatio) [334]. All SEQUEST™ .dta and .out files pertaining to an individual analysis were validated together through the ISB pipeline. Thus, gas phase separations derived from the same

analysis were analyzed concurrently to provide the most accurate protein probabilities and ASAP ratios. Following data processing through the ISB pipeline, a combined unified Protein Probability across all data sets was calculated using the following criteria. If a protein is identified by k experiments, labeled $r_1$, $r_2$,…$r_k$, then the summarized probability is calculated as:

$$P_{id} = 1 - \prod_{i=1}^{K}(1 - P_{ri}) \quad [1]$$

Where $P_{ri}$ is the probability measure from experiment $r_i$. Final relative abundance ratios were calculated by taking the average abundance ratio (ASAPRatio) over all data sets for each protein.

### 3.2. Microarray Analysis

3.2.1. Growth conditions

A *grr1Δ* strain (JH001) and a wild-type strain (DBY2059) were inoculated from stationary phase cultures into a synthetic defined minimal medium containing 2% dextrose, 0.17% yeast nitrogen base minus amino acids and ammonium sulfate, 0.25% L-glutamine, 0.025% magnesium sulfate and 25.2mg/L L-leucine. Four separate cultures of each strain were grown at 30°C, allowing between three and four doublings and cells were collected at approximately 8 x $10^6$cells/ml. Cells were centrifuged and immediately frozen in liquid nitrogen.

3.2.2. RNA extraction and cRNA construction

Cells were centrifuged and immediately frozen in liquid nitrogen. Total RNA was extracted using a hot acid phenol-chloroform protocol as previously described [335]. RNA quality was verified with $OD_{260/280}$ readings and a 1.5% agarose gel. The following portion of this microarray study was carried out using the facilities of the Center for Medical Genomics at Indiana University School of

Medicine. The Center for Medical Genomics is supported in part by the Indiana Genomics Initiative at Indiana University (INGEN®), which is supported in part by the Lilly Endowment, Inc. Briefly, cDNA was synthesized from the original RNA template by single cycle labeling using a T7 promoter-dT24 oligonucleotide as primer with the Invitrogen Life Technologies SuperScript Choice system (Invitrogen, California, USA) per the manufacturer's instructions. Following second strand cDNA synthesis and incubation with T4 DNA polymerase, the products were purified using an Affymetrix Cleanup Module (Affymetrix, California, USA) per the manufacturer's protocol. The cDNA was converted to cRNA using the Affymetrix IVT kit, again following the manufacturer's instructions. The cRNA was purified with Qiagen RNAeasy columns (Qiagen, California, USA), quantitated and then fragmented by incubating at high temperature with magnesium.

### 3.2.3. cRNA Hybridization and Data Analysis

Fifteen µg of biotinylated cRNA was added to a total hybridization cocktail of 300µl, and 200µl was hybridized to an Affymetrix Yeast 2.0 GeneChip after adding control oligonucleotides. The cRNA was hybridized at 45°C for 17 hours with constant rotation. The hybridization mixture was then removed and the Affymetrix Yeast 2.0 GeneChip were washed, stained with phycoerythrin-labeled streptavidin, washed, incubated with biotinylated anti-streptavidin, and then re-stained with phycoerythrin-labeled streptavidin for signal amplification. Balanced groups of samples were handled in parallel to reduce non-random error. The arrays were then scanned using the dedicated scanner, controlled by Affymetrix GCOS software. The Affymetrix Microarray Suite version 5 (MAS5) algorithms was used to analyze the hybridization intensity data from each array. The average intensity on each array was normalized by globally scaling to a target intensity of 1000. A student's t-test of the log base 2 transformed data was used to establish p-values.

### 3.3. Hxt3 and Hxt7 Western Blots

3.3.1. Strains, Growth Conditions, and Protein Extraction

Strains DBY2059 and JH001 (See Table 3.1 for genotype) were grown in 150ml of the same synthetic media described in Section 3.1.2 to a cell density of 1 x $10^7$cells/ml, allowing for four population doublings. Cells were then spun down at 3,000 X g and immediately flash frozen utilizing liquid nitrogen. The next day cells were thawed spun down and re-suspended in 1ml of lysis buffer (50mM Tris-HCL, pH 7.4, 250mM NaCl, 50 mM NaF, 5mM EDTA, .1% NP-40, 2mM EGTA, and proteasome inhibitors (Roche Diagnostics™). Protein extract was prepared the following day by manual bead beating using 300µm acid washed glass beads (Sigma™, St. Louis, MO.). Specifically, samples were subjected to 10 cycles consisting of 30 seconds on ice and 30 seconds of vortexing in the presence of glass beads. Glass beads and cellular debris were then spun down at 2000Xg and the supernatant was placed in 1ml Eppendorf tubes. Protein concentrations were determined using the Bradford protein assay.

3.3.2. Western Blot Analysis and Antibodies

Immediately following protein extraction, three 40µl (1µg/µl) aliquots of both DBY2059 and JH001 protein extract were mixed with 10µl of 5x Laemmli loading buffer, heated at 80°C for 5 minutes, and 20ul of each sample was loaded in replicate onto two hand cast 15% SDS-PAGE gels. Each gel was run at 60V in a BIO RAD™ Mini-Protean® II Cell until the resolving gel was reached at which time the voltage was increased to 100V. Each gel was cut in half and one side was stained with Coomassie to serve as a loading control while the other was wet transferred (25mM Tris-HCl, 192mM glycine, 15% methanol) onto a PVDF membrane for two hours at 28 Volts. The PVDF membrane was cut in half and each membrane was washed in three times for five minutes in 1 x KPBS-T. Membranes were blocked for one hour at room temperature in 5% dry milk dissolved in 1 X KPBS-T. One membrane was incubated for two hours at room temperature with primary antibody from the day 35 bleed of rabbit PA0661 (Hxt3; 1:2000 in 5% dry milk in 1X KPBST). The other membrane was incubated

as above with primary antibody from the day 35 bleed of rabbit PA0651 (Hxt7; 1:1000) (Table 3.2). The membranes were washed as before and then incubated at room temperature for one hour with horseradish peroxidase-conjugated goat anti-rabbit secondary antibody (1:10,000) (Santa Cruz Biotechnology, Santa Cruz, CA). Blots were then washed three times for 5 minutes with 1 X KPBST and then incubated for one minute at room temperature with ECL™ (Amersham™ Biosciences, Pittsburgh, PA). Exposure shown for Hxt3 is two minutes while the Hxt7 exposure is 30 seconds.

Polyclonal antibodies recognizing the Hxt3 protein and the Hxt7 protein were raised utilizing synthesized peptide antigens ($_{35}$KGVQDDFQAEADQVL$_{49}$ for Hxt3 and $_{33}$KAERDEIKAYGEGEEHE$_{49}$ for Hxt7) unique to the Hxt3 and Hxt7 protein sequences. Antibody preparation was conducted by Open Biosystems™ by injecting each peptide antigen into two independent rabbit hosts each and raw serum was drawn at day 35, 58, and upon termination. Crude antibody ELISA titers were measured pre-bleed and at the day 35 and 58 bleeds. These titers are shown below (Table 3.2). These titers are the reciprocal of the serum dilution at which the absorbance drops below 0.2 at OD 405. These ELISAs are conducted utilizing the peptide antigen coated directly onto the plate and antibodies are detected utilizing indirect enzyme immune assay utilizing anti-IgG-HRP and the ABTS substrate.

### 3.4. α-TAP Western Blots

#### 3.4.1. Strain Construction

TAP tagged constructs of Cat8, Ino2, Ino4, Glc7, and Sol1 were introduced into the *grr1Δ* strain using a mating and selection method derived from the synthetic genetic array methodology [336]. First, *GRR1* was knocked out in strain MT2112 (See Table 3.1) obtained from Dr. Mike Tyers using adaptamer mediated gene disruption as previously described [329]. Briefly, forward (5'-GGGA TTTTGAAAATAAAGGTGTAGTAGGACAGTAAGTATTCAATGAAATACAACACA CCGCAGGGTAATAACTG-3') and reverse (5'GGTAGTGAGGCTAAACAGTTTT GCGGTTTCCTTTATACTAAGAAGGTCTATAGATTCGGTAATCTCCGAACA-3')

| Animal/Antigen | Pre-Bleed | Day35 | Day58 |
|---|---|---|---|
| **PA0651/Hxt7** | 400 | >204,800 | >204,800 |
| **PA0652/Hxt7** | <50 | >204,800 | >204,800 |
| **PA0661/Hxt3** | <50 | >204,800 | >204,800 |
| **PA0662/Hxt3** | <50 | >204,800 | >204,800 |

**Table 3.2. Hxt3 and Hxt7 Antibody Titers**

adaptamers of 74 and 72 bp in length, respectively, were designed and purchased from MWG Biotech™ with ~20bp of DNA sequence at the 3' ends of each oligonucleotide complementary to flanking sequences of the *URA3* gene of plasmid PRS306. The remaining ~50 bp of 5' sequence on the forward and reverse oligonucleotides contains DNA sequence complementary to the 5' and 3' non-coding regions of the GRR1 locus, respectively. PCR amplification of the *URA3* containing disruption cassette, targeted to the *GRR1* locus was then performed utilizing plasmid PRS306 as the template. The disruption cassette was then transformed into strain MT2112 utilizing the lithium acetate method [330]. Strains harboring the disruption cassette were isolated by plating transformed cells on SD-URA for six days. Individual colonies were isolated a validated for *GRR1* disruption by phenotypic verification of the elongated bud morphology and by PCR confirmation. One strain was subsequently utilized in crosses with the TAP-tag library strains constructed by [337] and available through Open Biosystems™.

Before any crosses are made each TAP tagged strain was placed on YPD by taking 5ul of the culture from the appropriate plate coordinate and placing within a single square of the grid on a YPD plate. Strains were allowed to grow overnight at 30°C and were then replica plate onto each of the following medias.

SD (-ura), SD (-his), SD (-met), SD (-leu), YPD (+canavanine), SD (-lys) in order to verify auxotrophies and markers. The parental phenotypes for every strain reported in this volume exactly matched the indicated markers.

A lawn of JH020 cells was made on YPD media and allowed to grow three days until it was confluent. Once the JH020 lawn was confluent, the BY4741 (TAP tagged strains) strains from the SD (-his) selection plates were stamped onto a velvet. These plates contained each TAP tagged strain to be crossed in patch format arranged in a grid. The lawn of JH020 was then stamped onto the same velvet as the BY4741 stamp and this velvet was then replica plated onto YPD and allowed to grow overnight at 30°C. The next day, each strain was picked from its corresponding grid location and then struck onto its own individual SD –ura –his –lys plate for single colonies. This will allowed for selection of diploid colonies. Each strain was incubated at 30°C for two days. After two days, a single colony was picked from each diploid selection plate, patched on sporulation media (10g/L potassium acetate, 1g/L Bacto yeast extract, 0.5g/L glucose, 20g/L Bacto-agar, 1% adenine, 1% asparagine) in the same grid coordinate as before, and incubated at room temperature one week.

The following week, MAT α spore progeny were selected by streaking each sporulated diploid patch onto its own SD-leu-ura-his-lys plate. This plate was incubated at 30°C for three days. Each spore plate was then replica plated onto SD +canavanine (50µg/ml), -his, -arg and incubated for two days at 30°C. This selection revealed clones that were not resistant to canavanine which indicates that the histidine prototrophy is not conferred by the presence of the mating type selectable marker but the *ORF::TAP-HIS* construct. Canavanine sensitive colonies from each strain plate were individually and manually analyzed microscopically for the presence of the multiple elongated bud morphology of *grr1Δ* strains. Three clones for each *grr1Δ* Orf::TAP strain with the aforementioned characteristics were isolated and placed in liquid SD –leu, -his, -lys, -ura overnight at 30°C. The next day, 200ul of this culture was spread on YPD and incubated at 30°C overnight. The next day the cells were harvested and froze away at -80°C in 15% glycerol.

### 3.4.2. Growth Conditions and Sample Preparation

Protein extracts for western analysis of all *ORF::TAP grr1Δ* strains and the isogenic *ORF::TAP* containing wild-type strains were prepared from strains cultured as follows. Each, of the three clones for each *ORF::TAP grr1Δ* and the parental clone utilized to construct the *ORF::TAP grr1Δ* strain was struck from glycerol stocks onto YPD and incubated for three days at 30°C. A single colony was then picked and struck onto SD –leu, -ura, -his, -lys selection plates and incubated for two days at 30°C to verify auxotrophies and markers. After two days, a single colony from the selection plate was inoculated into 10ml of YPD + 0.5% glutamine and incubated at 30°C. Once the 10ml cultures reached stationary phase (~2 x $10^8$cells/ml), these cultures were utilized to inoculate a 250ml culture of YPD + 0.5% glutamine to 2 x $10^6$cells/ml. This culture was incubated at 30°C on an Orbital shaker set to 200 rpm allowing for three population doublings (~1.6 x $10^7$cells/ml or ~8hrs). Once the cultures reached 1.6 x $10^7$cells/ml, they were immediately spun down at 3,000xg, immediately flash frozen utilizing liquid nitrogen, and stored at -80°C overnight. The following day, protein extracts were prepared utilizing the protein extraction method of [338].

### 3.4.3. Western Blot Analysis and Antibodies

The procedures for western analysis of each TAP-tagged containing strain differed slightly because of the different sizes and pKas inherent to each of the proteins under analysis. For extracts prepared from Glc7::TAP, Ino2::TAP, Ino4::TAP, and Sol1::TAP containing strains, extracts were loaded onto a hand cast, large format, 10% SDS-Page gel model V16-2 (Bethesda Research Laboratories Life Technologies™). SDS-Page gels were then transferred onto PVDF (polyvinylidene fluoride; Immobilon-P from Millipore Corporation™) membrane at 12 volts in CAPS pH 11 buffer (2.2g/L CAPS, 10% methanol) for 60 minutes utilizing a semi-dry transfer apparatus (Fisher Biotech™). For extracts

prepared from Cat8::TAP containing strains, all conditions were identical to those described above with a few exceptions. First, 5% SDS-PAGE gels were utilized since the Cat8::TAP protein fusion has a predicted size of ~180,000 Da. Second, wet transfers of Cat8::TAP protein extracts were conducted at 25 volts overnight in a 4°C old room utilizing CAPS pH11 transfer buffer. All membranes were blotted utilizing a 1:2,000 dilution of rabbit polyclonal α-TAP primary antibody (Open Biosystems™) and a 1:5,000 dilution of polyclonal HRP-conjugated α-Rabbit secondary antibody (Santa Cruz Biotechnology, Inc.).

### 3.5. Glc7 Western Blots using α-Glc7 Antibodies

#### 3.5.1. Growth Conditions and Sample Preparation

Antibodies raised against endogenous Glc7 protein were obtained from Dr. John F. Cannon and western blots using these antibodies are pictured in Figure 7.6. For these blots, strains DBY2059 and JH001 were diluted to 2 x $10^6$cells/ml in 175mls of the synthetic media described in Section 3.1.2. Cells were incubated at 32°C on an Orbital shaker at 175 rpm for three population doublings until cells reached an approximate cell density of 2 x $10^7$cells/ml. Cells were spun down at 3000Xg, washed twice with ice cold water, and immediately flash frozen in liquid nitrogen. The next day cells were thawed and re-suspended in 300ul of RIPA lysis buffer (50mM Tris-HCL, pH 8, 0.1% SDS, 0.5% deoxycholate, 150mM NaCl, 1% Triton X100, 5mM EDTA, 50mM NaF, 10mM NEM) and cells were disrupted utilizing the bead beating method described in Section 3.3.1. NEM was chelated using 30µl of 100mM cysteine.

#### 3.5.2. Western Blot Analysis and Antibodies

Immediately preceding protein extraction, protein extracts were diluted to equal concentrations of 2µg/µl using RIPA buffer minus NEM and 64µl of extract from each strain was mixed with 16µl of 5 x Laemmli sample buffer. The samples were heated at 90°C for eight minutes and 40µg of extract from each strain was loaded in replicate onto a hand cast 10% SDS page gel. The gel was run at 65 volts through the stacking gel at which time the voltage was increased to 105 volts. Transfer conditions as well as washing and blocking conditions

were identical to those described in Section 3.3.2. Primary antibody to Glc7 was obtained from Dr. John Cannon and supplied in purified form by Dr. Anna De-Paoli-Roach. The membrane was cut in half after blocking and one half was incubated with a 1:500 dilution of rabbit anti-Glc7 antibody overnight at 4°C. The other membrane was incubated with a 1:20,000 dilution of purified α-Cdc34 which served as the loading control. The remaining procedures were identical to those described in Section 3.3.2. Exposures shown in Figure 7.6 B are seven minutes.

## 3.6. Spot Dilution Assays

### 3.6.1. Glucose + Antimycin A

Glucose concentration spot dilution assays conducted on *grr1Δ* and the representative wild-type strain (DBY2059) were carried out by first streaking for single colonies for both strains on YPD plates. Single colonies were picked for each strain and re-struck on YPD. After two days incubation at 30°C, four colonies were picked for each strain and struck on plates of the synthetic media described in Section 3.1.2 containing .02%, .2%, 1%, 2%, and 7% glucose, respectively. After four days incubation of these plates at 30°C, single colonies were picked from each plate and inoculated in to liquid cultures of the same composition from which they were picked. These liquid cultures were allowed to grow to mid-log phase at which time they were serial diluted in water to attain dilutions of the following cell concentrations (300, 30, 3, .3 cells/µl). 10µm of each dilution for each glucose concentration was then spotted onto plates of the same synthetic media with the same glucose concentration supplemented with 3µg/L of the respiratory inhibitor, Antimycin A (Sigma Aldrich Corporation). Pictures were taken using a Canon EOS digital SLR camera at 24 and 48 hrs post-incubation at 30°C.

### 3.6.2. Ethanol

Ethanol spot dilution assays conducted on strains, DBY2059, CenPK113-7D, JH001, and JH015 were carried out by first streaking for single colonies for

all strains on YPD plates. Single colonies were picked for each strain and re-struck on YPD. After two days incubation at 30°C, single colonies were picked for each strain and re-struck on YPE containing 3% ethanol. After seven days incubation of these plates at 30°C, single colonies were picked from each plate and inoculated in to liquid cultures of synthetic media (See Section 3.1.2) supplemented with 3% ethanol in place of glucose. These liquid cultures were allowed to grow to mid-log phase at which time they were serial diluted in water to attain dilutions of the following cell concentrations (6000, 600, 60, 6cells/ul). 10µm of each dilution for each glucose concentration was then spotted onto plates of synthetic media supplemented with 3% ethanol in place of glucose. Pictures were taken using a Canon EOS digital SLR camera at 72 hours post-incubation at 30°C.

### 3.7. Network Analysis

In order to facilitate physical and genetic network analyses, a database containing physical as well as genetic interaction data for all *Saccharomyces cerevisiae* proteins was constructed by importing the interaction data available through the *Saccharomyces* Genome Database ftp server. (http://downloads.yeastgenome.org/literature_curation/archive/) The following interaction file was utilized for all physical and genetic interaction networks; (interactions.tab.200606.gz). Additionally, transcription factor gene targets were manually imported into our database from the curated transcription factor/target gene repository of YEASTRACT (Yeast Search for Transcriptional Regulators And Consensus Tracking) [339].

Interaction networks were generated utilizing the network analysis tool ProteoLens 1.06 [340] which can be downloaded from the following URL. (http://bio.informatics.iupui.edu/proteolens/index.stm) Utilizing this tool we were able to overlay our proteomic and genomic expression information onto the interaction data from SGD and YEASTRACT in order to reveal nodes “proteins” possessing interactions with multiple proteins or genes observed to change at

either the gene or protein expression level. Relevant interaction networks were then rendered for publication utilizing Adobe Illustrator® CS4.

### 3.8. GO Analysis

GO (Gene Ontology) [341] annotations were obtained from the *Saccharomyces* Genome Database ftp server (http://downloads.yeastgenome.org/literature_curation/archive/orf_geneontology.tab.200606.gz). These annotations were utilized for GO component analysis as well as to direct our manual revised GO annotations for the genes and proteins with significantly altered expression in *grr1Δ* strains. GO enrichment analysis was conducted utilizing GenGO [342] which is openly available for use at the following URL; (http://www.sb.cs.cmu.edu/GenGO/).

### 3.9. Figure and Table Construction

All figures were rendered utilizing Adobe Illustrator® CS4. Scatter plots and bar graphs were generated utilizing the visual analysis and data visualization software, Tableau™.

### 3.10. Relational Database Tables

The sheer volume of data collected between our global genomic and proteomic analyses necessitated the need for a highly organized and relatively robust data storage infrastructure. Additionally, since many data processing steps and network analyses were to be carried out on these data, storage infrastructure had to be malleable allowing multiple queries and cross comparisons between many inter-related data sets. For these reasons, all data was imported into the open source database, MySQL (available for download at http://dev.mysql.com/downloads). A brief description of the data tables and the types of data stored in the "*GRR1 Database"* is provided as well as significant numbers and statistics for hand curated interaction and transcription factor tables.

### 3.10.1. Mass Spectrometry Data Tables

#### *3.10.1.1. Peptide Specific Data Tables*

All data describing each peptide detected and analyzed at any confidence level in our global proteomic analyses is captured in our database within the table "peptide_res". For each peptide instance, all results obtained from SEQUEST™, PeptideProphet™, and ASAPRatio™ are recorded here. Additionally, the analysis (specified as "run_id") as well as the specific MudPIT step and scan numbers that provided the MS/MS files for the peptides identification can be found within this table. The peptide sequence and its corresponding ORF or ORFs (if redundant) can also be found in this table. In all, this table consists of 67,201 records.

The number of peptides detected for a given protein utilizing MudPIT analysis has been shown to positively correlate with the number of protein molecules present within the cell [343,344]. Thus, more highly expressed proteins possess a greater number of positive peptide identifications in these analyses. Instances where a low protein molecule per cell estimate is accompanied by a high number of positive peptide identifications could convey biologically relevant information pertaining to differences between the media and/or strain utilized in our analysis compared to that utilized in the study where the protein molecule per cell estimates were made. Additionally, bias toward identification of labeled (wild-type) and/or un-labeled (*grr1Δ*) proteins could also provide an additional rough indicator of relative protein abundance. Total peptide counts across all analyses for non-redundant peptides with peptide probabilities greater than or equal to .75 for each ORF are provided in table "pepcount_protmolcell". Additionally, the estimated protein molecules per cell as determined by [337] are provided alongside peptide counts for *grr1Δ* and wild-type specific peptides for each ORF. In all, there are 2105 records in this table.

#### *3.10.1.2. Protein Specific Data Tables*

All protein data generated across all six analyses, prior to application of the multiple algorithms to combine these data, can be found in summarized,

filtered, or individual formats within the "*GRR1 Database"*. All protein data generated across all analyses as reported by ProteinProphet™ and ASAPRatio™ for proteins at all confidence levels can be found in the table "protein_total_res". Since data can be generated for a given protein in any one of the six analyses, multiple records for a single ORF may exist and in these instances the origins of the data can be distinguished by their "run_id" and "sample_id". Each record consists of the identified ORF, its protein probability as determined by ProteinProphet™, its percent coverage, its ratio and adjusted ratio mean with calculated standard deviations as determined by ASAPratio™, the number of unique and total number of peptides identified for the protein, the percent share of spectrum identifications for that protein relative to the total number of identifications in the analysis, a brief description of the ORF (gene name etc…), and whether the protein has redundant sequence with any other protein in the database ("alt_orf1", if blank is not redundant). An annotated and filtered version of this table is "protein_total_res_p75pp_filter_anno" and contains the same information as "protein_total_res" but only for those protein identifications with a protein probability greater than .75. This table also contains the "SGD_ID" for the ORF in order to fuse this information with SGD (*Saccharomyces* Genome Database) specific information such as details about the proteins function, half-life, translational frequency, codon bias, codon adaptation index, and gene expression level. This specific information has already been imported into this table to aid in elucidating relationships between protein characteristics and their ability to be detected and quantified by our analysis. Finally, the summarized results provided by "protein_total_res" are also provided in individual, analysis specific, tables to allow for individual evaluation of the results from each analysis. These tables are named "protein_analysis_(1_1-2_3)_results", respectively.

The protein identifications and relative abundances from each analysis for each ORF were combined utilizing the algorithms described in Sections *3.11.4.6 - 3.11.4.8* in order to generate proteomic data of higher confidence. The data from each of these stages is captured in a series of tables starting with

“protein_combined_res_all” which contains the calculated combined probability (Section *3.11.4.6*) of every ORF for which data was collected regardless of protein identification confidence. A wealth of additional data is also provided in this table including all data collected from each individual analysis for a given ORF (in column format rather than rows) as well as the number of times the ORF was identified across the six analyses (“Orf_count_6”). There is data for 3602 ORFs within this table. A filtered version of this table using a combined probability cutoff of .75 is named “protein_combined_res_detected” and contains data for the 1867 identified proteins in our analysis as reported in Section 4.1.3.

The combined analysis protein table named “protein_combined_res_quan-_anno” contains the final combined quantification data for the 1182 proteins quantitated in our analysis including “Gold”, “Silver”, and “Bronze” quantification categories (Section *3.11.4.7* and *3.11.4.8*). This table contains a wealth of data including all ProteinProphet™ and ASAPRatio™ data for every individual analysis for each ORF as well as summarized data from all of the analyses that may be utilized to assess the validity of the final relative abundance measure. For example, the number of total and unique peptides from which the protein was identified and quantified across all analyses is reported as well as the calculated quantification confidence and the z score. Additionally, the inter- and intra-analysis standard deviations are reported here. The inter-analysis standard deviation is calculated by considering each final adjusted ratio mean for a particular ORF for each individual analysis and is an indicator of quantitative reproducibility between replicate analyses. The intra analysis standard deviation is calculated by averaging the measured standard deviations from each analysis and is an indicator of peptide abundance measure variability across the six analyses.

### 3.10.2. Gene Expression Data Tables

We conducted whole genome expression studies comparing *grr1Δ* and wild-type strains using the Affymetrix™ yeast gene chips. These studies were conducted utilizing four replicates each of wild-type and *grr1Δ* RNA preps. All

raw data generated for each of these replicate analyses is provided in the "microarray_raw" table in the "*GRR1 Database"*. The term "raw data" refers to the numeric signal intensities, the presence or absence call, and the p-value for each gene in each replicate. This raw data was consolidated by calculating the mean signal intensity and standard deviation of the four replicate measures for both the wild-type and *grr1Δ* samples. The fold change was then determined by dividing the mean signal intensity for the *grr1Δ* samples by the mean signal intensity for the wild-type samples. Fold changes below 1 were converted to negative scale by taking the negative inverse of the fold change. Both the Welch's t-test and the Students t-test were applied and normalized to the log2 scale to determine the statistical relevance of the fold change. These summarized measures are reported in the table "microarray_grr1_vs_wt-_summary" and data for 5689 records is contained therein.

### 3.11. Development of the 2D-LC-MS/MS Based Quantitative Global Proteomics Approach: From Sample Preparation To Data Processing

The implementation of a liquid chromatography-mass spectrometry (LC-MS) based proteomic analysis platform is a stepwise process with the successful execution of each step pertinent to achieving reliable and comprehensive proteomic data. LC-MS based proteomics platforms can be divided into four main stages (Figure 3.1) defined generally as experimental design and sample preparation, chromatographic separation, mass spectrometric analysis, and data analysis and validation. Though these general stages of analysis are common to virtually every LC-MS based proteomics platform, the strategies that define these stages are highly customizable and often consist of multiple stepwise procedures, themselves. Additionally, these strategies can be utilized in multiple permutations; each with strengths and weaknesses specific to a given application. Thus, the design of a given proteomic platform must be tailored to specific experimental goals. In this regard, a great deal of effort was exerted in our laboratory to adopt and develop strategies that would allow an extensive and reliable quantitative analysis of a complex peptide mixture derived from a yeast

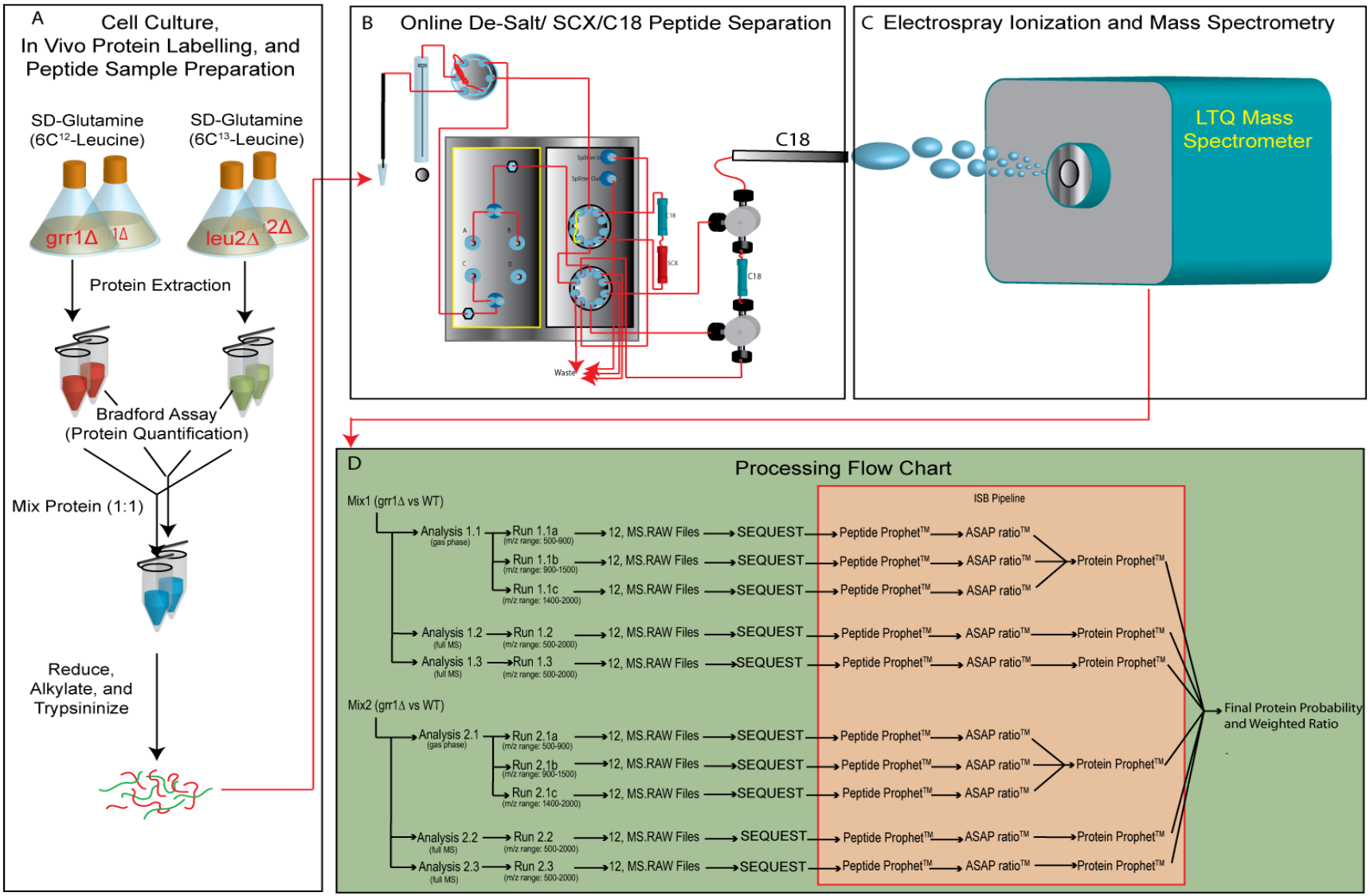
A
Cell Culture,
In Vivo Protein Labelling, and
Peptide Sample Preparation
SD-Glutamine
(6C12-Leucine)
SD-Glutamine
(6C13-Leucine)
grr1Δ
leu2Δ
Protein Extraction
Bradford Assay
(Protein Quantification)
Mix Protein (1:1)
Reduce,
Alkylate, and
Trypsininize
B
Online De-Salt/ SCX/C18 Peptide Separation
C18
Waste
C
Electrospray Ionization and Mass Spectrometry
LTQ Mass
Spectrometer
D
Processing Flow Chart
ISB Pipeline
Mix1 (grr1Δ vs WT)
Analysis 1.1
(gas phase)
Run 1.1a
(m/z range: 500-900)
Run 1.1b
(m/z range: 900-1500)
Run 1.1c
(m/z range: 1400-2000)
Analysis 1.2
(full MS)
Run 1.2
(m/z range: 500-2000)
Analysis 1.3
(full MS)
Run 1.3
(m/z range: 500-2000)
12, MS.RAW Files
SEQUEST
Peptide Prophet™
ASAP ratio™
Protein Prophet™
Mix2 (grr1Δ vs WT)
Analysis 2.1
(gas phase)
Run 2.1a
(m/z range: 500-900)
Run 2.1b
(m/z range: 900-1500)
Run 2.1c
(m/z range: 1400-2000)
Analysis 2.2
(full MS)
Run 2.2
(m/z range: 500-2000)
Analysis 2.3
(full MS)
Run 2.3
(m/z range: 500-2000)
Final Protein Probability
and Weighted Ratio

**Figure 3.1. Schematic Diagram of SILAC/2D-LC/MS-MS Proteomics Platform and Data Analysis Pipeline**. The proteomics platform employed in this study can be divided into four major components, each consisting of multiple stepwise procedures. **Sample preparation A:** Strains DBY2059 (Mat α *leu2-3, 112*) and JH001 (Mat α *grr1*::NAT) were grown in independent replicate batches of SD-Glutamine supplemented with 6-C13 leucine and 6-C12 leucine respectively to facilitate peptide labeling. Protein was extracted by bead beating for each culture and total protein concentration was determined utilizing a standard Bradford assay. Proteins from each batch (JH001 + DBY2059) were then mixed in a 1:1 ratio and reduced alkylated and trypsinized**. Online de-salt/SCX/C18 peptide separation B:** Approximately 150 ugs of each mixture (2 mixtures total) were then injected, separated, and analyzed six separate times utilizing an online desalting trap in line with a strong cation exchange column and finally a reverse phase (C18) column. Peptides from each injection (run) were sequentially fractionated utilizing the SCX trap by introducing Ammonium Formate concentrations of 0, 4, 8, 12, 15, 18, 21, 25, 50, and 100mM followed by two 1M steps. Each of these fractions was immediately separated on the C18 column utilizing a 90 minute Acetonitrile gradient from 5 to 50% at a 500nl/min flow rate. **Electrospray ionization and Mass spectrometry C:** As peptides eluted from the C18 column they were immediately ionized utilizing electrospray and analyzed utilizing an LTQ (Thermo Electron Corporation) mass spectrometer. The first three injections for each mixture were analyzed utilizing defined m/z scan windows of 500-1000 m/z, 900-1500 m/z, and 1400-2000m/z and together constituted one "gas phase" analysis. The final two injections for each mixture were analyzed utilizing the full m/z scan range and each individually constituted a "full scan range" analysis. In all, three analyses were performed on each mixture, one "gas phase" analysis and two "full scan range analyses". **Data Processing D:** Each injection (run) resulted in 12 ms.raw files that were each analyzed individually through SEQUEST (Thermo Electron Corporation) to facilitate peptide identification. SEQUEST results were then analyzed for validity and relative peptide quantification was measured utilizing a suite of software known as the Trans Proteomics Pipeline (TPP) available as open source from the Institute for Systems Biology. Statistical rules utilized by the TPP were then applied to the TPP results to combine protein identification probabilities and relative abundance ratios across all analyses into a final list of statistically valid protein identities and relative abundance ratios.

whole cell extract. In this chapter the stages of our proteomics platform are described in detail with emphasis placed on critical components of these stages and how they drove our decisions to adopt certain technologies. Additionally, suggestions for significant improvement of this system will be interjected.

### 3.11.1. Stage1: Experimental Design and Sample Preparation

#### *3.11.1.1. Experimental Question and Approach*

In order to drive the development of our customized proteomics platform we chose to characterize the proteomic response to deletion of the F-box protein, Grr1, in *S. cerevisiae.* Proteomic profiling of *GRR1* deleted *S. cerevisiae* strains was attractive for reasons both practical and biological. Practically, the *S. cerevisiae* genome was the first fully sequenced genome and is the most extensively annotated with 4718 verified genes, 1077 uncharacterized genes,

and 812 dubious open reading frames [345]. This translates to more reliable protein sequence databases to facilitate protein identification. Also, the yeast genome contains ~6000 open reading frames, offering a less complex eukaryotic protein mixture to analyze than its mammalian counterparts. Additionally, LC/MS systems have limited sensitivity that is typically accounted for by loading large amounts of protein (~150-200ug) that is easily obtained from yeast cell culture.

Biologically, our laboratory specializes in yeast genetics with particular interest in the SCF's (Skp, Cullin, F-box) role in coordinating both transcriptional and post-transcriptional responses to nutrient status. Thus, we were specifically interested in the discordance between transcript and protein levels in response to deletion of components involved in this regulatory pathway. With this in mind, we chose to characterize the proteomic response to deletion of the F-box protein, Grr1. Yeast deleted for *GRR1* remain viable, unlike many of the other SCF components, and thus, *grr1Δ* strains are amenable to analysis. Additionally, many substrates for the $SCF^{Grr1}$ complex have been elucidated. Therefore, the validity of data generated through our proteomics strategy could be ascertained since certain proteomic changes could be inferred from the known biological roles of Grr1. Finally, the eclectic group of substrates targeted by Grr1 includes multiple nutrient responsive transcription factors [56,168,57], cell polarity proteins [55,101], cell cycle regulators [346,347], and mitotic proteins [54,348]. We therefore predicted that a diverse array of proteins would be observed to have altered abundances in *grr1Δ* strains and that the inability of these strains to degrade Grr1 targeted transcription factors would lead to discordance between transcript and protein expression levels. Evaluation of this discordance would lead to a greater understanding of the role that Grr1 plays in coordinating these regulatory mechanisms.

In summary, our primary strategy pertaining to the development of the proteomics platform can be stated as follows. **We hypothesized that an application driven strategy for the development of a global quantitative proteomics platform utilizing *grr1Δ* mutants of *S. cerevisiae* would serve to**

**validate the utility of the platform and generate new biological insights into Grr1 function that could then be used to direct future experimentation.**

*3.11.1.2. Factors Influencing Strains and Media Conditions*

In order to provide a comprehensive and biologically relevant proteomic data set there were a number of considerations prior to sample preparation that influenced the strains and media conditions utilized. First, both the strains and media are dependent to some extent on the labeling strategy to be implemented. While many labeling approaches impose no restrictions on strain or media, others, such as SILAC (Stable Isotope Labeling of Amino Acids in Cell Culture) [349], in some circumstances, require specific strains and media to facilitate relative peptide quantification. Secondly, due to the known roles that Grr1 plays in extracellular sensing of both glucose and amino acids, both the genotype of the strain and the specific media conditions were tailored to minimize biological variables that would obfuscate the assessment of proteomic changes that arise as a direct result of Grr1 absence. In this section, I will briefly describe the labeling procedures that were available to us at the time of our analysis and detail the specific factors that led to the application of the chosen labeling procedure. Additionally, the specific growth and genetic concerns associated with the *grr1Δ* strain affected how we implemented the labeling procedure and will also be described.

The first strategic consideration that must be addressed when performing a quantitative proteomic analysis on a complex mixture is whether label free or isotopic labeling will be utilized. Both these methods can be employed to facilitate the relative quantitative comparison of two or more peptide samples and offer comparably accurate quantification. However, they differ remarkably in the degree of difficulty in reducing quantitative errors due to sample handling during preparation. This degree of difficulty is directly related to the theory by which each of these strategies relies on to facilitate relative peptide and finally protein quantification and underlies the most critical consideration when choosing between quantitative methods when both strategies are equally pursuable.

Label free strategies rely on the theories that relative peptide quantification can be measured by comparative quantification of extracted ion chromatograms (comparative LC-MS) [350] or by comparing the number of spectral counts (spectral counting) [343,351,352] from individual LC-MS analyses performed on the samples to be compared. In these procedures, samples are prepared and analyzed by HPLC-MS in parallel and as a result the reliability of the final quantitative results relies heavily on the ability to reproducibly prepare, chromatographically separate, ionize, detect, and measure peptides and their respective ion intensities across multiple HPLC-MS experiments. Variances in peptide quantification can be reduced significantly through multiple replicate analyses and extensive statistical analysis of the data but implementation of these measures drives up the price and time for each analysis [353,350]. Nevertheless, label free methodologies remain attractive and widely used for biological applications where label based strategies cannot be employed, such as the comparative analysis of more than three samples concurrently [354,355].

Quantitative labeling strategies rely on the theory that relative peptide quantification can be measured by comparing the extracted ion chromatograms of isotopically light and isotopically heavy labeled peptide pairs derived from the two samples to be compared, respectively. The introduction of an isotopic label to the peptides of one or possibly more samples allows for samples to be mixed prior to LC-MS analysis and analyzed concurrently [354,355], since the sample origin can now be distinguished by the shift in mass to charge ratio measured by the mass spectrometer. Samples can be mixed at the cell, protein, or peptide level, and prepared as one sample; minimizing errors introduced during sample handling and data acquisition. However, label based strategies, in some cases, vary in the degree of difficulty of performing the labeling reaction to completeness and thus suffer from incomplete labeling that compromises the accuracy of quantification [356,357]. Labels can also be costly and in most instances may only label a certain fraction of the protein or peptide mixture. Despite these drawbacks, label based methods remain the predominate strategies for conducting quantitative analysis on complex peptide mixtures.

Many label based strategies are currently applied for peptide quantification and a thorough review of all the technical alternatives is far beyond the scope of this volume [358,352]. However, these strategies can be classified generally based on the stage during sample preparation that the label is introduced and as a result the degree to which systematic and non-systematic variations can be reduced. Isotopic labels such as ICAT (Isotope Coded Affinity Tags) [359] are incorporated post cell lysis but before enzymatic digestion of the protein extract, enzyme facilitated labeling using trypsin or Glu-C in the presence of $^{18}O$ [356] incorporates the label during protein digestion, and chemical labels such as iTRAQ [355] are incorporated post-digestion. Each methodology provides viable peptide quantification, however the earliest stage at which a label can be incorporated into the proteome is during cell culture using a strategy known as SILAC (Stable Isotope Labeling of Amino Acids in Cell Culture) [349]. SILAC labeled samples can be mixed before or after cell lysis and, as a result, SILAC offers perhaps the most reliable quantification method if performed appropriately.

Due to the fact that our experiments were to be performed on yeast, the full toolkit of labeling strategies was available to facilitate relative peptide quantification. However, the ability to label proteins in vivo before systematic errors could be introduced was attractive to us and thus, we chose to implement a derivation of SILAC [360,349]. The SILAC strategy relies on the incorporation of a non-radioactive isotope of an essential amino acid into the proteome of one of the strains to be compared. This incorporation is engineered by supplementing the amino acid of choice into the growth medium of cultured cells for ~9-10 doublings. As a result, every instance of that amino acid in the proteome of the cultured cells occurs as the heavier isotopic version of the chosen amino acid. Samples can then be mixed after cell culture or after cell lysis and prepared and analyzed through HPLC-MS as a single sample. Since the mass spectrometer can distinguish between unlabelled and labeled peptide pairs based on the imposed mass difference; relative peptide quantification is realized by comparing their respective ion intensities across their chromatographic elution time.

Typically, SILAC is performed utilizing $C^{13}$ incorporated arginine and lysine residues [361,362]. The utilization of these amino acids for quantification of peptides generated from tryptic digestion is particularly attractive since trypsin cleaves at lysine and arginine residues which in theory would result in the incorporation of an isotopic label on every peptide. However, many organisms and cell lines can synthesize arginine and more often than not, lysine, de novo [363]. This ability leads to under-labeling and if left un-addressed can lead to inaccuracies in peptide quantification. Yeast, in particular, can synthesize every amino acid de novo and thus the successful implementation of SILAC in this organism relies on the construction of auxotrophic strains specific to the amino acid isotope to be utilized [364]. In addition, yeast will actively catabolize amino acids as primary sources of nitrogen and recycle the remaining carbon skeleton for the synthesis of other metabolites, including amino acids [365]. This can result in non-specific amino acid labeling through incorporation of $^{15}N$ or $^{13}C$ isotopes derived from catalysis of the isotopic amino acid. Thus, for any isotopic amino acid to be a viable label in yeast for whole proteome labeling, pathways required for synthesis and breakdown of the amino acid must be disabled.

The genetic engineering of yeast for the utilization of isotopic derivatives of arginine for relative peptide quantification is particularly challenging. Arginine can be synthesized de novo and is also a moderate nitrogen source in yeast (Figure 3.2). As a result, $^{15}N$ and $^{13}C$ isotopes incorporated into arginine can quickly become incorporated into other metabolites such as proline, and glutamate which lead to non-specific incorporation of isotopic labels into peptides (Figure 3.2). Thus, the effective use of arginine isotopes as quantitative labels requires at least two gene deletions (*arg*4 and *car*1) that together result in the inability of *Saccharomyces* to synthesize arginine de novo and catabolize arginine as a source of nitrogen. These gene deletions would not only affect arginine metabolism but the synthesis of proline and glutamate under certain nutrient conditions and as a result could introduce variations in protein or gene regulation that would be specific to the required gene deletions. However, it has been shown that supplementation of low amounts of proline in the growth

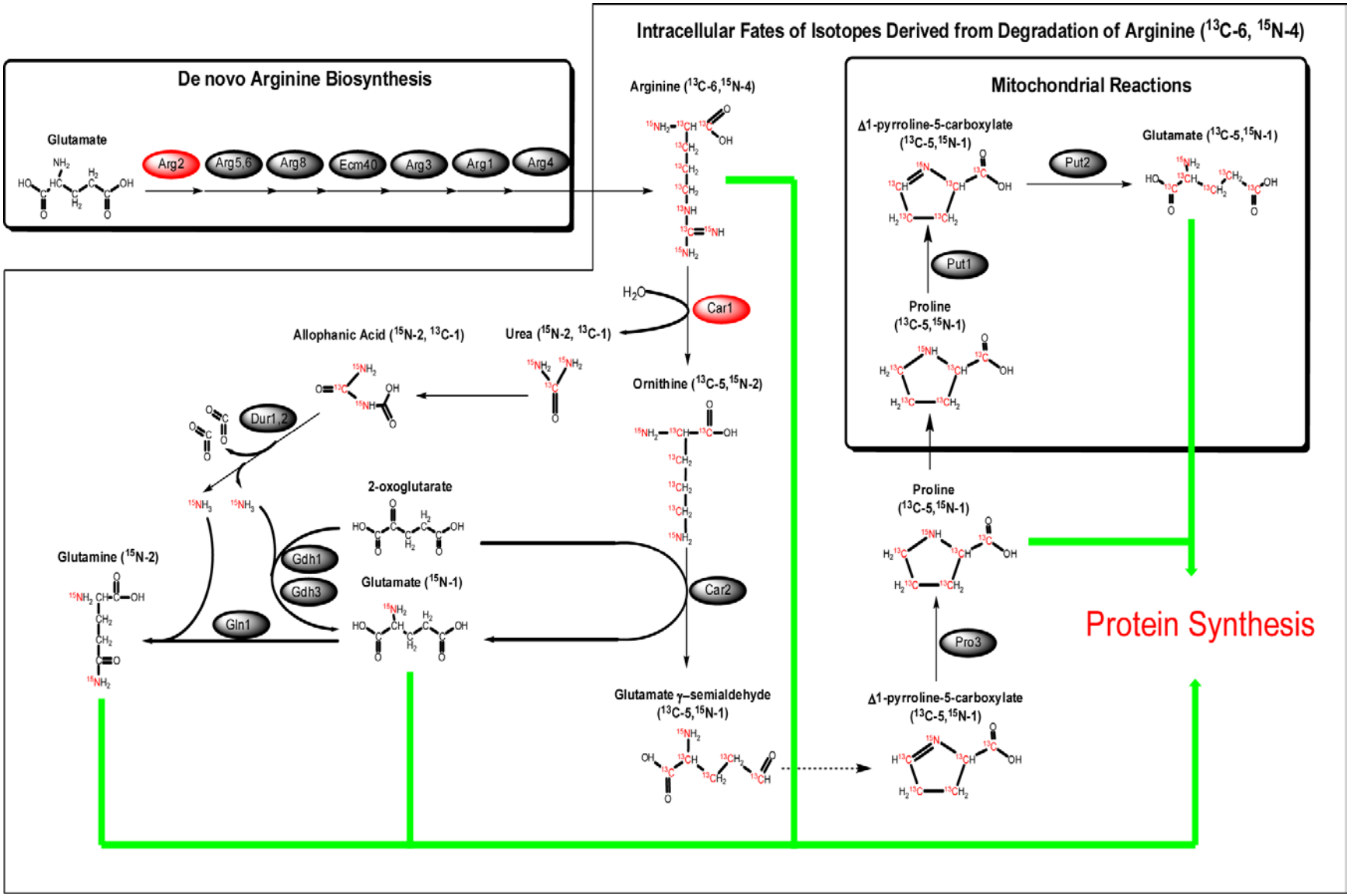
Intracellular Fates of Isotopes Derived from Degradation of Arginine ($^{13}$C-6, $^{15}$N-4)
De novo Arginine Biosynthesis
Glutamate
Arg2
Arg5,6
Arg8
Ecm40
Arg3
Arg1
Arg4
Arginine ($^{13}$C-6,$^{15}$N-4)
Mitochondrial Reactions
Δ1-pyrroline-5-carboxylate ($^{13}$C-5,$^{15}$N-1)
Put2
Glutamate ($^{13}$C-5,$^{15}$N-1)
Put1
Proline ($^{13}$C-5,$^{15}$N-1)
$H_2O$
Car1
Allophanic Acid ($^{15}$N-2, $^{13}$C-1)
Urea ($^{15}$N-2, $^{13}$C-1)
Ornithine ($^{13}$C-5,$^{15}$N-2)
Dur1,2
2-oxoglutarate
Proline ($^{13}$C-5,$^{15}$N-1)
Glutamine ($^{15}$N-2)
Gdh1
Gdh3
Glutamate ($^{15}$N-1)
Car2
Gln1
Protein Synthesis
Pro3
Glutamate γ–semialdehyde ($^{13}$C-5,$^{15}$N-1)
Δ1-pyrroline-5-carboxylate ($^{13}$C-5,$^{15}$N-1)

**Figure 3.2. Engineering *S. cerevisiae* for SILAC Arginine Labeling.** The successful utilization of arginine isotopes for peptide labeling utilizing the SILAC (Stable Isotope Labeling of Amino acids in cell Culture) method for yeast cell culture requires at least two gene deletions (nodes shown in red). The *ARG2* gene encodes for acetylglutamate synthase which catalyzes the first step in de novo arginine biosynthesis. Deletion of this gene is necessary to insure full incorporation of isotopically labeled arginine into newly synthesized proteins. The *CAR1* gene encodes for arginase and catalyzes the first step in arginine degradation. Strains containing a functional *CAR1* gene are able to utilize both the carbon skeleton and nitrogens of arginine for synthesis of other amino acids. Thus, in order to prevent incorporation of isotopic elements derived from arginine into other protein residues, deletion of *CAR1* is required. Isotopic elements derived from arginine are shown in red.

medium of cultured embryonic stem cells inhibits the conversion of arginine to proline [366] and thus proline supplementation in yeast medium could bypass the requirement for *CAR1* deletion.

To avoid the practical concerns associated with the utilization of arginine isotopes, we chose to utilize $^{13}$C-6 leucine (available from Cambridge Isotope Laboratories, Inc., Andover, MA, USA.) The utilization of isotopic derivatives of leucine to facilitate relative peptide quantification has been demonstrated recently [367] and is an extremely attractive alternative to arginine/lysine labeling for multiple reasons. First, de novo synthesis of leucine is easily avoided in yeast through utilization of a *leu2Δ* strain [364]. These strains are widely available in multiple *S. cerevisiae* backgrounds due to their widespread use as genetic markers [368]. Second, branched chain amino acid carbon skeletons are not recycled by yeast for biosynthesis and are metabolized to fusel alcohols and/or fusel acids that are simply excreted from the cell [369,370] (See Figure 3.3). No further gene deletions are required to remove leucine catabolic enzymes and thus, far less influence on nitrogen biosynthetic processes is exerted when implementing isotopic leucine derivatives as peptide labels. Finally, leucine is the most common amino acid comprising on average 9.1% of the amino acid residues in yeast proteins [367] and by our laboratories calculations would result in the labeling of ~65% of all tryptic peptides detectable.

In summary, the utilization of leucine isotopes to facilitate peptide labeling requires fewer gene deletions and influences central nitrogen metabolism to a much lesser extent than gene deletions required for utilization of arginine isotopes. In contrast, the implementation of isotopic leucine for peptide labeling

imposes limitations on the number of quantifiable peptides. We chose to error on the side of caution by utilizing isotopic leucine as a label due primarily to known issues that *grr1Δ* cells possess regarding nitrogen signaling and metabolism.

It is interesting to stress that, like leucine, valine and isoleucine are degraded to non-metabolizable fusel alcohols in yeast. Interestingly, an isoleucine/leucine/valine auxotrophic strain can be constructed through a single gene deletion at the *ILV3* locus encoding dihydroxyacid dehydratase which catalyzes the third step in the common pathway required for biosynthesis of all three branched chain amino acids. The utilization of isotopes of all three of these amino acids simultaneously would increase quantifiable tryptic peptide coverage to ~89%. Additionally, leucine and isoleucine are isobaric and as a result undistinguishable by mass spectrometry; implementation of isotopic leucine and isoleucine labels of different mass would bypass this issue leading to greater peptide identification confidence.

Additionally, when choosing between different amino acid labels containing elemental isotopes, it is wise to employ strictly $^{13}C$ derivatives that produce a mass shift greater than 4 Daltons. Labels with deuterated hydrogen impose chromatographic shifts in retention time that lead to difficulties in extracting ion chromatograms for quantification [371]. Due to the fact that primary amines on amino acids are often cleaved for nitrogen utilization and can ultimately be utilized for the anabolism of other amino acids [134], it is best to avoid $^{15}N$ incorporated labels when possible. Finally, ion traps are robust mass spectrometers and for this reason are popular mass analyzers utilized for the analysis of complex mixtures. However, these instruments have mass accuracies of approximately 1 Dalton and thus the ability to resolve isotopic envelopes of heavy and light peptide pairs becomes a greater challenge with labels less than 4 Daltons. This is because mass spectrometers measure m/z and thus a 3 Dalton label on a peptide with a charge equal to 3 would only shift the heavy label peptide 1 Dalton.

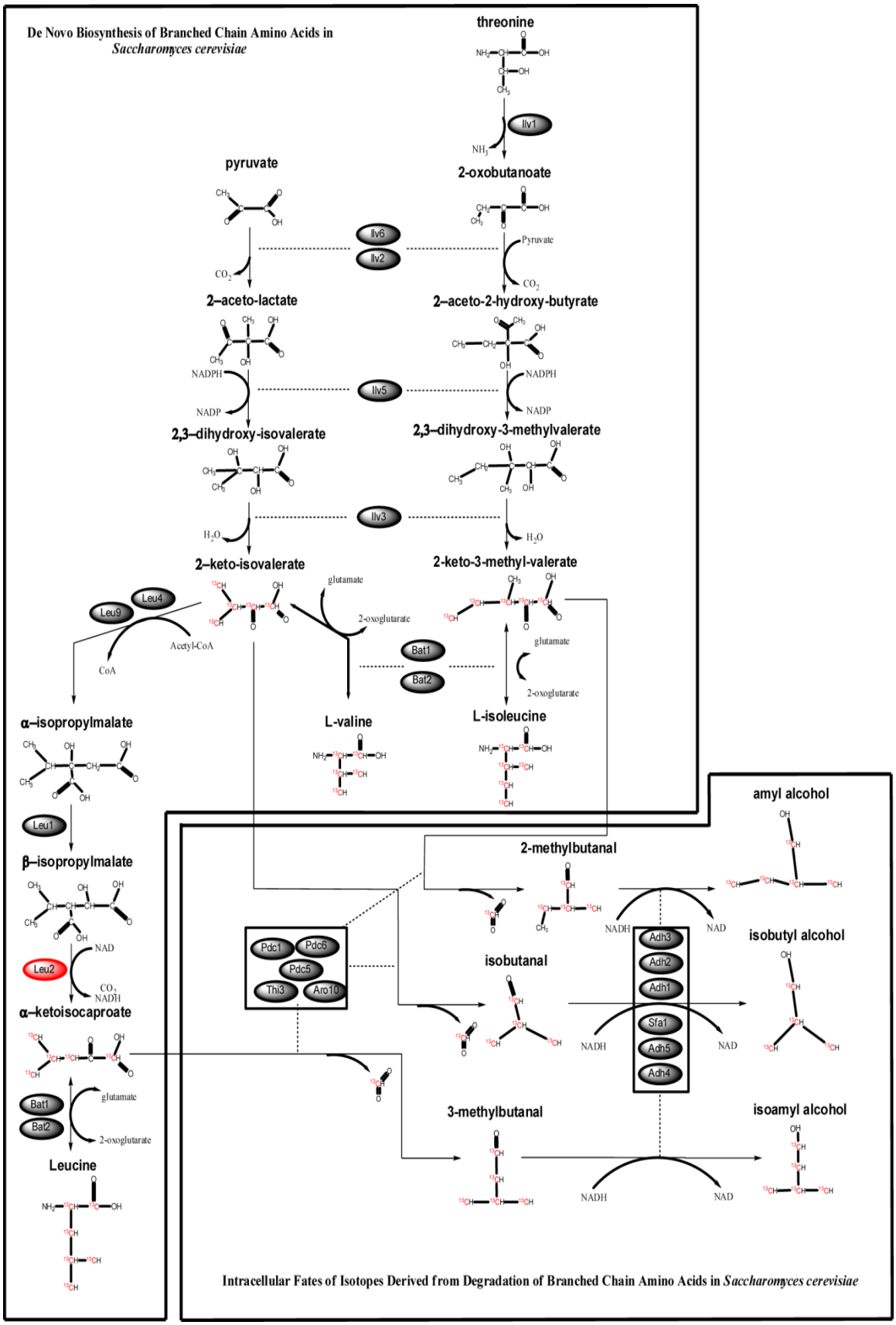
De Novo Biosynthesis of Branched Chain Amino Acids in
Saccharomyces cerevisiae
threonine
Ilv1
pyruvate
2-oxobutanoate
Ilv6
Ilv2
Pyruvate
2–aceto-lactate
2–aceto-2-hydroxy-butyrate
NADPH
NADP
Ilv5
2,3–dihydroxy-isovalerate
2,3–dihydroxy-3-methylvalerate
Ilv3
2–keto-isovalerate
2-keto-3-methyl-valerate
glutamate
2-oxoglutarate
Leu4
Leu9
Acetyl-CoA
CoA
Bat1
Bat2
α–isopropylmalate
L-valine
L-isoleucine
Leu1
β–isopropylmalate
NAD
Leu2
α–ketoisocaproate
Leucine
amyl alcohol
2-methylbutanal
NADH
Adh3
Adh2
Adh1
Sfa1
Adh5
Adh4
isobutyl alcohol
Pdc1
Pdc6
Pdc5
Thi3
Aro10
isobutanal
3-methylbutanal
isoamyl alcohol
Intracellular Fates of Isotopes Derived from Degradation of Branched Chain Amino Acids in Saccharomyces cerevisiae

**Figure 3.3. Engineering *S. cerevisiae* for SILAC Branched Chain Amino Acid Labeling.** The utilization of branched chain amino acid isotopes for SILAC labeling of peptides requires only a single gene deletion since the carbon skeleton of branched chain amino acids is not utilized for the synthesis of other amino acids. Branched chain amino acids are broken down to form fusel alcohols that are not utilized for protein synthesis therefore; inactivation of these pathways is not required. Utilization of isotopic leucine (utilized in our analysis) requires a single gene deletion of *LEU2,* which encodes for β-isopropylmalate dehydrogenase, or *LEU1*, which encodes for isopropylmalate isomerase. Theoretically, yeast could be engineered for concurrent utilization of isotopic valine, leucine, and isoleucine by deletion of *ILV5* or *ILV3* in order to increase the number of peptides quantitated. Intracellular, fates of isotopes derived from labeled valine, isoleucine, or leucine are shown in red.

In summary, the decision to employ a label based method facilitated by $^{13}$C-6 leucine SILAC was primarily driven by the concern to reduce systematic errors and their influence on data validity. We identified two potential sources ofsystematic errors that could be resolved early in the sample preparation stages. First, systematic errors due to sample handling are most easily minimized by preparing samples together in the same test tube at the earliest stages of sample preparation possible and the SILAC strategy is amenable to very early sample mixing. Second, non-specific isotopic labeling of peptides utilizing isotopic arginine labels is a known factor contributing to systematic errors in peptide quantification [372,358,371]. To bypass possible issues that would arise with their use we chose to utilize isotopic leucine whose carbon skeleton is known not to be recycled for biosynthetic reactions. The decision to implement this strategy imposed two restrictions on the media and strains that had to be utilized in our experiment. First, at least one of the strains had to be a leucine auxotroph. Thus, we chose to utilize strain DBY2059 (MAT α *leu2-3, 112)* as our comparative “wild-type” strain since a nonfunctional *leu2-3* allele was already present. Second, both strains culture media had to be supplemented with a significant amount of leucine and $^{13}$C-6 leucine, respectively, to facilitate peptide quantification. The remaining strains and media conditions were influenced strictly by the nature of the biological experiment and will be discussed in the following section.

Yeast requires a viable source of carbon, nitrogen, sulfur, and some essential vitamins to support growth and division. Interestingly, Grr1 is known to participate in coordinating cellular responses to both carbon and nitrogen source

fluctuations in the extra-cellular environment (Sections 1.9, 1.10, and 2.2). Specifically, *grr1Δ* strains have been shown to have defects in both glucose and nitrogen signaling and transport. This multi-faceted role for Grr1 in facilitating the intracellular response to these two critical metabolites presented an exceptional challenge to experimental design. The primary goal of our global analyses was to characterize changes in protein and transcript levels that were attributable to differential responses to glucose between *grr1Δ* and wild-type strains. Due to the role of Grr1 in both carbon and nitrogen signaling and the intimate relationship between these two nutrients in metabolism, it is difficult if not impossible to completely eliminate cross talk between the molecular responses that they elicit. Ergo, we sought to separate the molecular responses to carbon and nitrogen by choosing nitrogen and amino acid sources whose influence on *grr1Δ* physiology and transcriptional regulation had been previously defined.

As mentioned previously, the deletion of *GRR1* results in the inability to respond to extra-cellular amino acids through the SPS signaling pathway and therefore *grr1Δ* cells possess specific amino acid uptake deficiencies. It is well known that *ssy1Δ leu2Δ* strains do not grow on complex media despite the presence of leucine[112]. This phenotype has been attributed to the fact that Gap1 facilitated amino acid transport is the predominant transport mechanism in *ssy1Δ* cells and that amino acids compete for import through this transporter when multiple amino acids are present. Therefore, in the presence of multiple amino acids, the transport of leucine through Gap1in an *ssy1Δ leu2Δ* strain is insufficient to replace leucine biosynthesis. Strains deleted for *GRR1* share many of the attributes of *ssy1Δ* strains in regard to amino acid uptake. Like *ssy1Δ leu2Δ,* the *grr1Δ leu2Δ* strain (our laboratory, data not shown) shows a dramatic growth defect when grown in complex media when leucine is not provided at greater concentrations. Thus, we surmised that Gap1 was the predominant amino acid transporter in *grr1Δ* strains as well. We therefore chose not to utilize a *grr1Δ leu2Δ* strain in our global genomic and proteomic profiling experiments to avoid the effects that leucine deficiency would impose on the transcriptional and proteomic profiles of *grr1Δ* cells. The possible drawback of

this choice would be that the absence of leucine biosynthetic mutation in *grr1Δ* cells could lead to transcriptional and proteomic changes in leucine biosynthetic genes and proteins compared to “wild-type” (*leu2-114)* if leucine import was insufficient to supplement the intracellular leucine requirement in *grr1Δ* cells.

Due to the aforementioned competitive transport of amino acids through Gap1 we were limited in the number of amino acids that *grr1Δ* cells could be cultured with to avoid transcriptional and proteomic changes caused by deficiency of a particular amino acid. Furthermore, we wanted to culture *grr1Δ* in a media that was conducive to elicit nitrogen catabolite repression in order to avoid proteomic and transcriptional responses attributable to defective nitrogen signaling. Nitrogen catabolite repression is analogous to glucose repression in that certain nitrogen sources are defined as “preferred” nitrogen sources since their transport and metabolism exerts repression on genes required for the utilization of other “non-preferred” nitrogen sources. Leucine is a “non-preferred” nitrogen source and thus another nitrogen source that would elicit nitrogen catabolite repression was required. Strains of the S288C background show deficiencies in nitrogen catabolite repression when grown in ammonium sulfate which is normally a “preferred” nitrogen source in other strain backgrounds. Thus, even though *grr1Δ* strains show no deficiencies in transport of ammonium sulfate, this nitrogen source had to be avoided. Glutamine is a highly preferred nitrogen source in *S. cerevisiae* and has been shown in multiple studies to exert nitrogen repression [373]. Glutamine is also transported by the Gap1 amino acid transporter [121,374]. Due to these characteristics, we utilized glutamine as the primary source of nitrogen in our studies.

*3.11.1.3. Protein extraction*

Following cell culture, total cellular protein is extracted utilizing any number of alternative methods specific to the particular experimental application. An extensive review as well as experimental protocols for cell lysis of mammalian, bacterial, and yeast cells for common applications such as immunoprecipitation, immunoblotting, and liquid chromatography/mass

spectrometry can be found in [375]. This review provides an extensive and well outlined description of the critical issues that must be addressed for successful protein extraction. However, I will discuss some of the key issues I discovered, specifically for preparation of yeast whole cell lysates for LC-MS based global proteomic profiling experiments.

The ability to identify and determine the quantity of all proteins and peptides present in an entire cell is the “Holy Grail” of global proteomic profiling analysis. The comprehensiveness of these experiments completely relies on the ability to extract the entire set of proteins present in the cell. In order to analyze a given protein or peptide, it must first be present in the sample. There are two important factors that determine the thoroughness and applicability of a given extraction method. First, the efficiency of cell lysis must be high since unlysed cells lead to less protein and as a result make it harder to detect peptides derived from low abundance proteins. Second, and perhaps most importantly, lysis must be performed in a buffer that will solubilize the vast majority if not all proteins. This is particularly challenging given that cellular proteins exhibit radically diverse solubilities, pKas, hydrophobicity indices, and sub-cellular localizations.

A relatively simple procedure utilizing glass beads and a vortex provides a robust and efficient method for yeast cell lysis. Yeast cells are notoriously hard to lyse given the presence of a rigid cell wall in this organism and as a result require extraction methods that employ more “brute force” than procedures utilized for mammalian cell disruption. A number of viable alternatives are available to facilitate yeast cell breakage including the utilization of high pressure induced disruption facilitated by a French pressure cell or nitrogen cavitation. However, the abrasive lysis of yeast cells utilizing 0.5mm glass beads offered a simple and efficient method (yields of up to 95% cell breakage) [375] of protein extraction. Briefly, cells are suspended in an appropriate buffer and glass beads are added to the meniscus of this suspension. Cells are disrupted by ten consecutive rounds of 30 second vortexing and 30 second incubations on ice. The degree of cell breakage can be ascertained by examining an 8ul sample of the suspension under a phase contrast microscope.

As stated previously, the lysis buffer utilized during the glass bead disruption must promote solubilization of a wide array of proteins. Buffers containing 8M urea or 6M guanidinium chloride have been employed for quite some time for solubilizing notoriously insoluble proteins. Urea and guanidinium chloride are chaotrophic agents that greatly promote denaturation and thus enhance protein solubility. Therefore, we chose to utilize a lysis buffer comprised of 8M urea buffered to pH8.5 with 1mM ammonium bicarbonate.

*3.11.1.4. Determination of Protein Concentration and Sample Mixing*

Following cell lysis, the total protein concentration for each sample is determined to evaluate extraction yield and facilitate equal sample mixing. SILAC allows for sample mixing prior to cell lysis; however we were concerned about the variability in cell breakage efficiency between different strains (communications with the Roach lab). This was especially concerning given the gross morphological abnormalities observed in *grr1Δ* cells. We therefore decided to error on the side of caution and perform the mixing step post lysis where a relatively accurate protein concentration for each mixture could be determined utilizing any one of a number of available protein concentration assays.

The accuracy of relative peptide and protein concentration relies heavily on the ability to mix the samples to be compared in a 1:1 ratio during sample preparation. Thus, the given protein assay utilized to determine total protein concentration after cell lysis must be both robust and reliable. The protein concentration of each sample can be determined utilizing a number of techniques, including ultraviolet absorbance [376], the Lowry assay [377], the BCA assay [378,379], and the Bradford assay [380]. Each of these methods varies in sensitivity and the degree to which buffer constituents (i.e. salts and other biological materials) interfere with the measurement. Our protein mixtures were prepared in 8M urea and 100mM ammonium bicarbonate (salt) and therefore the protein assay we employed had to be both sensitive and compatible with salt. Among the possible methods, the Bradford assay offered both a highly sensitive

and buffer compatible means to determine protein concentration. Briefly, this assay is conducted utilizing Coomassie Brilliant Blue G-250 dye which binds to arginine, tryptophan, tyrosine, phenylalanine, and histidine residues in anionic form with an absorbance maximum at 595nm. An absorbance curve for a standard protein sample (normally Bovine Serum Albumin) at various concentrations is generated. It is important to seed the solutions for generating the standard curve with the same concentrations and volumes of the sample buffer that will be utilized (in this case 8M urea, .1M ammonium bicarbonate) when measuring the sample absorbance in order to minimize variability in absorbance attributable to the buffer constituents. The absorbance for the protein samples is then measured and protein concentration is calculated using the equation defining the standard curve. After protein concentrations are determined for each sample, the samples to be compared are mixed in a 1:1 ratio accordingly. Thus, in our experiment two independent mixtures have been created with each consisting of protein extracts derived from DBY2059 and JH001 mixed in a 1:1 ratio.

*3.11.1.5. Reduction, Alkylation, and Digestion*

Once the desired protein extracts have been mixed, these protein mixtures are prepared for proteolytic digestion. At this stage the proteins in the mixture exist in a semi-denatured state where both the secondary and tertiary structure has been disrupted by the presence of 8M urea. Secondary and tertiary structure is defined by non-covalent interactions, namely hydrophobic, hydrophilic, and Van der Waal's forces which are easily disrupted by urea. However, covalent bonds are not affected by urea and as a result disulfide bridges between cysteine residues are still intact. If these disulfide bridges are left intact, any reduction in the urea concentration could promote protein renaturation that would in some cases lead to protein aggregation and as a result sample loss. Additionally, the presence of disulfide bonds obstructs the protease during digestion resulting in inefficient protein cleavage. Proteolytic digestion cannot be conducted at urea concentrations exceeding 2M since the enzymes

utilized for digestion are themselves denatured and rendered inactive. Therefore, disulfide bridges must be disrupted and their reformation must be prohibited before the urea concentration can be reduced and digestion can proceed. Disulfide bridges are disrupted through chemically induced reductive cleavage utilizing dithiothreitol (DTT) [381,382]. Briefly, a 1:40 molar excess of DTT is introduced into the sample mixture and incubated at 50°C for ~30 minutes. The molarity of the protein mixture can be calculated utilizing the concentrations measured by the Bradford assay and by assuming an average protein molecular weight of 66,000 Daltons.

At this point the proteins present in the mixtures exist in a fully denatured state. Cysteines have been fully reduced and now exist with thiol groups present on the side chains. In order to prevent reformation of disulfide bridges that readily form from natural air oxidation reactions these thiol groups are alkylated utilizing iodoacetamide. Briefly, iodoactamide is added in an 80 fold molar excess to the reduced protein mixture and incubated in complete darkness on ice for ~2 hours. Reformation of disulfide bridges is now prohibited since the cysteines have been converted to S-carboxymethylcysteine [383,384].

Reduction and alkylation is proceeded by digestion of the protein mixture and is facilitated by any number of proteolytic enzymes (proteases) and chemicals (for review see [375]). Each of these enzymes and chemicals possess varying degrees of selectivity and specificity that determine the ability of the enzyme or chemical to generate peptide fragment mixtures amenable to analysis by a given global proteomics platform. The selectivity of a proteolytic enzyme or chemical is defined by the number of distinct sites (peptide bonds) that are recognized for hydrolysis. For example, chymotrypsin (EC 3.4.21.1) is a broadly selective protease that hydrolyzes peptide bonds C-terminal to tryptophan, tyrosine, phenylalanine, leucine, and methionine, whereas endoproteinase Lys-C (EC 3.4.21.50) is a highly selective protease hydrolyzing peptide bonds C-terminal to only lysine. Specificity refers to the efficiency of the hydrolysis at the selected sites and the degree to which “non-specific” peptide bonds are hydrolyzed inadvertently. Together, the selectivity and specificity of a particular

proteolytic enzyme or chemical determine the complexity of the final peptide mixture and the physical nature of the peptides generated. Both of these properties must be optimized and tailored to the proteomics platform to achieve valid and comprehensive global profiling data.

The comprehensiveness of a “global profiling” experiment is, in part, determined by the number of analyzable peptides generated during the digestion procedure: if more peptides are analyzable, then more proteins are detectable and quantifiable. The number of analyzable peptides is influenced greatly by the degree to which the physical properties of the peptides generated from a particular digestion strategy are amenable to the downstream separation, ionization, and analysis systems. Two important properties determine this amenability and are largely defined by the selectivity of the proteolytic enzyme or chemical.

First, it is favorable to generate peptides that can retain a significant number of positive charges. Most online two dimensional separation systems employ strong cation exchange chemistry to facilitate peptide separation in the first dimension [385]. This chemistry utilizes immobilized anions to retain positively charged peptides and therefore the generation of a peptide population containing a large number of peptides with anionic properties would decrease the efficiency of this separation step. Additionally, electrospray ionization is typically utilized in these systems in positive ionization mode which selectively ionizes positively charged peptides for mass spectrometric analysis [386]. For these reasons, digestion strategies that cleave C-terminal to basic residues (arginine and lysine) generate peptides that are quite amenable to analysis through these types of platforms. Second, ion trapping instruments are robust mass analyzers that are commonly employed in global profiling experiments. These mass analyzers possess functional scan ranges from 500 to 2000m/z. Scan limitations in this range would theoretically allow for the detection of peptides ranging from 500 to 6000 Daltons since peptides can hold multiple charges, usually ranging from 1 to 3. For this reason, it is favorable to choose a digestion strategy that produces the largest number of peptides within this molecular weight range. The optimal

proteolytic enzyme or chemical may vary for different proteomes since the average peptide size produced is a function of the number of cleavage sites the enzyme or chemical possesses and the frequency of these sites in a proteome.

Proteolytic enzymes or chemicals with broad selectivity and/or specificity generate diversified peptide populations which require larger peptide databases to facilitate efficient peptide identification. As the database gets larger and as a result more complex the statistical validity of peptide assignments made by database searching algorithms is adversely affected [387,388]. Thus, in order to increase the validity of peptide identifications it is wise to simplify the peptide mixture as much as possible to reduce database complexity but not at the detriment of proteome coverage. This is easily achieved by utilizing proteolytic enzymes of moderate to low selectivity and high specificity. Low selectivity and high specificity decreases the diversity of C-terminal and/or N-terminal amino acids which can be exploited when the peptide database is generated to reduce database size and complexity. To elaborate, during the mass spectrometric analysis of a complex peptide mixture, thousands of experimentally acquired "peptide fingerprints" known as MS/MS spectra are generated. Each of these spectra are unique to a given peptide sequence and as a result are utilized to reveal the peptides identity by comparing their pattern to theoretically derived MS/MS spectra generated from a protein sequence database (in our case the *S. cerevisiae* protein sequence database) [389]. The first step in the generation of theoretical MS/MS spectra is the computer assisted (*in silico*) digestion of the protein sequence database to generate the peptide database. Thus, the greater the number of non-specific cleavage events or recognized amino acids by a particular proteolytic enzyme or chemical, the larger the peptide database must become.

Tryptic digestion of protein mixtures generates a large number of peptides amenable to 2DLC-ESI-MS and is a highly selective and specific protease. Trypsin (EC 3.4.21.4) selectively hydrolyzes peptide bonds C-terminal to arginines and lysines which possess basic amine groups that increase the charge capacity of the peptides. This cleavage is highly specific and cleavage is

only known to be inhibited by the presence of proline residues C-terminally adjacent to arginine or lysine residues. For this reason, database searches can be performed utilizing a theoretical peptide database generated by specifying arginine and lysine cleavage with only two or three mis-cleavage events allowed. Furthermore, ~95% of the peptides generated from tryptic digestion of the yeast proteome fall within the mass window of ion trap instruments [390]. For these reasons, trypsin is utilized as the digestive enzyme for many "global profiling" experiments.

Despite the wide spread use of trypsin as the digestive enzyme for "global profiling" experiments it is important to emphasize that the implementation of multiple complementary enzymes on identical but separate protein mixtures could theoretically enhance proteome coverage and data validity. Thus, the same protein mixture would be digested by two separate digestive strategies and each of these peptide mixtures could then be analyzed separately to maintain database simplicity for each search. Amino acid sequences that are not detected and quantified by utilizing one digestion strategy due to the recalcitrance of the peptide to the analysis may be detected and quantified from another digestion strategy since the peptide properties would more than likely have changed. The results from these two analyses could then be combined to increase the statistical validity of protein identification and quantification as well as increase proteome coverage. The utilization of multiple digestion strategies to enhance "global profiling" analyses has received little attention despite the predicted benefits and hence optimization of this step in the analysis could provide large dividends with regards to enhanced proteome coverage.

In our experiment, for reasons described above, we chose to utilize trypsin to digest our protein mixture. Trypsin activity is inhibited at urea concentrations greater than 2M and thus before proceeding with digestion our samples were diluted four fold with 100mM ammonium bicarbonate to 2M urea. After dilution trypsin (TPCK treated to prevent autolysis) was added to achieve an enzyme to substrate ratio of 50:1. This mixture was incubated overnight at 37°C to allow digestion to proceed to completion.

*3.11.1.6. Sample De-Salting and Concentration*

Following digestion, the peptide mixture must be concentrated and buffer components that are incompatible with the separation strategy must be removed to insure realistic sample loading times and efficient peptide separation. The most effective liquid chromatography based separation strategies for complex peptide mixtures support low flow rates ranging from 100-300ηl/min. With 150 to 250µg of sample typically loaded per analysis, an 180µg peptide sample at 10ug/ul would take ~1 hour at a flow rate of 300ηl/min. The dilution steps needed to facilitate digestion typically dilute the peptide concentration to anywhere from 0.1-1µg/µl, thus these mixtures must be concentrated to minimize loading times. Additionally, liquid chromatography based separation strategies for the analysis of complex mixtures employ orthologous separation strategies performed in tandem, known as two-dimensional liquid chromatography. Strong cation exchange (SCX) chemistry comprises the first dimension of separation and retains peptides based on their positive charge. Peptides are then separated by increasing salt concentrations to divide the peptide mixtures into fractions. Thus, in order to retain the greatest number of peptides at the initial loading stage, the sample buffer must be largely devoid of salt and other buffer constituents that adversely affect peptide retention on SCX resin columns. Urea and ammonium bicarbonate at high concentrations are incompatible with SCX chromatography as is electrospray ionization and therefore great care must be exerted to insure the removal of these buffer components.

A number of methodologies can be employed to facilitate sample concentration and de-salting but solid phase extraction with a C18 or comparable micro-trap offers a simple strategy that is compatible with two dimensional chromatography separations consisting of SCX and reverse phase (RP) resins. In this procedure the peptide mixture is loaded onto a C18 micro-trap and peptides are retained on the column by hydrophobic interactions between the peptide and C18 stationary phase. Urea and ammonium bicarbonate are removed through subsequent washing steps after which the peptides are eluted utilizing the resin manufacturer's specifications. Often, the elution buffer is not

ideal for 2DLC-ESI-MS experiments and eluted peptide concentrations may not be ideal. In these instances the buffer can be exchanged and the peptide concentration increased by evaporating the elution buffer away from the peptides utilizing a speed vac. The dried peptide sample can then be re-suspended in a 2DLC-ESI-MS compatible buffer of appropriate volume.

There are a number of solid phase extraction strategies that can be employed with manufacturers promising increased retention of peptides with diverse physical properties. For instance, the Oasis$^{TM}$ HLB (Hydrophylic-Lypophylic Balance) cartridges from Waters Corporation employ N-vinylpyrrolidone and divinylbenzene stationary phases in the same column to retain peptides of neutral, basic, and acidic properties. However, the advantages of these preparatory columns are lost unless the same stationary phase chemistry is utilized in the second, reverse phase peptide separation. Peptides that are specifically retained on the Oasis HLB column due to the enhanced resin will not be retained if another C18 resin is utilized in the reverse phase separation. Therefore, to maintain peptide sample composition through all separation strategies it is wise to employ identical or similar stationary phases (typically C18) for de-salting and reverse phase separations.

De-salting procedures can be performed off-line utilizing gravimetric flow or vacuum manifolds, independent of the HPLC platform, or on-line where de-salting and two dimensional separations can be performed in tandem utilizing an HPLC system. Solid phase extraction columns for off-line de-salting can be purchased from numerous vendors, including Waters, Varian, GE Healthcare, and 3M Bio-analytical Technologies. Off-line de-salting strategies require more manual effort but reduce peptide sample cross-contamination problems and HPLC dead volumes that contribute to sample loss. Additionally, off-line strategies are more amenable to protocol development since multiple procedures utilizing varying chemistries can be performed simultaneously to assess the most robust and efficient de-salting method for a given application. On-line de-salting procedures, if implemented correctly, reduce manual sample preparation times through automation. The initial implementation and optimization of these

systems can be tedious since back pressure, buffer compatibility, flow rate, system volume, and plumbing must all be seamlessly integrated with downstream separation components. However, a carefully automated system can provide robust and sensitive analyses that require far less manual effort than off-line systems. The data reported in this work was generated utilizing an on-line de-salting and separation system and therefore the description of our de-salting and separation procedures will be discussed together in the next section.

### 3.11.2. Stage 2: Peptide Separation Strategies for the Analysis of Complex Peptide Mixtures

The comprehensiveness of a global proteomic profiling experiment is largely defined by the efficacy of sample preparation and the capacity of the analysis platform to detect, identify, and quantify the peptides present in the sample peptide mixture. These mixtures contain hundreds of thousands of peptides each present at specific concentrations that can vary by more than a thousand fold and therefore the complete analysis of every component in these mixtures presents a significant challenge to proteomic analysis platforms [337]. Employed alone, mass spectrometers lack the analytical capacity to measure even a small fraction of peptides present in these highly complex mixtures. To increase the analytical capacity of mass spectrometers, peptide separation strategies are implemented prior to mass spectrometric analysis. Separation systems act to temporally and spatially disperse peptides based on their inherent chemical properties. This serves to reduce the number of peptides available for analysis per unit of time in order to complement the analytical capacity of the ionization and analysis systems. This ultimately allows for measurements of a greater number of peptides to be carried out over the course of a separation. Therefore, the comprehensiveness of a global proteomics platform relies heavily on the effectiveness to which the separation components resolve the greatest number of peptides prior to mass spectrometric analysis.

The effectiveness of a given separation system to resolve the components of a mixture is primarily assessed by a metric termed peak capacity [391]. Peak

capacity in chromatographic separations is defined as the maximum number of peaks or separable components (in this case peptides) that can be sufficiently resolved within a given separation space. The maximum peak capacity of a chromatographic separation can be described by

$$N_C = \frac{L}{(4\sigma)R_s} \quad [2]$$

where L is defined as the theoretical total separation time or space, 4σ is the average time over which each peptide elutes or peak width, and $R_S$ is the desired resolution [392,393]. Thus, peak capacity can be increased by increasing separation space, by reducing the peak zone width, and/or by reducing the desired resolution. (Figure 3.4)

A number of peptide separation technologies have been developed in attempts to maximize peak capacity in order to provide complete proteomic coverage. HPLC (High Performance Liquid Chromatography) [394], UPLC (UltraPerformance Liquid Chromatography) [391], CZE (Capillary Zone Electrophoresis) [395], and CIEF (Capillary Isoelectric Focusing) [396] have all been utilized to analyze significant fractions of the peptides present in whole proteome digests but all of these technologies fall short of providing comprehensive proteome coverage. Nonetheless, these technologies allow for a substantial fraction of the proteome to be sampled and as a result can provide a wealth of biologically relevant proteomic measurements.Among these technologies, high performance liquid chromatography based separations have become the most widely employed. The widespread availability and relatively low cost of HPLC solvent delivery systems, the ease that these systems can be interfaced with mass spectrometers through electrospray ionization (ESI) or matrix assisted laser desorption ionization (MALDI), and the high sensitivities and peak capacities achievable by these systems are attributes that have contributed to this popularity. Within this category of liquid chromatography based separations

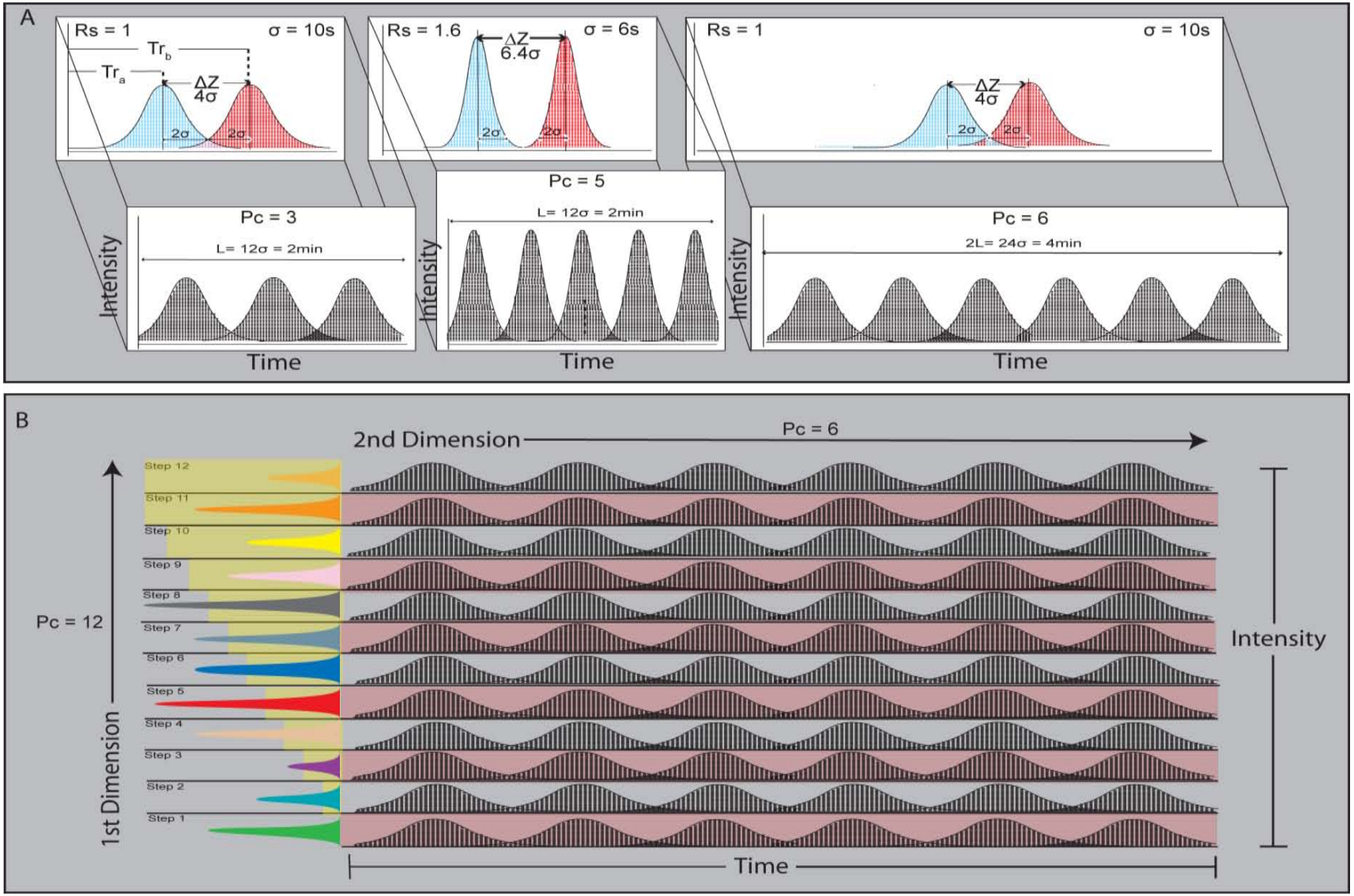
A
Rs = 1
σ = 10s
Tr_b
Tr_a
ΔZ
4σ
2σ
2σ
Rs = 1.6
σ = 6s
ΔZ
6.4σ
2σ
2σ
Rs = 1
σ = 10s
ΔZ
4σ
2σ
2σ
Pc = 3
L= 12σ = 2min
Intensity
Time
Pc = 5
L= 12σ = 2min
Intensity
Time
Pc = 6
2L= 24σ = 4min
Intensity
Time
B
2nd Dimension
Pc = 6
Step 12
Step 11
Step 10
Step 9
Step 8
Step 7
Step 6
Step 5
Step 4
Step 3
Step 2
Step 1
Pc = 12
1st Dimension
Intensity
Time

**Figure 3.4. Factors Defining Peak Capacity in Chromatographic Separations.** **A.** Peak capacity in single dimension chromatographic systems is defined by the number of components (i.e. peptides) than can be separated in a given separation space (in this case length = time = L). Peak capacity is a function of the length (L) divided by the resolution multiplied by the peak width (4σ). Resolution is calculated by taking the difference in retention times between two adjacent peaks (ΔZ = retention time of second peak ($Tr_b$) minus the retention time of the first peak ($Tr_a$)) and dividing by the sum of the half widths of each peak (2σ: sigma being a unit of time equal to 10 seconds in the left panel). In the left panel the baseline widths of each peak are uniform with each peak width equal to 4σ or 40s. Additionally, ΔZ, or the difference in retention time, is equal to 4σ and thus the resolution equals one (unit resolution). The separation space defined in this case by the length L in the left bottom panel is ~12σ or 2 minutes and thus the peak capacity of the example in the left panel is 3. A number of chromatographic properties can be altered to favor increased resolution including increasing the temperature and pressure of the mobile phase and decreasing the size and pore size of the chromatographic resin. The effects of increased resolution on peak capacity are exemplified in the middle panel. In the middle panel the peak width of each peptide has been reduced compared to the peak width observed in the left panel by altering one of the aforementioned chromatographic parameters (4σ now equal to 24s). By reducing the peak width, the ΔZ value relative to the peak width has now increased to 6.4σ or 38.4s and thus the resolution now equals 1.6. This increase in resolution leads to an increase in the peak capacity to 5 within the same 2 minute separation space. Peak capacity can also be increased by increasing the effective separation space or in this case length. If effective separation length can be achieved without a significant decrease in resolution, as can be achieved in certain types of chromatography, peak capacity can be increased as shown in the right panel. By doubling the effective separation space the peak capacity was also doubled (Pc = 6). **B.** Separation space can more effectively be increased by utilizing orthogonal separations in tandem. First, components (peptides) are separated utilizing a particular separation strategy that has a peak capacity of 12. Each of the components (peptides) from the first separation are then subject to another orthogonal (separation of components in the first dimension is retained in the second) separation strategy that further separates the components into additional components. This second separation strategy possesses a peak capacity of 6. The peak capacity of the two separation strategies utilized in tandem can now be calculated by taking the product of their individual peak capacities which in this case would be 72.

exists a multitude of configurations that employ unique separation chemistries in stand alone or tandem formats to enhance peptide detection. A complete review of the many HPLC configurations designed for proteomics applications is beyond the scope of this volume but can be found in the following excellent reviews [397,398]. HPLC strategies employing strong cation exchange (SCX) and reverse phase (RP) separation chemistries in tandem formats constitute the core of the most popular methodologies for shotgun based global proteomic profiling experiments and thus represent the mainstream class of global proteomics platforms. For our analysis, we chose to implement an on-line two dimensional SCX-RP HPLC based separation strategy.

The balance between high sensitivity, high peak capacity, and high resolution achievable utilizing capillary reverse phase HPLC on peptide mixtures

as well as the ease to which this separation can be coupled to mass spectrometric instrumentation through electrospray ionization (ESI) has made it a popular separation strategy for conducting global proteomic profiling experiments. Reverse phase peptide separations are often carried out utilizing micro capillary columns ranging in diameter from 50-100μm with varying lengths of 20-75cm. These small bore capillaries are densely packed with porous silica beads that are 5-10μm in size with pore sizes of ~300Å or greater and C18 surface coatings serving as the stationary phase chemistry. Initially, peptides are loaded onto the column dissolved in a predominately aqueous mobile phase environment that is continuously delivered through the column utilizing an HPLC pump at flow a rate ranging from 50-600ηl/min and pressures ranging from 500-1100psi. It is widely accepted that the water surrounding the dissolved peptides and the hydrophobic stationary phase must assume a highly structured lattice of unfavorable entropy [393]. The interaction of hydrophobic side chains present on peptides and the C18 stationary phase leads to a favorable increase in entropy for the system that leads to peptide retention on the column. Once bound, peptides are eluted differentially utilizing an organic solvent (typically acetonitrile) delivered by an HPLC pump that gradually increases the organic concentration of the mobile phase over time. As the organic concentration is increased, the increase in entropy associated with the peptides binding to the stationary phase C18 becomes minimized relative to the increase in entropy associated with the peptides interaction with the organic mobile phase. The mobile phase composition eventually reaches a critical organic phase concentration where it is entropically more favorable for the peptide to completely desorb back into the mobile phase and elute from the column. The organic phase concentration at which desorption occurs depends on the hydrophobic composition of each peptide and thus differential separation is achieved by exploiting the hydrophobic character of each peptide. The wide range of hydrophobicities present in peptide digests and the ability to implement capillary scale separations utilizing gradient elution under high pressures are the primary attributes of capillary reverse phase HPLC that contribute to its widespread success in providing sensitive separations

at high peak capacity. A more detailed and thorough treatment of separation theory by reverse phase chromatography can be found in the following volumes [399,393,400-402].

Initially, global proteomic profiling experiments were conducted utilizing one-dimensional capillary RP-HPLC, however due to the complexity of peptide mixtures generated from global proteome digests, the enhanced peak capacity achieved utilizing only one dimensional capillary RP- HPLC was insufficient to achieve comprehensive proteome coverage [403-405]. This insufficiency is best illustrated by computing the theoretical peak capacity of a one-dimensional RP-ESI-MS analysis. The peak capacity of a proteomics analysis platform is a product of the individual peak capacities of each orthogonal separation component. Separations are orthogonal if the resolution of the components in one dimension is retained and further enhanced in the second dimension [406]. In a typical one-dimensional RP-ESI-MS experiment the reverse phase chromatographic resin and the mass spectrometer can be considered as two orthogonal separations. Thus the peak capacity of the total proteomics platform is a product of the reverse phase separations peak capacity and the mass spectrometers peak capacity [393]. Assuming that the RP separation is performed utilizing a 90 min gradient run time and each peptide elutes over a 30 second time period ($30s = 4\sigma$) the ideal peak capacity at unit resolution ($R_s = 1$) of this one dimensional separation would be 180 (in this case 180 peptides could be resolved at unit resolution) using equation (1) for maximum peak capacity. The peak capacity of the mass spectrometer is determined by its duty cycle and the number of redundant peptide measurements that it is programmed to make. The duty cycle of a typical linear ion trap instrument is ~1s and commonly two redundant measurements are allowed, therefore the peak capacity of the mass spectrometer over a typical 30s chromatographic peak width is ~15 (in this case peptides). By multiplying the peak capacity of the reverse phase separation and the mass spectrometric analysis we arrive at a peak capacity of 2700 for a typical RP-ESI-MS proteomics analysis platform. Thus, even an ideal one dimensional

separation and analysis would only provide the peak capacity to analyze a fraction of the peptides present in a complex mixture.

In order to overcome the peak capacity limitations of one-dimensional separations, researchers have employed additional orthogonal separation stages prior to the RP-MS stage. For each additional, truly orthogonal, separation strategy employed, the peak capacity has the potential to increase by an order of magnitude. This concept is illustrated in (Figure 3.4 B) and is described here using 2D-gel electrophoresis as an example. In this separation, proteins are first separated by their pI using a pH gradient gel strip. This separation can be visualized with Coomassie stain which reveals that the proteins migrate in discrete zones along the gel (indicated as 12 peaks in Figure 3.4 B). Each zone can be comprised of multiple proteins but this cannot be confirmed visually utilizing only one dimension of separation. Application of a second orthogonal separation of the proteins by size reveals that each peak in fact consists of a myriad of proteins which can now be visually confirmed. The peak capacity of both separation strategies when employed together has now increased by an order of 12 which if multiplied by the peak capacity of our single reverse phase separation system results in a rise in peak capacity from 2,700 to 32,400. Most commonly, increases in peak capacity for global liquid chromatography based peptide separations are achieved utilizing an additional orthogonal peptide separation step prior to RP-ESI-MS. Among the many separation strategies available, peptide separation utilizing strong cation exchange (SCX) chromatography prior to RP-ESI-MS has become the most popular. Strong cation exchange (SCX) chromatographic separations, like reverse phase separations, are carried out in micro capillary columns densely packed with porous silica beads that are 5-10μm in size with pore sizes of ~300Å. However, SCX resins contain hydrophilic, anionic surface coatings (i.e. poly-(2-sulfoethyl aspartamide)) that retain peptides of net positive charge. Peptide retention is enhanced by loading peptide mixtures with a buffer at low pH (between 2 and 3) in order to insure that both aspartic and glutamic acid residues are neutralized and the net charge on the peptide is positive. Peptides can be eluted using a salt

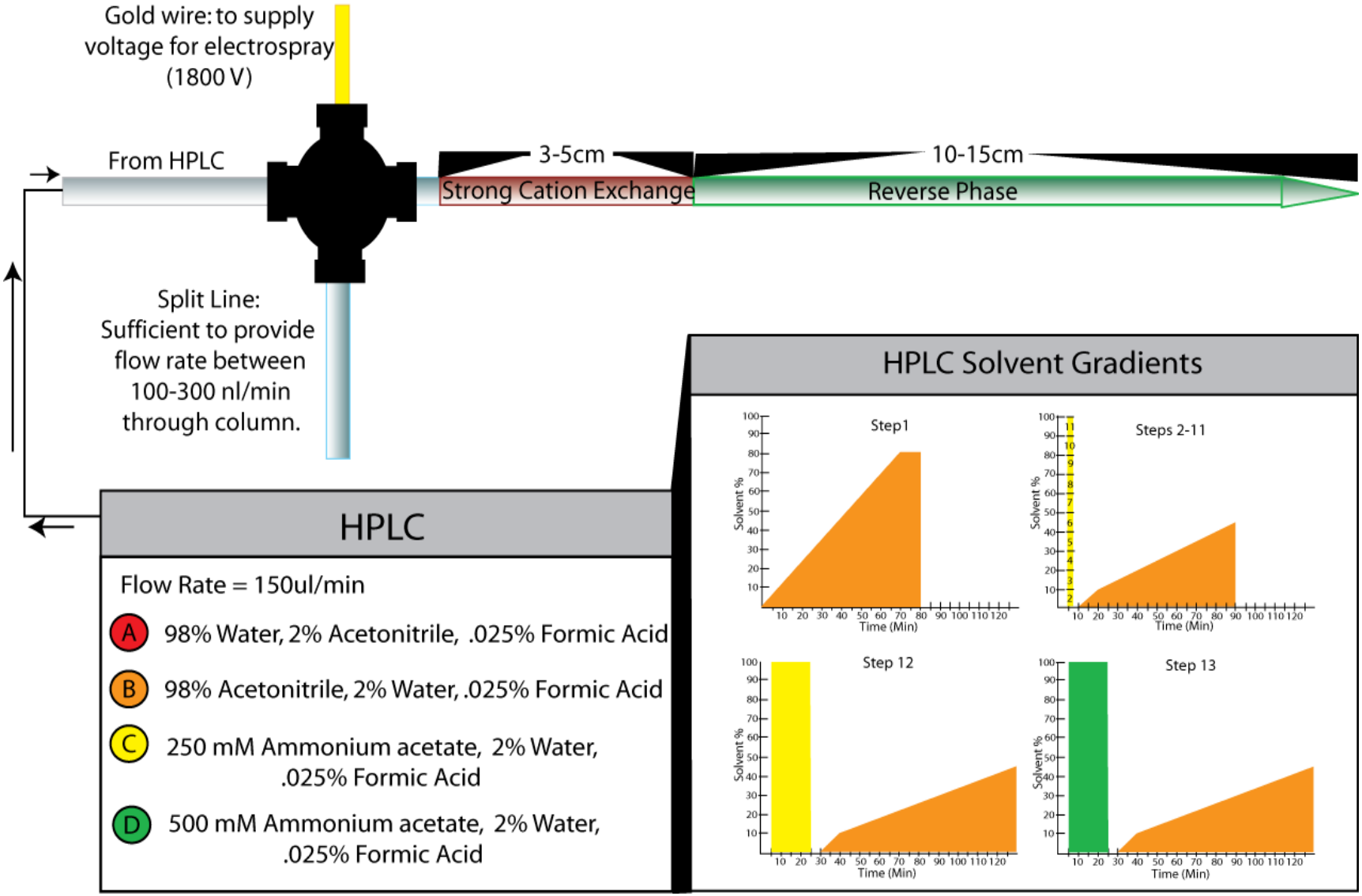
Gold wire: to supply voltage for electrospray (1800 V)
From HPLC
3-5cm
10-15cm
Strong Cation Exchange
Reverse Phase
Split Line: Sufficient to provide flow rate between 100-300 nl/min through column.
HPLC
Flow Rate = 150ul/min
A 98% Water, 2% Acetonitrile, .025% Formic Acid
B 98% Acetonitrile, 2% Water, .025% Formic Acid
C 250 mM Ammonium acetate, 2% Water, .025% Formic Acid
D 500 mM Ammonium acetate, 2% Water, .025% Formic Acid
HPLC Solvent Gradients
Step1
Steps 2-11
Step 12
Step 13
Solvent %
Time (Min)

**Figure 3.5. MudPIT (MultiDimensional Protein Identification Technology).** Increased chromatographic peak capacity to facilitate more comprehensive proteomic coverage is achieved utilizing orthogonal Strong Cation Exchange (SCX) and Reverse Phase (RP) separations juxtaposed in a single 50-100um i.d.. capillary. Initially, peptides are loaded onto the first 3-5cm of SCX packing utilizing mobile phase solvent A. Positively charged peptides are retained through ionic interactions with the negatively charged stationary phase (Polysulfoethyl A). During loading, a certain population of uncharged peptides will pass through the SCX packing and be retained by the RP packing through favorable hydrophobic interactions with the C18 stationary phase. This population of peptides is separated first utilizing a 70 minute acetonitrile gradient (Solvent B, Step1) and peptides are analyzed as they elute from the column using ESI-MS (Electrospray Ionization Mass Spectrometry). Populations of peptides are then eluted from the SCX packing based on their charge (peptides with less charge elute earlier) in a stepwise fashion onto the RP packing utilizing increasing salt (ammonium acetate) concentrations (Solvent C, Steps 2-11 and 12 yellow) (Solvent D, Step 13 green). Peptide populations eluted onto the RP packing after each salt step are then immediately separated and analyzed by acetonitrile gradient elution and ESI-MS (Steps 2-11, 12, and 13 orange).

(i.e. ammonium formate) gradient but are typically eluted using sequential isocratic (step-wise) elutions of increasing salt concentration. As the salt concentration increases peptides of greater net positive charge (acidic) are eluted from the column and thus, SCX chromatography separates peptides loosely by their inherent pIs with basic peptides eluting earlier than acidic. SCX chemistries are typically employed prior to reverse phase separations due to their superior binding capacity (~4 times greater than reverse phase resins) and can be integrated seamlessly with downstream reverse phase separations because peptide retention on either column is not affected by the elution buffers utilized in the other separation. These attributes led to the development of the popular two dimensional peptide separation strategy termed MudPIT (Multidimensional Protein Identification Technology) [407-409]. A version of this technology was utilized for our analysis and thus will be described further to illustrate the theory behind the peptide separation approach we employed.

The MudPIT separation strategy is schematically represented in (Figure 3.5). At the core of this technology is the separation column which consists of a 50-100µm diameter fused silica capillary possessing a hand pulled tip. This capillary is first packed with 15cm of C18 reverse phase resin followed by 3 -5cm of polysulfoethyl aspartamide SCX resin. The tandem juxtaposition of the two separation resins eliminates dead volumes that can greatly increase separation times and sample loss. Initially, the peptide sample, suspended in a low pH

buffer (~pH 2-3) is loaded directly onto the SCX resin phase of the column. During this initial sample loading stage, a large number of peptides with net positive charge are retained on the SCX phase while a small number of neutral or basic peptides slip through and are retained on the reverse phase column. Immediately after loading, a 90 minute reverse phase gradient from 5 to 50% acetonitrile is conducted to elute and analyze this fraction of peptides. Following the initial reverse phase separation, a pulse of 4mM ammonium formate is delivered across the column to elute the next fraction of peptides onto the reverse phase resin; another 90 minute gradient is run. This cycle proceeds for 12 steps consisting of 0, 4, 8, 12, 15, 18, 21, 25, 50, 100mM and finally two, 1M ammonium formate pulses. The application of MudPIT to global peptide separations has been reported to have a conservative theoretical peak capacity of 23,000 using an LCQ Deca [407,408] and would be at least 2 times higher if not more using the faster scanning LTQ for a peak capacity of 46,000.

### 3.11.3. Stage 3: Electrospray Ionization and Mass Spectrometry

Throughout each reverse phase separation, peptide ions eluting from the tip of the chromatographic column are immediately ionized using electrospray ionization. This ionization procedure utilizes a high voltage potential (~3 kV) between the tip of the chromatographic column and the capillary orifice of the mass spectrometer to release peptide ions from the mobile phase into the gas phase. This step is absolutely necessary for peptide ions to be amenable to mass spectrometric analysis and remained one of the last barriers preventing the application of mass spectrometry to large biomolecules until John Fenn and colleagues developed the procedure [410]; a feat for which he earned the Nobel prize in chemistry [411,412]. The mechanism by which peptides are liberated from the mobile phase solvent utilizing electrospray ionization is reviewed in the following volumes [411,413-415] and briefly described here.

In order to promote protonation of peptides the mobile phase normally contains a small amount of organic acid (0.0025%) and thus the mobile phase/peptide solution contains an excess of positive charge. As the

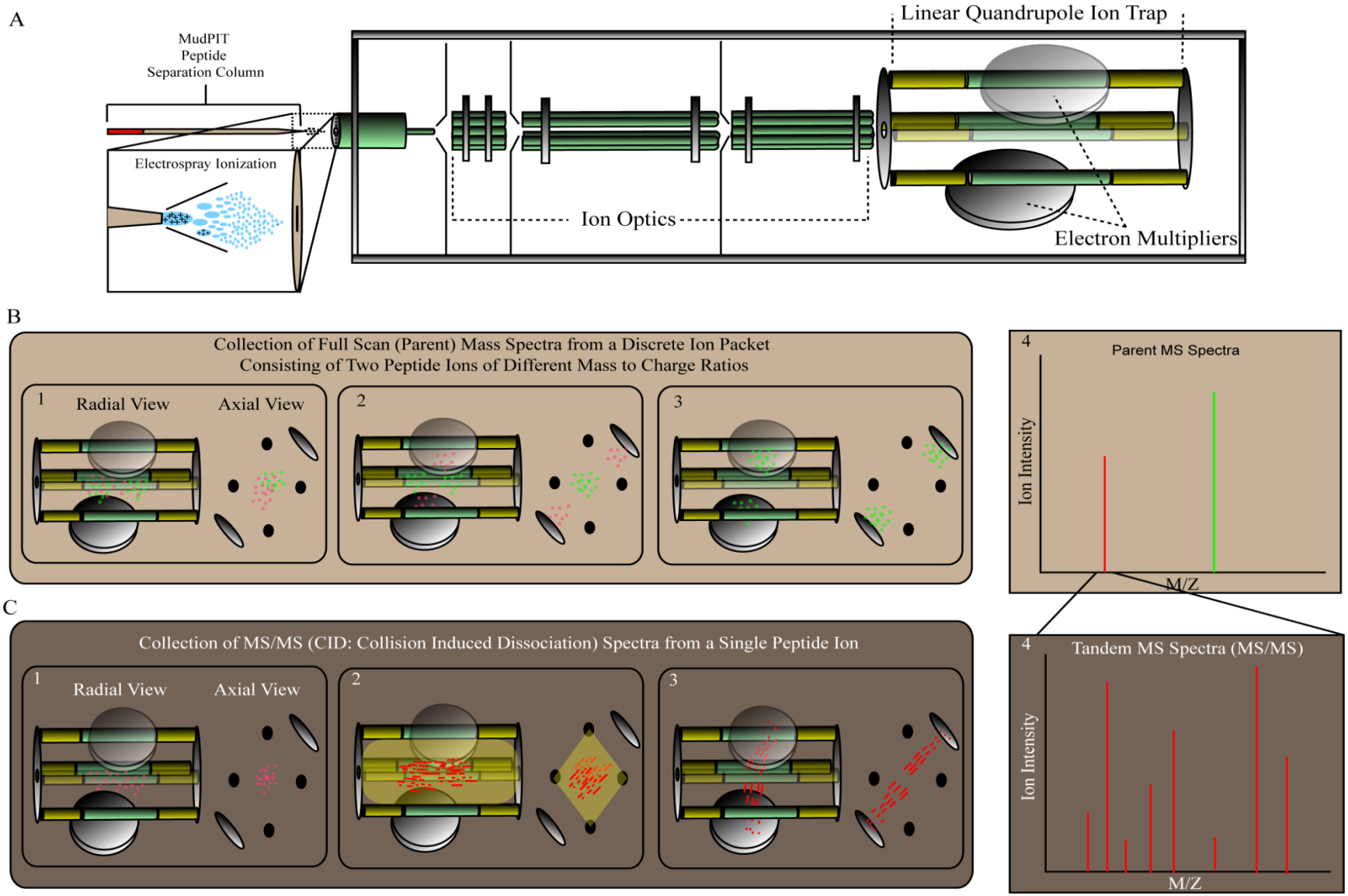
A
MudPIT
Peptide
Separation Column
Electrospray Ionization
Linear Quandrupole Ion Trap
Ion Optics
Electron Multipliers
B
Collection of Full Scan (Parent) Mass Spectra from a Discrete Ion Packet
Consisting of Two Peptide Ions of Different Mass to Charge Ratios
1
Radial View
Axial View
2
3
4
Parent MS Spectra
Ion Intensity
M/Z
C
Collection of MS/MS (CID: Collision Induced Dissociation) Spectra from a Single Peptide Ion
1
Radial View
Axial View
2
3
4
Tandem MS Spectra (MS/MS)
Ion Intensity
M/Z

**Figure 3.6. Overview of Mass Spectrometric Analysis Utilizing the Thermo Finnigan™ LTQ Linear Quadrupole Ion Trap (LTQ).** **A.** As peptides elute from the MudPIT column they are exposed to an electric field which promotes their conversion from liquid phase ions to gas phase ions. This process is known as electrospray ionization. These gas phase peptide ions enter into a heated capillary and are then guided through a series of ion optics into the linear quadrupole ion trap. **B. 1.** A discrete packet of ions of a specific mass to charge ratio range is trapped in the ion trap in a dynamic state of axial and radial motion between the quadrupoles of the trap through the combined application of direct-current (DC) and radio frequency (RF) fields. **B. 2 and 3.** Once trapped, the magnitude of the radio frequency amplitude and direct current voltage is ramped at a fixed ratio to eject peptide ions sequentially, based on their mass to charge ratio, towards the electron multipliers. The radio frequency and direct current ratio at which a particular peptide becomes unstable in the trap and hits the electron multiplier is utilized to determine the mass to charge ratio of the ion. The abundance of that ion in the trap is determined by the extent of the electric current produced from the ion populations bombardment of the electron multiplier. **B. 4.** The final output of the mass spectrometer is a two dimensional graph with the m/z ratio plotted on the x-axis and the ion intensity plotted on the y-axis. This is known as a parent ion mass spectrum. **C. 1.** If the abundance of the ion is larger than a pre-defined cutoff, the computerized control system will set the ratio of the RF and DC fields in the quadrupole trap to only allow for stability of that ion in the trap. Thus, the next packet of ions entering the trap will be effectively filtered to isolate only the peptide ion of interest. In terms of sequence, if multiple different ions are present in abundance above the cutoff, the most abundant ion will be isolated first and the remaining ions will be isolated in subsequent cycles of the trap. **C. 2.** Once isolated, the peptide ion is electrically accelerated in the presence of an inert gas such as argon. The accelerated ion collides with the argon molecules which leads to what is known as collision induced dissociation of the ion into ion fragments. **C. 3.** These ion fragments are then scanned as in the collection of the parent mass spectrum and their m/z ratios as well as their abundance are collected. **C. 4.** The final output of the mass spectrometer is a two dimensional graph with the m/z ratio plotted on the x-axis and the ion intensity plotted on the y-axis. This is known as the tandem mass spectrum or MS/MS spectrum. The pattern of a MS/MS spectrum is specific to the peptide ion sequence and can be utilized to determine the identity of the peptide by searching the MS/MS spectra against a library of theoretical MS/MS spectra generated computationally utilizing a protein sequence database.

peptide/mobile phase solution elutes from the capillary tip it is immediately exposed to the electric field and, due to the excess positive charge of the mobile phase/peptide solvent droplet, is pulled towards the lower potential mass spectrometer entrance orifice. As the peptide/mobile phase solvent droplet traverses toward the heated mass spectrometer capillary orifice, the thermal energy as well as the electric field promote solvent evaporation and the solvent droplet reduces in size. However, since ions are relatively involatile, the ions are retained in the droplet. The reduction in droplet size and the retention of positive ions within the droplet leads to an increase in charge density until the repulsive forces between the positive ions become greater than the cohesive forces acting to keep the solvent molecules together (known as the Rayleigh limit). Once the Rayleigh limit is reached, the solvent droplet begins to release peptide ions into

the gas phase. Peptide ions produced from electrospray ionization can possess multiple charges and peptides of +1, +2, +3 and even +4 charge are possible.

Peptides are continuously ionized by electrospray ionization during the course of each reverse phase separation and are analyzed “on the fly” utilizing mass spectrometry. Numerous mass spectrometers employing technologies in various formats exist and each possesses its own subset of characteristics that make it amenable for specialized applications (for review see [415,414]). The robustness and relatively fast scan rate of the linear ion trap mass spectrometer makes it particularly amenable to global shotgun based proteomic analyses. This type of instrument was utilized in our analysis and a basic schematic of the Thermo Finnigan™ LTQ linear ion trap that we utilized is depicted in Figure 3.6 A. An LTQ mass spectrometer is a complicated instrument consisting of a multitude of parts including pumping systems, electronic circuit boards, system gauges, and computer interfaces. Therefore, a thorough description of each of these systems is beyond the scope of this volume. However, the instrument can be broken down into three basic parts; the ion optics, the mass analyzer (in this case the linear quadrupole ion trap), and the detector (in this case the electron multiplier). In the following section, I will describe the processes that each of these parts facilitate in order to convey at a conceptual level how the mass spectrometer manipulates ions in order to measure their abundances and mass to charge ratios and to determine their identities.

Ionized peptides enter the mass spectrometer through a heated capillary tube which guides the peptides to a series of ion optics. The type and configuration of ion optics vary between mass spectrometers but in most instances serve to focus, accelerate, or de-accelerate the ion stream before the ions are subjected to analysis in the mass analyzer. The mass analyzer in this instance is the linear quadrupole ion trap which is comprised of four parallel rods spaced equidistant to form a hyperbolic cross section. In the Thermo Finnigan™ LTQ pictured in Figure 3.6 A, these four parallel rods are electrically and physically divided into three sections. The end sections (shown in yellow) are connected to a static DC voltage supply which is dynamically switched to gate

the ion stream from the ion optics into the central section of the mass analyzer (shown in green) and to trap ions within the centralized quadrupole region. Each pair of diagonal rods of the central quadrupole are connected together electrically and to RF and DC voltage sources and thus each pair of diagonal rods is oscillating between negative and positive polarity 180° out of phase. By modulating the amplitude of the RF and DC voltages at a fixed ratio, ions can be selectively trapped or excited out of the trap radially based on their mass to charge ratio. Ions that have been selectively excited from the trap hit either of the electron multipliers that are positioned perpendicular to the longitudinal axis of the linear ion trap. The collision of an emitted ion with the electron multiplier causes a chain reaction of electronic events that ultimately measure the presence and abundance of the emitted ion. Finally, the mass to charge ratio of the ion is determined by the RF amplitude at which the ion was ejected from the trap and hit the electron multiplier.

Throughout the course of the chromatographic separation peptides are continuously being ionized and injected in to the entrance of the mass spectrometer. However, it is important to emphasize that peptide ion analysis in the mass analyzer is not continuous but cyclic. Additionally, two types of cycles are carried out by the mass analyzer in order to facilitate ion detection (full scan or MS cycle) and to collect measurements to determine the identity of the peptide ion (product ion or MS/MS cycle). During the full scan analysis, peptide ions are accelerated into the linear ion trap by the ion optics for a specified amount of time. Once this time has been reached (trapping time), the end quadrupoles positive DC voltage is activated to trap the injected ions in the central quadrupole. Additionally, the amplitude of the central quadrupole's RF frequency is set to selectively stabilize all ions present in the trap (Figure 3.6 B panel 1). Once trapped the ions are in a dynamic state of motion; oscillating axially and radially but within the confines of the quadrupole trap. Each ion is then sequentially de-stabilized and emitted radially to the electron multiplier by linearly increasing the amplitude of the RF frequency but at a constant RF:DC ratio (Figure 3.6 B, panels 2 and 3). Peptide ions of smaller m/z ratio are emitted from

the mass analyzer first. This produces a single full MS parent scan which is represented on a graph with m/z on the x-axis and ion abundance (intensity) on the y-axis (Figure 3.6 B panel 4). These scans are collected continuously throughout the course of a given chromatographic separation.

If an ion is present in the full scan analysis at an abundance above a manually defined preset threshold, the mass spectrometer will perform two MS/MS (tandem MS) cycles on the selected ion (aka parent ion). (Note: The number of MS/MS cycles performed on a given ion (level of redundancy) is manually defined and subject to individual operator discretion.) Immediately following the acquisition of the full or “parent” ion spectrum, the end quadrupoles of the mass analyzer once again open to allow injection of a new packet of ions. However, the central quadrupole is now set to allow only the selected ion from the “parent” spectrum to be trapped and thus the linear ion trap fills with only the selected ion (Figure 3.6 C panel 1). Once filled, the selected ion is cooled or in other words the dynamic motion of the ion in the trap is slowed in preparation for fragmentation of the ion and a neutral gas is injected into the trap (Figure 3.6 C panel 2, yellow). Fragmentation or collision induced dissociation of the ion is achieved by heating the ion in the radial direction through application of a resonance excitation voltage to all rod sections on the x-axis of the quadrupoles. This excitation causes the parent ion to dissociate into fragments as it collides with the inert gas within the trap (Figure 3.6 C panel 2, yellow). These fragments are then selectively emitted from the trap as was described for the full scan MS analysis and detected (Figure 3.6 C panel 3). This scan produces what is known as an MS/MS (tandem MS) spectrum or peptide mass fingerprint (Figure 3.6 C panel 4) which can be utilized to identify the amino acid sequence of the peptide (Section *3.11.4.1*). As indicated above, two of these spectra are collected for each ion of sufficient abundance. After two MS/MS spectra have been collected, the parent ion is placed on an exclusion list for 2 minutes to prevent further analysis of the same parent ion.

### 3.11.4. Data Analysis and Validation

A brief overview of the data generated from each of the individual analyses conducted comparing *grr1Δ* to wild-type yeast as well as the software analysis pipeline utilized to process these data is shown in Figure 3.1 D. In order to provide a tangible assessment of the comprehensiveness and efficiency of our analysis, to describe the details of this analysis pipeline, and to describe the data analysis stages that we utilized to generate our final quantified list of proteins, I will briefly describe each of these stages and the specific tasks that each of the algorithms perform.

#### *3.11.4.1. Peptide Identification Utilizing SEQUEST™*

The first stage of data analysis requires the assignment of each tandem MS file and its respective parent ion to the correct peptide and thus the correct protein. Manual assignment of peptides to tandem mass spectra remains the most accurate method for assigning peptide identities but is tedious and time consuming and the vast number of MS and MS/MS files generated by our analysis required that a robust and accurate automated system be employed. Though multiple algorithms exist which will perform this process, we chose to utilize SEQUEST™ (Thermo Finnigan™, the manufacturer of the LTQ mass spectrometer that we utilized for data acquisition). SEQUEST™ employs a four step process to match experimentally acquired tandem MS spectra with their respective peptides. However, before these steps can be performed a protein sequence database must be available for theoretical generation of tandem MS files. The details of SEQUEST™ analytical capabilities have been eloquently described in the following papers [416] and will be briefly reviewed here.

The most popular search algorithm for peptide assignment from data generated from trap instruments, SEQUEST™ uses a correlation algorithm to match experimentally derived tandem mass spectra to the appropriate theoretically derived spectra; a process termed descriptive modeling [417]. Algorithms that employ descriptive models generate theoretical tandem MS files from a specified protein sequence database. In our case, a hand annotated

*Saccharomyces* protein sequence database was constructed utilizing the unaltered sequence database obtained through SGD (*Saccharomyces* Genome Database*)* by consolidating redundant protein sequences and removing some manually assessed dubious ORFs.

Theoretical tandem MS spectra were generated from this database *in-silico* utilizing the SEQUEST™ algorithm by first generating a theoretical tryptic digestion of all protein sequences, allowing for two mis-cleavage events. Additionally, at this stage, parameters specific to an experimental method are also specified when generating the theoretical peptide tandem MS database. The molecular mass of each of the hundreds of thousands of peptides generated is calculated for each of the three probable charge states (+1,+2, and +3) that may exist for each peptide during the experimental analysis. This calculation also includes any user specified parameters specific to the experiment that would influence the peptides mass. For instance, we utilized a 6-$C^{13}$-leucine label to distinguish between peptides derived from wild-type and *grr1Δ* strains. Thus, when generating the peptide database, additional peptide tandem MS files with this mass shift incorporated were also generated for every peptide containing a leucine residue to enable assignment of peptides derived from the wild-type strain. In addition, static carboxyamidomethylation of cysteine and dynamic carboxyamidomethylation of methionine residues is also specified. These modifications occur as a result of the iodoacetamide treatment of the peptides prior to analysis. Iodoacetamide, as discussed in Section *3.11.2.2*, is an alkylating agent used to prevent disulfide bond formation at cysteine residues; however, this compound can also randomly modify methionine residues as well. The molecular mass of peptides containing a single modified version of these residues increases by ~57 Daltons.

Once the experiment specific peptide database has been generated, SEQUEST™ proceeds by processing the tandem MS files into a more usable form that accelerates database searching. First, replicate tandem MS spectra are consolidated into one final higher quality tandem MS spectra for a given parent ion. The LTQ was configured during all of our analyses to collect replicate

tandem MS files for every parent ion that was selected for collision induced dissociation. Consolidation of these replicate measures increases the quality of the tandem MS spectra for a given parent ion since aberrations that may occur in the first collision reaction event may be reconciled by the second. After these replicate measures are consolidated the tandem MS spectra is reduced. This reduction step removes all fragment ion signals except the 200 most abundant for a given spectra. These 200 remaining fragment ion signals are then normalized to 100 and rounded to the nearest integer. A number of additional processing steps are also implemented in order to reduce the complexity of the tandem MS spectra and facilitate more expedient database searching. After these two processing steps are conducted SEQUEST™ generates files known as DTA files that contain the consolidated and reduced tandem MS spectra information. As can be seen in Figure 3.1 the number of DTA files produced by this processing step is, as expected, approximately one half of the number of tandem MS files collected.

After the DTA files are generated, the SEQUEST™ algorithm then sequentially searches the peptide database for peptides with masses (taking into account possible charge states as well) that match the experimentally acquired parent ion mass within a user specified mass tolerance. This tolerance is typically set between ± 0.05% and was the tolerance utilized in our analyses. All peptides with masses falling within this tolerance are then processed to produce theoretical tandem MS spectra using an algorithm based on empirical knowledge of peptides fragmentation during collision induced dissociation. These theoretical tandem MS spectra are then scored ($\mathrm{Sp}$) utilizing the following formula taken from [418].

$$\mathrm{Sp} = \left(\sum \mathrm{i_m}\right) \mathrm{n_i}(1+\beta)(1+\rho)/\mathrm{n_t} \qquad [3]$$

where ($n_i$) is the number of theoretical fragment ions matching within ± 1 amu of the experimentally acquired fragments, ($i_m$) is the abundances of these ions, (β)

is a 0.075 increment rewarded for every ion consecutive fragment ion matched, (ρ) is a 0.15 increment rewarded for every immonium ion matched between spectra, and ($n_t$) is the total number of predicted ions. Examination of this equation illustrates the specific characteristics of tandem MS spectra that are deemed to be important when determining the spectral match utilizing SEQUEST™. SEQUEST™ reports the *Sp* score and the *Sp* rank for each theoretical tandem MS spectra matched to a given experimental spectra.

The $S_p$ score provides an initial measure of the validity of a given spectral match. It was found that a number of experimentally acquired tandem MS spectra are not matched to the correct peptide because the correct theoretical tandem MS spectra do not produce the highest $S_p$ score in a list of possible matches. Therefore SEQUEST™ employs a cross correlation algorithm to further assess the top 500 theoretical tandem MS spectra matching a given experimental tandem MS spectra. The cross-correlation process utilized by SEQUEST™ is described in the following references [419,417] and is briefly summarized here. During collision induced dissociation, peptides fragment primarily along the peptide backbone to produce ions of a b and y ion distinction (For review see [420,375,421]). The b-and y- ions for the theoretical spectra are first generated with each of the primary ion series products assigned an intensity of 50. Any ions within a 1 amu mass window of these main fragments is assigned an abundance of 25 while the predicted water and ammonia ions are assigned an abundance value of 10. The theoretical and experimental tandem mass spectra are then cross-correlated using the following algorithm:

$$R_t = \sum_{i=0}^{n-1} x[i]y[i+\tau] \quad [4]$$

In essence, this algorithm measures the coherence of the experimental x[i] and theoretical y[i] discrete Fourier transforms utilizing fast Fourier transformation which superimposes the two functions across multiple displacement values (τ)

ranging from -75 -75. A positive match has the highest correlation score at zero displacement and the final score (known as Xcorr) is calculated by subtracting the mean correlation value from all displacements from the 0 displacement value [418,416]. This Xcorr value is also reported by SEQUEST™ and Xcorr cutoffs that are charge state specific are commonly utilized to filter positive identifications from less reliable matches. It is worth noting that the Xcorr value is database size independent and thus reflects the quality of the spectral match.

Another value of significance when assessing data validity generated from SEQUEST™ is the ΔCn value. A Cn value is calculated by normalizing the Xcorr value to 1 for a given spectral match. The difference of the Cn values from each theoretical spectral match to the next best theoretical spectral match for a given experimental spectra are calculated and reported as ΔCn. Thus, the ΔCn of the highest ranking spectral match can be used as an indication of its uniqueness in the database. The more unique (or greater the ΔCn) the match is, the greater the confidence that the experimental spectra is assigned to the correct theoretical spectra and the correct peptide.

*3.11.4.2. Statistical Analysis of SEQUEST Results using the Trans Proteomic Pipeline*

The accurate assignment of experimentally acquired tandem mass spectra (MS/MS) to the correct peptide and thus the correct protein is critical if the results of an LC-MS based experiment are to be valid. This necessitates the need for an automated analysis system that is both robust and accurate. The SEQUEST™ algorithm has been used extensively in global proteomics studies and has proven to be robust and is highly automated [419,417]. However, SEQUEST™, not unlike any other peptide identification software, reports multiple scoring parameters (i.e. Xcorr, Sp, RSP, and ΔCn) that individually assess a given attribute of the quality of the spectral match. Additionally, scores are biased by MS/MS quality, peptide mass, and charge state [332]. Thus, we sought to employ an additional layer of data evaluation that would serve to assess these

individual scores and derive an unbiased unified scoring parameter that we could use to assess the validity of our data systematically.

There are multiple data analysis algorithms available that will increase or assess the validity of peptide matches generated from SEQUEST™ including LIP (Logistic Identification of Peptides)[4], AMASS (Advanced Mass Spectrum Screener)[5], QSCORE [6], SEQUEST-NORM [7], and many more [8-12]. However, since we required programs that could facilitate relative peptide quantification as well as validate peptide search results we were drawn to utilize an analysis pipeline known as the TPP (Trans Proteomic Pipeline). The TPP, available as open source software from the Institute for Systems Biology (http://tools.proteomecenter.org/software.php), is a suite of software that was developed to provide a systematic analysis pipeline for global quantitative proteomic studies. Briefly, SEQUEST™ results for each peptide match are first analyzed by PeptideProphet™ which utilizes discriminate function analysis to combine the multiple scores generated by SEQUEST™ into a single unified probability that is based off of machine learning techniques from training data sets [332]. Peptide probabilities generated by PeptideProphet™ are then transferred into the program ProteinProphet™ which calculates a unified probability that a protein was successfully identified based on the probabilities of its representative peptides [333]. Finally, relative quantification is facilitated by ASAPRatio™ which utilizes rigorous numerical and statistical tests to assess peptide abundance ratios and their associated errors. Peptide ratios from peptides derived from the same protein are then weighted by their error and a protein abundance ratio is calculated using statistical methods for weighted samples [334].

In practice, SEQUEST™ can be utilized independently of the TPP (Trans Proteomic Pipeline) or within the TPP software pipeline. In order to process ".RAW" files produced by Xcaliber (the software package utilized to run and process mass spectrometric results generated from Thermo Finnigan mass spectrometers) through the TPP, these files must first be converted to what is known as the mzXML format by a program known as ReAdW (available from

http://tools.proteomecenter.org/wiki/index.php?title=Software:ReAdW) . The mzXML format was developed by the Seattle Proteome Center (SPC) at the Institute for Systems Biology to provide an open source file format for transfer and storage of mass spectrometry based proteomic data [422]. Like ReAdW, a number of file converters are available for many of the most popular instruments utilized for proteomic data analysis including, mzWiff (Analyst by ABI/MDS Sciex), massWolf (Water Masslynx), and trapper (Agilent MassHunter). Additionally, mzXML files can be viewed utilizing Pep3D (bundled with the TPP) which produces a graphical 2D gel type image that can be utilized for evaluating chromatographic separation efficiency and for interfacing with CID data and peptide probability information. It is important to note that the SPC's mzXML data format and the exclusive mzData format of the Proteomics Standards Initiative are in the process of consolidation, creating a new mzML format established by the HUPO Proteomics Standards Initiative (http://psidev.info/index.php?q=node/257) with participation by the ISB.

*3.11.4.3. Peptide Prophet*

Once the ".Raw" files are converted to mzXML they are processed utilizing SEQUEST™ within the TPP and passed to the PeptideProphet ™ algorithm. A thorough treatment of the statistical theories employed by this algorithm can be found in the following reference [332]. However, I will provide a brief, albeit surface level, review of the algorithm in order to convey some understanding of the process. Peptide Prophet™ was developed utilizing experimentally acquired data sets acquired from 22 LC/MS/MS runs on a sample of 18 purified and trypsinized proteins. These data sets were utilized to create training data sets where the attributes (SEQUEST™ scores) of known correct and incorrect spectral assignments could be defined. From these defined attributes, a discriminate function can be derived that can be utilized to combine the multiple scores generated by SEQUEST™ into a single discriminate score. Bayes law can then be applied to calculate the probability that a given peptide assignment is correct. This algorithm adjusts for changes in scores attributable

to charge state and peptide length. The algorithm also can be utilized to calculate peptide probabilities from data sets generated not utilizing enzymatic constraints on peptide identifications. For example, an unconstrained search is sometimes utilized to identify non-tryptic peptides in an experiment where trypsin was utilized. Additionally, error and sensitivity values are calculated across all probabilities in order to provide a means for users to specify a peptide acceptance cutoff. In short, PeptideProphet™ generates a single unified probability for each peptide assignment indicating the confidence of the spectral match. Error and sensitivity cutoffs are then applied to generate a user specified list of high confidence assignments. Thus, PeptideProphet™ provides a robust, fast, efficient, and unbiased means to filter peptide assignments generated by the SEQUEST™ algorithm.

*3.11.4.4. Protein Prophet*

The statistical results generated by PeptideProphet™ for each peptide of a given protein are then utilized by another algorithm named ProteinProphet™ to calculate a unified protein probability. The statistical theorems utilized by ProteinProphet™ have been described previously [333]. Using Bayesian statistics, ProteinProphet™ utilizes the highest probability of each unique peptide assignment for a given protein to calculate the probability that the protein was identified. Unique peptides are defined as those identified with distinctive amino acid sequence or charge state. This algorithm adjusts, in a data set specific manner, peptide probabilities obtained from PeptideProphet™ to account for the fact that the probability that a given peptide is correct is increased by the number of “sibling” peptides identified. This parameter, termed NSP (for Number of Sibling Peptides) is calculated by summing the individual probabilities of each distinct correct peptide assignment for a given “multi-hit” protein. Thus, peptides of “multi-hit” proteins have increased confidence adjusted according to the probabilities of its “sibling” peptides. De-generate peptides or peptide sequences identified that occur in multiple proteins are also accounted for and protein probabilities are adjusted accordingly. The final output of the ProteinProphet™

analysis for each protein is a final probability that a particular protein was identified correctly based on the individual probabilities of its peptides. Error and sensitivity data across all probabilities is also provided to allow user defined probability cutoffs to be assessed and applied.

*3.11.4.5. Determination of Peptide and Protein Relative Abundance Using ASAPratio*

The calculation of relative abundance ratios for peptides and proteins is facilitated in the TPP by an algorithm called ASAPratio™ (Automated Statistical Analysis of Protein ratios). The relative abundance of peptides labeled by a wide variety of chemical, enzymatic, or metabolic means can be determined utilizing this algorithm. The details of the calculations performed by ASAPratio™ have been described previously [334]. First, a single ion chromatogram is constructed across the entire elution time by summing the intensities of the first three isotopic peaks of the parent ion for a given tandem MS spectra (peptide). This process is repeated for the calculated labeled peptide pair as well as all charge states identified for each peptide. The chromatograms are then smoothed utilizing the Savitzky-Golay method and background noise is estimated based on the average of the signals measured outside the elution peak. A peak is accepted if the centered intensity is two fold higher than the background noise. If a peak is not accepted it is given a value of 0 however, the respective peptide partner is not excluded from measurement based on this assignment. In the cases where only one peptide of a pair is measured the final abundance ratio output is either 0 or 999 depending on which was quantified and which sample was set to be the numerator of the ratio (in our analysis a ratio of 0 would indicate that only the wild-type peptide was quantitated while a ratio of 999 would indicate the quantification of only the peptide derived from *grr1Δ)*. Peptide ratio abundance errors are calculated based on the difference in area between the raw and smoothed chromatograms. This algorithm additionally accounts for the identification of multiple charge states and the phenomena that a peptide is often found at different retention times and sometimes in different reverse phase

fractions during two dimensional analyses. Dixon's test is applied in these cases to omit outliers where three or more abundance ratios exist for the same peptide. The result of this analysis is the generation of a final weighted abundance ratio with a calculated error for every peptide identified and quantitated. The peptide abundance ratios corresponding to a given protein are then weighted by their errors and a final protein abundance measure with standard deviation is then calculated using statistical methods for weighted samples. P values are generated for each protein whose relative abundance was measured and provide a statistical means to evaluate significant abundance changes between samples.

*3.11.4.6. Generation of a Final Combined Protein Probability and Relative Abundance Ratio Utilizing Data Collected from All Analyses*

Though the TPP was designed to allow individual analyses to be combined and analyzed, we failed to get ten, twelve step, two dimensional, LC MS analyses through the pipeline simultaneously, presumably due to insufficient computational power. We therefore sought to combine the results from each analysis into a single high quality protein list using a multi-step processing scheme derived from algorithms utilized within the TPP computing architecture. Utilizing this processing scheme a final protein probability based off of the individual protein probabilities assessed in each analysis is calculated for every protein identified. Additionally, a unified relative abundance ratio with error analysis is also determined. The details of the processing steps utilized to generate these final scores are explained in the following section.

Since some proteins are identified in multiple analyses, the reliability and accuracy of multiple probability measures can be improved by combining the probability measures from each analysis. If a protein is identified by *k* analyses, labeled $r_1, r_2, \ldots r_k$, then the summarized probability is calculated as:

$$P_{id} = 1 - \prod_{i=1}^{k} (1 - P_{ri})$$

[5]

Where $P_{ri}$ is the probability measure from analysis $r_i$. Thus, utilizing this calculation, a protein identified in two separate analyses at 0.5 protein probability would have a final probability of 0.85. We deemed that a protein possessing a combined protein probability of 0.9 was successfully identified and valid. For example, using this cutoff for multiply sampled proteins this list, for example, would capture proteins whose confidence was assessed at 0.69 at least twice, at 0.6 at least three times, 0.5 at least four times, and 0.4 at least six times.

*3.11.4.7. Calculation of Combined Adjusted Ratio Means and Standard Errors*

We next wanted to combine the individual relative abundance ratios as well as their errors from each analysis into a single highly confident relative abundance measure for each protein. However, the confidence of the relative abundance ratio is determined by multiple factors and though the final calculation is relatively straightforward, consideration of all parameters contributing to its validity is not. First, a protein may be identified across multiple analyses at varying probabilities and it is possible for the relative abundance ratio to be derived from a low confidence protein identity despite the fact that the final protein probability is quite high. Second, though the extent of our analyses was quite substantial there still remain a number of proteins quantified by only a single peptide. Though these relative abundance ratios are deemed to be accurate for the single peptide, it is more difficult to assess the protein abundance ratio since multiple peptides ratios cannot be utilized for the calculation. Additionally, differential post-translational modifications occurring on a quantified peptide can create significant peptide abundance ratio changes that, if not accounted for, can be misinterpreted as protein abundance changes. In actuality, single peptide derived relative abundance ratios can be indicative of protein abundance changes or a change in the post-translational state of the peptide and nevertheless could represent significant biological changes attributable to the studied perturbation. Third, the error of the relative abundance

ratios within analyses as well as between multiple analyses must be assessed if a high confidence list of quantified proteins is to be constructed.

In order to construct a list of quantified proteins with tangible confidence parameters that could be assessed by the user, we first divided quantified proteins from all analyses into three different confidence groups termed “Gold”, “Silver” and “Bronze”. To construct the Gold list, we first filtered all protein assigned a probability across the six analysis by removing any proteins with probabilities less than our defined cutoff of 0.75. Proteins with no calculated abundance ratio or an abundance ratio of 0 or 999 were also removed. Thus, only protein identifications that possessed a valid relative abundance ratio and were highly confident were included in this list of quantified proteins. A combined relative abundance ratio and error was then determined in collaboration with Dr. Changyu Shen (Division of Biostatistics, IUSM) for the proteins within the “Gold” list using the procedure described in the next section. The “Silver” list includes those proteins that may not have possessed a single quantified instance where the protein probability was greater than 0.75 but were nevertheless quantified across multiple analyses below this cutoff threshold. To construct this list the combined abundance ratio was calculated as described in the next section by only considering those proteins with a valid abundance ratio and a combined protein probability of at least 0.9. There was no probability cutoff applied to the protein identification utilized for the quantified value and thus any quantification of a protein derived from this list is more suspect than the “Golden” list. It is important to justify the need for both the “Golden” list and the “Silver” list since both lists capture different types of high quality data. The “Golden” list, though highly confident, used alone would fail to consider any proteins that were detected reproducibly at moderate to high confidence which lends to an overall higher confidence that the protein was identified correctly. On the other hand, if the “Silver” list were used solely any protein identified and quantified only once at a probability below 0.9 would not be considered. Thus, the two lists together encapsulate distinct instances, leading to a more comprehensive quantified list of proteins. The final “Bronze” list includes the remainder of the proteins for which a

relative abundance ratio was determined and thus contains the lowest quality data with a presumed high false positive rate. Though this last list is indeed comprised of what is deemed low quality data we felt that it nonetheless should be included in the final results since some measures are indeed correct and could fortify significant changes in protein functional groups.

In order to combine the individual relative abundance ratios measured for a given protein across multiple analyses we employed the following method. The final relative abundance ratio as well as the associated error for proteins quantified in only one analysis is utilized for the final abundance ratio and error in the combined list. However, the determination of a final protein abundance ratio for proteins quantified multiple times presents a small dilemma. Each time a relative abundance ratio is determined for a given protein, the number of peptides that this ratio is based on most certainly varies. This is due to the stochastic process of obtaining valid parental mass spectra as well as tandem mass spectra for a given peptide each time an analysis is performed. Due to variations in the number of peptides contributing to a given abundance ratio, the standard deviation of the ratio varies as a function of the congruence observed across multiple peptide ratios. It is fair to make the assumption that a protein ratio with a low standard deviation provides a more accurate representation of the actual protein ratio than one containing a high standard deviation. Thus, the standard deviation associated with an abundance ratio can be utilized to weigh the significance of each independent measurement as well as the final protein ratio. With this in mind, final protein ratios as well as their standard deviations were calculated by combining multiple independent ratios across all analyses. The individual steps in this method are described below.

First, the adjusted ratio mean and the associated standard deviation for each independent measurement is logarithmically transformed by taking the natural logarithm of the adjusted ratio mean (denoted as $\ln R_i$) and dividing the standard deviation by the original adjusted ratio mean, respectively (denoted as $\ln SD_i$). Second, a weight is calculated for each adjusted ratio mean based on the standard deviation of the given adjusted ratio mean, using the following formula:

$$W_i = \frac{\frac{1}{(\ln SD_i)^2}}{\sum_{i=1}^{N}\left(\frac{1}{(\ln SD_i)^2}\right)}$$

[6]

Where $W_i$ is the weight score for each adjusted ratio mean determined for a given protein. Third, the final combined ratio in the natural log scale (denoted as lnR) is calculated using this weight score as follows:

$$\ln R = \sum_{i=1}^{N} W_i * \ln R_i$$

[7]

where $W_i$ is the weight calculated in equation 1 for a given ratio ($lnR_i$). Using this equation to sum each weighted instance of an adjusted ratio mean attained for a given protein; the final adjusted ration mean (R) for that protein is calculated and converted back to the normal scale. Finally, the final standard deviation (*lnSD*) is determined utilizing the following equation:

$$\ln SD = \sqrt{\frac{1}{\sum_{i=1}^{N}\frac{1}{(\ln SD_i)^2}}}$$

[8]

The final standard deviation (SD) is then calculated by multiplying the combined ratio (R) and the above calculated *lnSD*.

*3.11.4.8. Determination of Proteins with Significantly Altered Relative Abundance Changes*

We next sought to isolate those proteins whose relative abundance was altered either positively or negatively by *GRR1* deletion. To do this, a z-score

was calculated by dividing the final abundance ratio by its standard error for each protein. The local false discovery approach proposed by Effron (REF) is applied to the z-score to calculate the probability that the relative abundance ratio is different from 1- ($P_R$). Finally, we solve $P = P_{id} x P_{ratio}$ where $P_{id}$ is the combined protein probability that the protein is identified correctly and $P_{ratio}$ is the probability that the change in relative abundance is significant. In other words, to be claimed as "differentially expressed" in our analysis, a protein needs to have high confidence in its identification and high confidence in its differential abundance.

# CHAPTER 4: GLOBAL PROTEOMIC AND MICROARRAY RESULTS

## 4.1. Mass Spectrometry Analysis Numbers and Proteome Coverage

### 4.1.1. Raw Data and SEQUEST™ Totals

The completion of our LC/LC-MS analysis resulted in the production of 12 mass spectrometric raw files (denoted with a .RAW file extension) for each run. A total of 10 runs were performed ( 3 runs for each of two gas phase analyses as well as four single run full scan analyses) resulting in the generation of 120 ".RAW" files. Each of these ".RAW" files contains a file for every MS and MS/MS scan collected for the peptides eluting from one 90 minute reverse phase gradient from one salt step. Thus, not including wash steps, down time in between runs, and injection times; the entire LC/LC-MS procedure of the experiment took roughly 8 days of instrument time. Over one million scans (both MS and MS/MS scans as well as redundant scans), 500,716 of which were MS full scans, and 638,853 of which were MS/MS (tandem MS) scans were collected over the course of all six analyses (Figure 4.1). Comparison of the number of MS and MS/MS files generated from each analysis revealed, as expected, that the ample gas phase analysis (1.1), which consists of three runs with the mass spectrometer scanning a different third of the full scan range each run, generates ~ 3 times more MS and MS/MS files than a full scan single MS run (Figure 4.1). Also, as expected, consolidation of the redundant tandem MS scans by SEQUEST™ resulted in the production of approximately half the number of DTA files compared to the number of tandem MS files acquired for each analysis. In all, approximately 300,000 DTA files were generated and searched utilizing SEQUEST™.

We were curious to assess the proteome coverage achieved in our analysis by comparing our data to that of other global proteomic studies being performed on yeast at the time. Just prior to our proteomic analysis, a global analysis of the yeast proteome was reported [409]. At the time, this study represented the gold standard for protein identifications and their analyses most closely resembled our own, barring a few differences (i.e. we utilized more

analyses but did not fractionate and they utilized a less automated/more sensitive LC/LC separation).

Thus, we sought to compare our peptide and protein identifications totals utilizing their cutoff scores to validate the quality of our data. At that time, data was filtered using SEQUEST™ cutoffs and thus we utilized the same cutoffs applied by Washburn et.al to facilitate comparison of our data set with theirs. Washburn et.al deemed that peptides possessing the following criteria were valid. Peptides of +1, +2, and +3 charge states had to possess ΔCn values greater than or equal to 0.1 and the Xcorr value had to be greater than or equal to 1.9, 2.2, or 3.75, respectively [409]. In this study, Washburn et al. analyzed three fractions of a yeast whole cell lysate in three separate analyses. Utilizing this technique and these cutoffs they were able to identify 5,540 unique peptides corresponding to the identification of 1,484 proteins. In our analysis utilizing their SEQUEST™ filtering criteria we were able to successfully identify 19,861 total peptides (includes redundancies) corresponding to 5,200 unique peptide identifications and 1,722 non-redundant protein identifications. Surprisingly, we identified fewer unique peptides but more proteins than Washburn et al. (Figure 4.3).This would suggest that we successfully matched fewer peptides per protein or in other words increased protein coverage at the expense of the depth of coverage. Interestingly, on average the proteins we detected possessed over 10 peptide identifications per protein and we postulate that the replicate analyses greatly increased the depth of coverage for the most abundant proteins while the increase in coverage afforded to less abundant proteins was much more modest. However, given the added depth to which the gas phase analyses probe the proteome, it could be that we extended proteome coverage by detecting a new subset of peptides afforded by the added separation step in the gas phase analyses. Nevertheless, we believe that our analysis was at least as extensive as that of Washburn et al. if not more.

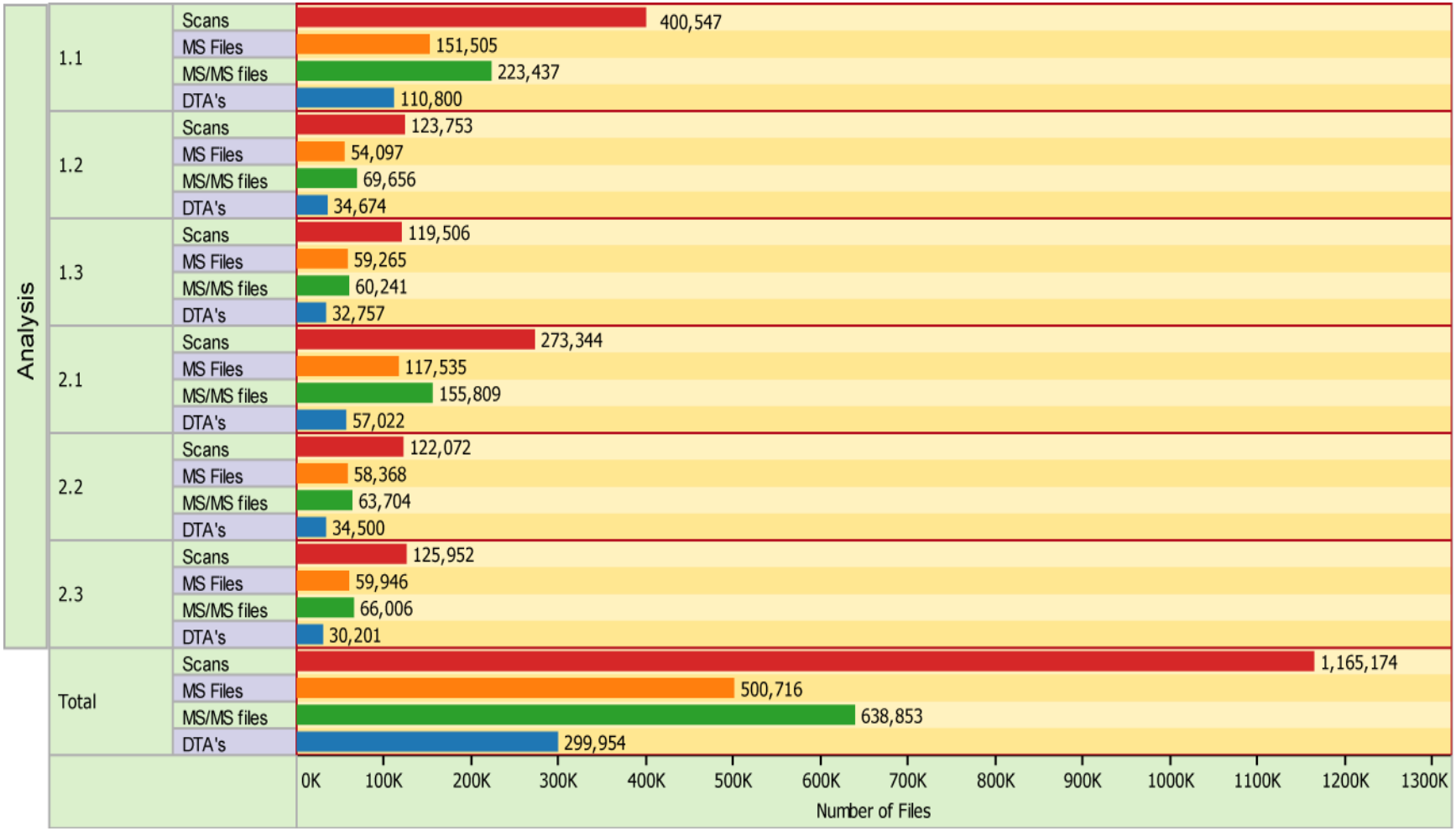


**Figure 4.1. Mass Spectrometry Scans and File Totals for All *grr1Δ* vs wild-type Proteomic Analyses.** The total number of scans, MS, tandem MS (MS/MS), and SEQUEST™ processed MS/MS (Dta) files generated per analysis as well as across all analyses are plotted and displayed.

### 4.1.2. Peptide Totals from Peptide Prophet™ and ASAPratio™

As indicated previously, all SEQUEST™ search results were immediately processed using peptide prophet to statistically assess the validity of the peptide matches. Subsequently, relative peptide abundance ratios were then determined using ASAPratio™. Our results as processed through these two algorithms are shown in Figure 4.2. PeptideProphet™ successfully calculated a peptide probability of at least 0.1 or greater for 67,201 of the 299,954 DTA files generated by SEQUEST™ (22.4%). Interestingly, 17,637 peptides were assigned a probability of at least 0.9 or higher. This represents 26% of all peptides for which a peptide probability was assigned and contains the most peptides of any probability bin. Interestingly, this number is 2224 peptides fewer than the total number of peptides detected using the SEQUEST™ cutoffs of Washburn et al., indicating that a 0.9 probability cutoff may eliminate a number of positive identifications. Additionally, the greatest number of peptides for which ASAPratio™ determined a relative abundance ratio also possessed peptide probabilities of at least 0.9 with 5,743 peptides quantitated at or above this probability. Thus, ~1/3 of the 17,637 peptides identified with probabilities greater than or equal to 0.9 were quantified as well. In summary, the high number of identified, as well as quantified, peptides assigned high probabilities in our analysis is a testament to the quality of the data generated.

Once again, as shown in Figure 4.2, the gas phase analysis (1.1 shown in orange) contributed greatly to both the number of identified and quantified peptides at all probabilities. This analysis alone accounted for ~66% of all the peptide identifications with probabilities greater than or equal to 0.9 across all runs. Given the fact that a single gas phase analysis consists of three independent runs, it can be presumed that one gas phase analysis would produce at least three times the number of peptide identifications as a normal full scan analysis. However, though the gas phase analysis produced approximately three times the number of DTA files as the other analyses (Figure 4.1), it produced approximately ten times the number of high quality peptide identifications (pep prob >= .9) (Figure 4.2). Thus, the increase in data

generated utilizing the gas phase analysis is not simply a byproduct of increased data acquisition but can be attributed, for the most part, to an increase in the quality of data collected. This increase in data quality is most likely due to the decreased number of ions that need to be trapped per MS scan due to the preset scan range limitations. Reduction of the number of ions that are trapped presumably leads to less space charge effects in the ion trap which allows for greater scan resolution and sensitivity. This disproportionally high contribution of the first gas phase analyses to the generation of high quality peptide data provides large support for the implementation of these type analyses on a greater scale.

### 4.1.3. Protein Results from Protein Prophet™ and ASAPratio™

Peptide probabilities as well as peptide relative abundance ratios are utilized by ProteinProphet™ and ASAPratio™ to arrive at the final protein probability and protein relative abundance ratio for each analysis. A summary of the final protein results from these algorithms can be seen in Figure 4.3. Utilizing a probability cutoff of .75 where the estimated average error and sensitivity across all six analyses was 5.6% and 60.1% respectively (Figure 4.4), we were able to successfully identify 1,810 proteins. Among those proteins identified at this probability, approximately 44% were quantified (796). Utilizing the ProteinProphet™ error and sensitivity estimates to determine the 0.75 protein probability cutoff, we were able to successfully include 88 statistically valid protein identifications that were not included utilizing the SEQUEST™ cutoff scores of Washburn et al. In summary, we were able to successfully identify 22% more proteins than that identified in the Washburn et al. analysis. Presently, other proteomic analyses are out performing our own, but given the time at which our data was collected this represented a significant achievement and is again a testament to the validity of the data collected.

As was the case for the peptide identifications and quantifications, the number of protein identifications and quantifications was facilitated by the gas

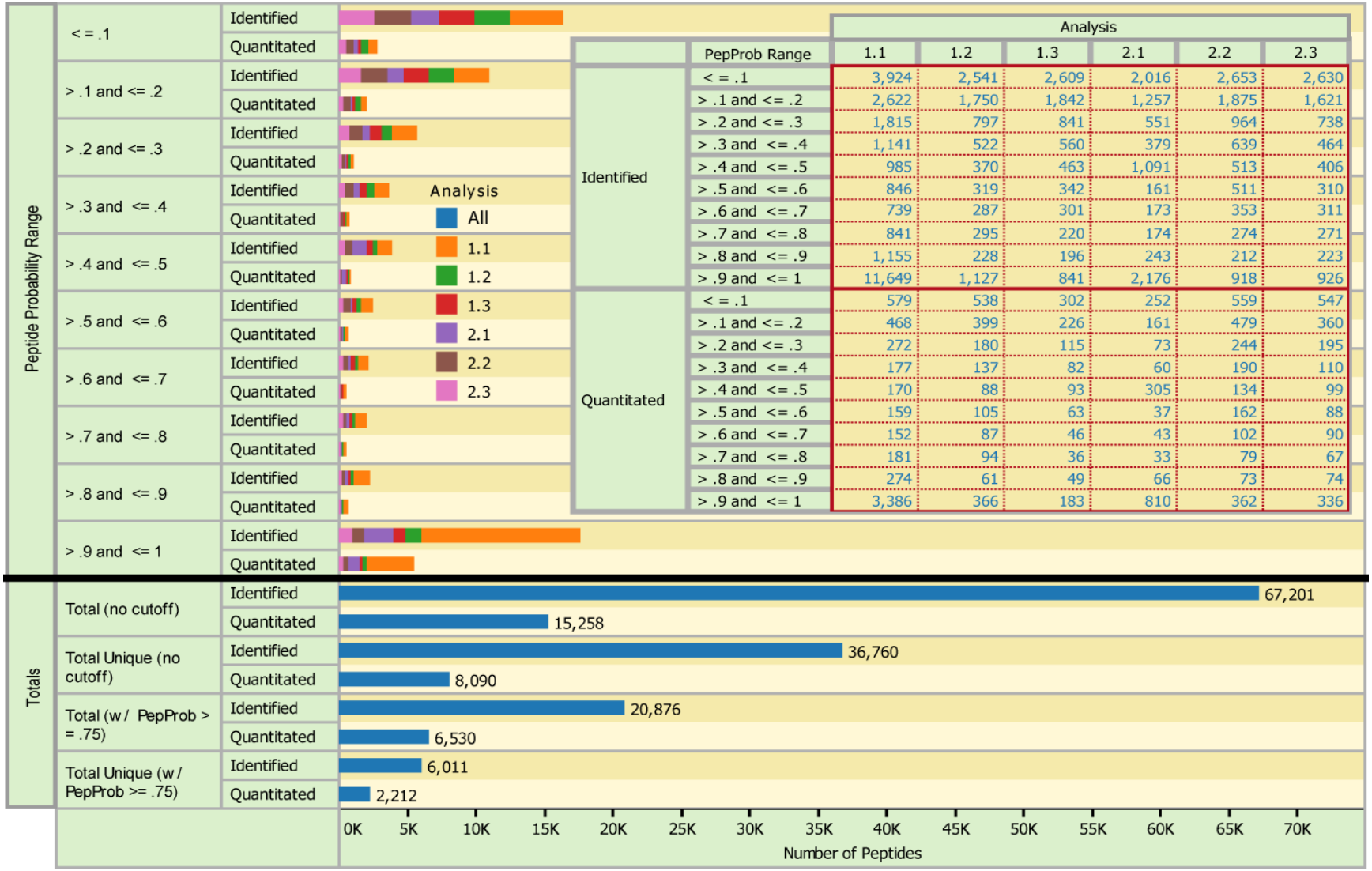


| | PepProb Range | Analysis 1.1 | 1.2 | 1.3 | 2.1 | 2.2 | 2.3 |
|---|---|---|---|---|---|---|---|
| Identified | < = .1 | 3,924 | 2,541 | 2,609 | 2,016 | 2,653 | 2,630 |
| | > .1 and <= .2 | 2,622 | 1,750 | 1,842 | 1,257 | 1,875 | 1,621 |
| | > .2 and <= .3 | 1,815 | 797 | 841 | 551 | 964 | 738 |
| | > .3 and <= .4 | 1,141 | 522 | 560 | 379 | 639 | 464 |
| | > .4 and <= .5 | 985 | 370 | 463 | 1,091 | 513 | 406 |
| | > .5 and <= .6 | 846 | 319 | 342 | 161 | 511 | 310 |
| | > .6 and <= .7 | 739 | 287 | 301 | 173 | 353 | 311 |
| | > .7 and <= .8 | 841 | 295 | 220 | 174 | 274 | 271 |
| | > .8 and <= .9 | 1,155 | 228 | 196 | 243 | 212 | 223 |
| | > .9 and <= 1 | 11,649 | 1,127 | 841 | 2,176 | 918 | 926 |
| Quantitated | < = .1 | 579 | 538 | 302 | 252 | 559 | 547 |
| | > .1 and <= .2 | 468 | 399 | 226 | 161 | 479 | 360 |
| | > .2 and <= .3 | 272 | 180 | 115 | 73 | 244 | 195 |
| | > .3 and <= .4 | 177 | 137 | 82 | 60 | 190 | 110 |
| | > .4 and <= .5 | 170 | 88 | 93 | 305 | 134 | 99 |
| | > .5 and <= .6 | 159 | 105 | 63 | 37 | 162 | 88 |
| | > .6 and <= .7 | 152 | 87 | 46 | 43 | 102 | 90 |
| | > .7 and <= .8 | 181 | 94 | 36 | 33 | 79 | 67 |
| | > .8 and <= .9 | 274 | 61 | 49 | 66 | 73 | 74 |
| | > .9 and <= 1 | 3,386 | 366 | 183 | 810 | 362 | 336 |

**Figure 4.2. PeptideProphet™ and ASAPratio™ Analysis Totals for Peptides Measured in all *grr1Δ* vs. wild-type Analyses.** (Top) Peptides assigned a peptide probability (Identified) by PeptideProphet™ as well as peptides whose relative abundance ratio was determined by ASAPratio™ (Quantified) across all *grr1Δ* vs. wild-type analyses were separated into ten bins based on their assigned peptide probabilities and plotted. The number of peptides contributed by each analysis for each bin is indicated by color and presented in the inset table. (Bottom) Total peptides as well as unique peptides using no probability cutoff as well as a probability cutoff of .75 (error = 6%) are plotted.

phase analysis (1.1 in orange) and exceeded the number acquired by any other analysis. However, the degree to which the number of protein identifications in analysis 1.1 exceeded the others on average (~2.8X the number of protein identifications at a protein probability of 0.9) was not as pronounced as the 10X improvement observed for peptide identifications. The decreased performance at the protein level most likely resulted from increased protein coverage in analysis 1.1 for proteins of high abundance that are commonly identified by multiple peptides at high probability. The identification of more high quality peptides for these proteins would only increase their protein probability incrementally since only one peptide of high probability is required to identify a protein at the same high probability. Thus, the accumulation of high quality peptide identifications for a single protein is not reflected strongly in the protein probability calculation and as a result those proteins identified by only a single peptide of high probability are not penalized. This assumption is supported by the fact that the average percentage of protein coverage in analysis 1.1 as well as 2.1 (also a gas phase analysis but 2.1 suffered from column clogging) for proteins possessing a 0.9 protein probability is approximately 21% and 18%, respectively, compared to the approximately 10% coverage obtained in the other full scan analyses.

The bias of global LC-MS based proteomic analyses towards proteins of high cellular abundance is well documented [423,424,389,425-427] and is illustrated utilizing our data in Figure 4.5. Utilizing the estimated proteins molecules per cell as determined by [428] we plotted the total number of proteins assigned a protein probability in each of fifteen protein abundance bins and visually overlaid the calculated average protein probability for each of those bins for each analysis

(Figure 4.5 A, the thicker and more red the bar, the greater the average protein probability determined for that bin). A couple of observations can be made from this graph. First, the average protein probability increases as the estimated number of protein molecules/cell increases across all analyses and this increase is directly correlated to an increase in the number of peptides identified per protein for all analyses (Figure 4.5 B). Second, the gas phase analyses (1.1 and 2.1) contain higher average protein probabilities across all bins. This indicates that these analyses greatly increase the dynamic range of the proteomics platform as proteins of lower abundance become more confidently identified. Again, this increase in dynamic range is a direct result of the increase in protein coverage at lower protein molecules/cell bins as the average number of peptides identified per protein is increased in lower abundance bins for the two gas phase analyses. Thus, as observed in other studies, our proteomics platform also is biased towards proteins of greater abundance and as a result possesses a limited dynamic range. However, the dynamic range is increased greatly by conducting “gas phase” analyses and would presumably increase to a greater extent as the number of replicate analyses of this type increased. Additionally, the gain in dynamic range conferred by this type of analysis utilizing newer separation technologies such as ultra high pressure liquid chromatography coupled to newer mass analyzers such as the Orbitrap may be immense.

### 4.1.4. Identification and Quantification Totals for the Final Combined Protein List

Until this point, our results have been reported regarding each analysis individually with final peptide and protein numbers calculated as the sum of the identifications obtained in each analysis. Additionally, we have assessed a probability cutoff of 0.75 based off of the average error and sensitivities achieved across all six analyses. Though the application of this cutoff alone is sufficient for individual analyses, it fails to consider those proteins that may have been identified in multiple analyses just below this cutoff. Since some proteins are identified in multiple analyses, the reliability and accuracy of multiple probability measures can be improved by combining the probability measures from each

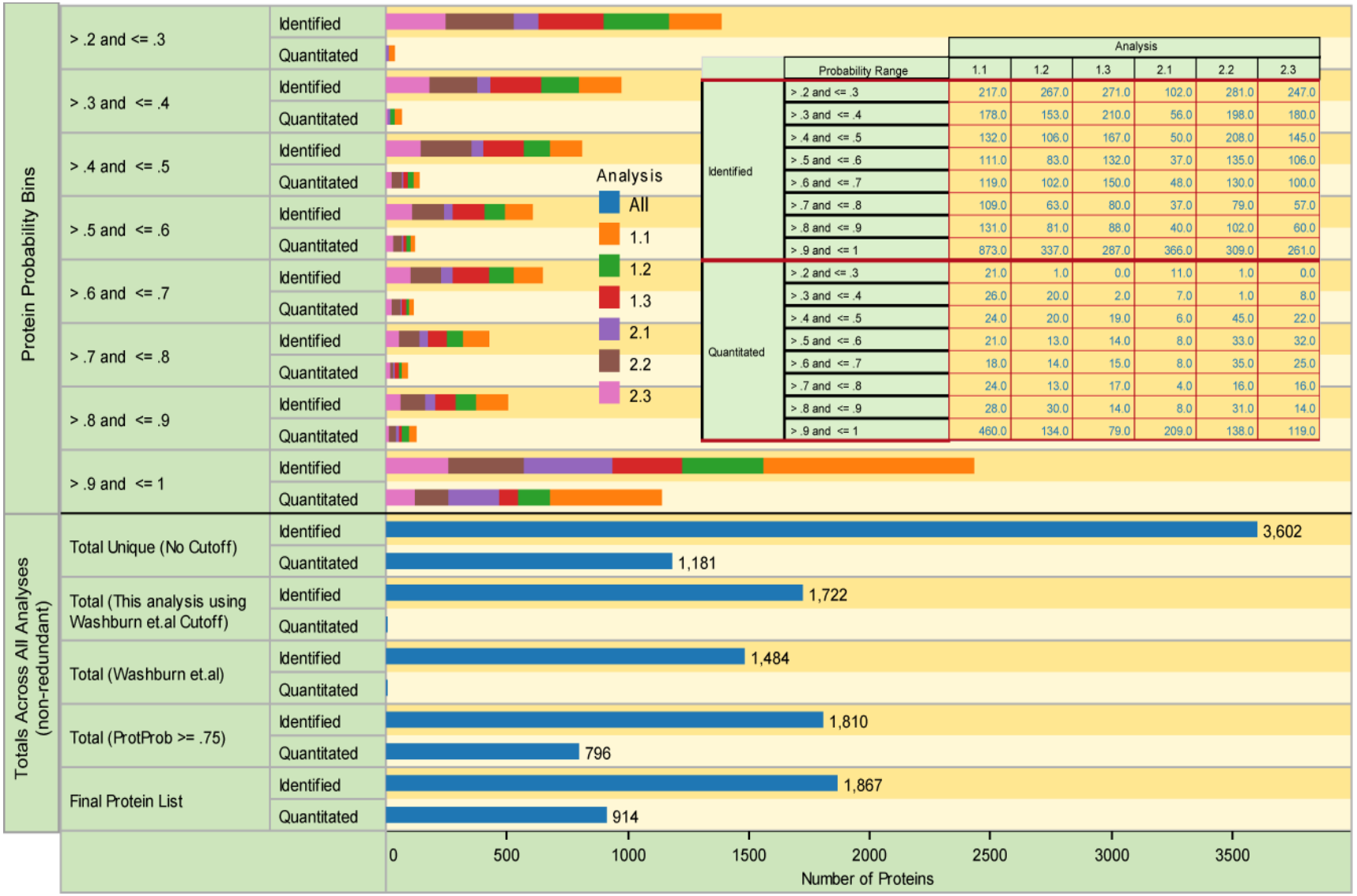


| | Probability Range | Analysis 1.1 | 1.2 | 1.3 | 2.1 | 2.2 | 2.3 |
|---|---|---|---|---|---|---|---|
| Identified | > .2 and <= .3 | 217.0 | 267.0 | 271.0 | 102.0 | 281.0 | 247.0 |
| | > .3 and <= .4 | 178.0 | 153.0 | 210.0 | 56.0 | 198.0 | 180.0 |
| | > .4 and <= .5 | 132.0 | 106.0 | 167.0 | 50.0 | 208.0 | 145.0 |
| | > .5 and <= .6 | 111.0 | 83.0 | 132.0 | 37.0 | 135.0 | 106.0 |
| | > .6 and <= .7 | 119.0 | 102.0 | 150.0 | 48.0 | 130.0 | 100.0 |
| | > .7 and <= .8 | 109.0 | 63.0 | 80.0 | 37.0 | 79.0 | 57.0 |
| | > .8 and <= .9 | 131.0 | 81.0 | 88.0 | 40.0 | 102.0 | 60.0 |
| | > .9 and <= 1 | 873.0 | 337.0 | 287.0 | 366.0 | 309.0 | 261.0 |
| Quantitated | > .2 and <= .3 | 21.0 | 1.0 | 0.0 | 11.0 | 1.0 | 0.0 |
| | > .3 and <= .4 | 26.0 | 20.0 | 2.0 | 7.0 | 1.0 | 8.0 |
| | > .4 and <= .5 | 24.0 | 20.0 | 19.0 | 6.0 | 45.0 | 22.0 |
| | > .5 and <= .6 | 21.0 | 13.0 | 14.0 | 8.0 | 33.0 | 32.0 |
| | > .6 and <= .7 | 18.0 | 14.0 | 15.0 | 8.0 | 35.0 | 25.0 |
| | > .7 and <= .8 | 24.0 | 13.0 | 17.0 | 4.0 | 16.0 | 16.0 |
| | > .8 and <= .9 | 28.0 | 30.0 | 14.0 | 8.0 | 31.0 | 14.0 |
| | > .9 and <= 1 | 460.0 | 134.0 | 79.0 | 209.0 | 138.0 | 119.0 |

**Figure 4.3. ProteinProphet™ and ASAPratio™ Analysis Totals for Proteins Measured in all *grr1Δ* vs. wild-type Analyses.** (Top) Proteins assigned a protein probability (Identified) by ProteinProphet™ as well as proteins whose relative abundance ratio was determined by ASAPratio™ (Quantified) across all *grr1Δ* vs. wild-type analyses were separated into eight bins based on their assigned protein probabilities and plotted . The number of proteins contributed by each analysis for each bin is indicated by color and presented in the inset table (Note: Redundant protein measures are included). (Bottom) Total non-redundant proteins detected using no probability cutoff as well as a probability cutoff of .75 (error = 6%) are plotted. Additionally, total proteins identified using the SEQUEST™ cutoffs specified by Washburn et al. for this analysis as well as their analysis are also plotted for comparison purposes. Finally, the totals for our combined probability and adjusted ratio means calculations are provided as the final protein list.

analysis. Thus, we sought to utilize the data processing scheme described in Section 4.4.6 to combine the protein probabilities of proteins identified multiple times in order to provide a more accurate unified probability. Utilizing a combined protein probability cutoff of 0.9 for multiply sampled proteins as well as the 0.75 cutoff for single analysis protein identifications we were able to increase the number of successfully identified proteins from 1810 to 1867. This list will be referred to as the final protein list throughout the rest of this volume.

The accuracy of the measured adjusted ratio mean for a given protein can also be improved by combining the multiple independent ratios obtained across all analyses into a single unified adjusted ratio mean. For proteins whose adjusted ratio mean was determined in more than one analysis we applied the data processing scheme described in Section 4.4.7. Through this process, a single adjusted ratio mean as well as its standard deviation is calculated from each individual relative abundance weighted by it standard deviation. Each protein for which an adjusted ratio mean was calculated was then categorized into one of three categories termed ‘Gold’, ‘Silver’, and ‘Bronze’ based on the confidence of the calculated ratio. “Gold” categorized proteins are considered the most reliable measures because they possess combined relative abundance ratios calculated from individual ratios whose corresponding protein probability was at least 0.75 or greater. This “Golden” protein list contained 797 quantified proteins. “Silver” categorized proteins possess a combined final protein probability greater than 0.9 but were not detected in any single analysis at a probability greater than 0.75. Thus, the relative abundance ratio is based off measurements from lower confidence protein identifications and as a result is

considered less reliable than those in the “Gold” list. This “Silver” list contained an additional 117 quantified proteins. The third and final list, denoted the “Bronze” list, contains the remainder of proteins for which an adjusted ratio mean was determined regardless of protein probability. This list contains 267 proteins and is expected to contain a high number of false positives. However, it most certainly contains a number of true positives that could provide useful biological evidence and was therefore included in the final protein list. The “Bronze” list is not included in any of the reported numbers for quantified proteins. Together, these categories indicate the confidence that a protein in our experiment was quantified correctly and can be utilized at the individual researcher’s discretion when interpreting the final results. Considering only the “Gold” and “Silver” lists we successfully quantified 914 proteins in a *S. cerevisiae* whole cell extract utilizing our proteomics analysis platform (Table 4.3). If the “Bronze list” is included in the total, 1181 proteins were quantified with the last 267 “Bronze” proteins containing many false positives.

Now that we had combined the data from all analyses into a unified list of proteins with unified confidence and relative abundance metrics we next wanted to isolate those proteins whose relative abundance changed significantly due to *GRR1* deletion. To do this, as described in Section 4.4.8, we calculated a “probability of change” that is calculated by taking the product of the combined probability that the protein was identified correctly and the probability that the relative abundance changed significantly ($P_{ratio}$). This second probability was calculated using the local false discovery approach of Effron [429] applied to the calculated z-score of the relative protein abundance. Thus, in order to possess a high “probability of change” in our analysis the protein had to both be identified at high confidence and its differential abundance had to be at high confidence. In order for a protein to be deemed “differentially expressed” in our analysis its “probability of change” had to be at least 0.9, the protein category had to be at least “Gold” or “Silver”, and the magnitude of its abundance change had to be at least 2.5X. Utilizing these cutoffs, 187 proteins were determined to be

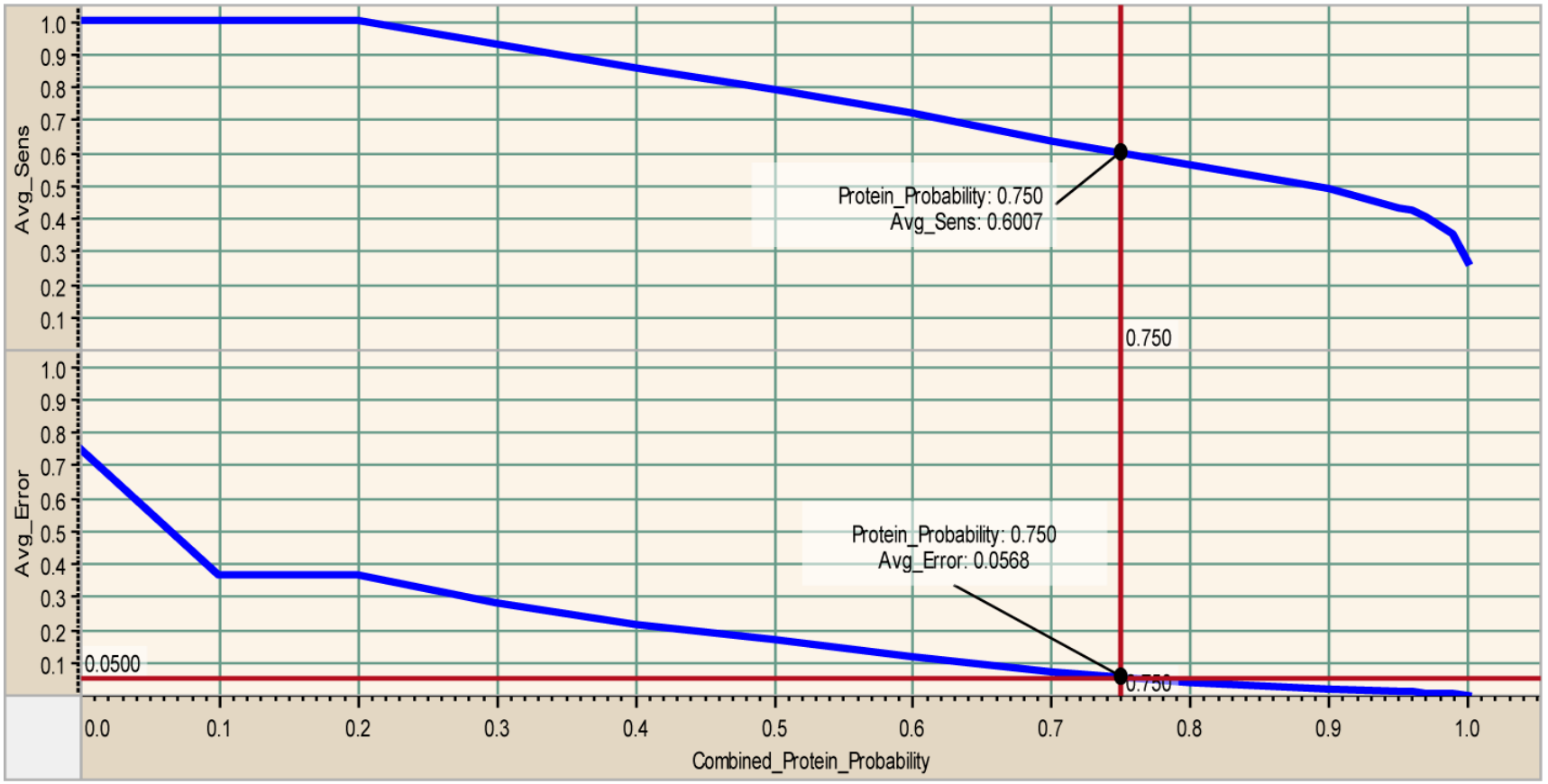


**Figure 4.4. Estimated Average Error and Sensitivity Plots from All Analyses.** Protein Prophet™ calculates an error and sensitivity estimation for each probability for each analysis. Utilizing these individual error and sensitivity estimates we calculated the average error and sensitivity across all six analyses (shown above with average sensitivity plot on top and average error plotted on bottom). Utilizing these averages we assessed a probability cutoff of .75 (red line) where the error was approximately 5.7% and the sensitivity was around 60% across all analyses. This cutoff was applied to those proteins only identified in a single analysis whereas those observed in multiple analyses were subjected to additional data processing (see text).

significantly changed due to *GRR1* deletion. Ninety one proteins have increased relative abundances in *grr1Δ* strains compared to wild-type while 96 proteins showed lower relative abundances in *grr1Δ*. Altogether, ~ 20.5 % of the proteins, for which we attained a relative abundance, were found to be "differentially expressed" due to *GRR1* deletion (Figure 4.6).

### 4.2. Micro-Array Totals

Our interests did not rest solely on determining the proteomic response to *GRR1* deletion but in comparing the correlation or lack thereof between transcriptional and proteomic changes attributable to loss of this gene. Microarray analyses have previously been reported for *grr1Δ* strains; however these analyses were conducted utilizing strains of the CenPK background which displays major differences with the S288C background regarding growth and nitrogen source preference. With this in mind, a genome wide transcriptional analysis (microarray) was conducted utilizing the same strains, media, and growth conditions as those utilized in our proteomic analysis. The details pertaining to how our microarray analysis was performed is described in detail in Section 3.2 and the results are summarized briefly here. Utilizing four biological replicates for each strain, we determined the relative levels of 5,593 gene transcripts including ~99% of the genes assayable on the microarray chip (Figure 4.6). A Welch significance test was applied to each measurement and only those transcripts possessing a Welch log 2 value equal to or below 0.05 as well as a 2 fold change in either direction were considered "differentially expressed". Utilizing these cutoffs we were able to measure 267 significant changes in gene expression of which, 197 were observed to increase and 70 were observed to decrease in *grr1Δ* strains. Altogether, ~ 4.8% of those genes whose relative expression level was measured were found to change significantly in the *grr1Δ* strain.

## 4.3. GO Enrichment Analyses for Proteomic and Genomic Data Sets

### 4.3.1. GO Component Enrichment Analysis of Global Proteomic Data

Global shotgun based proteomic analyses have previously displayed systematic biases against the identification of membrane proteins and/ or proteins of different sub-cellular locations [430]. This bias is attributable to both the inherent hydrophobicity of these proteins, which limits their solubility during extraction, and to the low abundance of these proteins within the cell. In order to assess whether this bias or if any other bias was present in our own analysis we determined the enrichment or lack thereof for proteins from different sub-cellular compartments. To do this, we individually categorized proteins detected, quantified, and changed in our analysis by their assigned GO (Gene Ontology) Slim component ontologies ("*Saccharomyces* Genome Database" ftp://genome-ftp.stanford.edu/pub/yeast/data_download/literature_curation/go_slim_mapping.tab (9/16/2009)). A percentage of protein coverage within a particular ontology was then determined by dividing our detected and quantified total by the total number of proteins in SGD assigned to the particular ontology. Additionally, given the bias already described towards proteins of higher abundance within the cell, we also calculated the average protein abundance as determined by [428] for each *Saccharomyces* GO Slim component category.

Empirical evaluation of each component in conjunction with the calculated enrichments for our analysis as well as the average protein abundance revealed that a high percentage of proteins annotated to the ribosome were detected (14.65% points above the mean) and quantified (15.26% points above the mean) and that this bias correlates with the increased average abundance of proteins annotated to the ribosomal component (Figure 4.7). Consistent with other analyses, proteins annotated to membranes as well as the nucleolus (7.35% below mean coverage) are observed to be underrepresented in our analysis including the plasma membrane (5.4% below), endoplasmic reticulum (10.76% below), membrane (10.18% below), membrane fraction (7.67% below),

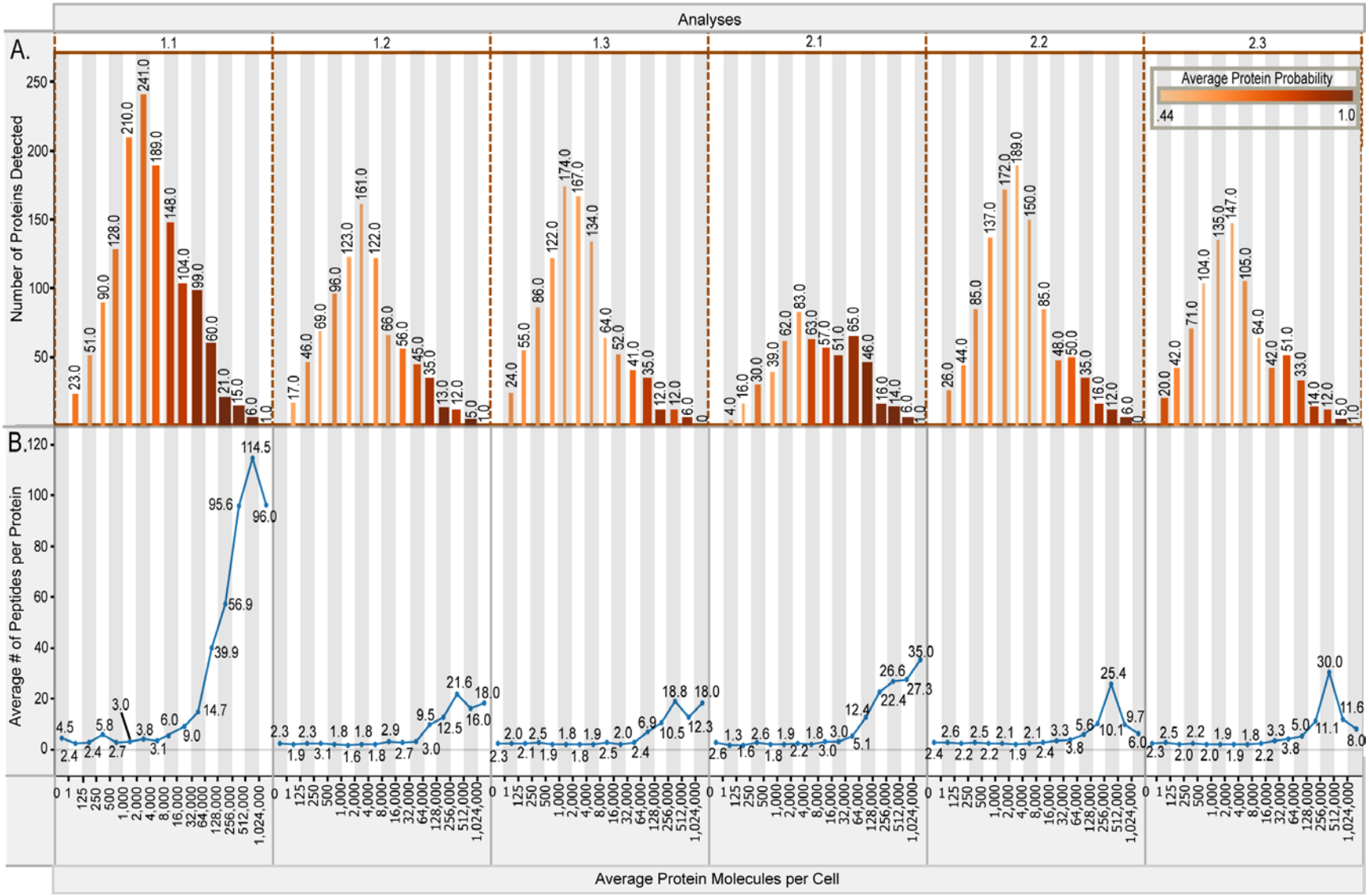
Analyses
1.1
1.2
1.3
2.1
2.2
2.3
A.
Number of Proteins Detected
Average Protein Probability
.44
1.0
B.
Average # of Peptides per Protein
Average Protein Molecules per Cell

**Figure 4.5. Assessment of the Inherent Bias Toward Proteins of Higher Abundance in the *grr1Δ* vs. wild-type Proteomic Analysis.** **A.** All proteins assigned a protein probability by Protein Prophet™ were divided by analysis and grouped into one of fifteen bins based on their estimated protein molecules per cell as determined by [428] The number of proteins within a given bin for a given analysis is represented by the height of the bar and annotated by the number at the top of the bar. The bars are colored by the average protein probability within that bin for that analysis. Higher average protein probability is represented by darker shades of red and thicker bars while lower average protein probability is represented by lighter shades of red and thinner bars. **B.** The average number of peptides identified for proteins within a given protein molecule per cell bin are plotted and separated by analysis.

mitochondrial envelope (10.46% below), and cytoplasmic membrane bound vesicle (5.42% below). This under enrichment does not correlate directly with the average protein abundance calculated for proteins within these components, suggesting that either the extraction procedure or our LC-LC-MS procedure possesses an inherent bias against the isolation or detection of proteins linked to these sub-cellular locations. This bias is most likely greater for proteins located in the endoplasmic reticulum, membrane, and membrane fraction since an exaggerated bias against their quantification is observed with values below the means of 5.58%, 12.26%, and 7.63%, respectively. Since our extraction procedures were not designed to include extracellular or excreted proteins, the lack of coverage for proteins annotated to extracellular region is expected. In summary, the bias of our proteomic analyses towards the detection and quantification of high abundance proteins is exemplified further in the GO component analysis due to the apparent preference for analyzing ribosomal proteins which are usually very abundant. Furthermore, the observed bias against membrane protein analysis for our platform is consistent with previous reports [431,432] and stresses the need for implementing extraction procedures ideal for membrane protein enrichment.

While the GO component enrichments discussed above are most likely due to systematic bias, the increased enrichment in the number of differentially expressed proteins annotated to cellular bud, cytoskeleton, and mitochondrial envelope most likely reflects biological differences between *grr1Δ* and wild-type strains. The percentage of proteins with significantly altered protein expression in these categories were 3.86% (cellular bud),

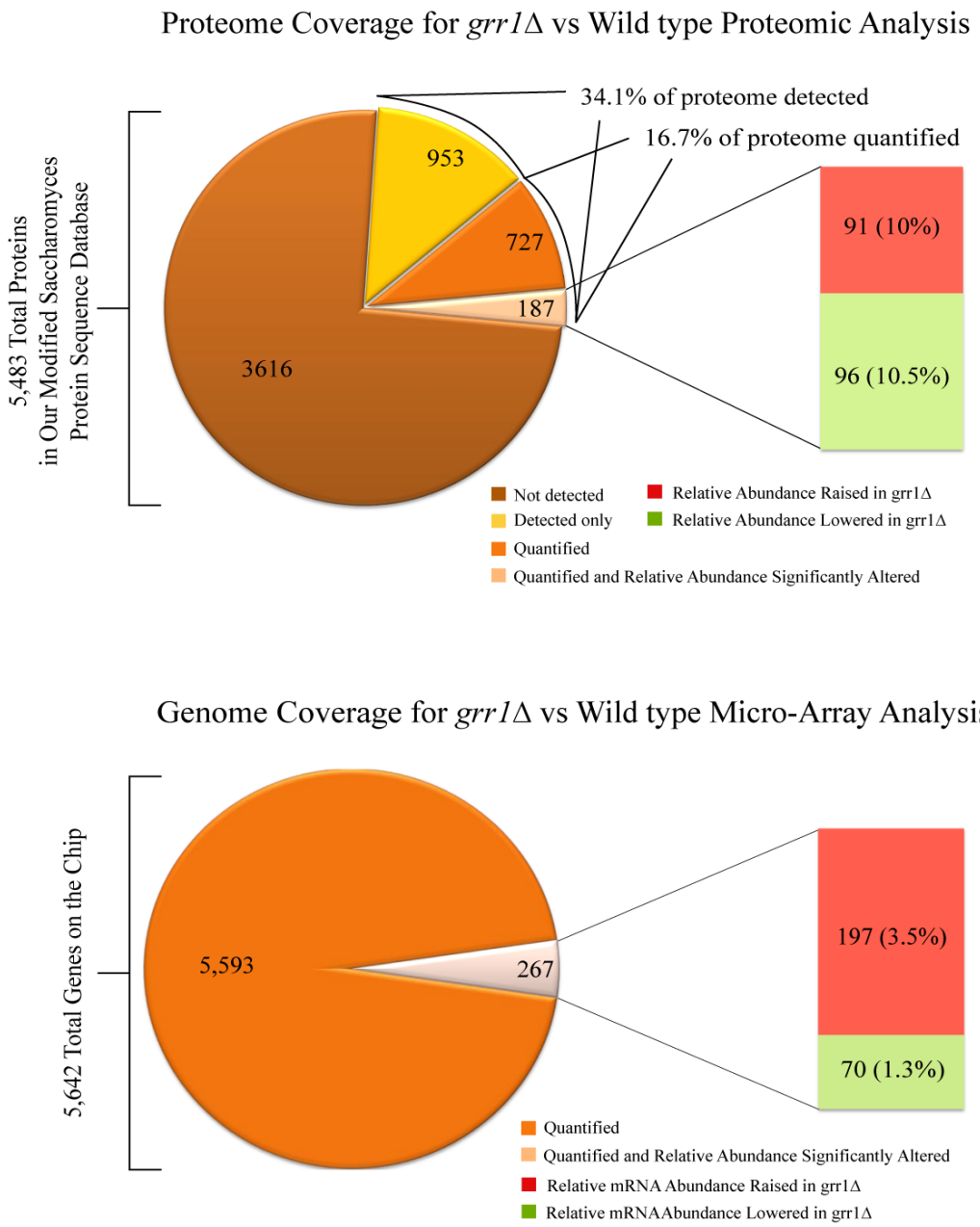


**Figure 4.6. Proteomic and Micro-array Analysis Totals for *grr1Δ* vs. wild-type Cells.** **Top.** Our hand annotated *Saccharomyces* Database contained 5,483 non-redundant protein entries of which 1867 were successfully identified in the *grr1Δ* vs. wild-type proteomic analysis utilizing our Protein Prophet™ cutoffs (see text). Of these 1867 identified proteins, 914 were quantified utilizing leucine SILAC™ and the ASAPRatio™ algorithm. Protein expression of 187 of these proteins was measured to significantly change in *grr1Δ* strains compared to wild-type with 91 proteins exhibiting increased expression and 96 exhibiting decreased expression. **Bottom.** A total of 5,642 non-redundant genes were represented on the Affymetrix Yeast 2.0 GeneChip. The relative expression of 5,593 of these genes was determined and 267 were measured to significantly change using a fold change cutoff of 2 and a Welch t-test cutoff of .05. The expression level of 197 genes was measured to increase in *grr1Δ* strains while 70 were measured to decrease.

9.56% (mitochondrial envelope), and 5.49% (cytoskeleton) above the mean percentage of significantly altered proteins across GO component categories. Phenotypically, *grr1Δ* strains exhibit an elongated bud morphology that requires altered regulation of bud and cytoskeletal proteins. Thus, the increased number of proteins annotated to these components that are observed to change is consistent with phenotypical manifestations of the *GRR1* deletion. This also holds true for proteins annotatedto the mitochondrial envelope as *grr1Δ* strains have been characterized by multiple laboratories to require enhanced mitochondrial function to support growth on glucose media [70,66,67]. Together, the observed enrichments attributable to lack of Grr1 function provide rudimentary validation of our proteomic analysis ability to measure relevant biological perturbations of protein expression.

### 4.3.2. GO Process Enrichments Achieved Utilizing GenGO on Changes in Global Gene Expression are Consistent with Previous Gene Expression Analyses of grr1Δ Cells

Given the fact that the GO component analysis was successful in revealing enrichments in protein groups that could be ascribed to Grr1 function; we next sought to identify more specific biological processes that *GRR1* deletion may perturb by extending this type of enrichment analysis to the entire "Process" category of GO ontologies [433]. Additionally, we were interested in comparing the enrichments achieved at the protein level to those at the transcriptional level in order to begin to evaluate the continuity between the transcriptional and post-transcriptional responses to *GRR1* deletion. To facilitate this analysis we first subjected our list of significantly changed proteins and transcripts to GO process analysis using the GenGO (GENerative GO analysis) algorithm [434]. This algorithm is available as a web based application (http://www.sb.cs.cmu.edu/GenGO) and utilizes a global likelihood function to identify a small subset of descriptive categories that together represent the major processes enriched in the supplied list of genes or proteins. We felt that a

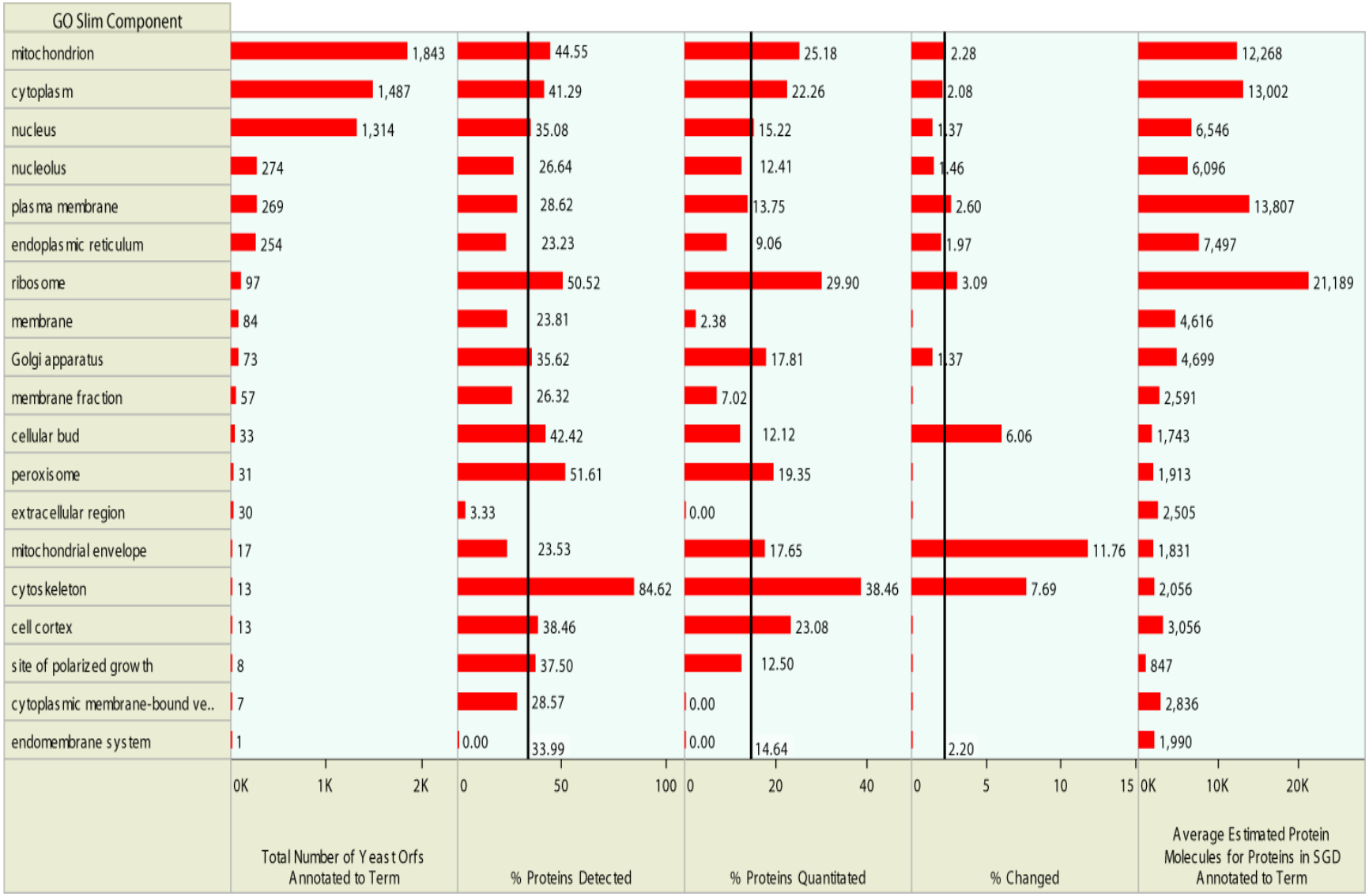
GO Slim Component
mitochondrion
cytoplasm
nucleus
nucleolus
plasma membrane
endoplasmic reticulum
ribosome
membrane
Golgi apparatus
membrane fraction
cellular bud
peroxisome
extracellular region
mitochondrial envelope
cytoskeleton
cell cortex
site of polarized growth
cytoplasmic membrane-bound ve..
endomembrane system
1,843
1,487
1,314
274
269
254
97
84
73
57
33
31
30
17
13
13
8
7
1
44.55
41.29
35.08
26.64
28.62
23.23
50.52
23.81
35.62
26.32
42.42
51.61
3.33
23.53
84.62
38.46
37.50
28.57
0.00
33.99
25.18
22.26
15.22
12.41
13.75
9.06
29.90
2.38
17.81
7.02
12.12
19.35
0.00
17.65
38.46
23.08
12.50
0.00
0.00
14.64
2.28
2.08
1.37
1.46
2.60
1.97
3.09
1.37
6.06
11.76
7.69
2.20
12,268
13,002
6,546
6,096
13,807
7,497
21,189
4,616
4,699
2,591
1,743
1,913
2,505
1,831
2,056
3,056
847
2,836
1,990
0K
1K
2K
0
50
100
0
20
40
0
5
10
15
0K
10K
20K
Total Number of Yeast Orfs Annotated to Term
% Proteins Detected
% Proteins Quantitated
% Changed
Average Estimated Protein Molecules for Proteins in SGD Annotated to Term

**Figure 4.7. GO Slim Component Analysis of Proteins Detected, Quantitated, and Significantly Changed between *grr1Δ* and wild-type Cells.**
The total number of proteins detected, quantitated, and measured to significantly change in protein expression between *grr1Δ* and wilt type strains were determined for each of 19 Go-Slim component annotations obtained from the "*Saccharomyces* Genome Database" ftp://genome-ftp.stanford.edu/pub/yeast/data_download/literature_curation/go_slim_mapping.tab (9/16/2009). Utilizing these totals the percent coverage within a given GO-Slim component category was calculated by dividing the total number of yeast genes in SGD annotated to the term. The total genes in SGD annotated to a given GO-Slim component are provided in the bar graph to the far left. The percent coverage for detected, quantitated, and changed proteins for the 19 GO-Slim component categories is plotted in the middle three bar graphs. The vertical black line in each of these graphs represents the mean percent coverage across all 19 GO-Slim Component categories. Deviations below or above the mean represent under-represented or enriched components in our proteomic analysis, respectively. The bar graph on the far right contains the average protein molecules per cell for proteins annotated to the given GO-Slim component. The average protein molecules per cell were calculated utilizing the individual protein molecule per cell estimates of [428].

comparison of the enriched GO processes generated by GenGO for the differentially expressed protein and transcript lists would provide a basic initial characterization of the discordance between transcript and protein in *grr1Δ* mutants.

In order to validate the ability of GenGO to elucidate biologically meaningful GO enrichments we first applied this algorithm to our *grr1Δ* gene expression data. The effects of *GRR1* deletion on gene expression have been eloquently revealed through the concerted effort of multiple laboratories [67,435,159,56,167] and thus the application of GenGO to our list of differentially expressed genes should reveal enriched GO processes consistent with these studies. To conduct our GenGO analysis we utilized three different lists of genes discriminated by the degree to which their expression level changed due to *GRR1* gene deletion. The implementation of the GenGO analysis in this way provides not only a more comprehensive list of enriched GO processes but also provides a hierarchy of the degree to which processes are most influenced by the absence of Grr1. As can be seen in Table 4.1, GenGO analysis of the list of gene transcripts differentially expressed by at least five fold in either direction revealed that the processes of “carboxylic acid transport”, “nitrogen utilization”, “glyoxylate metabolism”, “monosaccharide transport”, and “gluconeogenesis” were the most affected at the transcriptional level by *GRR1* deletion. The effects of *GRR1* deletion on the transcription of amino acid transporters as well as

nitrogen utilization genes through the SPS (Ssy1, Ptr3, Ssy5) signaling pathway [436,111,72,437] and the transcription of hexose transporters through the Snf3/Rgt2 signaling pathway [159,438,69,56] are well established. Thus, the enrichment of differentially expressed genes annotated to “carboxylic acid transport”, “monosaccharide transport”, (which encapsulates amino acid transport and hexose transport respectively) and “nitrogen utilization” is consistent with well characterized roles for Grr1. Genes annotated to “glyoxylate metabolism” and “gluconeogenesis” had also been measured to change in a previous *grr1Δ* micro-array [159]. Additionally, as the relative abundance cutoff was dropped from five fold, to three fold, and finally to two fold the list of GO enrichments expanded to include more processes known to be affected by *GRR1* deletion including, among others, heterocycle catabolic process (includes genes involved in allantoin metabolism) [63,159], siderophore transport (iron chelation for iron scavenging) [71], and disaccharide catabolic process [184]. Based on the ability of GenGO to isolate GO process ontologies from our genome wide expression data that are consistent with previous *grr1Δ* gene expression studies, we concluded that GenGO provided a very accurate and descriptive GO process enrichment analysis for our whole genome expression data.

### 4.3.3. Protein GO Process Enrichment Analysis Utilizing GenGO Reveals Previously Characterized Roles for Grr1 that are not Reflected at the Transcriptional Level

In order to reveal processes affected at the proteomic level, we applied the GenGO algorithm to lists of significantly altered proteins utilizing the fold change cutoffs applied to the transcriptional data (fold difference >= 2, 3, or 5) and the protein data validity cutoffs utilized to report our analysis totals (i.e. Probability of change >= 0.9, Category = Gold or Silver). Like the GenGO analysis of gene expression, the protein expression analysis also revealed GO process enrichments that correlate to known *grr1Δ* phenotypes. However, many of the processes enriched at the protein expression level were not significantly enriched at the gene expression level suggesting that these processes are

| Protein | | | | | | |
|---|---|---|---|---|---|---|
| **Gold or Silver and PC >= .9 and W_Ratio >= 5 or <=.2** | | | | | | |
| **ID** | **GO Category** | **GO ID** | **Score** | **Present** | **Total** | **Gene Names (Prot FC, mRNA FC)** |
| 5704 | Ergosterol metabolic process | GO:0008204 | 1.25E-05 | 5 | 26 | ERG1(.13, -1.22), ERG6(.13, 1.01 ), HMG2(6.31, -1.18), MCR1(.08, 2.04 ), ERG13(.09, -1 ) |
| 22805 | Spindle pole body organization and biogenesis | GO:0051300 | 0.00070739 | 3 | 15 | HCM1(.10, 1.22), BBP1(12.35, 1.49), CDC37(.19, -1) |
| 7727 | Membrane invagination | GO:0010324 | 0.00322056 | 5 | 83 | BZZ1(6.39, 1.05), CLC1(.11, -1.01 ), OSH2(9.40, -1.03), PAN1(8.87, -1.11), SDS24(.20, 1.09) |
| 18713 | Purine nucleoside monophosphate biosynthetic process | GO:0046040 | 0.00408725 | 3 | 15 | ADE16(6.48, -1.09), ADK1(6.98, -1.12), APT1(.31, 1.38) |
| 4570 | SRP-dependent cotranslational protein targeting to membrane translocation | GO:0006616 | 0.00616791 | 2 | 10 | SIL1(5.25, 1.14), SSA3(.10, -1.11) |
| 5034 | Budding cell apical bud growth | GO:0007118 | 0.01044205 | 2 | 13 | TPM1(.3, 1), CLA4(.10, -1.04) |
| **Gold or Silver and PC >= .9 and W_Ratio >= 3 or <=.33** | | | | | | |
| 4894 | Response to osmotic stress | GO:0006970 | 0.0002383 | 8 | 74 | BNR1(.25, 1.47), SSK2(8.94, 1.04), HSP12(2.78, 8.2), PTC1(.23, -1.19), CDC37(.19, -1), BZZ1(6.39, 1.05), TCO89(3.2, 1) |
| 5704 | Ergosterol metabolic process | GO:0008204 | 0.0002465 | 5 | 26 | ERG1(.13, -1), ERG6(.13, 1.01), HMG2(6.31, -1.18), MCR1(.08, 2.04), ERG13(.09, -1) |
| 12901 | Establishment and/or maintenance of cell polarity (sensu Fungi) | GO:0030467 | 0.0010288 | 9 | 114 | DNF1(.27, -1.11), AXL1(.32, -1.36), BNR1(.25, 1.47), PAN1(8.87, -1.11), CLA4(.10, -1.04), TPM2(.30, 1.01), RGA2(.19, -1.02), OSH2(9.40, -1.03), PCL2(5.34, 1.13) |
| 22832 | M phase of meiotic cell cycle | GO:0051327 | 0.00131665 | 10 | 142 | GLC7(4.35, -1.06), KAR3(5.97, 1.05), TOR1(23.10, 1.05), SCP160(3.60, -1.15), HOP1(3.05, -1.23), HOS4(3.20, 1.05), MEC1(4.20, 1.12), MSH5(5.69, -1.76), SLK19(.37, 1.11), REC114(.25, 1.14) |
| 6610 | Purine nucleoside monophosphate biosynthetic process | GO:0009168 | 0.00421895 | 3 | 15 | APT1(.31, 1.38), ADE16(6.48, -1.09) |
| 4072 | Acetyl-CoA metabolic process | GO:0006084 | 0.00973409 | 2 | 20 | CIT1(3.12, 2.7), IDH2(.16, 3.03) |
| **Gold or Silver and PC >= .9 and W_Ratio >= 2 or <=.5** | | | | | | |
| 5704 | Ergosterol metabolic process | GO:0008204 | 4.50E-06 | 8 | 26 | ERG1(.13, -1.22), ERG6(.13, 1.01), HMG2(6.31, -1.18), MCR1(.08, 2.04), ERG13(.09, -1), ERG9(.41, -1.09), ERG20(2.23, -1.05), MVD1(.41, -1.02) |
| 4341 | Transcription termination from RNA polymerase II promoter | GO:0006369 | 0.00052252 | 5 | 18 | GLC7(4.35, -1.06), RAT1(4.43, -1.02), SEN1(.19, 1), ESS1(.48, -1.01), PCF11(.33, -1.13) |
| 155 | MAPKKK cascade during osmolarity sensing | GO:0000161 | 0.00063398 | 4 | 11 | PTC1(.23, -1.19), SSK2(8.94, 1.04), CDC37(.19, -1), STE11(.43, -1.1) |
| 705 | Regulation of cell growth | GO:0001558 | 0.00063398 | 4 | 11 | AVO2(.38, -1.03), TCO89(3.20, 1), TOR1(23.10, 1.05), TOR2(2.28, -1.02) |
| 6517 | Aromatic amino acid family metabolic process | GO:0009072 | 0.00112591 | 5 | 21 | ARO10(2.52, 1.15), ARO2(.28, -1.23), ARO3(.48, -1.28), ARO1(.48, -1.05), PDC6(.23, -1.06) |
| 4101 | NADH oxidation | GO:0006116 | 0.00798115 | 3 | 11 | NDE1(2.47, 1.46), GPD2(2.97, -1.43), NDI1(.35, 3.76) |
| 8806 | Phospholipid transport | GO:0015914 | 0.01033433 | 3 | 12 | PDR17(.32, -1.49), DNF1(.27, -1.11), SEC14(.34, -1.1) |

**Table 4.1. GenGO Process Enrichment Analysis of Significant Gene and Protein Expression Changes Attributable to *GRR1* Deletion.** See page 158 for description.

| Microarray | | | | | | |
|---|---|---|---|---|---|---|
| **FC >=10 or <=-10 Welch t-test < .05** | | | | | | |
| **ID** | **GO Category** | **GO ID** | **Score** | **Present** | **total** | **Gene Names (Prot FC, mRNA FC)** |
| 19600 | Carboxylic acid transport | GO:0046942 | 6.89E-10 | 8 | 49 | ADY2(10.44), BAP2(-86.22), BAP3(-208.58), TAT1(-14.58), SFC1 (.96, 297.03), PUT4(2.04, 15.96), JEN1(26.84), AGP1(-22.64) |
| 11618 | Nitrogen utilization | GO:0019740 | 0.00017599 | 3 | 17 | ADY2(10.44), DAL80(21.13), MEP1(5.5) |
| 19158 | Glyoxylate metabolic process | GO:0046487 | 0.00042985 | 2 | 5 | ICL1(13.29), MLS1(88.33) |
| 8647 | Monosaccharide transport | GO:0015749 | 0.00050712 | 3 | 24 | HXT1(-209.98), HXT4(-11.98), HXT3(1.09, -19.86) |
| 4080 | Gluconeogenesis | GO:0006094 | 0.00080579 | 3 | 28 | FBP1(136.6), CAT8(18.92), PCK1(38.64) |
| **FC >=5 or <=-5 Welch t-test < .05** | | | | | | |
| 19600 | Carboxylic acid transport | GO:0046942 | 1.56E-10 | 10 | 49 | ADY2(10.44), BAP2(-86.22), BAP3(-208.58), TAT1(-14.58), SFC1 (.96, 297.03), PUT4(2.04, 15.96), JEN1(26.84), AGP1(-22.64), MUP1(-6.3), GNP1(-8.5) |
| 19363 | Heterocycle catabolic process | GO:0046700 | 2.64E-07 | 4 | 6 | DAL1(.51, 7.58), DAL2(6.9), DAL3(16.35), DAL7(7.14), DUR1,2 (4.14), PUT4(2.04, 15.96), PUT1(9.18), |
| 4080 | Gluconeogenesis | GO:0006094 | 1.59E-05 | 5 | 28 | FBP1(136.6), CAT8(18.92), PCK1(38.64), SIP4(6.19), PYC1(.91, 7.29) |
| 11618 | Nitrogen utilization | GO:0019740 | 3.80E-05 | 4 | 17 | ADY2(10.44), ATO2(3.55),DAL80(.78, 21.13), GAT1(1.38), MEP1(5.5), MEP2(14.34) |
| 8647 | Monosaccharide transport | GO:0015749 | 0.00015922 | 4 | 24 | HXT1(-209.98), HXT4(-11.98), HXT3(1.09,-19.86), HXK1(2.13, 8.28) |
| 4492 | Glutamate biosynthetic process | GO:0006537 | 0.00041587 | 3 | 13 | PUT1(9.18), IDP2(12.96), GDH3(8.35) |
| 19158 | Glyoxylate metabolic process | GO:0046487 | 0.00134693 | 2 | 5 | ICL1(13.29), MLS1(88.33) |
| 16690 | Vitamin B6 metabolic process | GO:0042816 | 0.0036857 | 2 | 8 | SNZ1(.32,-5.94), SNO1(-18.35) |
| 4055 | Ethanol metabolic process | GO:0006067 | 0.00707569 | 2 | 11 | NDE2(3.22), ALD4(1.04, 5.08) |
| **FC >=2 or <=-2 Welch t-test < .05** | | | | | | |
| 4079 | eneration of precursor metabolites and ener | GO:0006091 | 3.19E-25 | 44 | 180 | ACS1(2.63), COR1(2.34), COX4(2.51), COX6(2), COX12(2.08), COX7(2.45), COX13(2.08), ISF1(59.62), MAM33(2.1), MBR1(9.93), MDH1(2.24), MRPS217(2.13), PUF3(2.2), QCR2(2.35), QCR6(3), QCR10(3.6), RIP1(3.54), ATP3(2.26), ATP21(2.05), ATP17(2.24), ATP14(2.12), ATP19(2.5), ATP20(2.12), CYC1(1.52, 3.09), HXT4(-11.98), SDH1(3.94), SDH2(.68, 3.02), SDH3(2.07), SDH4(2.76), CAT8(18.92), HAP4(2.7), HMS1(2.89), MAL32(21.73), MRK1(16.93), MTH1(2.37), SRT1(2.69), SUC2(4.49), YEL057C(2.08), YNL144C(2.69), YNR034W-A(2.18), ADH2(27), NDE2(3.22), GSY1(2.86) GPH1(4.18) |
| 19600 | Carboxylic acid transport | GO:0046942 | 1.00E-10 | 15 | 49 | ADY2(10.44), DAL5(2.71), BAP2(-86.22), BAP3(-208.58), DIP5(-2.87), GAP1(4.71), TAT1(-14.58), GNP1(-8.5), TAT2(-4.24), SFC1 (.96, 297.03), PUT4(2.04, 15.96), JEN1(26.84), MUP1(-6.3), AGP1(-22.64), DIC1(2.82) |
| 4492 | Glutamate biosynthetic process | GO:0006537 | 3.28E-09 | 8 | 13 | ACO1(1.06, 2.41), CIT1(3.12, 2.7), CIT2(2.2), GDH3(8.35), IDH1(.89, 3.31), IDH2(.16, 3.03), IDP2(12.96), PUT1(9.18) |
| 15100 | Monocarboxylic acid metabolic process | GO:0032787 | 1.34E-08 | 20 | 122 | ALD4(1.04, 5.08), ACS1(2.63), ACH1(.18, 4.03), YAT1(4.15), YAT2(1.81, 4.01), POT1(3.05), POX1(4.82), SPS19(2.78), CRC1(6.17), FBP1(136.6), PCK1(38.64), PYC1(.91, 7.29), CIT2(2.2), ICL1(13.29), MLS1(88.33), CYB2(4.35), ALD4(1.04, 5.08), PDH1(4.67, 5.4), CIT3(2.43), ACO1(1.06, 2.41), CAT8(18.92), SIP4(6.19) |
| 6108 | Carbohydrate transport | GO:0008643 | 1.65E-07 | 10 | 33 | HXK1(2.13, 8.28), HXT1(-209.98), HXT3(1.09, -19.86), MIG2(-48.77), HXT4(-11.98), HXT5(4.4), HXT7(.39, 4.62), HXT10(4.82), MAL31(2.44), MTH1(2.37), STL1(5.28) |
| 11618 | Nitrogen utilization | GO:0019740 | 2.05E-05 | 6 | 17 | ADY2(10.44), ATO2(3.55),DAL80(21.13), GAT1(3.73), MEP1(5.5), MEP2(14.34) |
| 19363 | Heterocycle catabolic process | GO:0046700 | 2.54E-05 | 4 | 6 | DAL1(7.58), DAL2(6.9), DAL3(16.35), DAL7(7.14), DUR1,2 (4.14), PUT4(2.04, 15.96), PUT1(9.18), |
| 8784 | Siderophore transport | GO:0015891 | 1.95E-04 | 4 | 9 | FIT2(4.72), FIT3(2.71), ENB1(-3.2), SIT1(-3.81) |
| 12447 | Biological adhesion | GO:0022610 | 2.41E-03 | 3 | 8 | SAG1(-3.12), AGA1(-4.04), HSP12(2.78, 8.2) |
| 18663 | egulation of transcription by carbon catabolit | GO:0045990 | 1.07E-02 | 3 | 13 | ADR1(3.36), MIG2(-48.77), GAL3 (3.99) |
| 504 | Cytogamy | GO:0000755 | 1.26E-02 | 2 | 5 | FIG2 (-3.2), PRM1 (-6.49) |
| 8729 | Peptide transport | GO:0015833 | 1.26E-02 | 2 | 5 | PTR2 (-4.3), OPT1 (-20.6) |
| 19025 | Disaccharide catabolic process | GO:0046352 | 1.84E-02 | 2 | 6 | SUC2 (4.49), MAL32(21.73) |

**Table 4.1. GenGO Process Enrichment Analysis of Significant Gene and Protein Expression Changes Attributable to *GRR1* Deletion.** Continued. See page 158 for description.

**Table 4.1. GenGO Process Enrichment Analysis of Significant Gene and Protein Expression Changes Attributable to *GRR1* Deletion.** **Table 4.1, Page 155 (Blue).** GO "process" enrichment analysis was conducted on three different lists of proteins measured to exhibit significantly altered expression in *grr1Δ* cells relative to wild-type cells. The three protein lists are distinguished by the minimal fold change cutoff applied and thus were divided to include proteins whose expression level changed by greater than or equal to five fold (Blue/Top), greater than or equal to three fold (Blue/Middle), and greater than or equal to two fold (Blue/Bottom). A significance p-value for each enrichment is calculated by GenGO and reported here as "Score". The number of proteins in our experimental list is provided under "Present" as well as the total number of proteins in SGD annotated to the term ("total"). The common gene names for the proteins annotated to each term along with their protein and gene expression fold changes are provided in the final column in the following format (gene name (protein FC *grr1Δ*/WT, transcript FC *grr1Δ*/WT)). The existence of only one number in parentheses denotes that only the transcriptional fold change was measured and is reported in **Table 4.1, Page 156 (Pink).** GO "process" enrichment analysis was conducted on three different lists of transcripts measured to exhibit significantly altered expression in *grr1Δ* cells relative to wild-type cells. The three protein lists are distinguished by the minimal fold change cutoff applied and thus were divided to include proteins whose expression level changed by greater than or equal to ten fold (Pink/Top), greater than or equal to five fold (Pink/Middle), and greater than or equal to two fold (Pink/Bottom).

predominately regulated through post translational mechanisms. Significant GenGO process enrichments at the protein expression level that correlated with known *grr1Δ* phenotypes include "budding cell apical bud growth" (p-value = 0.01), "response to osmotic stress" (p-value = 2E-4), and "purine nucleoside mono-phosphate biosynthetic process" (p-value = 4E-3). Consistent with the enrichment of altered proteins annotated to the GO component of "cellular bud", the GenGO determined enrichment of "budding cell apical bud growth" is reflective of the role of Grr1 in negatively regulating hyperpolarized growth through ubiquitin targeted degradation of the cyclins, Cln1 and Cln2 [78,74], as well as the Cdc42 effectors, Gic1 and Gic2 [101,102]. Strains deleted for *GRR1* were originally characterized to exhibit enhanced sensitivity to osmotic stress [66]. Thus, altered protein expressions for proteins participating in the "response to osmotic stress" also correlate to a known phenotype of *grr1Δ* strains.

Evidence indicating that purine metabolic processes are altered in *grr1Δ* strains has also been previously detected. In metabolic profile experiments conducted on *grr1Δ* strains, xanthosine-5'-monophosphate, an important intermediate in purine and nucleoside metabolism, was determined to be the top reporter metabolite [67]. Also, in another global proteomic experiment utilizing GFP tagged proteins and microscopy, Ade17, which along with its redundant isozyme,

Ade16, catalyzes the penultimate step of purine biosynthesis (the metabolic synthesis of IMP from AICAR) was found to be increased at the protein level by a little over two fold [77]. Consistent with this observation, we measured Ade16 protein levels to increase by approximately six fold in our analysis. Together these results are not only a testament to the ability of our proteomics platform to determine relevant biological perturbations attributable to *GRR1* deletion but also a testament to the ability of GenGO to isolate these processes through GO analysis.

In addition to the observed enriched processes that can be directly ascribed to previously defined phenotypes of *grr1Δ* strains, a number of previously uncharacterized processes affected by *GRR1* deletion were observed to be enriched in the GenGO analysis of differentially expressed proteins. Multiple lines of evidence suggest that at least some if not all of these processes are indeed perturbed in *grr1Δ* cells. For instance, the second most affected process in *grr1Δ* strains was "spindle pole body organization and biogenesis" and a role for Grr1 in this process is supported by multiple lines of evidence. First, *GRR1* deletions are synthetically lethal with gene deletions of *PAC10* and *TUB3* [439]. The *PAC10* gene encodes Pac10/Gim2, a co-chaperone component of the GimC/prefoldin complex partially responsible for the proper folding of *β*-tubulin. The *TUB3* gene encodes *α*-tubulin. Deletion of either of these genes leads to increased levels of un-dimerized *β*-tubulin which is toxic to the cell and as a result causes growth defects in strains harboring either of these deletions [440,441]. The fact that deletion of *GRR1* exacerbates this growth defect suggests that *grr1Δ* strains may already be stressed by defects in microtubule function. This hypothesis is further supported by the fact that *grr1Δ* cells are observed to be hypersensitive to the microtubule destabilizing agent, benomyl [442]. Evidence that these defects in microtubule function are directly related to spindle pole body complications is provided by another independent study showing that ~ 23% of *grr1Δ* cells exhibit aberrant microtubules not connected to the spindle pole body or nucleus for that matter [442].

Interestingly, though they were not revealed in the GenGO process analysis, additional changes in protein abundance for other proteins involved in microtubule function and mitotic spindle migration were also measured in our analysis. Dyn1 and Kar3 which are microtubule motors found to be concentrated at spindle pole bodies and function in mitotic spindle migration [443-446] were found to be increased by ~39 and 6 fold, respectively. Additionally, components of the dynactin complex, Arp10 and Nip100, which are believed to participate in tethering microtubules to the spindle pole body as well as dynein (Dyn1) to endomembrane compartments [447], were found to increase by 4 fold and decrease by 10 fold, respectively. Taken together, these data provide compelling evidence for the presence of a previously undefined role for Grr1in spindle pole body and microtubule dynamics. The mechanistic role for Grr1 in these processes cannot be deduced utilizing These data alone but the fact that a number of proteins within the dynein/dynactin complex were observed to change suggests that Grr1 may be directly involved in regulating its function or the activity of a functionally redundant complex. This line of experimentation was not further explored in our research but nevertheless remains an exciting and extremely fertile experimental path.

The GO processes of membrane invagination (endocytosis) as well as purine metabolism are also most likely perturbed in *grr1Δ* cells. Grr1 was found by two hybrid analysis to bind to Bzz1 [448], which was measured to increase 6.39 fold in *grr1Δ* cells by our proteomic analysis. Bzz1 has been found to localize to actin paches and is implicated in the regulation of actin polymerization and endocytosis through its association with the yeast homolog to the human Wiskott-Aldrich syndrome protein (WASP), Las17 [449]. Interestingly, the Bzz1 protein is comprised of a N-terminal FCH bar domain, PEST sequences, and a C-terminal SH3 domain that are all present in a known Grr1 substrate, Hof1 [54]. Based on these observations it has been suggested that Bzz1 is a substrate for $SCF^{Grr1}$ mediated ubiquitylation and the increase in Bzz1 protein levels measured in our analysis is consistent with this hypothesis. Together these data support

that the altered protein levels measured for proteins involved in endocytosis are indeed representative of changes due to *GRR1* deletion.

Taken together the GO process enrichments as determined by GenGO analysis provide a biologically valid snapshot of transcriptional and proteomic processes affected by *GRR1* deletion, yet many of the processes most affected at the transcriptional level were not observed to be enriched at the protein level and visa versa. Interestingly, of the forty two proteins within a significantly enriched GenGO process whose protein abundance level was observed to change greater than three fold, only two showed concomitant changes in the included bronze categorized proteins under the assumption that a large number of significant changes in protein expression observed within a given expression of their encoding genes (Hsp12 and Cit1) (Tables 4.2 and 4.3). The expression level of genes encoding the remaining proteins either remained unaltered or significantly changed in the opposite direction. The enriched processes at both the transcriptional and proteomic levels reflect biological processes known to be perturbed in *grr1Δ* strains. This suggests that Grr1 may influence the molecular biology of the cell through both transcriptional and post-transcriptional mechanisms that in some instances are mutually exclusive. However, this analysis only provides a preliminary characterization of this phenomenon and by no means reflects the degree to which discordance is observed across the genome for *grr1Δ* cells since only 16.7 % of the proteome was quantitatively measured. Nevertheless, the instances of discordance observed in our GenGO analysis provide compelling support for the implementation of concurrent global genomic and proteomic profiling experiments to describe phenotypic manifestations of the molecular response to *GRR1* deletion.

### 4.3.4. Manual Curation and Comparative Analysis of the Transcriptional and Proteomic Response to *GRR1* Deletion

In order to provide a more intricate analysis of the transcriptional and proteomic discordance occurring in response to *GRR1* deletion, we manually annotated each gene and protein observed to change and utilized these manual

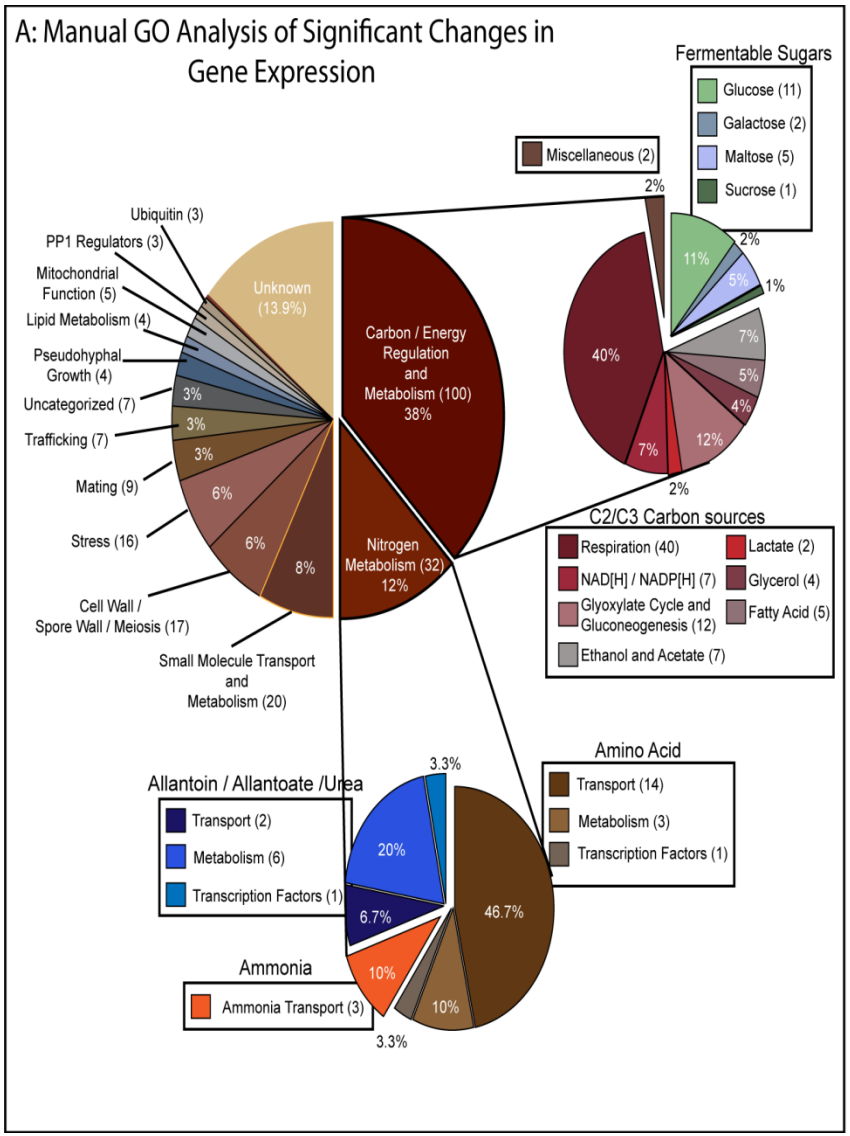
A: Manual GO Analysis of Significant Changes in Gene Expression
Ubiquitin (3)
PP1 Regulators (3)
Mitochondrial Function (5)
Lipid Metabolism (4)
Pseudohyphal Growth (4)
Uncategorized (7)
Trafficking (7)
Mating (9)
Stress (16)
Cell Wall / Spore Wall / Meiosis (17)
Small Molecule Transport and Metabolism (20)
Unknown (13.9%)
Carbon / Energy Regulation and Metabolism (100) 38%
Nitrogen Metabolism (32) 12%
Miscellaneous (2)
Fermentable Sugars
Glucose (11)
Galactose (2)
Maltose (5)
Sucrose (1)
C2/C3 Carbon sources
Respiration (40)
NAD[H] / NADP[H] (7)
Glyoxylate Cycle and Gluconeogenesis (12)
Ethanol and Acetate (7)
Lactate (2)
Glycerol (4)
Fatty Acid (5)
Amino Acid
Transport (14)
Metabolism (3)
Transcription Factors (1)
Allantoin / Allantoate /Urea
Transport (2)
Metabolism (6)
Transcription Factors (1)
Ammonia
Ammonia Transport (3)

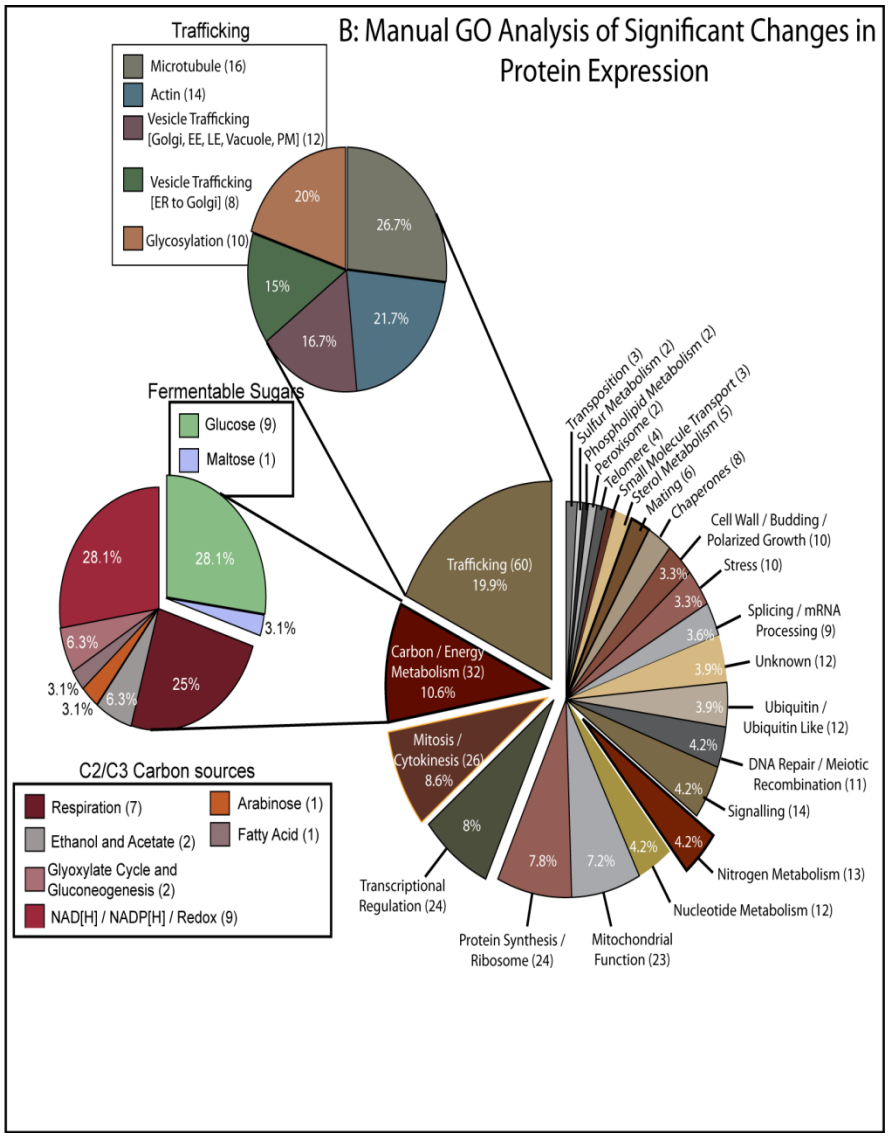
B: Manual GO Analysis of Significant Changes in Protein Expression
Trafficking
Microtubule (16)
Actin (14)
Vesicle Trafficking [Golgi, EE, LE, Vacuole, PM] (12)
Vesicle Trafficking [ER to Golgi] (8)
Glycosylation (10)
Fermentable Sugars
Glucose (9)
Maltose (1)
C2/C3 Carbon sources
Respiration (7)
Ethanol and Acetate (2)
Glyoxylate Cycle and Gluconeogenesis (2)
NAD[H] / NADP[H] / Redox (9)
Arabinose (1)
Fatty Acid (1)
Trafficking (60) 19.9%
Carbon / Energy Metabolism (32) 10.6%
Mitosis / Cytokinesis (26) 8.6%
Transcriptional Regulation (24)
Protein Synthesis / Ribosome (24)
Mitochondrial Function (23)
Nucleotide Metabolism (12)
Nitrogen Metabolism (13)
Signalling (14)
DNA Repair / Meiotic Recombination (11)
Ubiquitin / Ubiquitin Like (12)
Unknown (12)
Splicing / mRNA Processing (9)
Stress (10)
Cell Wall / Budding / Polarized Growth (10)
Chaperones (8)
Mating (6)
Sterol Metabolism (5)
Small Molecule Transport (3)
Telomere (4)
Peroxisome (2)
Phospholipid Metabolism (2)
Sulfur Metabolism (2)
Transposition (3)

**Figure 4.8. Manually Curated GO Process Enrichments for Gene and Protein Expression Changes Measured between *grr1Δ* and wild-type Yeast.** Manually assessed GO enrichments for Gene(A) and Protein(B) expression changes listed in tables 4.2 and 4.3 are presented. Genes and proteins annotated to a given process were totaled (found in parentheses next to the process name) and the percentage of genes or proteins within a given process was calculated by dividing this total by the total number of genes or proteins which were measured to change. Processes such as Carbon/Energy Regulation and Metabolism can be further subdivided into more granular processes and the percentages of genes or proteins in a particular sub-process within some select processes are also presented as expanded pie charts.

annotations to group genes and proteins by shared function and process. Additionally, in order to capture both the relevant changes in gene and protein expression in a format that allowed for the most facile comparison between the two we chose to present the data in two separate tables with one containing both proteomic and transcriptional information for relevant gene changes and the other containing the same information for relevant protein changes. The results of this work are presented in Table 4.2 (transcriptional changes) and Table 4.3 (proteomic changes). Together these tables contain all of the changes in gene and protein expression we measured as well as relevant results from our statistical analyses of each of these data sets. Within the proteomic table we process/function category would serve to strengthen the validity of those proteins quantitated within the same category at lower confidence. Genes and proteins were grouped by relevant shared processes and functions as curated by hand. Changes in gene expression are accompanied by the measured changes in protein expression where applicable and visa versa to allow comparison of transcriptional and proteomic information when both have been measured. Each table also contains annotated function/process and component descriptions collected from descriptions found in the *Saccharomyces* Genome Database as well as our own manual literature searches. Within the gene expression table is a field listing known transcription factors associated with each gene that were based off of annotations contained in the YEASTRACT database [339] and our own literature searches. Additionally, the protein expression table contains information allowing for individual discretion to be utilized when considering the validity and nature of each measured proteomic change. For instance, proteins changes determined by a single peptide could actually be indicative of a change

in a post-translational modification on the peptide being measured. Nevertheless, these instances still represent significant changes in the post-translational state of the protein and thus these instances are retained in our final analysis. However, in these instances the peptide sequence for the measured peptide is included to guide further inquiry.

As indicated in the GenGO analysis of the transcriptional response to *GRR1* deletion, our measured changes in gene expression are consistent with previous *grr1Δ* gene expression profiles. As reported in Figure 4.6, 267 genes were measured to change by two fold or more, of these, 132 (49.4%) could be ascribed to functions or processes involved in carbon or nitrogen metabolism while 51 (20.6%) of the transcriptional changes were in genes encoding for nutrient transporters. As indicated in the description of the GenGO analysis, the affect that *GRR1* deletion has on these processes has been previously characterized to be manifestations of defects in Snf3/Rgt2 signaling and SPS (Ssy1, Ptr3, Ssy5) signaling, respectively. The remainder of the genes observed to be altered in *grr1Δ* strains participate in eclectic cellular processes. These include “cell and spore wall organization and biogenesis /meiosis” (17 genes), “mating” (9 genes), “mitochondrial function” (5 genes), “protein trafficking” (7 genes), “pseudohyphal growth” (4 genes), “stress” (16 genes), “transport of small molecules” (20 genes), “lipid metabolism” (4 genes), “ubiquitin” (3 genes), and a small group of “protein phosphatase one (PP1) regulators” (3 genes). The majority of these processes are consistent with either known molecular roles for Grr1 or *grr1Δ* phenotypes. For instance, defects in mating and small molecule transport have been previously reported for *grr1Δ* cells [71,74]. Grr1 is also known to negatively regulate cell polarity through targeted degradation of the cyclins, Cln1 and Cln2 [346,74], and the Cdc42 effectors, Gic1 and Gic2 [55,101]. Additionally, the known Grr1 substrate, Ime2 [53,450], is a transcriptional regulator of meiotic genes and thus it is likely that Grr1 can influence meiotic gene expression through Ime2. Additionally, the known Grr1 substrate, Ime2 [53,450], is a transcriptional regulator of meiotic genes and thus a mechanism of Grr1’s influence on meiotic gene expression through Ime2 is likely.

Comparison of the list of manually categorized changes in protein abundance (Tables 4.2 and 4.3 and Figure 4.8) with the categorized changes in gene expression revealed accordance and discordance between and within the processes enriched in each list. The processes of carbon and energy metabolism (32), nitrogen metabolism (13), small molecule transport (4), mating (6), mitochondrial function (22), stress (10), ubiquitin (12), and trafficking (60), which were all found to be enriched at the transcriptional level were also enriched at the proteomic level. However, the extent to which these processes were enriched at each molecular level varied to a large degree. For instance, changes in gene expression for carbon and energy metabolism genes represented 38% of the transcriptional changes while they only represented 10.4% of the proteomic changes. Additionally, within this group the sub process of respiration represented 40% of all changes at the transcriptional level but only 25% of the changes observed at the proteomic level. Changes in gene expression for nitrogen metabolism related genes represented 12% of the transcriptional changes observed at the genetic level with changes in nitrogen/amino acid transporters representing 46.7% of all nitrogen related changes in gene expression. At the proteomic level, changes in nitrogen metabolism related proteins only constituted 4.2% of all proteomic changes and only one of the proteins (Put4) was an amino acid transporter. Interestingly, the expression level of proteins involved in “protein and vesicle trafficking” (60 proteins in this category representing 19.5% of all protein changes) process were highly influenced by *GRR1* deletion and yet only modestly reflected at the gene expression level (7 representing 3% of all transcriptional changes). Other processes, such as “mitosis and cytokinesis”, “transcriptional regulation” (constituted of chromatin remodeling and polymerase holo-enzymes as well as a handful of transcription factors), “protein synthesis/ribosome”, “nucleotide metabolism”, “DNA repair / meiotic recombination”, and “splicing / mRNA processing” were among a number of processes only observed to be influenced at the proteomic level (Figure 4.8).

Though these paradoxes distinguishing enriched processes in the proteomic and transcriptional data sets are striking, at least some of them are reflective of reduced proteomic coverage (16.7% of the proteome quantitated) relative to the coverage obtained at the genetic level (~99% of the genome quantitated). Fifty four of the two hundred and sixty seven (20.2%) changes in gene expression were measured at the protein level and, excepting Put4, no quantitative measurements for amino acid transporters were obtained. Thus, the influence that *GRR1* deletion has on amino acid transporters post-transcriptionally could not be assessed. However, contrary to nitrogen metabolism, 15 of the 40 significant changes in gene expression within the sub-process of respiration were measured at the protein level and only three (5%) were measured with significant changes in protein abundance. This would indicate a high level of discordance within the sub-process of respiration. Thus, the enrichments pictured in Figure 4.8 for changes in gene expression must be scrutinized when comparing our manually annotated processes that are highly enriched at the genetic level but underrepresented at the proteomic level.

### 4.3.5. Characterization of Discordance between Protein and Gene Expression Levels in *grr1Δ* Cells

In order to reveal valid instances of discordance systematically between perturbed processes at the genetic and proteomic levels, we plotted the log2 mRNA and protein expression ratios for the 914 genes where a measured protein expression ratio was acquired at high confidence (“Gold” or “Silver” category). Since all of the changes observed at the proteomic level were accompanied by transcriptional measurements, this analysis enabled a more thorough investigation of transcriptional and proteomic discordance. This analysis (Figure 1 A) revealed that a large majority of loci (664 of 914 “Gold” and “Silver”; ~73%) exhibited no significant change in protein or gene expression. Strikingly, only a handful of loci exhibiting significantly altered expression at the protein and mRNA levels showed positive correlation (perfect positive correlation is represented by the diagonal line). Loci exhibiting positive correlation between

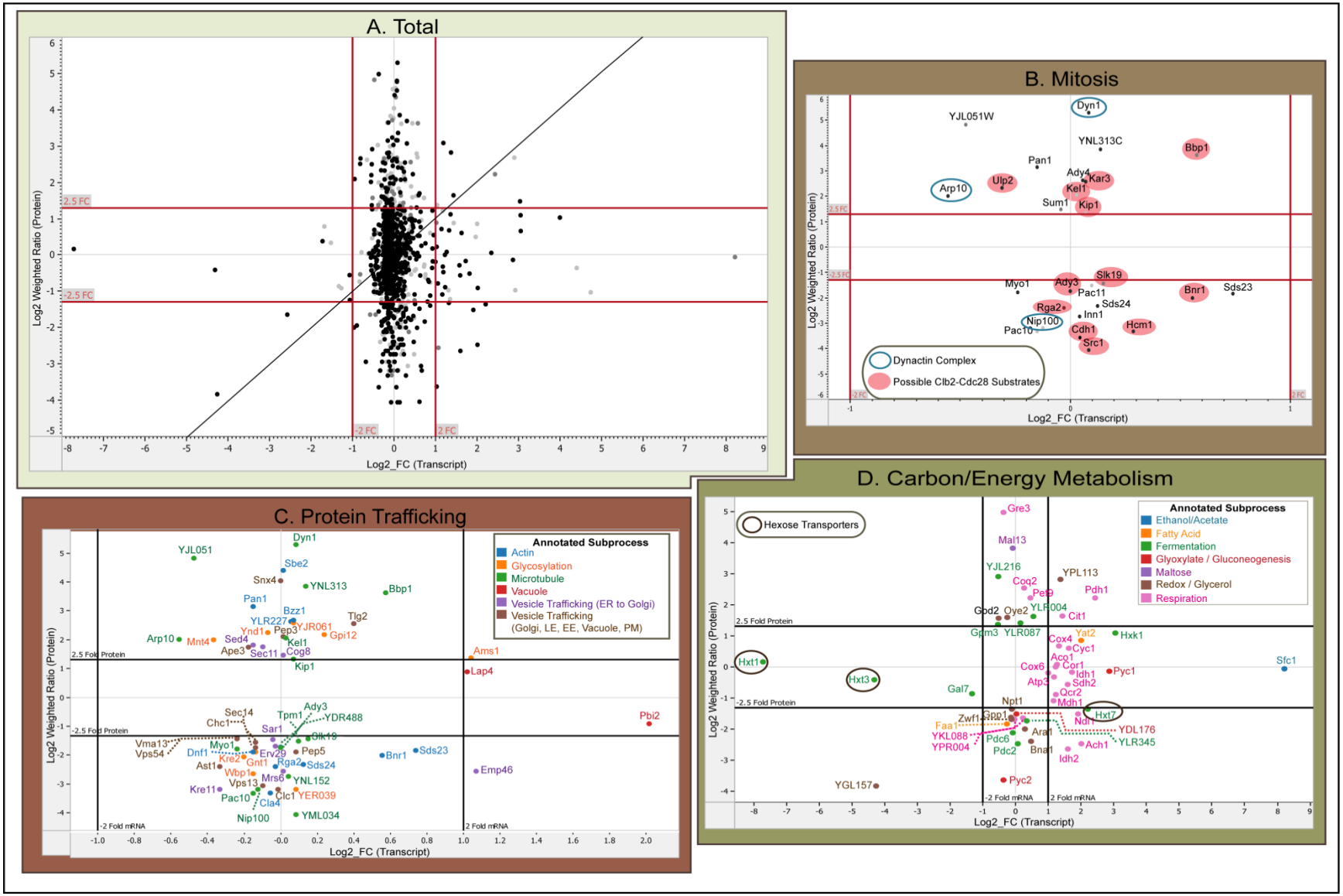
A. Total
Log2 Weighted Ratio (Protein)
Log2_FC (Transcript)
2.5 FC
2 FC
B. Mitosis
YJL051W
Dyn1
YNL313C
Bbp1
Pan1
Ady4
Kar3
Arp10
Ulp2
Kel1
Sum1
Kip1
Myo1
Ady3
Slk19
Pac11
Bnr1
Sds23
Rga2
Sds24
Inn1
Nip100
Pac10
Cdh1
Hcm1
Src1
Dynactin Complex
Possible Clb2-Cdc28 Substrates
C. Protein Trafficking
Annotated Subprocess
Actin
Glycosylation
Microtubule
Vacuole
Vesicle Trafficking (ER to Golgi)
Vesicle Trafficking (Golgi, LE, EE, Vacuole, PM)
YJL051
Dyn1
Sbe2
Snx4
YNL313
Bbp1
Pan1
Bzz1
YLR227
YJR061
Tlg2
Ynd1
Pep3
Gpi12
Arp10
Mnt4
Sed4
Kel1
Ape3
Sec11
Cog8
Kip1
Ams1
Lap4
Pbi2
Sec14
Chc1
Tpm1
Ady3
YDR488
Sar1
Glk19
Vma13
Vps54
Myo1
Erv29
Pep5
Dnf1
Kre2
Gnt1
Rga2
Sds24
Ast1
Wbp1
Mrs6
YNL152
Vps13
Kre11
Pac10
Cla4
Clc1
YER039
Nip100
YML034
Bnr1
Sds23
Emp46
2.5 Fold Protein
-2.5 Fold Protein
2 Fold mRNA
-2 Fold mRNA
Log2 Weighted Ratio (Protein)
Log2_FC (Transcript)
D. Carbon/Energy Metabolism
Annotated Subprocess
Ethanol/Acetate
Fatty Acid
Fermentation
Glyoxylate / Gluconeogenesis
Maltose
Redox / Glycerol
Respiration
Hexose Transporters
Gre3
Mal13
YJL216
YPL113
Coq2
Pet9
Pdh1
God2
Oye2
YLR004
Cit1
Gpm3
YLR087
Yat2
Hxk1
Cox4
Cyc1
Hxt1
Hxt3
Aco1
Cor1
Cox6
Idh1
Pyc1
Sfc1
Atp3
Sdh2
Gal7
Qcr2
Mdh1
Npt1
Hxt7
Zwf1
Gnd1
Nde1
Faa1
YKL088
YPR004
Ara1
YDL176
YLR345
Pdc6
Pdc2
Ach1
Bna1
Idh2
Pyc2
YGL157
2.5 Fold Protein
-2.5 Fold Protein
-2 Fold mRNA
2 Fold mRNA
Log2 Weighted Ratio (Protein)
Log2_FC (Transcript)

**Figure 4.9. Scatter Plots Reveal Discordance between Gene Expression and Protein Expression in *grr1Δ* Cells.** **A.** Scatter plot of the log2 of protein expression (y-axis) versus the log2 of gene expression (x-axis) among 914 loci of "Gold and Silver" confidence (black) and "Bronze" confidence (grey). The diagonal line represents perfect positive correlation. Discordance among the GO (Gene Ontology) "process" clusters of "mitosis", "trafficking", and "carbon/energy metabolism" are shown in panels **B.**, **C**, and **D.**, respectively.

changes in gene expression and their products included *CIT1*, *HSP12, GOR1, NSE5*, and *PDH1*. In each case increase was observed, both transcriptionally and proteomic ally. Furthermore, both Snz1 and Ari1 and their products decreased significantly. The remaining loci showed either little or no positive correlation between protein and mRNA expression levels and can be categorized into three groups based upon the nature of their discordance. The majority of discordant loci (176 of 914 quantitated "Gold" or "Silver") displayed either significantly increased (86) or decreased (90) protein expression with no significant change in gene expression measured. This type of discordance was exhibited by the majority of gene/proteins in all annotated GO processes enriched at the proteomic level (Figure 4.8) but the processes of "trafficking" (Figure 4.9 C), "carbon/energy metabolism" (Figure 4.9 D), "mitosis/cytokinesis" (Figure 4.9 B), "transcriptional regulation", "protein synthesis/ribosome", and "mitochondrial function" together contained over 54% of loci within this category. This suggests that *GRR1* deletion influences these particular processes almost exclusively through post-transcriptional mechanisms. The second type of discordance included loci that exhibit significantly increased or decreased gene expression with no concomitant change in protein expression and contained 26 of 914 loci quantitated at the proteomic level with "Gold" or "Silver" confidence. Though instances of this type of discordance are observed within a number of processes they are most highly enriched in "Carbon/energy metabolism" (Figure 4.9 D) genes/proteins as 15 of the 26 proteins within this category of discordance were annotated to this process. The last discordant category describes instances where the proteomic and genomic expression levels exhibit inverted responses. Interestingly, this type of inverse correlation was only observed for a handful of loci (7) which all displayed a significant decrease in protein expression despite a significant increase in their encoding genes. Once again the majority of

the loci within this group were those annotated to “carbon/energy metabolism” (Figure 4.9 D) (Ach1, Idh2, Hxt7, Ndi1, and Atp19) with one loci annotated to “trafficking” (Emp46) and the final loci annotated to “ergosterol metabolism” (Mcr1). Taken together, these data suggest not only that a number of processes are influenced by *GRR1* deletion exclusively at the protein expression level but also that many gene expression changes observed in response to *GRR1* deletion are not reflected in the expression of their products.

| | | Protein Results | | | | | Transcriptional Results | | | | | |
|---|---|---|---|---|---|---|---|---|---|---|---|---|
| Orf | Gene | Category | Final Protein Probability (Detected) | Probability of Change | SD (±) | Final Protein Ratio (*grr1*Δ/WT) | Fold change | Welch Significance Test | TTest Significance Test | Functions/Go terms | Localization | Transcription Factor |
| **Cell Cycle** | | | | | | | | | | | | |
| YMR199W | CLN1 | ------ | ------ | ------ | ------ | ------ | 2.31 | 0.005702 | 0.003591 | Cell cycle / G1 cyclin involved in regulation of the cell cycle G1-S | Cytoplasm | Xbp1 / |
| YJR090C | GRR1 | ------ | 0.997365 | ------ | ------ | ------ | -361.37 | 0.000965 | 0.000012 | Ubiquitin [F-box protein] / Glucose Repression / Glucose transport / Divalent cation transport / Amino Acid Signaling / Amino acid transport / Cell cycle / Morphogenesis / | Cytoplasm / Nucleus / Bud Neck / SCF Complex | ------ |
| **Cell Wall / Spore Wall / Meiosis** | | | | | | | | | | | | |
| YHL028W | WSC4 | ------ | ------ | ------ | ------ | ------ | -8.94 | 0.00161 | 0.000271 | Cell Wall Stress / Protein targeting to ER | ER membrane | Mal33? |
| YLR042C | YLR042 | ------ | 1 | ------ | ------ | ------ | 3.21 | 0.029662 | 0.023617 | Cell Wall Stress? | Cell Wall | ------ |
| YAR066W | YAR066 | ------ | ------ | ------ | ------ | ------ | 11.13 | 0.0000001 | 0.0000001 | Cell Wall Family / Putative GPI Protein | Unknown | Cat8 / Sok2 / Yap5 |
| YCL048W | SPS22 | ------ | ------ | ------ | ------ | ------ | 2.07 | 0.009868 | 0.003609 | Cell wall biogenesis / Ascospore wall assembly | Plasma Membrane | ------ |
| YOR338W | YOR388 | ------ | ------ | ------ | ------ | ------ | 3.46 | 0.007139 | 0.007139 | Ascospore formation / mRNA is Scp160 target | Unknown | ------ |
| YFL014W | HSP12 | GOLD | 1 | 1.00 | 0.13 | 2.78 | 8.2 | 0.021368 | 0.021368 | Cell Wall Stress | Plasma Membrane | MSN2 / Hap |
| YOR313C | SPS4 | GOLD | 1 | 1.00 | 0.06 | 1.58 | 8.3 | 0.000012 | 0.000012 | Sporulation / Ascospore Formation | Unknown | ------ |
| YPR030W | CSR2 | ------ | 0.7872 | ------ | ------ | ------ | 13.06 | 0.000006 | 0.0000001 | Cell Wall Organization and Biogenesis / Potential Cdc28 Substrate / Potential regulatory role in galactose and nonfermentable carbon source utilization / RSP5 Ubiquitylation | Nucleus | Rap1 / Ume6 |
| YKR076W | YKR076 | ------ | ------ | ------ | ------ | ------ | 2.09 | 0.000145 | 0.000048 | Cell wall / Omega class glutathione transferase | Cytoplasm | Msn / Rgt1 / Stp |
| YLR121C | YPS3 | GOLD | 0.98 | 1.00 | 0.18 | 1.64 | 2.21 | 0.038637 | 0.031754 | Cell wall / Plasma membrane attached aspartic protease | Plasma Membrane | ------ |
| YLR307W | CDA1 | ------ | ------ | ------ | ------ | ------ | 2.63 | 0.001729 | 0.000039 | Ascospore wall assembly / Chitin Deacetylase | Spore wall | Kar4 / Hap |
| YNR067C | DSE4 | ------ | 0.34 | ------ | ------ | ------ | -2.03 | 0.001465 | 0.001465 | Cytokinesis / Cell Separation [secreted glucanase from daughter] | Cell wall / Cell Septum / Extracellular | Ace2 / Swi5 / Yap5,6 / Yox1 |
| YHL024W | RIM4 | ------ | ------ | ------ | ------ | ------ | 3.71 | 0.00416 | 0.00416 | Meiosis / Sporulation / RNA binding? | Cytoplasm | Fhl1 / Fkh2 / Flo8 / Mga1 / Phd1 / Sok2 / Stb5 / Ste12 /Tec1 /Ume6 |
| YPR007C | REC8 | ------ | ------ | ------ | ------ | ------ | 2.35 | 0.024472 | 0.012534 | Meiosis / Component of meiosis specific sister chromatid cohesion complex | | Ste12 / Ino4 |
| YOL104C | NDJ1 | ------ | 0.61 | ------ | ------ | ------ | 2.29 | 0.015076 | 0.010978 | Meiosis / Homolog pairing / Crossover distribution Sister chromatid cohesion at meiotic telomeres | Nucleus / Telomere | Ste12 / Tec1 / Ume6 |
| YNL202W | SPS19 | ------ | ------ | ------ | ------ | ------ | 2.78 | 0.001628 | 0.001628 | Sporulation / Peroxisomal 2,4-dienoyl-CoA reductase, auxiliary enzyme of fatty acid beta-oxidation | Peroxisome | Adr1 / Mss11 |
| *Transcription Factors* | | | | | | | | | | | | |
| YPL230W | USV1 | ------ | ------ | ------ | ------ | ------ | 5.57 | 0.001742 | 0.000901 | Transcription / Cell Wall Biosynthesis Unknown | Unknown | ------ |
| **Mating** | | | | | | | | | | | | |
| YLR452C | SST2 | ------ | 0.995779 | ------ | ------ | ------ | -2.45 | 0.01899 | 0.008895 | Mating [Negatively regulates pheromone response] / GAP for Gpa1 | Plasma membrane | Ecm22 / Mcm1 / Rap1 / Ste12 |
| YJR004C | SAG1 | ------ | 1 | ------ | ------ | ------ | -3.12 | 0.00023 | 0.000083 | Mating [Agglutination] | Cell Wall | Mcm1 / Pho4 / Ste12 |
| YNR044W | AGA1 | ------ | ------ | ------ | ------ | ------ | -4.04 | 0.037033 | 0.011509 | Mating [Agglutination] | Cell Wall | Leu3 / Mbp1 / Mcm1 / Swi4 / Ste12 / Tec1 |
| YAR031W | PRM9 | ------ | ------ | ------ | ------ | ------ | -4.16 | 0.000001 | 0.000001 | Mating / Response to pheromone / Vesicle Organization and Biogenesis | ER / Plasma Membrane | Nrg1 / Ste12 |
| YCL027W | FUS1 | ------ | 0.5444 | ------ | ------ | ------ | -3.55 | 0.01441 | 0.010427 | Mating / Cell Fusion / Potential Cdc28 substrate | Plasma membrane / Mating Projection Tip | Ste12 / Tec1 |
| YCR089W | FIG2 | ------ | 0.98 | ------ | ------ | ------ | -3.2 | 0.049215 | 0.018527 | Mating [Cell wall integrity] | Cell Wall | Ste12 / Tec1 / Yap5 |
| YNL279W | PRM1 | ------ | ------ | ------ | ------ | ------ | -6.49 | 0.033084 | 0.009494 | Mating / Response to pheromone | Plasma Membrane / Mating projection tip | Aft1 / Dal82 / Ste12 / Tec1 |
| YPL156C | PRM4 | bronze | 0.5584 | 1.00 | 0.14 | 1.41 | 3.91 | 0.000797 | 0.000097 | Response to pheromone / Conjugation | Membrane | Aft2 / Hcm1 / Ixr1 / Put3 / Ste12 / Cat8 |
| *Transcription Factors* | | | | | | | | | | | | |

**Table 4.2. Categorized List of Gene Expression Level Changed Between *grr1Δ* and wild-type Yeast.** See page 180 for details.

| | | Protein Results | | | | | Transcriptional Results | | | | | |
|---|---|---|---|---|---|---|---|---|---|---|---|---|
| Orf | Gene | Category | Final Protein Probability (Detected) | Probability of Change | SD (±) | Final Protein Ratio (*grr1* Δ/WT) | Fold change | Welch Significance Test | TTest Significance Test | Functions/Go terms | Localization | Transcription Factor |
| **Metabolism** | | | | | | | | | | | | |
| *Carbon / Energy* | | | | | | | | | | | | |
| Fermentable Sugars | | | | | | | | | | | | |
| Galactose | | | | | | | | | | | | |
| *Metabolism* | | | | | | | | | | | | |
| YBR018C | GAL7 | bronze | 0.22 | 1.00 | 0.04 | 0.55 | -2.51 | 0.000355 | 0.000029 | Carbon [Galactose] | Cytoplasm | Gal4 / Nrg1 / Tos8 |
| *Transcription Factors* | | | | | | | | | | | | |
| YDR009W | GAL3 | ------ | 0.58 | ------ | ------ | ------ | 3.99 | 0.001568 | 0.00026 | Carbon / Transcriptional Activator / Galactose Degradation Genes | Cytoplasm | Gal4 / Mig1 / Pdr3 |
| GLUCOSE | | | | | | | | | | | | |
| *Transport* | | | | | | | | | | | | |
| YDR345C | HXT3 | GOLD | 1 | 0.95 | 0.04 | 1.09 | -19.86 | 0.000025 | 0.0000001 | Transport / Glucose [Low affinity] | | Rgt1 / Ino2 / Ino4 / Pdr1,3 / Phd1 / Sok2 / Stb5 / Ste12 / Swi4,5 / Tec1 |
| YHR092C | HXT4 | ------ | ------ | ------ | ------ | ------ | -11.98 | 0.002213 | 0.000062 | Transport / Glucose [High affinity] | | Rgt1 / Mig1 / Gcr1 / Mal33 / Sko1 / Sok2 / Tec1 / Yap6 |
| YHR094C | HXT1 | GOLD | 0.75 | ------ | 0.00 | 1.12 | -209.98 | 0.0000001 | 0.0000001 | Transport / Glucose [Low affinity] | | Rgt1 / Mig / Aro80 / Fkh1 / Flo8 / Ino4 / Rap1 / Sko1 / Sok2 / Ste12 / Tec1 |
| YDR342C | HXT7 | GOLD* | 1 | 0.16 | 0.44 | 0.39 | 4.62 | 0.003626 | 0.000162 | Transport / Glucose [High affinity] | Plasma Membrane | Crz1 / Hap1,4 / Phd1 / Sok2 / Ste12 / Tec1 /Tos8 |
| YFL011W | HXT10 | ------ | 0.8518 | ------ | ------ | ------ | 4.82 | 0.014196 | 0.002116 | Transport / Glucose? | Plasma membrane | Gts1 / Hap1 / Mbp1 / Tos8 |
| YHR096C | HXT5 | ------ | ------ | ------ | ------ | ------ | 4.4 | 0.001351 | 0.00021 | Transport / Glucose | Plasma Membrane | Hap / Ino4 / Ixr1 / Rap1 / Sko1 / Sok2 / Ste12 / Stp / Rgt |
| *Metabolism* | | | | | | | | | | | | |
| YFR053C | HXK1 | GOLD | 1 | 1.00 | 0.09 | 2.13 | 8.28 | 0.001821 | 0.000043 | Carbon / Glycolysis / Glucose repressed Hexokinase | | Adr1 / Msn2,4 / Gcr1 / Mig / Pdr1 / Sok2 / Ste12 / Tec1 / Neg_reg_by_cAMP and Hxk2 |
| *Transcription Factors* | | | | | | | | | | | | |
| YER028C | MIG3 | ------ | 0.5 | ------ | ------ | ------ | -23.34 | 0.000093 | 0.000004 | Transcription / Glucose Signalling | | Cin5 / Flo8 / Nrg1 / Phd1 / Rgt1 / Sok2 |
| YGL209W | MIG2 | ------ | ------ | ------ | ------ | ------ | -48.77 | 0.000036 | 0.000009 | Transcription / Glucose Signalling | | Rgt1 / Hcm1 / Pdr3 / Sok2 / Ste12 |
| YOR047C | STD1 | ------ | 0.3838 | ------ | ------ | ------ | -3.28 | 0.005809 | 0.0004 | Transcription / Glucose Signaling [Rgt2-Snf3] / Negative regulator of glucose transporter transcription | Nucleus / Plasma Membrane | Cin5 / Rgt1 / Sok2 / Yap6 |
| YDR277C | MTH1 | ------ | ------ | ------ | ------ | ------ | 2.37 | 0.044859 | 0.037501 | Transcription / Glucose Signalling [Rgt2-Snf3] / Negative regulator of glucose transporter transcription | Unknown | Gal4 / Hcm1 / Ino2,4 / Rap1 / Rgt1 / Ste12 |
| Maltose | | | | | | | | | | | | |
| *Transport* | | | | | | | | | | | | |
| YGR289C | MAL11 | ------ | ------ | ------ | ------ | ------ | 2.04 | 0.027915 | 0.022058 | Transport / Maltose Transport and Maltotriose / High affinity and broad specificity | Plasma membrane | Mal13 / Mig1 / Swi4 |
| YBR298C | MAL31 | ------ | 0.53 | ------ | ------ | ------ | 2.44 | 0.025037 | 0.012924 | Transport / Maltose [High affinity α-glucoside transporter] | Plasma Membrane | ------ |
| *Metabolism* | | | | | | | | | | | | |
| YBR299W | MAL32 | ------ | ------ | ------ | ------ | ------ | 21.73 | 0.000001 | 0.0000001 | Carbon / Maltose / alpha-D-glucosidase | Unknown | Mal33 |
| *Transcription Factors* | | | | | | | | | | | | |
| YBR297W | MAL33 | ------ | 0.33 | ------ | ------ | ------ | 6.2 | 0.000003 | 0.000003 | Transcription / Maltose Degradation Genes | Nucleus | ------ |

**Table 4.2.** Continued.

| | | Protein Results | | | | | Transcriptional Results | | | | | |
|---|---|---|---|---|---|---|---|---|---|---|---|---|
| Orf | Gene | Category | Final Protein Probability (Detected) | Probability of Change | SD (±) | Final Protein Ratio (*grr1* Δ/WT) | Fold change | Welch Significance Test | TTest Significance Test | Functions/Go terms | Localization | Transcription Factor |
| **Metabolism Continued** | | | | | | | | | | | | |
| *Carbon / Energy* | | | | | | | | | | | | |
| Fermentable Sugars | | | | | | | | | | | | |
| Sucrose | | | | | | | | | | | | |
| *Metabolism* | | | | | | | | | | | | |
| YIL162W | SUC2 | ------ | 0.9926 | ------ | ------ | ------ | 4.49 | 0.000066 | 0.000019 | Carbon / Sucrose Degradation | Extracellular Region | Gcr1/Hap/Mig |
| Storage Carbohydrates | | | | | | | | | | | | |
| Glycogen | | | | | | | | | | | | |
| YPR160W | GPH1 | ------ | 0.997806 | ------ | ------ | ------ | 4.18 | 0.034364 | 0.034364 | Carbon / Glycogen Degradation | | Stp / Neg_regulated_by_cAMP |
| C2 and C3 Carbon Energy Sources | | | | | | | | | | | | |
| Ethanol / Acetate | | | | | | | | | | | | |
| *Transport* | | | | | | | | | | | | |
| YJR095W | SFC1 | SILVER | 0.973757 | 0.21 | 0.04 | 0.96 | 297.03 | 0.0000001 | 0.0000001 | Transport / Carbon / Mit Transporter - Succinate in and Fumarate out / Required for Ethanol and Acetate based growth | Mitochondria | Cat8 / Sip4 / Ume6 |
| YLR348C | DIC1 | ------ | 0.6976 | ------ | ------ | ------ | 2.82 | 0.025603 | 0.006085 | Carbon/ Ethanol / Acetate / Mitochondrial Dicarboxylate carrier / Dicarboxylates in | Mitochondrial inner membrane | Adr1 |
| YCR010C | ADY2 | ------ | 0.53 | ------ | ------ | ------ | 10.44 | 0.000007 | 0.000001 | Transport / Carbon / Acetate | Plasma Membrane / Mitochondria | Cat8/Adr1 |
| *Metabolism* | | | | | | | | | | | | |
| YAL054C | ACS1 | ------ | 0.5136 | ------ | ------ | ------ | 2.63 | 0.000595 | 0.000595 | Carbon / Acetate / Acetyl-CoA synthetase / Nuclear source of Acetyl CoA for histone acetylation | Cytosol / Nucleus | Adr1 / Cat8 / Abf1 / Ume6 |
| YBL015W | ACH1 | GOLD | 1 | 1.00 | 0.01 | 0.18 | 4.03 | 0.001928 | 0.000352 | Carbon / Acetate Degradation / Acetyl-CoA Hydrolase | Mitochondria | Cat8 / Ume6 |
| YMR303C | ADH2 | ------ | 0.736 | ------ | ------ | ------ | 27 | 0.000049 | 0.000013 | Carbon / Ethanol / Alcohol Dehydrogenase | | Cat8/Gcr1/Adr1 |
| YOR374W | ALD4 | GOLD | 1 | 0.11 | 0.83 | 1.04 | 5.08 | 0.000057 | 0.000016 | Carbon / Ethanol / Aldehyde Dehydrogenase | Mitochondria | Adr1 |
| Fatty Acid | | | | | | | | | | | | |
| *Transport* | | | | | | | | | | | | |
| YAR035W | YAT1 | ------ | 0.69 | ------ | ------ | ------ | 4.15 | 0.000037 | 0.000037 | Carbon / Fatty Acid Ox. / Carnitine Acetyl transferase | Mitochondria / Outer Membrane | Adr1 / Gis1 |
| YER024W | YAT2 | bronze | 0.771058 | 1.00 | 0.11 | 1.81 | 4.01 | 0.000856 | 0.000107 | Carbon / Fatty Acid Ox. / Carnitine Acetyl transferase / Strong activity on Ethanol | Mitochondria / Outer membrane | Cat8 / Oaf |
| YOR100C | CRC1 | ------ | 0.982304 | ------ | ------ | ------ | 6.17 | 0.000008 | 0.000008 | Carbon / Fatty Acid Ox / Mit. Transport Carnitine | Mitochondria / Inner membrane | Adr1 / Cat8 / Oaf1 / Stp |
| *Metabolism* | | | | | | | | | | | | |
| YIL160C | POT1 | ------ | ------ | ------ | ------ | ------ | 3.05 | 0.000253 | 0.000092 | Carbon / Fatty Acid Ox | Peroxisome / Matrix | Adr1 / Oaf1 / Pip2 |
| YGL205W | POX1 | ------ | 0.924019 | ------ | ------ | ------ | 4.82 | 0.000754 | 0.000337 | Carbon / Fatty Acid Ox | Peroxisome | Adr1 / Cat8 / Oaf1 / Pip2 |

**Table 4.2.** Continued.

| | | Protein Results | | | | | Transcriptional Results | | | | | |
|---|---|---|---|---|---|---|---|---|---|---|---|---|
| Orf | Gene | Category | Final Protein Probability (Detected) | Probability of Change | SD (±) | Final Protein Ratio (*grr1* Δ/WT) | Fold change | Welch Significance Test | TTest Significance Test | Functions/Go terms | Localization | Transcription Factor |
| **Metabolism Continued** | | | | | | | | | | | | |
| *Carbon / Energy* | | | | | | | | | | | | |
| C2 and C3 Carbon Energy Sources | | | | | | | | | | | | |
| Glycerol | | | | | | | | | | | | |
| *Metabolism* | | | | | | | | | | | | |
| YER062C | GPP2 | ------ | 0.7 | ------ | ------ | ------ | 2.55 | 0.001766 | 0.000915 | Carbon / Glycerol Biosynthesis / Induced in response to osmotic and oxidative stress | Cytoplasm / Nucleus | ------ |
| YIL155C | GUT2 | ------ | ------ | ------ | ------ | ------ | 2.8 | 0.000063 | 0.000002 | Carbon / Glycerol / NAD metabolism / glycerol-3-phosphate dehydrogenase | Mitochondria | Adr1 / Hap / Neg_reg_by_cAMP / Pos regulated by Snf1 |
| YML087C | AIM33 | ------ | 0.22 | ------ | ------ | ------ | 3.59 | 0.032098 | 0.009013 | Carbon / Deletion Results in increased frequency of mitochondrial genome loss and severe growth defect on minimal glycerol media | Unknown | Hap |
| YFL053W | DAK2 | ------ | 0.985507 | ------ | ------ | ------ | -9.74 | 0.00155 | 0.00155 | Carbon / DHA Kinase | | ------ |
| YDR536W | STL1* | ------ | ------ | ------ | ------ | 0.00 | 5.28 | 0.084704 | 0.0441 | Transport/Glycerol | Plasma Membrane | Cat8 |
| Glyoxylate Cycle / Gluconeogenesis | | | | | | | | | | | | |
| *Metabolism* | | | | | | | | | | | | |
| YCR005C | CIT2 | ------ | 0.6808 | ------ | ------ | ------ | 2.2 | 0.010976 | 0.010976 | Carbon / Glyoxylate Cycle / Synthesis / Glutamate | Peroxisome | ------ |
| YER065C | ICL1 | ------ | 0.99684 | ------ | ------ | ------ | 13.29 | 0.000994 | 0.000013 | Carbon / Glyoxylate Cycle / Isocitrate Lyase | Unknown | Cat8 / Neg_reg_by_cAMP |
| YLR174W | IDP2 | ------ | 0.98 | ------ | ------ | ------ | 12.96 | 0.000689 | 0.000006 | Carbon / Glyoxylate Cycle / Isocitrate dehydrogenase (NADP) / Synthesis / Glutamate | Cytoplasm | Cat8 / Gcr1 |
| YFL030W | AGX1 | ------ | 0.27 | ------ | ------ | ------ | 6.42 | 0.001668 | 0.000285 | Carbon and Amino Acids / Gluconeogenesis / Glyoxylate Aminotransferase / Synthesis / Glycine and Serine | Cytoplasm | Cat8 / Mcm1 |
| YLR377C | FBP1 | ------ | 0.72 | ------ | ------ | ------ | 136.6 | 0.000003 | 0.000001 | Gluconeogenesis / Fructose bis Phosphatase | Cytoplasm | Cat8 / Gcr1 / Mig1 |
| YKR097W | PCK1 | ------ | 1 | ------ | ------ | ------ | 38.64 | 0.0000001 | 0.0000001 | Gluconeogenesis / PEP CarboxyKinase | Cytoplasm | Cat8 / Gcr1 |
| YNL117W | MLS1 | ------ | 0.69277 | ------ | ------ | ------ | 88.33 | 0.000001 | 0.000001 | Gluconeogenesis / Malate Synthase | | Cat8 / Hap1 / Stp1 / Stp2 |
| YGL062W | PYC1 | GOLD | 1 | 0.57 | 0.05 | 0.91 | 7.29 | 0.000006 | 0.000001 | Gluconeogenesis / NADPH Regeneration / Pyruvate Carboxylase | Cytoplasm | Gcr1 |
| *Transcription Factors* | | | | | | | | | | | | |
| YJL089W | SIP4 | ------ | ------ | ------ | ------ | ------ | 6.19 | 0.003752 | 0.000918 | Transcription / Cat8-like | | Cat8 / Gcr1 |
| YMR280C | CAT8 | ------ | 0.5243 | ------ | ------ | ------ | 18.92 | 0.001306 | 0.000022 | Transcription / Gluconeogenesis | | Mig1 / Hap2 |
| YDR216W | ADR1 | ------ | 0.9748 | ------ | ------ | ------ | 3.36 | 0.010127 | 0.006963 | Transcription / Carbon | | Adr1 / Stp |
| YGR067C | YGR067 | ------ | 0.5042 | ------ | ------ | ------ | 12.06 | 0.000166 | 0.00001 | Transcription / Adr1-Like | Unknown | Cat8 / Sok2 |
| Lactate | | | | | | | | | | | | |
| *Transport* | | | | | | | | | | | | |
| YKL217W | JEN1 | ------ | ------ | ------ | ------ | ------ | 26.84 | 0.000001 | 0.000001 | Transport / Carbon / Lactate | Plasma membrane | Adr1 / Cat8 / Hap2 |
| *Metabolism* | | | | | | | | | | | | |
| YML054C | CYB2 | ------ | 0.5644 | ------ | ------ | ------ | 4.35 | 0.00011 | 0.00011 | Carbon / Lactate / L-lactate cytochrome-c oxidoreductase | Mitochondria / Intermembrane space | Adr1 / Gcr1 / Hap |
| NAD[H] / NADP[H] | | | | | | | | | | | | |
| YDL085W | NDE2 | ------ | ------ | ------ | ------ | ------ | 3.22 | 0.00481 | 0.000279 | Redox / Carbon / NADH dehydrogenase [Oxidizes cytosolic NADH] | Mitochondria | Gis1 |
| YPL113C | GOR1 | GOLD | 0.86 | 1.00 | 0.32 | 7.07 | 2.59 | 0.001238 | 0.000184 | NAD / NADP / Glyoxylate and Hydroxypyruvate Reductase | | Adr1 |
| YPL171C | OYE3 | ------ | 0.9221 | ------ | ------ | ------ | 2.87 | 0.000386 | 0.000386 | NAD / NADP / Oxidoreductase for NADH and NADPH | | ------ |
| YJR078W | BNA2 | ------ | 0.33 | ------ | ------ | ------ | 2.59 | 0.001298 | 0.000638 | NAD / de Novo Biosynthesis / Putative tryptophan 2,3-dioxygenase or indoleamine 2,3-dioxygenase | Cytoplasm | Aft1 / Hap |
| YCL026C-B | HBN1 | ------ | ------ | ------ | ------ | ------ | 2.86 | 0.001072 | 0.001072 | NADPH nitroreductase ? | Cytoplasm / Nucleus | ------ |
| YGL157W | YGL157 | GOLD | 0.99 | 0.38 | 0.13 | 0.07 | -19.14 | 0.000001 | 0.0000001 | Oxidoreductase [NADPH Dependent] / Gre2-like | Cytoplasm / Nucleus | Rgt1 / Stp |
| YOL151W | GRE2 | ------ | 0.87 | ------ | ------ | ------ | -2.11 | 0.016925 | 0.016925 | Stress Induced [Oxidative, ionic, oxidative, heat shock, and heavy metals] / 3-methylbutanal reductase and | | ------ |

**Table 4.2.** Continued.

| | | Protein Results | | | | | Transcriptional Results | | | | | |
|---|---|---|---|---|---|---|---|---|---|---|---|---|
| Orf | Gene | Category | Final Protein Probability (Detected) | Probability of Change | SD (±) | Final Protein Ratio (*grr1*Δ/WT) | Fold change | Welch Significance Test | TTest Significance Test | Functions/Go terms | Localization | Transcription Factor |
| **Metabolism Continued** | | | | | | | | | | | | |
| *Carbon / Energy* | | | | | | | | | | | | |
| C2 and C3 Carbon Energy Sources | | | | | | | | | | | | |
| Respiration | | | | | | | | | | | | |
| *Transport* | | | | | | | | | | | | |
| YMR056C | AAC1 | ------ | 0.7768 | ------ | ------ | ------ | 2.11 | 0.029671 | 0.016217 | ATP / Transport / Mitochondrial inner membrane ADP/ATP translocator / ADP in ATP out | Mitochondria Inner membrane | ------ |
| *Metabolism* | | | | | | | | | | | | |
| YPR002W | PDH1 | SILVER | 0.958164 | 1.00 | 0.43 | 4.67 | 5.4 | 0.001971 | 0.000363 | Respiratory Growth / May convert 2-methylcitrate to 2-methylisocitrate | Mitochondria / Outer membrane | Adr1 / Rtg1 / Rtg3 |
| YNR001C | CIT1 | GOLD | 1 | 1.00 | 0.22 | 3.12 | 2.7 | 0.000812 | 0.000812 | Carbon / TCA Cycle / Citrate Synthase | Mitochondria | ------ |
| YPR001W | CIT3 | ------ | 0.97632 | ------ | ------ | ------ | 2.43 | 0.004497 | 0.00119 | Carbon / TCA Cycle / Citrate Synthase and methylcitrate synthase | Mitochondria | Adr1 |
| YLR304C | ACO1 | GOLD | 1 | 0.15 | 0.29 | 1.06 | 2.41 | 0.000577 | 0.00006 | Carbon / TCA Cycle / Aconitase | Mitochondria | Hap / Rtg |
| YGR244C | LSC2 | ------ | 1 | ------ | ------ | ------ | 4.67 | 0.0000001 | 0.0000001 | Carbon / TCA Cycle / Beta subunit of succinyl-CoA ligase | | Adr1 / Gcr1 |
| YDR178W | SDH4 | ------ | 0.6 | ------ | ------ | ------ | 2.76 | 0.000187 | 0.000065 | Carbon / TCA Cycle / Succinate dehydrogenase membrane anchor subunit | Mitochondria | ------ |
| YKL148C | SDH1 | ------ | 1 | ------ | ------ | ------ | 3.94 | 0.001589 | 0.000265 | Carbon / TCA Cycle / Flavoprotein subunit of succinate dehydrogenase | Mitochondria | Cat8 / Gcr1 |
| YLL041C | SDH2 | GOLD | 0.99955 | 1.00 | 0.05 | 0.68 | 3.02 | 0.00145 | 0.000727 | Carbon / TCA Cycle / Iron-sulfur protein subunit of succinate dehydrogenase | Mitochondria | Gcr1 / Neg_reg_by_cAMP |
| YKL141W | SDH3 | ------ | ------ | ------ | ------ | ------ | 2.07 | 0.000334 | 0.000027 | Carbon / TCA Cycle / Cytochrome b subunit of succinate dehydrogenase (Sdh1p, Sdh2p, Sdh3p, Sdh4p) | Mitochondria | Hap |
| YOR136W | IDH2 | GOLD | 1 | 1.00 | 0.01 | 0.16 | 3.03 | 0.000002 | 0.000002 | Carbon / TCA Cycle / Synthesis / Glutamate | Mitochondria | Gcr1 / Hap/Rtg |
| YNL037C | IDH1 | GOLD | 1 | 0.41 | 0.07 | 0.89 | 3.31 | 0.000008 | 0.000002 | Carbon / TCA Cycle / | Mitochondria | Cat8 / Hap |
| YKL085W | MDH1 | GOLD | 1 | 0.12 | 0.55 | 0.47 | 2.24 | 0.00001 | 0.000002 | Carbon / TCA Cycle / Malate Dehydrogenase | Mitochondria | Hap / Msn / Ace2 |
| YKR046C | PET10 | ------ | 0.31 | ------ | ------ | ------ | 3 | 0.008487 | 0.002923 | Respiratory Growth / "ATP/ADP" exchange? | Lipid Particle | Hap |
| YBR039W | ATP3 | GOLD | 1 | 1.00 | 0.03 | 0.80 | 2.26 | 0.000047 | 0.000013 | ATP / Gamma Subunit of F1 sector of F1F0 ATP Synthase | Mitochondria | ------ |
| YDR322C-A | ATP21 | ------ | ------ | ------ | ------ | ------ | 2.05 | 0.000033 | 0.000008 | ATP / Subunit e of mitochondrial F1F0-ATPase | Mitochondria | ------ |
| YDR377W | ATP17 | ------ | 0.77 | ------ | ------ | ------ | 2.24 | 0.000007 | 0.000007 | ATP / Subunit f of the F0 sector of mitochondrial F1F0 ATP synthase | Mitochondria | ------ |
| YLR295C | ATP14 | ------ | 0.999998 | ------ | ------ | ------ | 2.12 | 0.001287 | 0.000022 | ATP / Subunit e of mitochondrial F1F0-ATPase | Mitochondria | Hap |
| YPR020W | ATP20 | ------ | ------ | ------ | ------ | ------ | 2.12 | 0.000227 | 0.000227 | ATP / Subunit g of the F0 sector of mitochondrial F1F0 ATP synthase | Mitochondria | ------ |
| YOL077W-A | ATP19 | GOLD | 0.9998 | 1.00 | 0.03 | 0.40 | 2.5 | 0.00048 | 0.000197 | ATP / Subunit k of the F0 sector of mitochondrial F1F0 ATP synthase | Mitochondria | ------ |
| YDL130W-A | STF1 | ------ | ------ | ------ | ------ | ------ | 2.57 | 0.000957 | 0.000957 | ATP / Negative regulator of F1F0-ATP synthase | Mitochondria | ------ |
| YDL181W | INH1 | ------ | 0.56 | ------ | ------ | ------ | 11.04 | 0.000001 | 0.000001 | ATP / Negative regulator of F1F0-ATP synthase / Like Stf1 | Mitochondria | Hap2 |
| YEL024W | RIP1 | ------ | 1 | ------ | ------ | ------ | 3.54 | 0.000477 | 0.000045 | ATP / Respiratory Growth / Electron Transport Chain/ Transfers electrons from ubiquinol to cytochrome c1 during respiration | Mitochondria | Adr1 / Gcr1 / Hap |
| YBL045C | COR1 | GOLD | 1 | 0.99 | 0.04 | 1.11 | 2.34 | 0.000721 | 0.000084 | ATP / Respiratory Growth / Electron transport chain / Core subunit of ubiquinol-cytochrome c reductase complex | Mitochondria / Inner Membrane | ------ |
| YFR033C | QCR6 | ------ | ------ | ------ | ------ | ------ | 3 | 0.000009 | 0.000009 | ATP / Respiratory Growth / Electron Transport Chain / Subunit 6 of the ubiquinol cytochrome-c reductase complex | Mitochondria | Gcr1 / Hap |
| YHR001W-A | QCR10 | ------ | 1 | ------ | ------ | ------ | 3.6 | 0.000047 | 0.000012 | ATP / Respiratory Growth / Electron Transport Chain / Subunit of the ubiquinol-cytochrome c oxidoreductase complex | Mitochondria | Hap |
| YPR191W | QCR2 | GOLD | 1 | 0.10 | 0.59 | 0.54 | 2.35 | 0.000001 | 0.000001 | ATP / Respiratory Growth / Electron Transport Chain / Subunit 2 of the ubiquinol-cytochrome c oxidoreductase complex | Mitochondria | Hap |
| YML120C | NDI1 | GOLD | 0.8075 | 1.00 | 0.02 | 0.35 | 3.76 | 0.013977 | 0.005848 | Carbon / Electron Transport / NADH:ubiquinone oxidoreductase / | Mitochondria / Matrix | Gcr1 / Hap |
| YOR065W | CYT1 | ------ | ------ | ------ | ------ | ------ | 4.11 | 0.000015 | 0.000003 | Carbon / Electron Transport Chain / Cytochrome c1 | Mitochondria / Inner membrane | Hap / Mig1 |
| YPR151C | SUE1 | ------ | 0.99 | ------ | ------ | ------ | 2.32 | 0.008016 | 0.005322 | Required for degradation of unstable forms of cytochrome C | Mitochondria | Adr1 |

**Table 4.2.** Continued.

| | | Protein Results | | | | | Transcriptional Results | | | | | |
|---|---|---|---|---|---|---|---|---|---|---|---|---|
| Orf | Gene | Category | Final Protein Probability (Detected) | Probability of Change | SD (±) | Final Protein Ratio (*grr1* Δ/WT) | Fold change | Welch Significance Test | TTest Significance Test | Functions/Go terms | Localization | Transcription Factor |
| **Metabolism Continued** | | | | | | | | | | | | |
| *Carbon / Energy* | | | | | | | | | | | | |
| C2 and C3 Carbon Energy Sources | | | | | | | | | | | | |
| Respiration continued | | | | | | | | | | | | |
| *Metabolism continued* | | | | | | | | | | | | |
| YGL187C | COX4 | GOLD | 1 | 1.00 | 0.08 | 1.60 | 2.51 | 0.000015 | 0.000003 | ATP / Electron transport chain / Subunit IV of cytochrome c oxidase | Mitochondria | Hap |
| YHR051W | COX6 | GOLD | 1 | 1.00 | 0.03 | 0.88 | 2 | 0.00402 | 0.000198 | ATP / Electron transport chain / Subunit VI of cytochrome c oxidase | Mitochondria | Hap / Rtg |
| YLR038C | COX12 | ------ | ------ | ------ | ------ | ------ | 2.08 | 0.000001 | 0.000001 | ATP / Electron transport chain / Subunit VIb of cytochrome c oxidase | Mitochondria | Hap |
| YGL191W | COX13 | ------ | 0.81 | ------ | ------ | ------ | 2.08 | 0.000134 | 0.000007 | ATP / Electron transport chain / Subunit VIa of cytochrome c oxidase | Mitochondria | Hap |
| YMR256C | COX7 | ------ | ------ | ------ | ------ | ------ | 2.45 | 0.005542 | 0.000366 | ATP / Respiratory Growth / Electron Transport Chain/ Subunit VII of cytochrome c oxidase | Mitochondria | ------ |
| YIL070C | MAM33 | ------ | 0.96 | ------ | ------ | ------ | 2.1 | 0.004689 | 0.001263 | Unknown / Possible role in oxidative phosphorylation and respiratory growth | Mitochondria | Aft2 / Mcm1 / Met4 / Rtg ? / Adr1 ? |
| *Transcription Factors* | | | | | | | | | | | | |
| YKL109W | HAP4 | ------ | 0.36 | ------ | ------ | ------ | 2.7 | 0.000889 | 0.000114 | Transcription / Activator of Hap2/3/4/5 complex | | Cat8 / Mig1 |
| YKL093W | MBR1 | ------ | 0.36 | ------ | ------ | ------ | 9.93 | 0.00006 | 0.000002 | Respiratory Growth / Stress / Transcription / Hap2 Com Expression | Unknown | ------ |
| YMR081C | ISF1 | ------ | 0.2 | ------ | ------ | ------ | 59.62 | 0.000106 | 0.000005 | Respiratory Growth / Similar to Mbr1 / Transcription / Hap2 Com Expression | Unknown | ------ |
| Miscellaneous | | | | | | | | | | | | |
| YJL103C | GSM1 | ------ | 0.996208 | ------ | ------ | ------ | 3.55 | 0.000167 | 0.000056 | Transcription / Regulation of energy metabolism | Unknown | Gsm1 |
| YNL234W | YNL234 | ------ | 0.997984 | ------ | ------ | ------ | -3.15 | 0.004606 | 0.000257 | Carbon [Glucose] / Signalling and/or Metabolism | Cytoplasm | Rgt1 |
| YBR285W | YBR285 | ------ | ------ | ------ | ------ | ------ | 4.59 | 0.000127 | 0.000127 | Carbon / Deletion leads to poor growth on glucose-minimal medium | Unknown | ------ |
| *Nitrogen/Amino Acid* | | | | | | | | | | | | |
| Amino Acids | | | | | | | | | | | | |
| *Transport* | | | | | | | | | | | | |
| YBR068C | BAP2 | ------ | ------ | ------ | ------ | ------ | -86.22 | 0.000017 | 0.0000001 | Transport / L-I-V | Plasma membrane | Stp / Dal |
| YBR069C | TAT1 | ------ | 0.6524 | ------ | ------ | ------ | -14.58 | 0.000214 | 0.000001 | Transport / V-L-I-Y | Plasma membrane | Stp |
| YCL025C | AGP1 | ------ | ------ | ------ | ------ | ------ | -22.64 | 0.000015 | 0.0000001 | Transport / Amino Acids | Plasma membrane | Stp / Neg. reg. by cAMP |
| YDR046C | BAP3 | ------ | ------ | ------ | ------ | ------ | -208.58 | 0.0000001 | 0.0000001 | Transport / C-L-I-V | Plasma membrane | Stp / Dal |
| YDR508C | GNP1 | ------ | ------ | ------ | ------ | ------ | -8.5 | 0.001101 | 0.000016 | Transport / Q | Plasma membrane | Stp |
| YJL212C | OPT1 | ------ | ------ | ------ | ------ | ------ | -20.06 | 0.001796 | 0.000042 | Transport / Peptides | Plasma membrane | Stp |
| YKR093W | PTR2 | ------ | ------ | ------ | ------ | ------ | -4.3 | 0.020634 | 0.015682 | Transport / Peptides | Plasma membrane | Cat8 / Adr1 / Stp / Cup9 |
| YOL020W | TAT2 | ------ | 0.31 | ------ | ------ | ------ | -4.24 | 0.003972 | 0.000194 | Transport / W-Y | Plasma membrane | Stp |
| YOL163W | YOL163W | ------ | ------ | ------ | ------ | ------ | -4.89 | 0.010744 | 0.004063 | Transport / Dal5-like | Plasma membrane | ------ |
| | | | | | | | | | | | | |
| YGR055W | MUP1 | ------ | ------ | ------ | ------ | ------ | -6.3 | 0.001105 | 0.000156 | Transport / Methionine [High affinity] / Cysteine | Plasma membrane | ------ |
| YPL265W | DIP5 | ------ | ------ | ------ | ------ | ------ | -2.87 | 0.030232 | 0.024127 | Transport / Amino Acids Glutamate and Aspartate [High Affinity] / Also transports Gln, Asn, Ser, Ala, and Gly | Plasma membrane | ------ |
| YKR039W | GAP1 | ------ | 0.92 | ------ | ------ | ------ | 4.71 | 0.009485 | 0.003415 | Transport / Amino Acids [General] | Plasma Membrane | Cat8 / Dal |
| YOR348C | PUT4 | GOLD | 0.8922 | 1.00 | 0.12 | 2.04 | 15.90 | 0.003244 | 0.000131 | Transport / Proline | Plasma Membrane | Adr1 / Dal / Cat8 |
| YPL134C | ODC1 | ------ | 0.6 | ------ | ------ | ------ | 6.13 | 0.00001 | 0.0000001 | Transport / Alpha-ketoglutarate out of mit. / Synthesis / Lysine / Glutamate | Mitochondria / Inner membrane | Cat8 |
| *Metabolism* | | | | | | | | | | | | |
| YLR142W | PUT1 | ------ | 0.456 | ------ | ------ | ------ | 9.18 | 0.000357 | 0.000139 | Nitrogen / Proline Degradation | Mitochondria | Dal/Hap2/Stp/Put |
| YAL062W | GDH3 | ------ | 0.8518 | ------ | ------ | ------ | 8.35 | | | Nitrogen / Glutamate Synthesis | | Dal / Hap2 / Stp |
| YPL273W | SAM4 | ------ | 1 | ------ | ------ | ------ | -2.11 | 0.000001 | 0.0000001 | Synthesis / Methionine | Cytoplasm / Nucleus | ------ |
| *Transcription Fators* | | | | | | | | | | | | |

**Table 4.2.** Continued.

| | | Protein Results | | | | | Transcriptional Results | | | | | |
|---|---|---|---|---|---|---|---|---|---|---|---|---|
| Orf | Gene | Category | Final Protein Probability (Detected) | Probability of Change | SD (±) | Final Protein Ratio (*grr1* Δ/WT) | Fold change | Welch Significance Test | TTest Significance Test | Functions/Go terms | Localization | Transcription Factor |
| **Metabolism Continued** | | | | | | | | | | | | |
| *Nitrogen/Amino Acid* | | | | | | | | | | | | |
| Ammonia | | | | | | | | | | | | |
| *Transport* | | | | | | | | | | | | |
| YGR121C | MEP1 | ------ | 0.27 | ------ | ------ | ------ | 5.5 | 0.010084 | 0.001128 | Transport / NH3 | Plasma Membrane | Dal / Crz1 |
| YNL142W | MEP2 | ------ | 0.99 | ------ | ------ | ------ | 14.34 | 0.001254 | 0.000021 | Transport / NH3 | Plasma Membrane | Dal |
| YNR002C | ATO2 | ------ | ------ | ------ | ------ | ------ | 3.55 | 0.011015 | 0.004205 | Transport / NH3 Export | Plasma Membrane | Cat8 / Sip4 |
| Allantoin / Urea | | | | | | | | | | | | |
| *Transport* | | | | | | | | | | | | |
| YIR028W | DAL4 | ------ | ------ | ------ | ------ | ------ | 11.33 | 0.004591 | 0.001226 | Transport / Allantoin | Unknown | Dal / Stp |
| YJR152W | DAL5 | bronze | 0.6976 | 0.60 | 0.93 | 1.84 | 2.71 | 0.00802 | 0.002699 | Transport / Allantoate | | Dal80,81 / Gat1 / Gln3 / Stp1,2 |
| *Metabolism* | | | | | | | | | | | | |
| YIR027C | DAL1 | bronze | 0.8002 | 1.00 | 0.02 | 0.51 | 7.58 | 0.001522 | 0.000769 | Allantoin Degradation | Unknown | Dal / Stp |
| YIR029W | DAL2 | ------ | 0.93 | ------ | ------ | ------ | 6.9 | 0.002102 | 0.000057 | Allantoin Degradation / Urea | Unknown | Dal |
| YIR031C | DAL7 | ------ | ------ | ------ | ------ | ------ | 7.14 | 0.003218 | 0.000129 | Allantoin Degradation / Glyoxylate Cycle | | Dal |
| YIR032C | DAL3 | ------ | ------ | ------ | ------ | ------ | 16.35 | 0.000122 | 0.000006 | Allantoin Degradation | | Dal / Stp |
| YBR208C | "DUR1,2" | ------ | 1 | ------ | ------ | ------ | 4.14 | 0.00097 | 0.00097 | Allantoin Degradation / Urea | Cytoplasm | Dal |
| YIR030C | DCG1 | ------ | 0.53 | ------ | ------ | ------ | 3.03 | 0.001342 | 0.000208 | Unknown / Sensitive to nitrogen catabolite repression | Unknown | Dal80 / Hap |
| *Transcription Fators* | | | | | | | | | | | | |
| YKR034W | DAL80 | bronze | 0.69 | 0.80 | 0.08 | 0.78 | 21.13 | 0.000392 | 0.000034 | Transcription / Dal genes | Nucleus | GATA / STP |
| Pyrodoxine | | | | | | | | | | | | |
| YMR095C | SNO1 | ------ | ------ | ------ | ------ | ------ | -18.35 | 0.000001 | 0.000001 | Synthesis [Pyrodoxine] | Cytoplasm | ------ |
| YMR096W | SNZ1 | GOLD | 1 | 1.00 | 0.01 | 0.32 | -5.94 | 0.000035 | 0.000009 | Synthesis [Pyrodoxine] | Cytoplasm | ------ |
| *Lipid* | | | | | | | | | | | | |
| YDR018C | YDR018 | GOLD | 1 | 1.00 | 0.05 | 0.70 | 3.53 | 0.000006 | 0.000006 | Synthesis / Phospholipid | Unknown | ------ |
| YKL150W | MCR1 | GOLD | 1 | 1.00 | 0.00 | 0.08 | 2.04 | 0.004444 | 0.00117 | Ergosterol / Mitochondrial NADH-cytochrome b5 reductase | Mitochondria | ------ |
| YDR018C | YDR018 | GOLD | 1 | 1.00 | 0.05 | 0.70 | 3.53 | 0.000006 | 0.000006 | Synthesis / Phospholipid /Acetyltransferase? | Unknown | ------ |
| YPL057C | SUR1 | bronze | 0.56 | 0.08 | 1.07 | 0.51 | 2.48 | 0.001961 | 0.00036 | Lipid / sphingolipid / mannosylinositol phosphorylceramide (MIPC) synthase | Unknown | ------ |
| **Mitochondrial Function** | | | | | | | | | | | | |
| YJL102W | MEF2 | ------ | 0.6861 | ------ | ------ | ------ | 3.08 | 0.000025 | 0.000025 | Mitochondria Translation | Mitochondria | ------ |
| [redacted] | | | | | | | | | | | | |
| YML091C | RPM2 | ------ | ------ | ------ | ------ | ------ | 4.94 | 0.00528 | 0.000334 | Mitochondria organization and biogenesis / Transcription / mRNA processing / Translation | Mitochondria / Mitochondrial ribonuclease P complex / Nucleus / Cytoplasmic mRNA processing body | Hap2 |
| YEL059C-A | SOM1 | ------ | ------ | ------ | ------ | ------ | 2.11 | 0.001766 | 0.001766 | Proteolysis / Required for maturation of mitochondrial proteins of the intermembrane space | Mitochondria / Inner membrane | ------ |
| YGR110W | CLD1 | GOLD | 0.99 | 1.00 | 0.06 | 0.72 | 2.28 | 0.00344 | 0.001996 | Mitochondrial lipid synthesis / Cardiolipin phospholipase | Mitochondria / Inner membrane | |
| YLL013C | PUF3 | ------ | 1 | ------ | ------ | ------ | 2.2 | 0.010252 | 0.010252 | Mitochondria localization / Anterograde Mitochondrial movement / mRNA degradation | Mitochondria / Outer surface | Ste12 |
| **PP1 (Glc7) Regulators** | | | | | | | | | | | | |
| YOR178C | GAC1 | ------ | 0.26 | ------ | ------ | ------ | 14.82 | 0.000349 | 0.000349 | PP1 Regulator | | Neg regulated by cAMP |

**Table 4.2.** Continued.

| | | Protein Results | | | | | Transcriptional Results | | | | | |
|---|---|---|---|---|---|---|---|---|---|---|---|---|
| Orf | Gene | Category | Final Protein Probability (Detected) | Probability of Change | SD (±) | Final Protein Ratio (*grr1*Δ/WT) | Fold change | Welch Significance Test | TTest Significance Test | Functions/Go terms | Localization | Transcription Factor |
| **Protein Trafficking** | | | | | | | | | | | | |
| *Vacuole* | | | | | | | | | | | | |
| YNL015W | PBI2 | GOLD | 1 | 1.00 | 0.03 | 0.53 | 4.05 | 0.000231 | 0.000001 | Trafficking / Inhibitor Vacuolar proteinase B / Vacuolar fusion / SNARE Priming | Vacuole / Cytoplasm | Cat8 / Stp |
| YGL156W | AMS1 | bronze | 0.8404 | 1.00 | 0.20 | 2.59 | 2.06 | 0.000016 | 0.000016 | Carbohydrate Metabolism / Vacuolar alpha mannosidase / oligosaccharide degradation | Vacuolar Membrane | ------ |
| YMR174C | PAI3 | ------ | ------ | ------ | ------ | ------ | 2.24 | 0.000174 | 0.000174 | Vacuolar protein degradation / Cytoplasmic proteinase A (Pep4p) inhibitor | | Hog1 / Pbs2 dependent osmotic induction |
| YKL103C | LAP4 | SILVER | 0.939511 | 1.00 | 0.16 | 1.85 | 2.03 | 0.017044 | 0.012624 | Vacuolar protein degradation / Vacuolar aminopeptidase vscl | Vacuole | Dal80,81,82 / Gat1 /Msn |
| *Misc.* | | | | | | | | | | | | |
| YDL079C | MRK1 | ------ | ------ | ------ | ------ | ------ | 16.93 | 0.0005 | 0.000049 | RSP5 Ubiquitylation / Gsk3 Homolog | Unkown | Mig1 |
| YHR160C | PEX18 | ------ | ------ | ------ | ------ | ------ | 2.05 | 0.021811 | 0.021811 | Trafficking / Peroxisome biogenesis | Peroxisome / Cytoplasm | ------ |
| YLR080W | EMP46 | SILVER | 0.994984 | 1.00 | 0.02 | 0.17 | 2.1 | 0.007314 | 0.004789 | Trafficking / ER to Golgi CopII | Golgi / ER | - |
| **Pseudohyphal Growth** | | | | | | | | | | | | |
| YJR147W | HMS2 | ------ | 0.26 | ------ | ------ | ------ | -2.57 | 0.00062 | 0.000067 | Similar to heat shock transcription factors / Pseudohyphal growth | Cytoplasm / Nucleus | ------ |
| YPL021W | ECM23 | ------ | ------ | ------ | ------ | ------ | -2.59 | 0.0039 | 0.0039 | pre-rRNA processing / Pseudohyphal growth | Unknown | ------ |
| YPL021W | ECM23 | ------ | ------ | ------ | ------ | ------ | -2.59 | 0.0039 | 0.0039 | pre-rRNA processing / Pseudohyphal growth | Unknown | ------ |
| *Transcription Factors* | | | | | | | | | | | | |
| YOR032C | HMS1 | ------ | 0.61 | ------ | ------ | ------ | 2.89 | 0.004488 | 0.004488 | Transcription / Pseudohyphal growth | Unknown | ------ |
| **Stress** | | | | | | | | | | | | |
| Oxidative/ Osmotic / High Temperature | | | | | | | | | | | | |
| YGR154C | GTO1 | ------ | ------ | ------ | ------ | ------ | -2.12 | 0.015292 | 0.015292 | Stress / Oxidative / Glutathione transferase | Peroxisome | ------ |
| YBL064C | PRX1 | ------ | 0.98 | ------ | ------ | ------ | 2.49 | 0.000435 | 0.00004 | Oxidative stress / Respiratory Growth / Reduces hydroperoxides | Mitochondria | ------ |
| YBR046C | ZTA1 | ------ | ------ | ------ | ------ | ------ | 2.07 | 0.001105 | 0.001105 | Oxidative Stress / Quinone reductase activity [NADPH] | Cytoplasm / Nucleus | ------ |
| YLR364W | YLR364 | ------ | ------ | ------ | ------ | ------ | -2.16 | 0.006439 | 0.001981 | Stress ? / Oxidative? / Putative dithiol glutaredoxin / Induced by arsenic | Cytoplasm | ------ |
| YNL036W | NCE103 | ------ | ------ | ------ | ------ | ------ | 2.18 | 0.008766 | 0.005899 | Stress / Oxidative / Carbonic Anhydrase | Cytoplasm / Nucleus | ------ |
| YGL185C | YGL185 | ------ | ------ | ------ | ------ | ------ | 2.94 | 0.000159 | 0.000053 | Oxidoreductase / Hydroxyacid dehydrogenase? | Cytoplasm | ------ |
| YML131W | YML131 | ------ | 0.21 | ------ | ------ | ------ | 2.34 | 0.001217 | 0.001217 | Stress / Osmotic / DNA Damage | Cytoplasm | Yap1,6,7 |
| YOL052C-A | DDR2 | ------ | ------ | ------ | ------ | ------ | 8.28 | 0.008511 | 0.008511 | Stress / Multiple | Cytoplasm / Vacuole | Msn2 / Cad1 |
| YIL113W | SDP1 | bronze | 0.38 | 0.45 | 0.32 | 1.26 | -2.87 | 0.021613 | 0.021613 | Stess / MAPK Phosphatase [Negatively regulates Slt2 by de-phosphorylation] / Oxidative Stress / Heat Shock | Cytoplasm / Nucleus | ------ |
| YMR191W | SPG5 | ------ | 0.21 | ------ | ------ | ------ | 2.27 | 0.002387 | 0.000072 | Protein required for survival at high temperature during stationary phase | | ------ |
| YMR107W | SPG4 | ------ | ------ | ------ | ------ | ------ | 4.51 | 0.006223 | 0.003973 | Stress / Required for survival at high temperature | Unknown | Nothing |
| YOL052C-A | DDR2 | ------ | ------ | ------ | ------ | ------ | 8.28 | 0.008511 | 0.008511 | Stress / Multiple | Cytoplasm / Vacuole | MSN2 |
| YHR043C | DOG2 | ------ | ------ | ------ | ------ | ------ | 2.9 | 0.011691 | 0.004568 | Stress / Oxidative / Osmotic / 2-deoxyglucose-6-phosphate phosphatase / Confers 2-deoxyglucose resistance when overexpressed | Cytoplasm / Nucleus | Mig1,2 / Msn / Sip4 |
| YMR101C | SRT1 | ------ | 0.36 | ------ | ------ | ------ | 2.69 | 0.001496 | 0.001496 | Glycosylation / Cis-prenyltransferase involved in synthesis of long-chain dolichols | Lipid bodies | ------ |
| **Stress Continued** | | | | | | | | | | | | |
| Oxidative/ Osmotic / High Temperature | | | | | | | | | | | | |
| *Transcription Factors* | | | | | | | | | | | | |
| YPR065W | ROX1 | ------ | ------ | ------ | ------ | ------ | 2.01 | 0.001039 | 0.000143 | Transcription / Repressor of Hypoxic genes | Nucleus | Cin5 / Fhl1 / Flo8 / Hap1 / Msn4 / Rim101 / Rox1 / Skn7 / Sko1 / Sok2 / Ste12 / Tec1 / Yap1 / Yap6 |
| YIL101C | XBP1 | GOLD | 0.9504 | 0.98 | 0.60 | 2.17 | 2.57 | 0.029389 | 0.023373 | Transcription / Stress / Repressor of CYS3 and SMF2 / Increased duration of G1 upon overexpression / Transcription induced by multiple stresses includng heat shock, high osmolarity, oxidative stress, DNA damage, | Nucleus | Aft2 / Cin5 / Fhl1 / Ino4 / Mal33 / Mga1 / Nrg1 / Phd1 / Pip2 / Rap1 / Rox1 / Sok2 / Rgt1 / Ste12 / Yap5 |

**Table 4.2.** Continued

| | | Protein Results | | | | | Transcriptional Results | | | | | |
|---|---|---|---|---|---|---|---|---|---|---|---|---|
| Orf | Gene | Category | Final Protein Probability (Detected) | Probability of Change | SD (±) | Final Protein Ratio (*grr1*Δ/WT) | Fold change | Welch Significance Test | TTest Significance Test | Functions/Go terms | Localization | Transcription Factor |
| **Transport (Small Molecules)** | | | | | | | | | | | | |
| *Divalent Cations* | | | | | | | | | | | | |
| YGL258W | VEL1 | ------ | 0.67 | ------ | ------ | ------ | -2.09 | 0.003206 | 0.000733 | Unknown / Highly induced in zinc-depleted conditions | Unknown | ------ |
| YGL255W | ZRT1 | ------ | ------ | ------ | ------ | ------ | -3.13 | 0.00371 | 0.000904 | Transport / Zn [High Affinity] | Plasma membrane | Zap1 |
| YMR319C | FET4 | ------ | ------ | ------ | ------ | ------ | -10.31 | 0.000036 | 0.000036 | Transport / Fe [Low affininty] / Copper and Zinc | Plasma Membrane | ------ |
| YOR382W | FIT2 | ------ | ------ | ------ | ------ | ------ | 4.72 | 0.001976 | 0.001045 | Transport / Fe [Siderophore-iron] | Cell Wall | ------ |
| YOR383C | FIT3 | ------ | ------ | ------ | ------ | ------ | 2.71 | 0.00232 | 0.00046 | Transport / Fe [Siderophore] | Cell Wall | ------ |
| YOR384W | FRE5 | bronze | 0.44 | 0.61 | 1.60 | 2.32 | 2.26 | 0.00682 | 0.004417 | Fe / Ferric reductase / Induced by low Fe levels | Mitochondria | ------ |
| YOL158C | ENB1 | bronze | 0.55 | 1.00 | 0.14 | 1.72 | -3.2 | 0.013689 | 0.005682 | Transport [Endosomal ferric enterobactin transporter] / Response to Fe deprivation / Regulated by Rcs1 | Endosome | ------ |
| YEL065W | SIT1 | ------ | ------ | ------ | ------ | ------ | -3.81 | 0.000069 | 0.000003 | Transport / Fe [Ferrioxamine B] / Potential Cdc28 Substrate | Plasma Membrane | ------ |
| YLR136C | TIS11 | ------ | 0.21 | ------ | ------ | ------ | -2.65 | 0.005949 | 0.003771 | mRNA Degradation / Iron Homeostasis | Cytoplasm / Nucleus | ------ |
| *Multidrug* | | | | | | | | | | | | |
| YBR043C | AQR2 | ------ | 0.454 | ------ | ------ | ------ | -2.37 | 0.000035 | 0.000035 | Transport / Multidrug [quinidine, barban, cisplatin, and bleomycin] | | ------ |
| YHL035C | VMR1 | GOLD | 0.999696 | 0.99 | 0.07 | 0.68 | -2.1 | 0.007543 | 0.007543 | Transport? / Multidrug / Potential Cdc28 substrate | Mitochondria | ------ |
| YHR048W | YHK8 | ------ | 0.45 | ------ | ------ | ------ | -2.73 | 0.00575 | 0.003626 | Transport / Multidrug / Antiporter of the DHA1 family | Integral to Membrane | ------ |
| YOR378W | YOR378 | ------ | 0.44 | ------ | ------ | ------ | -6.94 | 0.000116 | 0.000036 | Transport / Belongs to the DHA2 family of drug:H+ antiporters/ Multidrug??? | Unknown | ------ |
| *Transcription Factors* | | | | | | | | | | | | |
| YOR028C | CIN5 | ------ | ------ | ------ | ------ | ------ | -2.2 | 0.018743 | 0.008738 | Transcription Factor / Pleiotropic drug resistance / Salt Tolerance | Nucleus | ------ |
| *Phosphate* | | | | | | | | | | | | |
| YBR296C | PHO89 | ------ | ------ | ------ | ------ | ------ | 23.76 | 0.015406 | 0.011252 | Transport / Pi and Na co transporter | Plasma Membrane | Crz1 / Pho / Stp |
| YBR092C | PHO3 | ------ | ------ | ------ | ------ | ------ | -6.52 | 0.000216 | 0.000014 | Transport / Acid phosphatase [hydrolyzes thiamin phosphates increasing thiamin uptake] | Cell wall bounded periplasmic spa | Thi2 / Pdc2 / Mig |
| YBR093C | PHO5 | ------ | ------ | ------ | ------ | ------ | 2.56 | 0.043866 | 0.015307 | Transport / Pi / Acid Phosphatase / Nucleoside-triphosphatase / Nucleoside-triphosphate diphosphatase | Cell Wall / Periplasmic Space | ------ |
| *Various* | | | | | | | | | | | | |
| YOR161C | PNS1 | ------ | 0.84 | ------ | ------ | ------ | -2.16 | 0.032857 | 0.018567 | Unknown [Postulated Cholin Transporter????] | Plasma Membrane | ------ |
| YLL052C | AQY2 | ------ | ------ | ------ | ------ | ------ | -2.01 | 0.014949 | 0.010872 | Transport / Water / Osmotically regulated | ER / Plasma Membrane | ------ |
| YLL053C | YLL053C | ------ | ------ | ------ | ------ | ------ | -2.37 | 0.000565 | 0.000239 | Unknown / Contiguous with Aqy2 | Unknown | ------ |
| **Transposon** | | | | | | | | | | | | |
| YGR109W-B | YGR109W-B | ------ | ------ | ------ | ------ | ------ | -3.06 | 0.037576 | 0.011797 | Ty [Retrotransposon TYA Gag and TYB Pol genes] | Retrotransposon nucleocaspid | Ste12 |
| **Ubiquitin** | | | | | | | | | | | | |
| YER098W | UBP9 | ------ | 0.9946 | ------ | ------ | ------ | 2.11 | 0.00447 | 0.00118 | Ubiquitin / Ubiquitin carboxyl-terminal hydrolase | Cytoplasm | ------ |
| YLL039C | UBI4 | GOLD | 1 | 0.89 | 0.09 | 1.17 | 2.04 | 0.037356 | 0.03058 | Ubiquitin / Polyubiquitin precursor | Cytoplasm | Hap / Msn / Ume6 |
| YEL012W | UBC8 | ------ | ------ | ------ | ------ | ------ | 2.02 | 0.008228 | 0.008228 | Ubiquitin / Negative regulation of gluconeogenesis / Mediates the glucose-induced ubiquitination of Fbp1 | Cytoplasm | ------ |
| **Uncategorized** | | | | | | | | | | | | |
| YBL097W | BRN1 | ------ | 0.862016 | ------ | ------ | ------ | 2.1 | 0.0000001 | 0.0000001 | Mitosis / Chromosome Condensation / tRNA condensation | Nucleus | ------ |
| YBR203W | COS111 | ------ | 0.715 | ------ | ------ | ------ | 2.67 | 0.012137 | 0.004812 | Required for ciclopirox olamine resistance | Mitochondria | ------ |
| YLR312C | QNQ1 | bronze | 0.54 | 1.00 | 0.30 | 6.41 | 7.46 | 0.000013 | 0.000003 | Null mutant exhibits reduced reproductive capacity | Unknown | Nothing |
| YEL066W | HPA3 | ------ | ------ | ------ | ------ | ------ | 2.12 | 0.003592 | 0.0021 | Histone Acetylase | Cytoplasm / Nucleus | ------ |
| YML023C | NSE5 | GOLD | 0.972708 | 1.00 | 0.75 | 8.48 | 2.28 | 0.036415 | 0.021265 | DNA Repair / Essential subunit of the Mms21-Smc5-Smc6 complex | Nucleus | ------ |
| YLR327C | TMA10 | ------ | ------ | ------ | ------ | ------ | 16.82 | 0.008691 | 0.000855 | Unknown / Associates with Ribosomes / Stf2-like [Blast] | Nucleus / Cytoplasm | Crz1 / Rox1 |

**Table 4.2.** Continued.

| | | Protein Results | | | | | Transcriptional Results | | | | | |
|---|---|---|---|---|---|---|---|---|---|---|---|---|
| Orf | Gene | Category | Final Protein Probability (Detected) | Probability of Change | SD (±) | Final Protein Ratio (*grr1*Δ/WT) | Fold change | Welch Significance Test | TTest Significance Test | Functions/Go terms | Localization | Transcription Factor |
| **Unknown** | | | | | | | | | | | | |
| YDR222W | YDR222 | ------- | ------- | ------ | ------- | ------- | -2.48 | 0.005988 | 0.0038 | Unknown | Unknown | ------- |
| YER064C | YER064 | ------- | 0.21 | ------ | ------- | ------- | -2.38 | 0.010261 | 0.003811 | Unknown | Nucleus | ------- |
| YGR121W-A | YGR121W-A | ------- | ------- | ------ | ------- | ------- | -2.72 | 0.008623 | 0.005789 | Unknown | Unknown | ------- |
| YGR131W | YGR131 | ------- | 0.35 | ------ | ------- | ------- | -2.2 | 0.00802 | 0.005325 | Unknown | Unknown | ------- |
| YHR210C | YHR210 | ------- | ------- | ------ | ------- | ------- | -2.05 | 0.000015 | 0.000003 | Unknown | Unknown | ------- |
| YGR204C-A | YGR204C-A | ------- | ------- | ------ | ------- | ------- | -2.18 | 0.003814 | 0.000179 | Unknown | Unknown | ------- |
| YHR022C | YHR022 | ------- | 0.21 | ------ | ------- | ------- | -2.48 | 0.011027 | 0.001331 | Unknown | Unknown | ------- |
| YJL078C | PRY3 | ------- | ------- | ------ | ------- | ------- | -2.35 | 0.009133 | 0.003239 | Unknown | Cell Wall | ------- |
| YKL068W-A | YKL068W-A | ------- | ------- | ------ | ------- | ------- | -2.65 | 0.000357 | 0.000357 | Unknown | Unknown | ------- |
| YLR108C | YLR108 | ------- | 0.34 | ------ | ------- | ------- | -3.18 | 0.000807 | 0.000099 | Unknown / Transcription? | Nucleus | ------- |
| YMR321C | YMR321 | ------- | ------- | ------ | ------- | ------- | -2.32 | 0.000462 | 0.000043 | Unknown | Unknown | ------- |
| YAL037C-A | YAL037C-A | ------- | ------- | ------ | ------- | ------- | -2.06 | 0.0000001 | 0.0000001 | Unknown | Unknown | ------- |
| YAL067W-A | YAL067W-A | ------- | ------- | ------ | ------- | ------- | 2.15 | 0.0000001 | 0.0000001 | Unknown | Unknown | ------- |
| YAR068W | YAR068 | ------- | ------- | ------ | ------- | ------- | 10.56 | 0.0000001 | 0.0000001 | Yhr214w-a-Like / Unknown | Unknown | Rim101 |
| YBL043W | ECM13 | ------- | ------- | ------ | ------- | ------- | 6.36 | 0.0000001 | 0.0000001 | Unknown | Unknown | Nothing |
| YBR230W-A | YBR230W-A | ------- | ------- | ------ | ------- | ------- | 2.4 | 0.000003 | 0.000003 | Unknown | Unknown | ------- |
| YDL037C | BSC1 | ------- | ------- | ------ | ------- | ------- | 2.25 | 0.00205 | 0.00205 | Unknown | Unknown | ------- |
| YDL169C | UGX | ------- | ------- | ------ | ------- | ------- | 3.74 | 0.001108 | 0.00053 | Stress | Unknown | ------- |
| YEL057C | YEL057 | ------- | 0.34 | ------ | ------- | ------- | 2.08 | 0.006606 | 0.002054 | Telomere Maintenance / Ume6 target | Unknown | ------- |
| YGR243W | FMP43 | ------- | ------- | ------ | ------- | ------- | 21.04 | 0.000008 | 0.000008 | YHR162w-Like | Unknown | ------- |
| YIL057C | YIL057 | ------- | ------- | ------ | ------- | ------- | 56.08 | 0.000264 | 0.000019 | Yer067w-like / Glucose Repressed | Unknown | Adr1 |
| YLR149C | YLR149 | ------- | 0.6766 | ------ | ------- | ------- | 3.44 | 0.007223 | 0.00472 | Unknown | Unknown | Adr1 |
| YLR307C-A | YLR307C-A | ------- | ------- | ------ | ------- | ------- | 40.12 | 0.000037 | 0.000001 | Unknown | Unknown | Nothing |
| YMR206W | YMR206 | ------- | 0.454 | ------ | ------- | ------- | 48.87 | 0.003868 | 0.000959 | Unknown | Unknown | Sok2 |
| YPL054W | LEE1 | bronze | 0.8677 | 0.37 | 0.25 | 0.49 | 26.71 | 0.000223 | 0.000015 | Unknown | Unknown | Rtg1/Rtg3 |
| YGL146C | YGL146 | ------- | ------- | ------ | ------- | ------- | 4.48 | 0.000034 | 0.000034 | Unknown | Unknown | Nothing |
| YPR036W-A | YPR036W-A | ------- | ------- | ------ | ------- | ------- | 2.35 | 0.002082 | 0.001111 | Unknown | | Pdr1 |
| YNL144C | YNL144 | ------- | ------- | ------ | ------- | ------- | 2.69 | 0.000058 | 0.000016 | Unknown | Mitochondria | ------- |
| YMR194C-B | YMR194C-B | ------- | ------- | ------ | ------- | ------- | 2.24 | 0.005423 | 0.003389 | Unknown | Unknown | ------- |
| YLR466C-B | YLR466C-B | ------- | ------- | ------ | ------- | ------- | 2.79 | 0.000015 | 0.000015 | Dubious | | ------- |
| YLR012C | YLR012 | ------- | ------- | ------ | ------- | ------- | 2.7 | 0.030065 | 0.016504 | Unknown | Unknown | ------- |
| YGL263W | COS12 | ------- | ------- | ------ | ------- | ------- | 2.6 | 0.01359 | 0.01359 | Unknown | Unknown | ------- |
| YHR054C | YHR054 | ------- | ------- | ------ | ------- | ------- | 2.17 | 0.000107 | 0.000107 | Unknown | Unknown | ------- |
| YHR126C | YHR126 | ------- | ------- | ------ | ------- | ------- | 2.91 | 0.007473 | 0.002444 | Unknown | Unknown | ------- |
| YKR015C | YKR015 | ------- | 0.728575 | ------ | ------- | ------- | 2.13 | 0.003292 | 0.003292 | Unknown | Unknown | ------- |
| YLL019C | KNS1 | ------- | 0.62 | ------ | ------- | ------- | 2.07 | 0.003072 | 0.000689 | Kinase / Unknown function | Unknown | ------- |
| YBR230C | OM14 | ------- | 0.32 | ------ | ------- | ------- | 4.98 | 0.000016 | 0.000003 | Abundance decreased in cells grown on glucose | Mitochondria / Outer Membrane | Cat8 |

**Table 4.2.** Continued.

**Table 4.2. Categorized List of Gene Expression Level Changes Between *grr1Δ* and wild-type Yeast.** Significant changes in gene expression (Welch log2 <=.05 and fold change >= 2 or <=-2) were categorized manually utilizing information obtained from the *Saccharomyces* Genome Database (SGD) or through manual literature curation. Genes are grouped at the highest level by shared process (highlighted in Peach). In some instances genes under a given process are further grouped into sub-classes (highlighted in Grey bars) and sub-sub classes (highlighted in Taupe). Under the process of metabolism within the sub-class of carbon/energy metabolism, genes involved in sugar fermentation are highlighted in blue, genes involved in storage carbohydrate metabolism are highlighted in green, and genes involved in respiratory metabolism are highlighted in red. For each gene, the ORF name (ORF) and common gene name (Gene) is provided when one has been assigned. Additionally, the Welch log2, the Student's T-test log2, and the measured fold change (+ = up in *grr1*, - = down in *grr1*) is provided for each measurement. When a measured protein expression level was attained for the gene product, information regarding the validity and degree of its fold change is provided. Relevant metrics pertaining to protein expression data include the "category" which contains the "Gold", "Silver", and "Bronze" designations as determined by the parameters (outlined in Section *3.11.4.7*), the "final protein probability (detected)" which contains the combined protein probability across all analyses (calculation outlined in Section *3.11.4.6*), the "quan confidence" which captures the calculated confidence of the measured protein fold change (calculation outlined in Section *3.11.4.8*), and the "final protein ratio (*grr1*/wt)" and the "SD (±)" which hold the combined relative protein expression and it's associated standard deviation, respectively (calculations outlined in Section *3.11.4.7*). Significant fold changes for both protein and gene expression data are colored red when expression was increased in *grr1* cells and green when expression was decreased in *grr1* cells. Proteins for which an expression level was measured but the expression level change was not significantly different between *grr1* and wild-type cells are colored blue. Each gene is also annotated with notes obtained from SGD as well as manual literature curation that pertain to the genes function and process as well as its localization and this information is captured in the "Functions/GO Terms" and "Localization" columns, respectively. Known transcription factors which contribute to the genes regulation were also obtained utilizing YEASTRACT and manual literature curation and are provided in the "Transcription Factor" column.

| Proteomic Results | | | | | | | Transcriptional Results | | | | | | | | | |
|---|---|---|---|---|---|---|---|---|---|---|---|---|---|---|---|---|
| Orf | Gene | Final Protein Probability (Detected) | Probability of Change | Category | SD (±) | Final Protein Ratio (*grr1* Δ/WT) | Fold change | Welch Significance Test (Log2) | TTest Significance test (Log2) | Functions | Localization of gene product | Peptide Quantitated | Charge | Mass Shift | Inter-experimental STDEV | Intra-experimental STDEV |
| **Cell Wall / Budding / Polarized Growth** | | | | | | | | | | | | | | | | |
| YDL055C | PSA1 | 1 | 0.98 | GOLD | 1.94 | 3.93 | -1.07 | 0.176646 | 0.1669 | Synthesis / Mannose / Glycosylation / Cell wall / Mutants are hypo-osmotic sensitive / Cell Cycle Regulated [Similar to Cln2] | ------ | | | | 0.00 | 1.94 |
| YGR189C | CRH1 | 0.9778 | 1.00 | GOLD* | 0.03 | 0.29 | 1.33 | 0.049273 | 0.049273 | Cell Wall / Bud Site / Chitin / Putative chitin transglycosidase | Cell Wall / Bud Site | K.TL[119]ASSSVTTSSSISSFEKQSSSSSKK.T | 3 | 2 | 0.00 | 0.03 |
| YMR215W | GAS3 | 0.53 | 1.00 | bronze* | 0.02 | 0.31 | 1.02 | 0.941231 | 0.938793 | Cell Wall Maintenance | Cell Wall | R.DAYAFQQLGVNTVR.I | 3 | 2 | 0.00 | 0.02 |
| YBR078W | ECM33 | 1 | 1.00 | GOLD | 0.01 | 0.23 | -1.03 | 0.466916 | 0.466916 | Cell Wall / GPI Anchored / Bud Growth? | Mitochondria / Plasma Membrane | | | | 0.00 | 0.01 |
| YDL019C | OSH2 | 1 | 1.00 | GOLD | 0.71 | 9.40 | -1.03 | 0.805497 | 0.805497 | Trafficking / Bud / Oxysterol Binding Protein | ER / Bud Neck / Plasma Membrane | | | | 0.00 | 0.71 |
| YBR162C | YBR162 | 1.000 | 1.00 | GOLD | 0.17 | 2.54 | 1.1 | 0.010188 | 0.010188 | Cell Wall / Covalently Bound | Cell Wall | | | | 0.00 | 0.17 |
| YOL113W | SKM1 | 0.882 | 0.18 | bronze | 0.41 | 0.39 | 1.12 | 0.435341 | 0.419763 | Polarized Growth / PAK kinase | Plasma Membrane | | | | 0.00 | 0.41 |
| YOR129C | AFI1 | 0.992312 | 1.00 | SILVER* | 0.30 | 3.11 | 1.12 | 0.320766 | 0.3128 | Polarization / Budding | Bud neck / Nucleus / Plasma Membrane | R.NGNTSVSM[147]NL[119]ASL[119]M[147]IPSSIER.N | 3 | 4 | 0.00 | 0.30 |
| YMR313C | TGL3 | 0.67 | 1.00 | bronze* | 0.02 | 0.22 | -1.18 | 0.217519 | 0.170664 | Budding / Lipase / Lipid Metabolism | Lipid particle | R.HRMEVLDNLGLLCSLIK.R | 3 | 10 | 0.00 | 0.02 |
| YLR083C | EMP70 | 0.56 | 1.00 | bronze* | 0.30 | 3.59 | -1.22 | 0.003126 | 0.003126 | Invasive / Pseudohyphal Growth | Endosome | R.IYNSPFQLNMLQEKECESLCK.T | 3 | 6 | 0.00 | 0.30 |
| **Chaperones** | | | | | | | | | | | | | | | | |
| YMR038C | CCS1 | 0.97595 | 1.00 | GOLD | 0.01 | 0.27 | -1.13 | 0.053309 | 0.021126 | Chaperone / Copper / Sod1 | Cytoplasm / Mitochondria / Inner membrane | | | | 0.02 | 0.01 |
| YDR171W | HSP42 | 1 | 1.00 | GOLD | 0.40 | 4.26 | -1.93 | 0.313292 | 0.313292 | Chaperone | ------ | | | | 0.00 | 0.40 |
| YDR168W | CDC37 | 0.99 | 1.00 | GOLD* | 0.01 | 0.19 | -1 | 0.898599 | 0.894356 | Chaperone / Cell Cycle / Osmotic Sensing / Spindle Pole Body Duplication | ------ | K.GGAKPLEATPSEALSSAAESNILNK.L | 2 | 9 | 0.00 | 0.01 |
| YBR169C | SSE2 | 1 | 1.00 | GOLD | 0.35 | 6.04 | -1.03 | 0.801135 | 0.801135 | Chaperone / HSP70 | ------ | | | | 0.00 | 0.35 |
| YBL075C | SSA3 | 1 | 1.00 | GOLD | 0.00 | 0.10 | -1.11 | 0.150521 | 0.140684 | Chaperone / HSP70 / SRP-dependent cotranslational protein targeting to membrane, translocation | ------ | | | | 0.00 | 0.00 |
| YOL031C | SIL1 | 0.82 | 1.00 | GOLD* | 0.53 | 5.25 | 1.14 | 0.15472 | 0.15472 | Chaperone / Nucleotide exchange factor for the endoplasmic reticulum (ER) lumenal Hsp70 chaperone Kar2p | Endoplasmic Reticulum | R.ILPIILSALSSK.L | 2 | 9 | 0.00 | 0.53 |
| YNL007C | SIS1 | 1 | 1.00 | GOLD | 2.14 | 5.65 | -1.45 | 0.202756 | 0.202756 | Chaperone / HSP40 / interacts with Ssa1 | Cytoplasm | | | | 0.00 | 2.14 |
| YHR064C | SSZ1 | 1 | 1.00 | GOLD | 0.01 | 0.24 | -1.06 | 0.212565 | 0.212565 | Chaperone [like Hsp70] / Translation/ Binds Zuo1 | ------ | | | | 0.37 | 0.16 |
| **Mating** | | | | | | | | | | | | | | | | |
| | | | | | | | | | | Mating / Invasive growth / [redacted] | | | | | | |
| YBL016W | FUS3 | 0.841954 | 1.00 | bronze* | 0.40 | 8.15 | -1.31 | | | Kinase [Serine/Threonine] / Activated by Ste7 / Substrates [Ste12, Far1, Bni1, Sst2] | Cytoplasm / Mating tip / Nucleus | K.SLPMYPAAPLEK.M | 3 | 2 | 0.00 | 0.40 |
| YDR103W | STE5 | 0.843712 | 1.00 | bronze | 0.02 | 0.22 | -1.21 | 0.027448 | 0.027448 | Mating Transport / A Mating Factor | ------ | | | | 0.00 | 0.02 |

**Table 4.3. Categorized List of Protein Expression Changes Between *grr1Δ* and wild-type Yeast.** See page 195 for details.

| | | Proteomic Results | | | | | Transcriptional Results | | | | | | | | | |
|---|---|---|---|---|---|---|---|---|---|---|---|---|---|---|---|---|
| Orf | Gene | Final Protein Probability (Detected) | Probability of Change | Category | SD (±) | Final Protein Ratio (*grr1* Δ/WT) | Fold change | Welch Significance Test (Log2) | TTest Significance test (Log2) | Functions | Localization of gene product | Peptide Quantitated | Charge | Mass Shift | Inter-experimental STDEV | Intra-experimental STDEV |
| **Mating Continued** | | | | | | | | | | | | | | | | |
| YPR122W | AXL1 | 0.9379 | 1.00 | SILVER* | 0.01 | 0.32 | -1.36 | 0.0288 | 0.0288 | Mating / 'A' factor maturation / Bud site selection | Bud Neck / Mating tip | R.RSKSLK.K | 1 | 6 | 0.00 | 0.01 |
| YLR389C | STE23 | 0.96373 | 1.00 | GOLD | 0.00 | 0.07 | -1.05 | 0.570683 | 0.559966 | Mating / Maturation of a-factor | Membrane | | | | 0.77 | 0.06 |
| YDR085C | AFR1 | 0.7192 | 1.00 | bronze | 0.01 | 0.27 | 1.12 | 0.453277 | 0.447372 | Mating | ------ | | | | 0.00 | 0.01 |
| **Metabolism** | | | | | | | | | | | | | | | | |
| **Carbon / Energy / Redox** | | | | | | | | | | | | | | | | |
| *Fermentation* | | | | | | | | | | | | | | | | |
| YLR087C | CSF1 | 0.7447 | 1.00 | bronze | 0.19 | 5.20 | 1.11 | 0.047757 | 0.040201 | Carbon / Fermentation | Mitochondria | | | | 4.93 | 0.41 |
| YOL056W | GPM3 | 1.000 | 1.00 | GOLD | 0.19 | 2.58 | -1.45 | 0.096358 | 0.053703 | Carbon / Glycolysis | Cytoplasm | | | | 0.00 | 0.19 |
| YJL216C | YJL216 | 0.9676 | 1.00 | GOLD* | 0.56 | 7.53 | -1.44 | 0.001704 | 0.000878 | Carbon / alpha-D-glucosidase | ------ | K.EMHNYM[147]LSQVPEGK.E | 3 | 2 | 0.00 | 0.56 |
| YLR345W | YLR345 | 0.75 | 0.90 | GOLD | 0.13 | 0.30 | 1.27 | 0.248313 | 0.248313 | Carbon / Glycolysis? / Similar to 6-phosphofructo-2-kinase / fructose-2,6-bisphosphatase enzymes responsible for the metabolism of fructoso-2,6-bisphosphate | Cytoplasm | | | | 0.00 | 0.13 |
| YDR081C | PDC2 | 0.8183 | 1.00 | bronze* | 0.01 | 0.18 | 1.05 | 0.429814 | 0.423554 | Transcription / Controls PDC Expression / Glucose to ethanol metabolism / Thiamin | Nucleus | R.YNICLM[147]AERHPK.W | 2 | 3 | 0.00 | 0.01 |
| YLR004C | THI73 | 0.813661 | 1.00 | bronze* | 0.24 | 3.09 | 1.46 | 0.056627 | 0.037726 | Transport / Carboxylic acid / Repressed by thiamine | Endoplasmic Reticulum | R.AL[119]L[119]NYAASMGIK.D | | | 0.00 | 0.24 |
| YGR087C | PDC6 | 0.986474 | 1.00 | SILVER* | 0.01 | 0.23 | -1.06 | 0.800571 | 0.796261 | Carbon / Pyruvate Decarboxylase | ------ | K.TPANKGVPASTPLK.Q | 3 | 2 | 0.00 | 0.01 |
| *Transport* | | | | | | | | | | | | | | | | |
| YDR342C | HXT7 | 1.000 | 0.16 | GOLD | 0.44 | 0.39 | 4.62 | 0.003626 | 0.000162 | Transport / Glucose / High Affinity | Plasma Membrane | | | | 0.00 | 0.44 |
| YMR011W | HXT2 | 0.922 | 0.34 | GOLD* | 0.26 | 0.25 | -1.09 | 0.300509 | 0.292233 | Transport / Glucose | Plasma membrane | R.IISGMGVGGIAVL[119]SPTL[119]ISETAPK.H | 2 | 6 | 0.00 | 0.26 |
| *Maltose* | | | | | | | | | | | | | | | | |
| YGR288W | MAL13 | 0.775 | 1.00 | bronze | 0.81 | 14.19 | -1.06 | 0.435062 | 0.403454 | Transcription / Maltose Degradation Genes | Nucleus | | | | 0.00 | 0.81 |
| *Respiration* | | | | | | | | | | | | | | | | |
| YNR041C | COQ2 | 0.996248 | 1.00 | GOLD | 0.82 | 5.83 | 1.2 | 0.03323 | 0.03323 | Carbon / Electron Transport / catalyzes the second step in ubiquinone (coenzyme Q) biosynthesis | Mitochondria | | | | 0.00 | 0.82 |
| YPR004C | AIM45 | 1 | 1.00 | GOLD | 0.02 | 0.32 | 1.17 | 0.172956 | 0.172956 | Carbon / Electron Transport / catalyzes the second step in ubiquinone (coenzyme Q) biosynthesis | Mitochondria | | | | 0.00 | 0.02 |
| YML120C | NDI1 | 0.808 | 1.00 | GOLD* | 0.02 | 0.35 | 3.76 | 0.013977 | 0.005848 | Carbon / Electron Transport / NADH:ubiquinone oxidoreductase | Mitochondria | | | | 0.00 | 0.02 |
| YBL030C | PET9 | 1 | 1.00 | GOLD | 0.32 | 4.67 | 1.37 | 0.000444 | 0.000041 | ADP IN / ATP OUT Carrier for Mit. | Mitochondria [Inner Membrane] | | | | 2.03 | 0.51 |

**Table 4.3.** Continued.

| Proteomic Results | | | | | | | Transcriptional Results | | | | | | | | | |
|---|---|---|---|---|---|---|---|---|---|---|---|---|---|---|---|---|
| Orf | Gene | Final Protein Probability (Detected) | Probability of Change | Category | SD (±) | Final Protein Ratio (*grr1* Δ/WT) | Fold change | Welch Significance Test (Log2) | TTest Significance test (Log2) | Functions | Localization of gene product | Peptide Quantitated | Charge | Mass Shift | Inter-experimental STDEV | Intra-experimental STDEV |
| Metabolism Continued | | | | | | | | | | | | | | | | |
| Carbon / Energy / Redox Continued | | | | | | | | | | | | | | | | |
| YOR136W | IDH2 | 1 | 1.00 | Bronze* | 0.01 | 0.16 | 3.03 | 0.000002 | 0.000002 | Carbon / TCA Cycle / Synthesis / Glutamate | Gcr1/Hap/Rtg | KTFGL[119]FANRVPAK | | | 0.00 | 0.01 |
| YPR002W | PDH1 | 0.958164 | 1.00 | SILVER | 0.43 | 4.67 | 5.4 | 0.001971 | 0.000363 | Respiratory Growth / May convert 2-methylcitrate to 2-methylisocitrate | Mitochondria /Outer membrane | | | | 0.00 | 0.43 |
| Acetate | | | | | | | | | | | | | | | | |
| YBL015W | ACH1 | 1 | 1.00 | GOLD* | 0.01 | 0.18 | 4.03 | 0.001928 | 0.000352 | Carbon [Acetate Degradation] | Mitochondria | AIAGHLVEFFR | | | 0.96 | 0.41 |
| YKL088W | YKL088 | 0.999637 | 1.00 | GOLD* | 0.03 | 0.31 | -1.02 | 0.772923 | 0.772923 | Synthesis / coenzyme A | ------ | K.KFHIL[119]IGATGSVATIK.V | 3 | 2 | 0.00 | 0.03 |
| Arabinose | | | | | | | | | | | | | | | | |
| YBR149W | ARA1 | 1 | 1.00 | GOLD* | 0.02 | 0.25 | 1.22 | 0.170342 | 0.170342 | Carbon [Arabinose] / NADP Dependent | Cytoplasm | R.AIGVSNFSIEYLER.L | 2 | 3 | 0 | 0.02 |
| Fatty Acid | | | | | | | | | | | | | | | | |
| YOR317W | FAA1 | 0.998974 | 1.00 | GOLD | 0.03 | 0.28 | -1.2 | 0.488315 | 0.488315 | Carbon / Synthesis / Fatty Acid / | Mitochondria / Outer membrane / lipid particle | | | | 0.00 | 0.03 |
| Gluconeogenesis | | | | | | | | | | | | | | | | |
| YDL176W | YDL176 | 0.990 | 1.00 | GOLD | 0.03 | 0.35 | 1.02 | 0.770156 | 0.768147 | Carbon / Gluconeogenesis? / Fbp1 degradation? | | | | | 0.00 | 0.03 |
| YBR218C | PYC2 | 1 | 1.00 | GOLD | 0.01 | 0.08 | -1.29 | 0.001943 | 0.001943 | Carbon / Gluconeogenesis / Pyruvate Carboxylase | Cytoplasm | | | | 0.00 | 0.01 |
| NAD[H] / NADP[H] / Redox | | | | | | | | | | | | | | | | |
| YHR104W | GRE3 | 1 | 1.00 | GOLD | 0.31 | 7.67 | -1.29 | 0.314706 | 0.314706 | Carbon [Xylose and Arabinose] / Detoxification / Methylglyoxal | ------ | | | | 15.21 | 0.86 |
| YNL241C | ZWF1/MET19 | 1 | 1.00 | GOLD | 0.02 | 0.31 | -1.09 | 0.655785 | 0.655785 | Carbon / Redox / Pentose Phosphate Shunt | Cytoplasm | | | | 0.00 | 0.02 |
| YIL053W | GPP1 | 1 | 1.00 | GOLD | 0.01 | 0.32 | -1.1 | 0.04668 | 0.04668 | Carbon / Glycerol / Osmotic Stress | Cytoplasm / Nucleus | | | | 0.05 | 0.02 |
| YOL059W | GPD2 | 1.000 | 1.00 | SILVER | 0.31 | 2.97 | -1.43 | 0.116689 | 0.116689 | Carbon / Glycerol / Phosphatitic Acid / NAD | Cytoplasm | | | | 0.00 | 0.31 |
| YJR025C | BNA1 | 1 | 0.74 | GOLD* | 0.14 | 0.19 | 1.39 | 0.023176 | 0.017885 | Synthesis / NAD [From tryptophan via kynurenine] | Cytoplasm | K.EAIL[119]DFENDVEKR.T | 2 | 3 | 0.00 | 0.14 |
| YOR209C | NPT1 | 1.000 | 0.40 | GOLD | 0.25 | 0.39 | -1.08 | 0.020087 | 0.015211 | NAD Salvage Pathway / Chromatin Silencing at Telomere | Nucleus | | | | 0.00 | 0.25 |
| YGL157W | YGL157 | 0.99 | 0.38 | GOLD | 0.13 | 0.07 | -19.14 | 0.000001 | 0 | Oxidoreductase [NADPH Dependent] / Gre2-like | Cytoplasm / Nucleus | | | | 0.00 | 0.13 |
| YHR179W | OYE2 | 1 | 1.00 | GOLD | 0.11 | 3.02 | -1.19 | 0.063246 | 0.043439 | Oxidoreductase [NADPH Dependent] | Cytoplasm / Nucleus / Mitochondria | | | | 1.40 | 0.24 |

**Table 4.3.** Continued.

| Proteomic Results | | | | | | | Transcriptional Results | | | | | | | | | |
|---|---|---|---|---|---|---|---|---|---|---|---|---|---|---|---|---|
| Orf | Gene | Final Protein Probability (Detected) | Probability of Change | Category | SD (±) | Final Protein Ratio (*grr1* Δ/WT) | Fold change | Welch Significance Test (Log2) | TTest Significance test (Log2) | Functions | Localization of gene product | Peptide Quantitated | Charge | Mass Shift | Inter-experimental STDEV | Intra-experimental STDEV |
| **Metabolism Continued** | | | | | | | | | | | | | | | | |
| **Nucleotide** | | | | | | | | | | | | | | | | |
| YJL055W | YJL055 | 0.47 | 1.00 | bronze* | 0.53 | 7.94 | -1.07 | 0.109668 | 0.100044 | Nucleotide Metabolism | Cytoplasm / Nucleus | K.LVYGGGTTGLMGKIAR.S | 2 | 3 | 0.00 | 0.53 |
| YNR034W | SOL1 | 0.84 | 0.25 | GOLD | 0.24 | 0.13 | -1.6 | 0.067438 | 0.047121 | Synthesis / Nucleotide / tRNA export from nucleus | Nucleus | | | | 0.00 | 0.24 |
| YML022W | APT1 | 1 | 1.00 | GOLD | 0.01 | 0.31 | 1.38 | 0.161369 | 0.151554 | Adenine salvage / Synthesis / AMP / Catalyzes condensation of adenine and PRPP | Cytoplasm / Nucleus | | | | 0.87 | 0.14 |
| YMR096W | SNZ1 | 1 | 1.00 | GOLD | 0.01 | 0.32 | -5.94 | 0.000035 | 0.000009 | Synthesis / Pyridoxine [Vitamin B6] / Interacts with Sno1 | Unknown | | | | 0.00 | 0.01 |
| YNR012W | URK1 | 0.576 | 0.87 | bronze* | 2.34 | 3.55 | 1.08 | 0.421055 | 0.404925 | Metabolism / Nucleotide | ------ | R.ILNAFDNKVNIFAGM[147]IISR.E | 3 | 2 | 0.00 | 2.34 |
| YHL011C | PRS3 | 0.999654 | 1.00 | GOLD* | 1.55 | 27.33 | 1.05 | 0.339899 | 0.320577 | Synthesis / Nucleotide, Histidine, Tryptophan | ------ | K.SVIAIVTHGVL[119]SGR.A | 2 | 3 | 0.00 | 1.55 |
| YBR248C | HIS7 | 1.000 | 0.32 | GOLD | 3.99 | 2.65 | -1.06 | 0.360405 | 0.341889 | Synthesis / Nucleotide / Histidine | Cytoplasm | | | | 0.00 | 3.99 |
| YLR028C | ADE16 | 1 | 1.00 | GOLD | 0.50 | 6.48 | -1.09 | 0.131691 | 0.107594 | Synthesis / Nucleotide [Purine] / Histidine | Cytoplasm | | | | 2.52 | 1.22 |
| YDR226W | ADK1 | 1 | 1.00 | GOLD | 0.38 | 6.98 | -1.12 | 0.024403 | 0.018957 | Synthesis / Nucleotide [ATP] | ------ | | | | 2.54 | 1.09 |
| YMR087W | YMR087 | 0.762 | 1.00 | bronze | 0.02 | 0.36 | 1.1 | 0.369122 | 0.361915 | Synthesis / ADP-Ribose / tRNA Splicing | | | | | 0.00 | 0.02 |
| *Transport* | | | | | | | | | | | | | | | | |
| YBR021W | FUR4 | 0.72 | 1.00 | bronze | 0.01 | 0.16 | 1.16 | 0.496617 | 0.491348 | Transport / Nucleotide / Uracil | Plasma Membrane | | | | 0.00 | 0.01 |
| **Phospholipid** | | | | | | | | | | | | | | | | |
| YER026C | CHO1 | 0.78 | 1.00 | GOLD* | 0.37 | 5.84 | -1.2 | 0.326035 | 0.318151 | Phospholipids | ER | R.FTLTGKPHYVQR.A | 2 | 3 | 0.00 | 0.37 |
| YNL264C | PDR17 | 0.945 | 1.00 | SILVER | 0.02 | 0.32 | -1.49 | 0.046486 | 0.016859 | Phospholipids | ------ | | | | 0.00 | 0.02 |
| **Nitrogen/Amino Acid** | | | | | | | | | | | | | | | | |
| YBR115C | LYS2 | 1 | 1.00 | GOLD | 2.02 | 23.07 | -1.23 | 0.018063 | 0.013485 | Synthesis / Amino Acid [Lysine] | ------ | | | | 12.92 | 1.86 |
| YBR263W | SHM1 | 1 | 1.00 | GOLD | 0.01 | 0.15 | -1.01 | 0.482349 | 0.454371 | Synthesis / Amino Acids [Serine and Glycine] / Glyoxylate Metabolism / Folate Metabolism | ------ | | | | 0.00 | 0.01 |
| YER081W | SER3 | 1 | 0.10 | GOLD | 0.46 | 0.12 | 1.57 | 0.014122 | 0.005931 | Synthesis / Amino Acids (Serine and Glycine) / Glyoxylate Metabolism | ------ | | | | 0.00 | 0.46 |
| YGL148W | ARO2 | 1 | 1.00 | GOLD | 0.02 | 0.28 | -1.23 | 0.000197 | 0.000197 | Synthesis / Amino Acids | ------ | | | | 0.00 | 0.02 |
| YGL009C | LEU1 | 1 | 0.98 | GOLD | 0.10 | 0.30 | -1.14 | 0.500455 | 0.473826 | Synthesis / Amino Acids (Branched Chains) | ------ | | | | 0.23 | 0.48 |
| YNL160W | YGP1 | 1 | 1.00 | GOLD* | 0.60 | 8.40 | 1.24 | 0.802874 | 0.801177 | Transport / Nitrogen / Stress | Cell Wall | K.WFFDASKPTL[119]ISSDSIIR.K | 2 | 3 | 0.00 | 0.60 |
| YML099C | ARG81 | 0.7228 | 1.00 | bronze | 0.00 | 0.07 | 1.35 | 0.167918 | 0.120203 | Synthesis / Amino Acids | ------ | | | | 0.27 | 0.01 |
| YEL062W | NPR2 | 0.6661 | 1.00 | bronze | 0.63 | 5.21 | 1.17 | 0.018302 | 0.00846 | Regulator / Nitrogen Permeases | ------ | | | | 0.00 | 0.63 |
| YMR250W | GAD1 | 0.23 | 1.00 | bronze* | 0.67 | 6.15 | -1.57 | 0.395384 | 0.395384 | Amino Acid Metabolism / Glutamate De-carboxylase / Oxidative Stress | Cytoplasm | R.KSSFIYEMLLALASPQDDIPTPDEIEKKNK.L | 3 | 6 | 0.00 | 0.67 |
| | | | | | | | | | | Nitrogen / NADP+ dependent | | | | | | |

**Table 4.3.** Continued.

| | | Proteomic Results | | | | | Transcriptional Results | | | | | | | | | |
|---|---|---|---|---|---|---|---|---|---|---|---|---|---|---|---|---|
| Orf | Gene | Final Protein Probability (Detected) | Probability of Change | Category | SD (±) | Final Protein Ratio (*grr1* Δ/WT) | Fold change | Welch Significance Test (Log2) | TTest Significance test (Log2) | Functions | Localization of gene product | Peptide Quantitated | Charge | Mass Shift | Inter-experimental STDEV | Intra-experimental STDEV |
| **Metabolism Continued** | | | | | | | | | | | | | | | | |
| **Nitrogen/Amino Acid Continued** | | | | | | | | | | | | | | | | |
| YDR380W | ARO10 | 0.912 | 1.00 | SILVER | 0.15 | 2.52 | 1.15 | 0.323567 | 0.303611 | Nitrogen / Amino Acid Degradation / Aromatic Amino Acid requiring/ NAD | Cytoplasm | | | | 0.00 | 0.15 |
| YHR208W | BAT1 | 1.000 | 1.00 | GOLD | 0.17 | 2.90 | -1.16 | 0.346384 | 0.307785 | Nitrogen / Branched Chain Amino Acid Degradation | Mitochondria | | | | 0.00 | 0.17 |
| YKL157W | APE2 | 1.000 | 1.00 | GOLD | 0.02 | 0.37 | 1.13 | 0.36031 | 0.34179 | Amino Acid / Leucine Scavenging / Aminopeptidase | Cell wall bounf periplasmic space / Extracellular | | | | 0.00 | 0.02 |
| **Sterol** | | | | | | | | | | | | | | | | |
| YML008C | ERG6 | 1 | 1.00 | GOLD | 0.01 | 0.13 | 1.01 | 0.819911 | 0.819911 | Synthesis / Sterol | Endoplasmic Reticulum / Mitochondria / Outer membrane | | | | 0.00 | 0.01 |
| YLR450W | HMG2 | 0.935056 | 1.00 | SILVER | 0.41 | 6.31 | -1.18 | 0.264037 | 0.241911 | Synthesis / Sterol | Endoplasmic reticulum | | | | 5.22 | 0.61 |
| YGR175C | ERG1 | 0.87 | 1.00 | GOLD | 0.01 | 0.13 | -1.22 | 0.013166 | 0.013166 | Synthesis / Sterol | ER | | | | 0.00 | 0.01 |
| YKL150W | MCR1 | 1 | 1.00 | GOLD* | 0.00 | 0.08 | 2.04 | 0.004444 | 0.00117 | Synthesis [Ergosterol] / NADH-cytochrome b5 reductase | Mitochondria | GSNVVRPYTPVSDLSQK | | | 1.52 | 0.34 |
| YNR043W | MVD1 | 1.000 | 1.00 | GOLD | 0.0100 | 0.2100 | -1.02 | 0.693342 | 0.686314 | Synthesis / Sterol | | | | | 0.42 | 0.03 |
| **Sulfur Metabolism** | | | | | | | | | | | | | | | | |
| YPL274W | SAM3 | 1 | 1.00 | GOLD | 0.03 | 0.26 | -1.86 | 0.003171 | 0.000721 | Sulfur / Transport / SAM [High Affinity] | Plasma membrane | | | | 0.00 | 0.03 |
| YLL057C | JLP1 | 0.9944 | 1.00 | GOLD* | 0.34 | 4.59 | -1.46 | 0.104249 | 0.104249 | Sulfur / Sulfonate Catabolism / Fe(II)-dependent sulfonate/alpha-ketoglutarate dioxygenase | Unknown | K.RRAPVTHIHPLVR.V | 3 | 2 | 0.00 | 0.34 |
| **Mitochondria** | | | | | | | | | | | | | | | | |
| YNL055C | POR1 | 1.000 | 1.00 | GOLD | 0.02 | 0.36 | 1.53 | 0.000586 | 0.00025 | Mitochondria / Porin | Mitochondria | | | | 0.95 | 0.57 |
| YLR259C | HSP60 | 1.000 | 1.00 | GOLD | 0.02 | 0.39 | -1.03 | 0.514119 | 0.501466 | Mitochondria / Chaperonin / Proteine folding | Mitochondria | | | | 0.24 | 0.21 |
| YGR132C | PHB1 | 1.000 | 1.00 | GOLD* | 0.02 | 0.36 | 1.22 | 0.005957 | 0.003777 | Mitochondrial Segregation / Prohibitin complex | Mitochondria | | | | 0.00 | 0.02 |
| YKL195W | MIA40 | 1.000 | 1.00 | GOLD | 0.04 | 0.39 | -1.02 | 0.926263 | 0.925652 | Mitochondria / Protein import and assembly | Mitochondrial intermembrane space | | | | 0.00 | 0.04 |
| [illegible] | | | | | | | | | | | | | | | | |
| YNL185C | MRPL19 | 0.71 | 1.00 | bronze* | 0.02 | 0.30 | 1.4 | 0.083619 | 0.043232 | Mitochondrial Translation | Mitochondria | K.SDERHSLLEM[147]LGSAPAK.G | 3 | 6 | 0.00 | 0.02 |
| YHR198C | FMP22 | 0.776 | 1.00 | bronze | 0.48 | 6.46 | 1.48 | 0.008553 | 0.005735 | Nothing | Mitochondria | | | | 0.00 | 0.48 |
| YHR194W | MDM31 | 0.7932 | 1.00 | bronze | 0.02 | 0.32 | -1.11 | 0.171012 | 0.171012 | Mitochondrial Inheritance / Ion homeostasis | Mitochondria / Inner Membrane | | | | 0.00 | 0.02 |
| YLR190W | MMR1 | 0.942 | 1.00 | SILVER | 0.25 | 2.70 | 1.17 | 0.134275 | 0.110132 | Mitochodria Inheritance / Interacts with Myo2 / mRNA targeted to bud by She2 dependent mechanism | Mitochondria of Bud | | | | 0.00 | 0.25 |
| YGR062C | COX18 | 0.44 | 1.00 | bronze* | 0.46 | 5.74 | 1.11 | 0.092545 | 0.083207 | Protein insertion into inner Mitochondrial Membrane | Mitochondria [Inner membrane] | K.QQELRKLVQPITPIIK.L | 3 | 4 | 0.00 | 0.46 |
| YOR187W | TUF1 | 1 | 1.00 | GOLD | 0.01 | 0.11 | 1.59 | 0.000614 | 0.000264 | Translation / Mit. / Mitochondrial translation elongation factor Tu | Mitochondria / Matrix | | | | 0.00 | 0.01 |
| [illegible] | | | | | | | | | | Reduced Growth rate on minimal | | | | | | |

**Table 4.3.** Continued.

| | | Proteomic Results | | | | | Transcriptional Results | | | | | | | | | |
|---|---|---|---|---|---|---|---|---|---|---|---|---|---|---|---|---|
| Orf | Gene | Final Protein Probability (Detected) | Probability of Change | Category | SD (±) | Final Protein Ratio (*grr1* Δ/WT) | Fold change | Welch Significance Test (Log2) | TTest Significance test (Log2) | Functions | Localization of gene product | Peptide Quantitated | Charge | Mass Shift | Inter-experimental STDEV | Intra-experimental STDEV |
| **Mitochondria Continued** | | | | | | | | | | | | | | | | |
| YNL310C | TIM15 | 0.9439 | 0.50 | GOLD | 0.20 | 0.22 | 1.17 | 0.087462 | 0.078241 | Mit. Chaperone / Mitochondria organization and biogenesis / Mitochondria protein import | Mitochondria | | | | 0.05 | 0.31 |
| YNL121C | TOM70 | 0.99918 | 1.00 | GOLD | 0.01 | 0.18 | -1.01 | 0.670799 | 0.670799 | Trafficking / Mitochondria protein import | Mitochondria / Outer membrane | | | | 0.00 | 0.01 |
| YER004W | YER004 | 0.49 | 1.00 | bronze* | 0.48 | 4.11 | 1.21 | 0.065347 | 0.056854 | Unknown | Mitochondria | K.HIIILRPGPLLGER.T | 2 | 9 | 0.00 | 0.48 |
| YDR116C | MRPL1 | 0.72 | 1.00 | bronze* | 0.31 | 3.01 | 1.36 | 0.10604 | 0.082751 | Mitochondrial Translation [Large Ribosomal Subunit) | Mitochondria | K.IAAFTNDESKL[119]EEL[119]R.E | 3 | 4 | 0.00 | 0.31 |
| YFL036W | RPO41 | 1.000 | 1.00 | GOLD | 0.01 | 0.39 | 1.42 | 0.000613 | 0.000613 | Mitochondiral RNA Polymerase | Mitochondria | | | | 2.70 | 0.28 |
| YOL027C | MDM38 | 1 | 1.00 | GOLD | 0.00 | 0.06 | 1.53 | 0.002248 | 0.002248 | Trafficking / Involved in membrane integration of a subset of mitochondrial proteins / K transport and homeostasis | Mitochondria / Inner membrane | | | | 0.60 | 0.18 |
| YKL011C | CCE4 | 0.832 | 1.00 | bronze | 0.20 | 2.63 | -1.05 | 0.68203 | 0.68203 | Recombination / Mitochondrial | Mitochondria Inner membrane | | | | 0.00 | 0.20 |
| YGR147C | NAT2 | 0.592 | 1.00 | bronze | 0.04 | 0.37 | 1.13 | 0.267047 | 0.245022 | Protein Methylation | Mitochondria | | | | 0.00 | 0.04 |
| YJR077C | MIR1 | 1.000 | 0.97 | GOLD | 2.4700 | 3.2400 | 1.53 | 0.000191 | 0.000191 | Mitochondria / Phospate carrier / Functionally redundant with Pic2 | | | | | 1.24 | 1.27 |
| YDL069C | CBS1 | 1.000 | 0.92 | GOLD | 0.0600 | 0.1500 | 1.18 | 0.077198 | 0.038186 | Mitochondria / Membrane bound translational activator / COB mRNA | Mitochondria | | | | 0.36 | 0.05 |
| **Peroxisome** | | | | | | | | | | | | | | | | |
| YLR191W | PEX13 | 0.9974 | 1.00 | GOLD | 0.02 | 0.20 | 1.14 | 0.14435 | 0.134513 | Peroxisome Biogenesis / Protein import into peroxisome matrix, docking | Peroxisomal membrane | | | | 0.00 | 0.02 |
| YGR004W | PEX31 | 0.8674 | 1.00 | bronze | 0.79 | 12.52 | -1.12 | 0.332572 | 0.292907 | Peroxisome Biogenesis / Negative Regulation of Peroxisome Size | Peroxisome | | | | 0.00 | 0.79 |
| **Protein Synthesis / Ribosome** | | | | | | | | | | | | | | | | |
| *Ribosome Biogenesis* | | | | | | | | | | | | | | | | |
| YLR276C | DBP9 | 0.901 | 1.00 | GOLD | 0.33 | 7.05 | -1.09 | 0.285451 | 0.27695 | Ribosome Biogenesis / rRNA processing | Nucleolus | | | | 0.00 | 0.33 |
| YPL043W | NOP4 | 0.88 | 1.00 | GOLD | 0.87 | 6.27 | 1 | 0.989104 | 0.989104 | Ribosome Biogenesis / rRNA processing | Nucleolus | | | | 0.00 | 0.87 |
| YAL025C | MAK16 | 0.997728 | 1.00 | GOLD* | 0.35 | 4.24 | 1.2 | 0.548828 | 0.544284 | Ribosome Biogenesis [rRNA maturation 25S and 5.8S] | Nucleolus | R.RL[119]AL[119]REEERHYVGVAPK.V | 3 | 4 | 0.00 | 0.35 |
| YPL239W | YAR1 | 1 | 1.00 | GOLD* | 0.18 | 5.00 | -1.17 | 0.006297 | 0.006297 | Ribosome Biogenesis / Osmotic Stress | Cytoplasm | K.ESESDSTALHMAAANGHIETVR.Y | 3 | 2 | 0.00 | 0.18 |
| YKL082C | RRP14 | 0.999823 | 1.00 | GOLD | 0.32 | 3.46 | -1.12 | 0.409623 | 0.393046 | Ribosome Biogenesis / Establishment of cell polarity | Nucleolus and Cytoplasm | | | | 0.00 | 0.32 |
| YGR159C | NSR1 | 1 | 1.00 | GOLD* | 0.00 | 0.15 | -1.06 | 0.183627 | 0.183627 | Ribosome Biogenesis / rRNA processing | Nucleolus | K.ALDALQGEYIDNRPVR.L | 2 | 6 | 0.00 | 0.00 |
| YIL019W | FAF1 | 0.805 | 1.00 | bronze | 0.01 | 0.13 | -1.13 | 0.56329 | 0.56329 | Ribosome Biogenesis / rRNA processing | Nucleolus | | | | 0.00 | 0.01 |
| YJL148W | RPA34 | 1 | 1.00 | GOLD | 0.02 | 0.13 | -1.09 | 0.087699 | 0.078472 | Ribosome Biogenesis / RNA Polymerase I | Nucleolus | | | | 0.00 | 0.02 |
| YDR239C | YDR239 | 0.63 | 1.00 | bronze | 0.76 | 6.81 | -1.05 | 0.537125 | 0.537125 | Ribosome Association? | Cytoplasm | | | | 0.00 | 0.76 |

**Table 4.3.** Continued.

| | | Proteomic Results | | | | | Transcriptional Results | | | | | | | | | |
|---|---|---|---|---|---|---|---|---|---|---|---|---|---|---|---|---|
| Orf | Gene | Final Protein Probability (Detected) | Probability of Change | Category | SD (±) | Final Protein Ratio (*grr1*Δ/WT) | Fold change | Welch Significance Test (Log2) | TTest Significance test (Log2) | Functions | Localization of gene product | Peptide Quantitated | Charge | Mass Shift | Inter-experimental STDEV | Intra-experimental STDEV |
| **Protein Synthesis / Ribosome** | | | | | | | | | | | | | | | | |
| *Ribosome Biogenesis* | | | | | | | | | | | | | | | | |
| YJL033W | HCA4 | 0.977 | 1.00 | GOLD | 0.03 | 0.35 | 1.08 | 0.668692 | 0.668692 | Ribosome Biogenesis / rRNA processing (18S) | Nucleolus | | | | 0.00 | 0.03 |
| YOR310C | NOP58 | 1.000 | 1.00 | GOLD | 0.02 | 0.39 | -1.14 | 0.02792 | 0.014954 | Ribosomal Biogenesis / pre-rRNA processing | Nucleolus / Processome | | | | 0.17 | 0.35 |
| YHL033C | RPL8A | 1.000 | 1.00 | GOLD | 0.4950 | 2.8422 | -1.1 | 0.017738 | 0.013209 | ------ | | | | | 1.52 | 0.88 |
| Translation | | | | | | | | | | | | | | | | |
| YKR057W | RPS21A | 1.000 | 1.00 | GOLD | 0.01 | 0.38 | -1.11 | 0.04063 | 0.033587 | Ribosome / small ribosomal subunit (40S) | Cytoplasm | | | | 0.28 | 0.29 |
| YJL190C | RPS22A | 1.000 | 1.00 | GOLD | 0.14 | 2.88 | -1.16 | 0.063893 | 0.028316 | Ribosome / Small subunit (40s) | ------ | | | | 1.23 | 0.28 |
| YPL079W | RPL21B | 1.000 | 1.00 | GOLD | 0.01 | 0.37 | -1.12 | 0.021131 | 0.021131 | Ribosome / large ribosomal subunit (60S) | Cytoplasm | | | | 0.42 | 0.05 |
| YNL244C | SUI1 | 1 | 1.00 | GOLD* | 0.28 | 4.23 | -1.17 | 0.003784 | 0.003784 | Translation Initiation [eIF1] | Cytoplasm / multi-eIF complex | K.TLTTVQGVPEEYDLKR.I | 2 | 6 | 0.00 | 0.28 |
| YMR309C | NIP1 | 0.9936 | 1.00 | SILVER* | 0.79 | 13.12 | -1.03 | 0.67385 | 0.658589 | Translation Initiation [eIF3] | Cytoplasm | R.LRDEQSIYNLILR.T | | | 0.00 | 0.79 |
| YOL139C | CDC33 | 1 | 1.00 | GOLD* | 0.08 | 0.33 | -1.06 | 0.215465 | 0.206048 | Translation Initiation / mRNA Cap binding / mRNA Catabolism | Cytoplasm / eIF-4F Complex [eIF-4E] | K.L[119]TDDGHL[119]EFFPHSSANGR.H K.LTDDGHLEFFPHSSANGR.H | | | 0.00 | 0.08 |
| YJL080C | SCP160 | 1 | 1.00 | GOLD | 0.16 | 3.60 | -1.15 | 0.035952 | 0.02091 | Translation/ RNA Binding [Localization] / Mating [Gpa1 effector / binding] / Spindle Pole Body /Chromatin Silencing / Chromosome Segregation | Nuclear Envelope and ER | | | | 1.29 | 0.37 |
| YER176W | ECM32 | 0.6976 | 1.00 | bronze* | 0.01 | 0.13 | -1.09 | 0.281934 | 0.260426 | Translation Termination / DNA-RNA Helicase | Polysome | K.FSSDKLNRSQK.T | | | 0.00 | 0.01 |
| YPL030W | YPL030 | 0.994 | 1.00 | GOLD | 0.03 | 0.39 | -1.17 | 0.198715 | 0.198715 | tRNA Methyltransferase / Serine | Cytoplasm | | | | 0.00 | 0.03 |
| Miscellaneous | | | | | | | | | | | | | | | | |
| YMR295C | YMR295 | 0.99 | 1.00 | GOLD* | 0.03 | 0.31 | 1.17 | 0.202908 | 0.179082 | Associates with ribosomes | Bud / Mating projection tip / ribosome | R.TASVADPILDAVQEAQPFEQAADTFHDNMNR.Q | | | 0.00 | 0.03 |
| **Signalling** | | | | | | | | | | | | | | | | |
| Cell Cycle | | | | | | | | | | | | | | | | |
| YPL194W | DDC1 | 0.89374 | 1.00 | bronze | 0.00 | 0.06 | 1.11 | 0.464491 | 0.450023 | Cell Cycle [G1-S, G2-M] / DNA Damage Checkpoint / Repair | Chromosomes | | | | 0.16 | 0.05 |
| YPL256C | CLN2 | 0.52 | 1.00 | bronze* | 0.01 | 0.12 | 1.26 | 0.282931 | 0.274393 | Cell Cycle [G1-S Phase] | Cytoplasm / Nucleus | R.QSQLSQDSDATVDER.P | 3 | 2 | 0.00 | 0.01 |
| YDR247W | VHS1 | 0.7723 | 1.00 | bronze | 0.20 | 3.62 | -1.06 | 0.77966 | 0.77966 | Cell Cycle [G1-S Phase] | Cytoplasm | | | | 0.43 | 0.28 |
| YDL127W | PCL2 | 0.73 | 1.00 | bronze | 0.21 | 5.34 | 1.13 | 0.664542 | 0.661425 | Cell Cycle [G1-S Phase] / Cell Polarity | Bud Neck / Bud Tip / Nucleus | | | | 0.00 | 0.21 |
| Miscellaneous | | | | | | | | | | | | | | | | |

**Table 4.3.** Continued**.**

| | | Proteomic Results | | | | | Transcriptional Results | | | | | | | | | |
|---|---|---|---|---|---|---|---|---|---|---|---|---|---|---|---|---|
| Orf | Gene | Final Protein Probability (Detected) | Probability of Change | Category | SD (±) | Final Protein Ratio (*grr1*Δ/WT) | Fold change | Welch Significance Test (Log2) | TTest Significance test (Log2) | Functions | Localization of gene product | Peptide Quantitated | Charge | Mass Shift | Inter-experimental STDEV | Intra-experimental STDEV |
| **Signalling Continued** | | | | | | | | | | | | | | | | |
| **PP1** | | | | | | | | | | | | | | | | |
| YBL058W | SHP1 | 0.9933 | 1.00 | GOLD* | 0.01 | 0.11 | -1.26 | | | Ubiquitin [Cdc48] / PP1(Glc7) Regulation | Cytoplasm / Nucleus | K.APTRKLGGFSGQGQR.L | 3 | 2 | 0.00 | 0.01 |
| YNL233W | BNI4 | 0.86 | 1.00 | GOLD | 0.32 | 5.31 | 1.07 | 0.256604 | 0.247693 | PP1 Regulator | ------ | | | | 0.00 | 0.32 |
| YER133W | GLC7 | 1 | 0.91 | GOLD | 3.07 | 4.35 | -1.06 | 0.232361 | 0.223138 | PP1 | ------ | | | | 0.00 | 3.07 |
| **RAS / cAMP** | | | | | | | | | | | | | | | | |
| YJL005W | CYR1 | 1 | 1.00 | GOLD | 0.13 | 3.00 | -1.21 | 0.192371 | 0.192371 | Ras1 Signaling / Adenylate Cyclase | ------ | | | | 4.66 | 0.59 |
| YOR101W | RAS1 | 0.7777 | 0.83 | bronze | 19.94 | 13.61 | -1.01 | 0.872509 | 0.871439 | Glucose Signaling / Adenylate Cyclase | Plasma Membrane | | | | 0.00 | 19.94 |
| **TOR** | | | | | | | | | | | | | | | | |
| YKL203C | TOR2 | 1.000 | 1.00 | GOLD | 0.4100 | 5.48 | -1.02 | 0.776201 | 0.774251 | TOR2 Signalling | | | | | 2.28 | 0.24 |
| YJR066W | TOR1 | 0.99032 | 1.00 | GOLD* | 2.07 | 23.10 | 1.05 | 0.392031 | 0.385184 | TOR1 Signaling | ------ | K.FEPLFSVISSKQRPR.K | 3 | 2 | 0.00 | 2.07 |
| YPL180W | TCO89 | 1 | 1.00 | SILVER | 0.30 | 3.20 | 1 | 0.918405 | 0.918405 | Torc1 Subunit / Glycerol Metabolism / Cell growth / Salt Stress | Vacuolar Membrane | | | | 0.00 | 0.30 |
| YMR068W | AVO2 | 1.000 | 1.00 | GOLD | 0.03 | 0.38 | -1.03 | 0.729189 | 0.723116 | TORII Complex | Cytoplasm | | | | 0.00 | 0.03 |
| **Stress (Oxidative / Osmotic / Cell Wall / Heavy Metal)** | | | | | | | | | | | | | | | | |
| YNL042W | BOP3 | 0.954325 | 0.25 | GOLD | 0.31 | 0.25 | -1.95 | 0.000173 | 0.000059 | Response to mercury / Potential Cdc28 substrate | Cytoplasm/ Nucleus | | | | 0.00 | 0.31 |
| YNL239W | LAP3 | 0.94265 | 0.10 | SILVER | 0.56 | 0.18 | 1.15 | 0.338577 | 0.330889 | Homocysteine resistance | Cytoplasm / Mitochondria | | | | 0.00 | 0.56 |
| YFL014W | HSP12 | 1.000 | 1.00 | GOLD | 0.13 | 2.78 | 8.2 | 0.021368 | 0.021368 | Stress / Cell wall, Osmotic, Oxidative, Glucose Depletion / HOG and RAS-PKA pathway regulated | Cytoplasm / Nucleus / Membrane | | | | 3.57 | 0.45 |
| YLR194C | YLR194 | 0.71 | 1.00 | bronze* | 0.04 | 0.31 | -1.06 | 0.638175 | 0.629572 | Cell Wall Stress / GPI Anchored | Cell Wall | K.STYTTTSGSTVETL[119]TTTYK.S | 3 | 2 | 0.00 | 0.04 |
| YDL006W | PTC1 | 1 | 1.00 | GOLD | 0.02 | 0.23 | -1.19 | 0.022862 | 0.022862 | Protein Phosphatase / Osmotic Stress [Inactivates osmosensing MAPK cascade by de-phosphorylating Hog1] | ------ | | | | 0.00 | 0.02 |
| YNR031C | SSK2 | 0.988358 | 1.00 | GOLD | 0.96 | 8.94 | 1.04 | 0.514379 | 0.501735 | Osmotic Stress / HOG1 mitogen-activated signaling pathway | Cytoplasm / Bud Neck / Bud tip | | | | 0.00 | 0.96 |
| YER042W | MXR1 | 0.95 | 1.00 | GOLD* | 0.34 | 6.31 | -1.75 | 0.03711 | 0.021801 | Detoxification [Oxidative Stress] / Oxidized methionine | Cytoplasm / Nucleus | K.NFYDAEEYHQL[119]YL[119]DK.N | | | 0.00 | 0.34 |
| YDR368W | YPR1 | 0.52 | 1.00 | bronze* | 0.60 | 5.95 | -1.21 | 0.035096 | 0.035096 | Oxidatve and Osmotic Stress [NADPH dependent aldo-keto reductase] | Cytoplasm / Nucleus | K.AGYRHIDAAAIYL[119]NEEEVGR.A | 3 | 2 | 0.00 | 0.60 |
| YIL010W | DOT5 | 0.56 | 1.00 | bronze* | 0.01 | 0.15 | 1.13 | 0.310668 | 0.29022 | Redox homeostasis / Oxidative Stress | Nucleus | K.KYAAVFGLSADSVTSQKK.F | 3 | 2 | 0.00 | 0.01 |
| YFR044C | DUG1 | 1.000 | 1.00 | GOLD | 0.30 | 2.69 | -1.13 | 0.006484 | 0.002001 | Stress / Oxidative / Redox / Glutathione degradation | Cytoplasm / Mitochondria | | | | 0.00 | 0.30 |
| **Small Molecule Transport** | | | | | | | | | | | | | | | | |
| YHR050W | SMF2 | 0.55 | 1.00 | bronze* | 1.65 | 12.25 | 1.26 | 0.000942 | 0.000427 | Transporter / Manganese | Plasma membrane / Cytoplasmic membrane | R.TTL[119]QPNSTSQSM | 3 | 4 | 0.00 | 1.65 |

**Table 4.3.** Continued.

| | | Proteomic Results | | | | | Transcriptional Results | | | | | | | | | |
|---|---|---|---|---|---|---|---|---|---|---|---|---|---|---|---|---|
| Orf | Gene | Final Protein Probability (Detected) | Probability of Change | Category | SD (±) | Final Protein Ratio (*grr1*Δ/WT) | Fold change | Welch Significance Test (Log2) | TTest Significance test (Log2) | Functions | Localization of gene product | Peptide Quantitated | Charge | Mass Shift | Inter-experimental STDEV | Intra-experimental STDEV |
| **Small Molecule Transport Continued** | | | | | | | | | | | | | | | | |
| YNL321W | VNX1 | 0.5734 | 1.00 | bronze* | 0.99 | 23.73 | -1.02 | 0.768979 | 0.76391 | Transport / Monovalent Cation Antiporter | Vacuole | K.GSM[147]L[119]IL[119]L[119]YIIIVVGFYFQGAL[119]S | 3 | 8 | 0.00 | 0.99 |
| YGL167C | PMR1 | 0.9 | 1.00 | GOLD* | 0.02 | 0.25 | -1.06 | 0.481545 | 0.467712 | Transprot [Ca-Mn] / Glycosylation / Trafficking | Golgi | K.L[119]WCL[119]DSM[147]SNKL[119]NVL[119]SL[119]DK.N | | | 0.00 | 0.02 |
| **Trafficking** | | | | | | | | | | | | | | | | |
| **Microtubule** | | | | | | | | | | | | | | | | |
| YHR158C | KEL1 | 0.504 | 1.00 | bronze* | 0.38 | 4.17 | 1.02 | 0.927496 | 0.925991 | Mitosis [Neg] / Morphogenesis | Cytolplasm / Bud Tip / Bud Neck | K.EPDLSETM[147]DPTVGNQR.I | 3 | 2 | 0.00 | 0.38 |
| YHR023W | MYO1 | 1 | 0.08 | GOLD | 0.95 | 0.29 | -1.18 | 0.208687 | 0.184982 | Trafficking / Cytokinesis / Cell Separation | Bud Neck / Contractile Ring | | | | 0.00 | 0.95 |
| YNL152W | INN1 | 0.985728 | 0.11 | GOLD | 0.45 | 0.15 | 1.03 | 0.446175 | 0.446175 | Mitosis / Cytokinesis / Chromosome organization and biogenesis / Hof1 interactor | Contractile actomyosin ring | | | | 0.00 | 0.45 |
| YML034W | SRC1 | 0.972 | 1.00 | GOLD | 0.00 | 0.06 | 1.06 | 0.678102 | 0.675138 | Mitosis / Chromosome Segregation / Spliced mRNA | Nuclear Envelope | | | | 0.00 | 0.00 |
| YOR195W | SLK19 | 0.955 | 0.15 | SILVER | 0.47 | 0.37 | 1.11 | 0.667179 | 0.65942 | Mitosis / Meiosis / Chromosomal Segregation / Component of FEAR regulatory network | Spindle / Kinetochore | | | | 0.00 | 0.47 |
| YDL239C | ADY3 | 0.974 | 1.00 | GOLD | 0.01 | 0.30 | 1 | 0.868301 | 0.867194 | Spindle Pole Body Interactor / Sporulation / Possible Cdc28 Substrate | —— | | | | 0.00 | 0.01 |
| YPL255W | BBP1 | 1 | 1.00 | SILVER | 0.49 | 12.35 | 1.49 | 0.071352 | 0.0506 | SPB Duplication / Mitosis [Cdc5] | Spindle pole body | | | | 0.00 | 0.49 |
| YPL174C | NIP100 | 0.8869 | 1.00 | bronze* | 0.01 | 0.11 | -1.09 | 0.436531 | 0.421 | Trafficking / Dynactin / Positioning Mitotic Spindle | Spindle pole body | R.YFDIDL[119]KKANSNGGYYGL[119]FCKK.D | 3 | 4 | 0.00 | 0.01 |
| YDR488C | PAC11 | 0.678 | 1.00 | bronze* | 0.03 | 0.35 | 1.07 | 0.736279 | 0.730389 | Trafficking / Microtubules / Dynein | Microtubule / Dynein Complex | | | | 0.00 | 0.03 |
| YKR054C | DYN1 | 0.999998 | 1.00 | GOLD | 25.72 | 39.24 | 1.06 | 0.467584 | 0.453232 | Trafficking / MTs / Mitosis / Spindle elongation / chromosome segregation | Cytoplasm | | | | 0.00 | 25.72 |
| YDR106W | ARP10 | 0.98 | 0.38 | GOLD* | 7.42 | 4.03 | -1.47 | 0.000316 | 0.000316 | Trafficking / Dynactin Complex | Cytoplasm | .M[147]SNTIVIVYL[119]GANRIEIGR.S | 3 | 2 | 0.00 | 7.42 |
| YPR141C | KAR3 | 0.971297 | 1.00 | GOLD | 0.56 | 5.97 | 1.05 | 0.660138 | 0.660138 | Trafficking / MTs / Mitosis / Potential Cdc28 substrate | Spindle pole body | | | | 0.00 | 0.56 |
| YNL313C | YNL313 | 0.990328 | 1.00 | GOLD* | 1.73 | 14.43 | 1.1 | 0.41618 | 0.409709 | Trafficking / Mts / Dyn1 related? | Cytoplasm / Nucleus | K.YQQKAHAGLIILAKSFTFQNFALR.T | 3 | 6 | 0.00 | 1.73 |
| YBL063W | KIP1 | 0.400 | 0.29 | bronze | 3.97 | 2.51 | 1.05 | 0.605785 | 0.601974 | Mitosis/spindle assembly/Kinesin related motor protein | Spindle Pole Body/ Microtubule | | | | 0.00 | 3.97 |
| YGR078C | PAC10 | 0.23 | 1.00 | bronze | 0.01 | 0.10 | -1.11 | 0.205647 | 0.19613 | Microtubules / Tubulin Complex Assembly | Cytoplasm | | | | 0.00 | 0.01 |
| YJL051W | YJL051 | 0.980457 | 1.00 | SILVER* | 2.32 | 28.31 | -1.39 | 0.147874 | 0.100598 | Trafficking / MTs | —— | R.SSQYVSRL[119]STISDISK.S | 3 | 2 | 0.00 | 2.32 |
| **Actin** | | | | | | | | | | | | | | | | |
| | | | | | | | | | | Trafficking / Arp2/3 Complex / | | | | | | |

**Table 4.3.** Continued.

| | | Proteomic Results | | | | | Transcriptional Results | | | | | | | | | |
|---|---|---|---|---|---|---|---|---|---|---|---|---|---|---|---|---|
| Orf | Gene | Final Protein Probability (Detected) | Probability of Change | Category | SD (±) | Final Protein Ratio (*grr1*Δ/WT) | Fold change | Welch Significance Test (Log2) | TTest Significance test (Log2) | Functions | Localization of gene product | Peptide Quantitated | Charge | Mass Shift | Inter-experimental STDEV | Intra-experimental STDEV |
| **Trafficking Continued** | | | | | | | | | | | | | | | | |
| **Actin continued** | | | | | | | | | | | | | | | | |
| YHR114W | BZZ1 | 0.99502 | 1.00 | SILVER* | 0.33 | 6.39 | 1.05 | 0.50441 | 0.49141 | Trafficking / Actin Polarization / Endocytosis / Actin Patches | Cytoplasm / Mating Projection Tip / Actin Patches | K.AASVENDLGANVSKR.L | 3 | 2 | 0.00 | 0.33 |
| YNL094W | APP1 | 0.849142 | 1.00 | bronze | 0.00 | 0.04 | -1.03 | 0.491681 | 0.491681 | Trafficking / Rvs161 Interactor / Actin Filament Organization / Bzz1 interactor | ------ | | | | 0.14 | 0.21 |
| YDR351W | SBE2 | 1 | 1.00 | GOLD | 1.79 | 21.12 | 1.01 | 0.902642 | 0.902642 | Trafficking [Golgi to PM] / Budding / Cell Wall | Golgi | | | | 0.00 | 1.79 |
| YGL056C | SDS23 | 0.9921 | 0.27 | GOLD | 0.31 | 0.28 | 1.67 | 0.032226 | 0.032226 | Trafficking / APC Cyclosome / Cytokinesis | ------ | | | | 0.00 | 0.31 |
| YBR214W | SDS24 | 1 | 1.00 | GOLD | 0.02 | 0.20 | 1.09 | 0.953613 | 0.953613 | Trafficking [endocytosis] / APC Cyclosome | ------ | | | | 0.00 | 0.02 |
| YNL079C | TPM1 | 1 | 1.00 | GOLD | 0.05 | 0.30 | 1 | 0.970695 | 0.969484 | Trafficking / Binds and stabilizes actin cables and filaments / Budding / Filamentous growth / Mitochondria and Vacuole inheritance / mRNA localization | Bud neck / Contractile ring | | | | 0.13 | 0.37 |
| YDR379W | RGA2 | 0.982082 | 1.00 | GOLD* | 0.01 | 0.19 | -1.02 | 0.741372 | 0.735612 | Trafficking / Rho GAP [Cdc42] / Budding / Pheromone Response / Septin Organization / Pseudohyphal Growth / Actin filament organization / Regulated by Cdc28 and Pho85 | Bud Neck | R.STNAL[119]L[119]EDDSTK.V | 2 | 6 | 0.00 | 0.01 |
| YIL159W | BNR1 | 0.999959 | 1.00 | GOLD | 0.01 | 0.25 | 1.47 | 0.03482 | 0.028268 | Trafficking / Formin / Budding / Mitotic Spindle formation / Actin Filament Organization / Osmotic Stress | Bud neck / Contractile ring | | | | 0.07 | 0.02 |
| YER166W | DNF1 | 0.9164 | 1.00 | SILVER | 0.03 | 0.27 | -1.11 | 0.017956 | 0.013394 | Trafficking [Phospholipid flippase] / Endocytosis / Establishment of cell polarity | Plasma Membrane | | | | 0.00 | 0.03 |
| YDL231C | BRE4 | 0.8845 | 1.00 | bronze | 0.00 | 0.06 | -1.08 | 0.146515 | 0.122227 | Trafficking / Endocytosis | Membrane | | | | 0.12 | 0.01 |
| YLR227C | ADY4 | 1 | 1.00 | GOLD | 2.10 | 6.19 | 1.04 | 0.811117 | 0.807054 | Meiosis / Structural component of the meiotic outer plaque | Spindle Pole Body | | | | 0.00 | 2.10 |
| YIR006C | PAN1 | 1 | 1.00 | GOLD | 0.40 | 8.87 | -1.11 | 0.30699 | 0.286402 | Trafficking / Bud / Cytokinesis / Endocytosis / Actin Patches / Cell polarity | Cytoplasm / Nucleus / Cortical actin patches | | | | 0.00 | 0.40 |
| YNL298W | CLA4 | 0.933 | 1.00 | SILVER | 0.00 | 0.10 | -1.04 | 0.64806 | 0.644755 | Trafficking / Septin ring assembly / cytokinesis / Vacuole inheritence / Cell polarity | Bud / Vacuole | | | | 0.05 | 0.01 |
| **Glycosylation** | | | | | | | | | | | | | | | | |
| YEL002C | WBP1 | 1 | 1.00 | GOLD* | 0.00 | 0.16 | -1.11 | 0.053221 | 0.04533 | Trafficking / Glycosylation | ER Membrane / OST Complex | R.HGVFTFL[119]TDYR.K | 2 | 3 | 0.00 | 0.00 |
| YDR483W | KRE2 | 0.89 | 1.00 | GOLD* | 0.02 | 0.24 | -1.15 | 0.019021 | 0.003593 | Trafficking / Glycosylation / Mannosylation | Golgi | R.HELLEEYDWYWR.V | 2 | 6 | 0.00 | 0.02 |
| YOR320C | GNT1 | 1 | 1.00 | GOLD* | 0.03 | 0.27 | -1.1 | 0.37543 | 0.339112 | Trafficking / Glycosylation | Golgi Medial Cisterna | R.EKQPINLQSYTKVLTK.R | 3 | 4 | 0.00 | 0.03 |

**Table 4.3.** Continued.

| | | Proteomic Results | | | | | Transcriptional Results | | | | | | | | | |
|---|---|---|---|---|---|---|---|---|---|---|---|---|---|---|---|---|
| Orf | Gene | Final Protein Probability (Detected) | Probability of Change | Category | SD (±) | Final Protein Ratio (*grr1*Δ/WT) | Fold change | Welch Significance Test (Log2) | TTest Significance test (Log2) | Functions | Localization of gene product | Peptide Quantitated | Charge | Mass Shift | Inter-experimental STDEV | Intra-experimental STDEV |
| **Trafficking Continued** | | | | | | | | | | | | | | | | |
| **Glycosylation** | | | | | | | | | | | | | | | | |
| YNR059W | MNT4 | 0.42 | 0.99 | bronze* | 1.84 | 3.99 | -1.29 | 0.015193 | 0.006558 | Trafficking / Glycosylation / Putative alpha-1,3-mannosyltransferase | Unknown | K.GVVM[147]SVSEYL[119]VADTIRL[119]IR.V | 3 | 4 | 0.00 | 1.84 |
| YGL167C | PMR1 | 0.9 | 1.00 | GOLD* | 0.02 | 0.25 | -1.06 | 0.481545 | 0.467712 | Trafficking / Transprot [Ca-Mn] / Glycosylation | Golgi | K.L[119]WCL[119]DSM[147]SNKL[119]NVL[119]SL[119]DK.N | | | 0.00 | 0.02 |
| YMR281W | GPI12 | 0.53 | 1.00 | bronze* | 0.21 | 4.52 | 1.18 | 0.385941 | 0.368433 | GPI Anchor / Lipid Metabolism | ER | K.NNIVLK.Y | 1 | 6 | 0.00 | 0.21 |
| YJR061W | YJR061 | 0.999996 | 1.00 | GOLD | 0.54 | 5.99 | 1.05 | 0.528796 | 0.52398 | Cell Wall / Mnn4-like? / Glycosylation | Unknown | | | | 0.00 | 0.54 |
| YER039C | HVG1 | 0.85 | ------ | GOLD* | 0.00 | 0.11 | 1.06 | 0.496028 | 0.496028 | Transporter / GTP-Mannose [based on sequence similarity to Vrg4] | Unknown | K.LPIALAGLVFFDAPK.N | 2 | 9 | 0.00 | 0.00 |
| YGL156W | AMS1 | 0.840 | 1.00 | bronze | 0.20 | 2.59 | 2.06 | 0.000016 | 0.000016 | Free oligosaccharide degradation / Alpha-mannosidase | Vacuolar Membrane | | | | 0.00 | 0.20 |
| **Vesicle Trafficking (ER to Golgi)** | | | | | | | | | | | | | | | | |
| YIR022W | SEC11 | 0.678 | 1.00 | bronze | 0.20 | 2.76 | 1.01 | 0.788687 | 0.786856 | Trafficking / ER signal Peptidase Complex Catalytic Enzyme | Endoplasmic Reticulum | | | | 0.00 | 0.20 |
| YPL218W | SAR1 | 1.000 | 1.00 | GOLD | 0.04 | 0.36 | -1.03 | 0.483234 | 0.469463 | Trafficking [ER to Golgi Transport] / COPII Coated Vesicles | Endoplasmic Reticulum / Golgi | | | | 1.35 | 1.31 |
| YCR067C | SED4 | 0.9788 | 1.00 | GOLD | 0.27 | 3.29 | -1.11 | 0.264281 | 0.242162 | Trafficking [ER to Golgi] / Activates Sar1 | ER membrane | | | | 1.54 | 0.24 |
| YGR284C | ERV29 | 0.9658 | 1.00 | GOLD* | 0.03 | 0.31 | -1.02 | 0.640012 | 0.640012 | Trafficking [ER to Golgi] / CopII Vesicles | ------ | K.SWFTVVL[119]TIIGTICFAIGYK.T | 3 | 2 | 0.00 | 0.03 |
| YLR080W | EMP46 | 0.994984 | 1.00 | SILVER* | 0.02 | 0.17 | 2.1 | 0.007314 | 0.004789 | Trafficking [ER to Golgi] / Cop II Vesicles | Endoplasmic Reticulum / Golgi | K.QGNEGDSTEL[119]FGGSSK.K | 3 | 2 | 0.00 | 0.02 |
| YGR166W | KRE11 | 0.55 | 1.00 | bronze* | 0.01 | 0.11 | -1.26 | 0.055783 | 0.022747 | Trafficking [ER-Golgi] / TAPP complex | Trans-Golgi-Network / TRAPP Complex | R.FVLQNMIILINEAQVTR.T | 3 | 4 | 0.00 | 0.01 |
| YML071C | COG8 | 0.33 | 1.00 | bronze | 0.18 | 3.37 | -1.07 | 0.544231 | 0.539625 | Trafficking [Golgi] | Golgi Transport Complex | | | | 0.00 | 0.18 |
| YOR370C | MRS6 | 0.53 | 1.00 | bronze* | 0.01 | 0.17 | 1.01 | 0.863597 | 0.857828 | Trafficking [ER to Golgi] / Rab Escort | Cytoplasm | K.NDYYGDTSATLTVDQIKR.W | 3 | 2 | 0.00 | 0.01 |
| **Vesicle Trafficking (Golgi, EE, LE, Vacuole, PM)** | | | | | | | | | | | | | | | | |
| YLL040C | VPS13 | 1 | 1.00 | GOLD | 0.00 | 0.12 | -1.07 | 0.50798 | 0.495108 | Trafficking [Late endosome to vacuole] / Protein retention in Golgi | Endosome | | | | 0.00 | 0.00 |
| YMR231W | PEP5 | 0.999863 | 1.00 | GOLD | 0.01 | 0.27 | 1.06 | 0.574025 | 0.563418 | Trafficking [Golgi to endosome and late endosome to vacuole] | Vacuole membrane / CORVET complex / HOPS complex | | | | 0.21 | 0.20 |
| YLR148W | PEP3 | 0.7984 | 1.00 | bronze | 0.36 | 4.31 | 1.01 | 0.989586 | 0.989371 | Trafficking [Golgi to endosome and late endosome to vacuole] | Vacuole membrane / CORVET complex / HOPS complex | | | | 0.00 | 0.36 |
| YDR058C | TLG2 | 0.906088 | 1.00 | SILVER | 0.51 | 5.89 | 1.32 | 0.014587 | 0.002224 | Trafficking [Golgi to Vacuole] / Inositol Phosphorylceramide Metabolic Process | trans-Golgi-Network / Early Endosome | | | | 4.69 | 0.73 |
| YJL036W | SNX4 | 0.41 | 1.00 | bronze* | 0.66 | 16.47 | -1 | 0.997719 | 0.997719 | Trafficking / EE to vacuole to golgi | Vacuole / Golgi / Early endosome | R.FPTCIIPPLPDK.K | 2 | 3 | 0.00 | 0.66 |
| YDR027C | VPS54 | 0.998 | 1.00 | SILVER | 0.03 | 0.38 | 1.18 | 0.016217 | 0.011939 | Trafficking / GARP complex / Recycling from Endosomes to | Golgi / GARP complex | | | | 0.00 | 0.03 |

**Table 4.3.** Continued.

| | | Proteomic Results | | | | | Transcriptional Results | | | | | | | | | |
|---|---|---|---|---|---|---|---|---|---|---|---|---|---|---|---|---|
| Orf | Gene | Final Protein Probability (Detected) | Probability of Change | Category | SD (±) | Final Protein Ratio (*grr1*Δ/WT) | Fold change | Welch Significance Test (Log2) | TTest Significance test (Log2) | Functions | Localization of gene product | Peptide Quantitated | Charge | Mass Shift | Inter-experimental STDEV | Intra-experimental STDEV |
| **Trafficking Continued** | | | | | | | | | | | | | | | | |
| **Vesicle Trafficking (Golgi, EE, LE, Vacuole, PM) Continued** | | | | | | | | | | | | | | | | |
| YGL206C | CHC1 | 1 | 0.34 | GOLD | 0.27 | 0.30 | -1.1 | 0.378576 | 0.378576 | Trafficking / Clathrin / Endocytosis / Vesicle Mediated Transport | ------ | | | | 0.00 | 0.27 |
| YGR167W | CLC1 | 1 | 0.27 | SILVER* | 0.21 | 0.11 | -1.01 | 0.747311 | 0.741702 | Trafficking / Clathrin / Endocytosis / Vesicle Mediated Transport | Cytoplasm / Clathrin coated vesicles | R.AL[119]QL[119]INQDD ADIIGGR.D | 2 | 6 | 0.00 | 0.21 |
| YBL069W | AST1 | 0.68 | 1.00 | bronze* | 0.02 | 0.19 | -1.26 | | | Trafficking / Targets Pma1 to plasma membrane | Extrinsic to interior of Plasma membrane | K.EIPM[147]DAPVL[119] KRVAR.P | 3 | 2 | 0.00 | 0.02 |
| YMR079W | SEC14 | 1.000 | 1.00 | GOLD | 0.02 | 0.34 | -1.1 | 0.396989 | 0.379916 | Trafficking / Lipid / Phosphatidyl inositol and phosphatidylcholine transfer protein | Cytoplasm / Golgi | | | | 0.00 | 0.02 |
| YPR036W | VMA13 | 1.000 | 0.66 | GOLD | 0.18 | 0.37 | -1.18 | 0.067619 | 0.047281 | Vacuolar H+-ATPase / Subunit H | Vacuolar Membrane | | | | 0.00 | 0.18 |
| YBR286W | APE3 | 1 | 1.00 | GOLD | 0.21 | 3.34 | -1.13 | 0.109962 | 0.086502 | Vacuolar Aminopeptidase Y | Vacuole | | | | 0.68 | 0.42 |
| **Transcriptional Regulation** | | | | | | | | | | | | | | | | |
| **Transcription Factors / Polymerases** | | | | | | | | | | | | | | | | |
| YDR123C | INO2 | 1 | 1.00 | GOLD* | 0.00 | 0.06 | 1.1 | 0.616191 | 0.612508 | Transcription Factor [De-repression of Phospholipid Biosynthetic Genes] | ------ | K.RIPKHIL[119]L[119]TC VM[147]NDIKSIR.S | 3 | 4 | 0.00 | 0.00 |
| YCR065W | HCM1 | 0.9947 | 1.00 | GOLD* | 0.01 | 0.10 | 1.22 | 0.220673 | 0.211314 | Transcription Factor [In S-phase drives expression of Spindle Pole Body, Chromosome Segragation, and Budding genes] / Cdc28-Clb2 Substrate / Telomere | ------ | K.RTLEDEKEMITPPSST VR.K | 3 | 2 | 0.00 | 0.01 |
| YGL131C | SNT2 | 0.851 | 1.00 | bronze | 0.04 | 0.37 | 1.22 | 0.039234 | 0.023452 | Transcription? / Regulates gene expression of amine transporters | Nucleus / Cytoplasm | | | | 0.00 | 0.04 |
| YAL051W | OAF1 | 1.000 | 1.00 | GOLD | 0.04 | 0.36 | -1.09 | 0.133436 | 0.133436 | Transcription / Oleate activated transcription factor / Fatty acid oxidation / Peroxisome biogenesis | Nucleus | | | | 0.00 | 0.04 |
| YPL048W | CAM1 | 1.000 | 1.00 | GOLD | 0.09 | 2.63 | -1.03 | 0.611355 | 0.611355 | Transcription / Binds Calcium and phospholipids | Nucleus | | | | 0.00 | 0.09 |
| [illegible] | [illegible] | [illegible] | [illegible] | [illegible] | [illegible] | [illegible] | [illegible] | [illegible] | [illegible] | Transcription / Fatty Acid | Cytoplasm / Mitochondria | [illegible] | [illegible] | [illegible] | [illegible] | [illegible] |
| YKR064W | OAF3 | 0.983907 | 1.00 | GOLD | 0.01 | 0.26 | -1.23 | 0.038036 | 0.038036 | Metabolism / Response to Oleate | [illegible] / Nucleus | | | | 0.00 | 0.01 |
| YOR172W | YRM1 | 0.99715 | 1.00 | GOLD* | 0.05 | 0.15 | -1.2 | 0.00843 | 0.002895 | Transcription / Multidrug resistant genes | Cytoplasm / Nucleus | K.FLIMLTGLSTAK.V | 2 | 9 | 0.00 | 0.05 |
| YLR179C | YLR179 | 0.9295 | 1.00 | GOLD | 0.70 | 12.52 | -1.1 | 0.291447 | 0.248764 | Multidrug Resistance ? / Transcription activated by Yrm1 and Yrr1 | Cytoplasm / Nucleus | | | | 0.00 | 0.70 |
| YIL128W | MET18/MMS19 | 0.998024 | 0.84 | GOLD* | 3.40 | 4.23 | 1.03 | 0.726777 | 0.724333 | DNA Repair [NER] / RNA Polymerase II / Telomere | ------ | R.ILDTPNVLAISYAK.I | 3 | 4 | 0.00 | 3.40 |
| YIL143C | SSL2 | 0.75 | 1.00 | GOLD* | 0.41 | 8.92 | 1.06 | 0.405807 | 0.405807 | RNA Polymerase II / DNA Repair | ------ | K.VKLVIK.H | 1 | 6 | 0.00 | 0.41 |
| YGL151W | NUT1 | 0.989664 | 1.00 | GOLD | 0.01 | 0.20 | -1.17 | 0.053787 | 0.045865 | RNA Polymerase II | Nucleus / Mitochondria | | | | 0.00 | 0.01 |
| YPR186C | PZF1 | 0.610 | 1.00 | bronze | 0.24 | 2.91 | -1.09 | 0.4731 | 0.4731 | Transcription / TFIII A | Nucleus | | | | 0.00 | 0.24 |
| YPL007C | TFC8 | 0.78 | 1.00 | GOLD | 1.71 | 27.80 | 1.05 | 0.617976 | 0.608763 | RNA Polymerase III | Nucleus / Transcription factor TFIIIC complex | | | | 0.00 | 1.71 |
| [illegible] | [illegible] | [illegible] | 1.00 | [illegible] | 0.05 | [illegible] | [illegible] | [illegible] | [illegible] | Transcription Factor / [illegible] | [illegible] | K.VM[147]KSKKL[119]EQ | [illegible] | [illegible] | [illegible] | 0.05 |

**Table 4.3.** Continued.

| | | Proteomic Results | | | | | Transcriptional Results | | | | | | | | | |
|---|---|---|---|---|---|---|---|---|---|---|---|---|---|---|---|---|
| Orf | Gene | Final Protein Probability (Detected) | Probability of Change | Category | SD (±) | Final Protein Ratio (*grr1*Δ/WT) | Fold change | Welch Significance Test (Log2) | TTest Significance test (Log2) | Functions | Localization of gene product | Peptide Quantitated | Charge | Mass Shift | Inter-experimental STDEV | Intra-experimental STDEV |
| **Transcriptional Regulation Continued** | | | | | | | | | | | | | | | | |
| **Chromatin** | | | | | | | | | | | | | | | | |
| YOR290C | SNF2 | 1 | 1.00 | GOLD | 0.01 | 0.25 | 1.1 | 0.034896 | 0.034896 | Transcription / Chromatin remodeling | Nucleus [Swi/Snf complex] | | | | 0.09 | 0.06 |
| YGR275W | RTT102 | 0.6436 | 1.00 | bronze | 0.26 | 6.89 | -1.1 | 0.008596 | 0.002976 | Chromatin Remodelling / Chromosome Segregation | Nucleus [SWI-SNF / RSC Complexes] | | | | 0.00 | 0.26 |
| YNL021W | HDA1 | 0.6612 | 0.43 | bronze* | 0.20 | 0.18 | -1.07 | 0.487552 | 0.482153 | Chromatin / Histone Deacetylase | | R.DTRAVTKTVINFLGDK QLK.P | 3 | 4 | 0.00 | 0.20 |
| YCR033W | SNT1 | 0.719 | 0.28 | bronze* | 5.40 | 2.87 | -1 | 0.987031 | 0.987031 | Histone deacetylase / Set3C Complex | Nucleus / Set3C complex | | | | 0.00 | 5.40 |
| YHR119W | SET1 | 0.32 | 1.00 | bronze | 1.43 | 24.17 | 1.03 | 0.840223 | 0.836827 | Chromatin Silencing [Methylation] / Telomere Maintenance | Nucleus [SET1-COMPASS Complex] | | | | 0.00 | 1.43 |
| YDR469W | SDC1 | 0.8068 | 1.00 | bronze | 0.01 | 0.26 | 1.15 | 0.018554 | 0.018554 | Chromatin Silencing at Telomere | Nucleus [SET1/COMPASS Complex] | | | | 0.48 | 0.06 |
| YFR037C | RSC8 | 0.6175 | 0.49 | bronze | 0.16 | 0.13 | -1.02 | 0.498031 | 0.498031 | Chromatin Remodelling / Cell Cylce [G1-S] / Doube strand Break Repair | Nucleus [RSC Complex] | | | | 0.00 | 0.16 |
| YPR031W | NTO1 | 0.42 | 1.00 | bronze | 0.01 | 0.25 | 1.03 | 0.931939 | 0.931376 | Histone Acetyltransferase | Cytoplasm / Nucleus | | | | 0.00 | 0.01 |
| YBR231C | SWC5 | 0.8812 | 1.00 | bronze | 0.05 | 0.09 | 1.08 | 0.535474 | 0.53075 | Chromatin Remodelling / Histone exchange | Nucleus [SWR1 Complex] | | | | 0.01 | 0.12 |
| YDR310C | SUM1 | 0.964 | 0.99 | SILVER | 0.93 | 2.80 | -1.03 | 0.685426 | 0.67818 | Mitosis / Sporulation transcriptional repressor / Telomere maintenance / chromatin silencing | Nucleus | | | | 0.00 | 0.93 |
| **Splicing / mRNA Processing and Transport** | | | | | | | | | | | | | | | | |
| YHR015W | MIP6 | 0.62 | 1.00 | bronze | 0.61 | 6.92 | 1.46 | 0.053317 | 0.045421 | mRNA Export | Nuclear Pore | | | | 0.00 | 0.61 |
| YGL094C | PAN2 | 0.7011 | 1.00 | bronze | 0.19 | 3.62 | -1.06 | 0.720146 | 0.720146 | mRNA Processing / Postreplication Repair | Cytoplasm [PAN Complex] | | | | 0.00 | 0.19 |
| YMR080C | UPF1 | 1.000 | 0.54 | GOLD | 2.20 | 2.55 | -1.05 | 0.545444 | 0.522041 | mRNA / Nonsense mediated decay / Translation termination at nonsense codons | Cytoplasm / Polysome | | | | 0.00 | 2.20 |
| YOL021C | DIS3 | 1.000 | 1.00 | GOLD | 0.33 | 2.91 | -1.04 | 0.258642 | 0.249759 | mRNA / 3'-5' RNA processing and degradation | Cytoplasm / Nucleus / Exosome | | | | 0.95 | 0.42 |
| YDR482C | CWC21 | 0.914 | 1.00 | SILVER | 0.03 | 0.34 | 1.06 | 0.225978 | 0.225978 | mRNA / Splicing | Spliceasomal complex | | | | 0.00 | 0.03 |
| YOR048C | RAT1 | 0.996569 | 1.00 | GOLD* | 0.43 | 4.43 | -1.02 | 0.631203 | 0.631203 | RNA Metabolism / rRNA and snRNA processing / mRNA transcription termination | Nucleus | K.TWDSNAITPGTPFMD KL[119]AAAL[119]R.Y | 3 | 4 | 0.00 | 0.43 |
| YLR430W | SEN1 | 1 | 1.00 | GOLD | 0.01 | 0.19 | 1 | 0.988977 | 0.988977 | RNA Metabolism / RNA polymerase II Transcription Termination / RNA processing | Nucleus | | | | 0.00 | 0.01 |
| YDR464W | SPP41 | 1 | 1.00 | SILVER* | 1.86 | 20.31 | 1.03 | 0.818385 | 0.816831 | Splicing | Nucleus [Spliceosome] | K.KPYRRWTPEELLK.R | 3 | 4 | 0.00 | 1.86 |
| YBR152W | SPP381 | 1.000 | 1.00 | GOLD | 0.0100 | 0.3300 | 1.17 | 0.637171 | 0.619746 | mRNA Splicing / U4/U6 | | | | | 2.16 | 0.17 |
| **DNA Repair / Meiotic Recombination** | | | | | | | | | | | | | | | | |
| YDR314C | RAD34 | 0.988904 | 1.00 | GOLD | 0.18 | 3.30 | 1.11 | 0.537179 | 0.537179 | DNA Repair [NER] | ------ | | | | 0.00 | 0.18 |
| YML023C | NSE5 | 0.972708 | 1.00 | GOLD | 0.75 | 8.48 | 2.28 | 0.036415 | 0.021265 | DNA Repair / Mms21-Smc5-Smc6 complex | Nucleus | | | | 0.00 | 0.75 |
| YLR376C | PSY3 | 0.98 | 1.00 | GOLD* | 0.02 | 0.29 | 1.32 | 0.036281 | 0.036281 | DNA repair | Cytoplasm / Nucleus | K.SGVTLYPTKLPDSYM[147]K.G | 2 | 6 | 0.00 | 0.02 |

**Table 4.3.** Continued.

| | | Proteomic Results | | | | | Transcriptional Results | | | | | | | | | |
|---|---|---|---|---|---|---|---|---|---|---|---|---|---|---|---|---|
| Orf | Gene | Final Protein Probability (Detected) | Probability of Change | Category | SD (±) | Final Protein Ratio (*grr1*Δ/WT) | Fold change | Welch Significance Test (Log2) | TTest Significance test (Log2) | Functions | Localization of gene product | Peptide Quantitated | Charge | Mass Shift | Inter-experimental STDEV | Intra-experimental STDEV |
| **DNA Repair / Meiotic Recombination Continued** | | | | | | | | | | | | | | | | |
| YER041W | YEN1 | 0.4 | 1.00 | bronze | 0.20 | 3.54 | -1.13 | 0.061188 | 0.061188 | Repair/ Recombination / Crossover Junction Endodeoxyribonuclease activity | Nucleus | | | | 0.00 | 0.20 |
| YBR136W | MEC1 | 0.99998 | 1.00 | GOLD | 0.42 | 4.20 | 1.12 | 0.191861 | 0.144276 | PI Kinase / DNA Damage Checkpoint / Telomere Maintenance / Meiotic Recombination | Nucleus | | | | 0.00 | 0.42 |
| YDL154W | MSH5 | 0.938222 | 1.00 | GOLD | 0.33 | 5.69 | -1.76 | 0.005102 | 0.003157 | DNA / Meiotic Recombination | Nucleus | | | | 0.00 | 0.33 |
| YIL072W | HOP1 | 0.999762 | 0.98 | GOLD | 1.26 | 3.05 | -1.23 | 0.283184 | 0.239935 | Meiosis / Synapsis [Chromosome Condensation] | Synaptonemal complex | | | | 0.00 | 1.26 |
| YGL251C | HFM1 | 1.000 | 1.00 | GOLD | 0.16 | 2.80 | -1.08 | 0.429063 | 0.422791 | Meiosis / Recombination | Nucleus | | | | 0.00 | 0.16 |
| YMR133W | REC114 | 0.877367 | 1.00 | bronze* | 0.01 | 0.25 | 1.14 | 0.603987 | 0.600154 | Meiosis | Chromosome | R.KEASPSEGLTIRVKNVNR.N | 3 | 2 | 0.00 | 0.01 |
| YNL204C | SPS18 | 0.54 | 1.00 | bronze | 0.33 | 6.16 | -1.13 | 0.309044 | 0.309044 | Sporulation | Ubnkown | | | | 0.00 | 0.33 |
| **Telomere** | | | | | | | | | | | | | | | | |
| YBR233W | PBP2 | 0.9097 | 1.00 | GOLD | 0.00 | 0.05 | 1.24 | 0.061536 | 0.053214 | Telomere / RNA [Poly-Adenylation] | ------ | | | | 6.42 | 0.50 |
| YBR275C | RIF1 | 1 | 1.00 | GOLD | 0.34 | 4.90 | 1.18 | 0.153258 | 0.143425 | Telomere [Rap1 and Rif2] | ------ | | | | 1.19 | 5.01 |
| YLR453C | RIF2 | 0.66 | 0.45 | bronze* | 0.18 | 0.15 | 1.4 | 0.035329 | 0.020434 | Telomere Maintenance | Telomere | K.VVDSDKIVKAISDDL[119]EQK.N | 3 | 2 | 0.00 | 0.18 |
| YBR225W | YBR225 | 0.889915 | 1.00 | bronze | 0.19 | 4.27 | -1.15 | 0.016715 | 0.012347 | Telomere Capping? | Cytoplasm | | | | 0.00 | 0.19 |
| **Transposition** | | | | | | | | | | | | | | | | |
| YPR164W | MMS1 | 0.999979 | 1.00 | GOLD | 0.01 | 0.29 | 1.12 | 0.02452 | 0.02452 | DNA Repair / Regulation of Ty1 transposition [Negative] | Unknown | | | | 0.58 | 0.08 |
| YJR142W | YJR142 | 0.999307 | 1.00 | GOLD* | 0.00 | 0.11 | -1.06 | 0.544917 | 0.533337 | Restricts Ty1 transposition | Unknown | R.KMYL[119]ESSLSGVKGWR.N | | | 0.00 | 0.00 |
| YAR009C | Ty | 1 | 1.00 | GOLD* | 0.24 | 6.06 | 1.79 | 0.068568 | 0.048122 | Transposable Element | | R.APGQPGL[119]YIDQDEL[119]EIDEDEYK.E | | | 0.00 | 0.24 |
| **Ubiquitin / Ubiquitin like** | | | | | | | | | | | | | | | | |
| YDL132W | CDC53 | 0.99766 | 1.00 | GOLD | 0.02 | 0.29 | -1.16 | 0.139536 | 0.139536 | Ubiquitin / SCF Component | ------ | | | | 0.00 | 0.02 |
| YDR177W | UBC1 | 1 | 1.00 | GOLD | 0.01 | 0.17 | 1.07 | 0.143775 | 0.119509 | Ubiquitin | ------ | | | | 0.00 | 0.01 |
| YFL007W | BLM10 | 1 | 1.00 | GOLD | 0.47 | 5.74 | -1.16 | 0.154085 | 0.129761 | Proteasome [activator subunit] | ------ | | | | 0.00 | 0.47 |
| YOR261C | RPN8 | 1 | 1.00 | GOLD* | 0.02 | 0.33 | -1.1 | 0.15191 | 0.127593 | Ubiquitin / Proteasome regulatory subunit | Proteasome | K.VTIAPL[119]VL[119]L[119]SAL[119]DHYER.T K.VTIAPLVLLSALDHYER.T | 3 | 8 | 0.00 | 0.02 |
| YJL197W | UBP12 | 0.7112 | 1.00 | bronze | 0.17 | 3.15 | -1.13 | 0.031558 | 0.031558 | Ubiquitin Protease | ------ | | | | 0.00 | 0.17 |
| YJL001W | PRE3 | 0.699168 | 1.00 | bronze* | 0.36 | 4.54 | -1.11 | 0.385675 | 0.368157 | Ubiquitin / Proteasome | ------ | K.RAIM[147]L[119]SSQRISL[119]R.Q | 3 | 4 | 0.00 | 0.36 |
| YGL141W | HUL5 | 0.6826 | 1.00 | bronze* | 0.23 | 3.54 | -1.07 | 0.623502 | 0.619907 | Ubiquitin [E4] / Polyubiquitylation / ERAD | Cytoplasm / Nucleus | R.FRKL[119]EIL[119]L[119]EL[119]PFFIPFEER.V | 3 | 8 | 0.00 | 0.23 |
| YIL030C | DOA10 | 0.9814 | 1.00 | GOLD* | 0.01 | 0.16 | -1.15 | 0.088101 | 0.078864 | Ubiquitin / ERAD | ------ | K.PL[119]L[119]ERYWKTIFK.L | 3 | 4 | 0.00 | 0.01 |
| YMR161W | HLJ1 | 0.25 | 1.00 | bronze | 0.69 | 12.24 | 1.13 | 0.415022 | 0.398656 | ERAD | ER | | | | 0.00 | 0.69 |

**Table 4.3.** Continued.

| | | Proteomic Results | | | | | Transcriptional Results | | | | | | | | | |
|---|---|---|---|---|---|---|---|---|---|---|---|---|---|---|---|---|
| Orf | Gene | Final Protein Probability (Detected) | Probability of Change | Category | SD (±) | Final Protein Ratio (*grr1* Δ/WT) | Fold change | Welch Significance Test (Log2) | TTest Significance test (Log2) | Functions | Localization of gene product | Peptide Quantitated | Charge | Mass Shift | Inter-experimental STDEV | Intra-experimental STDEV |
| Ubiquitin / Ubiquitin like Continued | | | | | | | | | | | | | | | | |
| SUMO | | | | | | | | | | | | | | | | |
| YIL031W | ULP2 | 1 | 1.00 | GOLD* | 0.34 | 5.03 | -1.24 | 0.001592 | 0.000811 | Sumoylation / Mitosis [Spindle assembly checkpoint] / Chromosome Condensation | ------ | K.FNSL[119]KPL[119]DTL[119]NSSR.A | 3 | 6 | 0.00 | 0.34 |
| YOR191W | ULS1 | 1 | 1.00 | GOLD | 0.94 | 10.27 | 1.07 | 0.568955 | 0.568955 | Chromatin / Ubiquitin ligase for SUMO Conjugates / Mating | Nucleus | | | | 0.00 | 0.94 |
| Unknown | | | | | | | | | | | | | | | | |
| YKR018C | YKR018 | 0.996024 | 1.00 | GOLD* | 0.01 | 0.17 | -1.05 | 0.598044 | 0.58821 | Unknown / Interacts with Rsp5 | Cytoplasm / Nucleus | R.AQGYADDYELSTRVGM[147]K.I | 3 | 2 | 0.00 | 0.01 |
| YLL007C | YLL007 | 0.999435 | 1.00 | SILVER | 0.42 | 3.64 | -1.1 | 0.159243 | 0.111648 | Unknown | Unknown | | | | 0.00 | 0.42 |
| YDR307W | YDR307 | 0.46 | 1.00 | bronze* | 0.02 | 0.33 | 1.14 | 0.214787 | 0.214787 | Unknown | ER | .M[147]KDLR.L | 1 | 6 | 0.00 | 0.02 |
| YLR312C | YLR312 | 0.54 | 1.00 | bronze | 0.30 | 6.41 | 7.46 | 0.000013 | 0.000003 | Nothing | Nothing | | | | 0.00 | 0.30 |
| YGL235W | YGL235 | 0.370 | 1.00 | bronze | 0.28 | 2.97 | 1.65 | 0.257761 | 0.248866 | Unknown | Unknown | | | | 0.00 | 0.28 |
| YJL162C | JJJ2 | 0.800 | 1.00 | bronze | 0.34 | 2.88 | -1.09 | 0.444382 | 0.444382 | Unknown | Unknown | | | | 0.00 | 0.34 |
| YOR118W | RTC5 | 0.926 | 1.00 | SILVER | 0.14 | 2.59 | -1.3 | 0.017328 | 0.003038 | Unknown | Cytoplasm | | | | 0.00 | 0.14 |
| YPL105C | YPL105 | 0.210 | 1.00 | bronze | 0.13 | 2.72 | -1.03 | 0.675145 | 0.667612 | Unknown | Cytoplasm / Mitochondria | | | | 0.00 | 0.13 |
| YBR204C | YBR204 | 0.700 | 1.00 | bronze | 0.01 | 0.38 | 1.21 | 0.119967 | 0.119967 | Unknown | Unknown | | | | 0.00 | 0.01 |
| YIL158W | YIL158 | 0.740 | 0.21 | bronze* | 0.37 | 0.35 | -1.03 | 0.885718 | 0.884763 | Unknown | Vacuole | | | | 0.00 | 0.37 |
| YJL218W | YJL218 | 0.71 | 1.00 | bronze* | 0.02 | 0.18 | 1.11 | 0.67117 | 0.67117 | Oleate Induced | ------ | K.LHEYNTLSPADENKKSQVIR.E | 3 | 4 | 0.00 | 0.02 |
| YER158C | YER158 | 0.978 | 1.00 | GOLD | 0.2800 | 0.3800 | 1.83 | 0.008563 | 0.008563 | Unknown | | | | | | |



**Table 4.3. Categorized List of Protein Expression Level Changes Between *grr1Δ* and wild-type Yeast.** Changes in protein expression (including "Gold", "Silver", and "Bronze" categories; Fold changes >= 2.5 or <=.4) were categorized manually utilizing information obtained from the *Saccharomyces* Genome Database (SGD) or through manual literature curation. Descriptions for the semantics of the table structure as well as the data descriptions for the proteomic and transcriptional data presented can be found in the **Table 4.2** legend. Proteins identified and quantitated from a single peptide are denoted with an asterisk within the "category" field and in these instances the peptide sequence, its' charge, and the predicted mass shift of the labeled peptide are provided. Inter-experimental standard deviation is also reported and indicates the deviation between protein abundance ratios determined between separate analyses for the same protein. An interexperimental standard deviation of 0 is reported for proteins that were only quantitated in one analysis. Additionally, intra-experimental standard deviation indicates the average standard deviation among peptides whose relative abundance ratios were utilized to calculate the final protein abundance ratio across all analyses. Proteins which participate in mitotic processes are highlighted in brown**.**

# CHAPTER 5: PROTEIN AND GENE EXPRESSION DISCORDANCE IN *grr1Δ* CELLS AND ITS IMPLICATIONS FOR *GRR1'S* ROLE IN GLUCOSE REPRESSION

## 5.1 Introduction

In the previous sections we determined that 22% of the loci where protein expression was determined exhibited discordance between gene and protein expression in *grr1Δ* strains. Each occurrence of measured discordance potentially represents an instance where protein steady state levels cannot be inferred from gene expression data. Thus, inferences made by whole genome expression analyses may either be inaccurate or fail to detect perturbations in processes that may be strictly regulated post-translationally. Since analysis of each individual locus remains a practical challenge, we implemented a GO enrichment analysis to determine the processes exhibiting the highest degree of discordance in terms of the number of proteins with measured discordance annotated to a given process. The GO process of "Carbon and Energy Metabolism" was found to be highly enriched among discordant loci in our analysis with 44 discordant loci annotated to this process. Discordant loci among the "Carbon and Energy Metabolism" cluster could be grouped into each of the three discordance types with 4 loci exhibiting type 1 discordance, 23 loci exhibiting type 2 discordance, and 21 loci exhibiting type 3 discordance.

As indicated previously, Grr1 plays a predominate role in the regulation of the cellular response to glucose and *grr1Δ* strains exhibit glucose repression resistant expression of a number of glucose repressed genes. However, much of what is known about the role for Grr1 in glucose repression and the effects of *GRR1* deletion on glucose dependent signaling and metabolism have been limited to transcriptional and phenotypic studies with little attention devoted to the proteomic response to *GRR1*deletion. From these studies, the effects of *GRR1* deletion on metabolic and signaling processes can only be inferred which could lead to inaccurate descriptions of the actual state of *grr1Δ* cells. The extent of discordance between gene and protein expression that we measured among loci

annotated to “Carbon and Energy Metabolism” processes suggests that descriptions of the role for Grr1 in glucose repression based solely off transcriptional studies may indeed be inaccurate or incomplete. In this chapter, we present a thorough analysis of the discordances measured among loci annotated to the “Carbon and Energy Metabolism” cluster in *grr1Δ* strains. Through this analysis we reveal a number of relevant instances of discordance that necessitate the re-assessment of the role for Grr1 in glucose repression.

## 5.2. Expression Levels for the Hexose Transporters, Hxt3 and Hxt7, are Discordant with *HXT3* and *HXT7* Gene Expression Levels in *grr1Δ* Strains

Strains harboring deletions of *GRR1* have been extensively characterized to possess defects in high affinity glucose transport that lead to severely reduced growth on low glucose or raffinose media. Additionally, *grr1Δ* strains display increased doubling times on high glucose media (~2%) with reported increases ranging from 75-100% of that of wild-type strains [159,66,67]. Consistent with these phenotypes, high affinity transport has been found to be completely absent in *grr1Δ* cells while defects in low affinity glucose uptake have been reported to be reduced 35% of that of wild-type strains [69,70]. These defects in *grr1Δ* strains are a consequence of the inability to de-repress transcription through the Snf3/Rgt2 dependent inactivation of the transcriptional repressor Rgt1 in response to glucose availability [56,167,160]. Thus, despite the presence of glucose, Rgt1 remains constitutively bound to *HXT* gene promoters and as a result a number of hexose transporter genes, including both low (*HXT1* and *HXT3*) and high (*HXT2*, and *HXT4*) affinity transporter genes, remain constitutively repressed in *grr1Δ* cells [167]. While the constitutive repression of glucose transporters genes certainly contributes to the glucose growth defects of *grr1Δ* cells, it does not completely account for a number of phenotypes. First, while the high affinity hexose transporter genes, *HXT2* and *HXT4*, are constitutively repressed in *grr1Δ* cells, the gene expression of the remaining functional high affinity hexose transporter gene(s), *HXT6/7,* has been measured in multiple independent experiments to be higher in *grr1Δ* strains by approximately four fold ([159] and

present study). This is inconsistent with the lack of high affinity glucose transport in *grr1Δ* strains. Second, despite significant large decreases in low affinity (*HXT1* and *HXT3*) [167] hexose transporter gene expression, *grr1Δ* cells grow more robustly on high concentrations of glucose with only a decrease in glucose uptake at these concentrations of ~35% [69,70].

In the experiments described above, we compared the gene expression and protein expression profiles of *grr1Δ* and wild-type cells on a system wide level. As noted, a high degree of discordance was observed between gene expression and protein expression, especially among genes and proteins annotated to the GO process of "carbon and energy metabolism". Among the loci within this category, discordance between gene expression and protein expression for hexose transporters and the encoding genes was observed. Interestingly, despite significant large decreases in gene expression for the low affinity hexose transporters, *HXT1* (-209.98) and *HXT3* (-19.86), the protein expression level of these transporters remained relatively unaltered (1.12 ± 0.01 and 1.09 ± 0.01, respectively) (Figure 5.1 middle) in *grr1Δ* cells. Additionally, while expression of the high affinity transporter gene, *HXT7,* was observed to increase in *grr1Δ* cells relative to wild-type (4.62), the relative expression of Hxt7 was observed to decrease (0.39 ± .44).

In order to confirm that the protein expression ratios obtained by our proteomic analysis for Hxt3 and Hxt7 were indeed reflective of changes in the steady state level of these proteins, we performed western analysis of Hxt3 and Hxt7 protein levels in *grr1Δ* strains utilizing rabbit polyclonal antibodies raised against synthesized peptide sequences unique to Hxt3 and Hxt7 (Open Biosystems™) (Section 3.3.2). Western blots were performed utilizing raw sera from these antibody preparations on protein extracts obtained from both wild-type and *grr1Δ* cells grown on defined medium containing 2% glucose. As can be seen in Figure 5.1 (right), western analysis confirmed that the relative protein expression measurements obtained in our global proteomic analysis were in fact reflective of the steady state protein level of both Hxt3 and Hxt7. Hxt7 steady state levels were observed to decrease while Hxt3 steady state protein levels

remained unaltered in *grr1Δ* strains. These data are in contrast to the transcriptional regulation of each of these transporters. The steady state protein levels for Hxt3 and Hxt7 in *grr1Δ* strains are consistent with both the glucose transport defects as well as the growth defects observed on glucose media for *grr1Δ* strains. Since our strains and media condition were slightly different than those utilized previously, we sought to confirm that our *grr1Δ* strain exhibited these same growth properties on the synthetic medium we utilized in our global analyses. To do this, we utilized spot dilution assays to compare *grr1Δ* and wild-type growth on the synthetic defined media utilized in our global analyses supplemented with glucose concentrations of 0.02, 0.2, 1, and 2% in the presence of the respiratory inhibitor, Antimycin A. As can be seen in Figure 5.1 (left), consistent with previous studies, defects in glucose based growth were exhibited at all concentrations of glucose assayed. However, growth of *grr1Δ* cells deteriorated precipitously as the glucose concentration decreased. These data are consistent with the growth phenotypes of *grr1Δ* cells reported by others. Together these data suggest that glucose transport and as result growth on high glucose concentrations is supported by Hxt3 and possibly Hxt1 mediated glucose transport despite large decreases in their transcriptional expression. At the same time, the severe growth defect of *grr1Δ* cells on low glucose seems to be a consequence of constitutive repression of *HXT2* and *HXT4* (Hxt2 protein expression was measured to decrease in accordance with its reduced gene expression (Figure 5.1)) and the reduced protein steady state levels of Hxt6/7.

### 5.3. Analysis of Discordance between Gene and Protein Expression for Mitochondrial Function in *grr1Δ* Cells

Previous genetic analyses monitoring the effect that *GRR1* deletion has on gene expression on high glucose media (~2%) have revealed widespread de-repression of a number of enzymes and transporters required for the utilization of an eclectic array of alternative energy sources. Genes necessary for growth on other fermentable sugars such as maltose, sucrose, and galactose as well as

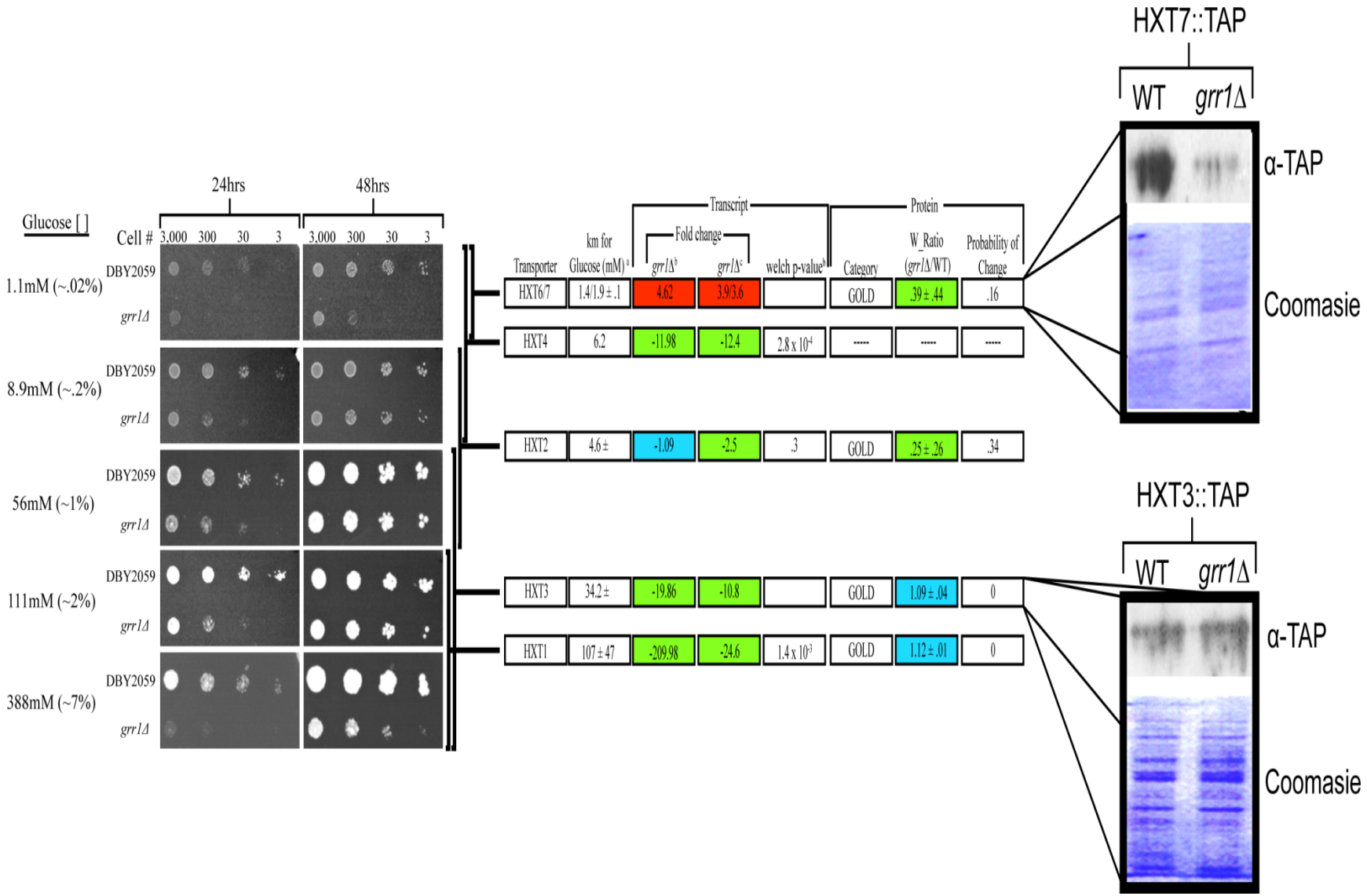
24hrs
48hrs
Glucose [ ]
Cell # 3,000 300 30 3 3,000 300 30 3
1.1mM (~.02%)
8.9mM (~.2%)
56mM (~1%)
111mM (~2%)
388mM (~7%)
DBY2059
grr1Δ
Transcript
Protein
Transporter
km for Glucose (mM)[a]
Fold change
grr1Δ[b]
grr1Δ[c]
welch p-value[b]
Category
W_Ratio (grr1Δ/WT)
Probability of Change
HXT6/7 1.4/1.9 ± .1 4.62 3.9/3.6 GOLD .39 ± .44 .16
HXT4 6.2 -11.98 -12.4 2.8 x 10-4 ----- ----- -----
HXT2 4.6 ± -1.09 -2.5 .3 GOLD .25 ± .26 .34
HXT3 34.2 ± -19.86 -10.8 GOLD 1.09 ± .04 0
HXT1 107 ± 47 -209.98 -24.6 1.4 x 10-3 GOLD 1.12 ± .01 0
HXT7::TAP
WT grr1Δ
α-TAP
Coomasie
HXT3::TAP
WT grr1Δ
α-TAP
Coomasie

**Figure 5.1. *HXT3* and *HXT7* Gene Expression is Discordant with Hxt3 and Hxt7 Protein Expression in *grr1Δ* Cells.** **Left:** Spot dilution assays were performed at various concentrations of glucose in the presence of the respiratory inhibitor, Antimycin A (3 µg/L), comparing growth of *grr1Δ* and the representative wild-type strain, DBY2059. Pictures were taken at 24 and 48 hours post incubation at 30°C. **Middle:** The hexose transporters facilitating the majority of glucose transport at the glucose concentrations utilized in the spot dilution assays was inferred from gene expression [167] and kinetic studies [173,451] and indicated by black bars. The Km values (Km[a]) for each hexose transporter as determined by [173], the relative gene expression levels (*grr1Δ*[b]) and their respective p-values (Welch p-value[b]) as measured in this study and by [159] (*grr1Δ*[c]), and the relative protein expression levels as measured in our proteomic analysis (W_Ratio) are indicated . Red denotes significant increased expression in *grr1Δ* strains, blue indicates no significant change in expression, and green indicates significant decreased expression in *grr1Δ* strains. **Right:** Western blots utilizing rabbit polyclonal antibody raised against synthetic peptides unique to Hxt3 and Hxt7 confirm the mass spectrometry based protein expression data.

genes needed for respiratory growth on C2 and C3 carbon sources such as pyruvate, lactate, acetate, glycerol and ethanol have all been measured to have increased gene expression in *grr1Δ* cells grown on high glucose concentrations (~2%) [159]. The changes we measured in gene expression for *grr1Δ* cells under our media conditions (synthetic media containing 2% glucose and 5mg/ml glutamine) were consistent with these analyses. Figure 5.2 and table 5.1 show the significant relative gene and protein expression changes measured in our global profiling experiments of *grr1Δ* cells for select metabolic processes including glycolysis, ethanol fermentation, the TCA cycle, the electron transport chain, gluconeogenesis, the glyoxylate cycle, and the pentose phosphate shunt as well as glycerol, ethanol, acetate, pyruvate, lactate, and maltose metabolism. Proteins are represented as ovals with the color of the oval filling indicating the change in protein expression measured and the color of the oval border representing the change in gene expression measured for the specific enzyme or transporter encoding gene (Red = up in *grr1*, Green = down in *grr1*, Blue = unchanged, and Black = not measured). As can be seen in Figure 5.2, glucose insensitive expression of a number of genes within these processes was measured including genes necessary for the utilization of maltose (*MAL11, MAL31, MAL32,* and *MAL33*), sucrose (*SUC2*), galactose (*GAL3*), ethanol and acetate (*SFC1, DIC1, ADY2, ACS1, ACH1, ADH2,* and *ALD4*), fatty acids (*YAT1, YAT2, CRC1, POT1,* and *POX1*), glycerol (*GPP2* and *GUT2*), and lactate and pyruvate (*JEN1* and *CYB2*). Additionally, glucose insensitive expression of

respiratory and TCA cycle genes (*AAC1, PDH1, CIT1, CIT3, ACO1, LSC2, SDH1, SDH2, SDH3, SDH4, IDH1, IDH2, MDH1, PET10, ATP3, ATP21, ATP17, ATP14, ATP20, ATP19, STF1, INH1, RIP1, COR1, QCR6, QCR10, QCR2, NDI1, CYT1, SUE1, CYC1, COX4, COX6, COX12, COX13,* and *COX7*) as well as glyoxylate cycle and gluconeogenesis genes (*CIT2, ICL1, IDP2, AGX1, FBP1, PCK1, MLS1,* and *PYC1*) were also measured in *grr1Δ* strains.

The increased expression of respiratory genes has been suggested to result in increased respiratory metabolism in *grr1Δ* cells grown on glucose as the sole carbon source [70]. However, recent glucose fermentation profiles of *grr1Δ* cells have measured no significant decrease in overall ethanol yield [67]. This suggests that, despite increased expression of TCA cycle and respiratory genes, respiration rate remains unaltered in *grr1Δ* strains. The measured discordance between gene and protein expression among loci of the TCA cycle and respiratory chain as well as loci involved in mitochondrial function support the metabolic data and further suggest that though flux through the TCA cycle is increased in *grr1Δ* cells respiratory capacity is decreased in *grr1Δ* cells (Figure 5.2 and table 5.1). Discordance among TCA cycle and respiratory chain genes/proteins can be categorized into three types based on the nature of the discordance. The majority of loci exhibited increased gene expression with no concomitant change in protein expression and included *ACO1*/Aco1 (+2.41 gene expression in *grr1Δ*, +1.06 protein expression in *grr1Δ*), *IDH1*/Idh1 (+3.31, -1.12), *SDH2*/Sdh2 (+3.02, -1.5), *MDH1*/Mdh1 (+2.24, -2.1), *ATP3*/Atp3 (+2.26, -1.25), *QCR2*/Qcr2 (+2.35, -1.9), *COR1*/Cor1 (+2.34, +1.11), *CYC1*/Cyc1 (+3.09, +1.52), *COX4*/Cox4 (+2.51, +1.59), and *COX6*/Cox6 (+2, -1.14). A smaller group of proteins, including Pet9 (+1.37, +4.67) and Coq2 (+1.2, +5.83), were measured to significantly increase in expression with no significant change in the expression of their encoding. Finally, Ach1 (+4.03, -5.6), Ndi1 (+3.76, -2.86), Idh2 (+3.03, -6.25), and Atp19 (+2.5, -2.5) were measured to significantly decrease in protein expression despite significant increases in the expression of their encoding genes. With the exception of Pet9 and Coq2, the measured protein expression levels of the remainder of TCA cycle and respiratory enzymes

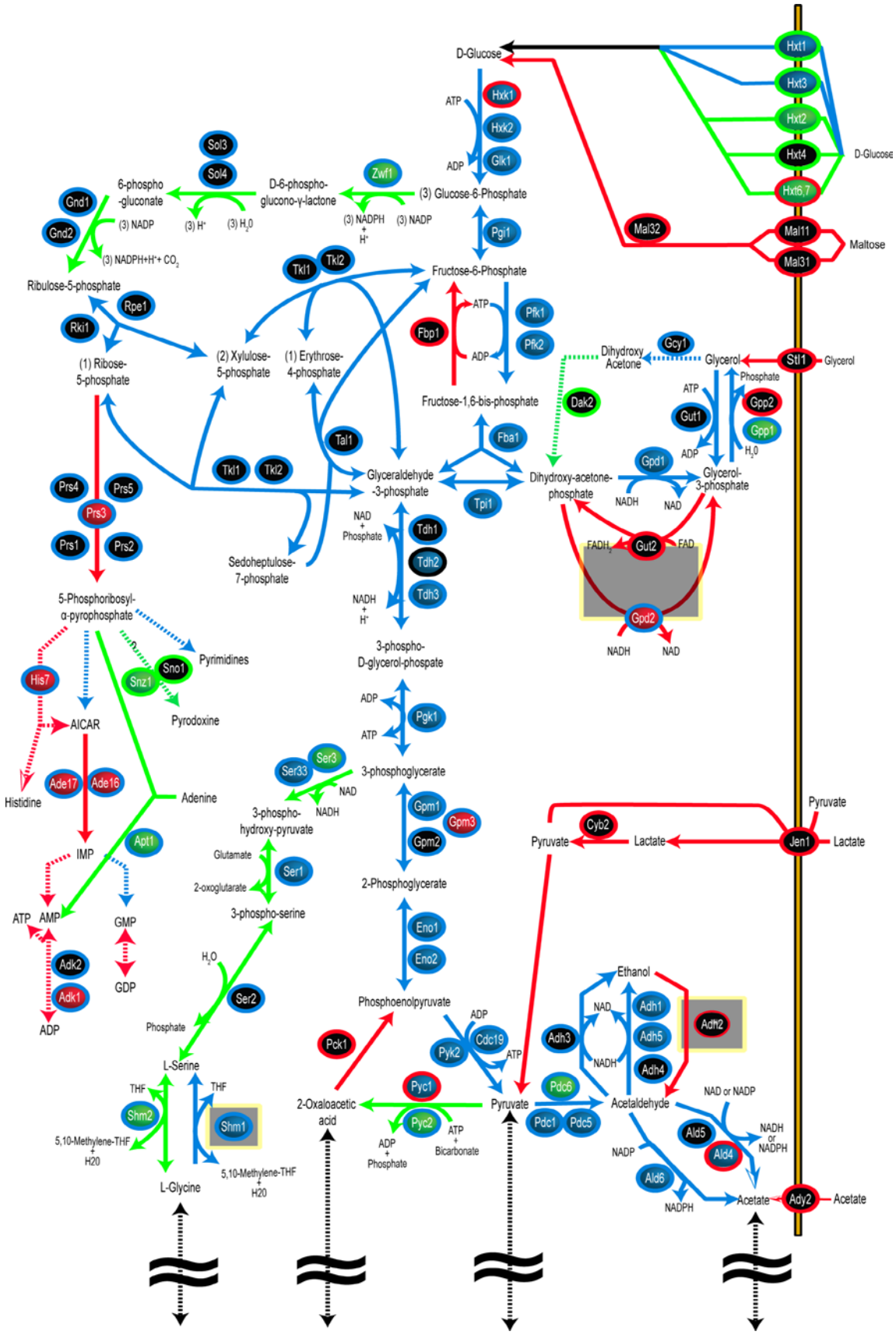
D-Glucose
Hxt1
Hxt3
Hxt2
Hxt4
Hxt6,7
D-Glucose
Mal32
Mal11
Mal31
Maltose
ATP
Hxk1
Hxk2
Glk1
ADP
(3) Glucose-6-Phosphate
Pgi1
Fructose-6-Phosphate
Pfk1
Pfk2
Fbp1
Fructose-1,6-bis-phosphate
Fba1
Tpi1
Glyceraldehyde -3-phosphate
Dihydroxy-acetone-phosphate
Dihydroxy Acetone
Gcy1
Glycerol
Stl1
Glycerol
Dak2
Gut1
Gpp2
Gpp1
Phosphate
Gpd1
Glycerol-3-phosphate
NADH
NAD
FADH2
Gut2
FAD
Gpd2
Tdh1
Tdh2
Tdh3
NAD + Phosphate
NADH + H+
3-phospho-D-glycerol-phospate
Pgk1
3-phosphoglycerate
Ser3
Ser33
NAD
NADH
3-phospho-hydroxy-pyruvate
Gpm1
Gpm3
Gpm2
2-Phosphoglycerate
Glutamate
2-oxoglutarate
Ser1
3-phospho-serine
Eno1
Eno2
Phosphoenolpyruvate
H2O
Ser2
Phosphate
L-Serine
Tkl1
Tkl2
(1) Ribose-5-phosphate
Rki1
Rpe1
Ribulose-5-phosphate
(2) Xylulose-5-phosphate
(1) Erythrose-4-phosphate
Sedoheptulose-7-phosphate
Zwf1
(3) NADPH + H+
(3) NADP
D-6-phospho-glucono-γ-lactone
Sol3
Sol4
(3) H+
(3) H2O
6-phospho-gluconate
Gnd1
Gnd2
(3) NADP
(3) NADPH+H+ + CO2
Prs4
Prs5
Prs3
Prs1
Prs2
5-Phosphoribosyl-α-pyrophosphate
Pyrimidines
Sno1
Snz1
Pyrodoxine
His7
Histidine
AICAR
Ade17
Ade16
Adenine
Apt1
IMP
ATP
AMP
GMP
GDP
ADP
Adk2
Adk1
Tal1
Shm2
Shm1
THF
5,10-Methylene-THF + H20
L-Glycine
Pck1
2-Oxaloacetic acid
Pyc1
Pyc2
ADP + Phosphate
ATP + Bicarbonate
Pyk2
Cdc19
Pyruvate
Cyb2
Lactate
Jen1
Pdc6
Pdc1
Pdc5
Adh3
Adh1
Adh5
Adh4
Adh2
Ethanol
Acetaldehyde
NAD or NADP
NADH or NADPH
Ald5
Ald4
Ald6
NADPH
Acetate
Ady2
Acetate

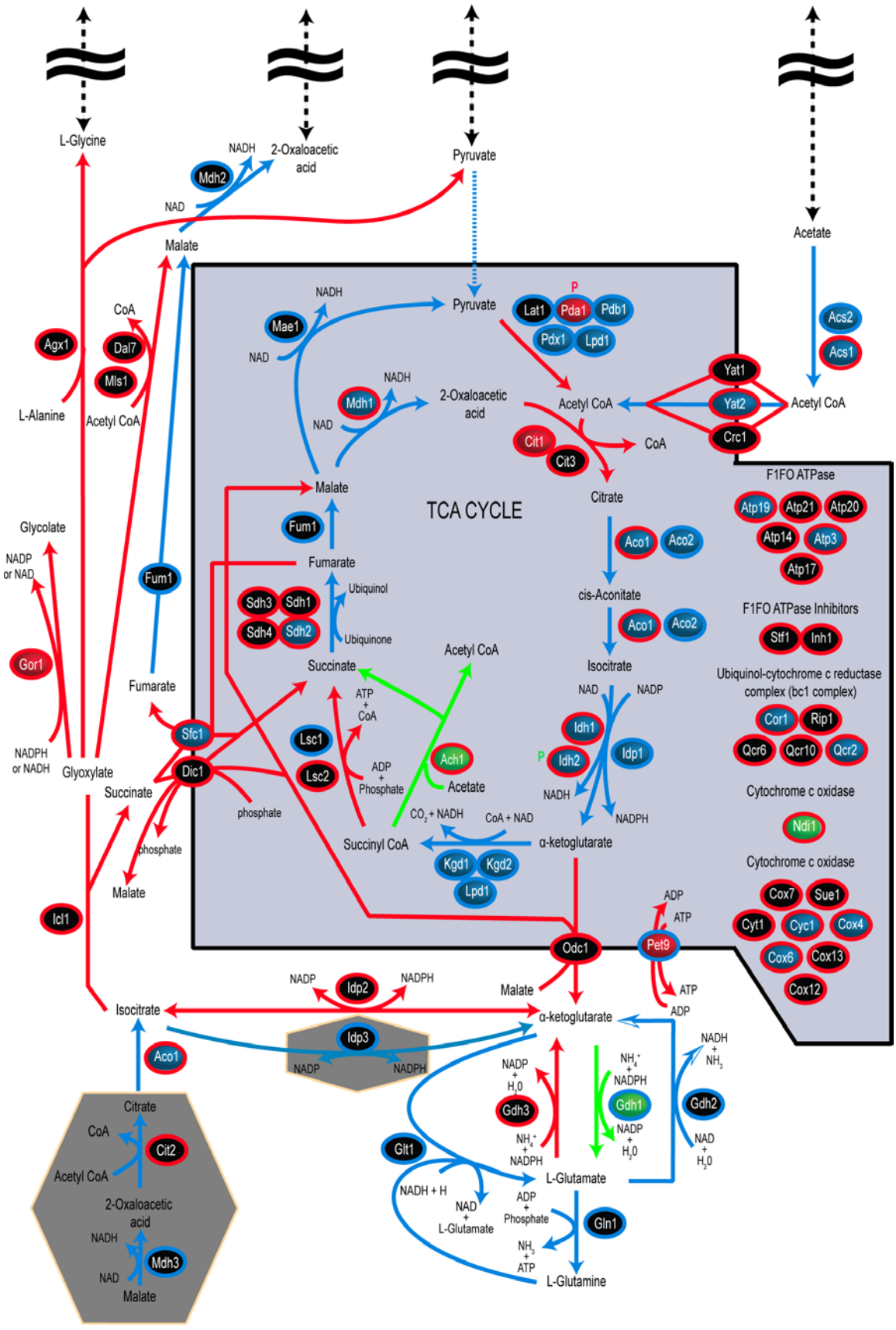
L-Glycine
NADH
2-Oxaloacetic acid
Pyruvate
Acetate
Mdh2
NAD
Malate
CoA
Agx1
Dal7
Mls1
L-Alanine
Acetyl CoA
Mae1
Lat1
Pda1
Pdb1
Pdx1
Lpd1
P
Acs2
Acs1
Mdh1
Yat1
Yat2
Crc1
Cit1
Cit3
Citrate
TCA CYCLE
F1FO ATPase
Atp19
Atp21
Atp20
Atp14
Atp3
Atp17
Fum1
Fumarate
Aco1
Aco2
cis-Aconitate
F1FO ATPase Inhibitors
Stf1
Inh1
Ubiquinol
Ubiquinone
Sdh3
Sdh1
Sdh4
Sdh2
Isocitrate
Ubiquinol-cytochrome c reductase complex (bc1 complex)
Cor1
Rip1
Qcr6
Qcr10
Qcr2
Glycolate
NADP or NAD
Gor1
Succinate
Acetyl CoA
Lsc1
Lsc2
ATP + CoA
ADP + Phosphate
Ach1
Acetate
Idh1
Idh2
Idp1
NADPH
Sfc1
Dic1
Glyoxylate
NADPH or NADH
phosphate
Succinyl CoA
CO2 + NADH
CoA + NAD
α-ketoglutarate
Kgd1
Kgd2
Lpd1
Cytochrome c oxidase
Ndi1
Cytochrome c oxidase
Cox7
Sue1
Cyt1
Cyc1
Cox4
Cox6
Cox13
Cox12
Icl1
ADP
ATP
Odc1
Pet9
Idp2
Idp3
Aco1
Gdh3
Gdh1
Gdh2
Glt1
L-Glutamate
NADH + H
ADP + Phosphate
Gln1
L-Glutamine
Citrate
Cit2
2-Oxaloacetic acid
Mdh3

**Figure 5.2. Metabolic Map of *grr1Δ* Cells Grown on 2% Glucose.** (Previous page) Gene and protein expression measurements were overlaid onto a metabolic map of *S. cerevisiae* metabolism. Enzymes are represented by nodes with the color of the node denoting increased (red), decreased (green), unchanged (blue), or un-measured (black) protein expression. Changes in gene expression are represented by the color of the ring or edge around each node utilizing the same color scheme as that used for protein expression. Reactions are denoted with solid lines with the direction of the reaction denoted by the arrowhead (bi-directional reactions contain an arrowhead at both ends). The color of the reaction line denotes whether the flux through the reaction is presumed to be increased (red), decreased (green), or unchanged (blue). Flux through a particular reaction is presumed based off of gene expression data when no protein expression data is present. However, if protein expression is measured for an enzyme of a particular reaction it is utilized over gene expression data to infer flux through the reaction. Dotted reaction lines represent multiple metabolic steps. Increased line weight for the reaction catalyzed by Gdh1 is utilized to denote that maximum flux capacity for this reaction is catalyzed by Gdh1 whereas Gdh3 catalyzes the reaction at a much slower rate. Proteins bound by yellow bordered squares are mitochondrial localized proteins whereas those bound by a yellow bordered hexagon are peroxisomal. Proteins highlighted in grey with the green boarder represent proteins involved in glycolysis and fermentation. Transcriptional targets of Cat8 are also indicated (black dotted line with double arrow heads). For protein expression and gene expression values see Table 5.1.

and acetyl-CoA (Cit1). Thus, it is possible that the increases in these enzymes are sufficient to suggest that respiratory rate may not be significantly altered in *grr1Δ* cells. However, it is likely that the discordances measured of the last type, where decreased protein expression was measured despite an increase in gene expression, may be attributable to noise in the proteomic measurements contributed by differential post-translational modification of the peptides analyzed since these proteins were only quantified by single peptide hits. Nevertheless, disregarding these instances of discordance, Aco1, Sdh2, Qcr2, Cor1, and Cox4 were quantified utilizing 19, 3, 8, 9, and 6 peptides, respectively. Each of these proteins expression has been found to increase as respiratory capacity increases [452] and thus the absence of an observed increase in their protein expression suggests that respiratory capacity may be unaltered in *grr1Δ* cells.

It must be noted that while many of the TCA cycle genes and proteins exhibited discordance, citrate synthase (Cit1) and the E1 alpha subunit of the pyruvate dehydrogenase complex (Pda1) were measured to have an accordant increase in protein expression and of the encoding gene of approximately three fold each. Together these two proteins catalyze the initial, rate limiting, reactions of the TCA cycle; the synthesis of acetyl Co-A from pyruvate (Pda1 in conjunction with the pyruvate dehydrogenase complex) and the synthesis of

citrate from oxaloacetate increase flux through the TCA cycle without concomitant increases in the remaining TCA cycle enzymes. Concurrent with this hypothesis, increased flux through the TCA cycle has been observed during $^{13}$C-labeled glucose experiments monitoring metabolic flux through the TCA cycle in *grr1Δ* cells [174]. Together these data suggest that despite increases in flux through the TCA cycle, respiration rate is unaltered in *grr1Δ* cells.

In addition to proteins involved in metabolic processes of the mitochondrial TCA cycle and respiratory chain, fourteen proteins involved in various aspects of maintaining mitochondrial integrity were also measured to be discordant with the expression of their encoding genes (Table 5.2). All fourteen of these proteins exhibited either increased or decreased protein expression with no significant change observed in the expression of the encoding genes, suggesting that these proteins may be regulated post-transcriptionally in *grr1Δ* cells. Proteins within this group included the mitochondrial porin, Por1 (+1.53, -2.78), six proteins involved in mitochondrial protein import, Hsp60 (-1.03, -2.56), Phb1 (+1.22, -2.78), Mia40 (-1.02, -2.56), Tim15(+1.17, -4.55), Tom70 (-1.01, -9.09), and Mdm38 (+1.53, -16.67), three proteins involved in mitochondrial translation, Msk1 (+1.01, +4.11), Tuf1 (+1.59, -9.09), and Cbs1 (+1.18, -6.67), and four proteins involved in other aspects of mitochondrial function, Mir1 (+1.53, +3.24), Rpo41 (+1.42, -2.56), Fmp26 (+1.51, +3.13), and Mmr1 (+1.17, +2.70). All of these proteins were quantified by multiple discrete peptides with the exception of Phb1. Msk1 (lysine-tRNA synthetase), Mir1 (mitochondrial phosphate carrier), Mmr1 (localizes exclusively to mitochondria in the bud), and Fmp26 (unknown) displayed increased protein expression levels. Among these proteins, the protein expression level of the mitochondrial porin, Por1, has been measured to increase with increased respiratory capacity [452] and this protein plays a central role in regulating respiratory capacity [453]. Por1 or the TOM complex both mediate the permeability of the outer mitochondrial membrane to NADH and have roles in mediating mitochondrial protein import. Interestingly, Tom70, the receptor component of the TOM complex, was also shown to decrease in protein

| | | | | | | | | | | Transcriptional Results | | | | | | | | | | | |
|---|---|---|---|---|---|---|---|---|---|---|---|---|---|---|---|---|---|---|---|---|---|
| Orf | Gene | Final Protein Probability (Detected) | Probability of Change | Trans Freq | Hallife | PMC | Category | SD (±) | Final Protein Ratio (*grr1Δ*/WT) | fold change | Welch Significance Test (Log2) | TTest Significance Test (Log2) | SGD Annotations | Localization | Transcription Factor | ORF Identification Count | # Unique Peps Identified | Total # Peps Identified | Ratio ORF Count | Combined Ratio # of Peps | Inter-experimental STDEV | Intra-experimental STDEV |
| Glycolysis / Fermentation | | | | | | | | | | | | | | | | | | | | | | |
| Transport | | | | | | | | | | | | | | | | | | | | | | |
| YHR094C | HXT1 | 0.750 | ------ | | 41.00 | 10.00 | 23300.00 | GOLD | 0.00 | 1.120000 | -209.98 | 0 | 0 | Transport/Glucose in | Plasma Membrane | Rgt1/Mig | 1 | 2 | 2 | 1 | 2 | 0 | 0.430000007 |
| YDR345C | HXT3 | 1.000 | 0.95 | 37.50 | 13.00 | 37200.00 | GOLD | 0.04 | 1.087383 | -19.86 | 0.000025 | 0 | Transport/Glucose in | Plasma Membrane | Rgt1 | 4 | 6 | 16 | 4 | 7 | 0.564358027 | 0.297500004 |
| YMR011W | HXT2 | 0.922 | 0.34 | 12.40 | 21.00 | 0.00 | GOLD | 0.26 | 0.250000 | -1.09 | 0.300509 | 0.292233 | Transport/Glucose in | Plasma Membrane | ------ | 2 | 2 | 2 | 1 | 1 | 0 | 0.25999999 |
| YHR092C | HXT4 | ------ | ------ | 10.60 | 11.00 | 0.00 | ------ | ------ | ------ | -11.98 | 0.002213 | 0.000062 | Transport/Glucose in | Plasma Membrane | Rgt1/Mig/Gcr1 | ------ | ------ | ------ | ------ | ------ | ------ | ------ |
| YDR342C | HXT7 | 1.000 | 0.16 | 15.10 | 24.00 | 7350.00 | GOLD | 0.44 | 0.390000 | 4.62 | 0.003626 | 0.000162 | Transport/Glucose in | Plasma Membrane | ------ | 2 | 7 | 14 | 1 | 1 | 0 | 0.439999998 |
| YEL069C | HXT13 | ------ | ------ | ------ | ------ | 0.00 | ------ | ------ | ------ | 2.47 | 0.473292 | 0.459153 | Transport/Glucose in (?) | Plasma Membrane | ------ | ------ | ------ | ------ | ------ | ------ | ------ | ------ |
| YNL318C | HXT14 | ------ | ------ | ------ | ------ | 0.00 | ------ | ------ | ------ | -1.03 | 0.860514 | 0.859339 | Transport/Glucose in (?) | Plasma Membrane | ------ | ------ | ------ | ------ | ------ | ------ | ------ | ------ |
| YDL245C | HXT15 | ------ | ------ | ------ | ------ | 0.00 | ------ | ------ | ------ | 1.14 | 0.972071 | 0.971841 | Transport/Glucose in (?) | Plasma Membrane | ------ | ------ | ------ | ------ | ------ | ------ | ------ | ------ |
| YHR096C | HXT5 | ------ | ------ | ------ | ------ | 0.00 | ------ | ------ | ------ | 4.4 | 0.001351 | 0.00021 | Transport/Glucose in (?) | Plasma Membrane | Hap/Stp/Rgt | ------ | ------ | ------ | ------ | ------ | ------ | ------ |
| YFL011W | HXT10 | 0.852 | ------ | 0.40 | 15.00 | 0.00 | ------ | ------ | ------ | 4.82 | 0.014196 | 0.002116 | Transport/Glucose in (?) | Plasma Membrane | Hap1 | 2 | 2 | 3 | ------ | ------ | ------ | ------ |
| YNR072W | HXT17 | ------ | ------ | ------ | 14.00 | 0.00 | ------ | ------ | ------ | -1.33 | 0.375353 | 0.368244 | Transport/Glucose in (?) | Plasma Membrane | ------ | ------ | ------ | ------ | ------ | ------ | ------ | ------ |
| YJL219W | HXT9 | ------ | ------ | ------ | 13.00 | 0.00 | ------ | ------ | ------ | 1.15 | 0.500758 | 0.500758 | Transport/Glucose in (?) | Plasma Membrane | ------ | ------ | ------ | ------ | ------ | ------ | ------ | ------ |
| YJL214W | HXT8 | 0.550 | ------ | 0.80 | 12.00 | 623.00 | ------ | ------ | ------ | -1.34 | 0.023267 | 0.01171 | Transport/Glucose in (?) | Plasma Membrane | ------ | 1 | 1 | 1 | ------ | ------ | ------ | ------ |
| YOL156W | HXT11 | ------ | ------ | ------ | 11.00 | 0.00 | ------ | ------ | ------ | 1.41 | 0.276899 | 0.255213 | Transport/Glucose in (?) | Plasma Membrane | ------ | ------ | ------ | ------ | ------ | ------ | ------ | ------ |
| YGR289C | MAL11 | ------ | ------ | 0.30 | 25.00 | 0.00 | ------ | ------ | ------ | 2.04 | 0.027915 | 0.022058 | Transport / Maltose in | Plasma Membrane | ------ | ------ | ------ | ------ | ------ | ------ | ------ | ------ |
| YBR298C | MAL31 | 0.530 | ------ | ------ | ------ | 0.00 | ------ | ------ | ------ | 2.44 | 0.025037 | 0.012924 | Transport / Maltose in | Plasma Membrane | ------ | 1 | 1 | 1 | ------ | ------ | ------ | ------ |
| Metabolism | | | | | | | | | | | | | | | | | | | | | | |
| YBR299W | MAL32 | ------ | ------ | ------ | 23.00 | 4030.00 | ------ | ------ | ------ | 21.73 | 0.000001 | 0 | Carbon/ Maltose / alpha-D-glucosidase / maltose -> 2 glucose | Plasma Membrane enriched fraction | Mal33 | ------ | ------ | ------ | ------ | ------ | ------ | ------ |
| YFR053C | HXK1 | 1.000 | 1.00 | 5.80 | 23.00 | 40800.00 | GOLD | 0.09 | 2.133595 | 8.28 | 0.001821 | 0.000043 | glucose + ATP -> glucose-6-phosphate + ADP | Cytoplasm | Gcr1/Mig/Neg_reg_by_cAMP | 6 | 46 | 136 | 3 | 11 | 0.55403574 | 0.683333347 |
| YGL253W | HXK2 | 1.000 | 0.16 | 71.90 | 10.00 | 114000.00 | GOLD | 0.16 | 0.851937 | -1.1 | 0.078662 | 0.057192 | glucose + ATP -> glucose-6-phosphate + ADP | Cytoplasm | ------ | 5 | 40 | 80 | 2 | 14 | 0.175000012 | 0.25500001 |
| YCL040W | GLK1 | 1.000 | 0.52 | 3.80 | 36.00 | 21100.00 | GOLD | 0.50 | 1.440000 | 1.53 | 0.171191 | 0.146914 | glucose + ATP -> glucose-6-phosphate + ADP | Cytoplasm | ------ | 4 | 22 | 33 | 1 | 9 | 0 | 0.5 |
| YBR196C | PGI1 | 1.000 | 1.00 | 30.70 | 18.00 | 91600.00 | GOLD | 0.05 | 1.277830 | -1.13 | 0.051486 | 0.019955 | glucose-6-phosphate -> fructose-6-phosphate | Cytoplasm | ------ | 6 | 60 | 198 | 6 | 32 | 0.76820138 | 0.659999998 |
| YGR240C | PFK1 | 1.000 | 1.00 | 23.00 | 14.00 | 89800.00 | GOLD | 0.12 | 1.429028 | -1.19 | 0.049442 | 0.018669 | fructose-6-phosphate + ATP -> fructose-1,6-bisphosphate | Cytoplasm | | 5 | 33 | 56 | 3 | 17 | 0.31930482 | 0.536666669 |
| YMR205C | PFK2 | 1.000 | 1.00 | 20.00 | 13.00 | 90200.00 | GOLD | 0.18 | 2.002126 | -1.1 | 0.114696 | 0.069675 | fructose-6-phosphate + ATP -> fructose-1,6-bisphosphate | Cytoplasm | ------ | 6 | 43 | 87 | 3 | 15 | 0.648810879 | 0.346666674 |
| YIL107C | PFK26 | 0.999 | 0.99 | ------ | ------ | 1710.00 | GOLD | 0.11 | 1.280000 | 1.31 | 0.151319 | 0.127004 | 6-phosphofructo-2-kinase / syntesizes fructose-2,6-bisphosphate | Cytoplasm | ------ | 3 | 6 | 7 | 1 | 2 | 0 | 0.109999999 |
| YOL136C | PFK27 | 0.250 | ------ | 4.50 | 14.00 | 0.00 | ------ | ------ | ------ | 1.09 | 0.620859 | 0.620859 | 6-phosphofructo-2-kinase / syntesizes fructose-2,6-bisphosphate | Cytoplasm | ------ | 1 | 1 | 1 | ------ | ------ | ------ | ------ |
| YKL060C | FBA1 | 1.000 | 0.22 | 167.90 | 16.00 | 1020000.00 | GOLD | 0.29 | 0.626030 | -1.12 | 0.034596 | 0.034596 | fructose-1,6-bisphosphate -> dihydroxy-acetone-phosphate + glyceraldehyde-3-phosphate | Cytoplasm | ------ | 6 | 73 | 529 | 2 | 20 | 0.00999999 | 0.434999987 |
| YDR050C | TPI1 | 1.000 | 0.49 | 130.40 | 15.00 | 207000.00 | GOLD | 0.14 | 0.731380 | -1.1 | 0.043908 | 0.027166 | dihydroxy-acetone-phosphate <-> glyceraldehyde-3-phosphate | Cytoplasm | ------ | 6 | 95 | 271 | 5 | 36 | 0.386967685 | 0.518000008 |
| YJL052W | TDH1 | 0.978 | ------ | 12.70 | 10.00 | 120000.00 | ------ | ------ | ------ | -1.06 | 0.724428 | 0.72196 | glyceraldehyde-3-phosphate + NAD + phosphate -> 3-phospho-D-glyceroyl-phosphate + NAD | Cytoplasm | ------ | 2 | 2 | 2 | ------ | ------ | ------ | ------ |
| YGR192C | TDH3 | 1.000 | 0.77 | 188.10 | 18.00 | 169000.00 | GOLD | 0.07 | 0.823994 | -1.09 | 0.105216 | 0.105216 | glyceraldehyde-3-phosphate + NAD + phosphate -> 3-phospho-D-glyceroyl-phosphate + NAD | Cytoplasm | ------ | 6 | 103 | 638 | 6 | 22 | 0.198529337 | 0.291666664 |
| YCR012W | PGK1 | 1.000 | 0.12 | 110.50 | 20.00 | 314000.00 | GOLD | 0.14 | 0.904202 | -1.12 | 0.021684 | 0.021684 | 3-phospho-D-glyceroyl-phosphate +ADP -> 3-phospho-glycerate + ATP | Cytoplasm | ------ | 6 | 187 | 932 | 6 | 81 | 0.221766902 | 0.439999995 |

**Table 5.1. Gene and Protein Expression Levels in *grr1Δ* Cells for Select Loci of Central Metabolism.** See page 213 for details.

| | | | | | | | | | | Transcriptional Results | | | | | | | | | | | |
|---|---|---|---|---|---|---|---|---|---|---|---|---|---|---|---|---|---|---|---|---|---|
| Orf | Gene | Final Protein Probability (Detected) | Probability of Change | Trans Freq | Hallife | PMC | Category | SD (±) | Final Protein Ratio (*grr1* Δ/WT) | fold change | Welch Significance Test (Log2) | TTest Significance Test (Log2) | SGD Annotations | Localization | Transcription Factor | ORF Identification Count | # Unique Peps Identified | Total # Peps Identified | Ratio ORF Count | Combined Ratio # of Peps | Inter-experimental STDEV | Intra-experimental STDEV |
| Metabolism Continued | | | | | | | | | | | | | Glycolysis / Fermentation continued | | | | | | | | | |
| YDL021W | GPM2 | 0.460 | ------ | 0.30 | 16.00 | 2020.00 | ------ | ------ | ------ | 2.53 | 0.198376 | 0.188791 | 3-phospho-glycerate -> 2-phospho-glycerate | Cytoplasm | ------ | 1 | 1 | 1 | ------ | ------ | ------ | ------ |
| YOL056W | GPM3 | 1.000 | 1.00 | 3.00 | 11.00 | 3730.00 | GOLD | 0.19 | 2.580000 | -1.45 | 0.096358 | 0.053703 | 3-phospho-glycerate -> 2-phospho-glycerate | Cytoplasm | ------ | 1 | 1 | 6 | 1 | 1 | 0 | 0.189999998 |
| YGR254W | ENO1 | 1.000 | 0.76 | 48.10 | 13.00 | 76700.00 | GOLD | 0.11 | 1.158154 | -1.11 | 0.223106 | 0.223106 | 2-phospho-glycerate -> phosphoenolpyruvate + H2O | Cytoplasm | ------ | 5 | 112 | 885 | 4 | 41 | 0.383340598 | 0.334999999 |
| YHR174W | ENO2 | 1.000 | 0.86 | 134.70 | 17.00 | 2610.00 | GOLD | 0.11 | 0.643629 | -1.15 | 0.014856 | 0.014856 | 2-phospho-glycerate -> phosphoenolpyruvate + H2O | Cytoplasm | ------ | 4 | 163 | 1519 | 4 | 55 | 0.104253301 | 0.232499998 |
| YAL038W | CDC19 | 1.000 | 1.00 | 101.30 | 18.00 | 291000.00 | GOLD | 0.04 | 0.547095 | -1.11 | 0.055113 | 0.055113 | phosphoenolpyruvate + ADP -> pyruvate + ATP | Cytoplasm | ------ | 6 | 129 | 483 | 6 | 42 | 0.072667441 | 0.173333334 |
| YOR347C | PYK2 | 0.885 | 0.20 | 1.00 | 12.00 | 2130.00 | bronze | 0.11 | 1.040000 | 1.31 | 0.124939 | 0.124939 | phosphoenolpyruvate + ADP -> pyruvate + ATP | Cytoplasm | Neg_reg_by_cAMP | 2 | 3 | 5 | 1 | 2 | 0 | 0.109999999 |
| YLR044C | PDC1 | 1.000 | 1.00 | 103.20 | 16.00 | 8970.00 | GOLD | 0.03 | 0.594692 | -1.12 | 0.016481 | 0.01215 | pyruvate -> acetaldehyde + CO2 | Cytoplasm | ------ | 6 | 141 | 669 | 6 | 47 | 0.111317861 | 0.183333336 |
| YLR134W | PDC5 | 1.000 | 0.54 | 2.10 | 16.00 | 471000.00 | GOLD | 0.18 | 0.570000 | -1.26 | 0.104027 | 0.094482 | pyruvate -> acetaldehyde + CO2 | Cytoplasm | ------ | 2 | 13 | 19 | 1 | 7 | 0 | 0.180000007 |
| YGR087C | PDC6 | 0.986 | 1.00 | ------ | 15.00 | 1520.00 | SILVER | 0.01 | 0.230000 | -1.06 | 0.800571 | 0.796261 | pyruvate -> acetaldehyde + CO3 | Cytoplasm | ------ | 4 | 7 | 8 | 1 | 1 | 0 | 0.01 |
| YDR081C | PDC2 | 0.818 | 1.00 | ------ | ------ | 572.00 | bronze | 0.01 | 0.180000 | 1.05 | 0.429814 | 0.423554 | Transcription Factor for pyruvate decarboxylases | Cytoplasm | ------ | 2 | 3 | 3 | 1 | 1 | 0 | 0.01 |
| YOL086C | ADH1 | 1.000 | 1.00 | 125.60 | 15.00 | 0.00 | GOLD | 0.08 | 0.522782 | -1.1 | 0.070967 | 0.070967 | acetaldehyde + NADH -> ethanol + NAD | Cytoplasm | ------ | 6 | 123 | 959 | 6 | 34 | 0.048189443 | 0.218333339 |
| YMR083W | ADH3 | 1.000 | ------ | 22.20 | 13.00 | 11600.00 | ------ | ------ | ------ | -1.01 | 0.870055 | 0.864571 | acetaldehyde + NADH -> ethanol + NAD | Cytoplasm | ------ | 3 | 11 | 20 | ------ | ------ | ------ | ------ |
| YGL256W | ADH4 | 0.994 | ------ | 11.00 | 13.00 | 125.00 | ------ | ------ | ------ | -1.18 | 0.034286 | 0.034286 | acetaldehyde + NADH -> ethanol + NAD | Cytoplasm | ------ | 2 | 2 | 4 | ------ | ------ | ------ | ------ |
| YBR145W | ADH5 | 1.000 | 0.28 | 1.90 | 12.00 | 1310.00 | GOLD | 0.15 | 1.080000 | -1.42 | 0.189892 | 0.165832 | acetaldehyde + NADH -> ethanol + NAD | Cytoplasm | ------ | 3 | 6 | 9 | 1 | 3 | 0 | 0.150000006 |
| YMR318C | ADH6 | 1.000 | 1.00 | 23.00 | 13.00 | 21700.00 | GOLD | 0.10 | 1.760000 | 1.37 | 0.018157 | 0.003305 | acetaldehyde + NADPH -> ethanol + NADP | Cytoplasm | ------ | 3 | 10 | 14 | 1 | 4 | 0 | 0.100000001 |
| YCR105W | ADH7 | 0.750 | ------ | 0.50 | 26.00 | 2870.00 | ------ | ------ | ------ | -1.03 | 0.840611 | 0.840611 | acetaldehyde + NADPH -> ethanol + NADP | Cytoplasm | ------ | 1 | 2 | 2 | ------ | ------ | ------ | ------ |
| YMR303C | ADH2 | 0.736 | ------ | 2.90 | 17.00 | 1620.00 | ------ | ------ | ------ | 27 | 0.000049 | 0.000013 | ethanol + NAD -> acetaldehyde + NADH | Cytoplasm | Cat8/Gcr1/Adr1 | 2 | 3 | 4 | ------ | ------ | ------ | ------ |
| | | | | | | | | | | | | | Pyruvate Dehydrogenase | | | | | | | | | |
| YNL071W | LAT1 | 1.000 | ------ | 7.50 | 20.00 | 5440.00 | ------ | ------ | ------ | 1.07 | 0.246451 | 0.246451 | pyruvate + CoA + NAD -> acetyl-CoA + NADH + CO2 | Mitochondria | ------ | 1 | 4 | 8 | ------ | ------ | ------ | ------ |
| YER178W | PDA1 | 1.000 | 1.00 | 12.70 | 21.00 | 100000.00 | GOLD | 0.14 | 3.313222 | -1.01 | 0.698914 | 0.692038 | pyruvate + CoA + NAD -> acetyl-CoA + NADH + CO3 | Mitochondria | ------ | 3 | 7 | 10 | 2 | 4 | 1.070000052 | 0.170000002 |
| YBR221C | PDB1 | 1.000 | 0.54 | 13.00 | 24.00 | 9970.00 | GOLD | 0.06 | 1.060785 | 1.02 | 0.519109 | 0.506633 | pyruvate + CoA + NAD -> acetyl-CoA + NADH + CO4 | Mitochondria | ------ | 2 | 6 | 8 | 2 | 5 | 0.085000038 | 0.139999999 |
| YGR193C | PDX1 | 0.260 | ------ | 2.30 | 16.00 | 414.00 | ------ | ------ | ------ | 1.08 | 0.228565 | 0.219296 | pyruvate + CoA + NAD -> acetyl-CoA + NADH + CO5 | Mitochondria | ------ | 1 | 1 | 1 | ------ | ------ | ------ | ------ |
| YFL018C | LPD1 | 1.000 | 0.35 | 4.20 | 22.00 | 24600.00 | GOLD | 0.09 | 0.871355 | 1.2 | 0.004466 | 0.000242 | pyruvate + CoA + NAD -> acetyl-CoA + NADH + CO6 | Mitochondria | ------ | 4 | 17 | 24 | 2 | 7 | 0.139999986 | 0.315000013 |
| | | | | | | | | | | | | | TCA Cycle | | | | | | | | | |
| YNR001C | CIT1 | 1.000 | 1.00 | 5.50 | 25.00 | 0.00 | GOLD | 0.22 | 3.120000 | 2.7 | 0.000812 | 0.000812 | acetyl CoA + oxaloacetate -> citrate (Rate Limiting Step) | Mitochondria | ------ | 2 | 5 | 7 | 1 | 6 | 0 | 0.219999999 |
| YPR001W | CIT3 | 0.976 | ------ | 0.30 | 18.00 | 0.00 | ------ | ------ | ------ | 2.43 | 0.004497 | 0.00119 | acetyl CoA + oxaloacetate -> citrate, propionyl CoA + oxaloacetate -> methylcitrate | Mitochondria | Adr1 | 3 | 5 | 7 | ------ | ------ | ------ | ------ |
| YLR304C | ACO1 | 1.000 | 0.15 | 5.00 | 23.00 | 96700.00 | GOLD | 0.29 | 1.058638 | 2.41 | 0.000577 | 0.00006 | citrate -> cis-aconitate -> isocitrate | Mitochondria / Cytoplasm | ------ | 6 | 33 | 59 | 3 | 19 | 0.271784219 | 0.766666651 |
| YJL200C | ACO2 | 1.000 | 1.00 | 4.30 | 12.00 | 4670.00 | GOLD | 0.02 | 0.494707 | -1.4 | 0.006412 | 0.001969 | citrate -> cis-aconitate -> isocitrate | Mitochondria | ------ | 3 | 10 | 14 | 2 | 7 | 2.399999976 | 0.190000002 |
| YDL066W | IDP1 | 1.000 | 0.13 | 4.60 | 20.00 | 0.00 | GOLD | 0.30 | 1.038400 | 1.48 | 0.011793 | 0.004624 | NADP + Isocitrate -> α-ketoglutarate + NADPH | Mitochondria | ------ | 5 | 16 | 24 | 2 | 8 | 0.064999968 | 0.500000015 |
| YNL037C | IDH1 | 1.000 | 0.41 | 4.00 | 19.00 | 10500.00 | GOLD | 0.07 | 0.890000 | 3.31 | 0.000008 | 0.000002 | NAD + Isocitrate -> α-ketoglutarate + NADH | Mitochondria | Cat8/Hap | 2 | 8 | 13 | 1 | 4 | 0 | 0.07 |
| YOR136W | IDH2 | 1.000 | 1.00 | 10.40 | 20.00 | 43100.00 | GOLD* | 0.01 | 0.160000 | 3.03 | 0.000002 | 0.000002 | NAD + Isocitrate -> α-ketoglutarate + NADH | Mitochondria | Gcr1/Hap/Rtg | 2 | 7 | 11 | 1 | 3 | 0 | 0.01 |
| | | | | | | | | | | | | | [redacted] | | | | | | | | | |
| YIL125W | KGD1 | 1.000 | 0.22 | 1.10 | 29.00 | 14300.00 | GOLD | 0.30 | 0.600000 | 1.79 | 0.0009 | 0.0009 | [illegible] CO2+ Succinyl-CoA | Mitochondria | ------ | 3 | 15 | 18 | 1 | 10 | 0 | 0.300000012 |
| YDR148C | KGD2 | 1.000 | 1.00 | 1.30 | 21.00 | 7970.00 | GOLD | 0.09 | 1.460000 | 1.94 | 0.000343 | 0.000028 | NAD +CoA+α-ketoglutarate -> NADH + CO2+ Succinyl-CoA | Mitochondria | ------ | 5 | 7 | 11 | 1 | 1 | 0 | 0.090000004 |
| YFL018C | LPD1 | 1.000 | 0.35 | 4.20 | 22.00 | 24600.00 | GOLD | 0.09 | 0.871355 | 1.2 | 0.004466 | 0.000242 | NAD +CoA+α-ketoglutarate -> NADH + CO2+ Succinyl-CoA | Mitochondria | ------ | 4 | 17 | 24 | 2 | 7 | 0.139999986 | 0.315000013 |
| YOR142W | LSC1 | 1.000 | ------ | 2.10 | 25.00 | 18400.00 | ------ | ------ | ------ | 1.35 | 0.002732 | 0.000094 | Succinyl-CoA + ADP + Phosphate -> Succinate + ATP + CoA | Mitochondria | ------ | 3 | 7 | 11 | ------ | ------ | ------ | ------ |
| YGR244C | LSC2 | 1.000 | ------ | 3.50 | 16.00 | 0.00 | ------ | ------ | ------ | 4.67 | 0 | 0 | Succinyl-CoA + ADP + Phosphate -> Succinate + ATP + CoA | Mitochondria | Adr1/Gcr1 | 1 | 6 | 9 | ------ | ------ | ------ | ------ |
| YKL148C | SDH1 | 1.000 | ------ | 1.00 | 22.00 | 10400.00 | ------ | ------ | ------ | 3.94 | 0.001589 | 0.000265 | Succinate + Ubiquinone -> Ubiquinol + Fumarate | Mitochondria | Cat8/Gcr1 | 2 | 4 | 5 | ------ | ------ | ------ | ------ |
| YLL041C | SDH2 | 1.000 | 1.00 | 0.60 | 71.00 | 9540.00 | GOLD | 0.05 | 0.676772 | 3.02 | 0.00145 | 0.000727 | Succinate + Ubiquinone -> Ubiquinol + Fumarate | Mitochondria | Gcr1/Neg_reg_by_cAMP | 3 | 6 | 11 | 2 | 3 | 0.205000013 | 0.070000002 |

**Table 5.1.** Continued.

| | | | | | | | | | | Transcriptional Results | | | | | | | | | | | |
|---|---|---|---|---|---|---|---|---|---|---|---|---|---|---|---|---|---|---|---|---|---|
| Orf | Gene | Final Protein Probability (Detected) | Probability of Change | Trans Freq | Hallife | PMC | Category | SD (±) | Final Protein Ratio (*grr1* Δ/WT) | fold change | Welch Significance Test (Log2) | TTest Significance Test (Log2) | SGD Annotations | Localization | Transcription Factor | ORF Identification Count | # Unique Peps Identified | Total # Peps Identified | Ratio ORF Count | Combined Ratio # of Peps | Inter-experimental STDEV | Intra-experimental STDEV |
| **TCA Cycle continued** | | | | | | | | | | | | | | | | | | | | | | |
| YDR178W | SDH4 | 0.600 | ------ | 3.00 | 24.00 | 7920.00 | ------ | ------ | ------ | 2.76 | 0.000187 | 0.000065 | Succinate + Ubiquinone -> Ubiquinol + Fumarate | Mitochondria | ------ | 1 | 1 | 1 | ------ | ------ | ------ | ------ |
| YPL262W | FUM1 | 1.000 | ------ | 5.20 | 22.00 | 6920.00 | ------ | ------ | ------ | 1.46 | 0.001112 | 0.001112 | Fumarate + H2O -> Malate | Mitochondria / Cytoplasm | ------ | 2 | 5 | 5 | ------ | ------ | ------ | ------ |
| YKL085W | MDH1 | 1.000 | 0.12 | 11.60 | 16.00 | 28100.00 | GOLD | 0.55 | 0.470000 | 2.24 | 0.00001 | 0.000002 | Malate + NAD -> Oxaloacetate + NADH | Mitochondria | ------ | 6 | 16 | 42 | 1 | 5 | 0 | 0.550000012 |
| **Gluconeogenesis** | | | | | | | | | | | | | | | | | | | | | | |
| YLR174W | IDP2 | 0.980 | ------ | ------ | ------ | 2620.00 | ------ | ------ | ------ | 12.96 | 0.000689 | 0.000006 | NADP + isocitrate <-> α-ketoglutarate + NADPH | Cytoplasm | Cat8/Gcr1 | 1 | 1 | 2 | ------ | ------ | ------ | ------ |
| YOL126C | MDH2 | ------ | ------ | 7.40 | 14.00 | 5260.00 | ------ | ------ | ------ | 1.2 | 0.257674 | 0.248778 | malate + NAD -> oxaloacetate + NADH | Cytoplasm | Cat8/Neg_reg_by_cAMP | ------ | ------ | ------ | ------ | ------ | ------ | ------ |
| YGL062W | PYC1 | 1.000 | 0.57 | 2.20 | 19.00 | 12500.00 | GOLD | 0.05 | 0.909211 | 7.29 | 0.000006 | 0.000001 | pyuvate + ATP + bicarbonate -> oxaloacetate + ADP +Phosphate | Cytoplasm | Gcr1 | 4 | 11 | 17 | 2 | 6 | 0.245000005 | 0.08 |
| YBR218C | PYC2 | 1.000 | 1.00 | 6.70 | 13.00 | 17000.00 | GOLD | 0.01 | 0.060000 | -1.29 | 0.001943 | 0.001943 | pyuvate + ATP + bicarbonate -> oxaloacetate + ADP +Phosphate | Cytoplasm | ------ | 1 | 15 | 20 | 1 | 9 | 0 | 0.01 |
| YKR097W | PCK1 | 1.000 | ------ | 0.20 | 30.00 | 0.00 | ------ | ------ | ------ | 38.64 | 0 | 0 | oxaloacetate + ATP -> phosphoenolpyruvate + ADP | Cytoplasm | Cat8/Gcr1 | 3 | 4 | 5 | ------ | ------ | ------ | ------ |
| YLR377C | FBP1 | 0.720 | ------ | ------ | ------ | 589.00 | ------ | ------ | ------ | 136.6 | 0.000003 | 0.000001 | fructose-1,6-bisphosphate + H20 -> fructose-6-phosphate + phosphate | Cytoplasm | Cat8/Gcr1/Mig1 | 1 | 2 | 3 | ------ | ------ | ------ | ------ |
| YKL029C | MAE1 | 1.000 | ------ | 5.80 | 9.00 | 10500.00 | ------ | ------ | ------ | -1.02 | 0.885261 | 0.885261 | malate + NAD -> pyruvate + NADH | Mitochondria | ------ | 1 | 6 | 7 | ------ | ------ | ------ | ------ |
| **Glyoxylate Cycle** | | | | | | | | | | | | | | | | | | | | | | |
| YCR005C | CIT2 | 0.681 | ------ | ------ | ------ | 2310.00 | ------ | ------ | ------ | 2.2 | 0.010976 | 0.010976 | acetyl CoA + oxaloacetate -> citrate | Peroxisome | ------ | 2 | 2 | 2 | ------ | ------ | ------ | ------ |
| YNL009W | IDP3 | 1.000 | ------ | 0.40 | 22.00 | 0.00 | ------ | ------ | ------ | 1.59 | 0.002887 | 0.002887 | NADP + isocitrate -> α-ketoglutarate + NADPH | Peroxisome / Cytoplasm | Adr1 | 2 | 6 | 10 | ------ | ------ | ------ | ------ |
| YDL078C | MDH3 | 0.990 | ------ | 10.20 | 12.00 | 3300.00 | ------ | ------ | ------ | 1.24 | 0.007518 | 0.004943 | malate + NAD -> oxaloacetate + NADH | Peroxisome | ------ | 1 | 2 | 3 | ------ | ------ | ------ | ------ |
| YER065C | ICL1 | 0.997 | ------ | 0.60 | 13.00 | 0.00 | ------ | ------ | ------ | 13.29 | 0.000994 | 0.000013 | Isocitrate -> glyoxylate + succinate | Gluconeogenesis/Isocitrate Lyase | Cat8/Neg_reg_by_cAMP | 3 | 3 | 3 | ------ | ------ | ------ | ------ |
| YIR031C | DAL7 | ------ | ------ | 0.30 | 28.00 | 0.00 | ------ | ------ | ------ | 7.14 | 0.003218 | 0.000129 | glyoxylate + H2O + Acetyl CoA -> malate + CoA | Nitrogen/Allantoin Degradation | Dal | ------ | ------ | ------ | ------ | ------ | ------ | ------ |
| YNL117W | MLS1 | 0.693 | ------ | ------ | 18.00 | 0.00 | ------ | ------ | ------ | 88.33 | 0.000001 | 0.000001 | glyoxylate + H2O + Acetyl CoA -> malate + CoA | Gluconeogenesis/ Malate Synthase | Cat8/Hap1/Stp1/Stp2 | 3 | 3 | 4 | ------ | ------ | ------ | ------ |
| YFL030W | AGX1 | 0.270 | ------ | ------ | 11.00 | 339.00 | ------ | ------ | ------ | 6.42 | 0.001668 | 0.000285 | glyoxylate+ alanine -> glycine + pyruvate | Gluconeogenesis/ Glyoxylate Aminotransferase | ------ | 1 | 1 | 1 | ------ | ------ | ------ | ------ |
| **Glycerol** | | | | | | | | | | | | | | | | | | | | | | |
| Transport | | | | | | | | | | | | | | | | | | | | | | |
| YDR536W | STL1 | ------ | ------ | ------ | ------ | 0.00 | ------ | ------ | ------ | 5.28 | 0.084704 | 0.0441 | Glycerol in | Plasma Membrane | Cat8 | ------ | ------ | ------ | ------ | ------ | ------ | ------ |
| Metabolism | | | | | | | | | | | | | | | | | | | | | | |
| YOR120W | GCY1 | 0.994 | ------ | 1.20 | 17.00 | 2600.00 | ------ | ------ | ------ | -1.17 | 0.408235 | 0.391604 | NADP coupled glycerol dehydrogenase? | Cytoplasm | ------ | 2 | 2 | 2 | ------ | ------ | ------ | ------ |
| YFL053W | DAK2 | 0.986 | ------ | ------ | 20.00 | 0.00 | ------ | ------ | ------ | -9.74 | 0.00155 | 0.00155 | Carbon / DHA Kinase | Unknown | ------ | 5 | 5 | 5 | ------ | ------ | ------ | ------ |
| YER062C | GPP2 | 0.700 | ------ | 6.40 | 12.00 | 5000.00 | ------ | ------ | ------ | 2.55 | 0.001766 | 0.000915 | dihydrox-yacetone kinase | Cytoplasm | ------ | 1 | 2 | 2 | ------ | ------ | ------ | ------ |
| YIL053W | GPP1 | 1.000 | 1.00 | 84.90 | 11.00 | 193000.00 | GOLD | 0.01 | 0.324430 | -1.1 | 0.04668 | 0.04668 | glycerol-3-phosphate + H2O -> glycerol + phosphate | Cytoplasm | ------ | 5 | 25 | 56 | 2 | 3 | 0.049999997 | 0.02 |
| YHL032C | GUT1 | 1.000 | ------ | 1.10 | 14.00 | 0.00 | ------ | ------ | ------ | 1.68 | 0.00059 | 0.000062 | glycerol + ATP -> glycerol-3-phosphate + ADP | Cytoplasm | Adr1 | 2 | 3 | 4 | ------ | ------ | ------ | ------ |
| YIL155C | GUT2 | ------ | ------ | ------ | ------ | 1670.00 | ------ | ------ | ------ | 2.8 | 0.000063 | 0.000002 | glycerol-3-phosphate + FAD -> dihydroxy-acetone-phosphate + FADH2 | Mitochondrial Inner Membrane Catalytic component faces | Adr1/Neg_reg_by_cAMP | ------ | ------ | ------ | ------ | ------ | ------ | ------ |
| YDL022W | GPD1 | 1.000 | 0.89 | 18.70 | 15.00 | 807.00 | GOLD | 0.11 | 1.204096 | -1.31 | 0.451584 | 0.451584 | dihydrox-yacetone-phosphate + NADH -> glycerol-3-phosphate + NAD | Peroxisome / cytoplasm | ------ | 3 | 8 | 29 | 2 | 5 | 3.129999936 | 2.834999971 |

**Table 5.1.** Continued.

| | | | | | | | | | | Transcriptional Results | | | | | | | | | | | | |
|---|---|---|---|---|---|---|---|---|---|---|---|---|---|---|---|---|---|---|---|---|---|---|
| Orf | Gene | Final Protein Probability (Detected) | Probability of Change | Trans Freq | Halflife | PMC | Category | SD (±) | Final Protein Ratio (grr1 Δ/WT) | fold change | Welch Significance Test (Log2) | TTest Significance Test (Log2) | SGD Annotations | Localization | Transcription Factor | ORF Identification Count | # Unique Peps Identified | Total # Peps Identified | Ratio ORF Count | Combined Ratio # of Peps | Inter-experimental STDEV | Intra-experimental STDEV |
| **Glycerol continued** | | | | | | | | | | | | | | | | | | | | | | |
| Regulation continued | | | | | | | | | | | | | | | | | | | | | | |
| YPL180W | TCO89 | 1.000 | 1.00 | 8.00 | 10.00 | 521.00 | SILVER | 0.30 | 3.200000 | 1 | 0.918405 | 0.918405 | Subunit of TORC1 / involved in glycerol regulation | Vacuolar Membrane / Extrinsic to internal side of Plasma Membrane | ------ | 4 | 12 | 14 | 1 | 4 | 0 | 0.300000012 |
| **Acetate / Acetyl Co-A** | | | | | | | | | | | | | | | | | | | | | | |
| YAL054C | ACS1 | 0.514 | ------ | 0.50 | 24.00 | 2890.00 | ------ | ------ | ------ | 2.63 | 0.000595 | 0.000595 | acetate + CoA + ATP -> acetyl-CoA + pyrophosphate + AMP | Cytoplasm/ Mitochondria | Adr1/Cat8 | 2 | 2 | 2 | ------ | ------ | ------ | ------ |
| YLR153C | ACS2 | 1.000 | 0.95 | 14.70 | 12.00 | 225000.00 | GOLD | 0.05 | 0.830000 | 1.01 | 0.895542 | 0.895542 | acetate + CoA + ATP -> acetyl-CoA + pyrophosphate + AMP | Cytoplasm/ Mitochondria | ------ | 2 | 21 | 31 | 2 | 11 | 0 | 0.325000012 |
| YBL015W | ACH1 | 1.000 | 1.00 | 1.70 | 20.00 | 4890.00 | GOLD | 0.01 | 0.179997 | 4.03 | 0.001928 | 0.000352 | succinyl-CoA + acetate -> succinate + acetyl-CoA | Mitochondria | Cat8 | 5 | 12 | 22 | 2 | 7 | 0.964999951 | 0.410000001 |
| YER073W | ALD5 | 0.392 | ------ | 7.20 | 11.00 | 23300.00 | ------ | ------ | ------ | -1.2 | 0.358304 | 0.320635 | acetaldehyde + NADP -> acetate + NADPH | Mitochondria | ------ | 2 | 2 | 2 | ------ | ------ | ------ | ------ |
| YOR374W | ALD4 | 1.000 | 0.11 | 1.00 | 55.00 | 22200.00 | GOLD | 0.83 | 1.040000 | 5.08 | 0.000057 | 0.000016 | acetaldehyde + NADP or NAD -> acetate + NADPH or NADH | Mitochondria | Adr1 | 5 | 9 | 13 | 1 | 4 | 0 | 0.829999983 |
| YPL061W | ALD6 | 1.000 | 1.00 | 22.10 | 15.00 | 135000.00 | GOLD | 0.14 | 2.330926 | 1.9 | 0.097857 | 0.074989 | acetaldehyde + NADP -> acetate + NADPH | Cytoplasm | Cat8 | 4 | 36 | 67 | 2 | 8 | 0.644999981 | 0.519999988 |
| **Mitochondrial Transporters** | | | | | | | | | | | | | | | | | | | | | | |
| YBL030C | PET9 | 1.000 | 1.00 | 30.70 | 17.00 | 0.00 | GOLD | 0.32 | 4.673166 | 1.37 | 0.000444 | 0.000041 | ATP out / ADP in | Mitochondria Inner Membrane | ------ | 3 | 17 | 49 | 2 | 11 | 2.030000031 | 0.50999999 |
| YJR095W | SFC1 | 0.974 | 0.21 | 0.40 | 12.00 | 0.00 | SILVER | 0.04 | 0.960000 | 297.03 | 0 | 0 | Succinate in / Fumarate out | Mitochondria Inner Membrane | Cat8 | 5 | 5 | 6 | 1 | 2 | 0 | 0.039999999 |
| YPL134C | ODC1 | 0.600 | ------ | 1.70 | 15.00 | 2840.00 | ------ | ------ | ------ | 6.13 | 0.00001 | 0 | alpha-ketoglutarate out of mit. / malate in | Mitochondria Inner Membrane | Cat8 | 1 | 2 | 2 | ------ | ------ | ------ | ------ |
| YLR348C | DIC1 | 0.698 | ------ | 2.80 | 12.00 | 3390.00 | ------ | ------ | ------ | 2.82 | 0.025603 | 0.006085 | malate or succinate in / phosphate out | Mitochondria Inner Membrane | Adr1 | 2 | 2 | 2 | ------ | ------ | ------ | ------ |
| YAR035W | YAT1 | 0.690 | ------ | 0.40 | 25.00 | 0.00 | ------ | ------ | ------ | 4.15 | 0.000037 | 0.000037 | activated acyl groups in | Mitochondria Inner Membrane | Gis1 | 1 | 1 | 2 | ------ | ------ | ------ | ------ |
| YER024W | YAT2 | 0.771 | 1.00 | 1.20 | 17.00 | 319.00 | bronze | 0.11 | 1.810000 | 4.01 | 0.000856 | 0.000107 | activated acyl groups in | Mitochondria Inner Membrane | Cat8 | 3 | 3 | 4 | 1 | 2 | 0 | 0.109999999 |
| YOR100C | CRC1 | 0.982 | ------ | ------ | 20.00 | 0.00 | ------ | ------ | ------ | 6.17 | 0.000008 | 0.000008 | carnitine dependent transport of acetyl co-A from peroxisome to mitochondria | Mitochondria Inner Membrane | Cat8/Oaf/Stp | 3 | 5 | 6 | ------ | ------ | ------ | ------ |
| YCR010C | ADY2 | 0.530 | ------ | ------ | ------ | 0.00 | ------ | ------ | ------ | 10.44 | 0.000007 | 0.000001 | acetate in | Mitochondria Inner Membrane | Cat8/Adr1 | 1 | 1 | 1 | ------ | ------ | ------ | ------ |
| **Respiratory Chain** | | | | | | | | | | | | | | | | | | | | | | |
| F1 F0 ATP synthase | | | | | | | | | | | | | | | | | | | | | | |
| YBL099W | ATP1 | 1.000 | 1.00 | 6.40 | 20.00 | 41500.00 | GOLD | 0.11 | 1.455207 | 1.22 | 0.003164 | 0.001811 | α-subunit of F1-ATP synthase complex | Mitochondria | ------ | 6 | 31 | 65 | 4 | 20 | 0.434770055 | 0.300000008 |
| YJR121W | ATP2 | 1.000 | 0.10 | 9.90 | 16.00 | 164000.00 | GOLD | 0.05 | 0.974876 | 1.52 | 0.000336 | 0.000027 | β-subunit of F1-ATP synthase complex | Mitochondria | ------ | 5 | 51 | 119 | 5 | 30 | 0.466235968 | 0.594000009 |
| YBR039W | ATP3 | 1.000 | 1.00 | 9.00 | 22.00 | 28100.00 | GOLD | 0.03 | 0.800000 | 2.26 | 0.000047 | 0.000013 | γ-subunit of F1-ATP synthase complex | Mitochondria | ------ | 3 | 11 | 13 | 1 | 5 | 1.214422552 | 1.469999999 |
| YPL271W | ATP15 | 1.000 | ------ | 11.20 | 18.00 | 4280.00 | ------ | ------ | ------ | 1.73 | 0.000007 | 0.000007 | ε-subunit of F1-ATP synthase complex | Mitochondria | ------ | 6 | 9 | 23 | ------ | ------ | ------ | ------ |
| YPL078C | ATP4 | 1.000 | 1.00 | 9.40 | 21.00 | 12900.00 | GOLD | 0.02 | 0.674969 | 1.55 | 0.000031 | 0.000008 | subunit b of the stator stalk of the F1F0-ATP synthase complex | Mitochondria | ------ | 6 | 9 | 20 | 2 | 5 | 0.354999989 | 0.049999999 |
| YDR298C | ATP5 | 1.000 | 1.00 | 7.90 | 24.00 | 32400.00 | GOLD | 0.02 | 0.460000 | 1.83 | 0.000363 | 0.00003 | subunit 5 of the stator stalk of the F1F0-ATP synthase complex | Mitochondria | ------ | 5 | 12 | 20 | 1 | 4 | 0 | 0.02 |
| YKL016C | ATP7 | 1.000 | 0.24 | 6.70 | 16.00 | 6820.00 | GOLD | 0.07 | 0.922004 | 1.91 | 0.000044 | 0.000011 | subunit d of the stator stalk of the F1F0-ATP synthase complex | Mitochondria | ------ | 4 | 6 | 8 | 3 | 3 | 1.012356968 | 0.466666671 |
| YDL004W | ATP16 | 1.000 | 0.11 | 11.90 | 17.00 | 0.00 | GOLD | 0.63 | 0.410000 | 1.75 | 0.000644 | 0.000006 | δ-subunit of the central stalk of the F1F0-ATP synthase complex | Mitochondria | ------ | 2 | 6 | 15 | 1 | 3 | 0 | 0.629999995 |
| YLR295C | ATP14 | 1.000 | ------ | 10.60 | 16.00 | 6140.00 | ------ | ------ | ------ | 2.12 | 0.001287 | 0.000022 | subunit h of the F0-ATP synthase complex | Mitochondria | ------ | 4 | 4 | 6 | ------ | ------ | ------ | ------ |
| YDR377W | ATP17 | 0.770 | ------ | 6.90 | 19.00 | 14600.00 | ------ | ------ | ------ | 2.24 | 0.000007 | 0.000007 | subunit f of the F0-ATP synthase complex | Mitochondria | ------ | 1 | 2 | 2 | ------ | ------ | ------ | ------ |
| YML081C-A | ATP18 | ------ | ------ | ------ | ------ | 6540.00 | ------ | ------ | ------ | 1.91 | 0.001454 | 0.000729 | subunit i/j of the F1F0-ATP synthase complex | Mitochondria | ------ | ------ | ------ | ------ | ------ | ------ | ------ | ------ |
| YOL077W-A | ATP19 | 1.000 | 1.00 | ------ | ------ | 1320.00 | GOLD* | 0.0300 | 0.4000 | 2.5 | 0.00048 | 0.000197 | subunit k of the F1F0-ATP synthase complex | Mitochondria | ------ | 2 | 2 | 7 | 1 | 1 | 0 | 0.029999999 |
| YPR020W | ATP20 | ------ | ------ | 3.30 | 18.00 | 0.00 | ------ | ------ | ------ | 2.12 | 0.000227 | 0.000227 | subunit g of the F1F0-ATP synthase complex | Mitochondria | ------ | ------ | ------ | ------ | ------ | ------ | ------ | ------ |
| YDR322C-A | ATP21 | ------ | ------ | ------ | ------ | 4590.00 | ------ | ------ | ------ | 2.05 | 0.000033 | 0.000008 | Subunit e of mitochondrial F1F0-ATPase complex | Mitochondria | ------ | ------ | ------ | ------ | ------ | ------ | ------ | ------ |

**Table 5.1.** Continued.

| Orf | Gene | Final Protein Probability (Detected) | Probability of Change | Trans Freq | Halflife | PMC | Category | SD (±) | Final Protein Ratio (*arrt* Δ/WT) | Transcriptional Results: fold change | Welch Significance Test (Log2) | TTest Significance Test (Log2) | SGD Annotations | Localization | Transcription Factor | ORF Identification Count | # Unique Peps Identified | Total # Peps Identified | Ratio ORF Count | Combined Ratio # of Peps | Inter-experimental STDEV | Intra-experimental STDEV |
|---|---|---|---|---|---|---|---|---|---|---|---|---|---|---|---|---|---|---|---|---|---|---|
| **Respiratory Chain continued** | | | | | | | | | | | | | | | | | | | | | | |
| **Regulation of F1 F0 ATP synthase continued** | | | | | | | | | | | | | | | | | | | | | | |
| YDL130W-A | STF1 | ------ | ------ | ------ | ------ | 0.00 | ------ | ------ | ------ | 2.57 | 0.000957 | 0.000957 | neg regulation of mitochondrial F1F0-ATPase complex | Mitochondria | | ------ | ------ | ------ | ------ | ------ | ------ | ------ |
| YDL181W | INH1 | 0.560 | ------ | 4.50 | 10.00 | 981.00 | ------ | ------ | ------ | 11.04 | 0.000001 | 0.000001 | neg regulation of mitochondrial F1F0-ATPase complex | Mitochondria | Hap2 | 1 | 1 | 1 | ------ | ------ | ------ | ------ |
| YGR008C | STF2 | 1.000 | ------ | 7.60 | 29.00 | 5330.00 | ------ | ------ | ------ | 1.19 | 0.62045 | 0.62045 | neg regulation of mitochondrial F1F0-ATPase complex | Mitochondria | | 2 | 2 | 10 | ------ | ------ | ------ | ------ |
| **Ubiquinol-cytochrome c reductase complex** | | | | | | | | | | | | | | | | | | | | | | |
| YBL045C | COR1 | 1.000 | 0.99 | 3.80 | 27.00 | 19300.00 | GOLD | 0.04 | 1.108430 | 2.34 | 0.000721 | 0.000084 | core subunit of the ubiquinol-cytochrome c reductase complex (bc1 complex) | Mitochondria | ------ | 6 | 15 | 40 | 3 | 9 | ------ | ------ |
| YPR191W | QCR2 | 1.000 | 0.10 | 2.60 | 26.00 | 35700.00 | GOLD | 0.59 | 0.540000 | 2.35 | 0.000001 | 0.000001 | subunit 2 of the ubiquinol cytochrome-c reductase complex | Mitochondria | ------ | 5 | 17 | 25 | 1 | 8 | ------ | ------ |
| YHR001W-A | QCR10 | 1.000 | ------ | 2.80 | 15.00 | 5590.00 | ------ | ------ | ------ | 3.6 | 0.000047 | 0.000012 | subunit of the ubiqunol-cytochrome c oxidoreductase complex | Mitochondria | ------ | 2 | 3 | 4 | ------ | ------ | ------ | ------ |
| YFR033C | QCR6 | ------ | ------ | 17.30 | 12.00 | 4490.00 | ------ | ------ | ------ | 3 | 0.000009 | 0.000009 | subunit 6 of the ubiquinol cytochrome-c reductase complex | Mitochondria | ------ | ------ | ------ | ------ | ------ | ------ | ------ | ------ |
| YGR183C | QCR9 | ------ | ------ | 8.40 | 25.00 | 4550.00 | ------ | ------ | ------ | 1.84 | 0.000089 | 0.000027 | subunit 9 of the ubiquinol cytochrome-c reductase complex | Mitochondria | ------ | ------ | ------ | ------ | ------ | ------ | ------ | ------ |
| YJL166W | QCR8 | ------ | ------ | 10.00 | 21.00 | 6140.00 | ------ | ------ | ------ | 1.43 | 0.001416 | 0.000706 | subunit 8 of ubiquinol cytochrome-c reductase complex | Mitochondria | ------ | ------ | ------ | ------ | ------ | ------ | ------ | ------ |
| YDR529C | QCR7 | 1.000 | ------ | 0.70 | 16.00 | 1770.00 | ------ | ------ | ------ | 1.61 | 0.000031 | 0.000031 | reductase complex | Mitochondria | ------ | 4 | 6 | 9 | ------ | ------ | ------ | ------ |
| YOR065W | CYT1 | ------ | ------ | ------ | ------ | 39900.00 | ------ | ------ | ------ | 4.11 | 0.000015 | 0.000003 | Cytochrome c1 | Mitochondria | ------ | ------ | ------ | ------ | ------ | ------ | ------ | ------ |
| YEL024W | RIP1 | 1.000 | ------ | 4.40 | 15.00 | 0.00 | ------ | ------ | ------ | 3.54 | 0.000477 | 0.000045 | ubiquinol-cytochrome-c reductase | Mitochondria | ------ | 1 | 3 | 4 | ------ | ------ | ------ | ------ |
| **Cytochrome c oxidase complex** | | | | | | | | | | | | | | | | | | | | | | |
| YJR048W | CYC1 | 1.000 | 0.27 | 10.00 | 10.00 | 7330.00 | GOLD | 1.22 | 1.520000 | 3.09 | 0.006496 | 0.000494 | Cytochrome c isoform 1; electron carrier | Mitochondria | ------ | 1 | 2 | 5 | 1 | 1 | ------ | ------ |
| YGL187C | COX4 | 1.000 | 1.00 | 10.70 | 17.00 | 9410.00 | GOLD | 0.08 | 1.597910 | 2.51 | 0.000015 | 0.000003 | subunit 4 of cytochrome c oxidase | Mitochondria | ------ | 4 | 13 | 25 | 3 | 6 | ------ | ------ |
| YNL052W | COX5A | 0.998 | ------ | 3.60 | 12.00 | 0.00 | ------ | ------ | ------ | 1.75 | 0.00106 | 0.000502 | subunit 5a of cytochrome c oxidase | Mitochondria | ------ | 4 | 4 | 4 | ------ | ------ | ------ | ------ |
| YIL111W | COX5B | 0.592 | ------ | 2.60 | 18.00 | 2250.00 | ------ | ------ | ------ | -1.43 | 0.289236 | 0.280791 | subunit 5b of cytochrome c oxidase | Mitochondria | ------ | 2 | 2 | 2 | ------ | ------ | ------ | ------ |
| YHR051W | COX6 | 1.000 | 1.00 | 7.40 | 20.00 | 12500.00 | GOLD | 0.03 | 0.876216 | 2 | 0.00402 | 0.000198 | subunit 6 of cytochrome c oxidase | Mitochondria | ------ | 2 | 3 | 7 | 2 | 3 | ------ | ------ |
| YGL191W | COX13 | 0.810 | ------ | 3.10 | 27.00 | 0.00 | ------ | ------ | ------ | 2.08 | 0.000134 | 0.000007 | subunit 6a of cytochrome c oxidase | Mitochondria | ------ | 1 | 2 | 2 | ------ | ------ | ------ | ------ |
| YLR038C | COX12 | ------ | ------ | 13.80 | 16.00 | 1390.00 | ------ | ------ | ------ | 2.08 | 0.000001 | 0.000001 | subunit 6b of cytochrome c oxidase | Mitochondria | ------ | ------ | ------ | ------ | ------ | ------ | ------ | ------ |
| YMR256C | COX7 | ------ | ------ | 0.90 | 22.00 | 2730.00 | ------ | ------ | ------ | 2.45 | 0.005542 | 0.000366 | subunit 7 of cytochrome c oxidase | Mitochondria | ------ | ------ | ------ | ------ | ------ | ------ | ------ | ------ |
| YDL067C | COX9 | ------ | ------ | 10.70 | 17.00 | 35500.00 | ------ | ------ | ------ | 1.78 | 0.001567 | 0.000796 | subunit 7a of cytochrome c oxidase | Mitochondria | ------ | ------ | ------ | ------ | ------ | ------ | ------ | ------ |
| YLR395C | COX8 | 0.390 | ------ | 13.90 | 14.00 | 672.00 | ------ | ------ | ------ | 1.63 | 0.000235 | 0.000235 | subunit 8 of cytochrome c oxidase | Mitochondria | ------ | 1 | 1 | 2 | ------ | ------ | ------ | ------ |
| YGR062C | COX18 | 0.440 | 1.00 | 1.90 | 11.00 | 468.00 | bronze | 0.46 | 5.740000 | 1.11 | 0.092545 | 0.083207 | required for membrane insertion of C-terminus of Cox2p | Mitochondria | ------ | 1 | 1 | 1 | 1 | 1 | 0 | 0.460000008 |
| **NADH:ubiquinone oxidoreductase** | | | | | | | | | | | | | | | | | | | | | | |
| YML120C | NDI1 | 0.808 | 1.00 | ------ | ------ | 5240.00 | GOLD | 0.02 | 0.350000 | 3.76 | 0.013977 | 0.005848 | NADH:ubiquinone oxidoreductase | Mitochondria | ------ | 2 | 3 | 5 | 1 | 4 | 0 | 0.02 |
| YDL085W | NDE2 | ------ | ------ | ------ | 19.00 | 0.00 | ------ | ------ | ------ | 3.22 | 0.00481 | 0.000279 | NADH:ubiquinone oxidoreductase | Inner Membrane Catalytic | ------ | ------ | ------ | ------ | ------ | ------ | ------ | ------ |
| YMR145C | NDE1 | 1.000 | 1.00 | 12.80 | 18.00 | 4930.00 | GOLD | 0.12 | 2.468439 | 1.46 | 0.004237 | 0.002544 | NADH:ubiquinone oxidoreductase | Mitochondrial Inner Membrane Catalytic component faces intermembrane space | ------ | 5 | 13 | 17 | 2 | 2 | 2.2299999 | 0.215000007 |
| **Serine/Glycine** | | | | | | | | | | | | | | | | | | | | | | |
| YER081W | SER3 | 1.000 | 0.10 | ------ | ------ | 7670.00 | GOLD | 0.46 | 0.120000 | 1.57 | 0.014122 | 0.005931 | 3-phosphoglycerate + NAD -> 3-phospho-hydroxypyruvate + NADH | Cytoplasm | ------ | 2 | 3 | 4 | 1 | 2 | 0 | 0.460000008 |
| YIL074C | SER33 | 1.000 | 0.11 | 3.10 | 14.00 | 2010.00 | GOLD | 0.26 | 0.820000 | -1.36 | 0.002055 | 0.002055 | 3-phosphoglycerate + NAD -> 3-phospho-hydroxypyruvate + NADH | Cytoplasm | ------ | 2 | 10 | 19 | 1 | 5 | 0 | 0.25999999 |
| YOR184W | SER1 | 1.000 | 1.00 | 12.10 | 13.00 | 15900.00 | GOLD | 0.05 | 1.140277 | -1.29 | 0.033492 | 0.009696 | 3-phospho-hydroxypyruvate + glutamate -> 2-oxoglutarate + 3-phospho-serine | Cytoplasm | ------ | 4 | 14 | 22 | 2 | 7 | 0.270000011 | 0.070000002 |
| YGR208W | SER2 | ------ | ------ | 4.10 | 21.00 | 13800.00 | ------ | ------ | ------ | -1.49 | 0.003887 | 0.003887 | 3-phospho-serine + H2O -> serine + phosphate | Cytoplasm | ------ | ------ | ------ | ------ | ------ | ------ | ------ | ------ |
| YBR263W | SHM1 | 1.000 | 1.00 | 6.60 | 17.00 | 17700.00 | GOLD | 0.01 | 0.150000 | -1.01 | 0.482349 | 0.454371 | serine + THF <-> glycine + 5,10-methylene-THF | Mitochondria | ------ | 3 | 7 | 9 | 1 | 5 | 0 | 0.01 |
| YLR058C | SHM2 | 1.000 | 0.96 | 46.00 | 12.00 | 67600.00 | GOLD | 0.08 | 1.180368 | -1.07 | 0.013886 | 0.009995 | serine + THF <-> glycine + 5,10-methylene-THF | Cytoplasm | ------ | 6 | 80 | 181 | 4 | 24 | 0.3043333 | 0.244999995 |

**Table 5.1.** Continued.

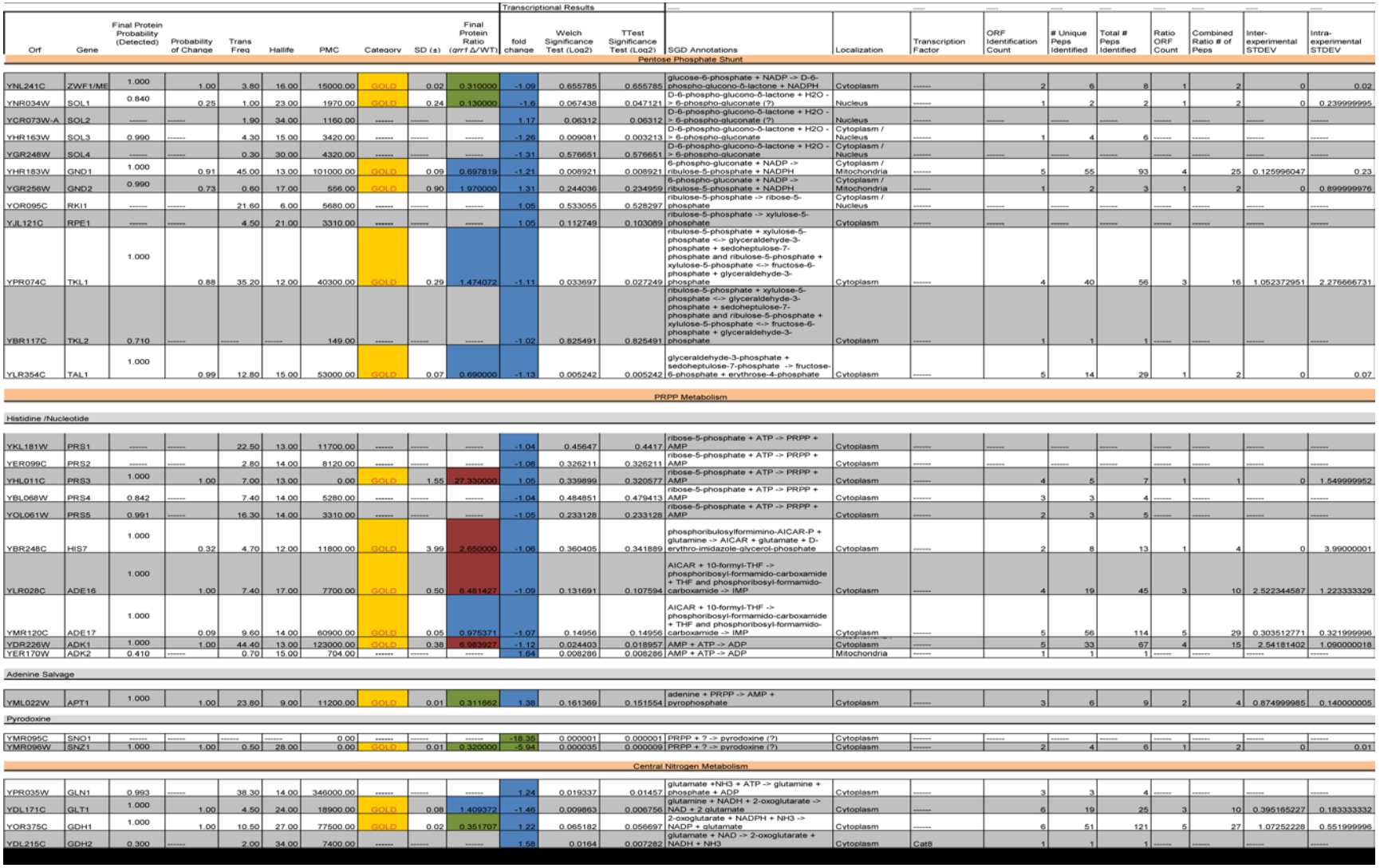

| | | | | | | | | | | Transcriptional Results | | | | | | | | | | | |
|---|---|---|---|---|---|---|---|---|---|---|---|---|---|---|---|---|---|---|---|---|---|
| Orf | Gene | Final Protein Probability (Detected) | Probability of Change | Trans Freq | Halflife | PMC | Category | SD (±) | Final Protein Ratio (grr1 Δ/WT) | fold change | Welch Significance Test (Log2) | TTest Significance Test (Log2) | SGD Annotations | Localization | Transcription Factor | ORF Identification Count | # Unique Peps Identified | Total # Peps Identified | Ratio ORF Count | Combined Ratio # of Peps | Inter-experimental STDEV | Intra-experimental STDEV |
| **Pentose Phosphate Shunt** | | | | | | | | | | | | | | | | | | | | | | |
| YNL241C | ZWF1/ME | 1.000 | 1.00 | 3.80 | 16.00 | 15000.00 | GOLD | 0.02 | 0.310000 | -1.09 | 0.655785 | 0.655785 | glucose-6-phosphate + NADP -> D-6-phospho-glucono-δ-lactone + NADPH | Cytoplasm | ------ | 2 | 6 | 8 | 1 | 2 | 0 | 0.02 |
| YNR034W | SOL1 | 0.840 | 0.25 | 1.00 | 23.00 | 1970.00 | GOLD | 0.24 | 0.130000 | -1.6 | 0.067438 | 0.047121 | D-6-phospho-glucono-δ-lactone + H2O -> 6-phospho-gluconate (?) | Nucleus | ------ | 1 | 2 | 2 | 1 | 2 | 0 | 0.239999995 |
| YCR073W-A | SOL2 | ------ | ------ | 1.90 | 34.00 | 1160.00 | ------ | ------ | ------ | 1.17 | 0.06312 | 0.06312 | D-6-phospho-glucono-δ-lactone + H2O -> 6-phospho-gluconate (?) | Nucleus | ------ | ------ | ------ | ------ | ------ | ------ | ------ | ------ |
| YHR163W | SOL3 | 0.990 | ------ | 4.30 | 15.00 | 3420.00 | ------ | ------ | ------ | -1.26 | 0.009081 | 0.003213 | D-6-phospho-glucono-δ-lactone + H2O -> 6-phospho-gluconate | Cytoplasm / Nucleus | ------ | 1 | 4 | 6 | ------ | ------ | ------ | ------ |
| YGR248W | SOL4 | ------ | ------ | 0.30 | 30.00 | 4320.00 | ------ | ------ | ------ | -1.31 | 0.576651 | 0.576651 | D-6-phospho-glucono-δ-lactone + H2O -> 6-phospho-gluconate | Cytoplasm / Nucleus | ------ | ------ | ------ | ------ | ------ | ------ | ------ | ------ |
| YHR183W | GND1 | 1.000 | 0.91 | 45.00 | 13.00 | 101000.00 | GOLD | 0.09 | 0.697819 | -1.21 | 0.008921 | 0.008921 | 6-phospho-gluconate + NADP -> ribulose-5-phosphate + NADPH | Cytoplasm / Mitochondria | ------ | 5 | 55 | 93 | 4 | 25 | 0.125996047 | 0.23 |
| YGR256W | GND2 | 0.990 | 0.73 | 0.60 | 17.00 | 556.00 | GOLD | 0.90 | 1.970000 | 1.31 | 0.244036 | 0.234959 | 6-phospho-gluconate + NADP -> ribulose-5-phosphate + NADPH | Cytoplasm / Mitochondria | ------ | 1 | 2 | 3 | 1 | 2 | 0 | 0.899999976 |
| YOR095C | RKI1 | ------ | ------ | 21.60 | 6.00 | 5680.00 | ------ | ------ | ------ | 1.05 | 0.533055 | 0.528297 | ribulose-5-phosphate -> ribose-5-phosphate | Cytoplasm / Nucleus | ------ | ------ | ------ | ------ | ------ | ------ | ------ | ------ |
| YJL121C | RPE1 | ------ | ------ | 4.50 | 21.00 | 3310.00 | ------ | ------ | ------ | 1.05 | 0.112749 | 0.103089 | ribulose-5-phosphate -> xylulose-5-phosphate | Cytoplasm | ------ | ------ | ------ | ------ | ------ | ------ | ------ | ------ |
| YPR074C | TKL1 | 1.000 | 0.88 | 35.20 | 12.00 | 40300.00 | GOLD | 0.29 | 1.474072 | -1.11 | 0.033697 | 0.027249 | ribulose-5-phosphate + xylulose-5-phosphate <-> glyceraldehyde-3-phosphate + sedoheptulose-7-phosphate and ribulose-5-phosphate + xylulose-5-phosphate <-> fructose-6-phosphate + glyceraldehyde-3-phosphate | Cytoplasm | ------ | 4 | 40 | 56 | 3 | 16 | 1.052372951 | 2.276666731 |
| YBR117C | TKL2 | 0.710 | ------ | ------ | ------ | 149.00 | ------ | ------ | ------ | -1.02 | 0.825491 | 0.825491 | ribulose-5-phosphate + xylulose-5-phosphate <-> glyceraldehyde-3-phosphate + sedoheptulose-7-phosphate and ribulose-5-phosphate + xylulose-5-phosphate <-> fructose-6-phosphate + glyceraldehyde-3-phosphate | Cytoplasm | ------ | 1 | 1 | 1 | ------ | ------ | ------ | ------ |
| YLR354C | TAL1 | 1.000 | 0.99 | 12.80 | 15.00 | 53000.00 | GOLD | 0.07 | 0.690000 | -1.13 | 0.005242 | 0.005242 | glyceraldehyde-3-phosphate + sedoheptulose-7-phosphate -> fructose-6-phosphate + erythrose-4-phosphate | Cytoplasm | ------ | 5 | 14 | 29 | 1 | 2 | 0 | 0.07 |
| **PRPP Metabolism** | | | | | | | | | | | | | | | | | | | | | | |
| Histidine /Nucleotide | | | | | | | | | | | | | | | | | | | | | | |
| YKL181W | PRS1 | ------ | ------ | 22.50 | 13.00 | 11700.00 | ------ | ------ | ------ | -1.04 | 0.45647 | 0.4417 | ribose-5-phosphate + ATP -> PRPP + AMP | Cytoplasm | ------ | ------ | ------ | ------ | ------ | ------ | ------ | ------ |
| YER099C | PRS2 | ------ | ------ | 2.80 | 14.00 | 8120.00 | ------ | ------ | ------ | -1.08 | 0.326211 | 0.326211 | ribose-5-phosphate + ATP -> PRPP + AMP | Cytoplasm | ------ | ------ | ------ | ------ | ------ | ------ | ------ | ------ |
| YHL011C | PRS3 | 1.000 | 1.00 | 7.00 | 13.00 | 0.00 | GOLD | 1.55 | 27.330000 | 1.05 | 0.339899 | 0.320577 | ribose-5-phosphate + ATP -> PRPP + AMP | Cytoplasm | ------ | 4 | 5 | 7 | 1 | 1 | 0 | 1.549999952 |
| YBL068W | PRS4 | 0.842 | ------ | 7.40 | 14.00 | 5280.00 | ------ | ------ | ------ | -1.04 | 0.484851 | 0.479413 | ribose-5-phosphate + ATP -> PRPP + AMP | Cytoplasm | ------ | 3 | 3 | 4 | ------ | ------ | ------ | ------ |
| YOL061W | PRS5 | 0.991 | ------ | 16.30 | 14.00 | 3310.00 | ------ | ------ | ------ | -1.05 | 0.233128 | 0.233128 | ribose-5-phosphate + ATP -> PRPP + AMP | Cytoplasm | ------ | 2 | 3 | 5 | ------ | ------ | ------ | ------ |
| YBR248C | HIS7 | 1.000 | 0.32 | 4.70 | 12.00 | 11800.00 | GOLD | 3.99 | 2.650000 | -1.06 | 0.360405 | 0.341889 | phosphoribulosylformimino-AICAR-P + glutamine -> AICAR + glutamate + D-erythro-imidazole-glycerol-phosphate | Cytoplasm | ------ | 2 | 8 | 13 | 1 | 4 | 0 | 3.99000001 |
| YLR028C | ADE16 | 1.000 | 1.00 | 7.40 | 17.00 | 7700.00 | GOLD | 0.50 | 6.481427 | -1.09 | 0.131691 | 0.107594 | AICAR + 10-formyl-THF -> phosphoribosyl-formamido-carboxamide + THF and phosphoribosyl-formamido-carboxamide -> IMP | Cytoplasm | ------ | 4 | 19 | 45 | 3 | 10 | 2.522344587 | 1.223333329 |
| YMR120C | ADE17 | 1.000 | 0.09 | 9.60 | 14.00 | 60900.00 | GOLD | 0.05 | 0.975371 | -1.07 | 0.14956 | 0.14956 | AICAR + 10-formyl-THF -> phosphoribosyl-formamido-carboxamide + THF and phosphoribosyl-formamido-carboxamide -> IMP | Cytoplasm | ------ | 5 | 56 | 114 | 5 | 29 | 0.303512771 | 0.321999996 |
| YDR226W | ADK1 | 1.000 | 1.00 | 44.40 | 13.00 | 123000.00 | GOLD | 0.38 | 6.583927 | -1.12 | 0.024403 | 0.018957 | AMP + ATP -> ADP | Cytoplasm | ------ | 5 | 33 | 67 | 4 | 15 | 2.54181402 | 1.090000018 |
| YER170W | ADK2 | 0.410 | ------ | 0.70 | 15.00 | 704.00 | ------ | ------ | ------ | 1.04 | 0.008286 | 0.008286 | AMP + ATP -> ADP | Mitochondria | ------ | 1 | 1 | 1 | ------ | ------ | ------ | ------ |
| Adenine Salvage | | | | | | | | | | | | | | | | | | | | | | |
| YML022W | APT1 | 1.000 | 1.00 | 23.80 | 9.00 | 11200.00 | GOLD | 0.01 | 0.311662 | 1.38 | 0.161369 | 0.151554 | adenine + PRPP -> AMP + pyrophosphate | Cytoplasm | ------ | 3 | 6 | 9 | 2 | 4 | 0.874999985 | 0.140000005 |
| Pyrodoxine | | | | | | | | | | | | | | | | | | | | | | |
| YMR095C | SNO1 | ------ | ------ | ------ | ------ | 0.00 | ------ | ------ | ------ | -18.35 | 0.000001 | 0.000001 | PRPP + ? -> pyrodoxine (?) | Cytoplasm | ------ | ------ | ------ | ------ | ------ | ------ | ------ | ------ |
| YMR096W | SNZ1 | 1.000 | 1.00 | 0.50 | 28.00 | 0.00 | GOLD | 0.01 | 0.320000 | -5.94 | 0.000035 | 0.000009 | PRPP + ? -> pyrodoxine (?) | Cytoplasm | ------ | 2 | 4 | 6 | 1 | 2 | 0 | 0.01 |
| **Central Nitrogen Metabolism** | | | | | | | | | | | | | | | | | | | | | | |
| YPR035W | GLN1 | 0.993 | ------ | 38.30 | 14.00 | 346000.00 | ------ | ------ | ------ | 1.24 | 0.019337 | 0.01457 | glutamate +NH3 + ATP -> glutamine + phosphate + ADP | Cytoplasm | ------ | 3 | 3 | 4 | ------ | ------ | ------ | ------ |
| YDL171C | GLT1 | 1.000 | 1.00 | 4.50 | 24.00 | 18900.00 | GOLD | 0.08 | 1.409372 | -1.46 | 0.009863 | 0.006756 | glutamine + NADH + 2-oxoglutarate -> NAD + 2 glutamate | Cytoplasm | ------ | 6 | 19 | 25 | 3 | 10 | 0.395165227 | 0.183333332 |
| YOR375C | GDH1 | 1.000 | 1.00 | 10.50 | 27.00 | 77500.00 | GOLD | 0.02 | 0.351707 | 1.22 | 0.065182 | 0.056697 | 2-oxoglutarate + NADPH + NH3 -> NADP + glutamate | Cytoplasm | ------ | 6 | 51 | 121 | 5 | 27 | 1.07252228 | 0.551999996 |
| YDL215C | GDH2 | 0.300 | ------ | 2.00 | 34.00 | 7400.00 | ------ | ------ | ------ | 1.58 | 0.0164 | 0.007282 | glutamate + NAD -> 2-oxoglutarate + NADH + NH3 | Cytoplasm | Cat8 | 1 | 1 | 1 | ------ | ------ | ------ | ------ |



**Table 5.1.** Continued.

**Table 5.1. Gene and Protein Expression Levels in *grr1Δ* Cells for Select Loci of Central Metabolism.** Protein and gene expression data for loci of central carbon and energy metabolism from the comparative analysis of wild-type and *grr1Δ* cells is captured in this table. Fields are as described in Tables 4.2 and 4.3.

expression by ~9fold in *grr1Δ* strains. Taken together, this further suggests that respiratory capacity may be decreased in strains lacking Grr1 function. Interestingly, the degree to which many of the mitochondrial import proteins decrease in protein expression (-2.78, -2.56, -2.78, -2.56, -4.55 for Por1, Hsp60, Phb1, Mia40, and Tim15, respectively) correlate well with the degree to which increases in gene expression for many of the TCA cycle and respiratory genes changed (+2.4 average increase).

In order to empirically assess the respiratory competence of *grr1Δ* cells we performed spot dilution assays comparing wild-type and *grr1Δ* cells of the S288C and the CenPK genetic backgrounds on ethanol medium. The S288C background possesses known respiratory defects [454] and thus we included wild-type and *grr1Δ* cells of the CenPK background, which does not possess these defects, in our spot dilution analysis. Cells for each strain were grown on YPD to mid log phase and then spotted onto SD-3% ethanol plates at cell counts of 60,000, 6,000, 600, and 60 and incubated at 32°C for 40hrs. As can be seen in Figure 5.3, both the wild-type and *grr1Δ* strains of the CenPK background, as predicted, grew much more robustly on ethanol medium than the respective strains of the S288C background. Little growth was observed for *grr1Δ* (S288C), confirming that respiratory growth on ethanol is indeed compromised. Additionally, though growth was far more robust for *grr1Δ* strains of the CenPK background on ethanol, slower growth was observed for this strain compared to the isogenic wild-type strain. These data further suggest that, though the respiratory deficiencies of the S288C background exacerbate the growth defect of *grr1Δ* strains, they cannot completely account for all of the growth deficiencies of *grr1Δ* strains on ethanol based medium. The discordance between gene and protein expression on glucose medium as well as the growth defects of *grr1Δ* cells on ethanol together provide compelling evidence for a reduced respiratory capacity inherent in *grr1Δ* cells.

### 5.4. Glycerol Metabolism in grr1Δ Cells

As indicated previously, ethanol production is not affected during fermentations with *grr1Δ* cells, however, the production of glycerol has been measured to be significantly decreased during fermentive growth of these strains. In this same experiment glycerol-3-phosphate was identified as a "reporter metabolite" based on a genome scale metabolic model [67]. Additionally, metabolic flux during the conversion of glycerol-3-phosphate to glycerol has been found to be reduced in *grr1Δ* cells [174]. Concurrent with these data, we were able to detect significant increases and decreases among genes and proteins required for glycerol metabolism. The transcriptional and post-transcriptional regulation of glycerol metabolic enzymes measured in our genomic and proteomic analysis correlate well with the previously measured changes in metabolic flux through this pathway in *grr1Δ* cells. Together these data suggest that this pathway is regulated to increase NADH oxidation via the glycerol-3-phosphate shuttle. The first step in glycerol biosynthesis is catalyzed by two isoforms of NAD-dependent glycerol-3-phosphate dehydrogenase, known as Gpd1 and Gpd2 [455]. Together these two enzymes catalyze the rate limiting step of glycerol biosynthesis, glycerol phospholipid biosynthesis, and the glycerol-3-phosphate shuttle (NADH oxidation to NAD) which entails the conversion of the glycolytic intermediate dihydroxy-acetone-phosphate to glycerol-3-phosphate accompanied by the re-oxidation of excess NADH to NAD. Interestingly, Gpd1 has been shown to play a major role in osmoadaptation [456,457] and we measured no significant changes in either the protein or its encoding gene. On the other hand, Gpd2, whose proteins levels were measured to significantly increase in *grr1Δ* cells by ~3 fold, plays a different physiological role as its production is stimulated by anoxia or excess NADH [456]. The increase in Gpd2 protein expression suggests that the production of glycerol-3-phosphate is increased in *grr1Δ* cells in order to enhance oxidation of NADH to NAD.

Glycerol-3-phosphate can be further metabolized to produce either glycerol for osmoadaptation, to produce phospholipids, or oxidized back to dihydroxy-acetone-phosphate by the glycerol-3-phosphate dehydrogenase, Gut2,

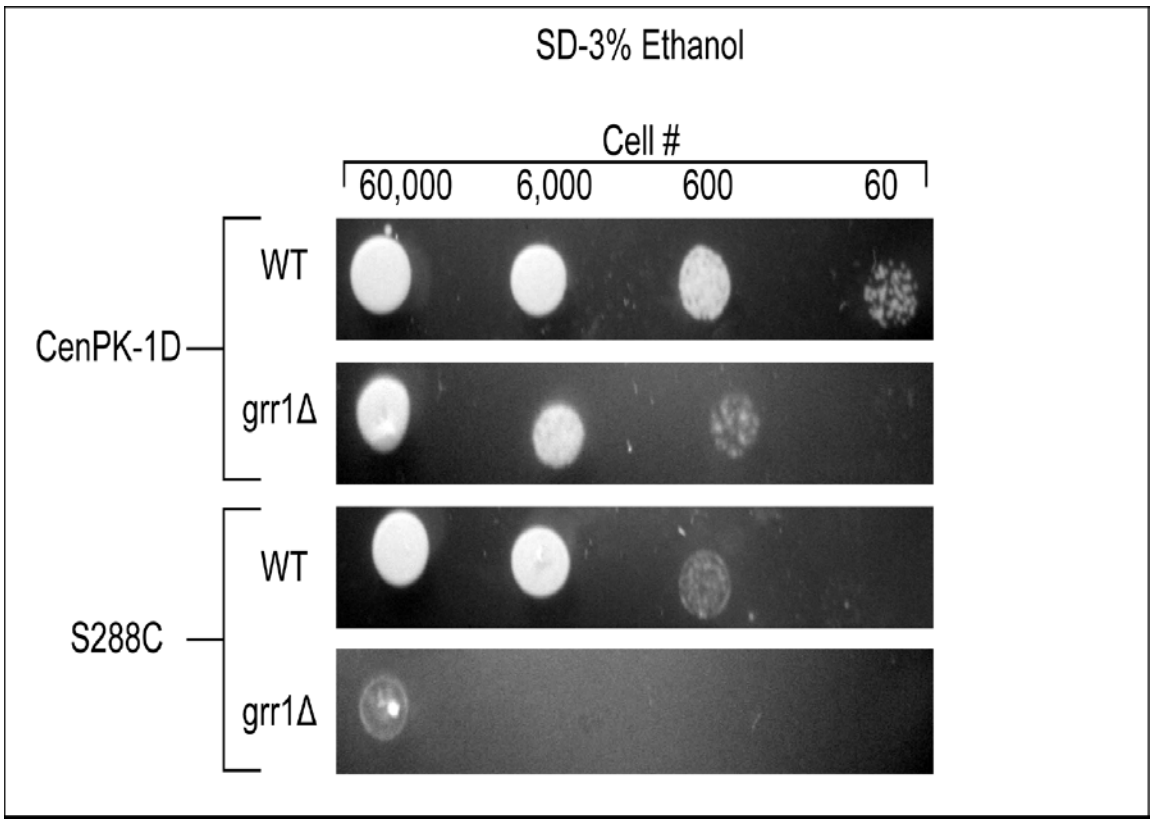


**Figure 5.3. Respiratory Deficiency in *grr1Δ* Cells.** Due to conflicting reports, we determined the respiratory competence of *grr1Δ* cells of the CenPK genetic background and the S288C genetic background. Wild-type and *grr1Δ* CenPK and wild-type and grr1Δ S288C strains were spot diluted onto synthetic defined medium containing 3% ethanol as the carbon source and incubated at 32° C . At 40 hours pictures were taken using a Canon EOS digital SLR camera. The S288C background contains a ty1 insertion in the gene encoding the respiratory transcription factor HAP1 [454] and thus differences in strain background could explain the respiratory deficient phenotype of grr1Δ cells reported by some labs [68] . While the S288C strains did exhibit decreased respiratory growth on ethanol media compared to the CenPK strains, the grr1Δ strains exhibited deficient respiratory growth in both strain backgrounds compared to the isogenic wild-type strains. Thus, GRR1 deletion does confer a respiratory deficiency to both strain backgrounds.

which couples glycerol-3-phosphate oxidation to the electron transport chain and along with Gpd1 and Gpd2 comprises the glycerol-3-phosphate shuttle [453,456,458]. A number of observations suggest that glycerol metabolism may be regulated in *grr1Δ* strains to increase flux through the latter pathway. Both glycerol production and flux from glycerol-3-phosphate to glycerol have been measured to decrease in *grr1Δ* strains by approximately 2.4 fold [67] and 4.6 fold [174], respectively. Together our proteomic and genomic data suggest a possible mechanism for this decreased flux. Glycerol-3-phosphate is metabolized to glycerol by two isoforms of glycerol-3-phosphatase, Gpp1 and Gpp2. We measured a significant increase in *GPP2* expression (+2.55 fold), however Gpp1 has been shown to be the major isoform contributing to greater than 70% of glycerol-3-phosphatase activity in this *S. cerevisiae* and deletion of *GPP1* leads to significant increases in glycerol-3-phosphate accordingly [459]. Interestingly, we measured no significant change in *GPP1* expression in *grr1Δ* cells compared to wild-type, yet Gpp1 protein expression decreased to the same extent that Gpd2 protein expression increased; approximately 3 fold. These measurements are strikingly similar to the fold decreases in glycerol output and flux between glycerol-3-phosphate and glycerol suggesting that the glycerol pathway has been modulated in *grr1Δ* cells at the post-transcriptional level to increase glycerol-3-phosphate concentration. Finally, we measured a significant ~3 fold increase in *GUT2* expression as well, but failed to measure its product expression level. This is not surprising given the fact that it is an integral mitochondrial inner membrane protein and our proteomic analysis was slightly biased against the detection of membrane proteins. Nevertheless, based off of the measurements acquired for the other glycerol pathway enzymes it is highly likely that Gut2 protein expression is indeed increased in *grr1Δ* cells. These data suggest that flux through the glycerol-3-phosphate shuttle is increased by at least 3 fold in *grr1Δ* cells. Furthermore, this increase in flux implies that *grr1Δ* strains differ from wild-type strains regarding glycerol metabolism; choosing to utilize glycerol-3-phosphate for respiration instead of the production of glycerol.

## 5.5. Flux through Gluconeogenesis and the Glyoxylate Cycle May be Increased in *grr1Δ* Cells on Glucose Media

Previously, GenGO enrichment analysis of our *grr1Δ* global gene expression analysis revealed that the processes of “gluconeogenesis” (p-value = 8E-4) and “glyoxylate metabolism” (pvalue = 4E-4) were among the most affected processes at the transcriptional level in *grr1Δ* cells grown on 2% glucose. Large transcriptional increases in the gluconeogenesis genes encoding for fructose-1,6-bisphosphatase (*FBP1*, +136.6), pep carboxy kinase (*PCK1*, +38.64), cytosolic NADP dependent isocitrate dehydrogenase (*IDP2*, +12.96), and pyruvate carboxylase (*PYC1*, +7.29) as well as the glyoxylate cycle genes encoding for isocitrate lyase (*ICL1,* +13.29) and malate synthase (*MLS1,* +88.33) were measured. Increases in gene expression for these genes were measured in a previous *grr1Δ* microarray [159] but were not analyzed further.

Despite these large increases in transcriptional expression we were unable to successfully measure the protein steady state levels for these enzymes. However, a number of independent observations suggest that the transcript levels for these genes may reflect the steady state level of their respective encoded proteins. First, previous analyses have found that the steady state level of Fbp1 is controlled by two distinct proteolytic pathways; one which is active after prolonged periods of glucose starvation (1-3 days) and another that is active after short term glucose starvation (~24 hrs) [460]. Glucose addition to cells exposed to long periods of glucose starvation induces degradation of Fbp1 by targeting Fbp1 to vacuolar import and degradation vesicles (Vid vesicles) which results in its’ degradation in the vacuole [461]. Our cells were not exposed to long term glucose starvation (see materials and methods) and thus Fbp1 degradation through this pathway is unlikely. The second pathway targets Fbp1 for proteasomal degradation after glucose is added to cells starved for glucose less than 24 hours. This pathway requires Grr1 and as a result Fbp1 protein levels are stabilized in *grr1Δ* cells [462].

Second, we measured significant increases and decreases in proteins of metabolic pathways that suggest increased flux through gluconeogenesis and

the glyoxylate cycle. Both Ser3 and Shm2 were measured in our proteomic analysis of *grr1Δ* strains to decrease by ~8 and 7 fold, respectively. Ser3 is one of two isoforms of 3-phosphoglycerate dehydrogenase in yeast [463] whereas Shm2 is the mitochondrial isoform for serine hydroxymethyltransferase [464]. Both of these enzymes contribute to the biosynthesis of glycine and serine on glucose grown cells [463]. On ethanol or other respiratory carbon sources, glycine and serine are synthesized via the glyoxylate pathway. Thus, the decrease in Ser3 and Shm2 protein levels are consistent with a decreased need to synthesize serine and glycine from 3-phosphoglycerate which can be supplied via the glyoxylate pathway.

We also measured differential regulation of the cytosolic NADP+ dependent glutamate dehydrogenases, Gdh1 and Gdh3. These two proteins together form a hetero-hexameric enzyme that catalyzes the synthesis of glutamate from ammonia and α-ketoglutarate [465,466]. It has been shown that the enzymatic rate of α-ketoglutarate utilization is much higher for Gdh1 than Gdh3 and the ratio of these two enzymes is intricately controlled by post-transcriptional modification of Gdh1 [467] and regulation of *GDH3* expression [466], in a carbon source dependent manner. On glucose or ethanol, the transcriptional expression of *GDH1* is unaltered; however the ratio of Gdh1 to Gdh3 protein decreases as glucose is depleted from the media. On the other hand, *GDH3*, transcriptional expression is low on glucose and markedly higher on ethanol. This transcriptional increase corresponds to an ethanol dependent increase in Gdh3 protein. Taken together, these data suggest that during fermentive growth, when energy contributed via the TCA cycle is minimal, a higher rate of α-ketoglutarate utilization for the synthesis of glutamate can be supported and is facilitated predominately by Gdh1. However, as glucose becomes limiting and aerobic growth on ethanol becomes the major energy providing pathway, the metabolic flux of α-ketoglutarate to glutamate is reduced by increasing the abundance of the less active isoenzyme, Gdh3, through transcriptional de-repression of its encoding gene. The decrease in flux through this pathway most likely leads to higher cytosolic α-ketoglutarate levels which can serve as a source of cytosolic

isocitrate for the glyoxylate cycle and gluconeogenesis since the gluconeogenic, cytosolic, NADP dependent, isocitrate dehydrogenase, Idp2, is a bi-directional enzyme that catalyzes the interconversion of isocitrate and α-ketoglutarate in a substrate concentration dependent manner [468]. Our data is consistent with the mode of regulation for the two isozymes as Gdh1 protein expression in *grr1Δ* cells was decreased ~3 fold (Table 5.1) with no significant change in *GDH1* expression measured, while *GDH3* expression increased ~8 fold (Table 5.1 and Figure 5.2). We were unable to successfully measure Gdh3 expression level, however Gdh3 expression has been shown to correlate with *GDH3* expression and thus it is likely that Gdh3 protein expression is increased in *grr1Δ* cells. The differential regulation of Gdh1 and Gdh3 observed in *grr1Δ* cells is consistent with the differential regulation of these two proteins observed in wild-type strains grown on a respiratory carbon source where the glyoxylate cycle and gluconeogenesis are needed for metabolism. Thus, these data further suggest that metabolic flux through these two pathways is increased in *grr1Δ* cells despite the fact that glucose is actively fermented in these strains.

Finally, perhaps the most compelling piece of evidence supporting increased flux through gluconeogenesis and the glyoxylate cycle is supplied by a significant and correlated increase in both the gene and protein expression of the glyoxylate reductase encoded by *YPL113C* [469]. In our global transcriptional and proteomic analysis, *YPL113C* expression was measured to increase by ~2.6 fold with an accordant increase in protein expression of 5.1 fold also measured. The YPl113C protein has been shown to be an isoform of a number of glyoxylate reductases in yeast that may be differentially localized [469]. The increased protein expression of YPL113C suggests that *grr1Δ* cells are producing excess glyoxylate through the glyoxylate cycle.

## 5.6. Network Analysis of the Transcripts Observed to Increase in *grr1Δ* Cells Reveals that Direct Targets of the Gluconeogenic Transcription Factors, Cat8 and Adr1, are Significantly Increased in *grr1Δ* Cells

Prior to glucose exhaustion, glucose exerts repression on genes necessary for utilizing of C2 carbon sources such as glycerol, ethanol and acetate. Growth on these carbon sources requires the enzymes of both the glyoxylate cycle and gluconeogenesis which together catalyze the biosynthesis of four carbon compounds which are subsequently utilized to synthesize sugars such as glucose and other essential compounds. These enzymes however, are dispensable for fermentive growth and thus the genes encoding these enzymes as well as the enzymes themselves are highly sensitive to glucose repression and glucose dependent inactivation, respectively. In fact, glucose repression of gluconeogenic genes has been shown to be triggered on glucose concentrations as low as 0.005% [170] and glucose induced degradation of gluconeogenic mRNA's has been found to occur at glucose concentrations as low as 0.001% [171]. Additionally, gene expression profiles of fermentive metabolism have shown that the gluconeogenic and glyoxylate cycle genes are among the last to be de-repressed; requiring almost complete depletion of glucose before increases in gene expression are detected [135]. In our analysis of *grr1Δ* cells the glucose concentration when we isolated our cells was well above 1% glucose; a concentration at which only a 30% deficiency in glucose transport is measured in *grr1Δ* cells[470]. Despite these conditions, we measured significant increases in gene expression for the gluconeogenic genes, *FBP1, PCK1, PYC1,* and *IDP2* as well as the glyoxylate cycle genes, *MLS1* and *ICL1*. Furthermore, a number of observations suggest that these transcripts indeed reflect the protein expression level of their respective products in *grr1Δ* cells (see Section 5.5). Together, these data suggest that glucose repression of gluconeogenic and glyoxylate cycle genes and glucose induced inactivation of gluconeogenic proteins is inactive in *grr1Δ* cells despite the presence of glucose and glucose transport. Interestingly, studies monitoring *FBP1* gene expression in yeast strains defective to varying degrees for glucose transport have shown that the complete absence

of glucose transport is required to eliminate glucose repression of *FBP1* [140]. Thus the glucose insensitive expression of gluconeogenic and glyoxylate cycle genes in *grr1Δ* cells is unlikely to be an indirect consequence of the glucose transport deficiency of this strain.

In order to determine the mechanism by which gluconeogenic and glyoxylate cycle genes are induced in *grr1Δ* cells, we first sought to determine the specific transcription factor(s) responsible for their expression. Interestingly, we determined the expression of the gluconeogenic and glyoxylate cycle transcription factor genes *ADR1, CAT8,* and *SIP4* to increase in gene expression by 3.4, 18.9, and 6.2 fold, respectively in *grr1Δ* cells. Together Adr1, Cat8, and Sip4 are responsible for the induction of gluconeogenic and glyoxylate cycle genes after glucose exhaustion [471-473]. Recently, Tachibana et al. conducted an extensive analysis where they identified those genes that exhibit both Adr1 and/or Cat8 binding to their promoter regions and showed significant decreases in transcriptional expression due to *ADR1* or *CAT8* deletion [474]. Thirty three genes were identified as direct targets of Adr1 of which 18 (55%) were significantly increased (as determined by Welchlog2 t-test < 0.05) in *grr1Δ* cells. Strikingly, 28 out of 34 (82%) of those genes found to be direct targets of Cat8 were significantly up-regulated in the *grr1Δ* cells.(Figure 5.4) Together these two transcription factors account for 32% of all genes up-regulated in response to GRR1 deletion at least 3 fold with a Welch log2 t-test <= 0.05. Thus, these data suggest that the glucose insensitive transcription of gluconeogenic and glyoxylate cycle genes is due to increased Adr1 and Cat8 dependent transcription.

## 5.7. Cat8 and Phosphorylated Cat8 Protein Levels are Increased in *grr1Δ* Strains

The extent to which Cat8 dependent genes are induced in *grr1Δ* cells despite the presence of high concentrations of extracellular glucose, prompted us to confirm if Cat8 protein levels were indeed higher in *grr1Δ* cells under these same conditions. To do this, we constructed *grr1Δ* cells containing a

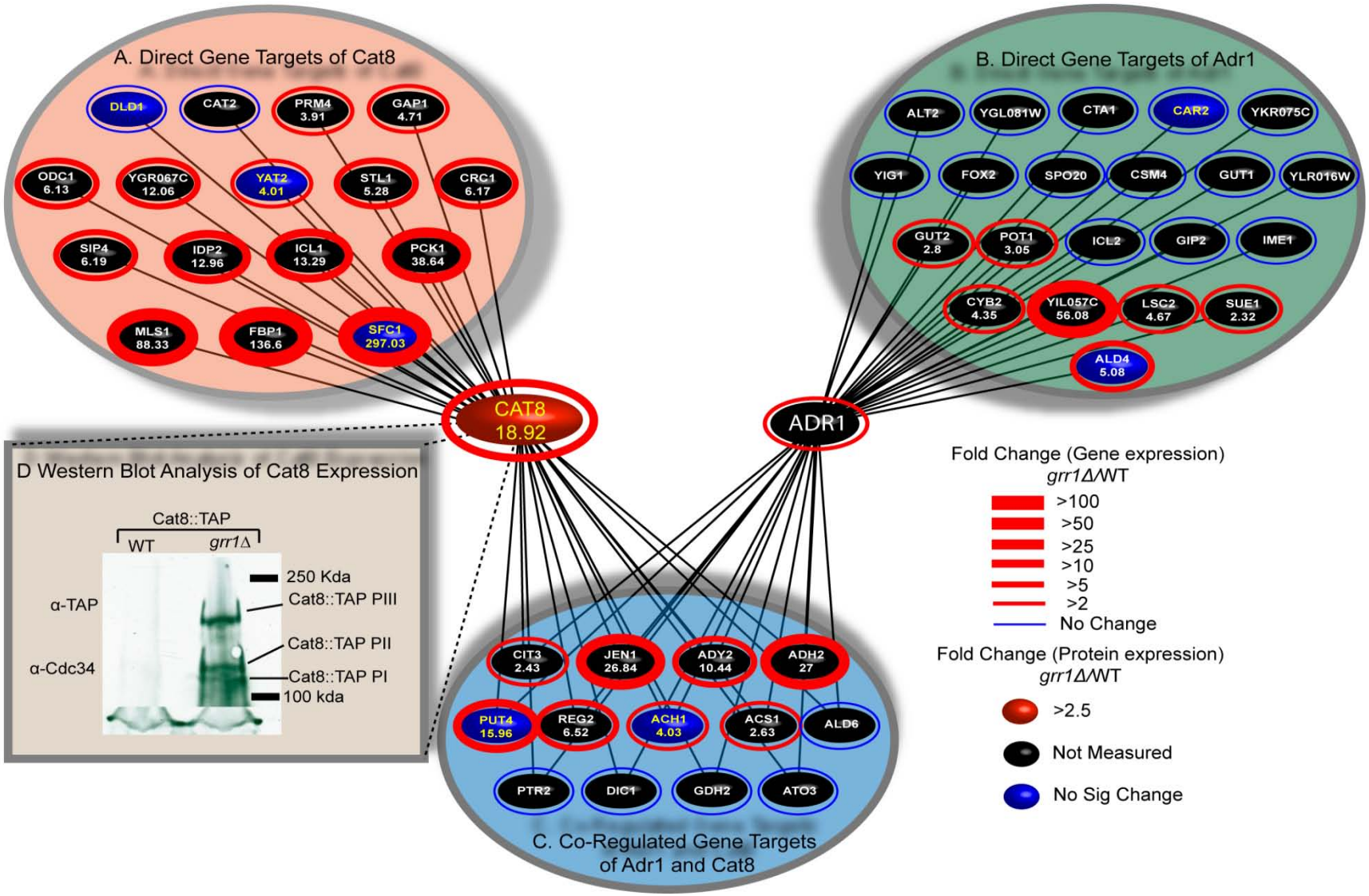
A. Direct Gene Targets of Cat8
DLD1
CAT2
PRM4 3.91
GAP1 4.71
ODC1 6.13
YGR067C 12.06
YAT2 4.01
STL1 5.28
CRC1 6.17
SIP4 6.19
IDP2 12.96
ICL1 13.29
PCK1 38.64
MLS1 88.33
FBP1 136.6
SFC1 297.03
B. Direct Gene Targets of Adr1
ALT2
YGL081W
CTA1
CAR2
YKR075C
YIG1
FOX2
SPO20
CSM4
GUT1
YLR016W
GUT2 2.8
POT1 3.05
ICL2
GIP2
IME1
CYB2 4.35
YIL057C 56.08
LSC2 4.67
SUE1 2.32
ALD4 5.08
CAT8 18.92
ADR1
D Western Blot Analysis of Cat8 Expression
Cat8::TAP
WT
grr1Δ
250 Kda
α-TAP
Cat8::TAP PIII
Cat8::TAP PII
α-Cdc34
Cat8::TAP PI
100 kda
CIT3 2.43
JEN1 26.84
ADY2 10.44
ADH2 27
PUT4 15.96
REG2 6.52
ACH1 4.03
ACS1 2.63
ALD6
PTR2
DIC1
GDH2
ATO3
C. Co-Regulated Gene Targets of Adr1 and Cat8
Fold Change (Gene expression)
grr1Δ/WT
>100
>50
>25
>10
>5
>2
No Change
Fold Change (Protein expression)
grr1Δ/WT
>2.5
Not Measured
No Sig Change

**Figure 5.4. Glucose Insensitive Transcription of Gluconeogenic and Glyoxylate Cycle Genes in *grr1Δ* Cells is Due to Increased Cat8 and Adr1 Dependent Transcription.** Genes directly regulated by the gluconeogenic transcription factors Cat8 (**A.**), Adr1 (**B.**), or both (**C.**) as determined by [474] are displayed as nodes connected to their respective transcription factors by black edges. Protein and gene expression measurements from global analysis of *grr1Δ* cells are denoted by the color of the node (protein) and the color of the ring around the node (gene) as indicated. **D.** The protein expression level of Cat8 in wild-type and *grr1Δ* cells grown on glucose media is shown utilizing wild-type and *grr1Δ* cells containing the Cat8::TAP fusion construct and α-Tap antibodies obtained from Open Biosystems™. The transcriptionally active, phosphorylated species are indicated.

*CAT8::TAP::HIS3* construct that could then be detected utilizing α-TAP antibodies available commercially through Open Biosystems™. In order to construct this strain as well as *grr1Δ* strains containing other TAP tagged protein constructs in a high throughput manner we implemented a derivative of the selective screening procedure utilized to perform high throughput synthetic lethal screens [336]. Briefly, the *GRR1* locus was deleted by adaptamer mediated gene disruption by inserting the *URA3* gene into the *GRR1* locus of the mating type selectable marker strain, MT2112, to construct strain JH020 (*mfα1Δ::MFα1pr-LEU2 can1Δ::MFA1pr-HIS3, his3Δ1, leu2Δ0, ura3Δ0, grr1Δ::URA3, met15Δ0, lys2Δ0*). This strain was then crossed to a BY4741 strain containing the *CAT8::TAP::HIS3* (*MATA his3Δ1 leu2Δ0 met15Δ0 ura3Δ0 CAT8::TAP::HIS3*) fusion construct that was obtained from the Open Biosystems™ TAP-tagged yeast strain library. Diploids were then selected on synthetic media lacking uracil, histidine, and lysine. Diploids were sporulated and *MAT α* spore progeny were selected by streaking spore tetrads on synthetic medium lacking leucine, uracil, histidine, and lysine. Finally, *grr1Δ* cells containing the *CAT8::TAP::HIS3* construct were isolated by replica plating the *MAT α* strains onto synthetic medium containing canavanine and lacking histidine and arginine. Colonies exhibiting no resistance to canavanine are positive for growth on media containing histidine due to the presence of the *CAT8::TAP::HIS3* construct. Each colony, exhibiting canavanine sensitivity, was examined for the characteristic elongated bud morphology of *grr1Δ* strains by microscopic examination and isolated (strain = JH006).

Cat8 protein levels were determined by western blotting utilizing α-TAP antibodies against protein extracts from strain JH006

(*grr1Δ::URA3 CAT8::TAP::HIS3*) and the original progenitor BY4741 (*CAT8::TAP::HIS3*) strain utilized to construct JH006. As can be seen in Figure 4.1 D we measured a drastic increase in Cat8 protein levels in *grr1Δ* strains grown on high glucose (~2%) media compared to the progenitor wild-type strain. Additionally, we observed two slower migrating species of Cat8 protein reminiscent of the phosphorylated species characterized by [320]. In this study, it was determined that the amount of hyper-phosphorylated Cat8 (Cat8 pIII) correlated with the gene expression as well as the enzymatic levels of PEPCK and FBPase. Also, Cat8 hyper-phosphorylation is regulated by the carbon source as hyper-phosphorylation is lost upon introduction of glucose to cells growing on ethanol. Together, the glucose insensitive expression of the *CAT8* gene, the glucose insensitive expression of gluconeogenic genes directly controlled by Cat8 dependent transcriptional induction, the measured increase in Cat8 protein levels on glucose media, and the prevalence of hyper-phosphorylated Cat8 pIII on glucose media in *grr1Δ* cells confirm that the glucose repression mechanism acting to repress *CAT8* gene expression as well as the catabolite inactivation mechanism responsible for inhibition of Cat8 dependent transcriptional activation are compromised in *grr1Δ* cells.

### 5.8. Network Analysis of Significantly Changed Proteins in *grr1Δ* Strains Reveals Enrichment for Glc7/Reg1 Interactors

It has been well established that Cat8 transcriptional expression as well as Cat8 transcriptional activity both require Snf1 catalytic activity [316,320,317,475]. Thus, the increased expression of *CAT8*, the increased protein expression of Cat8, and the existence of hyper-phosphorylated Cat8 in *grr1Δ* cells suggest that Snf1 catalytic activity must be active in this strain despite the presence of glucose and glucose transport. With this in mind, we were curious to reveal the particular mechanism by which Snf1 could be activated in *grr1Δ* cells. In order to do this we utilized the genetic and physical interaction data available through SGD to populate a relational database that could be interfaced with the network analysis tool ProteoLens™ [340]. Utilizing ProteoLens™ we then overlaid the protein and

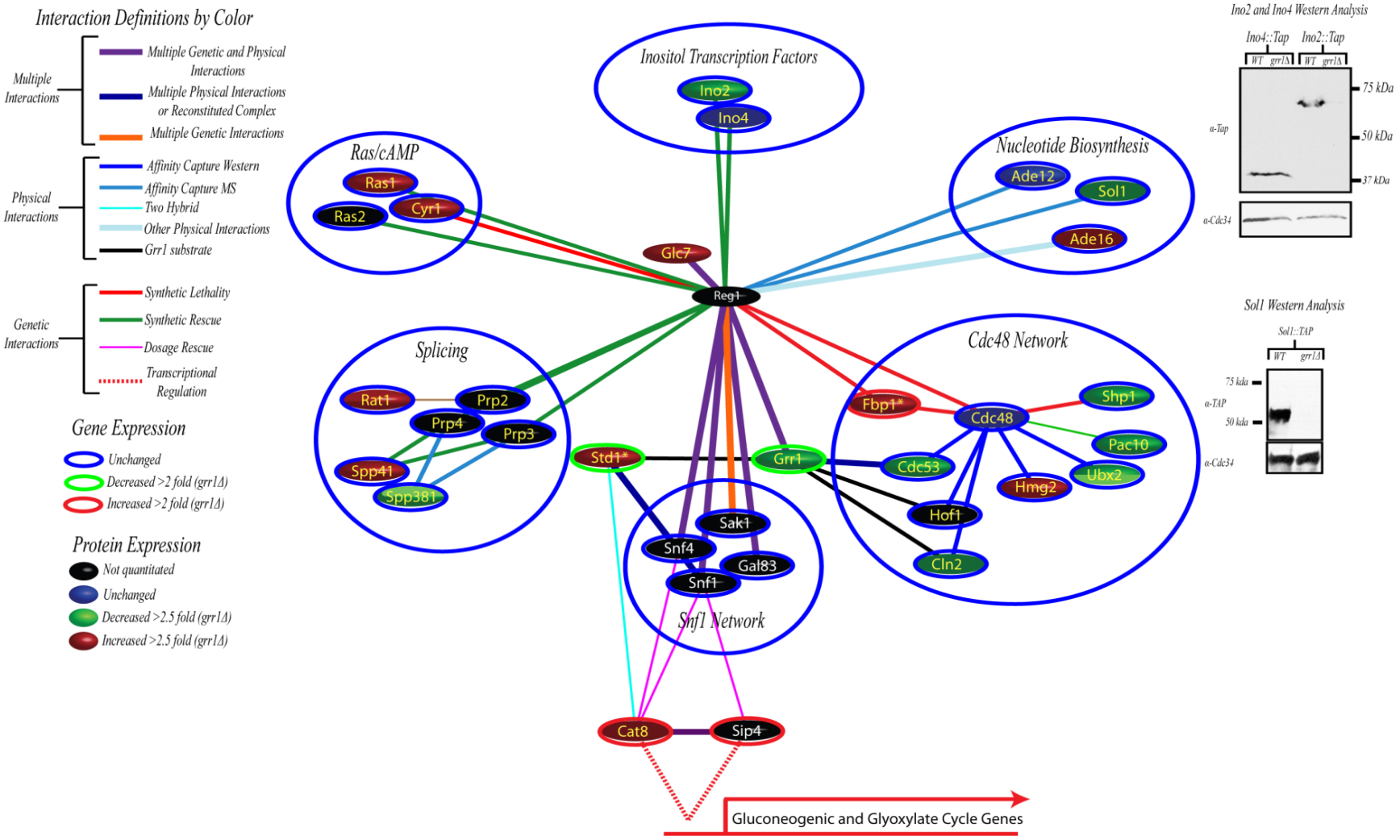
Interaction Definitions by Color
Multiple Interactions
Multiple Genetic and Physical Interactions
Multiple Physical Interactions or Reconstituted Complex
Multiple Genetic Interactions
Physical Interactions
Affinity Capture Western
Affinity Capture MS
Two Hybrid
Other Physical Interactions
Grr1 substrate
Genetic Interactions
Synthetic Lethality
Synthetic Rescue
Dosage Rescue
Transcriptional Regulation
Gene Expression
Unchanged
Decreased >2 fold (grr1Δ)
Increased >2 fold (grr1Δ)
Protein Expression
Not quantitated
Unchanged
Decreased >2.5 fold (grr1Δ)
Increased >2.5 fold (grr1Δ)
Inositol Transcription Factors
Ino2
Ino4
Ras/cAMP
Ras1
Ras2
Cyr1
Nucleotide Biosynthesis
Ade12
Sol1
Ade16
Glc7
Reg1
Splicing
Rat1
Prp2
Prp4
Prp3
Spp41
Spp381
Cdc48 Network
Fbp1*
Cdc48
Shp1
Pac10
Cdc53
Ubx2
Hmg2
Hof1
Cln2
Std1*
Grr1
Snf1 Network
Sak1
Snf4
Gal83
Snf1
Cat8
Sip4
Gluconeogenic and Glyoxylate Cycle Genes
Ino2 and Ino4 Western Analysis
Ino4::Tap
Ino2::Tap
WT
grr1Δ
75 kDa
50 kDa
37 kDa
α-Tap
α-Cdc34
Sol1 Western Analysis
Sol1::TAP
75 kda
α-TAP
50 kda
α-Cdc34

**Figure 5.5. Network Analysis of Gene and Protein Expression Changes in *grr1Δ* Cells Reveals Enrichment among Proteins Associated with the PP1 Targeting Subunit, Reg1.** A Reg1 protein interaction network was constructed utilizing the protein interaction data available through SGD and the network visualization tool ProteoLens™ [340]. Utilizing ProteoLens™, global gene and protein expression data from our analysis of *grr1Δ* strains was overlaid onto the yeast interaction map and manually assessed for "hot spots" where a high degree of expression changes were observed surrounding particular nodes. Utilizing this method, many proteins directly (first degree) and indirectly (second degree) associated with Reg1 were revealed to exhibit changes in protein expression. The legend for edges and nodes is provided (inset) as well as western blots confirming the protein expression level changes for Ino2 and Sol1.

gene expression data from our global *grr1Δ* genomic and proteomic data sets onto the *Saccharomyces* interaction network and looked for enrichment of protein or gene expression level changes among interactors of known Snf1 regulatory proteins. Interestingly, we measured no enrichment for protein or gene expression changes among interactors of the activating gamma subunit of the Snf1 kinase complex, Snf4, or the beta subunits; Gal83, Sip1, and Sip2. Additionally, we observed no enrichments of protein or gene expression level changes among interactors of the upstream Snf1 activating kinases Elm1, Tos3, or Sak1. However, a number of significant alterations in protein expression were observed among first degree and second degree interactors of the Glc7 regulatory subunit Reg1 including Glc7 (Figure 5.5).

Significant changes in protein expression measured in *grr1Δ* cells for proteins directly (first degree) interacting with Reg1 included components of the Ras/cAMP (Ras1 and Cyr1) pathway, enzymes involved in nucleotide biosynthesis (Ade16 and Sol1), the inositol transcription factor, Ino2, fructose-bis-phosphatase (Fbp1), and the catalytic subunit of the Reg1-Glc7 phosphatase, Glc7. Indirect interactions (second degree = separated by at most one shared node) with measured changes in protein expression included the splicing components, Spp41, Spp381, and Rat1, a number of Cdc48 interactors including Cdc53, Cln2, Pac10, Ubx2, Hmg2, and Shp1, and finally the downstream targets of Snf1, Cat8 and Sip4, which regulate gluconeogenic and glyoxylate cycle genes. Together, the multiple changes in protein expression measured among proteins with first or second degree interactions with Reg1 suggested that aspects of Reg1-Glc7 function were indeed altered in *grr1Δ* cells.

### 5.9. Western Analysis of Glc7 Reveals the Presence of a Modified Form of Glc7 that is Significantly Reduced in Abundance in *grr1Δ* Strains

The measured protein expression level changes among proteins exhibiting either genetic or physical interactions with Reg1 suggested that Reg1 function was somehow altered in *grr1Δ* cells. Interestingly, we measured increased protein expression of Glc7 whose phosphatase activity is required for the majority of Reg1 functions. This alteration in Glc7 expression is perplexing given the fact that Glc7 is a stable protein whose abundance has not been measured to change in any conditions previously assayed. However, Glc7 was quantitated in our global proteomic analysis by only one peptide (pep sequence) and thus the measured change in Glc7 abundance could either be due to the absence of an unknown modification of Glc7 on this peptide in *grr1Δ* cells or indeed reflect Glc7 protein expression levels. We therefore sought to resolve this discrepancy by constructing a *grr1Δ* strain harboring a Glc7::TAP fusion construct which could then be assayed by western analysis using anti-TAP antibodies. This strain (JH007) was constructed utilizing the same method utilized to construct JH006 (*grr1Δ* Cat8::TAP).

Strain JH007 and its progenitor wild-type strain were grown to early mid-log phase in liquid YPD+N media (see materials and methods) and whole cell protein extracts were prepared. Interestingly, western analysis of these extracts utilizing the α-Tap antibodies obtained from Open Biosystems ™revealed that while Glc7::TAP in *grr1Δ* strains migrated at the predicted size ~36, the Glc7::TAP fusion in the progenitor wild-type strain displayed a much slower migrating form and no signal was measured at the predicted size of Glc7 in wild-type strains. In order to confirm that these bands were indeed the Glc7 protein and that the altered migration in wild-type was not a consequence of the presence of the Tap tag fusion construct we obtained antibodies raised against the endogenous Glc7 protein from two independent laboratories. We first conducted western analysis on protein extracts isolated from strains DBY2059 (*leu2-3)* and JH001 (*grr1Δ::NAT)* grown on the SD+N media utilized in the global genomic and proteomics experiments with purified α-Glc7 antibodies obtained

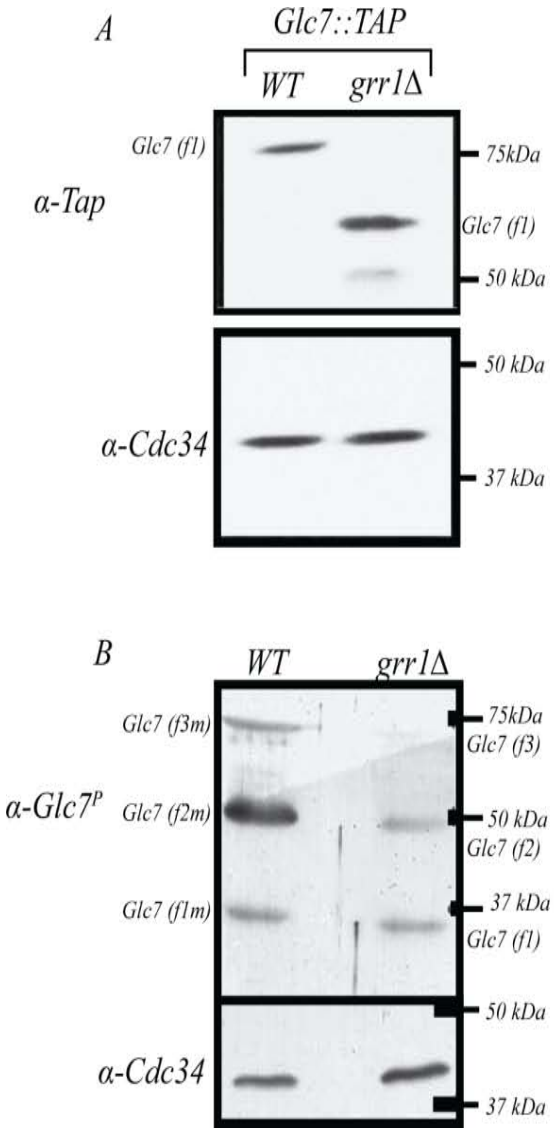
A
Glc7::TAP
WT
grr1Δ
Glc7 (f1)
75kDa
α-Tap
Glc7 (f1)
50 kDa
50 kDa
α-Cdc34
37 kDa
B
WT
grr1Δ
Glc7 (f3m)
75kDa
Glc7 (f3)
α-Glc7P
Glc7 (f2m)
50 kDa
Glc7 (f2)
Glc7 (f1m)
37 kDa
Glc7 (f1)
50 kDa
α-Cdc34
37 kDa

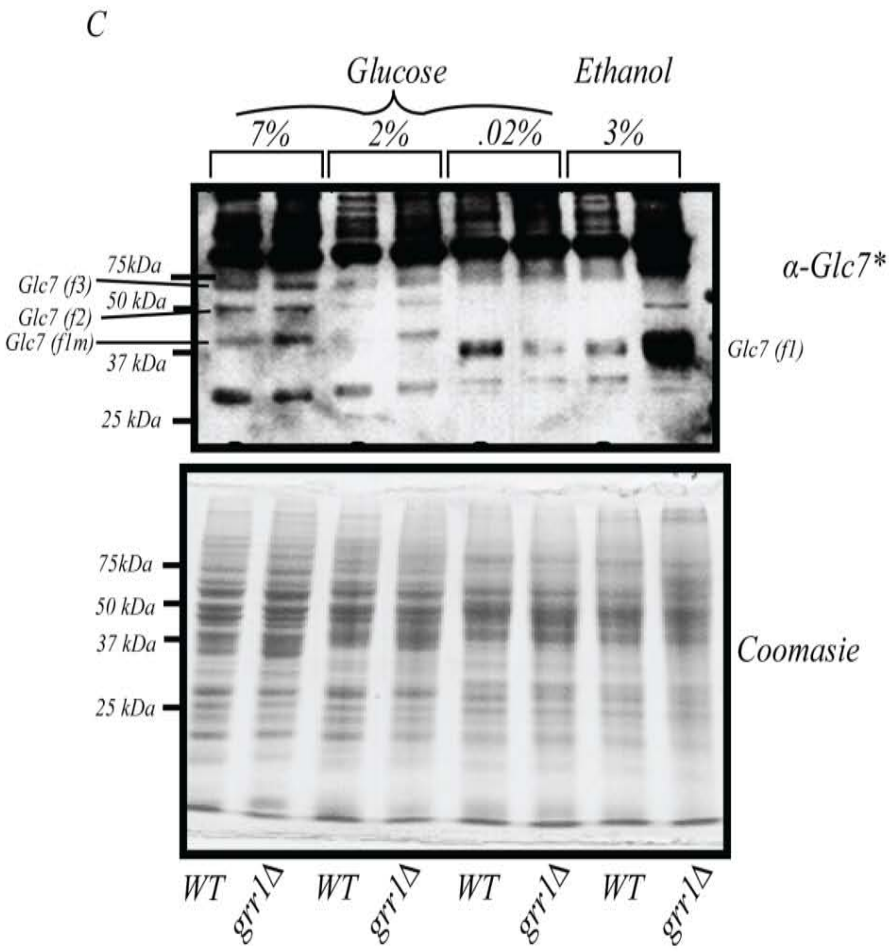
C
Glucose
Ethanol
7%
2%
.02%
3%
75kDa
Glc7 (f3)
50 kDa
Glc7 (f2)
Glc7 (f1m)
37 kDa
25 kDa
α-Glc7*
Glc7 (f1)
75kDa
50 kDa
37 kDa
25 kDa
Coomasie
WT
grr1Δ
WT
grr1Δ
WT
grr1Δ
WT
grr1Δ

**Figure 5.6. Glc7 Western Blots Comparing *grr1Δ* and wild-type Cells** **A.** Western analysis of wild-type and *grr1Δ* strains grown on YPD+N (see materials and methods) harboring the Glc7::Tap construct using rabbit polyclonal antibodies against the Tap protein reveal the presence of a slower migrating form of Glc7 (Glc7 (f1)) that is estimated to be 10-15kDa bigger than the Glc7 unmodified form found in *grr1Δ* strains (Glc7 (u)). **B:** Western analysis of wild-type and *grr1Δ* strains grown on SD+N (see materials and methods) using antibodies against the endogenous Glc7 protein (α-Glc7$^{P}$) reveals the presence of multiple forms of Glc7 all of which are differentially expressed in *grr1Δ* strain. Glc7(f1) represents the endogenous unmodified form of Glc7 and this form seems to migrate slightly slower in wild-type strains perhaps representing a phosphorylated form of Glc7 (Glc7(f1M)). A slower migrating form of Glc7 ( Glc7 (f2)) which is estimated to be 10-15kDa bigger than the predicted 36kDa form, Glc7 (f2), is detected in the *grr1Δ* and the wild-type strain. However, once again the wild-type Glc7 (f2m) seems to slightly migrate slower and is much more prevalent than in *grr1Δ* strains. Finally, a third , slower migrating form of Glc7 estimated to be at least 30 kDa larger than Glc7(f1) is found in wild-type strains but absent in *grr1Δ* strains. **C:** Western analysis of wild-type and *grr1Δ* strains on various concentrations of glucose and on ethanol media (see materials and methods) using another antibody raised against endogenous Glc7 (Glc7*) reveals that the presence of the different forms of Glc7 are differentially regulated according to carbon source. On 7% glucose forms f1m,f2, and f3 are measured to be equally present and the unmodified form of Glc7 (Glc7 (f1)) is absent in both wild-type and *grr1Δ* strains. Both the f2 and f3 forms of Glc7 are present in wild-type strains grown on 2% glucose but the f1m and the f1form is absent. In *grr1Δ* strains all forms except the f1 form are present on 2% glucose. On .02% glucose only the f1 form of Glc7 is present in wild-type and *grr1Δ* strains. Finally, as on .02% glucose, on 3% ethanol media the wild-type strain contains only the f1 form. However, the *grr1Δ* strain contains much more of the f1 form and both the f2 and f3 forms can be detected.

from Dr. John Cannon. As can be seen in Figure 5.6 B utilizing these antibodies we were able to detect Glc7 at the normal migration size in both the wild-type and *grr1Δ* strains which was in contrast to the pattern observed utilizing the α-TAP antibodies against the Glc7::TAP fusion construct in wild-type and *grr1Δ* strains. We were also able to detect the slower migrating form of Glc7 (Glc7 (f2)) in both strains under these conditions. However, this form was much more prevalent in the wild-type strain than in the *grr1Δ* strain indicating that this form was differentially regulated in *grr1Δ* strains. Additionally, another even slower migrating form of Glc7 was also detected in the wild-type utilizing these antibodies and this form was completely absent in *grr1Δ* strains. This same banding pattern was also observed utilizing raw sera from another independent Glc7 antibody preparation obtained from Dr. Ron Wek (α-Glc7$^{*}$). Together, these data prove the existence of multiple forms of Glc7, the identity of which remains to be elucidated. These data also suggests that the measured change in relative abundance of Glc7 in our mass spectrometric analysis of *grr1Δ* and wild-type strains may in fact reflect a difference in the relative abundance of different forms of the Glc7 protein between these two strains.

Due to the fact that *grr1Δ* strains display increased expression of genes directly controlled by the Snf1 kinase, that *grr1Δ* strains show changes in protein expression among Reg1 interactors, and that these changes are coincident with reduced expression of the second and third forms of Glc7, we speculated that the predicted faster migrating form of Glc7 may not interact with Reg1 and that Glc7 interaction with Reg1 may be facilitated by the increased expression of either of the second and/or third forms of Glc7. Additionally, the fact that these forms showed reduced expression in *grr1Δ* strains suggested that the expression of these forms may not be directly controlled by Grr1 but a consequence of reduced glucose transport in *grr1Δ* cells. If this is indeed the case then the expression of these alternative forms would likely respond to the concentration of glucose provided to the cell and thus the regulation of these alternative forms may be a novel mechanism to control glucose repression of Snf1 dependent genes.
In order to determine if these alternative forms were differentially regulated in response to glucose we grew the wild-type and *grr1Δ* strains on YPD media containing 7%, 2%, and .02% glucose as well as YP ethanol media. We then compared the expression level of these alternative forms of Glc7 through western analysis utilizing the Glc7* antibodies. As can be seen in Figure 5.6 C, on 7% glucose, we detected both the second and third forms of Glc7 in both the *grr1Δ* and wild-type strains. Interestingly the predicted 36kDa from of Glc7 was not detected and yet another slower migrating form of Glc7 with an estimated molecular weight of 38-40kDa was detected in both strains. On 2% glucose the expression of the second and third forms of Glc7 was reduced but present in both strains. Once again the predicted 36kDa form of Glc7 was absent in both strains. Interestingly, the 38-40kDa from of Glc7 was absent in wild-type cells but present in the *grr1Δ* cells at this glucose concentration. We currently have no explanation for this difference other than the wild-type lane may be under loaded. Remarkably, when both the wild-type and the *grr1Δ* cells were grown on glucose de-repressing media (0.02% glucose and ethanol media), the second and third forms of Glc7 were absent as well as the 38-40kDa form in both strains. In fact the only form of Glc7 observed on 0.02% glucose in both strains was the

predicted 36 kDa form of Glc7. This form was also only present in the wild-type on ethanol media, however the *grr1Δ* strain displayed a tremendous increase in expression of this from on ethanol and additional forms of Glc7 were also observed in *grr1Δ* cells on ethanol media. Together this data provides compelling evidence that multiple forms of Glc7 exist in *Saccharomyces* and that the expression of these forms is differentially regulated by the concentration and type of carbon source.

# CHAPTER 6: DISCUSSION: THE ROLE OF *GRR1* IN GLUCOSE REPRESSION

## 6.1. Glucose Transport in *grr1Δ* Cells

In our analysis of discordance among loci annotated to the "carbon and energy metabolism" cluster, discordance among hexose transporters was measured. Multiple studies have eloquently revealed that *grr1Δ* cells are defective in high affinity glucose transport; however low affinity glucose transport has not been shown to be affected in *grr1Δ* cells. This phenotype is counter to the changes in gene expression measured in *grr1Δ* cells among hexose transporter genes. In previous studies, the affect that *GRR1* deletion had on the high affinity transporter, *HXT6/7,* was either undetermined or not discussed. Interestingly, despite the lack of high affinity hexose transport in *grr1Δ* cells, we as well as others detect increased expression of *HXT6/7*. In our analysis, we reveal that despite increases in *Hxt6/7* gene expression, Hxt6/7 protein expression is significantly decreased in *grr1Δ* cells. Though the origins of the discordance between gene and protein expression of Hxt6/7 in *grr1Δ* cells are not revealed by our analysis, network analysis of nutrient transporters post-translationally controlled by Grr1 suggests that Grr1 may regulate trafficking of these transporters through a Las17 dependent mechanism (Section *5.4.3.1*). In the case of Hxt6/7, Grr1 would presumably promote the stability of Hxt6/7 at the membrane.

Changes in gene expression measured for the low affinity hexose transporters are also inconsistent with the glucose transport phenotype of *grr1Δ* cells. In *grr1Δ* cells, the expression of the low affinity hexose transporters, *HXT1* and *HXT3*, are fully and partially repressed, respectively. Once again, these decreases in low affinity gene expression are inconsistent with the lack of a deficiency in low affinity glucose transport in *grr1Δ* cells. We revealed that, despite a significant decrease in *HXT3* gene expression, Hxt3 protein levels are not measured to change significantly in *grr1Δ* cells at the growth phase we measured. Thus, the decreased gene expression of *HXT3* is compensated in

*grr1Δ* cells by a currently unknown mechanism that most likely influences either the translational rate of Hxt3 synthesis or the trafficking and stability of Hxt3. We therefore conclude that low affinity glucose transport in *grr1Δ* cells is, in part, facilitated by Hxt3. (Figure 8.1 for model) However, the presence of Hxt3 facilitated glucose transport in *grr1Δ* cells does not completely provide wild-type levels of glucose transport as a 30-40% deficiency in glucose transport is measured at high glucose concentrations. This would suggest that either a fraction of glucose transport at high glucose levels is provided by one or more high affinity glucose transporters, whose expression is defective in *grr1Δ* cells, and/or that Hxt1 facilitated glucose transport may be compromised in *grr1Δ* cells. Interestingly, our quantitative proteomics analysis measured no significant change in protein expression of Hxt1 in *grr1Δ* cells.

### 6.2. Discordance among Carbon and Energy Metabolism Genes and its Implications for Grr1 Metabolism

Our discovery that Hxt3 protein levels are unaffected in *grr1Δ* cells despite a significant decrease in *HXT3* expression provides a mechanistic explanation for the sustainability of glucose based growth in *grr1Δ* cells. However, it also presents a perplexing paradigm regarding the role of Grr1 in glucose repression. Recently, utilizing an array of *S. cerevisiae* strains expressing individual hexose transporters with different glucose transport rates, it was shown that the transcriptional expression (and thus release from glucose repression) of the gluconeogenic gene, *FBP1,* required the complete lack of glucose transport [140]. Additionally, a number of other studies have revealed that gluconeogenic and glyoxylate cycle genes are extremely sensitive to glucose repression [476,170,172,135]. We presented multiple lines of evidence that indicate gluconeogenic and glyoxylate cycle genes are expressed, that their gene products are expressed, and that the enzymatic activity of these proteins is active in *grr1Δ* cells despite the presence of glucose and Hxt3 facilitated glucose transport. These data pose the question; what causes glucose insensitive expression of gluconeogenic genes and their products in *grr1Δ* cells? Our data and that of others suggests

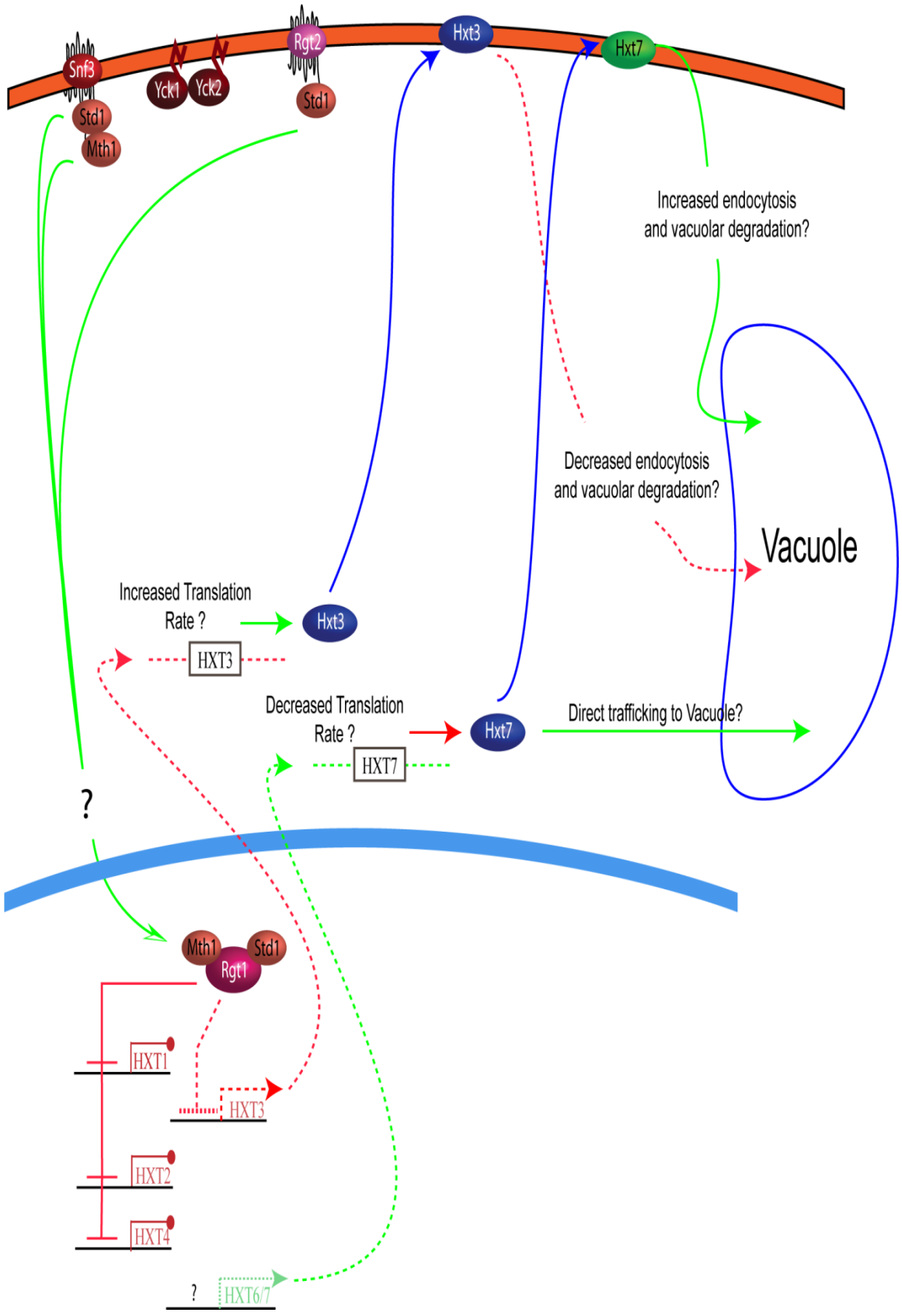
Snf3
Std1
Mth1
Yck1
Yck2
Rgt2
Std1
Hxt3
Hxt7
Increased endocytosis
and vacuolar degradation?
Decreased endocytosis
and vacuolar degradation?
Vacuole
Increased Translation
Rate ?
Hxt3
HXT3
Decreased Translation
Rate ?
Hxt7
HXT7
Direct trafficking to Vacuole?
?
Mth1
Std1
Rgt1
HXT1
HXT3
HXT2
HXT4
?
HXT6/7

**Figure 6.1. Model for Post-Transcriptional Regulation of Hxt3 and Hxt6/7 in *grr1Δ* Cells.** In *grr1Δ* cells the transcriptional repressor, Rgt1, is free to associate with both Mth1 and Std1. This leads to constitutive and full repression of the hexose transporter gene *HXT1* while *HXT2, HXT4, HXT3* are repressed but not to the full extent. Rgt1's influence on *HXT6,7* has not been determined but must not be repressing since *HXT6,7* expression is increased 4.6 fold in *grr1Δ* cells. On glucose media, the inability to fully de-repress *HXT3* transcription leads to a lag in the accumulation of Hxt3 protein and a deficiency in Hxt3 mediated glucose transport. An increase in the translational rate or decrease in the vacuolar degradation of Hxt3 acts to compensate for this deficiency in *HXT3* transcription in order to facilitate glucose transport in *grr1Δ* cells. At the same time, despite the fact that *HXT6,7* transcription is increased by almost 5 fold in *grr1Δ* cells the protein expression level of Hxt6,7 is decreased in *grr1Δ* cells by greater than 3 fold. This decrease in Hxt6,7 may be due to either a decrease in the rate of synthesis of the protein or an increase in the vacuolar degradation of the protein. These data are consistent with the ability of *grr1Δ* cells to grow on moderate to high glucose concentrations where Hxt3 facilitates glucose transport and the inability of *grr1Δ* cells to grow on low glucose concentrations where Hxt6,7 facilitate glucose transport.

that flux through gluconeogenic and glyoxylate cycle pathways may be needed in *grr1Δ* cells to provide TCA cycle intermediates to the mitochondria in response to a deficiency in respiration in *grr1Δ* cells. This respiratory deficiency may be caused by the inability to permeabilize the mitochondrial outer membrane to NADH and is remedied utilizing the less energy efficient glycerol-3-phosphate shuttle.

Comparison of protein and gene expression levels among loci annotated to the "carbon and energy metabolism" cluster revealed multiple instances of discordance which were subsequently overlaid onto a metabolic map of central carbon and energy metabolism. Comparison of this metabolic map with previous analyses of metabolic flux in *grr1Δ* cells together suggested that despite increased flux through the TCA cycle, respiratory capacity is decreased in *grr1Δ* cells. These conclusions are supported by multiple lines of evidence.

In our proteomic and genomic analysis of *grr1Δ* cells we measured a significant amount of discordance between gene and protein expression of a number of mitochondrial proteins. Significant increases in gene expression were measured for a number of TCA cycle genes yet correlative increases in protein expression were only observed for *CIT1*/Cit1 (2.70, 3.12). These two enzymes catalyze the rate limiting steps of the TCA cycle and thus increased flux through the TCA cycle is likely despite the measured insignificant changes in the remaining TCA cycle proteins. Consistent with this interpretation is the fact that

increased flux through the TCA cycle has been measured for *grr1Δ* cells previously [477,174].

Despite increased flux through the TCA cycle in *grr1Δ* cells, our data as well as that of others supports that respiratory capacity in *grr1Δ* cells is compromised. While some labs report normal growth of *grr1Δ* cells on respiratory carbon sources [66] others have found that *GRR1* is required for respiratory growth [68]. We postulated that these discrepancies may be due to differences between strains backgrounds as cells of the S288C lineage are known to possess an inactivating Ty1 insertion in the respiratory *HAP1* gene [454]. However, while defects in respiratory growth for *grr1Δ* cells of the S288C background were more severe than those of the Cen.PK background a noticeable defect in respiratory growth was still present in Cen.PK *grr1Δ* cells.

Consistent with a decreased respiratory capacity of *grr1Δ* cells, we also measured that expression of a number of proteins necessary for respiratory growth were observed to decrease. The decreases in protein expression measured for mitochondrial proteins combined with the changes in protein expression for proteins involved in glycerol metabolism suggest that redox metabolism in *grr1Δ* cells is drastically altered. The most notable of mitochondrial protein expression changes supporting an altered redox metabolism in *grr1Δ* cells are the mitochondrial porin, Por1, and the mitochondrial protein import receptor, Tom70. Together, these two proteins, among other functions, serve to regulate the flux of NADH through the outer mitochondrial membrane [478,479,453,480], thus controlling the accessibility of NADH to the mitochondrial inner membrane NADH dehydrogenases, Nde1 and Nde2. The catalytic sites of these two dehydrogenases face the inter membrane space and thus these two enzymes couple the oxidation of cytosolic NADH to the mitochondrial electron transport chain. Thus, reduction of Por1 and Tom70 protein levels would suggest that the permeability of the mitochondrial outer membrane to NADH was reduced and that NADH oxidation through Nde1 and Nde2 is also coordinately reduced. Interestingly, it has been found that the enzymatic activity of Nde1 and Nde2 inhibits the glycerol-3-phosphate

dehydrogenase, Gut2 [458], which was measured to increase in gene expression in *grr1Δ* cells. Gut2 enzymatic activity is required for glycerol utilization and the glycerol-3-phosphate shuttle, which serves as an alternative pathway to couple NADH oxidation to the electron transport chain. Interestingly, this pathway does not require NADH but glycerol-3-phosphate to traverse the mitochondrial outer membrane. It has been reported that glycerol production in *grr1Δ* cells grown on glucose is reduced [67] and our protein expression data suggest that this reduction in glycerol production may be a consequence of increased flux through the glycerol-3-phosphate shuttle as Gpd2, whose protein expression is stimulated by excess cytosolic NADH [456], was measured to increase by 3 fold in *grr1Δ* cells. Additionally, we also measured decreased protein expression of Gpp1 in *grr1Δ* cells, which is the major isoform of glycerol-3-phosphatase catalyzing the biosynthesis of glycerol from glycerol-3-phosphate. Together, this data suggests that decreased glycerol production in *grr1Δ* cells is a consequence of increased flux through the glycerol-3-phosphate shuttle in *grr1Δ* cells.

The origins of decreased respiratory capacity in *grr1Δ* cells are difficult to ascertain from our present analysis. However, a number of potential roles for Grr1 in regulating respiratory capacity are supported by various lines of evidence. Interestingly, Grr1 as well as the cullin protein of the SCF, Cdc53, have been discovered to physically interact with the Por1 protein in a large scale mass spectrometry based screen for protein interactions [481]. This data suggests that altered redox metabolism may be a consequence of some as of yet to be defined role for the $SCF^{Grr1}$ complex in directly regulating the mitochondrial porin. Additionally, cells deleted for *GRR1* have been shown to possess defects in the transport of divalent cations including, $Ni^{2+}$, $Co^{2+}$, $Zn^{2+}$, and $Mn^{2+}$ [71]. Furthermore, significant increases in gene expression for transporters involved in iron import were measured in *grr1Δ* cells, including Fre7, Fit2, Fit3, and Fre5. Together, this data suggests that *grr1Δ* cells are depleted of intracellular cations. Decreased intracellular iron, in particular, would decrease the formation of iron-sulfur cluster proteins which decreases respiratory capacity and activates the retrograde response pathway.

It has been previously discovered that Grr1 is required for activation of mitochondrial retrograde signaling in response to mitochondrial respiratory dysfunction by catalyzing the degradation of the negative regulator of retrograde signaling, Mks1 [57]. Retrograde signaling is an adaptive response to deficiencies in mitochondrial respiration arising from changes in intracellular cation dynamics or defects in enzymes of the TCA cycle and/or respiratory chain [123,122]. The TCA cycle fails to function as a full cycle in respiratory deficient mitochondria since succinate would fail to be oxidized to fumarate. Thus, through the retrograde signaling pathway, mitochondria can induce changes in nuclear gene expression to enhance production of enzymes of anapleurotic metabolic pathways that serve to provide TCA cycle intermediates to the mitochondria. Utilizing the gluconeogenic and glyoxylate cycle pathways, the oxidation of succinate to fumarate in the TCA cycle can be bypassed to allow production of essential TCA cycle metabolites such as glutamate in the absence of respiratory function. In *grr1Δ* cells the retrograde response is inactive and thus up-regulation of *CAT8* gene expression, which is not under retrograde control but Snf1 and Hap2/Hap3/Hap4/Hap5 control, may serve as a compensatory pathway to defects in retrograde response. Nevertheless, the need for increased respiratory capacity in *grr1Δ* strains grown on glucose is not explained by these phenomena and a direct role for Grr1 in modulating Cat8 and Cat8 dependent transcription cannot be eliminated at this time.

### 6.3. Glc7 Regulation in *grr1Δ* Cells

The intracellular signal that leads to Cat8 dependent transcriptional induction of gluconeogenic and glyoxylate cycle genes in *grr1Δ* cells remains a mystery but our data suggests that this signal acts to regulate Snf1 kinase activity through inhibition of Reg1-Glc7 activity. We presented data that strongly suggests that transcriptional activation of gluconeogenic genes in *grr1Δ* cells is facilitated through Cat8 dependent transcriptional induction as *CAT8* expression was increased in *grr1Δ* cells, Cat8 dependent genes were significantly increased in *grr1Δ* cells, and accumulation of the hyper-phosphorylated transcriptionally

active form of Cat8 was measured to increase in *grr1Δ* cells. Since *CAT8* gene expression and phosphorylation of Cat8 requires Snf1 kinase activity we deduced that the Snf1 kinase was indeed active in *grr1Δ* cells. Finally, we presented evidence suggesting that *grr1Δ* cells possess alterations in the activity of the Reg1-Glc7 phosphatase, possibly through post-translational modification of Glc7, which most likely lead to increased Snf1 catalytic activity. These data suggest that the signal acting to de-repress gluconeogenic and glyoxylate cycle genes in *grr1Δ* cells acts to modulate Reg1-Glc7 activity by controlling the levels of the alternative forms of Glc7.

The identity of the alternative forms of Glc7 detected in our analysis is presently unknown but one promising possibility can be conceived. The migration shift between form one of Glc7 and form two of Glc7 is estimated to correlate to a difference in protein size between 10-15 kDa. Though many post-translational modifications cause slower migration of proteins through SDS-Page gels the extent to which the migratory shift occurs is in most cases is more subtle than that observed for Glc7. However, sumo, which is a protein that is covalently attached to protein substrates like ubiquitin, has a molecular weight of 11,597 Da. Thus, it is possible that Glc7 may be sumoylated and that Glc7 form three may possess two of these modifications since the difference in migration between form two and form three is roughly equal to the difference in migration between form one and form two. It is also interesting to note that the SUMO peptidase, Ulp2, which de-conjugates SUMO modifications from proteins, was measured to increase in expression in *grr1Δ* cells by 5 fold. Additionally, Uls1, which is a RING finger protein involved in ubiquitin dependent proteolysis of SUMO conjugated proteins, is also measured to increase in expression by ~10 fold. Together, these data provide preliminary evidence that the processes mediating sumoylation may be affected in *grr1Δ* strains and that Glc7 may be a target for sumoylation in response to glucose availability and/or increased glycolytic flux. However, further investigation is required to confirm or deny this hypothesis.

### 6.4. Final Model for Hexose Transport in *grr1Δ* Cells

The results pertaining to post-transcriptional control of hexose transporters, the decreased respiratory capacity, and the regulation of gluconeogenic and glyoxylate cycle genes through modulation of Glc7 in *grr1Δ* strains together provide an in depth analysis of the regulatory and metabolic state of *grr1Δ* cells grown on glucose. However, the direct cause of the glucose insensitivity of these alterations is not apparent in our analysis. Previous analyses have provided compelling evidence that the resistance to glucose repression observed in *grr1Δ* strains is an indirect consequence of decreased glucose transport and as a result decreased glycolytic flux in this strain. Our results do not refute this explanation but provide a possible explanation for the absence of glucose repression of the highly glucose sensitive gluconeogenic and glyoxylate cycle genes. Considering these prior analyses as well as our own, we propose the following model for the glucose repression resistant phenotype of *grr1Δ* strains.

During the initial phases of glucose based growth when stationary phase cells have just been diluted in fresh glucose medium there is a measurable lag in cell replication until the cells adjust the external environment as well as their own intracellular environment to support efficient utilization of the available nutrients. Once adjusted, the yeast cell enters logarithmic growth where the rate of cellular replication is increased substantially. Depending on the metabolic and regulatory state of the cell this adjustment phase varies in length. For example, if the inoculated cells were from stationary phase cultures, the transport and metabolic state of the cell is most likely adjusted for growth on low glucose or even ethanol depending on how long the cells were allowed to incubate in stationary phase. Thus, inoculation of these cells into fresh (2% glucose) cultures would require a more extensive remodeling of the transport and metabolic state of the cell. However, if the inoculated cells were from cultures of cells in mid-log phase, the transport and metabolic state of the cell is adjusted for fermentive growth on glucose (glucose concentrations ranging from 0.5-1.5%). Thus, the amount of transport and metabolic remodeling required to adjust to fermentive growth on

the higher glucose concentration present in the fresh medium would be far less extensive.

With this in mind, we believe that the glucose repression resistant phenotype of *grr1Δ* strains is a manifestation of two independent defects. First, the relief from glucose repression in *grr1Δ* strains is a manifestation of the decreased ability of *grr1Δ* strains to adjust their glucose transport capacity in response to changes in extracellular glucose concentration. When *grr1Δ* stationary phase cells are inoculated into fresh, 2% glucose media, there is a significant lag in the onset of logarithmic growth compared to wild-type cells. We believe this lag is at least partially caused by the inability to de-repress hexose transporter transcription in response to glucose availability through the Snf3/Rgt2 pathway. However, the expression of the low affinity hexose transporter gene, *HXT3*, is not fully repressed in *grr1Δ* strains and therefore its protein product can be synthesized albeit at a much slower rate. This slower rate of Hxt3 synthesis contributes to the lag in the onset of logarithmic growth of *grr1Δ* cells since glycolytic flux would presumably be decreased coordinately with the glucose transport capacity supplied by Hxt3. Once Hxt3 protein levels reach wild-type levels in *grr1Δ* cells, we presume that glucose transport capacity would be sufficient for logarithmic growth on glucose to begin. It is critical to emphasize that in our analyses we adjusted for the lag in the onset of logarithmic growth by allowing *grr1Δ* cells to grow for approximately 6 hours longer than wild-type (this was the point where cell densities were equal) before protein extraction. Thus, at the time points where we measured Hxt3 and Hxt7 levels the *grr1Δ* strain had entered logarithmic growth and thus, under our model, differences in Hxt3 protein levels at this point would be absent. Considering the above model for the decreased rate of glucose transport capacity adjustment in *grr1Δ* strains, the need for increased respiratory capacity in *grr1Δ* strains is an indirect consequence of this delay. The slow response to the availability of glucose in *grr1Δ* strains would lead to an increased dependence of these strains to support the energy demands of the cell through respiration during the prolonged adjustment phase.

Second, the glucose insensitive expression of the highly glucose sensitive gluconeogenic and glyoxylate cycle genes is most likely a consequence of the need for increased respiratory capacity in *grr1Δ* strains and the inability to effectively increase respiratory capacity in *grr1Δ* strains due to an undefined role for Grr1 in regulating respiration. As indicated previously, the glyoxylate cycle provides metabolic intermediates to the TCA cycle and can serve to bypass the oxidation of succinate to fumarate in respiratory deficient cells in order to support synthesis of essential metabolites such as glutamate and glutamine. Our data suggests that *grr1Δ* cells possess defects in respiration that may be due to one or more roles for Grr1 in respiratory function. Thus, gluconeogenic and glyoxylate cycle enzymes may be needed in *grr1Δ* cells to provide anapleurotic pathways in order to compensate for the respiratory defect of *grr1Δ* strains.

The patterns of Glc7 modification throughout our various experiments also provide support for the increased lag phase model. We showed that that the levels of the modified forms of Glc7 were reduced considerably as wild-type and *grr1Δ* cells were grown on decreasing glucose concentrations. However, in this set of experiments, we did not measure differences in the levels of the modified forms of Glc7 between wild-type and *grr1Δ* strains. This is in contrast to the previous two blots (Figure 5.6 A and 5.6 B) where a difference in the expression levels of the modified forms of Glc7 was observed between wild-type and *grr1Δ* cells. We believe that these differences can be explained by the differences in the way in which these experiments were conducted. In the first experiments (Figure 5.6 A and B), cells were grown to stationary phase, inoculated into fresh culture and protein extraction was carried out at the indicated cell density. In the second set of experiments (Figure 5.6 C) each culture was grown to mid-log phase in media of the appropriate glucose concentration, inoculated into fresh media of the same glucose concentration, and protein was extracted at the indicated cell density. Thus, we believe that the *grr1Δ* cells in the second set of experiment were not compromised by their inability to re-adjust to the change in media conditions because these cultures were inoculated from mid-log phase cultures. Therefore, the difference in expression of the modified forms of Glc7

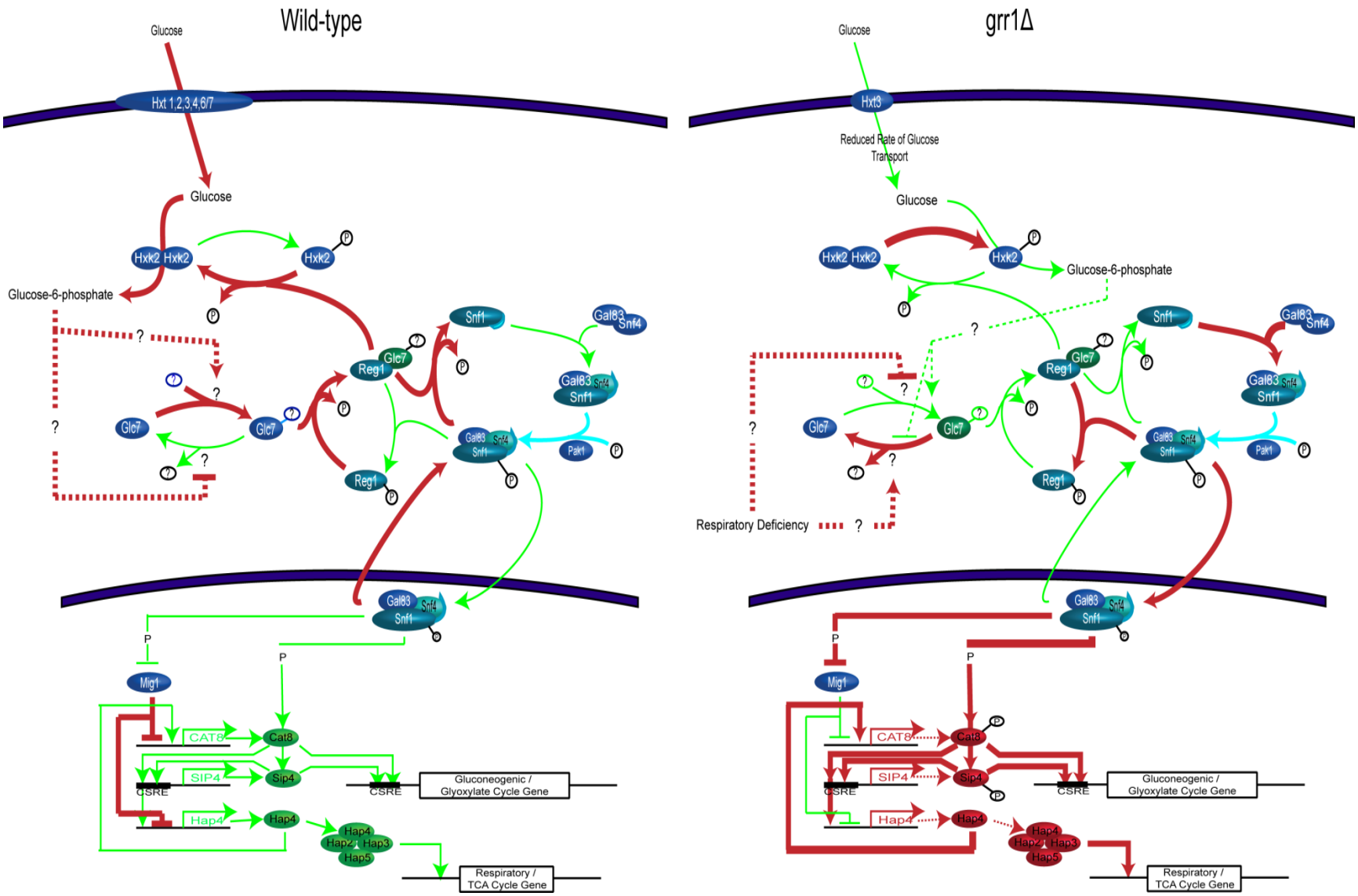
Wild-type
Glucose
Hxt 1,2,3,4,6/7
Glucose
Hxk2 Hxk2
Hxk2
Glucose-6-phosphate
Glc7
Reg1
Snf1
Gal83 Snf4
Pak1
Mig1
CAT8
Cat8
SIP4
Sip4
Hap4
Hap2/3/4/5
CSRE
Gluconeogenic / Glyoxylate Cycle Gene
Respiratory / TCA Cycle Gene
grr1Δ
Hxt3
Reduced Rate of Glucose Transport
Respiratory Deficiency

**Figure 6.2. Final Model for Intracellular Glucose Signaling Through the Hxk2/Reg1-Glc7/Snf1 Dependent Pathway in wild-type and *grr1Δ* Cells.** A model for intracellular glucose signaling through the Hxk2/Reg1-Glc7/Snf1 dependent pathway in *grr1Δ* and wild-type strains is proposed based off of data from our present analysis as well as the current literature regarding regulation of this pathway. Increased and decreased pathways are indicated by solid red lines and green lines, respectively. Constitutively, active pathways are indicated in blue. Unknown regulatory events are indicated by dashed lines and the presumed activity of these regulatory events are indicated by color with red indicating increased activity and green indicating decreased activity. Decreased expression of a particular gene or protein is indicated by the color of the gene (bent arrow) or protein (node) with red indicating increased expression, green indicating decreased expression, and blue indicating no change in expression. The circled question mark indicated as a modification of Glc7 represents the modified forms of Glc7 detected in our analysis. See text for description.

between wild-type and *grr1Δ* strains is dependent on the precise phase at which the protein extracts are taken. Though we presently favor this model, it is possible that one or a number of the pleiotrophic nutrient defects inherent in *grr1Δ* strains leads to the differential expression of modified forms of Glc7. Thus, further analysis is needed to determine the specific conditions that lead to differential expression of the modified forms of Glc7. Nevertheless, the expression levels of these modified forms decreases as the glucose concentration decreases suggesting that the intracellular signal modulating the presence of these forms is in some way influenced by glucose.

Given these data the following model is proposed for intracellular glucose signaling through the Hxk2/Reg1/Glc7/Snf1 pathway in *grr1Δ* and wild-type strains grown on glucose. In the presence of glucose, in wild-type strains, glucose is transported through any one of the hexose transporters, Hxt1, 2, 3, 4, and/or 6/7 depending on the external glucose concentration. Transport of glucose in wild-type strains is of sufficient capacity to support high glycolytic flux which through an unknown mechanism (possibly increased glucose-6-phosphate) leads to increased expression of the modified forms of Glc7. Presumably, the modified forms of Glc7 would interact more favorably with Reg1. Reg1-Glc7 then catalyzes the de-phosphorylation of Hxk2 leading to Hxk2 dimerization which supports higher glycolytic flux and thus serves as a positive feedback loop promoting further Reg1-Glc7 interaction. Reg1-Glc7 also de-activates Snf1 kinase through de-phosphorylation of threonine-210 in the activation loop of Snf1. De-phosphorylation of Snf1 leads to auto-inhibition as

the regulatory domain of Snf1 is now free to mask threonine-210 preventing phosphorylation by the Snf1 activating kinase, Pak1. Inactivation of Snf1 also prevents its Gal83 dependent nuclear translocation thus preventing Snf1 dependent phosphorylation and de-activation of the nuclear localized Mig1 repressor. Active Mig1 represses expression of the respiratory transcription factor gene, *HAP4*, as well as the gluconeogenic and glyoxylate cycle transcription factor genes, *CAT8* and *SIP4*.

In the presence of glucose, in *grr1Δ* cells, glucose based growth is facilitated predominately by the low affinity glucose transporter, Hxt3. However, glucose transport through Hxt3 is insufficient to support a high glycolytic flux. Reduced glycolytic flux in *grr1Δ* strains leads to an increased dependency on respiration to fulfill the energy demands of the cell but *grr1Δ* strains possess a respiratory deficiency and thus cannot appropriately increase respiratory capacity. The combination of decreased glycolytic flux in the presence of decreased respiratory capacity leads to reduced expression of the modified forms of Glc7 (again through an unknown mechanism). The reduced expression of the modified forms of Glc7 reduces Reg1-Glc7 interaction which subsequently reduces the accumulation of dimerized Hxk2. The presence of monomeric Hxk2 reduces the glycolytic flux in accordance with the reduced transport capacity. At the same time, the reduction of Reg1-Glc7 interaction leads to enhanced Snf1 phosphorylation and Gal83 dependent nuclear localization. Catalytically active nuclear localized Snf1-Gal83-Snf4 phosphorylates Mig1, inhibiting Mig1 repression of the respiratory transcription factor gene, *HAP4*, as well as the gluconeogenic and glyoxylate cycle transcription factor genes, *CAT8* and *SIP4*. Additionally, catalytically active nuclear localized Snf1-Gal83-Snf4 phosphorylates and activates the transcriptional activity of Cat8 and Sip4 leading to gluconeogenic and glyoxylate cycle gene expression. Gluconeogenic and glyoxylate cycle enzymes are then actively expressed in *grr1Δ* cells to provide metabolic intermediates to the TCA cycle to support supplementation of respiratory capacity through glycerol based growth.

# CHAPTER 7: DISCUSSION: GENE AND PROTEIN DISCORDANCE AND ITS IMPLICATIONS IN *grr1Δ* CELLS

## 7.1. Reasons for Discordance between Protein Expression and Gene Expression

While the high degree of discordance between mRNA and protein expression levels in our analysis is counter-intuitive, the lack of accordance between protein and mRNA expression levels has been observed in other studies. Several studies have been conducted comparing transcriptional expression levels to protein expression levels with only weak positive correlations observed [482-487]. This absence of correlation is perplexing and raises a number of questions. First, what are the origins of discordance? Are they biological or are they simply a byproduct of the inherent noise of our analyses? If biological, from what molecular regulatory level does most discordance arise? These and many other questions must be addressed in order to begin to predict protein expression levels from transcriptional expression levels. However, based on the primary type of discordance observed in our analysis (no change in gene expression despite large changes in protein expression) it seems doubtful that extrapolation from gene expression for a large percentage of the proteome will ever be able to be achieved, thus necessitating the need for independent protein measurements.

Regarding the origins of discordance, at least four sources can be hypothesized. Perhaps the most obvious factors contributing to protein and gene expression discordance is the existence of independent regulation of protein synthesis and protein degradation. Early investigators showed that dynamic regulation of both of these processes serves as an important mechanism governing the activity of enzymes, transporters, and regulatory proteins, and multiple examples illustrating uncoupled regulation of transcriptional and post-transcriptional regulation exist. For instance, regulation of the transcriptional activator, Gcn4, is almost exclusively controlled by translational rate and the rate of protein degradation [488] and regulated proteolysis of cell cycle regulators such

as the cyclins and cyclin dependent kinase inhibitors is critical to proper cell cycle progression [489,80,490,491]. Furthermore, numerous nutrient transporters and enzymes are rapidly inactivated by protein degradation in response to changes in the extracellular nutrient composition [492-496]. Thus, if any model for extrapolating gene expression levels to determine protein expression levels is to be viable, rates of both protein synthesis and degradation under the conditions utilized must be taken into account.

A number of computational analyses have been conducted in an effort to corroborate the discordance between protein and gene expression by taking into account protein synthesis and degradation rates. While insightful, these analyses have had limited success. Independent studies have provided estimates for translation rate [497], ribosome density [498], and protein half life [499] across the yeast genome. In order to account for differences in translational rate that most likely contribute to discordance, correlations of protein and mRNA abundance have been conducted by accounting for ribosome density (distribution of ribosomes on a mRNA) and ribosome occupancy (number of ribosomes bound to an mRNA) of yeast mRNA concertedly. Higher correlations were observed for ORFs possessing high levels of ribosomal occupancy and lower correlations observed for those transcripts possessing low occupancy [482,486]; however, even considering these attributes the increase in correlation was subtle and only applied to a fraction of the genome. In a more extensive analysis, conducted by [486], these measurements as well as other parameters such as protein abundance, mRNA abundance, and transcript length were utilized to calculate a protein half life descriptor (PHD) measure. This value was constructed to provide a calculated protein half life measure that could be utilized to corroborate the lack of correlation between protein and mRNA expression levels. However, while the “PHD” measure correlated well with known half-lives and underscored the tremendous variability between individual proteins with regards to protein turnover rate, it was not utilized to correct for discordance observed between individual transcripts and their respective proteins.

Nevertheless, the authors noted that protein turnover as well as protein synthesis rates are the most correlative predictors of steady state protein levels in the cell.

The third and perhaps most under appreciated contributor to discordance is the mRNA degradation rate of the transcript. A number of transcripts including *SDH2* which encodes the iron protein subunit of succinate dehydrogenase [500], *CYC1* which encodes cytochrome c [501,502], *MAL62* which encodes maltase [503], *SUC2* which encodes invertase [504], *PCK1* which encodes pep carboxy-kinase, *FBP1* which encodes fructose-1,6-bisphosphatase [476], and the meiotic mRNA of *SPO13* [505] are promoted for rapid degradation when glucose is introduced to cells growing on respiratory carbon sources. Though examples of control of mRNA degradation are limited to transcripts subject to glucose repression, it seems reasonable to think that more mRNAs in yeast will be found subject to this type of regulation. If so, the steady state level of the mRNA abundance contributed to by both mRNA synthesis (transcription) and mRNA degradation could be potential regulatory points where discordance could be elicited.

A fourth factor potentially contributing to mRNA/protein discordance is the presence of manufactured systematic noise in global gene and protein expression data sets. Systematic noise in protein expression data sets is most likely much greater than noise present in genomic data sets given the relative immaturity of the experimental processes utilized to attain quantitative protein measurements. In my descriptions of our proteomic analyses I mentioned that differential post-translational modifications on peptides for a given protein could contribute to inaccurate estimates of the protein steady state level. I believe that these phenomena may be the most important factor contributing to what would be considered experimental noise in shotgun based proteomic analyses. Here I will describe the technical origins of this problem and provide biological support for the existence of this phenomena in the *grr1Δ* proteomic data set.

Differential modification of peptides (i.e. phosphorylated in one sample but not the other) can lead to differences in chromatographic retention times between the modified (i.e. phosphorylated) and unmodified peptide. In shotgun based proteomic analyses, proteins are digested utilizing proteolytic enzymes to

produce more readily analyzable peptide fragments and these peptides are then separated utilizing any number of chromatographic separation techniques. In this study we utilized a two dimensional separation system known as MudPIT (For review see Section 3.11.3). The first phase of this separation system utilizes a strong cation exchange stationary phase to retain peptides based on their charge. The more positive the charge the higher the affinity the peptide has for the stationary phase. The total yeast peptide population bound to the SCX column is then separated into 12 discrete populations by utilizing isocratic elutions of increasing salt concentration. Thus, the average positive charge/peptide between peptide populations would increase as the salt concentration increases in later elutions. The presence of a modification of either negative or positive polarity substantially alters the peptides charge state and thus the affinity of that peptide for the SCX stationary phase. For instance, a phosphorylated serine or threonine would decrease the net positive charge of the peptide compared to the un-phosphorylated version of the peptide. This phosphopeptide would thus, in most instances, elute in an earlier isocratic salt fraction than its respective un-phosphorylated version [506]. Each isocratic salt elution is followed by a 90 minute reverse phase separation which resolves peptides based on their hydrophobicity. Peptide modifications such as phosphorylation have been found to decrease or increase a peptides retention time in reverse phase columns as well [507].

As peptides elute from the reverse phase column their mass to charge ratio as well as their CID (collision induced dissociation) spectra are acquired through mass spectrometric analysis. Identification of the peptide is facilitated by searching the experimentally acquired CID spectra against a theoretically determined CID spectral library. This theoretical library is generated computationally utilizing protein sequence information obtained for the appropriate organism (in our case *S. cerevisiae*) obtained from the appropriate protein sequence database (in our case the *Saccharomyces* Genome Database ftp://ftp.yeastgenome.org/yeast/(July 2006)).Theoretical digestion of the protein sequences is performed by specifying the particular enzymatic protease. Each

protease targets defined sites for proteolytic cleavage (i.e. trypsin cleaves C-terminal to arginine and lysine residues) and thus proteins from the sequence database can be computationally digested based upon these specificities. The particular algorithm then calculates the theoretical mass to charge ratio of the theoretical, in this case, tryptic peptide. At this stage, since post-translational modifications alter the mass to charge ratio of the peptide, post-translational modifications must be specified *a priori*. Thus, in order to identify a modified peptide, knowledge of its modification would have to be known in order generate an *in silico* theoretical library that included the specific modification on the peptide with the correct mass to charge ratio. Given the large number of different types of modifications as well as the combinations and number of modifications that could occur on a particular peptide, a theoretical library containing these permutations would be immense and practically unsearchable. As a result, most searches are performed utilizing only a few modifications and thus many modified peptides remain unidentifiable. Additionally, post-translational modifications greatly alter the experimentally acquired CID pattern of the peptide further complicating the ability to successfully identify these modified forms [508].

The altered chromatographic retention time, mass to charge ratio, and CID spectra of modified forms of a particular peptide together lead to relative quantitative peptide measures that are not reflective of the relative protein abundance but of the extent of post-translational modification of the peptide between the samples being compared. Typically, due to the aforementioned complications, only the unmodified peptide is detectable. Once a peptide has been detected, its chromatographic elution profile is reconstructed using the ion intensities for the parent ion across multiple MS scans. This typically creates a bell shaped curve whose area is determined through integration. The chromatographic elution profile of the peptide partner from the other sample is then also reconstructed by utilizing the same steps. However, if the peptide partner was not identified, the partner is assumed to elute with the identified peptide at a mass to charge ratio calculated by the size of the label utilized. A relative quantitative measure of the particular peptide is then generated by

dividing the area of one peptide elution profile by the other. Thus, if a peptide were differentially modified and thus undetectable, quantification utilizing these methods would lead to a relative peptide measure that would indicate that the peptide is more abundant in the sample containing the unmodified version of the peptide. This would therefore either completely bias the relative protein measure (if it was one of only a few peptides measured for a given protein) or skew the relative protein abundance (if it was one of multiple peptides identified for a given protein) toward a higher or lower relative abundance difference.

In order to reduce the bias contributed by peptide modifications to relative protein expression measures, analysis of shotgun based proteomic data must be restricted to only those proteins for which multiple distinct peptide sequences were identified and quantitated. However, these restrictions severely reduce proteomic coverage due to the dynamic range (sensitivity) limitations of these analyses and eliminate potentially valuable biological information pertaining to differential post-translational regulation of the protein. A solution to the dynamic range problem inherent in shotgun based whole proteome analyses known as SRM, for selected reaction monitoring, can be applied to increase coverage of a predetermined set of proteins and offers a valuable follow up method to global analyses. Recently, a variation of this technique was applied to successfully detect and quantify low abundance proteins of the TCA cycle, gluconeogenesis, glycolysis, and the glyoxylate cycle with extremely accurate results [509].

## 7.2. Type 1 Discordance: Instances of Inverted Gene and Protein Expression Levels are Likely Due to Manufactured Systematic Noise from Peptide Modifications in Proteomic Data Sets

Our comparative analysis of global gene and protein expression levels revealed a large degree of discordance between these two regulatory levels in *grr1Δ* cells. The discordance measured can be grouped into three different types depending upon the nature of the discordance. The first type includes those loci where mRNA was observed to significantly increase and the change in the gene product expression level was measured to show an inverse correlation,

decreasing in abundance. This group of loci was smallest among discordant loci and included *EMP46* and its product involved in COPII ER to Golgi transport protein (mRNA +2.1 in *grr1Δ*, protein -5.9 in *grr1Δ*), *MCR1* and its product, the mitochondrial NADH-cytochrome b5 reductase (+2.04, -12.5), *ATP19* an its product, the k subunit of the F1F0 ATP synthase (+2.5, -2.5), *NDI1* and its product, the NADH:ubiquinone oxidoreductase (+3.76, -2.86), *IDH2* and its product, the mitochondrial NAD(+)-dependent isocitrate dehydrogenase (+3.03, -6.25), *ACH1* and its product, the mitochondrial acetate detoxification enzyme (+4.03, -5.56), and *HXT7* and its product, the high affinity hexose transporter (+4.62, -2.56). Though in the instance of Hxt7, the measured discordance is indeed true, as shown in our results (Figure 5.1), the other instances for the most part likely represent discordance attributed to systematic noise due to possible post-translational modifications. Idh2 was quantified as bronze by one peptide (KTFGLFANRVPAK) with a peptide probability of 0.59. However, it is interesting to note that another peptide (pTGDLAGTATTSSFTEAVIK) for this protein was also identified and quantitated in our analysis with a relative abundance of 0 (these are not included in our analysis due to a high degree of noise among proteins quantitated with 0 or 999 values). The peptide phosphorylation (indicated by the lowercase p) was identified in a mass spectrometry screen mapping sites of phosphorylation on mitochondrial proteins [510]. Thus our data suggest that it is phosphorylated in *grr1Δ* cells. The remaining proteins Ndi1 (ARPVITDLFK), Emp46 (QGNEGDSTELFGGSSK), Ach1 (AIAGHLVEFFR), Mcr1 (GSNVVRPYTPVSDLSQK), and Atp19 (AIPPHQLAIGTLGLLGLLVVPNPF-K) were all quantified by a single peptide (indicated in parentheses). Taken together the majority of the instances of discordance measured within this group are probably false positives for significant changes in protein abundance as the relative peptide abundances are most likely due to differential modification of the quantitated peptide. Nevertheless, these data may indeed reflect the actual steady state protein level or may indicate important regulatory modifications of these proteins on these peptide sequences. Therefore, these data were included in the analysis.

### 7.3. Type 2 Discordance: Changes in Protein Expression Occurring in the Absence of Significant Changes in Gene Expression

The second type of discordance measured included loci where no change in gene expression was measured while protein expression was measured to significantly increase or decrease. This type of discordance was the most prominent in our analysis including 86% (286 of 333) of all discordant loci. Loci within this discordance group were closely split between proteins measured to significantly increase (48.6%) and proteins measured to significantly decrease (51.4%). These data suggest that a large number of proteins may be exclusively controlled through post-transcriptional mechanisms and that these post-transcriptional regulatory mechanisms are affected by the absence of Grr1.

Given the role that Grr1 plays in regulating protein stability through ubiquitin dependent degradation, a number of the proteins measured to increase could in fact be direct targets of Grr1 mediated ubiquitylation. At the same time, a number of the alterations in protein steady state levels within this category of discordance could be affected in *grr1Δ* strains indirectly as part of a compensatory response to correct for deficiencies that are directly caused by *GRR1* deletion. Distinguishing between these two possibilities for each discordant locus poses a significant challenge, since extensive scientific analyses must be implemented to unravel the direct cause of each perturbation individually. However, biological insight pertaining to the role that Grr1 plays in the biology of the cell can be extracted from large scale datasets by determining the processes most affected by the absence of *GRR1*. To this end, we implemented an automated as well as a manual GO (Gene Ontology) annotation strategy to group proteins with significantly altered expression in *grr1Δ* strains by shared molecular processes. The enrichment for each process among significantly changed protein was then determined. Enrichment of several molecular processes was found among proteins exhibiting discordance of the second type described above and the role of Grr1 in several processes is supported by previous analyses.

### 7.3.1. Type 2 Discordance among Trafficking Proteins in *grr1Δ* Cells

Manual GO analysis of enriched processes revealed that the process "trafficking" encompassed 19.9% (60 total proteins) of all discordant loci of the second type. This was the most highly enriched process within this group and included proteins involved in the dynamics of actin, microtubule, vesicle, and glycosylation function. Thus our definition of "trafficking" encompassed a diverse array of processes that all affect the movement of proteins and vesicles within the cell. GenGO analysis revealed more specifically that the processes "membrane invagination" and "budding cell apical bud growth", which fall under our manual annotation of "trafficking" proteins, were significantly enriched among these discordant loci. As can be seen in Figure 1.4, *grr1Δ* cells exhibit multiple elongated buds which is a phenotype attributed to the role of Grr1 in degrading the G1 cyclins, Cln1 and Cln2, as well as the Cdc42 effectors Gic1 and Gic2. Given this role for Grr1, the enrichment observed for proteins annotated to "budding cell apical bud growth" is well substantiated. In fact, the majority of protein expression changes within the enriched process of "trafficking" may be attributable to downstream events initiated from stabilization of the Clns and the Gics in *grr1Δ* cells as drastic alterations in actin, microtubule, and secretory processes are necessary to promote polarized growth [511].

The role of Grr1 in "trafficking" is not strictly limited to its function in regulating Cln and Gic stability. The glucose induced inactivation of the maltose transporter, Mal61 [512], and the galactose transporter, Gal2 [512], has been shown to require Grr1. In response to glucose both of these proteins are ubiquitylated by the HECT type ubiquitin ligase, Rsp5, which promotes their internalization and vacuolar degradation [513,514]. Therefore, Grr1 does not catalyze the ubiquitylation of these transporters directly, suggesting an indirect mechanism for Grr1 mediated control of maltose and galactose transporter stability.

Interestingly, the GO process of membrane invagination (endocytosis) was found to be enriched by GenGO analysis of protein expression changes in *grr1Δ* cells. Grr1 was found by two hybrid analysis to bind to Bzz1 [448], which was measured to increase 6.39 fold in *grr1Δ* cells by our proteomic analysis. Bzz1

has been found to localize to actin patches and is implicated in the regulation of actin polymerization and endocytosis through its association with the yeast homolog to the human Wiskott-Aldrich syndrome protein (WASP), Las17 [449]. Interestingly, the Bzz1 protein contains a N-terminal FCH bar domain, PEST sequences, and a C-terminal SH3 domain that are all present in a known Grr1 substrate, Hof1 [54]. Based on these observations it has been suggested that Bzz1 may be a substrate for $SCF^{Grr1}$ mediated ubiquitylation and the increase in Bzz1 protein levels measured in our analysis is consistent with this hypothesis. It is tempting to speculate that the role of Grr1 in glucose dependent de-activation of the maltose and galactose permeases is through de-stabilization of Bzz1 or another Bzz1 or Hof1-like protein.

We were curious to determine through network analysis whether a link could be made between Las17/Bzz1 function and the maltose and galactose transporters (Figure 7.1). Interestingly, physical interactions have been detected between Las17 and only two transporters, Gal2 and Hxt6/7. No interaction between Las17 and the maltose transporter is in our database. Nevertheless, since Gal2 inactivation is known to be Grr1 dependent, since Hxt6/7 may be differentially trafficked in Grr1 strains, and since these two proteins interact physically with Las17 suggests that Grr1 influences Las17 function to control endocytosis of these proteins. This control may be exerted through Grr1 dependent degradation of the Las17 effector, Bzz1, or through another unknown protein. Interestingly, Yck2, which is involved in several Grr1 dependent processes, most notably the Snf3/Rgt2 pathway and the SPS pathway, also has biochemical activity towards Las17 and Bzz1 [515]. Additionally, a Las17/Bzz1/Vrp1 complex has been found to regulate cortical actin patch assembly by activating the Arp2/3 complex [516]. This complex is recruited to Cdc42 and activated by a Cdc42 dependent mechanism [517]. Grr1 controls Cdc42 activity by controlling Cln2 stability [346,104] and Gic1 and Gic2 stability [55,101]. Together, this data suggests that Grr1 may play a multifaceted role in regulating membrane dynamics through regulation of cortical actin patches in a Cdc42/Las17 dependent manner.

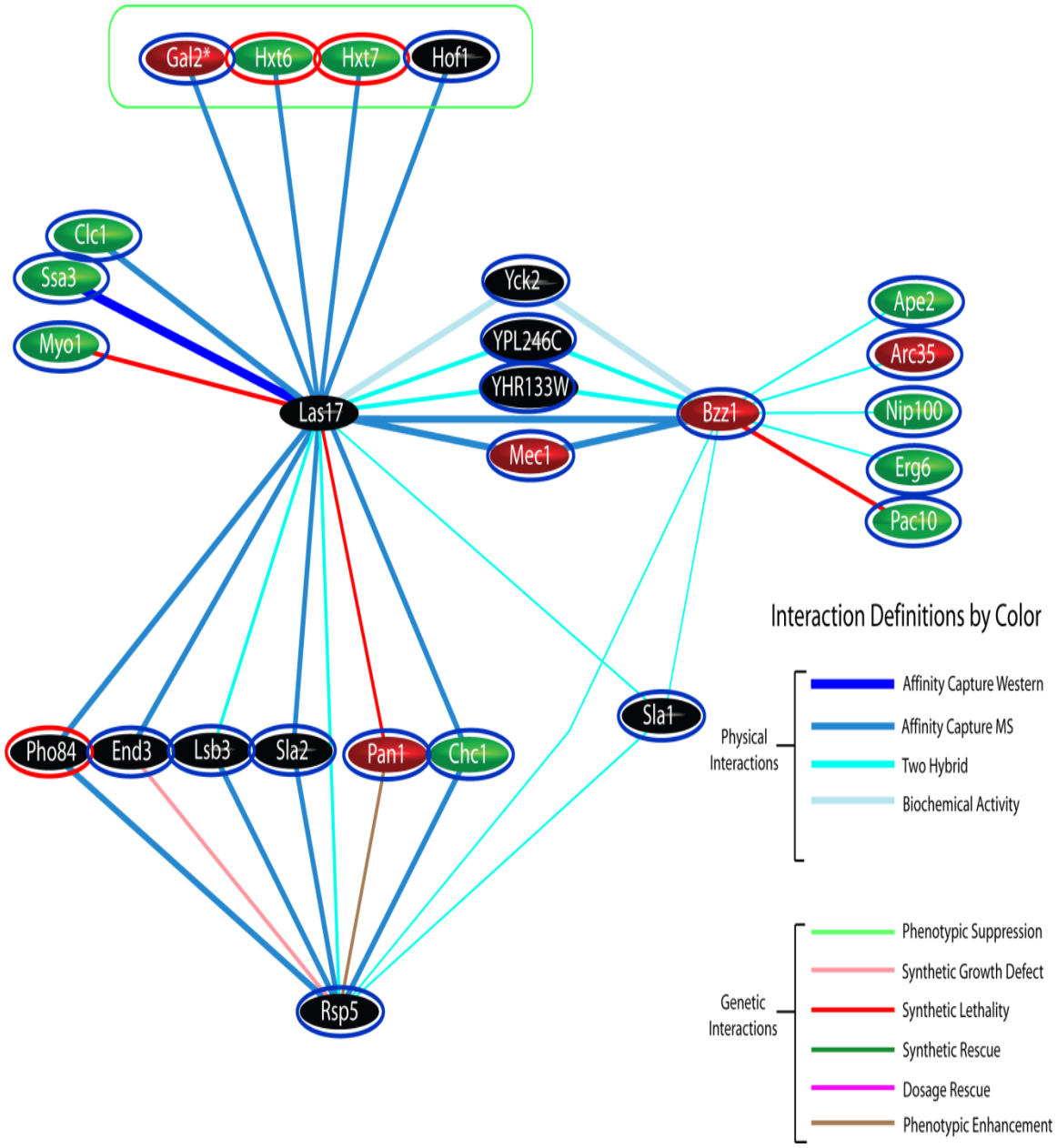


**Figure 7.1. Interaction Network Linking Las17/Bzz1 to Transporter Proteins Affected in *grr1Δ* Cells.** An interaction network was constructed utilizing interaction data from the *Saccharomyces* Genome Database (July, 2006 version) and the network visualization tool, ProteoLens™. Physical interactions between the Las17 and the transporters Gal2 and Hxt6/7 were found in previous analyses. Trafficking of the Gal2 transporter has been shown to be effected in *grr1Δ* cells through an unknown mechanism leading to Gal2 stability *[495,518]. In our analysis, Hxt6/7 stability is also affected in *grr1Δ* strains (see Section 5.2). Hof1 is a known Grr1 substrate [54] and Bzz1 contains many of the protein domains present in Hof1 (see text). Bzz1 is a known Las17 effector that is thought to recruit actin polymerization machinery during endocytosis [449]. Given these facts and the fact that a number of proteins which interact with Bzz1 and Las17 are measured to have increased (red) or decreased (green) protein levels, a role for Grr1 in endocytosis through Bzz1 is highly likely.

7.3.2. Type 2 Discordance among Proteins Annotated to “Mitosis” or “M phase of the Meiotic Cell Cycle”

An interesting observation from the gene expression data is that, despite the well studied role for Grr1 in mediating the proteasomal degradation of the G1 cyclins Cln1 and Cln2 to regulate G1/S phase progression, no changes in cell cycle genes are measured as significantly changed. In fact, no evidence of Grr1’s role in cell cycle regulation is apparent at the transcriptional level with the exception of the 2 fold increase in *CLN1* expression. Overall, these data are commensurate with previous gene expression studies performed on *grr1Δ* cells [159].

Interestingly, 8.6% of the significant changes in protein expression in *grr1Δ* strains possessed known roles in mitosis. Our manual GO annotation and GenGO analysis revealed that the process “M phase of the meiotic cell cycle” was significantly enriched among proteins with significant changes in protein expression in *grr1Δ* cells. Proteins within this GO process of “Gold” or “Silver” confidence included proteins involved in regulating microtubule and spindle dynamics (Myo1 (-3.45 fold change in protein expression in *grr1Δ* cells), Inn1 (-6.67), Src1 (-16.67), Slk19 (-2.70), Ady3 (-3.33), Bbp1 (+12.35), Dyn1 (+39.24), Arp10 (+4.03), Kar3 (+5.97), YNL313 (+14.43), and YJL051 (+28.31)), proteins involved in regulating actin dynamics (Sds23 (-3.57), Sds24 (-5.00), Rga2 (-5.26), Bnr1 (-4.00), Ady4 (+6.19), Pan1 (+8.87), and Cla4 (-10.00)), transcription factors regulating mitotic genes (Hcm1 (-10.00) and Sum1 (+2.80)), the APC/Cyclosome activating protein Cdh1 (-4.35), and various other proteins involved in some capacity in mediating mitosis (Ulp2 (+5.03), Cdc37 (-5.26), Glc7 (+4.35), Tor1 (+23.10), Hop1 (+3.05), Scp160 (+3.60), Msh5 (+5.69), and Mec1(+4.20)). Interestingly, of these proteins, no significant change in gene expression was measured for any. Together this data suggests that the cell cycle defects associated with *grr1Δ* strains manifest at the post-transcriptional level in M phase of the cell cycle.

It has been previously established that a significant fraction of *grr1Δ* cells possess a 2N DNA content (92% compared to 55% of wild-type) [78,77] which has

been suggested to be a consequence of premature entry into S phase. This hypothesis is based on the fact that premature advancement through the G1-S phase transition is observed in cells expressing stabilized versions of Cln2 [82] and that Cln2 stability is increased in *grr1Δ* cells from a half life of 10 minutes to over 30 minutes [78]. Stabilization of Cln1 and Cln2 promote premature phosphorylation and degradation of the Clb-Cdc28 inhibitor Sic1 which promotes early entry into S phase. Interestingly, many of the mitotic proteins with significantly altered protein expression have been found to be potential substrates of the Sic1 inhibited Clb2-Cdc28 kinase (Figure 4.9 B) suggesting that hyperactive Clb2-Cdc28 kinase activity may contribute to many of the protein expression level changes in mitotic proteins measured in *grr1Δ* cells. Additionally, Grr1 has been shown to mediate the timely degradation of the Hof1 protein required for cytokinesis and a fraction of cells harboring stabilized versions of Hof1 arrest in cytokinesis. Thus, the mother and the daughter cell continue to share the same cytoplasm [54]. Therefore, it is possible that many of the measured changes in protein expression are a consequence of Grr1's role in degrading the Clns and Hof1. However given the extent to which mitotic protein expression levels are altered and the number measured to change it seems likely that additional roles for Grr1 in regulating mitosis remain to be uncovered; specifically with regards to regulating spindle dynamics.

### 7.4. Type 3 Discordance: Changes in Gene Expression Occurring in the Absence of Significant Changes in Protein Expression

The third type of discordance measured in our analysis included significant changes in gene expression with no concomitant change in the gene products expression. This type of discordance was observed exclusively among loci annotated to "carbon and energy metabolism". The biological relevance of this discordance was studied in Chapter 5 and discussed in Chapter 6.

## REFERENCES


1. Huynh MA, Stegmüller J, Litterman N, Bonni A. Regulation of Cdh1-APC function in axon growth by Cdh1 phosphorylation. *J. Neurosci*. 2009;29(13):4322-4327.

2. Fu W, Ma Q, Chen L, et al. MDM2 acts downstream of p53 as an E3 ligase to promote FOXO ubiquitination and degradation. *J. Biol. Chem*. 2009;284(21):13987-14000.

3. Bhoj VG, Chen ZJ. Ubiquitylation in innate and adaptive immunity. *Nature*. 2009;458(7237):430-437.

4. Choi K, Bae M, Jeong J, Moon H, Kim K. Hypoxia-induced angiogenesis during carcinogenesis. *J. Biochem. Mol. Biol*. 2003;36(1):120-127.

5. Petroski MD. The ubiquitin system, disease, and drug discovery. *BMC Biochem*. 2008;9 Suppl 1:S7.

6. Miki Y, Swensen J, Shattuck-Eidens D, et al. A strong candidate for the breast and ovarian cancer susceptibility gene BRCA1. *Science*. 1994;266(5182):66-71.

7. Futreal PA, Liu Q, Shattuck-Eidens D, et al. BRCA1 mutations in primary breast and ovarian carcinomas. *Science*. 1994;266(5182):120-2.

8. Liu J, Stevens J, Rote CA, et al. Siah-1 mediates a novel beta-catenin degradation pathway linking p53 to the adenomatous polyposis coli protein. *Mol Cell*. 2001;7(5):927-36.

9. Latres E, Chiaur DS, Pagano M. The human F box protein beta-Trcp associates with the Cul1/Skp1 complex and regulates the stability of beta-catenin. *Oncogene*. 1999;18(4):849-54.

10. Winston JT, Strack P, Beer-Romero P, et al. The SCFbeta-TRCP-ubiquitin ligase complex associates specifically with phosphorylated destruction motifs in IkappaBalpha and beta-catenin and stimulates IkappaBalpha ubiquitination in vitro. *Genes Dev*. 1999;13(3):270-83.

11. Beaudenon S, Huibregtse JM. HPV E6, E6AP and cervical cancer. *BMC Biochem*. 2008;9 Suppl 1:S4.

12. Wang J, Sampath A, Raychaudhuri P, Bagchi S. Both Rb and E7 are regulated by the ubiquitin proteasome pathway in HPV-containing cervical tumor cells. *Oncogene*. 2001;20(34):4740-9.

13. Margottin F, Bour SP, Durand H, et al. A novel human WD protein, h-beta TrCp, that interacts with HIV-1 Vpu connects CD4 to the ER degradation pathway through an F-box motif. *Mol Cell*. 1998;1(4):565-74.

14. Schubert U, Antón LC, Bacík I, et al. CD4 glycoprotein degradation induced by human immunodeficiency virus type 1 Vpu protein requires the function of proteasomes and the ubiquitin-conjugating pathway. *J Virol*. 1998;72(3):2280-8.

15. Yu X, Yu Y, Liu B, et al. Induction of APOBEC3G ubiquitination and degradation by an HIV-1 Vif-Cul5-SCF complex. *Science*. 2003;302(5647):1056-60.

16. Belaïdouni N, Marchal C, Benarous R, Besnard-Guérin C. Involvement of the betaTrCP in the ubiquitination and stability of the HIV-1 Vpu protein. *Biochem Biophys Res Commun*. 2007;357(3):688-93.

17. Sheehy AM, Gaddis NC, Malim MH. The antiretroviral enzyme APOBEC3G is degraded by the proteasome in response to HIV-1 Vif. *Nat Med*. 2003;9(11):1404-7.

18. Shirakawa K, Takaori-Kondo A, Kobayashi M, et al. Ubiquitination of APOBEC3 proteins by the Vif-Cullin5-ElonginB-ElonginC complex. *Virology*. 2006;344(2):263-6.

19. Coscoy L, Sanchez DJ, Ganem D. A novel class of herpesvirus-encoded membrane-bound E3 ubiquitin ligases regulates endocytosis of proteins involved in immune recognition. *J Cell Biol*. 2001;155(7):1265-73.

20. Coscoy L, Ganem D. Kaposi's sarcoma-associated herpesvirus encodes two proteins that block cell surface display of MHC class I chains by enhancing their endocytosis. *Proc Natl Acad Sci U S A*. 2000;97(14):8051-6.

21. Duncan LM, Piper S, Dodd RB, et al. Lysine-63-linked ubiquitination is required for endolysosomal degradation of class I molecules. *EMBO J*. 2006;25(8):1635-45.

22. Hewitt EW, Duncan L, Mufti D, et al. Ubiquitylation of MHC class I by the K3 viral protein signals internalization and TSG101-dependent degradation. *EMBO J*. 2002;21(10):2418-29.

23. Tank EMH, True HL. Disease-associated mutant ubiquitin causes proteasomal impairment and enhances the toxicity of protein aggregates. *PLoS Genet*. 2009;5(2):e1000382.

24. Muñoz U, Bartolomé F, Bermejo F, Martín-Requero A. Enhanced proteasome-dependent degradation of the CDK inhibitor p27(kip1) in immortalized lymphocytes from Alzheimer's dementia patients. *Neurobiol Aging*. 2008;29(10):1474-84.

25. Gong C, Liu F, Grundke-Iqbal I, Iqbal K. Post-translational modifications of tau protein in Alzheimer's disease. *J Neural Transm*. 2005;112(6):813-38.

26. Arias-Vásquez A, de Lau L, Pardo L, et al. Relationship of the Ubiquilin 1 gene with Alzheimer's and Parkinson's disease and cognitive function. *Neurosci Lett*. 2007;424(1):1-5.

27. Hristova VA, Beasley SA, Rylett RJ, Shaw GS. Identification of a novel Zn2+-binding domain in the autosomal recessive juvenile parkinson's related E3 ligase parkin. *J Biol Chem*. 2009. Available at: http://www.ncbi.nlm.nih.gov/pubmed/19339245 [Accessed April 18, 2009].

28. Li H, Guo M. Protein degradation in Parkinson disease revisited: it's complex. *J Clin Invest*. 2009;119(3):442-5.

29. Wong HK, Bauer PO, Kurosawa M, et al. Blocking acid-sensing ion channel 1 alleviates Huntington's disease pathology via an ubiquitin-proteasome system-dependent mechanism. *Hum Mol Genet*. 2008;17(20):3223-35.

30. Finkbeiner S, Mitra S. The ubiquitin-proteasome pathway in Huntington's disease. *ScientificWorldJournal*. 2008;8:421-33.

31. Ciechanover A, Heller H, Elias S, Haas AL, Hershko A. ATP-dependent conjugation of reticulocyte proteins with the polypeptide required for protein degradation. *Proc. Natl. Acad. Sci. U.S.A*. 1980;77(3):1365-8.

32. Hershko A, Ciechanover A, Heller H, Haas AL, Rose IA. Proposed role of ATP in protein breakdown: conjugation of protein with multiple chains of the polypeptide of ATP-dependent proteolysis. *Proc. Natl. Acad. Sci. U.S.A*. 1980;77(4):1783-6.

33. Chau V, Tobias JW, Bachmair A, et al. A multiubiquitin chain is confined to specific lysine in a targeted short-lived protein. *Science*. 1989;243(4898):1576-83.

34. Thrower JS, Hoffman L, Rechsteiner M, Pickart CM. Recognition of the polyubiquitin proteolytic signal. *EMBO J*. 2000;19(1):94-102.

35. van Nocker S, Vierstra RD. Multiubiquitin chains linked through lysine 48 are abundant in vivo and are competent intermediates in the ubiquitin proteolytic pathway. *J. Biol. Chem*. 1993;268(33):24766-73.

36. Arnason T, Ellison MJ. Stress resistance in Saccharomyces cerevisiae is strongly correlated with assembly of a novel type of multiubiquitin chain. *Mol. Cell. Biol*. 1994;14(12):7876-83.

37. Pickart CM. Mechanisms underlying ubiquitination. *Annu. Rev. Biochem*. 2001;70:503-33.

38. Johnson ES, Ma PC, Ota IM, Varshavsky A. A proteolytic pathway that recognizes ubiquitin as a degradation signal. *J. Biol. Chem*. 1995;270(29):17442-56.

39. Hicke L. Protein regulation by monoubiquitin. *Nat. Rev. Mol. Cell Biol*. 2001;2(3):195-201.

40. Ciechanover A, Elias S, Heller H, Hershko A. "Covalent affinity" purification of ubiquitin-activating enzyme. *J. Biol. Chem*. 1982;257(5):2537-42.

41. McGrath JP, Jentsch S, Varshavsky A. UBA 1: an essential yeast gene encoding ubiquitin-activating enzyme. *EMBO J*. 1991;10(1):227-36.

42. Patton EE, Willems AR, Tyers M. Combinatorial control in ubiquitin-dependent proteolysis: don't Skp the F-box hypothesis. *Trends Genet*. 1998;14(6):236-43.

43. Mathias N, Steussy CN, Goebl MG. An essential domain within Cdc34p is required for binding to a complex containing Cdc4p and Cdc53p in Saccharomyces cerevisiae. *J. Biol. Chem*. 1998;273(7):4040-5.

44. Zheng N, Schulman BA, Song L, et al. Structure of the Cul1-Rbx1-Skp1-F boxSkp2 SCF ubiquitin ligase complex. *Nature*. 2002;416(6882):703-9.

45. Lammer D, Mathias N, Laplaza JM, et al. Modification of yeast Cdc53p by the ubiquitin-related protein rub1p affects function of the SCFCdc4 complex. *Genes Dev*. 1998;12(7):914-26.

46. Skowyra D, Koepp DM, Kamura T, et al. Reconstitution of G1 cyclin ubiquitination with complexes containing SCFGrr1 and Rbx1. *Science*. 1999;284 (5414):662-5.

47. Bai C, Sen P, Hofmann K, et al. SKP1 connects cell cycle regulators to the ubiquitin proteolysis machinery through a novel motif, the F-box. *Cell*. 1996;86(2):263-74.

48. Spielewoy N, Flick K, Kalashnikova TI, Walker JR, Wittenberg C. Regulation and recognition of SCFGrr1 targets in the glucose and amino acid signaling pathways. *Mol. Cell. Biol*. 2004;24(20):8994-9005.

49. Skowyra D, Craig KL, Tyers M, Elledge SJ, Harper JW. F-box proteins are receptors that recruit phosphorylated substrates to the SCF ubiquitin-ligase complex. *Cell*. 1997;91(2):209-19.

50. Deshaies RJ, Chau V, Kirschner M. Ubiquitination of the G1 cyclin Cln2p by a Cdc34p-dependent pathway. *EMBO J*. 1995;14(2):303-12.

51. Kus BM, Caldon CE, Andorn-Broza R, Edwards AM. Functional interaction of 13 yeast SCF complexes with a set of yeast E2 enzymes in vitro. *Proteins*. 2004;54(3):455-67.

52. Barral Y, Jentsch S, Mann C. G1 cyclin turnover and nutrient uptake are controlled by a common pathway in yeast. *Genes Dev*. 1995;9(4):399-409.

53. Purnapatre K, Gray M, Piccirillo S, Honigberg SM. Glucose inhibits meiotic DNA replication through SCFGrr1p-dependent destruction of Ime2p kinase. *Mol. Cell. Biol*. 2005;25(1):440-50.

54. Blondel M, Bach S, Bamps S, et al. Degradation of Hof1 by SCF(Grr1) is important for actomyosin contraction during cytokinesis in yeast. *EMBO J*. 2005;24(7):1440-52.

55. Jaquenoud M, Gulli MP, Peter K, Peter M. The Cdc42p effector Gic2p is targeted for ubiquitin-dependent degradation by the SCFGrr1 complex. *EMBO J*. 1998;17(18):5360-73.

56. Flick KM, Spielewoy N, Kalashnikova TI, et al. Grr1-dependent inactivation of Mth1 mediates glucose-induced dissociation of Rgt1 from HXT gene promoters. *Mol. Biol. Cell*. 2003;14(8):3230-41.

57. Liu Z, Spírek M, Thornton J, Butow RA. A novel degron-mediated degradation of the RTG pathway regulator, Mks1p, by SCFGrr1. *Mol. Biol. Cell*. 2005;16(10):4893-904.

58. La Rue J, Tokarz S, Lanker S. SCFGrr1-mediated ubiquitination of Gis4 modulates glucose response in yeast. *J. Mol. Biol*. 2005;349(4):685-98.

59. Jiang H, Tatchell K, Liu S, Michels CA. Protein phosphatase type-1 regulatory subunits Reg1p and Reg2p act as signal transducers in the glucose-induced inactivation of maltose permease in Saccharomyces cerevisiae. *Mol. Gen. Genet*. 2000;263(3):411-22.

60. Horak J, Wolf DH. The ubiquitin ligase SCF(Grr1) is required for Gal2p degradation in the yeast Saccharomyces cerevisiae. *Biochem. Biophys. Res. Commun*. 2005;335(4):1185-90.

61. Iraqui I, Vissers S, Bernard F, et al. Amino acid signaling in Saccharomyces cerevisiae: a permease-like sensor of external amino acids and F-Box protein Grr1p are required for transcriptional induction of the AGP1 gene, which encodes a broad-specificity amino acid permease. *Mol Cell Biol*. 1999;19(2):989-1001.

62. Poulsen P, Wu B, Gaber RF, Kielland-Brandt MC. Constitutive signal transduction by mutant Ssy5p and Ptr3p components of the SPS amino acid sensor system in Saccharomyces cerevisiae. *Eukaryot Cell*. 2005;4(6):1116-24.

63. Bernard F, André B. Ubiquitin and the SCF(Grr1) ubiquitin ligase complex are involved in the signalling pathway activated by external amino acids in Saccharomyces cerevisiae. *FEBS Lett*. 2001;496(2-3):81-5.

64. Bailey RB, Benitez T, Woodward A. Saccharomyces cerevisiae Mutants Resistant to Catabolite Repression: Use in Cheese Whey Hydrolysate Fermentation. *Appl. Environ. Microbiol*. 1982;44(3):631-639.

65. Bailey RB, Woodword A. Isolation and characterization of a pleiotropic glucose repression resistant mutant of Saccharomyces cerevisiae. *Mol. Gen. Genet*. 1984;193(3):507-12.

66. Flick JS, Johnston M. GRR1 of Saccharomyces cerevisiae is required for glucose repression and encodes a protein with leucine-rich repeats. *Mol. Cell. Biol*. 1991;11(10):5101-5112.

67. Westergaard SL, Oliveira AP, Bro C, Olsson L, Nielsen J. A systems biology approach to study glucose repression in the yeast Saccharomyces cerevisiae. *Biotechnol Bioeng*. 2007;96(1):134-45.

68. Dimmer KS, Fritz S, Fuchs F, et al. Genetic basis of mitochondrial function and morphology in Saccharomyces cerevisiae. *Mol. Biol. Cell*. 2002;13(3):847-853.

69. Vallier LG, Coons D, Bisson LF, Carlson M. Altered regulatory responses to glucose are associated with a glucose transport defect in grr1 mutants of Saccharomyces cerevisiae. *Genetics*. 1994;136(4):1279-85.

70. Ozcan S, Schulte F, Freidel K, Weber A, Ciriacy M. Glucose uptake and metabolism in grr1/cat80 mutants of Saccharomyces cerevisiae. *Eur J Biochem*. 1994;224(2):605-11.

71. Conklin DS, Kung C, Culbertson MR. The COT2 gene is required for glucose-dependent divalent cation transport in Saccharomyces cerevisiae. *Mol. Cell. Biol*. 1993;13(4):2041-9.

72. Bernard F, André B. Ubiquitin and the SCFGrr1 ubiquitin ligase complex are involved in the signalling pathway activated by external amino acids in Saccharomyces cerevisiae. *FEBS Letters*. 2001;496(2-3):81-85.

73. Blondel M, Bach S, Bamps S, et al. Degradation of Hof1 by SCF(Grr1) is important for actomyosin contraction during cytokinesis in yeast. *EMBO J*. 2005;24(7):1440-52.

74. Schweitzer K, Cocklin R, Garrett L, Desai F, Goebl M. The ubiquitin ligase SCFGrr1 is necessary for pheromone sensitivity in Saccharomyces cerevisiae. *Yeast*. 2005;22(7):553-64.

75. Outten CE, Falk RL, Culotta VC. Cellular factors required for protection from hyperoxia toxicity in Saccharomyces cerevisiae. *Biochem. J*. 2005;388(Pt 1):93-101.

76. Kim YJ, Francisco L, Chen GC, Marcotte E, Chan CS. Control of cellular morphogenesis by the Ip12/Bem2 GTPase-activating protein: possible role of protein phosphorylation. *J Cell Biol*. 1994;127(5):1381-94.

77. Benanti JA, Cheung SK, Brady MC, Toczyski DP. A proteomic screen reveals SCFGrr1 targets that regulate the glycolytic-gluconeogenic switch. *Nat Cell Biol*. 2007;9(10):1184-91.

78. Barral Y, Jentsch S, Mann C. G1 cyclin turnover and nutrient uptake are controlled by a common pathway in yeast. *Genes Dev*. 1995;9(4):399-409.

79. Tyers M, Tokiwa G, Nash R, Futcher B. The Cln3-Cdc28 kinase complex of S. cerevisiae is regulated by proteolysis and phosphorylation. *EMBO J*. 1992;11(5):1773-1784.

80. Barral Y, Jentsch S, Mann C. G1 cyclin turnover and nutrient uptake are controlled by a common pathway in yeast. *Genes Dev*. 1995;9(4):399-409.

81. Deshaies RJ, Kirschner M. G1 cyclin-dependent activation of p34CDC28 (Cdc28p) in vitro. *Proc Natl Acad Sci U S A*. 1995;92(4):1182-6.

82. Hadwiger JA, Wittenberg C, Richardson HE, de Barros Lopes M, Reed SI. A family of cyclin homologs that control the G1 phase in yeast. *Proc. Natl. Acad. Sci. U.S.A*. 1989;86(16):6255-6259.

83. Richardson HE, Wittenberg C, Cross F, Reed SI. An essential G1 function for cyclin-like proteins in yeast. *Cell*. 1989;59(6):1127-1133.

84. Cross FR. Cell cycle arrest caused by CLN gene deficiency in Saccharomyces cerevisiae resembles START-I arrest and is independent of the mating-pheromone signalling pathway. *Mol. Cell. Biol*. 1990;10(12):6482-6490.

85. Benton BK, Tinkelenberg AH, Jean D, Plump SD, Cross FR. Genetic analysis of Cln/Cdc28 regulation of cell morphogenesis in budding yeast. *EMBO J*. 1993;12(13):5267-75.

86. Hartwell LH. Saccharomyces cerevisiae cell cycle. *Bacteriol Rev*. 1974;38(2):164-198.

87. Schwob E, Böhm T, Mendenhall MD, Nasmyth K. The B-type cyclin kinase inhibitor p40SIC1 controls the G1 to S transition in S. cerevisiae. *Cell*. 1994;79(2):233-244.

88. Tyers M, Tokiwa G, Futcher B. Comparison of the Saccharomyces cerevisiae G1 cyclins: Cln3 may be an upstream activator of Cln1, Cln2 and other cyclins. *EMBO J*. 1993;12(5):1955-68.

89. Blondel M, Mann C. G2 cyclins are required for the degradation of G1 cyclins in yeast. *Nature*. 1996;384(6606):279-282.

90. Willems AR, Lanker S, Patton EE, et al. Cdc53 targets phosphorylated G1 cyclins for degradation by the ubiquitin proteolytic pathway. *Cell*. 1996;86(3):453-463.

91. Bai C, Sen P, Hofmann K, et al. SKP1 connects cell cycle regulators to the ubiquitin proteolysis machinery through a novel motif, the F-box. *Cell*. 1996;86(2):263-274.

92. Deshaies RJ, Chau V, Kirschner M. Ubiquitination of the G1 cyclin Cln2p by a Cdc34p-dependent pathway. *EMBO J*. 1995;14(2):303-312.

93. Skowyra D, Craig KL, Tyers M, Elledge SJ, Harper JW. F-box proteins are receptors that recruit phosphorylated substrates to the SCF ubiquitin-ligase complex. *Cell*. 1997;91(2):209-219.

94. Skowyra D, Koepp DM, Kamura T, et al. Reconstitution of G1 cyclin ubiquitination with complexes containing SCFGrr1 and Rbx1. *Science*. 1999;284(5414):662-665.

95. Tyson CB, Lord PG, Wheals AE. Dependency of size of Saccharomyces cerevisiae cells on growth rate. *J. Bacteriol*. 1979;138(1):92-8.

96. Johnston GC, Ehrhardt CW, Lorincz A, Carter BL. Regulation of cell size in the yeast Saccharomyces cerevisiae. *J. Bacteriol*. 1979;137(1):1-5.

97. Li FN, Johnston M. Grr1 of Saccharomyces cerevisiae is connected to the ubiquitin proteolysis machinery through Skp1: coupling glucose sensing to gene expression and the cell cycle. *EMBO J*. 1997;16(18):5629-5638.

98. Barral Y, Jentsch S, Mann C. G1 cyclin turnover and nutrient uptake are controlled by a common pathway in yeast. *Genes Dev*. 1995;9(4):399-409.

99. Schmidt MC, McCartney RR, Zhang X, et al. Std1 and Mth1 proteins interact with the glucose sensors to control glucose-regulated gene expression in Saccharomyces cerevisiae. *Mol Cell Biol*. 1999;19(7):4561-71.

100. Smith GR, Givan SA, Cullen P, Sprague GF. GTPase-activating proteins for Cdc42. *Eukaryot Cell*. 2002;1(3):469-80.

101. Brown JL, Jaquenoud M, Gulli MP, Chant J, Peter M. Novel Cdc42-binding proteins Gic1 and Gic2 control cell polarity in yeast. *Genes Dev*. 1997;11(22):2972-82.

102. Kawasaki R, Fujimura-Kamada K, Toi H, Kato H, Tanaka K. The upstream regulator, Rsr1p, and downstream effectors, Gic1p and Gic2p, of the Cdc42p small GTPase coordinately regulate initiation of budding in Saccharomyces cerevisiae. *Genes Cells*. 2003;8(3):235-50.

103. Lew DJ, Reed SI. Morphogenesis in the yeast cell cycle: regulation by Cdc28 and cyclins. *J. Cell Biol*. 1993;120(6):1305-1320.

104. Queralt E, Igual JC. Functional distinction between Cln1p and Cln2p cyclins in the control of the Saccharomyces cerevisiae mitotic cycle. *Genetics*. 2004;168(1):129-140.

105. Cabib E, Mol PC, Shaw JA, Choi WJ. Biosynthesis of cell wall and septum during yeast growth. *Arch. Med. Res*. 1993;24(3):301-303.

106. Henar Valdivieso M, Durán A, Roncero C. Chitin synthases in yeast and fungi. *EXS*. 1999;87:55-69.

107. Lippincott J, Li R. Dual function of Cyk2, a cdc15/PSTPIP family protein, in regulating actomyosin ring dynamics and septin distribution. *J. Cell Biol*. 1998;143(7):1947-1960.

108. Vallen EA, Caviston J, Bi E. Roles of Hof1p, Bni1p, Bnr1p, and myo1p in cytokinesis in Saccharomyces cerevisiae. *Mol Biol Cell*. 2000;11(2):593-611.

109. Forsberg H, Gilstring CF, Zargari A, Martínez P, Ljungdahl PO. The role of the yeast plasma membrane SPS nutrient sensor in the metabolic response to extracellular amino acids. *Mol. Microbiol*. 2001;42(1):215-228.

110. Didion T, Regenberg B, Jørgensen MU, Kielland-Brandt MC, Andersen HA. The permease homologue Ssy1p controls the expression of amino acid and peptide transporter genes in Saccharomyces cerevisiae. *Mol. Microbiol*. 1998;27(3):643-50.

111. Iraqui I, Vissers S, Bernard F, et al. Amino acid signaling in Saccharomyces cerevisiae: a permease-like sensor of external amino acids and F-Box protein Grr1p are required for transcriptional induction of the AGP1 gene, which encodes a broad-specificity amino acid permease. *Mol. Cell. Biol*. 1999;19(2):989-1001.

112. Klasson H, Fink GR, Ljungdahl PO. Ssy1p and Ptr3p Are Plasma Membrane Components of a Yeast System That Senses Extracellular Amino Acids. *Mol. Cell. Biol.* 1999;19(8):5405-5416.

113. Forsberg H, Ljungdahl PO. Genetic and biochemical analysis of the yeast plasma membrane Ssy1p-Ptr3p-Ssy5p sensor of extracellular amino acids. *Mol. Cell. Biol*. 2001;21(3):814-26.

114. Liu Z, Thornton J, Spírek M, Butow RA. Activation of the SPS amino acid-sensing pathway in Saccharomyces cerevisiae correlates with the phosphorylation state of a sensor component, Ptr3. *Mol. Cell. Biol*. 2008;28(2):551-63.

115. Poulsen P, Lo Leggio L, Kielland-Brandt MC. Mapping of an internal protease cleavage site in the Ssy5p component of the amino acid sensor of Saccharomyces cerevisiae and functional characterization of the resulting pro- and protease domains by gain-of-function genetics. *Eukaryotic Cell*. 2006;5(3):601-8.

116. Abdel-Sater F, El Bakkoury M, Urrestarazu A, Vissers S, André B. Amino acid signaling in yeast: casein kinase I and the Ssy5 endoprotease are key determinants of endoproteolytic activation of the membrane-bound Stp1 transcription factor. *Mol. Cell. Biol*. 2004;24(22):9771-85.

117. Andréasson C, Ljungdahl PO. Receptor-mediated endoproteolytic activation of two transcription factors in yeast. *Genes Dev*. 2002;16(24):3158-72.

118. Boban M, Ljungdahl PO. Dal81 enhances Stp1- and Stp2-dependent transcription necessitating negative modulation by inner nuclear membrane protein Asi1 in Saccharomyces cerevisiae. *Genetics*. 2007;176(4):2087-97.

119. Abdel-Sater F, Iraqui I, Urrestarazu A, André B. The external amino acid signaling pathway promotes activation of Stp1 and Uga35/Dal81 transcription factors for induction of the AGP1 gene in Saccharomyces cerevisiae. *Genetics*. 2004;166(4):1727-39.

120. Grenson M, Hou C, Crabeel M. Multiplicity of the amino acid permeases in Saccharomyces cerevisiae. IV. Evidence for a general amino acid permease. *J. Bacteriol*. 1970;103(3):770-7.

121. Regenberg B, Düring-Olsen L, Kielland-Brandt MC, Holmberg S. Substrate specificity and gene expression of the amino-acid permeases in Saccharomyces cerevisiae. *Curr. Genet*. 1999;36(6):317-28.

122. Butow RA, Avadhani NG. Mitochondrial signaling: the retrograde response. *Mol. Cell*. 2004;14(1):1-15.

123. Epstein CB, Waddle JA, Hale W, et al. Genome-wide responses to mitochondrial dysfunction. *Mol. Biol. Cell*. 2001;12(2):297-308.

124. Sekito T, Liu Z, Thornton J, Butow RA. RTG-dependent mitochondria-to-nucleus signaling is regulated by MKS1 and is linked to formation of yeast prion [URE3]. *Mol. Biol. Cell*. 2002;13(3):795-804.

125. Liu Z, Butow RA. A transcriptional switch in the expression of yeast tricarboxylic acid cycle genes in response to a reduction or loss of respiratory function. *Mol. Cell. Biol*. 1999;19(10):6720-6728.

126. Liao XS, Small WC, Srere PA, Butow RA. Intramitochondrial functions regulate nonmitochondrial citrate synthase (CIT2) expression in Saccharomyces cerevisiae. *Mol. Cell. Biol*. 1991;11(1):38-46.

127. Jia Y, Rothermel B, Thornton J, Butow RA. A basic helix-loop-helix-leucine zipper transcription complex in yeast functions in a signaling pathway from mitochondria to the nucleus. *Mol. Cell. Biol*. 1997;17(3):1110-1117.

128. Sekito T, Thornton J, Butow RA. Mitochondria-to-nuclear signaling is regulated by the subcellular localization of the transcription factors Rtg1p and Rtg3p. *Mol. Biol. Cell*. 2000;11(6):2103-2115.

129. Liu Z, Sekito T, SpI[combining acute accent]rek M, Thornton J, Butow RA. Retrograde Signaling Is Regulated by the Dynamic Interaction between Rtg2p and Mks1p. *Molecular Cell*. 2003;12(2):401-411.

130. Komeili A, Wedaman KP, O'Shea EK, Powers T. Mechanism of metabolic control. Target of rapamycin signaling links nitrogen quality to the activity of the Rtg1 and Rtg3 transcription factors. *J. Cell Biol*. 2000;151(4):863-878.

131. Dilova I, Aronova S, Chen JC, Powers T. Tor signaling and nutrient-based signals converge on Mks1p phosphorylation to regulate expression of Rtg1.Rtg3p-dependent target genes. *J. Biol. Chem*. 2004;279(45):46527-46535.

132. Cooper TG. Transmitting the signal of excess nitrogen in Saccharomyces cerevisiae from the Tor proteins to the GATA factors: connecting the dots. *FEMS Microbiol. Rev*. 2002;26(3):223-238.

133. Powers T, Dilova I, Chen CY, Wedaman K. Yeast TOR signaling: a mechanism for metabolic regulation. *Curr. Top. Microbiol. Immunol*. 2004;279:39-51.

134. Strathern J. *The Molecular biology of the yeast Saccharomyces : metabolism and gene expression*. Cold Spring Harbor N.Y.: Cold Spring Harbor Laboratory; 1982.

135. DeRisi JL, Iyer VR, Brown PO. Exploring the metabolic and genetic control of gene expression on a genomic scale. *Science*. 1997;278(5338):680-6.

136. Yin Z, Smith RJ, Brown AJ. Multiple signalling pathways trigger the exquisite sensitivity of yeast gluconeogenic mRNAs to glucose. *Mol Microbiol*. 1996;20(4):751-64.

137. Johnston M. Feasting, fasting and fermenting: glucose sensing in yeast and other cells. *Trends in Genetics*. 1999;15(1):29-33.

138. Cereghino GP, Scheffler IE. Genetic analysis of glucose regulation in saccharomyces cerevisiae: control of transcription versus mRNA turnover. *EMBO J*. 1996;15(2):363-74.

139. Daran-Lapujade P, Jansen MLA, Daran J, et al. Role of transcriptional regulation in controlling fluxes in central carbon metabolism of Saccharomyces cerevisiae. A chemostat culture study. *J Biol Chem*. 2004;279(10):9125-38.

140. Elbing K, Ståhlberg A, Hohmann S, Gustafsson L. Transcriptional responses to glucose at different glycolytic rates in Saccharomyces cerevisiae. *Eur J Biochem*. 2004;271(23-24):4855-64.

141. Wang Y, Pierce M, Schneper L, et al. Ras and Gpa2 mediate one branch of a redundant glucose signaling pathway in yeast. *PLoS Biol*. 2004;2(5):E128.

142. Moriya H, Johnston M. Glucose sensing and signaling in Saccharomyces cerevisiae through the Rgt2 glucose sensor and casein kinase I. *Proc. Natl. Acad. Sci. U.S.A*. 2004;101(6):1572-1577.

143. Kim J, Johnston M. Two glucose-sensing pathways converge on Rgt1 to regulate expression of glucose transporter genes in Saccharomyces cerevisiae. *J. Biol. Chem*. 2006;281(36):26144-26149.

144. Ozcan S, Dover J, Rosenwald AG, Wölfl S, Johnston M. Two glucose transporters in Saccharomyces cerevisiae are glucose sensors that generate a signal for induction of gene expression. *Proc. Natl. Acad. Sci. U.S.A*. 1996;93(22):12428-12432.

145. Flick JS, Johnston M. Two systems of glucose repression of the GAL1 promoter in Saccharomyces cerevisiae. *Mol. Cell. Biol*. 1990;10(9):4757-4769.

146. Carlson M, Osmond BC, Botstein D. Mutants of yeast defective in sucrose utilization. *Genetics*. 1981;98(1):25-40.

147. Rahner A, Schöler A, Martens E, Gollwitzer B, Schüller HJ. Dual influence of the yeast Cat1p (Snf1p) protein kinase on carbon source-dependent transcriptional activation of gluconeogenic genes by the regulatory gene CAT8. *Nucleic Acids Res*. 1996;24(12):2331-2337.

148. Lesage P, Yang X, Carlson M. Yeast SNF1 protein kinase interacts with SIP4, a C6 zinc cluster transcriptional activator: a new role for SNF1 in the glucose response. *Mol. Cell. Biol*. 1996;16(5):1921-1928.

149. Wright RM, Poyton RO. Release of two Saccharomyces cerevisiae cytochrome genes, COX6 and CYC1, from glucose repression requires the SNF1 and SSN6 gene products. *Mol. Cell. Biol*. 1990;10(3):1297-1300.

150. Ulery TL, Jang SH, Jaehning JA. Glucose repression of yeast mitochondrial transcription: kinetics of derepression and role of nuclear genes. *Mol. Cell. Biol*. 1994;14(2):1160-1170.

151. Young ET, Dombek KM, Tachibana C, Ideker T. Multiple pathways are co-regulated by the protein kinase Snf1 and the transcription factors Adr1 and Cat8. *J. Biol. Chem*. 2003;278(28):26146-26158.

152. De Winde JH, Crauwels M, Hohmann S, Thevelein JM, Winderickx J. Differential requirement of the yeast sugar kinases for sugar sensing in establishing the catabolite-repressed state. *Eur J Biochem*. 1996;241(2):633-43.

153. Ma H, Botstein D. Effects of null mutations in the hexokinase genes of Saccharomyces cerevisiae on catabolite repression. *Mol Cell Biol*. 1986;6(11):4046-52.

154. Entian KD. Genetic and biochemical evidence for hexokinase PII as a key enzyme involved in carbon catabolite repression in yeast. *Mol Gen Genet*. 1980;178(3):633-7.

155. Entian KD, Mecke D. Genetic evidence for a role of hexokinase isozyme PII in carbon catabolite repression in Saccharomyces cerevisiae. *J Biol Chem*. 1982;257(2):870-4.

156. Rose M, Albig W, Entian KD. Glucose repression in Saccharomyces cerevisiae is directly associated with hexose phosphorylation by hexokinases PI and PII. *Eur. J. Biochem*. 1991;199(3):511-518.

157. Terrell SL, Bernard A, Bailey RB. Ethanol from Whey: Continuous Fermentation with a Catabolite Repression-Resistant Saccharomyces cerevisiae Mutant. *Appl Environ Microbiol*. 1984;48(3):577-580.

158. Bailey RB, Woodword A. Isolation and characterization of a pleiotropic glucose repression resistant mutant of Saccharomyces cerevisiae. *Mol Gen Genet*. 1984;193(3):507-12.

159. Westergaard SL, Bro C, Olsson L, Nielsen J. Elucidation of the role of Grr1p in glucose sensing by Saccharomyces cerevisiae through genome-wide transcription analysis. *FEMS Yeast Res*. 2004;5(3):193-204.

160. Ozcan S, Johnston M. Two different repressors collaborate to restrict expression of the yeast glucose transporter genes HXT2 and HXT4 to low levels of glucose. *Mol Cell Biol*. 1996;16(10):5536-45.

161. Ozcan S, Dover J, Johnston M. Glucose sensing and signaling by two glucose receptors in the yeast Saccharomyces cerevisiae. *EMBO J*. 1998;17(9):2566-2573.

162. Kim J, Brachet V, Moriya H, Johnston M. Integration of transcriptional and posttranslational regulation in a glucose signal transduction pathway in Saccharomyces cerevisiae. *Eukaryotic Cell*. 2006;5(1):167-173.

163. Santangelo GM. Glucose signaling in Saccharomyces cerevisiae. *Microbiol Mol Biol Rev*. 2006;70(1):253-82.

164. Rolland F, Winderickx J, Thevelein JM. Glucose-sensing and -signalling mechanisms in yeast. *FEMS Yeast Res*. 2002;2(2):183-201.

165. Trumbly RJ. Glucose repression in the yeast Saccharomyces cerevisiae. *Mol. Microbiol*. 1992;6(1):15-21.

166. Erickson JR, Johnston M. Suppressors reveal two classes of glucose repression genes in the yeast Saccharomyces cerevisiae. *Genetics*. 1994;136(4):1271-8.

167. Ozcan S, Johnston M. Three different regulatory mechanisms enable yeast hexose transporter (HXT) genes to be induced by different levels of glucose. *Mol Cell Biol*. 1995;15(3):1564-72.

168. Spielewoy N, Flick K, Kalashnikova TI, Walker JR, Wittenberg C. Regulation and recognition of SCFGrr1 targets in the glucose and amino acid signaling pathways. *Mol Cell Biol*. 2004;24(20):8994-9005.

169. Ozcan S, Freidel K, Leuker A, Ciriacy M. Glucose uptake and catabolite repression in dominant HTR1 mutants of Saccharomyces cerevisiae. *J Bacteriol*. 1993;175(17):5520-8.

170. Yin Z, Smith RJ, Brown AJ. Multiple signalling pathways trigger the exquisite sensitivity of yeast gluconeogenic mRNAs to glucose. *Mol. Microbiol*. 1996;20(4):751-764.

171. Yin Z, Hatton L, Brown AJ. Differential post-transcriptional regulation of yeast mRNAs in response to high and low glucose concentrations. *Mol. Microbiol*. 2000;35(3):553-565.

172. Meijer MM, Boonstra J, Verkleij AJ, Verrips CT. Glucose repression in Saccharomyces cerevisiae is related to the glucose concentration rather than the glucose flux. *J. Biol. Chem*. 1998;273(37):24102-24107.

173. Reifenberger E, Boles E, Ciriacy M. Kinetic characterization of individual hexose transporters of Saccharomyces cerevisiae and their relation to the triggering mechanisms of glucose repression. *Eur J Biochem*. 1997;245(2):324-33.

174. Raghevendran V, Gombert AK, Christensen B, Kötter P, Nielsen J. Phenotypic characterization of glucose repression mutants of Saccharomyces cerevisiae using experiments with 13C-labelled glucose. *Yeast*. 2004;21(9):769-79.

175. Ozcan S, Johnston M. Function and regulation of yeast hexose transporters. *Microbiol. Mol. Biol. Rev*. 1999;63(3):554-569.

176. Reifenberger E, Freidel K, Ciriacy M. Identification of novel HXT genes in Saccharomyces cerevisiae reveals the impact of individual hexose transporters on glycolytic flux. *Mol Microbiol*. 1995;16(1):157-67.

177. Liang H, Gaber RF. A novel signal transduction pathway in Saccharomyces cerevisiae defined by Snf3-regulated expression of HXT6. *Mol. Biol. Cell*. 1996;7(12):1953-1966.

178. Reifenberger E, Ciriacy M. The roles of multiple hexose transporters in S. cerevisiae. *Folia Microbiol (Praha)*. 1994;39(6):541-2.

179. Ko CH, Liang H, Gaber RF. Roles of multiple glucose transporters in Saccharomyces cerevisiae. *Mol Cell Biol*. 1993;13(1):638-48.

180. Bisson LF, Fraenkel DG. Transport of 6-deoxyglucose in Saccharomyces cerevisiae. *J Bacteriol*. 1983;155(3):995-1000.

181. Maier A, Völker B, Boles E, Fuhrmann GF. Characterisation of glucose transport in Saccharomyces cerevisiae with plasma membrane vesicles (countertransport) and intact cells (initial uptake) with single Hxt1, Hxt2, Hxt3, Hxt4, Hxt6, Hxt7 or Gal2 transporters. *FEMS Yeast Res*. 2002;2(4):539-550.

182. Bisson LF, Fraenkel DG. Expression of kinase-dependent glucose uptake in Saccharomyces cerevisiae. *J. Bacteriol*. 1984;159(3):1013-1017.

183. Boles E, Hollenberg CP. The molecular genetics of hexose transport in yeasts. *FEMS Microbiol. Rev*. 1997;21(1):85-111.

184. Neigeborn L, Carlson M. Genes affecting the regulation of SUC2 gene expression by glucose repression in Saccharomyces cerevisiae. *Genetics*. 1984;108(4):845-858.

185. Neigeborn L, Schwartzberg P, Reid R, Carlson M. Null mutations in the SNF3 gene of Saccharomyces cerevisiae cause a different phenotype than do previously isolated missense mutations. *Mol. Cell. Biol*. 1986;6(11):3569-3574.

186. Bisson LF, Neigeborn L, Carlson M, Fraenkel DG. The SNF3 gene is required for high-affinity glucose transport in Saccharomyces cerevisiae. *J. Bacteriol*. 1987;169(4):1656-1662.

187. Celenza JL, Marshall-Carlson L, Carlson M. The yeast SNF3 gene encodes a glucose transporter homologous to the mammalian protein. *Proc. Natl. Acad. Sci. U.S.A*. 1988;85(7):2130-2134.

188. Marshall-Carlson L, Neigeborn L, Coons D, Bisson L, Carlson M. Dominant and recessive suppressors that restore glucose transport in a yeast snf3 mutant. *Genetics*. 1991;128(3):505-512.

189. Schmidt MC, McCartney RR, Zhang X, et al. Std1 and Mth1 proteins interact with the glucose sensors to control glucose-regulated gene expression in Saccharomyces cerevisiae. *Mol. Cell. Biol*. 1999;19(7):4561-4571.

190. Lafuente MJ, Gancedo C, Jauniaux JC, Gancedo JM. Mth1 receives the signal given by the glucose sensors Snf3 and Rgt2 in Saccharomyces cerevisiae. *Mol. Microbiol*. 2000;35(1):161-172.

191. Ganster RW, Shen W, Schmidt MC. Isolation of STD1, a high-copy-number suppressor of a dominant negative mutation in the yeast TATA-binding protein. *Mol. Cell. Biol*. 1993;13(6):3650-3659.

192. Hubbard EJ, Jiang R, Carlson M. Dosage-dependent modulation of glucose repression by MSN3 (STD1) in Saccharomyces cerevisiae. *Mol. Cell. Biol*. 1994;14(3):1972-1978.

193. Sabina J, Johnston M. Asymmetric signal transduction through paralogs that comprise a genetic switch for sugar sensing in S. cerevisiae. *J. Biol. Chem*. 2009. Available at: http://www.ncbi.nlm.nih.gov/pubmed/19720826 [Accessed September 8, 2009].

194. Johnston M. Feasting, fasting and fermenting. Glucose sensing in yeast and other cells. *Trends Genet*. 1999;15(1):29-33.

195. Lakshmanan J, Mosley AL, Ozcan S. Repression of transcription by Rgt1 in the absence of glucose requires Std1 and Mth1. *Curr Genet*. 2003;44(1):19-25.

196. Geladé R, Van de Velde S, Van Dijck P, Thevelein JM. Multi-level response of the yeast genome to glucose. *Genome Biol*. 2003;4(11):233.

197. Polish JA, Kim J, Johnston M. How the Rgt1 transcription factor of Saccharomyces cerevisiae is regulated by glucose. *Genetics*. 2005;169(2):583-594.

198. Mosley AL, Lakshmanan J, Aryal BK, Ozcan S. Glucose-mediated Phosphorylation Converts the Transcription Factor Rgt1 from a Repressor to an Activator. *J. Biol. Chem.* 2003;278(12):10322-10327.

199. Ozcan S, Leong T, Johnston M. Rgt1p of Saccharomyces cerevisiae, a key regulator of glucose-induced genes, is both an activator and a repressor of transcription. *Mol. Cell. Biol*. 1996;16(11):6419-6426.

200. Johnston M, Kim J. Glucose as a hormone: receptor-mediated glucose sensing in the yeast Saccharomyces cerevisiae. *Biochem Soc Trans*. 2005;33(Pt 1):247-52.

201. Ozcan S, Johnston M. Function and regulation of yeast hexose transporters. *Microbiol. Mol. Biol. Rev*. 1999;63(3):554-569.

202. Treitel MA, Kuchin S, Carlson M. Snf1 protein kinase regulates phosphorylation of the Mig1 repressor in Saccharomyces cerevisiae. *Mol. Cell. Biol*. 1998;18(11):6273-6280.

203. Ostling J, Ronne H. Negative control of the Mig1p repressor by Snf1p-dependent phosphorylation in the absence of glucose. *Eur. J. Biochem*. 1998;252(1):162-168.

204. Alms GR, Sanz P, Carlson M, Haystead TA. Reg1p targets protein phosphatase 1 to dephosphorylate hexokinase II in Saccharomyces cerevisiae: characterizing the effects of a phosphatase subunit on the yeast proteome. *EMBO J*. 1999;18(15):4157-4168.

205. Jiang R, Carlson M. Glucose regulates protein interactions within the yeast SNF1 protein kinase complex. *Genes Dev*. 1996;10(24):3105-3115.

206. Ludin K, Jiang R, Carlson M. Glucose-regulated interaction of a regulatory subunit of protein phosphatase 1 with the Snf1 protein kinase in Saccharomyces cerevisiae. *Proc. Natl. Acad. Sci. U.S.A*. 1998;95(11):6245-6250.

207. Tu J, Carlson M. REG1 binds to protein phosphatase type 1 and regulates glucose repression in Saccharomyces cerevisiae. *EMBO J*. 1995;14(23):5939-46.

208. Alms GR, Sanz P, Carlson M, Haystead TA. Reg1p targets protein phosphatase 1 to dephosphorylate hexokinase II in Saccharomyces cerevisiae: characterizing the effects of a phosphatase subunit on the yeast proteome. *EMBO J*. 1999;18(15):4157-68.

209. Sanz P, Alms GR, Haystead TA, Carlson M. Regulatory interactions between the Reg1-Glc7 protein phosphatase and the Snf1 protein kinase. *Mol Cell Biol*. 2000;20(4):1321-8.

210. Tomás-Cobos L, Sanz P. Active Snf1 protein kinase inhibits expression of the Saccharomyces cerevisiae HXT1 glucose transporter gene. *Biochem J*. 2002;368(Pt 2):657-63.

211. Lobo Z, Maitra PK. Physiological role of glucose-phosphorylating enzymes in Saccharomyces cerevisiae. *Archives of Biochemistry and Biophysics*. 1977;182(2):639-645.

212. Gancedo JM, Clifton D, Fraenkel DG. Yeast hexokinase mutants. *J Biol Chem*. 1977;252(13):4443-4.

213. Herrero P, Galíndez J, Ruiz N, Martínez-Campa C, Moreno F. Transcriptional regulation of the Saccharomyces cerevisiae HXK1, HXK2 and GLK1 genes. *Yeast*. 1995;11(2):137-44.

214. Rodríguez A, De La Cera T, Herrero P, Moreno F. The hexokinase 2 protein regulates the expression of the GLK1, HXK1 and HXK2 genes of Saccharomyces cerevisiae. *Biochem. J*. 2001;355(Pt 3):625-631.

215. Westergaard SL, Oliveira AP, Bro C, Olsson L, Nielsen J. A systems biology approach to study glucose repression in the yeast Saccharomyces cerevisiae. *Biotechnol. Bioeng*. 2007;96(1):134-145.

216. Belinchón MM, Gancedo JM. Glucose controls multiple processes in Saccharomyces cerevisiae through diverse combinations of signaling pathways. *FEMS Yeast Res*. 2007;7(6):808-818.

217. Ma H, Botstein D. Effects of null mutations in the hexokinase genes of Saccharomyces cerevisiae on catabolite repression. *Mol. Cell. Biol*. 1986;6(11):4046-4052.

218. Petit T, Diderich JA, Kruckeberg AL, Gancedo C, Van Dam K. Hexokinase regulates kinetics of glucose transport and expression of genes encoding hexose transporters in Saccharomyces cerevisiae. *J Bacteriol*. 2000;182(23):6815-8.

219. Schuurmans JM, Boorsma A, Lascaris R, Hellingwerf KJ, Teixeira de Mattos MJ. Physiological and transcriptional characterization of Saccharomyces cerevisiae strains with modified expression of catabolic regulators. *FEMS Yeast Res*. 2008;8(1):26-34.

220. Raamsdonk LM, Diderich JA, Kuiper A, et al. Co-consumption of sugars or ethanol and glucose in a Saccharomyces cerevisiae strain deleted in the HXK2 gene. *Yeast*. 2001;18(11):1023-33.

221. Randez-Gil F, Herrero P, Sanz P, Prieto JA, Moreno F. Hexokinase PII has a double cytosolic-nuclear localisation in Saccharomyces cerevisiae. *FEBS Lett*. 1998;425(3):475-478.

222. Ahuatzi D, Herrero P, de la Cera T, Moreno F. The glucose-regulated nuclear localization of hexokinase 2 in Saccharomyces cerevisiae is Mig1-dependent. *J. Biol. Chem*. 2004;279(14):14440-14446.

223. Herrero P, Martínez-Campa C, Moreno F. The hexokinase 2 protein participates in regulatory DNA-protein complexes necessary for glucose repression of the SUC2 gene in Saccharomyces cerevisiae. *FEBS Lett*. 1998;434(1-2):71-76.

224. Randez-Gil F, Sanz P, Entian KD, Prieto JA. Carbon source-dependent phosphorylation of hexokinase PII and its role in the glucose-signaling response in yeast. *Mol. Cell. Biol*. 1998;18(5):2940-2948.

225. Ma H, Bloom LM, Walsh CT, Botstein D. The residual enzymatic phosphorylation activity of hexokinase II mutants is correlated with glucose repression in Saccharomyces cerevisiae. *Mol Cell Biol*. 1989;9(12):5643-9.

226. Mayordomo I, Sanz P. Hexokinase PII: structural analysis and glucose signalling in the yeast Saccharomyces cerevisiae. *Yeast*. 2001;18(10):923-930.

227. Kraakman LS, Winderickx J, Thevelein JM, De Winde JH. Structure-function analysis of yeast hexokinase: structural requirements for triggering cAMP signalling and catabolite repression. *Biochem J*. 1999;343 Pt 1:159-68.

228. Walsh RB, Clifton D, Horak J, Fraenkel DG. Saccharomyces cerevisiae null mutants in glucose phosphorylation: metabolism and invertase expression. *Genetics*. 1991;128(3):521-7.

229. Gancedo JM. Yeast carbon catabolite repression. *Microbiol. Mol. Biol. Rev*. 1998;62(2):334-361.

230. Gancedo JM. The early steps of glucose signalling in yeast. *FEMS Microbiol Rev*. 2008;32(4):673-704.

231. Celenza JL, Carlson M. A yeast gene that is essential for release from glucose repression encodes a protein kinase. *Science*. 1986;233(4769):1175-1180.

232. Hedbacker K, Carlson M. SNF1/AMPK pathways in yeast. *Front Biosci*. 2008;13:2408-20.

233. Carling D, Aguan K, Woods A, et al. Mammalian AMP-activated protein kinase is homologous to yeast and plant protein kinases involved in the regulation of carbon metabolism. *J. Biol. Chem*. 1994;269(15):11442-11448.

234. Hedbacker K, Carlson M. SNF1/AMPK pathways in yeast. *Front Biosci*. 2008;13:2408-20.

235. Hardie DG, Carling D, Carlson M. The AMP-activated/SNF1 protein kinase subfamily: metabolic sensors of the eukaryotic cell? *Annu Rev Biochem*. 1998;67:821-55.

236. Celenza JL, Carlson M. Structure and expression of the SNF1 gene of Saccharomyces cerevisiae. *Mol. Cell. Biol*. 1984;4(1):54-60.

237. Rubenstein EM, McCartney RR, Zhang C, et al. Access denied: Snf1 activation loop phosphorylation is controlled by availability of the phosphorylated threonine 210 to the PP1 phosphatase. *J. Biol. Chem*. 2008;283(1):222-230.

238. Wilson WA, Hawley SA, Hardie DG. Glucose repression/derepression in budding yeast: SNF1 protein kinase is activated by phosphorylation under derepressing conditions, and this correlates with a high AMP:ATP ratio. *Curr. Biol*. 1996;6(11):1426-1434.

239. McCartney RR, Schmidt MC. Regulation of Snf1 kinase. Activation requires phosphorylation of threonine 210 by an upstream kinase as well as a distinct step mediated by the Snf4 subunit. *J. Biol. Chem*. 2001;276(39):36460-36466.

240. Sanz P, Alms GR, Haystead TA, Carlson M. Regulatory interactions between the Reg1-Glc7 protein phosphatase and the Snf1 protein kinase. *Mol. Cell. Biol*. 2000;20(4):1321-1328.

241. Jiang R, Carlson M. Glucose regulates protein interactions within the yeast SNF1 protein kinase complex. *Genes Dev*. 1996;10(24):3105-3115.

242. Schmidt MC, McCartney RR. beta-subunits of Snf1 kinase are required for kinase function and substrate definition. *EMBO J*. 2000;19(18):4936-4943.

243. Hedbacker K, Townley R, Carlson M. Cyclic AMP-dependent protein kinase regulates the subcellular localization of Snf1-Sip1 protein kinase. *Mol Cell Biol*. 2004;24(5):1836-43.

244. Vincent O, Carlson M. Gal83 mediates the interaction of the Snf1 kinase complex with the transcription activator Sip4. *EMBO J*. 1999;18(23):6672-6681.

245. Vincent O, Townley R, Kuchin S, Carlson M. Subcellular localization of the Snf1 kinase is regulated by specific beta subunits and a novel glucose signaling mechanism. *Genes Dev*. 2001;15(9):1104-1114.

246. Estruch F, Treitel MA, Yang X, Carlson M. N-terminal mutations modulate yeast SNF1 protein kinase function. *Genetics*. 1992;132(3):639-650.

247. Leech A, Nath N, McCartney RR, Schmidt MC. Isolation of mutations in the catalytic domain of the snf1 kinase that render its activity independent of the snf4 subunit. *Eukaryotic Cell*. 2003;2(2):265-273.

248. McCartney RR, Schmidt MC. Regulation of Snf1 kinase. Activation requires phosphorylation of threonine 210 by an upstream kinase as well as a distinct step mediated by the Snf4 subunit. *J. Biol. Chem*. 2001;276(39):36460-36466.

249. Celenza JL, Carlson M. Mutational analysis of the Saccharomyces cerevisiae SNF1 protein kinase and evidence for functional interaction with the SNF4 protein. *Mol. Cell. Biol*. 1989;9(11):5034-5044.

250. Celenza JL, Eng FJ, Carlson M. Molecular analysis of the SNF4 gene of Saccharomyces cerevisiae: evidence for physical association of the SNF4 protein with the SNF1 protein kinase. *Mol. Cell. Biol*. 1989;9(11):5045-5054.

251. Hong S, Leiper FC, Woods A, Carling D, Carlson M. Activation of yeast Snf1 and mammalian AMP-activated protein kinase by upstream kinases. *Proc. Natl. Acad. Sci. U.S.A*. 2003;100(15):8839-8843.

252. Elbing K, Rubenstein EM, McCartney RR, Schmidt MC. Subunits of the Snf1 kinase heterotrimer show interdependence for association and activity. *J. Biol. Chem*. 2006;281(36):26170-26180.

253. Bouquin N, Barral Y, Courbeyrette R, et al. Regulation of cytokinesis by the Elm1 protein kinase in Saccharomyces cerevisiae. *J. Cell. Sci*. 2000;113 ( Pt 8):1435-1445.

254. Koehler CM, Myers AM. Serine-threonine protein kinase activity of Elm1p, a regulator of morphologic differentiation in Saccharomyces cerevisiae. *FEBS Lett*. 1997;408(1):109-114.

255. Garrett JM. The control of morphogenesis in Saccharomyces cerevisiae by Elm1 kinase is responsive to RAS/cAMP pathway activity and tryptophan availability. *Mol. Microbiol*. 1997;26(4):809-820.

256. Kim M, Hong S, Carlson M. Role of Tos3, a Snf1 protein kinase kinase, during growth of Saccharomyces cerevisiae on nonfermentable carbon sources. *Eukaryotic Cell*. 2005;4(5):861-866.

257. Hedbacker K, Hong S, Carlson M. Pak1 protein kinase regulates activation and nuclear localization of Snf1-Gal83 protein kinase. *Mol. Cell. Biol*. 2004;24(18):8255-8263.

258. McCartney RR, Rubenstein EM, Schmidt MC. Snf1 kinase complexes with different beta subunits display stress-dependent preferences for the three Snf1-activating kinases. *Curr. Genet*. 2005;47(6):335-344.

259. Nigavekar SS, Tan YSH, Cannon JF. Glc8 is a glucose-repressible activator of Glc7 protein phosphatase-1. *Arch. Biochem. Biophys*. 2002;404(1):71-79.

260. Gilbert W, Guthrie C. The Glc7p nuclear phosphatase promotes mRNA export by facilitating association of Mex67p with mRNA. *Mol Cell*. 2004;13(2):201-12.

261. Feng ZH, Wilson SE, Peng ZY, et al. The yeast GLC7 gene required for glycogen accumulation encodes a type 1 protein phosphatase. *J. Biol. Chem*. 1991;266(35):23796-23801.

262. Kozubowski L, Panek H, Rosenthal A, et al. A Bni4-Glc7 phosphatase complex that recruits chitin synthase to the site of bud emergence. *Mol. Biol. Cell*. 2003;14(1):26-39.

263. Knaus M, Cameroni E, Pedruzzi I, et al. The Bud14p-Glc7p complex functions as a cortical regulator of dynein in budding yeast. *EMBO J*. 2005;24(17):3000-3011.

264. Wu X, Hart H, Cheng C, Roach PJ, Tatchell K. Characterization of Gac1p, a regulatory subunit of protein phosphatase type I involved in glycogen accumulation in Saccharomyces cerevisiae. *Mol. Genet. Genomics*. 2001;265(4):622-635.

265. Sassoon I, Severin FF, Andrews PD, et al. Regulation of Saccharomyces cerevisiae kinetochores by the type 1 phosphatase Glc7p. *Genes Dev*. 1999;13(5):545-55.

266. Nedea E, He X, Kim M, et al. Organization and function of APT, a subcomplex of the yeast cleavage and polyadenylation factor involved in the formation of mRNA and small nucleolar RNA 3'-ends. *J. Biol. Chem*. 2003;278(35):33000-33010.

267. Peggie MW, MacKelvie SH, Bloecher A, et al. Essential functions of Sds22p in chromosome stability and nuclear localization of PP1. *J. Cell. Sci*. 2002;115(Pt 1):195-206.

268. Sanz M, Castrejón F, Durán A, Roncero C. Saccharomyces cerevisiae Bni4p directs the formation of the chitin ring and also participates in the correct assembly of the septum structure. *Microbiology (Reading, Engl.)*. 2004;150(Pt 10):3229-3241.

269. Lin JT, Lis JT. Glycogen synthase phosphatase interacts with heat shock factor to activate CUP1 gene transcription in Saccharomyces cerevisiae. *Mol. Cell. Biol*. 1999;19(5):3237-3245.

270. Tung HY, Wang W, Chan CS. Regulation of chromosome segregation by Glc8p, a structural homolog of mammalian inhibitor 2 that functions as both an activator and an inhibitor of yeast protein phosphatase 1. *Mol. Cell. Biol*. 1995;15(11):6064-6074.

271. Wu X, Tatchell K. Mutations in yeast protein phosphatase type 1 that affect targeting subunit binding. *Biochemistry*. 2001;40(25):7410-20.

272. Tu J, Carlson M. The GLC7 type 1 protein phosphatase is required for glucose repression in Saccharomyces cerevisiae. *Mol. Cell. Biol*. 1994;14(10):6789-6796.

273. Neigeborn L, Carlson M. Mutations causing constitutive invertase synthesis in yeast: genetic interactions with snf mutations. *Genetics*. 1987;115(2):247-253.

274. Zimmermann FK, Scheel I. Mutants of Saccharomyces cerevisiae resistant to carbon catabolite repression. *Mol. Gen. Genet*. 1977;154(1):75-82.

275. Egloff MP, Johnson DF, Moorhead G, et al. Structural basis for the recognition of regulatory subunits by the catalytic subunit of protein phosphatase 1. *EMBO J*. 1997;16(8):1876-1887.

276. Dombek KM, Voronkova V, Raney A, Young ET. Functional analysis of the yeast Glc7-binding protein Reg1 identifies a protein phosphatase type 1-binding motif as essential for repression of ADH2 expression. *Mol. Cell. Biol*. 1999;19(9):6029-6040.

277. Erickson JR, Johnston M. Suppressors reveal two classes of glucose repression genes in the yeast Saccharomyces cerevisiae. *Genetics*. 1994;136(4):1271-1278.

278. Neigeborn L, Carlson M. Mutations causing constitutive invertase synthesis in yeast: genetic interactions with snf mutations. *Genetics*. 1987;115(2):247-253.

279. Sanz P, Alms GR, Haystead TA, Carlson M. Regulatory interactions between the Reg1-Glc7 protein phosphatase and the Snf1 protein kinase. *Mol. Cell. Biol*. 2000;20(4):1321-1328.

280. Ludin K, Jiang R, Carlson M. Glucose-regulated interaction of a regulatory subunit of protein phosphatase 1 with the Snf1 protein kinase in Saccharomyces cerevisiae. *Proc Natl Acad Sci U S A*. 1998;95(11):6245-50.

281. Rubenstein EM, McCartney RR, Zhang C, et al. Access denied: Snf1 activation loop phosphorylation is controlled by availability of the phosphorylated threonine 210 to the PP1 phosphatase. *J Biol Chem*. 2008;283(1):222-30.

282. McCartney RR, Schmidt MC. Regulation of Snf1 Kinase. *Journal of Biological Chemistry*. 2001;276(39):36460-36466.

283. McCartney RR, Schmidt MC. Regulation of Snf1 kinase. Activation requires phosphorylation of threonine 210 by an upstream kinase as well as a distinct step mediated by the Snf4 subunit. *J. Biol. Chem*. 2001;276(39):36460-36466.

284. Jiang R, Carlson M. The Snf1 protein kinase and its activating subunit, Snf4, interact with distinct domains of the Sip1/Sip2/Gal83 component in the kinase complex. *Mol. Cell. Biol*. 1997;17(4):2099-2106.

285. Wilson WA, Hawley SA, Hardie DG. Glucose repression/derepression in budding yeast: SNF1 protein kinase is activated by phosphorylation under derepressing conditions, and this correlates with a high AMP:ATP ratio. *Curr. Biol*. 1996;6(11):1426-1434.

286. Bloecher A, Tatchell K. Dynamic localization of protein phosphatase type 1 in the mitotic cell cycle of Saccharomyces cerevisiae. *J. Cell Biol*. 2000;149(1):125-140.

287. Nehlin JO, Ronne H. Yeast MIG1 repressor is related to the mammalian early growth response and Wilms' tumour finger proteins. *EMBO J*. 1990;9(9):2891-2898.

288. Griggs DW, Johnston M. Regulated expression of the GAL4 activator gene in yeast provides a sensitive genetic switch for glucose repression. *Proc. Natl. Acad. Sci. U.S.A*. 1991;88(19):8597-8601.

289. Flick JS, Johnston M. Analysis of URSG-mediated glucose repression of the GAL1 promoter of Saccharomyces cerevisiae. *Genetics*. 1992;130(2):295-304.

290. Johnston M, Flick JS, Pexton T. Multiple mechanisms provide rapid and stringent glucose repression of GAL gene expression in Saccharomyces cerevisiae. *Mol. Cell. Biol*. 1994;14(6):3834-3841.

291. Lundin M, Nehlin JO, Ronne H. Importance of a flanking AT-rich region in target site recognition by the GC box-binding zinc finger protein MIG1. *Mol. Cell. Biol*. 1994;14(3):1979-1985.

292. Hu Z, Nehlin JO, Ronne H, Michels CA. MIG1-dependent and MIG1-independent glucose regulation of MAL gene expression in Saccharomyces cerevisiae. *Curr. Genet*. 1995;28(3):258-266.

293. Klein CJ, Olsson L, Rønnow B, Mikkelsen JD, Nielsen J. Alleviation of glucose repression of maltose metabolism by MIG1 disruption in Saccharomyces cerevisiae. *Appl Environ Microbiol*. 1996;62(12):4441-9.

294. Sierkstra LN, Verbakel JM, Verrips CT. Analysis of transcription and translation of glycolytic enzymes in glucose-limited continuous cultures of Saccharomyces cerevisiae. *J Gen Microbiol*. 1992;138(12):2559-66.

295. de Winde JH, Grivell LA. Global regulation of mitochondrial biogenesis in Saccharomyces cerevisiae. *Prog. Nucleic Acid Res. Mol. Biol*. 1993;46:51-91.

296. Kratzer S, Schüller HJ. Transcriptional control of the yeast acetyl-CoA synthetase gene, ACS1, by the positive regulators CAT8 and ADR1 and the pleiotropic repressor UME6. *Mol. Microbiol*. 1997;26(4):631-641.

297. Mercado JJ, Gancedo JM. Regulatory regions in the yeast FBP1 and PCK1 genes. *FEBS Lett*. 1992;311(2):110-114.

298. Mercado JJ, Vincent O, Gancedo JM. Regions in the promoter of the yeast FBP1 gene implicated in catabolite repression may bind the product of the regulatory gene MIG1. *FEBS Lett*. 1991;291(1):97-100.

299. Lundin M, Nehlin JO, Ronne H. Importance of a flanking AT-rich region in target site recognition by the GC box-binding zinc finger protein MIG1. *Mol. Cell. Biol*. 1994;14(3):1979-1985.

300. Hedges D, Proft M, Entian KD. CAT8, a new zinc cluster-encoding gene necessary for derepression of gluconeogenic enzymes in the yeast Saccharomyces cerevisiae. *Mol. Cell. Biol*. 1995;15(4):1915-1922.

301. Rahner A, Schöler A, Martens E, Gollwitzer B, Schüller HJ. Dual influence of the yeast Cat1p (Snf1p) protein kinase on carbon source-dependent transcriptional activation of gluconeogenic genes by the regulatory gene CAT8. *Nucleic Acids Res*. 1996;24(12):2331-2337.

302. Schöler A, Schüller HJ. A carbon source-responsive promoter element necessary for activation of the isocitrate lyase gene ICL1 is common to genes of the gluconeogenic pathway in the yeast Saccharomyces cerevisiae. *Mol. Cell. Biol*. 1994;14(6):3613-3622.

303. Klein CJ, Olsson L, Nielsen J. Glucose control in Saccharomyces cerevisiae: the role of Mig1 in metabolic functions. *Microbiology*. 1998;144 ( Pt 1):13-24.

304. Turcotte B, Liang XB, Robert F, Soontorngun N. Transcriptional regulation of nonfermentable carbon utilization in budding yeast. *FEMS Yeast Res*. 2009.

305. Gancedo JM. Carbon catabolite repression in yeast. *Eur. J. Biochem*. 1992;206(2):297-313.

306. Rosenkrantz M, Kell CS, Pennell EA, Devenish LJ. The HAP2,3,4 transcriptional activator is required for derepression of the yeast citrate synthase gene, CIT1. *Mol. Microbiol*. 1994;13(1):119-131.

307. Schlaepfer IR, Mattoon JR, Bajszár G. The sequence and potential regulatory elements of the HEM2 promoter of Saccharomyces cerevisiae. *Yeast*. 1994;10(2):227-229.

308. Kaniak A, Xue Z, Macool D, Kim J, Johnston M. Regulatory network connecting two glucose signal transduction pathways in Saccharomyces cerevisiae. *Eukaryotic Cell*. 2004;3(1):221-231.

309. De Vit MJ, Waddle JA, Johnston M. Regulated nuclear translocation of the Mig1 glucose repressor. *Mol. Biol. Cell*. 1997;8(8):1603-1618.

310. DeVit MJ, Johnston M. The nuclear exportin Msn5 is required for nuclear export of the Mig1 glucose repressor of Saccharomyces cerevisiae. *Curr. Biol*. 1999;9(21):1231-1241.

311. Schüller H. Transcriptional control of nonfermentative metabolism in the yeast Saccharomyces cerevisiae. *Curr. Genet*. 2003;43(3):139-160.

312. Vallier LG, Carlson M. Synergistic release from glucose repression by mig1 and ssn mutations in Saccharomyces cerevisiae. *Genetics*. 1994;137(1):49-54.

313. Smith FC, Davies SP, Wilson WA, Carling D, Hardie DG. The SNF1 kinase complex from Saccharomyces cerevisiae phosphorylates the transcriptional repressor protein Mig1p in vitro at four sites within or near regulatory domain 1. *FEBS Lett*. 1999;453(1-2):219-223.

314. Treitel MA, Kuchin S, Carlson M. Snf1 protein kinase regulates phosphorylation of the Mig1 repressor in Saccharomyces cerevisiae. *Mol Cell Biol*. 1998;18(11):6273-80.

315. Ahuatzi D, Riera A, Peláez R, Herrero P, Moreno F. Hxk2 regulates the phosphorylation state of Mig1 and therefore its nucleocytoplasmic distribution. *J. Biol. Chem*. 2007;282(7):4485-4493.

316. Rahner A, Schöler A, Martens E, Gollwitzer B, Schüller HJ. Dual influence of the yeast Cat1p (Snf1p) protein kinase on carbon source-dependent transcriptional activation of gluconeogenic genes by the regulatory gene CAT8. *Nucleic Acids Res*. 1996;24(12):2331-2337.

317. Young ET, Dombek KM, Tachibana C, Ideker T. Multiple pathways are co-regulated by the protein kinase Snf1 and the transcription factors Adr1 and Cat8. *J Biol Chem*. 2003;278(28):26146-58.

318. Vincent O, Carlson M. Sip4, a Snf1 kinase-dependent transcriptional activator, binds to the carbon source-responsive element of gluconeogenic genes. *EMBO J*. 1998;17(23):7002-7008.

319. Klein CJ, Rasmussen JJ, Rønnow B, Olsson L, Nielsen J. Investigation of the impact of MIG1 and MIG2 on the physiology of Saccharomyces cerevisiae. *J Biotechnol*. 1999;68(2-3):197-212.

320. Randez-Gil F, Bojunga N, Proft M, Entian KD. Glucose derepression of gluconeogenic enzymes in Saccharomyces cerevisiae correlates with phosphorylation of the gene activator Cat8p. *Mol. Cell. Biol*. 1997;17(5):2502-2510.

321. Schöler A, Schüller HJ. A carbon source-responsive promoter element necessary for activation of the isocitrate lyase gene ICL1 is common to genes of the gluconeogenic pathway in the yeast Saccharomyces cerevisiae. *Mol. Cell. Biol*. 1994;14(6):3613-3622.

322. Niederacher D, Schüller HJ, Grzesitza D, et al. Identification of UAS elements and binding proteins necessary for derepression of Saccharomyces cerevisiae fructose-1,6-bisphosphatase. *Curr. Genet*. 1992;22(5):363-370.

323. Haurie V, Perrot M, Mini T, et al. The transcriptional activator Cat8p provides a major contribution to the reprogramming of carbon metabolism during the diauxic shift in Saccharomyces cerevisiae. *J Biol Chem*. 2001;276(1):76-85.

324. Roth S, Schüller HJ. Cat8 and Sip4 mediate regulated transcriptional activation of the yeast malate dehydrogenase gene MDH2 by three carbon source-responsive promoter elements. *Yeast*. 2001;18(2):151-62.

325. Kratzer S, Schüller HJ. Transcriptional control of the yeast acetyl-CoA synthetase gene, ACS1, by the positive regulators CAT8 and ADR1 and the pleiotropic repressor UME6. *Mol. Microbiol*. 1997;26(4):631-641.

326. Bojunga N, Kötter P, Entian KD. The succinate/fumarate transporter Acr1p of Saccharomyces cerevisiae is part of the gluconeogenic pathway and its expression is regulated by Cat8p. *Mol. Gen. Genet*. 1998;260(5):453-461.

327. Bojunga N, Entian KD. Cat8p, the activator of gluconeogenic genes in Saccharomyces cerevisiae, regulates carbon source-dependent expression of NADP-dependent cytosolic isocitrate dehydrogenase (Idp2p) and lactate permease (Jen1p). *Mol. Gen. Genet*. 1999;262(4-5):869-875.

328. Brons JF, De Jong M, Valens M, et al. Dissection of the promoter of the HAP4 gene in S. cerevisiae unveils a complex regulatory framework of transcriptional regulation. *Yeast*. 2002;19(11):923-932.

329. Reid R, Lisby M, Rothstein R. Cloning-free genome alterations in Saccharomyces cerevisiae using adaptamer-mediated PCR. In: *Methods in Enzymology*.Vol 350. New York: Academic Press; 2002:258-277.

330. Fairhead C, Llorente B, Denis F, Soler M, Dujon B. New vectors for combinatorial deletions in yeast chromosomes and for gap-repair cloning using 'split-marker' recombination. *Yeast*. 1996;12(14):1439-1457.

331. Harsha HC, Molina H, Pandey A. Quantitative proteomics using stable isotope labeling with amino acids in cell culture. *Nat Protoc*. 2008;3(3):505-16.

332. Keller A, Nesvizhskii AI, Kolker E, Aebersold R. Empirical statistical model to estimate the accuracy of peptide identifications made by MS/MS and database search. *Anal Chem*. 2002;74(20):5383-92.

333. Nesvizhskii AI, Keller A, Kolker E, Aebersold R. A statistical model for identifying proteins by tandem mass spectrometry. *Anal Chem*. 2003;75(17):4646-58.

334. Li X, Zhang H, Ranish JA, Aebersold R. Automated statistical analysis of protein abundance ratios from data generated by stable-isotope dilution and tandem mass spectrometry. *Anal Chem*. 2003;75(23):6648-57.

335. Schmitt ME, Brown TA, Trumpower BL. A rapid and simple method for preparation of RNA from Saccharomyces cerevisiae. *Nucleic Acids Res*. 1990;18(10):3091-3092.

336. Tong AHY, Evangelista M, Parsons AB, et al. Systematic Genetic Analysis with Ordered Arrays of Yeast Deletion Mutants. *Science*. 2001;294(5550):2364-2368.

337. Ghaemmaghami S, Huh W, Bower K, et al. Global analysis of protein expression in yeast. *Nature*. 2003;425(6959):737-741.

338. Horvath A, Riezman H. Rapid protein extraction from Saccharomyces cerevisiae. *Yeast*. 1994;10(10):1305-1310.

339. Teixeira MC, Monteiro P, Jain P, et al. The YEASTRACT database: a tool for the analysis of transcription regulatory associations in Saccharomyces cerevisiae. *Nucl. Acids Res.* 2006;34(suppl_1):D446-451.

340. Huan T, Sivachenko A, Harrison S, Chen J. ProteoLens: a visual analytic tool for multi-scale database-driven biological network data mining. *BMC Bioinformatics*. 2008;9(Suppl 9):S5.

341. Ashburner M, Ball CA, Blake JA, et al. Gene ontology: tool for the unification of biology. The Gene Ontology Consortium. *Nat. Genet*. 2000;25(1):25-29.

342. Lu Y, Rosenfeld R, Simon I, Nau GJ, Bar-Joseph Z. A probabilistic generative model for GO enrichment analysis. *Nucleic Acids Res*. 2008;36(17):e109.

343. Liu H, Sadygov RG, Yates JR. A model for random sampling and estimation of relative protein abundance in shotgun proteomics. *Anal Chem*. 2004;76(14):4193-201.

344. Bridges SM, Magee GB, Wang N, et al. ProtQuant: a tool for the label-free quantification of MudPIT proteomics data. *BMC Bioinformatics*. 2007;8 Suppl 7:S24.

345. Saccharomyces Genome Database. 2008. Available at: http://www.yeastgenome.org/ [Accessed August 6, 2008].

346. Barral Y, Jentsch S, Mann C. G1 cyclin turnover and nutrient uptake are controlled by a common pathway in yeast. *Genes Dev*. 1995;9(4):399-409.

347. Kishi T, Yamao F. An essential function of Grr1 for the degradation of Cln2 is to act as a binding core that links Cln2 to Skp1. *J Cell Sci*. 1998;111 ( Pt 24):3655-61.

348. Höfken T, Schiebel E. Novel regulation of mitotic exit by the Cdc42 effectors Gic1 and Gic2. *J Cell Biol*. 2004;164(2):219-31.

349. Ong S, Blagoev B, Kratchmarova I, et al. Stable isotope labeling by amino acids in cell culture, SILAC, as a simple and accurate approach to expression proteomics. *Mol Cell Proteomics*. 2002;1(5):376-86.

350. America AHP, Cordewener JHG. Comparative LC-MS: a landscape of peaks and valleys. *Proteomics*. 2008;8(4):731-49.

351. Old WM, Meyer-Arendt K, Aveline-Wolf L, et al. Comparison of label-free methods for quantifying human proteins by shotgun proteomics. *Mol Cell Proteomics*. 2005;4(10):1487-502.

352. Bantscheff M, Schirle M, Sweetman G, Rick J, Kuster B. Quantitative mass spectrometry in proteomics: a critical review. *Anal Bioanal Chem*. 2007;389(4):1017-31.

353. Finney GL, Blackler AR, Hoopmann MR, et al. Label-free comparative analysis of proteomics mixtures using chromatographic alignment of high-resolution muLC-MS data. *Anal Chem*. 2008;80(4):961-71.

354. Choe L, D'Ascenzo M, Relkin NR, et al. 8-plex quantitation of changes in cerebrospinal fluid protein expression in subjects undergoing intravenous immunoglobulin treatment for Alzheimer's disease. *Proteomics*. 2007;7(20):3651-60.

355. Ross PL, Huang YN, Marchese JN, et al. Multiplexed protein quantitation in Saccharomyces cerevisiae using amine-reactive isobaric tagging reagents. *Mol Cell Proteomics*. 2004;3(12):1154-69.

356. López-Ferrer D, Ramos-Fernández A, Martínez-Bartolomé S, García-Ruiz P, Vázquez J. Quantitative proteomics using 16O/18O labeling and linear ion trap mass spectrometry. *Proteomics*. 2006;6 Suppl 1:S4-11.

357. Johnson KL, Muddiman DC. A method for calculating 16O/18O peptide ion ratios for the relative quantification of proteomes. *J Am Soc Mass Spectrom*. 2004;15(4):437-45.

358. Mirza SP, Olivier M. Methods and approaches for the comprehensive characterization and quantification of cellular proteomes using mass spectrometry. *Physiol Genomics*. 2008;33(1):3-11.

359. Gygi SP, Rist B, Gerber SA, et al. Quantitative analysis of complex protein mixtures using isotope-coded affinity tags. *Nat Biotech*. 1999;17(10):994-999.

360. Ong S, Mann M. Stable isotope labeling by amino acids in cell culture for quantitative proteomics. *Methods Mol Biol*. 2007;359:37-52.

361. Schmidt F, Hustoft HK, Strozynski M, et al. Quantitative proteome analysis of cisplatin-induced apoptotic Jurkat T cells by stable isotope labeling with amino acids in cell culture, SDS-PAGE, and LC-MALDI-TOF/TOF MS. *Electrophoresis*. 2007;28(23):4359-68.

362. Graumann J, Hubner NC, Kim JB, et al. Stable Isotope Labeling by Amino Acids in Cell Culture (SILAC) and Proteome Quantitation of Mouse Embryonic Stem Cells to a Depth of 5,111 Proteins. *Mol Cell Proteomics*. 2008;7(4):672-683.

363. Ong S, Mann M. A practical recipe for stable isotope labeling by amino acids in cell culture (SILAC). *Nat. Protocols*. 2007;1(6):2650-2660.

364. Jones E, Fink GR. Regulation of amino acid and nucleotide biosynthesis in yeast. In: *The Molecular Biology of the Yeast Saccharomyces: Metabolism and Gene Expression*. Cold Spring Harbor Laboratory Press, Cold Spring Harbor, NY; 1982:181-299.

365. Godard P, Urrestarazu A, Vissers S, et al. Effect of 21 different nitrogen sources on global gene expression in the yeast Saccharomyces cerevisiae. *Mol Cell Biol*. 2007;27(8):3065-86.

366. Bendall SC, Hughes C, Stewart MH, et al. Prevention of amino acid conversion in SILAC experiments with embryonic stem cells. *Mol Cell Proteomics*. 2008.

367. Jiang H, English AM. Quantitative analysis of the yeast proteome by incorporation of isotopically labeled leucine. *J Proteome Res*. 2002;1(4):345-50.

368. Sikorski RS, Hieter P. A system of shuttle vectors and yeast host strains designed for efficient manipulation of DNA in Saccharomyces cerevisiae. *Genetics*. 1989;122(1):19-27.

369. Webb AAIJ. Fusel Oil. *Adv. Appl. Microbiol.* 1963;(5):317-353.

370. Sentheshanuganathan S. The mechanism of the formation of higher alcohols from amino acids by Saccharomyces cerevisiae. *Biochem. J*. 1960;(74):568-576.

371. Gevaert K, Impens F, Ghesquière B, et al. Stable isotopic labeling in proteomics. *Proteomics*. 2008;8(23-24):4873-4885.

372. Hamdan M, Righetti PG. Modern strategies for protein quantification in proteome analysis: advantages and limitations. *Mass Spectrometry Reviews*. 21(4):287-302.

373. Magasanik B, Kaiser CA. Nitrogen regulation in Saccharomyces cerevisiae. *Gene*. 2002;290(1-2):1-18.

374. Jauniaux J, Grenson M. GAP1, the general amino acid permease gene of Saccharomyces cerevisiae.. *European Journal of Biochemistry*. 1990;190(1):39-44.

375. Simpson RJ. *Proteins and Proteomics: A Laboratory Manual*. Cold Spring Harbor Laboratory Press; 2003.

376. Layne E. In: *Methods in Enzymology*.Vol 3.; 1957:447.

377. Lowry O, Rosebrough N, Randall R. *J. Biol. Chem*. 1951;(193):265.

378. Smith PK, Krohn RI, Hermanson GT, et al. Measurement of protein using bicinchoninic acid. *Anal. Biochem*. 1985;150(1):76-85.

379. Wiechelman KJ, Braun RD, Fitzpatrick JD. Investigation of the bicinchoninic acid protein assay: identification of the groups responsible for color formation. *Anal. Biochem*. 1988;175(1):231-7.

380. Bradford MM. A rapid and sensitive method for the quantitation of microgram quantities of protein utilizing the principle of protein-dye binding. *Anal. Biochem*. 1976;72:248-54.

381. Cleland WW. Dithiothreitol, A New Protective Reagent for SH Groups. *Biochemistry*. 1964;3:480-2.

382. Konigsberg W. Reduction of disulfide bonds in proteins with dithiothreitol. In: *Methods in Enzymology*.Vol 25.; 1972:185-188.

383. Hirs C. Determination of cystine as as cysteic acid. In: *Methods in Enzymology*.Vol 11.; 1967:59-62.

384. Crestfield AM, Moore S, Stein WH. The preparation and enzymatic hydrolysis of reduced and S-carboxymethylated proteins. *J. Biol. Chem*. 1963;238:622-7.

385. Nägele E, Vollmer M, Hörth P, Vad C. 2D-LC/MS techniques for the identification of proteins in highly complex mixtures. *Expert Review of Proteomics*. 2004;1(1):37-46.

386. Fenn JB, Mann M, Meng CK, Wong SF, Whitehouse CM. Electrospray ionization for mass spectrometry of large biomolecules. *Science*. 1989;246(4926):64-71.

387. Resing KA, Meyer-Arendt K, Mendoza AM, et al. Improving reproducibility and sensitivity in identifying human proteins by shotgun proteomics. *Anal. Chem*. 2004;76(13):3556-68.

388. Yen C, Russell S, Mendoza A, et al. Improving Sensitivity in Shotgun Proteomics Using a Peptide-Centric Database with Reduced Complexity: Protease Cleavage and SCX Elution Rules from Data Mining of MS/MS Spectra. *Anal. Chem.* 2006;78(4):1071-1084.

389. Resing KA, Ahn NG. Proteomics strategies for protein identification. *FEBS Lett*. 2005;579(4):885-9.

390. Fischer F, Poetsch A. Protein cleavage strategies for an improved analysis of the membrane proteome. *Proteome Science*. 2006;4:2.

391. Sandra K, Moshir M, D'hondt F, et al. Highly efficient peptide separations in proteomics: Part 1. Unidimensional high performance liquid chromatography. *Journal of Chromatography B*. 2008;866(1-2):48-63.

392. Wolters DA, Washburn MP, Yates JR. An automated multidimensional protein identification technology for shotgun proteomics. *Anal Chem*. 2001;73(23):5683-90.

393. Giddings JC. *Unified Separation Science*. New York: John Wiley & Sons; 1991.

394. Mitulovic G, Mechtler K. HPLC techniques for proteomics analysis--a short overview of latest developments. *Brief Funct Genomic Proteomic*. 2006;5(4):249-60.

395. Kascaronička V. Capillary electrophoresis of peptides. *Electrophoresis*. 1999;20(15-16):3084-3105.

396. Simpson DC, Smith RD. Combining capillary electrophoresis with mass spectrometry for applications in proteomics. *Electrophoresis*. 2005;26(7-8):1291-305.

397. Issaq HJ, Conrads TP, Janini GM, Veenstra TD. Methods for fractionation, separation and profiling of proteins and peptides. *Electrophoresis*. 2002;23(17):3048-61.

398. Issaq HJ, Chan KC, Janini GM, Conrads TP, Veenstra TD. Multidimensional separation of peptides for effective proteomic analysis. *J Chromatogr B Analyt Technol Biomed Life Sci*. 2005;817(1):35-47.

399. Scott RPW. *Liquid Chromatography Column Theory*. 1st ed. John Wiley & Sons; 1991.

400. Jandera P(. *Gradient Elution in Column Liquid Chromatography: Theory and Practice*. Elsevier; 1985.

401. Rachinskii VV(V. *The General Theory of Sorption Dynamics and Chromatography. Authorized Translation from the Russian*. Consultants Bureau; 1965.

402. Krstulovi*c AM. *Reversed-Phase High-Performance Liquid Chromatography: Theory, Practice, and Biomedical Applications*. Wiley; 1982.

403. Davis JM, Giddings JC. Origin and characterization of departures from the statistical model of component-peak overlap in chromatography. *J Chromatogr*. 1984;289:277-98.

404. Davis JM, Giddings JC. Statistical method for estimation of number of components from single complex chromatograms: application to experimental chromatograms. *Anal Chem*. 1985;57(12):2178-82.

405. Davis JM, Giddings JC. Statistical method for estimation of number of components from single complex chromatograms: theory, computer-based testing, and analysis of errors. *Anal Chem*. 1985;57(12):2168-77.

406. Giddings JC. Two-dimensional separations: concept and promise. *Anal Chem*. 1984;56(12):1258A-1260A, 1262A, 1264A passim.

407. Wolters DA, Washburn MP, Yates JR. An automated multidimensional protein identification technology for shotgun proteomics. *Anal Chem*. 2001;73(23):5683-90.

408. Peng J, Elias JE, Thoreen CC, Licklider LJ, Gygi SP. Evaluation of multidimensional chromatography coupled with tandem mass spectrometry (LC/LC-MS/MS) for large-scale protein analysis: the yeast proteome. *J Proteome Res*. 2(1):43-50.

409. Washburn MP, Wolters D, Yates JR. Large-scale analysis of the yeast proteome by multidimensional protein identification technology. *Nat Biotechnol*. 2001;19(3):242-7.

410. Fenn JB, Mann M, Meng CK, Wong SF, Whitehouse CM. Electrospray ionization for mass spectrometry of large biomolecules. *Science*. 1989;246(4926):64-71.

411. Fenn J. Electrospray ionization mass spectrometry: How it all began. *J Biomol Tech*. 2002;13(3):101-118.

412. Fenn JB. Electrospray wings for molecular elephants (Nobel lecture). *Angew. Chem. Int. Ed. Engl*. 2003;42(33):3871-3894.

413. Annesley TM. Ion Suppression in Mass Spectrometry. *Clin Chem*. 2003;49(7):1041-1044.

414. Watson JT. *Introduction to Mass Spectrometry*. 3rd ed. Lippincott-Raven; 1997.

415. Herbert CG. *Mass Spectrometry Basics*. CRC Press; 2003.

416. Sadygov RG, Cociorva D, Yates JR. Large-scale database searching using tandem mass spectra: looking up the answer in the back of the book. *Nat. Methods*. 2004;1(3):195-202.

417. Sadygov RG, Cociorva D, Yates JR. Large-scale database searching using tandem mass spectra: looking up the answer in the back of the book. *Nat Methods*. 2004;1(3):195-202.

418. Eng JK, McCormack AL, Yates JR. An approach to correlate tandem mass spectral data of peptides with amino acid sequences in a protein database. *Journal of the American Society for Mass Spectrometry*. 1994;5(11):976-989.

419. Eng JK, McCormack AL, Yates III JR. An approach to correlate tandem mass spectral data of peptides with amino acid sequences in a protein database. *Journal of the American Society for Mass Spectrometry*. 1994;5(11):976-989.

420. Johnson RS, Martin SA, Biemann K, Stults JT, Watson JT. Novel fragmentation process of peptides by collision-induced decomposition in a tandem mass spectrometer: differentiation of leucine and isoleucine. *Analytical Chemistry*. 1987;59(21):2621-2625.

421. P. Lee Ferguson and and Richard D. Smith, Proteome Analysis by Mass Spectrometry, *Annual Review of Biophysics and Biomolecular Structure* 32 (June 2003): 399-424.

422. Pedrioli PGA, Eng JK, Hubley R, et al. A common open representation of mass spectrometry data and its application to proteomics research. *Nat. Biotechnol*. 2004;22(11):1459-1466.

423. Khalsa-Moyers G, McDonald WH. Developments in mass spectrometry for the analysis of complex protein mixtures. *Briefings in Functional Genomics & Proteomics*. 2006;5(2):98-111.

424. Olsen JV, Mann M. Improved peptide identification in proteomics by two consecutive stages of mass spectrometric fragmentation. *Proc Natl Acad Sci U S A*. 2004;101(37):13417-22.

425. Washburn MP, Wolters D, Yates JR. Large-scale analysis of the yeast proteome by multidimensional protein identification technology. *Nat Biotechnol*. 2001;19(3):242-7.

426. Fournier ML, Gilmore JM, Martin-Brown SA, Washburn MP. Multidimensional separations-based shotgun proteomics. *Chem. Rev*. 2007;107(8):3654-86.

427. Picotti P, Bodenmiller B, Mueller LN, Domon B, Aebersold R. Full dynamic range proteome analysis of S. cerevisiae by targeted proteomics. *Cell*. 2009;138(4):795-806.

428. Ghaemmaghami S, Huh W, Bower K, et al. Global analysis of protein expression in yeast. *Nature*. 2003;425(6959):737-741.

429. Efron B, Tibshirani R, Storey JD, Tusher V. Empirical Bayes Analysis of a Microarray Experiment. *Journal of the American Statistical Association*. 2001;96(456):1151-1160.

430. Issaq HJ, Chan KC, Janini GM, Conrads TP, Veenstra TD. Multidimensional separation of peptides for effective proteomic analysis. *Journal of Chromatography B*. 2005;817(1):35-47.

431. Trimpin S, Brizzard B. Analysis of insoluble proteins. *BioTechniques*. 2009;46(6):409-419.

432. Rabilloud T. Membrane proteins and proteomics: love is possible, but so difficult. *Electrophoresis*. 2009;30 Suppl 1:S174-180.

433. Ashburner M, Ball CA, Blake JA, et al. Gene Ontology: tool for the unification of biology. *Nat Genet*. 2000;25(1):25-29.

434. Lu Y, Rosenfeld R, Simon I, Nau GJ, Bar-Joseph Z. A probabilistic generative model for GO enrichment analysis. *Nucleic Acids Res*. 2008;36(17):e109.

435. Zimmermann FK, Kaufmann I, Rasenberger H, Haubetamann P. Genetics of carbon catabolite repression in Saccharomycess cerevisiae: genes involved in the derepression process. *Mol Gen Genet*. 1977;151(1):95-103.

436. Poulsen P, Wu B, Gaber RF, et al. Amino acid sensing by Ssy1. *Biochem. Soc. Trans*. 2005;33(Pt 1):261-4.

437. Kodama Y, Omura F, Takahashi K, Shirahige K, Ashikari T. Genome-wide expression analysis of genes affected by amino acid sensor Ssy1p in Saccharomyces cerevisiae. *Curr. Genet*. 2002;41(2):63-72.

438. Ozcan S. Two different signals regulate repression and induction of gene expression by glucose. *J Biol Chem*. 2002;277(49):46993-7.

439. Lacefield S, Solomon F. A novel step in beta-tubulin folding is important for heterodimer formation in Saccharomyces cerevisiae. *Genetics*. 2003;165(2):531-41.

440. Lacefield S, Magendantz M, Solomon F. Consequences of defective tubulin folding on heterodimer levels, mitosis and spindle morphology in Saccharomyces cerevisiae. *Genetics*. 2006;173(2):635-46.

441. Burke D, Gasdaska P, Hartwell L. Dominant effects of tubulin overexpression in Saccharomyces cerevisiae. *Mol. Cell. Biol*. 1989;9(3):1049-1059.

442. Kim YJ, Francisco L, Chen GC, Marcotte E, Chan CS. Control of cellular morphogenesis by the Ip12/Bem2 GTPase-activating protein: possible role of protein phosphorylation. *J. Cell Biol*. 1994;127(5):1381-1394.

443. Eshel D, Urrestarazu LA, Vissers S, et al. Cytoplasmic dynein is required for normal nuclear segregation in yeast. *Proc. Natl. Acad. Sci. U.S.A*. 1993;90(23):11172-11176.

444. Saunders WS, Koshland D, Eshel D, Gibbons IR, Hoyt MA. Saccharomyces cerevisiae kinesin- and dynein-related proteins required for anaphase chromosome segregation. *J. Cell Biol*. 1995;128(4):617-624.

445. Page BD, Satterwhite LL, Rose MD, Snyder M. Localization of the Kar3 kinesin heavy chain-related protein requires the Cik1 interacting protein. *J. Cell Biol*. 1994;124(4):507-519.

446. Gardner MK, Haase J, Mythreye K, et al. The microtubule-based motor Kar3 and plus end-binding protein Bim1 provide structural support for the anaphase spindle. *J. Cell Biol*. 2008;180(1):91-100.

447. Schroer TA. DYNACTIN. *Annu. Rev. Cell Dev. Biol.* 2004;20(1):759-779.

448. Tong AHY, Drees B, Nardelli G, et al. A combined experimental and computational strategy to define protein interaction networks for peptide recognition modules. *Science*. 2002;295(5553):321-324.

449. Soulard A, Lechler T, Spiridonov V, et al. Saccharomyces cerevisiae Bzz1p is implicated with type I myosins in actin patch polarization and is able to recruit actin-polymerizing machinery in vitro. *Mol. Cell. Biol*. 2002;22(22):7889-7906.

450. Honigberg SM. Ime2p and Cdc28p: co-pilots driving meiotic development. *J. Cell. Biochem*. 2004;92(5):1025-33.

451. Diderich JA, Schepper M, van Hoek P, et al. Glucose uptake kinetics and transcription of HXT genes in chemostat cultures of Saccharomyces cerevisiae. *J Biol Chem*. 1999;274(22):15350-9.

452. Ohlmeier S, Kastaniotis AJ, Hiltunen JK, Bergmann U. The yeast mitochondrial proteome, a study of fermentative and respiratory growth. *J. Biol. Chem*. 2004;279(6):3956-3979.

453. Rigoulet M, Aguilaniu H, Avéret N, et al. Organization and regulation of the cytosolic NADH metabolism in the yeast Saccharomyces cerevisiae. *Mol. Cell. Biochem*. 2004;256-257(1-2):73-81.

454. Gaisne M, Bécam AM, Verdière J, Herbert CJ. A 'natural' mutation in Saccharomyces cerevisiae strains derived from S288c affects the complex regulatory gene HAP1 (CYP1). *Curr. Genet*. 1999;36(4):195-200.

455. Nevoigt E, Stahl U. Osmoregulation and glycerol metabolism in the yeast Saccharomyces cerevisiae. *FEMS Microbiol. Rev*. 1997;21(3):231-241.

456. Ansell R, Granath K, Hohmann S, Thevelein JM, Adler L. The two isoenzymes for yeast NAD+-dependent glycerol 3-phosphate dehydrogenase encoded by GPD1 and GPD2 have distinct roles in osmoadaptation and redox regulation. *EMBO J.* 1997;16(9):2179–2187.

457. Hohmann S, Krantz M, Nordlander B. Yeast Osmoregulation. In: *Osmosensing and Osmosignaling*.Vol Volume 428.

458. Påhlman I, Larsson C, Averét N, et al. Kinetic regulation of the mitochondrial glycerol-3-phosphate dehydrogenase by the external NADH dehydrogenase in Saccharomyces cerevisiae. *J. Biol. Chem*. 2002;277(31):27991-27995.

459. Pahlman AK, Granath K, Ansell R, Hohmann S, Adler L. The yeast glycerol 3-phosphatases Gpp1p and Gpp2p are required for glycerol biosynthesis and differentially involved in the cellular responses to osmotic, anaerobic, and oxidative stress. *J. Biol. Chem*. 2001;276(5):3555-3563.

460. Hung G, Brown CR, Wolfe AB, Liu J, Chiang H. Degradation of the gluconeogenic enzymes fructose-1,6-bisphosphatase and malate dehydrogenase is mediated by distinct proteolytic pathways and signaling events. *J. Biol. Chem*. 2004;279(47):49138-49150.

461. Brown CR, Wolfe AB, Cui D, Chiang H. The vacuolar import and degradation pathway merges with the endocytic pathway to deliver fructose-1,6-bisphosphatase to the vacuole for degradation. *J Biol Chem*. 2008;283(38):26116-27.

462. Horak J, Regelmann J, Wolf DH. Two distinct proteolytic systems responsible for glucose-induced degradation of fructose-1,6-bisphosphatase and the Gal2p transporter in the yeast Saccharomyces cerevisiae share the same protein components of the glucose signaling pathway. *J Biol Chem*. 2002;277(10):8248-54.

463. Albers E, Laizé V, Blomberg A, Hohmann S, Gustafsson L. Ser3p (Yer081wp) and Ser33p (Yil074cp) are phosphoglycerate dehydrogenases in Saccharomyces cerevisiae. *J. Biol. Chem*. 2003;278(12):10264-72.

464. McNeil JB, McIntosh EM, Taylor BV, et al. Cloning and molecular characterization of three genes, including two genes encoding serine hydroxymethyltransferases, whose inactivation is required to render yeast auxotrophic for glycine. *J. Biol. Chem*. 1994;269(12):9155-9165.

465. Hollenberg CP, Riks WF, Borst P. The glutamate dehydrogenases of yeast: Extra-mitochondrial enzymes. *Biochimica et Biophysica Acta (BBA) - General Subjects*. 1970;201(1):13-19.

466. DeLuna A, Avendano A, Riego L, Gonzalez A. NADP-glutamate dehydrogenase isoenzymes of Saccharomyces cerevisiae. Purification, kinetic properties, and physiological roles. *J Biol Chem*. 2001;276(47):43775-83.

467. Mazón MJ, Hemmings BA. Regulation of Saccharomyces cerevisiae nicotinamide adenine dinucleotide phosphate-dependent glutamate dehydrogenase by proteolysis during carbon starvation. *J. Bacteriol.* 1979;139(2):686-9.

468. Contreras-Shannon V, Lin A, McCammon MT, McAlister-Henn L. Kinetic properties and metabolic contributions of yeast mitochondrial and cytosolic NADP+-specific isocitrate dehydrogenases. *J Biol Chem*. 2005;280(6):4469-75.

469. Rintala E, Pitkänen J, Vehkomäki M, Penttilä M, Ruohonen L. The ORF YNL274c (GOR1) codes for glyoxylate reductase in Saccharomyces cerevisiae. *Yeast*. 2007;24(2):129-136.

470. Nathalie Spielewoy et al., “Regulation and recognition of SCFGrr1 targets in the glucose and amino acid signaling pathways,” *Molecular and Cellular Biology* 24, no. 20 (October 2004): 8994-9005.

471. Hiesinger M, Roth S, Meissner E, Schüller HJ. Contribution of Cat8 and Sip4 to the transcriptional activation of yeast gluconeogenic genes by carbon source-responsive elements. *Curr Genet*. 2001;39(2):68-76.

472. Tachibana C, Yoo JY, Tagne J, et al. Combined global localization analysis and transcriptome data identify genes that are directly coregulated by Adr1 and Cat8. *Mol Cell Biol*. 2005;25(6):2138-46.

473. Young ET, Dombek KM, Tachibana C, Ideker T. Multiple pathways are co-regulated by the protein kinase Snf1 and the transcription factors Adr1 and Cat8. *J Biol Chem*. 2003;278(28):26146-58.

474. Tachibana C, Yoo JY, Tagne J, et al. Combined global localization analysis and transcriptome data identify genes that are directly coregulated by Adr1 and Cat8. *Mol Cell Biol*. 2005;25(6):2138-46.

475. Schüller H. Transcriptional control of nonfermentative metabolism in the yeast Saccharomyces cerevisiae. *Curr. Genet*. 2003;43(3):139-160.

476. Yin Z, Hatton L, Brown AJ. Differential post-transcriptional regulation of yeast mRNAs in response to high and low glucose concentrations. *Mol. Microbiol*. 2000;35(3):553-565.

477. Heyland J, Fu J, Blank LM. Correlation between TCA cycle flux and glucose uptake rate during respiro-fermentative growth of Saccharomyces cerevisiae. *Microbiology (Reading, Engl.)*. 2009.

478. Lee AC, Xu X, Blachly-Dyson E, Forte M, Colombini M. The role of yeast VDAC genes on the permeability of the mitochondrial outer membrane. *J. Membr. Biol*. 1998;161(2):173-181.

479. Kmita H, Stobienia O, Michejda J. The access of metabolites into yeast mitochondria in the presence and absence of the voltage dependent anion selective channel (YVDAC1). *Acta Biochim. Pol*. 1999;46(4):991-1000.

480. Kmita H, Budzińska M. Involvement of the TOM complex in external NADH transport into yeast mitochondria depleted of mitochondrial porin1. *Biochim. Biophys. Acta*. 2000;1509(1-2):86-94.

481. Ho Y, Gruhler A, Heilbut A, et al. Systematic identification of protein complexes in Saccharomyces cerevisiae by mass spectrometry. *Nature*. 2002;415(6868):180-183.

482. Greenbaum D, Colangelo C, Williams K, Gerstein M. Comparing protein abundance and mRNA expression levels on a genomic scale. *Genome Biol*. 2003;4(9):117.

483. Gygi SP, Rochon Y, Franza BR, Aebersold R. Correlation between protein and mRNA abundance in yeast. *Mol. Cell. Biol*. 1999;19(3):1720-1730.

484. Ideker T, Thorsson V, Ranish JA, et al. Integrated Genomic and Proteomic Analyses of a Systematically Perturbed Metabolic Network. *Science*. 2001;292(5518):929-934.

485. Wu G, Nie L, Zhang W. Integrative Analyses of Posttranscriptional Regulation in the Yeast Saccharomyces cerevisiae Using Transcriptomic and Proteomic Data. *Current Microbiology*. 2008;57(1):18-22.

486. Beyer A, Hollunder J, Nasheuer H, Wilhelm T. Post-transcriptional Expression Regulation in the Yeast Saccharomyces cerevisiae on a Genomic Scale. *Mol Cell Proteomics*. 2004;3(11):1083-1092.

487. Washburn MP, Koller A, Oshiro G, et al. Protein pathway and complex clustering of correlated mRNA and protein expression analyses in Saccharomyces cerevisiae. *Proc Natl Acad Sci U S A.* 2003;100(6):3107–3112.

488. Hinnebusch AG. Translational Regulation of Gcn4 and the General Amino Acid Control of Yeast*. *Annu. Rev. Microbiol.* 2005;59(1):407-450.

489. Wittenberg C. Cell cycle: cyclin guides the way. *Nature*. 2005;434(7029):34-5.

490. Mendenhall MD, Hodge AE. Regulation of Cdc28 cyclin-dependent protein kinase activity during the cell cycle of the yeast Saccharomyces cerevisiae. *Microbiol. Mol. Biol. Rev*. 1998;62(4):1191-1243.

491. King RW, Deshaies RJ, Peters JM, Kirschner MW. How proteolysis drives the cell cycle. *Science*. 1996;274(5293):1652-9.

492. Hicke L. Ubiquitin-dependent internalization and down-regulation of plasma membrane proteins. *FASEB J*. 1997;11(14):1215-1226.

493. Dupré S, Urban-Grimal D, Haguenauer-Tsapis R. Ubiquitin and endocytic internalization in yeast and animal cells. *Biochim Biophys Acta*. 2004;1695(1-3):89-111.

494. Horák J. Yeast nutrient transporters. *Biochim Biophys Acta*. 1997;1331(1):41-79.

495. Horak J, Wolf DH. The ubiquitin ligase SCF(Grr1) is required for Gal2p degradation in the yeast Saccharomyces cerevisiae. *Biochem Biophys Res Commun*. 2005;335(4):1185-90.

496. Brondijk TH, Konings WN, Poolman B. Regulation of maltose transport in Saccharomyces cerevisiae. *Arch Microbiol*. 2001;176(1-2):96-105.

497. Arava Y, Wang Y, Storey JD, et al. Genome-wide analysis of mRNA translation profiles in Saccharomyces cerevisiae. *Proc. Natl. Acad. Sci. U.S.A*. 2003;100(7):3889-3894.

498. Arava Y, Boas FE, Brown PO, Herschlag D. Dissecting eukaryotic translation and its control by ribosome density mapping. *Nucleic Acids Res*. 2005;33(8):2421-2432.

499. Belle A, Tanay A, Bitincka L, Shamir R, O'Shea EK. Quantification of protein half-lives in the budding yeast proteome. *Proc Natl Acad Sci U S A.* 2006;103(35):13004–13009.

500. Cereghino GP, Atencio DP, Saghbini M, Beiner J, Scheffler IE. Glucose-dependent turnover of the mRNAs encoding succinate dehydrogenase peptides in Saccharomyces cerevisiae: sequence elements in the 5' untranslated region of the Ip mRNA play a dominant role. *Mol. Biol. Cell*. 1995;6(9):1125-1143.

501. Zitomer RS, Nichols DL. Kinetics of glucose repression of yeast cytochrome c. *J. Bacteriol*. 1978;135(1):39-44.

502. Zitomer RS, Montgomery DL, Nichols DL, Hall BD. Transcriptional regulation of the yeast cytochrome c gene. *Proc. Natl. Acad. Sci. U.S.A*. 1979;76(8):3627-3631.

503. Federoff HJ, Eccleshall TR, Marmur J. Carbon catabolite repression of maltase synthesis in Saccharomyces carlsbergensis. *J. Bacteriol*. 1983;156(1):301-307.

504. Cereghino GP, Scheffler IE. Genetic analysis of glucose regulation in saccharomyces cerevisiae: control of transcription versus mRNA turnover. *EMBO J*. 1996;15(2):363-374.
505. Surosky RT, Strich R, Esposito RE. The yeast UME5 gene regulates the stability of meiotic mRNAs in response to glucose. *Mol. Cell. Biol*. 1994;14(5):3446-3458.

506. Paradela A, Albar JP. Advances in the analysis of protein phosphorylation. *J. Proteome Res*. 2008;7(5):1809-1818.

507. Kim J, Petritis K, Shen Y, et al. Phosphopeptide elution times in reversed-phase liquid chromatography. *Journal of Chromatography A*. 2007;1172(1):9-18.

508. Froelich JM, Reid GE. The effect of post-translational and process-induced modifications on the multistage gas-phase fragmentation reactions of protonated peptides. *Comb. Chem. High Throughput Screen*. 2009;12(2):175-184.

509. Picotti P, Bodenmiller B, Mueller LN, Domon B, Aebersold R. Full dynamic range proteome analysis of S. cerevisiae by targeted proteomics. *Cell*. 2009;138(4):795-806.

510. Reinders J, Wagner K, Zahedi RP, et al. Profiling Phosphoproteins of Yeast Mitochondria Reveals a Role of Phosphorylation in Assembly of the ATP Synthase. *Mol Cell Proteomics*. 2007;6(11):1896-1906.

511. Fischer R, Zekert N, Takeshita N. Polarized growth in fungi--interplay between the cytoskeleton, positional markers and membrane domains. *Mol. Microbiol*. 2008;68(4):813-826.

512. Jiang H, Medintz I, Michels CA. Two glucose sensing/signaling pathways stimulate glucose-induced inactivation of maltose permease in Saccharomyces. *Mol Biol Cell*. 1997;8(7):1293-304.

513. Medintz I, Jiang H, Michels CA. The role of ubiquitin conjugation in glucose-induced proteolysis of Saccharomyces maltose permease. *J Biol Chem*. 1998;273(51):34454-62.

514. Horak J, Wolf DH. Glucose-induced monoubiquitination of the Saccharomyces cerevisiae galactose transporter is sufficient to signal its internalization. *J Bacteriol*. 2001;183(10):3083-8.

515. Ptacek J, Devgan G, Michaud G, et al. Global analysis of protein phosphorylation in yeast. *Nature*. 2005;438(7068):679-684.

516. Soulard A, Lechler T, Spiridonov V, et al. Saccharomyces cerevisiae Bzz1p is implicated with type I myosins in actin patch polarization and is able to recruit actin-polymerizing machinery in vitro. *Mol. Cell. Biol*. 2002;22(22):7889-7906.

517. Lechler T, Jonsdottir GA, Klee SK, Pellman D, Li R. A two-tiered mechanism by which Cdc42 controls the localization and activation of an Arp2/3-activating motor complex in yeast. *J. Cell Biol*. 2001;155(2):261-270.

# CURRICULUM VITAE

Joshua William Heyen

**Education:**

| | |
|---|---|
| Aug. 1977-May 1999 | B.S. Illinois State University<br>Department of Biology |
| Aug. 2001-May 2010 | Ph.D. Indiana University<br>Department of Biochemistry and Molecular Biology |

**Research Experience:**

| | |
|---|---|
| June 1999-May 2000 | Laboratory Technician<br>Zebrafish Physical Mapping<br>Genome Sequencing Center<br>Washington University School of Medicine |
| May 2000-Aug. 2001 | Human Sequence Finisher<br>Human Genome Project<br>Genome Sequencing Center<br>Washington University School of Medicine |

**Training Assignments:**

| | |
|---|---|
| Cara Magnabosco, Brebeuf HS student | 2007 |
| Nick Brenner, SEED Student | 2009 |

**Presentations:**

Analysis of Proteome Changes by CapLC-ESI-FTICR-MS, 2002. Yeast Genetics and Molecular Biology Meeting, July30-Aug. 4, University of Wisconsin, Madison, WI.

Dropping Yeast in a MudPIT and Cleaning Up the Mess, Aug. 2004. Invited Speaker, Miami of Ohio, Cincinatti, OH.

**Professional Experience:**

Selected and Participated in “The Graduate and Postdoctoral Summer Institute in Preparation for Carreers in Microbiology”, American Society for Microbiology, July 31-Aug. 4, 2004.

Lecturer and course instructor for the graduate course “Methods in Proteomics” at the Indiana University School of Medicine, Jan.-May 2010.

**Publications:**


Radivojac, P., Vacic, V., Haynes, C., Cocklin, R., Mohan, A., Heyen, J., Goebl, M., and Iakoucheva, L. 2010. Identification, analysis, and prediction of protein ubiquitination sites. *Protein:Struct. Func. Bioinform*. 78(2):365-380.

Yan, Zhong, Jake Y. Chen, Josh Heyen, Lee W Ott, Cary Woods, Maureen A Harrington, and Mark G Goebl (2007) Data Management in Expression-based Proteomics, in Biological Database Modeling. 2007.

Ott, L.W., Resing, K.A., Sizemore, A.W., Heyen, J.W., Cocklin, R.R., Pedrick, N.M., Woods, H.C., Chen, J.Y., Goebl, M.G., Witzmann, F.A., and Harrington, M.A. 2007. Tumor necrosis factor-α- and interleukin 1-induced cellular responses: Coupling proteomic and genomic information. J. Proteome Res. 6: 2176-2185.

International Human Genome Sequencing Consortium, 2001. Initial sequencing and analysis of the human genome. *Nature* 409, 861 – 921.

Barbazuk, B.W., Korf, I., Kadavi, C., Heyen, J., Tate, S., Wun, E., Bedell, J.A., McPherson, J.D., Johnson, S.L. 2000. The Syntenic Relationship of the Zebrafish and Human Genomes. *Genome Research* 10, 1351 – 1358.